

ALKALINE INTRUSIVES

from the

TUGELA TERRANE, NATAL METAMORPHIC PROVINCE

by


Andrew John Scogings

Submitted in fulfilment of the requirements for the degree
of Doctor of Philosophy in the Department of Geology,
University of Durban-Westville.

Durban, October 1991



FRONTISPIECE : PANORAMIC VIEW NORTHWARDS ONTO THE CENTRAL PART OF THE BULLS RUN COMPLEX. FIELD OF VIEW ABOUT 6 km , TOTAL RELIEF IS SOME 400m ABOVE THE MHLATUZE RIVER.

ABSTRACT

Three gneissose alkaline granitoid intrusives at Ngoye, Bulls Run and Wangu are described. They are located within the Nkomo Nappe of the Tugela Terrane, near the northern margin of the Natal Metamorphic Province.

The Ngoye Complex comprises alkaline granites, with minor syenite and monzodiorite phases. According to modal and geochemical criteria the Ngoye granites range from peraluminous (muscovite-bearing), through metaluminous (biotite- and/or hornblende-bearing), to peralkaline (riebeckite-, aegirine- and magnetite-bearing). The granites are A-types according to their modal and geochemical characteristics. Rb-Sr isotopic data for the hornblende granites indicate an age of 1063 ± 17 Ma and the initial ratio ($R_0 = 0.7025$) provides evidence for derivation from a mantle source. Plotting of the Ngoye geochemistry on tectonic-discrimination diagrams suggests intrusion into rifted continental crust. It is concluded that the gneissose Ngoye granites constitute a deformed central complex, similar to anorogenic complexes in Nigeria and the Sudan.

The Bulls Run Complex is situated 30 km west of the Ngoye Complex. A concentric outcrop pattern has been mapped, according to which an envelope of silica-saturated biotite-muscovite syenite surrounds a core of nepheline-bearing syenites. Minor intrusive phases include biotite-rich dykes, sövite carbonatite sheets, silica-oversaturated microsyenite dykes and feldspathic ijolite. The outer envelope of muscovite-rich syenite is interpreted as fenitised pelitic country rock. An alkali-lamprophyre origin is suggested for the biotite-rich dykes. Geochemically the syenites are predominantly miaskitic, apart from the microsyenite dykes which are mildly peralkaline. Rb-Sr isotopic data for the nepheline syenites indicate an age of 1138 ± 45 Ma ($R_0 = 0.70322$). Carbonate separates from the carbonatites provide a similar low initial ratio ($R_0 = 0.70319$) which supports a comagmatic mantle origin. A comparison is drawn between the Bulls Run Complex and miaskitic nepheline syenite gneisses in the mid-Proterozoic Grenville

(ii)

Province of Canada. From this, it is suggested that the Bulls Run Complex is pre-tectonic and was intruded into the rifted passive margin of a continent.

The Wangu Granite Gneiss is situated 3 km southwest of the Bulls Run Complex. The granites are fine grained and contain aegirine-augite and/or magnetite, and classify as alkali-feldspar granite. Peralkaline chemistry is characteristic of the Wangu granites, with trace-element contents indicating a distinct A-type signature. Biotite-rich mafic dykes intrude the southern part of the Wangu outcrop and, on the basis of major- and trace-element signatures, are suggested to be metamorphosed volatile-rich alkaline lamprophyres similar to those at Bulls Run. Geochemical similarities between the Wangu granites and certain comendites from the Kenya Rift are noted. It is suggested that the Wangu granites were emplaced as high-level dykes, within rifted continental crust.

It is proposed that the Ngoye, Bulls Run and Wangu intrusives be united as the Nkwaleni Suite.

Comparison of the Tugela Terrane with the Grenville Province reveals many similarities, particularly their mid- to late-Proterozoic age and the occurrence of pre-tectonic anorogenic continental magmatism. It is concluded that, unlike the current model which would have the Tugela Terrane as obducted ophiolite, these new data indicate that the Tugela Terrane is a metamorphosed continental rift system.

UITTREKSEL

Drie gneisagtige granitoïed intrusiewe liggame by Ngoye, Bulls Run en Wangu word beskryf. Die liggame kom voor in die Nkomo Nappe in die Tugela Terrein naby die noordelike grens van die Natal Metamorfe Provinsie.

Die Ngoye Kompleks bestaan uit alkali graniete met ondergeskikte sieniet en monzodioriet fases. Volgens modale en geochemiese analyses varieer die Ngoye graniete in samestelling van per-aluminieus (met muskoviet) na met-aluminieus (biotiet en/of hornblende-bevattend) tot per-alkalies (met riebeckiet, egirien en magnetiet). Gebaseer op modale en geochemiese kenmerke word die graniete as A-tipes geklassifiseer. Die Rb-Sr isotoop data van die hornblende graniete dui op 'n ouderdom van 1063 ± 17 Ma en die aanvangsverhouding (R_0) dui op 'n mantel oorsprong ($R_0 = 0,7025$). Verspreiding van die Ngoye geochemiese data op tektoniese onderskeidsdiagramme dui op intrusie in 'n kontinentale slenkdalomgewing. Die gevolgtrekking kan derhalwe gemaak word dat die gneisagtige Ngoye graniete verteenwoordigend is van 'n vervormde sentrale kompleks wat vergelykbaar is met anorogenetiese komplekse in Nigerië en Sudan.

Die Bulls Run Kompleks is 30km wes van die Ngoye Kompleks geleë. 'n Konsentriese dagsoom patroon van 'n nefelienryke siënietskern word omring deur 'n silika versadigde biotiet-muskoviet sieniet. Ondergeskikte intrusiewe fases sluit in biotietryke gange, söviet karbonatietplate, silika oorversadigde mikro-siëniëtgange en veldspatiese ijoliet. Die buitenste sone bestaan uit muskoviet-ryke siëniët en word geïnterpreteer as gefenitiseerde pelitiese omgewingsgesteente. Dit word voorgestel dat die biotietryke gange 'n alkaliese lamprofier-oorsprong het. Geochemies is die siëniëte hoofsaaklik miaskities, behalwe die mikro-siëniëtgange wat effens na peralkalies neig. Die Rb-Sr isotoop data van die nefelien siëniëte dui op 'n ouderdom van 1138 ± 45 Ma ($R_0 = 0,70322$). Karbonaat skeidings van karbonatiete toon ook 'n soortgelyke aanvangsverhouding ($R_0 = 0,70319$) wat 'n ko-magmatiese mantel oorsprong ondersteun. Die Bulls Run Kompleks kan vergelyk word

met die miaskitiese nefelien siënië gneise van die Proterosoiese Grenville Provinsie in Kanada. Aldus word voorgestel dat die Bulls Run Kompleks 'n pre-tektoniese slenkdal intrusie is in die randsones van 'n passiewe kontinent.

Die Wangu Graniet Gneis is 3km suidwes van die Bulls Run Kompleks geleë. Die fynkorrelrige graniete bevat egerien-ougiet en/of magnetiet en klassifiseer as 'n alkali-veldspaat graniet. Die peralkaliese chemiese karakter is tipies van die Wangu graniete, terwyl die spoorelement-samestelling dit as 'n A-tipe graniet kenmerk. Biotietryke mafiese intrusies in die suidelike gedeelte van die Wangu dagsoom word aan die hand van hoof- en spoorelemente-inhoud geklassifiseer as gemetamorfiseerde alkaliese mafiese gesteente met 'n hoë vluiginhoud soortgelyk aan dié van die Bulls Run Kompleks. Geochemiese ooreenkomste is ook opgemerk tussen die Wangu graniete en sekere "comenditiese" gesteentes van die Kenia Slenkdal. Dit word voorgestel dat die Wangu graniete waarskynlik ingeplaas is as hoë vlak gange in die kontinentale kors van die slenkdal.

Dit word voorgestel dat die Ngoye, Bulls Run en Wangu intrusies gesamentlik bekend sal staan as die Nkwaleni Suite.

'n Vergelyking tussen die Tugela Terrein en die Grenville Provinsie toon heelwat ooreenkomste in besonder die middel- tot laat-Proterosoiese ouderdom sowel as die voorkoms van pre-tektoniese anorogenetiese kontinentale magmatisme. Die slotsom is dat die Tugela Terrein 'n gemetamorfiseerde kontinentale slenkdal sisteem is en nie soos die huidige model voorstel, 'n geobdiseerde ofioliet nie.

TABLE OF CONTENTS

	Page
FRONTISPICE	
ABSTRACT	i
UITTREKSEL	iii
CONTENTS	v
ACKNOWLEDGEMENTS	vii
 Chapter 1: INTRODUCTION	
1.1 Aims and methodology	1
1.2 Structure of the dissertation	3
1.3 Regional geological setting	4
1.4 Nappes of the Tugela Group	6
1.5 Alkaline granitoids: their characteristics	9
 Chapter 2: THE NGOYE COMPLEX	
2.1 Introduction	19
2.2 Field and petrographic descriptions	23
2.3 Geochemistry	33
2.4 Rb-Sr isotopes	53
2.5 Tectono-magmatic discrimination	57
2.6 Summary of salient features	63
 Chapter 3: THE BULLS RUN COMPLEX	
3.1 Introduction	64
3.2 Structural considerations	67
3.3 Field and petrographic descriptions	72
3.4 Geochemistry	92
3.5 Rb-Sr isotopes	115
3.6 Discussion of fenites and lamprophyres	119
3.7 Tectono-magmatic discrimination	123
3.8 Summary of salient features	128

	Page
Chapter 4: THE WANGU GRANITE	
4.1 Introduction	129
4.2 Field and petrographic descriptions	132
4.3 Geochemistry	136
4.4 Tectono-magmatic discrimination	150
4.5 Summary of salient features	157
Chapter 5: SUMMARY, DISCUSSION AND CONCLUSIONS	
5.1 Summary	159
5.2 Discussion	166
5.3 Conclusions	172
REFERENCES	173

APPENDICES

APPENDIX 1

Sample identification (Tables I, II, III)	
Modal analyses (Tables A1.1, A1.2, A1.3)	1

APPENDIX 2

Geochemistry (Tables A2.1, A2.2, A2.3)	15
--	----

APPENDIX 3

CIPW norms and mesonorms (Tables A3.1, A3.2, A3.3)	32
--	----

APPENDIX 4

Publications and symposium abstracts	47
--------------------------------------	----

ACKNOWLEDGEMENTS

Sincere thanks are extended to my promoters Prof. Mike Cooper and Dr John Dunlevey for their valued assistance and encouragement during the past five years. Dr Andrew Mitchell is thanked for informative discussions. I am indebted to Dr Ingo Forster for having made available for me the post of research assistant at the University of Durban-Westville, during the period 1984 to 1987. To Stanley and Ashwin, many thanks for the excellent thin sections and polished rock slabs produced.

Bruce Eglington and Jock Harmer are thanked for their invaluable assistance with the Rb-Sr isotope data, as well as useful discussions regarding carbonatites.

Mona Heine is thanked for her assistance with the photographs. Alfred Ahrens, Nic Thirion and Matt du Toit are thanked for their help with translating the abstract.

I would like to thank the Mineral Development Division of STK for having funded the geochemical analysis of some of the Bulls Run samples during 1987. Mr V. E. Viljoen kindly allowed me access to the laser printer at STK, a tremendous benefit. To Mr J-D. Germiquet, thanks for understanding my situation during the past few months. Helen de Jager, thanks for willing assistance in typing numerous tables, and for printing this document.

For accommodation so generously offered during my field trips, my gratitude is extended to John Adlam and the Parkers of Port Durnford State Forest, as well as to Jamie and Tessa Chance at Nkwaleneni.

To my parents David and Irene Scogings for encouraging me in the pursuit of further education, and to my parents'-in-law Philip and Cherie for their moral support, my heartfelt thanks.

This thesis is dedicated to my wife Renee, for all her support and encouragement, particularly during my period of leave away from home while completing this thesis. Without her I would not have persevered to this stage.

Chapter 1

INTRODUCTION

1.1 Aims and methodology

This study forms part of an ongoing research programme at the University of Durban-Westville (UDW), aimed at investigating alkaline granitoid intrusive bodies in the northern part of the Natal Metamorphic Province (hereafter referred to as the NMP). The results of field mapping, petrographical, geochemical and isotope studies carried out over an area of some 200 km² across the Ngoye, Bulls Run and Wangu intrusives (Fig. 1.1) are presented and collated, as a logical extension to earlier research on the Ngoye Complex (Scogings 1985).

Following the initial discovery of alkaline granitoids at Ngoye, and realisation of their importance with regard to the tectonic history of the NMP, a reconnaissance sampling and mapping exercise was commenced in 1985 to screen the area to the west of Ngoye. By the end of 1986 several interesting alkaline outcrops had been located (Fig. 1.1) and, for the purposes of this thesis, it was decided to restrict work to three of these, with the remainder targeted for research at a later date.

In view of the wealth of detailed structural and metamorphic data available from previous investigations of this part of the NMP (Charlesworth 1981, Matthews & Charlesworth 1981, Scogings 1985) this study has been directed towards "seeing" through the superimposed metamorphic and deformational "screen", so as to elucidate the

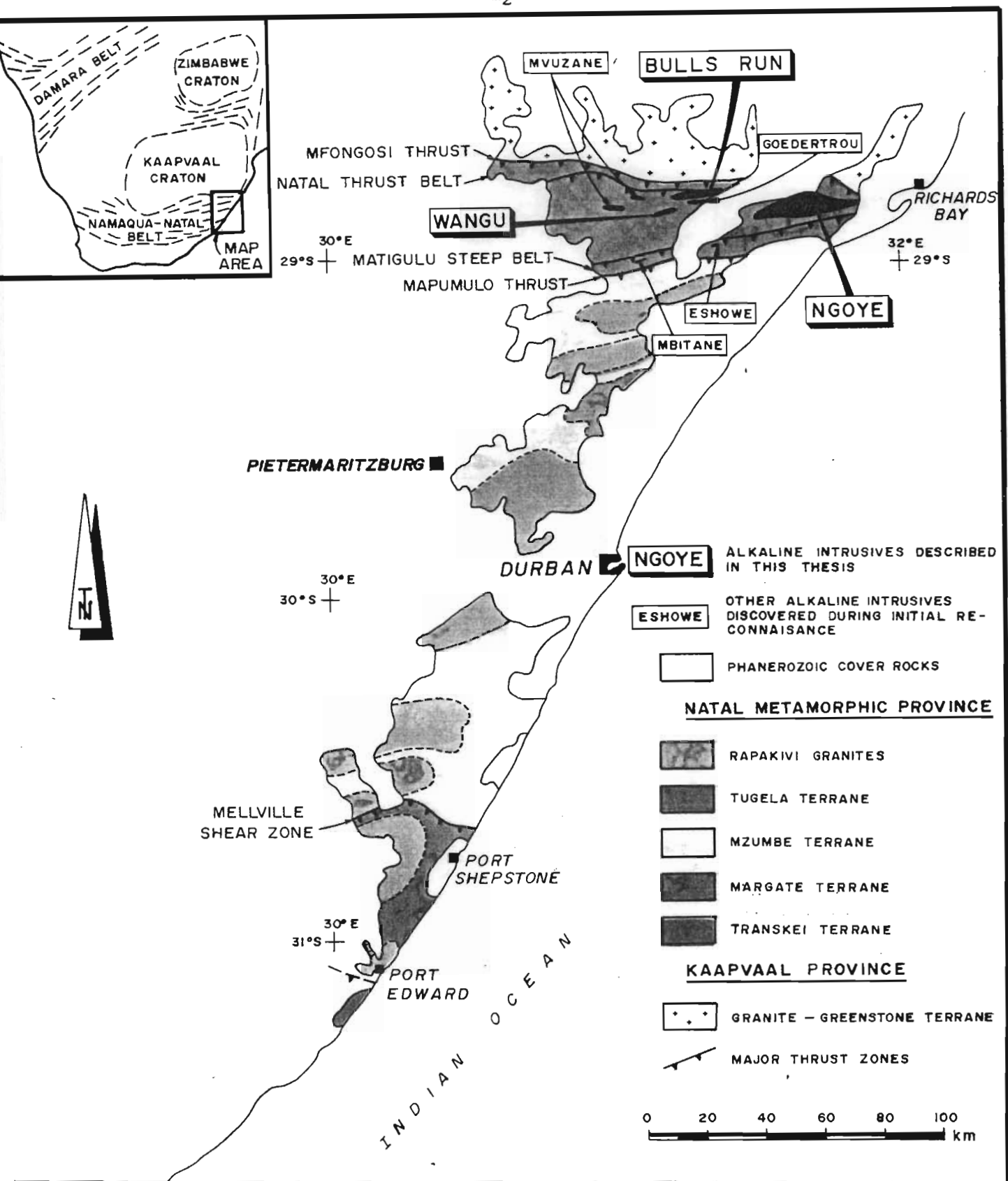


Figure 1.1. Location of the Ngoye, Bull's Run and Wangu alkaline intrusives within the Tugela Terrane. Other alkaline occurrences discovered during initial reconnaissance are also shown. Subdivision of the Natal Metamorphic Province after Thomas (1990), Thomas *et al.* (1990).

pre-deformational character of the granitoid intrusives. The term "granitoid" is used here in the broadest sense to describe all leucocratic crystalline rocks of granitic field appearance, including undersaturated syenite, syenite and granite. The majority of the rocks mapped display gneissose fabrics and, as they are of igneous origin, should strictly be classified as gneissic granitoids, meta-granitoids, or orthogneisses. However, the gneissosity is heterogeneous and tends to be concentrated in mylonitic zones of high strain, with some of the outcrops virtually devoid of any visible fabric. Therefore, as the purpose of this thesis is to define the original character of the various lithologies, the term "gneissic" is omitted for brevity (cf. Scogings 1985).

1.2 Structure of the dissertation

Chapter 1 introduces the topic, describing and outlining the regional geological setting. As the Ngoye, Bulls Run and Wangu granitoid bodies are located in the northern portion of the NMP, this area is treated in more detail than the southern reaches of the province. Due to the alkaline nature of the granitoids, attention is given to highlighting the general characteristics of alkaline (A-type) granitoid suites, as a basis for discussion in subsequent chapters.

Chapters 2, 3 and 4 are devoted to the descriptive geology of the Ngoye and Bulls Run Complexes and the Wangu Granite respectively. Much of the data have been published during the duration of the research project (Scogings 1986, 1989, 1990b, 1991a, 1991b, Scogings & Forster 1989), and this part of the dissertation aims to summarise earlier reports and to update the published database. Additional hitherto unpublished data presented for the Ngoye Complex includes certain whole-rock analyses, REE data, Rb-Sr isotopic interpretation, microprobe mineral analyses and some revisions to the earlier geological map. The Bulls Run database has been augmented by additional field mapping and the discovery of feldspathic ijolite, REE analyses, microprobe mineral data, Rb-Sr isotopic data and interpretation of structural information. The Wangu data have been published recently in some detail (Scogings

1989) and this thesis includes new information which is related mainly to additional field mapping and the interpretation of previously unpublished geochemistry. Due to financial and logistical constraints the Wangu granitoids have not yet been subjected to Rb-Sr isotopic investigation. This facet will be addressed during the subsequent phase of this ongoing study and does not materially affect this dissertation.

Chapter 5 is largely interpretational and uses geochemical and isotopic data to gain insight into tectonic regimes operational when the alkaline granitoids were intruded. A model embracing continental-rift concepts, similar to that for the mid-Proterozoic Grenville Province, is suggested in order to account for the spatial and temporal relationships of the observed lithologies.

1.3 Regional geological setting

1.3.1 Introduction

The mid-Proterozoic NMP crops out as an elongate basement inlier parallel to the eastern seaboard of Natal and is exposed for some 300 km in a north-south direction, between Port Edward in the south and Richards Bay in the north (Fig. 1.1). Whereas the exposed northern margin of the NMP is known to be in thrust contact with the Archaean Kaapvaal Craton, elsewhere it passes beneath younger sedimentary cover and its true extent is conjectural. However, it is believed to extend westwards, beneath this younger cover, to connect with the coeval Namaqua Province (Nicolaysen & Burger 1965). Although the NMP is restricted to a narrow north-south outcrop, a good transverse section is available across the structural grain of the belt, allowing subdivision into four major zones (Matthews 1981).

On the basis of lithological, metamorphic and structural characteristics, including the discovery of a previously-unknown gneissic terrane to the south of Port Edward (Thomas & Mawson 1989), Matthews' (1981) classification was modified and redefined by Thomas (1989 1990) who recognised four tectonostratigraphic terranes described from south to north as:

1.3.2 Transkei Terrane

This is an amphibolite-grade terrane intruded by S-type granitoids, distinctly different from the granulite-grade Margate Terrane to the north (Thomas & Mawson 1989).

1.3.3 Margate Terrane

This corresponds to the Granulite Zone of Matthews (1981) and is characterized by granulite-grade supracrustal gneisses, calc-silicates, marbles and metapelites of the Mzinkulu Group, into which leucogranites, charnockites, mafic sheets and large plutons and batholiths of megacrystic rapakivi granite were intruded (Grantham 1983, Mendonidis & Grantham 1989, Mendonidis & Strydom 1989, Thomas 1989, 1990). The northern margin of this terrane is marked by a prominent structural discontinuity known as the Melville Shear Zone (Thomas 1989).

1.3.4 Mzumbe Terrane

This unit embraces both the Migmatite and the Granite Gneiss and Granite Zones of Matthews (1981). It is characterized by felsic, semi-pelitic and pelitic paragneisses and minor amphibolites of the Mapumulo Group that have been metamorphosed to amphibolite grade by intrusion of a variety of I- and S-type granitoid suites, mafic dykes and A-type rapakivi-granite plutons (Kerr 1985, Eglington 1987, Eglington & Kerr 1989, Evans *et al.* 1987, Thomas 1989, 1990). The northern limit of the Mzumbe Terrane is drawn at the Mapumulo Thrust (Fig. 1.1).

1.3.5 Tugela Terrane

Essentially equivalent to the Northern Frontal Zone of Matthews (1981) and the Northern Marginal Zone of Tankard *et al.* (1982), this terrane is bounded in the south by the Mapumulo Thrust and to the north by the Mfongosi Thrust. As defined originally by Matthews (1981) and subsequently modified by Thomas (1990), it comprises three major structural components, namely the Natal Thrust Belt, the Natal Nappe Complex and the Matigulu Steep Belt (Fig. 1.2):

- (i) **Natal Thrust Belt:** This is a 2 to 5km-wide imbricate zone that forms the northern border of the Tugela Terrane. It comprises southward-dipping tectonic slices of greenschist-

grade material in which Mfongosi Group meta-pelites and metabasalts have been thrust northwards onto conglomerates, grits, shales and marine carbonates of the Ntingwe Group (Matthews 1972, 1981).

- (ii) **Natal Nappe Complex:** This extends southwards from the Natal Thrust Belt and is a 30 km-wide package of westward-plunging, northward-verging thrust nappes rooted in the Matigulu Steep Belt (Matthews 1972 1981). Based largely on mapping by Rigotti (1977), Schulze-Hulbe (1977), Harmer (1979), Smalley (1980) and Charlesworth (1981), Matthews (1981) constructed a schematic down-plunge section through the Tugela Terrane to illustrate the tectonostratigraphy of the Tugela Group nappes (Fig. 1.3).

The nappes are predominantly amphibolitic in composition, with infolded elements of granitic gneiss, metapelite, magnetite quartzite, and marble (Matthews 1981). In general, from the uppermost Tugela Nappe downwards to the basal Nkomo Nappe, the proportion of felsic rocks increases (Tankard *et al.* 1982).

- (iii) **Matigulu Steep Belt:** This structural unit marks the southern limit of the Tugela Terrane and is an elongate E-W zone of highly deformed, steep-dipping gneisses, of dominantly felsic composition (the Buhleni, Mpisi and Intuze Formations), with subordinate amphibole gneisses and amphibolites constituting the Sequembi and Thondo Formations (Matthews & Charlesworth 1981). The Buhleni Formation is developed extensively throughout the Steep Belt and is interpreted as a deformed S-type granite (Charlesworth 1981). The amphibolitic Sequembi Formation contains thin carbonate and magnetite quartzite layers.

1.4 Nappes of the Tugela Group

As the Ngoye, Bulls Run and Wangu granitoids, that form the basis of this thesis, are confined to the lowermost (Nkomo) nappe of the Tugela

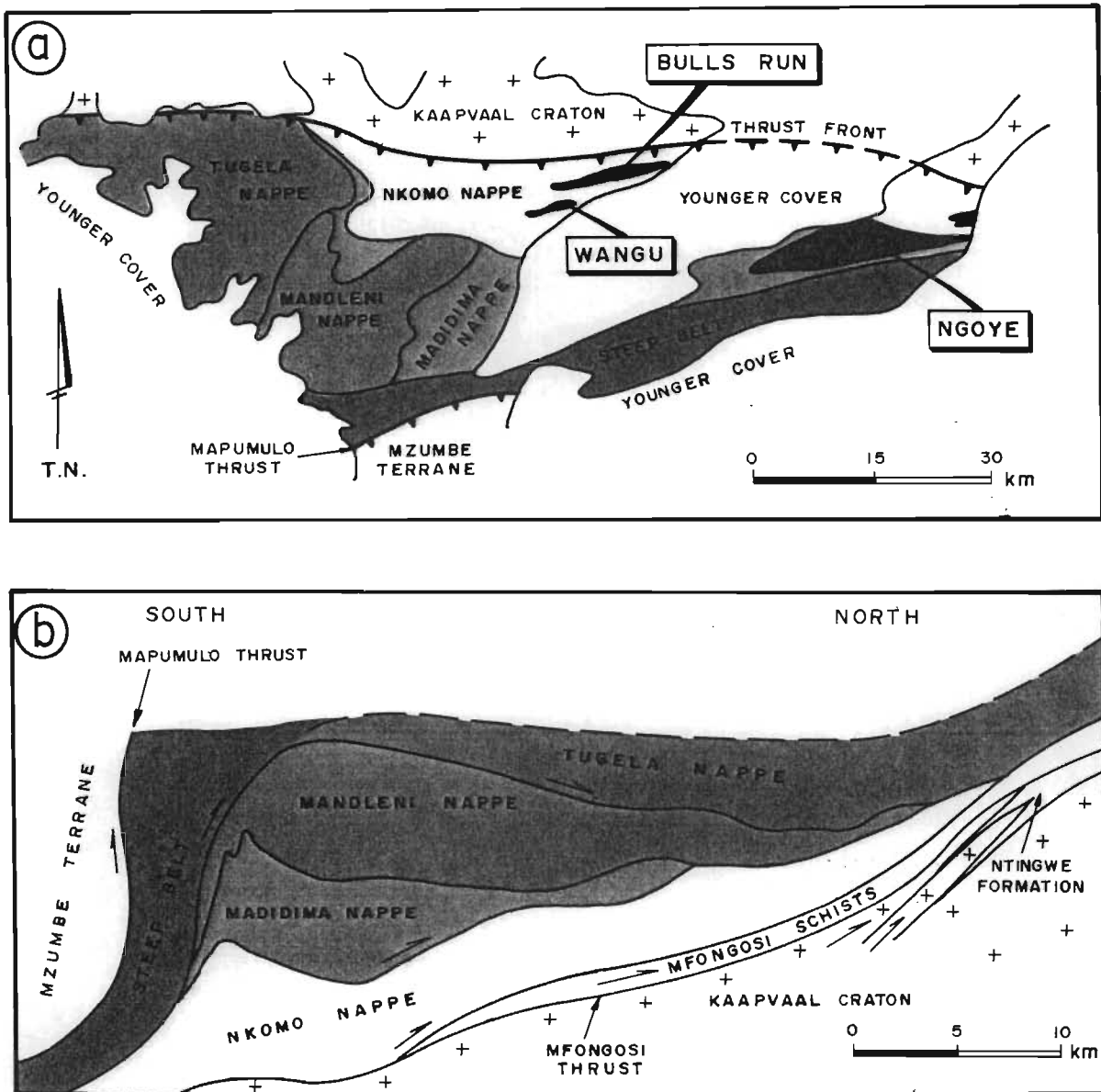


Figure 1.2. Simplified geological map (Fig. 1.2a) and schematic down-plunge structural profile (Fig. 1.2b) of the Tugela Terrane, after Matthews (1981) and Matthews & Charlesworth (1981).

Terrane, the lithological components of this and the other nappes are outlined in some detail:

1.4.1 Tugela Nappe

This is the uppermost nappe of the Tugela Group. It is largely mafic in composition and comprises two tectonic slices (Matthews 1981, Tankard et al. 1982). Whereas the lower tectonic slice, designated the Tuma Formation, is relatively felsic, with pelitic, psammitic and mafic schists, the upper slice comprises amphibolitic gneisses of the Manyane Formation. The western part of the Tugela Nappe is intruded by the Kotongweni tonalite, the enderbitic Mkondene diorite and the layered Tugela Rand Suite, the latter a predominantly norite/bronzitite/troctolite/gabbro body (Harmer 1979, Matthews & Charlesworth 1981, Wilson 1990).

1.4.2 Mandleni Nappe

Lithologically this nappe is similar to the Tugela Nappe, with mafic lithologies predominant (Matthews & Charlesworth 1981). Whereas the mafic rocks are contained within the Wosi, Dondwana and Tondweni Formations, as well as the Sithilo Serpentinite Complex, felsic semi-pelitic gneisses are exposed mainly in the western part of the nappe as the Dulumbe Formation. Magnetite quartzites and quartzites occur interlayered with the Wosi amphibolites. The intrusive Mambulu Complex is a prominent feature of the southern part of the nappe and is a saucer-shaped, well-layered, gabbro/pyroxenite/anorthosite/magnetitite body with amphibolitized margins that is exposed over some 25 km² (Schulze-Hulbe 1977).

1.4.3 Madidima Nappe

This nappe contains approximately equal proportions of mafic (Zwaneni, Endlovini and Silambo Formations) and felsic gneiss (the Thawini, Zidoni and Gazeni Formations). A large (10 x 5 km) metagabbro/serpentinite body, known as the Mlalazi Complex, crops out to the west of the Ngoye granite (Charlesworth 1981).

1.4.4 Nkomo Nappe

The Nkomo Nappe contains the three prominent granitoid bodies previously designated the Ngoye Granite, Halambu Granodiorite and Bulls Run Syenite Gneiss Formations (SACS 1980, Matthews & Charlesworth 1981), that form the basis of this dissertation. These granitoids constitute the bulk of the Nkomo Nappe, with the remainder essentially amphibolitic (the Mtengu and Khomo Formations). An olivine-norite/troctolite body, known as the Hlobane Complex, is located immediately to the north of the Ngoye granite.

Although previously the granitoids of the Nkomo Nappe were suggested to be calc-alkaline (Charlesworth 1981), this research not only has demonstrated the alkaline character of the Ngoye and Bulls Run granitoids, but also of a large proportion of the Halambu Formation in the Wangu area (Scogings 1986, 1989, Scogings & Forster 1989).

Reclassification of the Ngoye and Bulls Run Formations, as the Ngoye and Bulls Run Complexes, has been ratified by the South African Committee for Stratigraphy (Scogings 1990b, 1991a). In addition, the Wangu Granite Gneiss has been discriminated as a separate entity, distinctly different from the surrounding Halambu granodiorite (Scogings 1991b).

1.5 Alkaline granitoids: their characteristics

As alkaline "A-type" granitoid rocks are central to this thesis, an overview of their mineralogy, geochemistry, geological associations and tectonic setting is presented, to facilitate discussion of the rocks described from Ngoye, Bulls Run and Wangu.

1.5.1 Geochemistry and mineralogy

A-type granitoids are distinguished from I-, S- and M-types by their low alumina/alkali ratios, low CaO and Sr contents, and metaluminous to peralkaline compositions. In addition, as indicated in Table 1.1 and Figure 1.3, high Fe/Mg ratios, high alkalis and elevated Zr, Y, Nb, Ta, REE, Zn and Ga contents are characteristic (Loiselle & Wones 1979, Collins *et al.* 1982, Whalen *et al.* 1987, Sylvester 1989, Eby 1990).

TABLE 1.1

AVERAGE GRANITE TYPES

	M-type	I-type	Felsic-I	S-type	Felsic-S	A-type
SiO ₂	67.24	69.17	73.39	70.27	73.39	73.81
TiO ₂	0.49	0.43	0.26	0.48	0.28	0.26
Al ₂ O ₃	15.18	14.33	13.43	14.10	13.45	12.40
Fe ₂ O ₃	1.94	1.04	8.60	0.56	0.36	1.24
FeO	2.35	2.29	1.32	2.87	1.73	1.58
MnO	0.11	0.07	0.05	0.06	0.04	0.06
MgO	1.73	1.42	0.55	1.42	0.58	0.20
CaO	4.27	3.20	1.71	2.03	1.28	0.75
Na ₂ O	3.97	3.13	3.33	2.41	2.81	4.07
K ₂ O	1.26	3.40	4.13	3.96	4.56	4.65
P ₂ O ₅	0.09	0.11	0.07	0.15	0.14	0.04
Total	98.63	98.59	98.84	98.31	98.62	99.06
Zn	56	49	35	62	44	120
Ga	15	16	16	17	17	25
Nb	1	11	12	12	13	37
Zr	108	151	144	165	136	528
Y	22	28	34	32	33	75
U	<1	4	5	4	6	5
Th	1	18	22	18	18	23
Pb	5	19	23	27	28	24
Rb	18	151	194	217	277	169
Sr	282	247	143	120	81	48
Ba	263	538	510	468	388	352
Ce	16	64	68	64	53	137
Ga/Al	1.87	2.1	2.25	2.28	2.39	3.75
P.I.	0.52	0.62	0.74	0.59	0.71	0.95

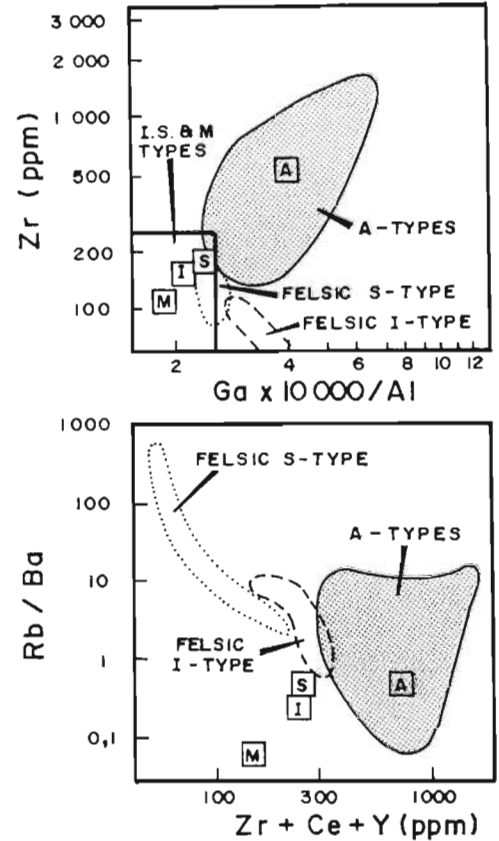


Figure 1.3. Examples of diagrams for discrimination between A-type granites and I-, S- and M-type granites, from Whalen *et al.* (1987)

Average M-, I-, S- and A-type granitoids from Whalen *et al.* (1987).

- M-type:** Derived directly from melting of subducted oceanic crust. Low K₂O, low SiO₂, hornblende-bearing.
- I-type:** Derived by partial melting of igneous protolith. Metaluminous, wide SiO₂ range, biotite- and hornblende-bearing, normative diopside, high Na₂O/K₂O ratios, moderate initial ⁸⁷Sr/⁸⁶Sr ratios (0.704-0.706). Highly fractionated I-types can have characteristics of A-types.
- S-type:** Derived from partially-melted sedimentary protolith. Peraluminous, muscovite+/-garnet bearing, normative corundum. Low Na₂O/K₂O ratios, less than 3.5% Na₂O. High initial Sr ratios >0.708 (Chappel & White 1974). Highly fractionated S-types can have A-type characteristics.
- A-type:** Derived from mantle-sourced basalt, interaction of mantle basalt with continental crust, remelting of crust that has previously had a melt extracted during previous orogenic event. Syenitic to peralkaline granite, alkali-rich mafic minerals. Enriched in Nb, Zn, Zr, REE and Ga/Al and depleted in CaO, Sr and Eu compared with I- and S-types.

It is noted that highly fractionated, felsic, S- and I-type granites (with $\text{SiO}_2 > 64\%$) can have chemistries that overlap those of A-types, particularly with respect to major elements such as Na, K and Ca. However, Fe/Mg ratios and concentrations of trace elements, eg. Nb, Zn, Ta and Y, are distinctive for A-types at high silica levels (Whalen et al. 1987, Eby 1990).

Mineralogically, A-type suites are distinguished from I- and S- types by the presence of alkali amphiboles and pyroxenes, together with iron-rich minerals such as fayalite, ferrohastingsite and annitic biotite. Whereas I- and S-type granites are hydrous minimum-melt magmas, most A-type granites form from water-undersaturated high-temperature melts enriched in F, Cl and CO_2 . A natural result of their anhydrous nature is that A-types intrude higher crustal levels than I- and S-types and, as a result, volcanic equivalents of plutonic A-types are common (Whalen et al. 1987). Both the plutonic and volcanic expressions of A-type magmatism are characterised by bimodal salic-mafic associations, with little development of rocks of intermediate composition.

Although initial $^{87}\text{Sr}/^{86}\text{Sr}$ ratios for A-type granitoids are variable and generally low ($R_0=0.703$ to 0.712), values as high as 0.739 have been recorded (Eby 1990). This broad spread of isotopic data is indicative of varying degrees of interaction between mantle-derived magmas and radiogenic crust (Eby 1990).

1.5.2 Form of intrusion and geological association

A-type granites and associated silica-undersaturated alkaline granitoids often form composite, multi-phase plugs, ring dykes and central complexes (Bowden 1974, Eby 1990). Although silica-undersaturated rocks were not included in the original definition of A-type granitoids (Loiselle & Wones 1979), the spatial and temporal relationship between undersaturated alkaline magmatism, viz. syenites, carbonatites and alkaline lamprophyres, and A-type granitoids is well documented (Collins et al. 1982, Lameyre & Bowden 1982, Eby 1984, 1985, 1990, Fitton 1987, Upton & Emeleus 1987).

1.5.3 Tectonic setting

Geological evidence indicates that A-type granites and related rocks are intruded predominantly into tensional (rifted, anorogenic or non-compressional) within-plate environments in continental crust or oceanic basins (Middlemost 1974, Macdonald 1975b, Petersen 1978, Petro *et al.* 1979, Pearce *et al.* 1984, Sawkins 1986, Thompson & Fowler 1986, Nielsen 1987, Upton & Emeeus 1987, Whalen *et al.* 1987, Elby 1990, Cooper 1991). A-type magmatism also has been ascribed to crustal relaxation at the end of compressive orogenic cycles (Whalen *et al.* 1987, Sylvester 1989, Elby 1990, Rogers & Greenberg 1990).

1.5.4 Tectonic discrimination diagrams

Numerous attempts have been made, particularly during the last decade, to devise geochemical and mineralogical plots that can be used to discriminate between granitoids emplaced in different tectonic settings (eg. Petro *et al.* 1979, Pearce *et al.* 1984, Batchelor & Bowden 1985, Whalen *et al.* 1987, Maniar & Piccoli 1989, Elby 1990, Rogers & Greenberg 1990). Salient features of various schemes are described below, with reference to selected discrimination diagrams that will be used in succeeding chapters of this thesis.

Pearce *et al.* (1984) used trace-element data, from Phanerozoic granitoid suites of known tectonic setting, to distinguish statistically between collision (COLG), volcanic-arc (VAG), ocean-ridge (ORG), and within-plate (WPG) granitoids (Table 1.2, Fig. 1.4). In their original description of WPG granites, Pearce *et al.* (1984) discriminated several tectonic settings according to the type of crust into which the granite was emplaced. These were:

- (i) **Continental crust of normal thickness**, such as that intruded by the younger granites of Nigeria, Sudan and the Oslo graben. Pearce *et al.* (1984) noted that Oslo-graben/ORG-normalised patterns are similar to those exemplified by within-plate oceanic island granites, eg. Ascension Island (Fig. 1.4). These patterns are "mantle dominated" and marked by elevated and approximately equal abundance of Rb, Th and

TABLE 1.2

COMPARISON OF GRANITES FROM DIFFERENT TECTONIC SETTINGS

	ORG:A	ORG:B	VAG:A	VAG:B	COLG:A	COLG:B	WPG:A	WPG:B
SiO ₂	72.47	75.33	70.10	74.50	74.56	71.73	71.61	76.02
TiO ₂	0.33	0.23	0.53	0.16	0.18	0.25	0.19	0.29
Al ₂ O ₃	14.17	12.92	12.00	12.52	13.34	14.55	11.68	12.60
Fe ₂ O ₃	3.16	3.65	4.85	1.00	1.63	2.17	4.48	1.95
FeO	nd	nd	nd	nd	nd	nd	nd	nd
MnO	0.08	0.05	0.13	0.01	0.05	0.03	0.14	0.02
MgO	1.39	0.37	0.80	0.07	0.44	0.46	0.17	0.08
CaO	1.48	2.66	3.06	0.29	1.58	0.69	0.13	0.06
Na ₂ O	5.55	5.18	4.41	3.56	2.92	2.52	5.50	4.07
K ₂ O	0.24	0.14	0.28	5.51	4.45	5.50	4.68	4.40
P ₂ O ₅	0.06	0.04	0.11	0.01	0.03	0.23	nd	nd
LOI	1.00	nd	2.55	0.94	0.81	1.36	0.08	0.76
Total	99.93	100.57	98.82	98.57	99.99	99.49	98.66	100.25
Nb	42	5	2	17	16	13	168	24
Zr	285	93	99	184	99	80	1089	258
Y	55	35	44	30	25	13	92	57
Th	3	1	<1	20	35	20	24	9
Rb	<2	<2	<2	169	243	488	94	97
Sr	89	130	200	93	75	96	1	75
Ba	149	137	56	331	389	nd	53	545
La	44	nd	4	40	32	34	91	39
Ce	82	15	11	86	56	70	274	96
Nd	35	11	10	36	22	34	122	39

ORG:A = Ocean-ridge granite, Mid Atlantic Ridge.

ORG:B = Ocean-ridge granite, Troodos .

VAG:A = Volcanic-arc granite, Oman.

VAG:B = Volcanic-arc granite, Chile.

COLG:A = Syn-collision granite, Tibet

COLG:B = Syn-collision granite, SW England

WPG:A = Within-plate granite, Ascension Islands

WPG:B = Within-plate granite, Skaergaard, Greenland

Granites from different tectonic settings, from Pearce et al. (1984).

ORG: Granitic rocks from either oceanic crust or ophiolite sequences predominantly calcic to calc-alkaline, hornblende-bearing quartz diorite to tonalite, metaluminous or peraluminous.

VAG: Oceanic to continental arcs, quartz diorite and tonalite through to quartz monzonite and granite. Tholeiitic to high-K calc-alkaline or shoshonitic. Hornblende- and biotite-bearing, enriched in K, Rb, Ba, Th and depleted in Nb, Zr, Y relative to ORG. Metaluminous to slightly peraluminous.

COLG: Continent-continent and continent-arc collision, essentially biotite- and muscovite-bearing quartz monzonite to granite. Calc-alkaline to alkali-calcic and have I- and S-type features. Apart from elevated Rb, geochemical patterns are similar to VAG, depleted in Nb, Zr, Ce, Sm.

WPG: Intrude normal and attenuated continental crust, also oceanic crust. Essentially of syenite to alkali-feldspar granite composition, generally metaluminous to peralkaline, may be peraluminous. Characteristic Fe-rich mafic minerals annite, hastingsite, soda amphiboles. Enriched in Nb, Zr, Sm, Y, Yb relative to VAG and COLG; marked Ba depletion in WPG's intruded into normal continental crust. Rb enrichment may reflect crustal contamination.

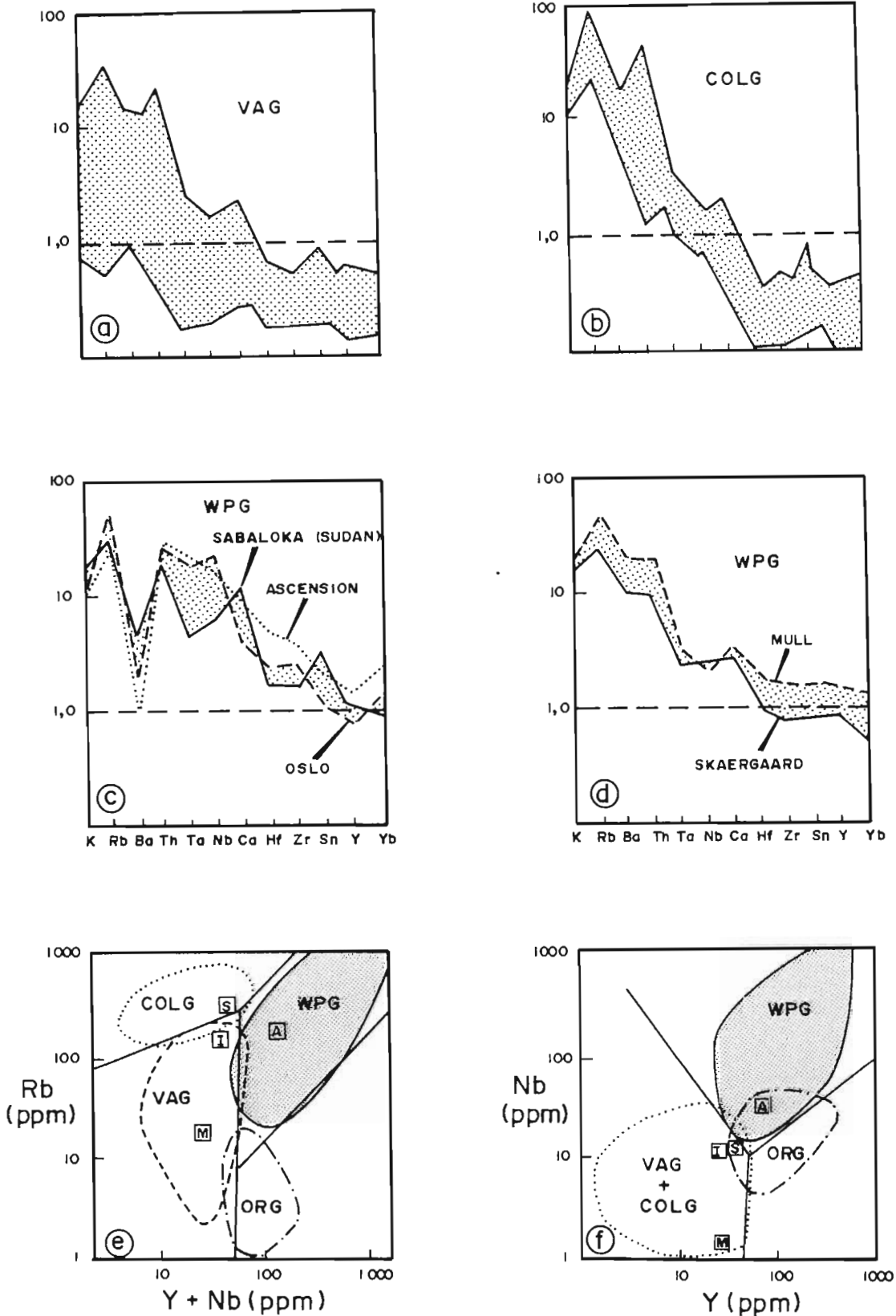


Figure 1.4. Ocean-ridge granite (ORG) normalized geochemical patterns for volcanic-arc granites (Fig. 1.4a), collision granites (Fig. 1.4b), within-plate granites intruded into crust of normal thickness (Fig. 1.4c) and within-plate granites intruded into attenuated continental crust (Fig. 1.4d). Comparison of average I-, S-, M- and A-type granites from Whalen *et al.* (1987), with the fields derived by Pearce *et al.* (1984) for VAG, COLG, ORG and WPG granites (Figs 1.4e & f).

Nb, a feature that also typifies most within-plate basalts. This type of granite magmatism is explained as being derived directly from incompatible-element enriched mantle, with little evidence of significant crustal involvement.

In contrast, the Sabaloka (Sudan) pattern is markedly different, with Rb, Th, Ce and Sm enriched relative to Ta, Nb, Zr and Y respectively (Fig. 1.4). Pearce et al. (op cit.) attribute this selective enrichment and the subsequent "spikes" on the WPG pattern to crustal involvement. Notwithstanding the spikes in the Sabaloka pattern, the crustal- and mantle-dominated patterns have common characteristics that set them apart from COLG and VAG, viz. a large negative Ba anomaly and general decrease in abundances from Rb to Yb.

- (ii) **Strongly attenuated continental crust**, at the edge of a continent that has rifted apart. The Tertiary granites of Scotland and Greenland (Skaergaard and Mull) are examples from this tectonomagmatic environment. ORG-normalised patterns exhibit high ratios of Rb and Th relative to Nb, that Pearce et al. (1984) consider to be characteristic of "crust-dominated" WPG (Fig. 1.4). However a noteworthy difference is the much smaller negative Ba anomaly and a flatter more "MORB-like" trend from Ta to Yb.
- (iii) **Oceanic crust**, into which oceanic island granites, such as constitute Ascension and Reunion, are intruded (Fig. 1.4). As described above, the patterns for oceanic granites (comendites) are similar to those for granites intruded into normal crust (eg. Oslo rift).

Whalen et al. (1987) assessed the Pearce et al. (1984) tectonic-discrimination diagrams and demonstrated that the average A-type granite plots as WPG, in contrast to the M-, I- and S-types that fall within the VAG+COLG and VAG fields (Figs 1.4e & 1.4f). A-type granites were noted

to have occurred "world-wide throughout geological time and do not necessarily indicate an anorogenic or rifting environment" (Whalen et al. 1987, p. 407).

Maniar & Piccoli (1989) have categorized granitoids by their tectonic environment as follows: (1) island-arc granitoids (IAG), (2) continental-arc granitoids (CAG), (3) continental-collision granitoids (CCG), (4) post-orogenic granitoids (POG), (5) rift-related granitoids (RRG), (6) continental epeirogenic-uplift granitoids (CEUG) and (7) oceanic plagiogranites (OP). These categories are further refined so that Group I (IAG+CAG+CCG) can be distinguished geochemically from Group II (RRG+CEUG) using plots such as Al_2O_3 vs SiO_2 and $FeO(tot)/FeO(tot)+MgO$ v SiO_2 (Fig. 1.5). The distinction of Group III (POG) is less satisfactory, in that it does not have a unique field and consequently has characteristics of both Groups I and II. With respect to the chemistry of Group II granitoids, Maniar & Piccoli (1989) noted a bimodal silica range, compared with unimodal silica distribution in Groups I & III.

Eby (1990) summarised the range of geological environments in which A-type granite magmatism could occur, as (i) continental rifts (Oslo graben, White Mountains, Gardar Province), (ii) intra-continental ring complexes (Younger Granites of Nigeria, Corsica, Sudan), (iii) attenuated crust (Mull, Skaergaard), (iv) oceanic islands, (Ascension, Reunion), (v) postorogenic (Saudi Arabia, Lachlan Fold Belt).

Eby (op cit.) noted that Y/Nb ratios are relatively constant for each particular A-type suite although metasomatism, which is common in peralkaline complexes, may result in dispersed ratios. He suggested that A-type suites with $Y/Nb < 1.2$ are derived from sources similar to ocean-island basalts (OIB), whereas suites with $Y/Nb > 4.8$ are derived from sources similar to island arc basalts (IAB). Intermediate Y/Nb ratios are taken to indicate crustal interaction with the A-type magma during emplacement (Fig. 1.5). From the examples presented in Figure 1.5, it is apparent that A-type suites emplaced into rifted continental settings (eg. Oslo graben, White Mountains), oceanic islands (eg. Ascension), and intracontinental ring complexes (eg. Sabaloka) generally

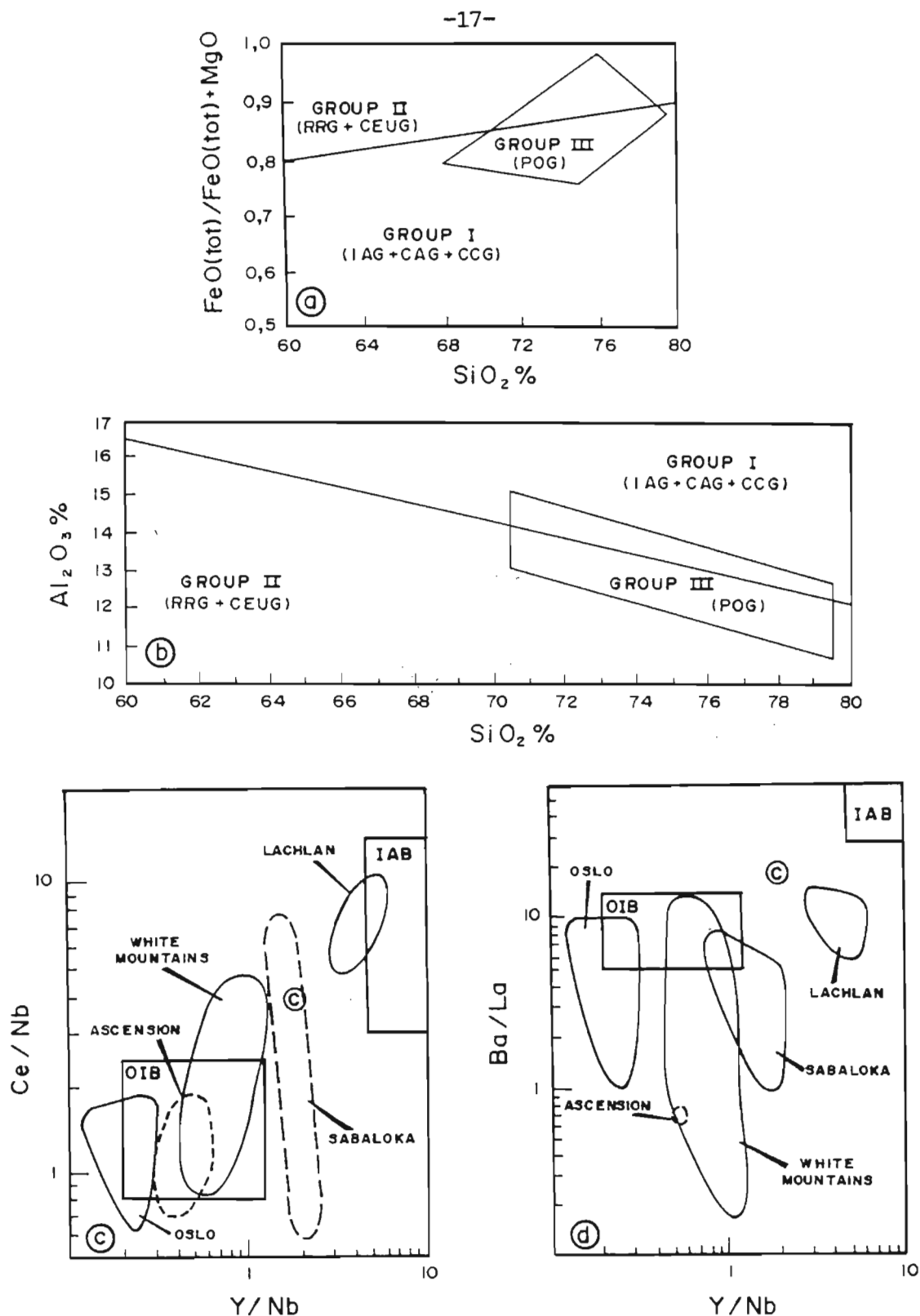


Figure 1.5. Examples of major- and trace-element diagrams for the tectonic discrimination of granitoids. Figs 1.5a & b discrimination between Groups I, II and III on the basis of major-element chemistry, from Maniar & Piccoli (1989). Note the restricted SiO_2 range of Group III compared with Group II. Figs 1.5c & d are from Eby (1990) and discriminate between granitoids with low Y/Nb emplaced into rifted continental crust (Oslo, White Mountains), as intracontinental ring complexes (Sabaloka), into oceanic crust (Ascension) and high Y/Nb granitoids of post-orogenic settings (Lachlan).

have $Y/Nb < 1.2$, although crustal involvement may increase this ratio to about 3.0. Those suites that fall at the high end of the Y/Nb spectrum are modelled as having been generated from previously melted crust, eg. the Lachlan Fold Belt postorogenic A-type granites. Similarly, the Mull granites intruded into attenuated crust have high Y/Nb ratios, interpreted to result from the mixing of a mantle plume with crustal material.

CHAPTER 2

THE NGOYE COMPLEX

2.1 Introduction

The Ngoye Complex is the easternmost of the three alkaline granitoids described here and is located between Eshowe and Empangeni (Fig. 2.1). The geology of the complex has been described previously in some detail (Scogings 1985, 1986, 1990b). Therefore the aim of this chapter is to summarise published information and to review additional data collected during this study, particularly whole-rock and REE geochemistry, microprobe mineral analyses of representative samples, and Rb-Sr isotopes. The present study involved field mapping and the collection of 31 additional rock samples for major- and trace-element analysis, so as to consolidate the foundation laid in the original study (Scogings 1985). Of the 59 samples available for this study, 19 representative specimens were analysed for 12 rare earth elements (REE) plus Y, and modal analyses were conducted on a routine basis (for sampling and analytical procedures, see appendix). Microprobe analyses were undertaken on selected samples at Rhodes University during 1988, in order to confirm optical mineral identification.

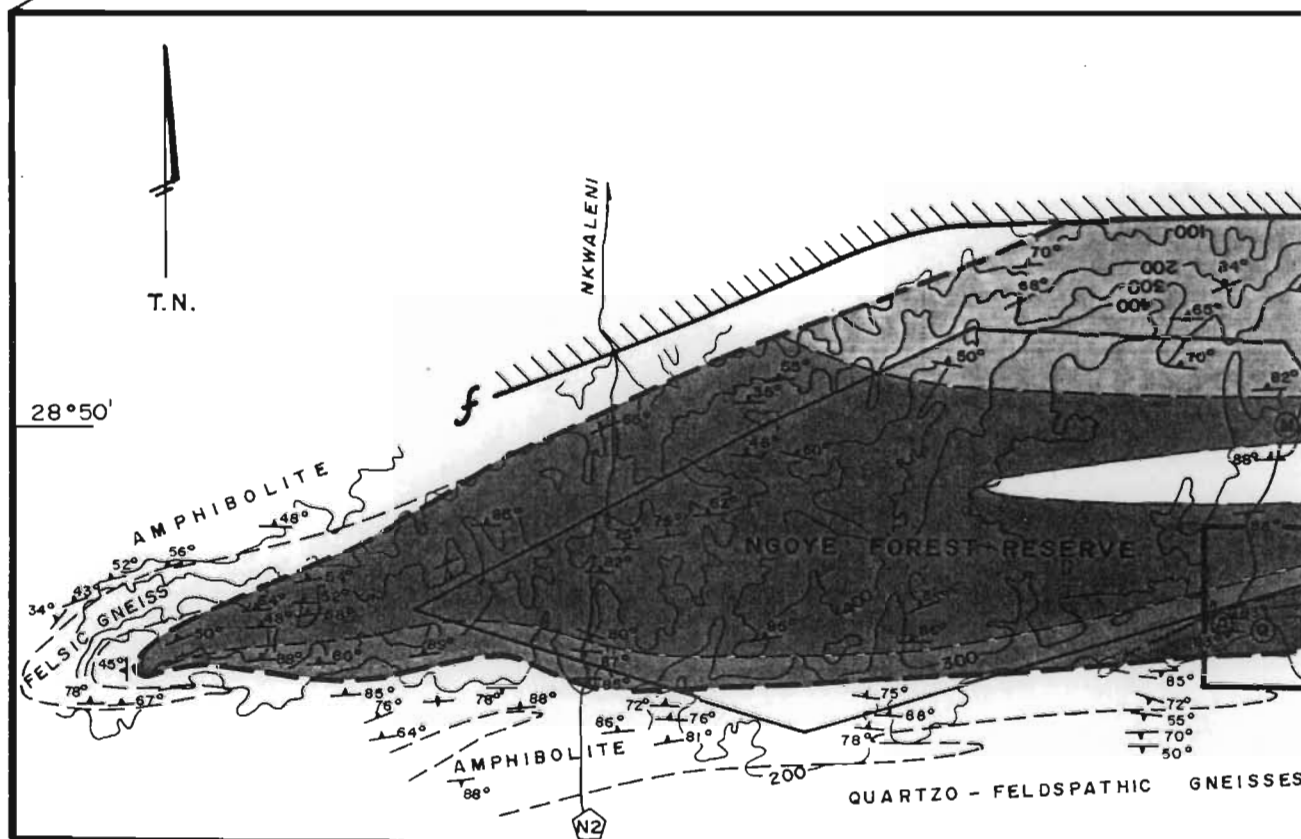
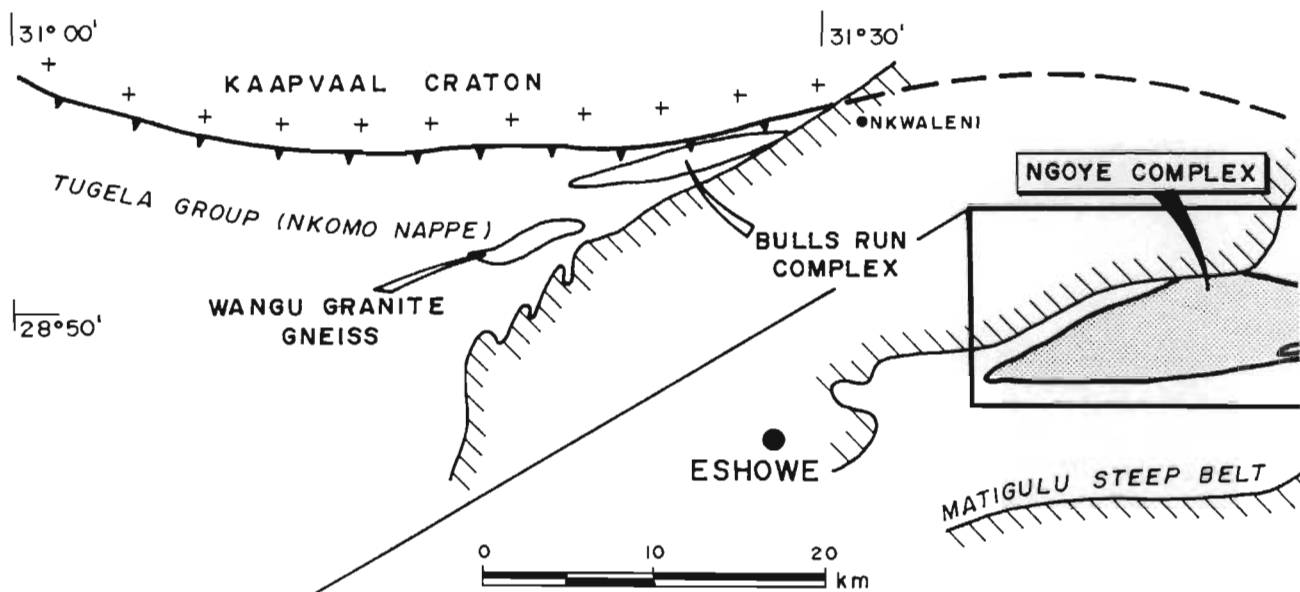
A brief historical review of the results of earlier research in this area is presented:

- (i) William Anderson (1901) first noted the granitic composition of the Ngoye Hills.
- (ii) McCarthy (1961) described the typical Ngoye lithology as

biotite-granite gneiss, noting the occurrence of garnetiferous aplite in the northeastern part of the body. Apparently gradational contacts with the surrounding amphibolites were used to suggest an "in-situ" metasomatic origin for the Ngoye granite by granitisation processes.

- (iii) Charlesworth (1981), from the results of a structural investigation of the Eshowe - Empangeni area, noted that deformation of the Ngoye Formation (SACS 1980) had produced mylonitic gneisses around the margins of the body, and interpreted these as thrust zones. On the basis of limited petrographical and geochemical data, Charlesworth classified the Ngoye gneisses as calc-alkaline, I-type, quartz monzonites and granites.
- (iv) Barton (1983) offered a Rb/Sr mean-emplacement age of 1060 Ma, with an R_0 of 0.7058 ± 0.002 . The fairly low initial ratio supported an I-type origin.
- (v) Scogings (1985, 1986) conducted a detailed field-mapping and petrographical investigation, combined with preliminary geochemical analyses and defined twelve different granitoids within the Ngoye "Formation". On the basis of alumina-saturation criteria, the granites were classed into three groups ranging from peraluminous, through metaluminous, to peralkaline compositions. An overall alkaline character, in conjunction with elevated incompatible trace-element contents (Nb, Y, Zr, Zn) led to re-interpretation of the Ngoye "Formation" as a metamorphosed A-type granite central complex. Similarities were noted with the classic "younger-granite" ring complexes of Nigeria and Saudi Arabia.

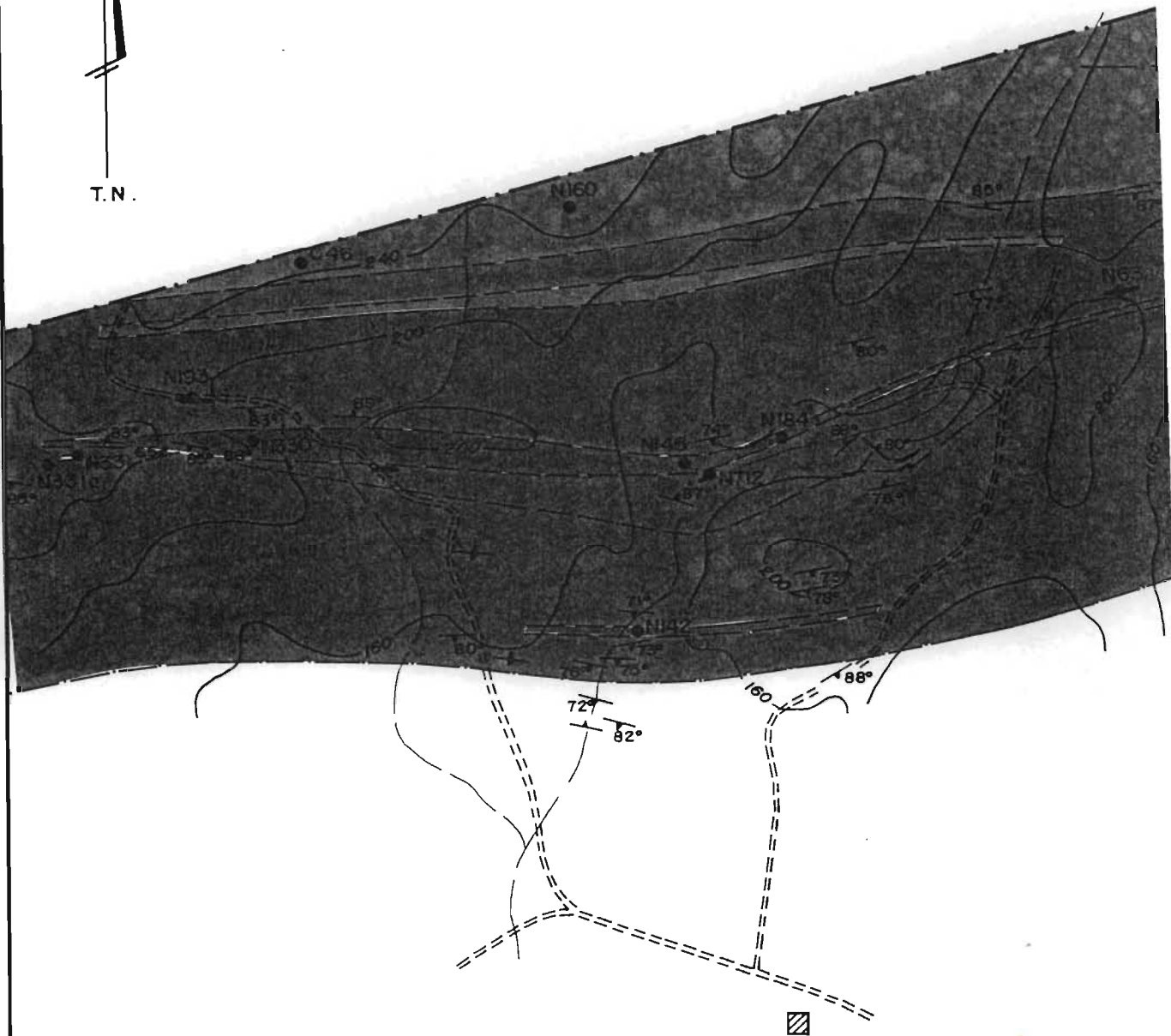
A detailed structural investigation of shear zones and mylonites in the Ngoye Complex led to the detection of a prominent left-lateral shear component. This discovery was based on both macro- and micro-structural textures, such as S- and C-fabrics, asymmetric pressure shadows around mylonite clasts, rotated fold



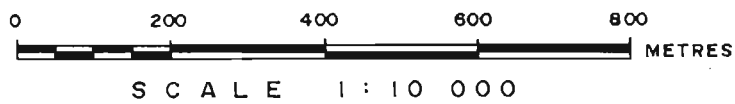
NGOYE FOREST RESERVE



T.N.



AMANZAMNYAMA
MISSION



axes which parallel the shear direction, and boudinaged magnetite grains (Scogings 1985). The elongate shape of the Ngoye body was suggested to be the result of lateral shearing and stretching of an originally circular complex.

The discovery of alkaline granites in the Tugela Group raised the possibility that the Ngoye lithologies were intruded into rifted continental crust, either in an intracratonic or back-arc setting on an attenuated continental margin (Scogings 1985). This postulate provided an alternate model to the ophiolite-obduction/thrusting events envisaged by Matthews (1972, 1981).

- (vi) Scogings (1990b) proposed that the Ngoye Granite Gneiss Formation be renamed the "Ngoye Complex", in accordance with terminology used to describe alkaline granite intrusions (Bowden *et al.* 1987). This proposal was accepted by the South African Committee for Stratigraphy.

2.2 Field and petrographic descriptions

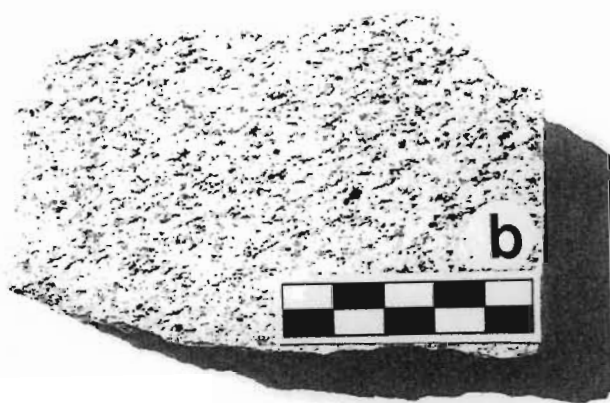
2.2.1 Introduction

The Ngoye granitoids are subdivided into five major and six minor lithologies on the basis of modal mineralogy and relative areal distribution (Figs 2.1, 2.2 & 2.4). Representative modal analyses are presented as Table 2.1 (a complete modal data set is given in Appendix 1, Table A1.1), and classification according to the QAP system of Streckeisen (1976a) is illustrated in Figure 2.4.

With respect to the QAP classifications given previously (Scogings 1985), an important point concerning the optical identification of alkali-feldspar has arisen subsequent to obtaining microprobe data for the Ngoye granites. This is related to the fundamental premise of the Streckeisen (1976a) proposals, whereby plagioclase with an Ab content of greater than 95% is combined with K-feldspar and which together form the alkali feldspar component for classification purposes. The microprobe analyses show that, apart from oligoclase in the mesocrystic biotite granite, some of the biotite-hornblende granites and in the



MESOCRYSTIC BIOTITE GRANITE



GARNET - MUSCOVITE GRANITE



BIOTITE - HORNBLLENDE GRANITE



RIEBECKITE - BIOTITE GRANITE



RIEBECKITE GRANITE



MAGNETITE - QUARTZ ROCK



MAGNETITE GRANITE

Figure 2.3. Polished slabs of representative Ngoye granitoids. Scale in cm.

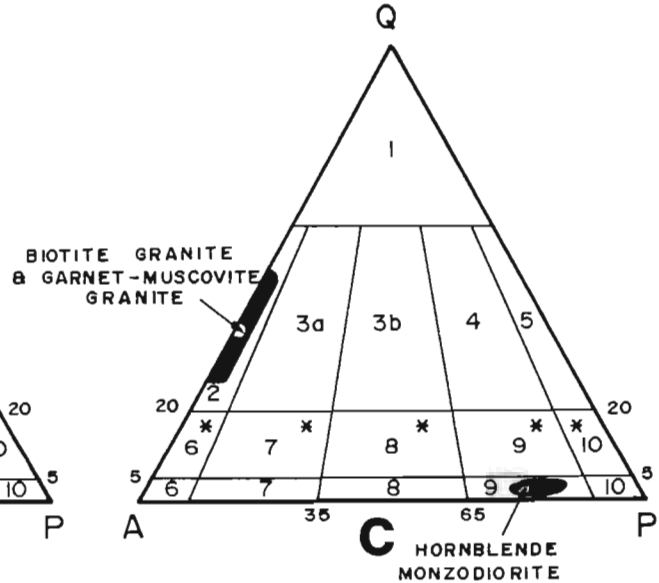
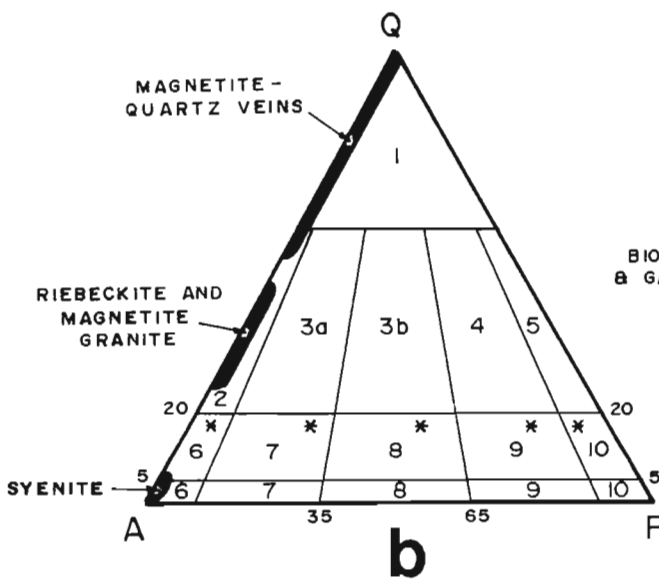
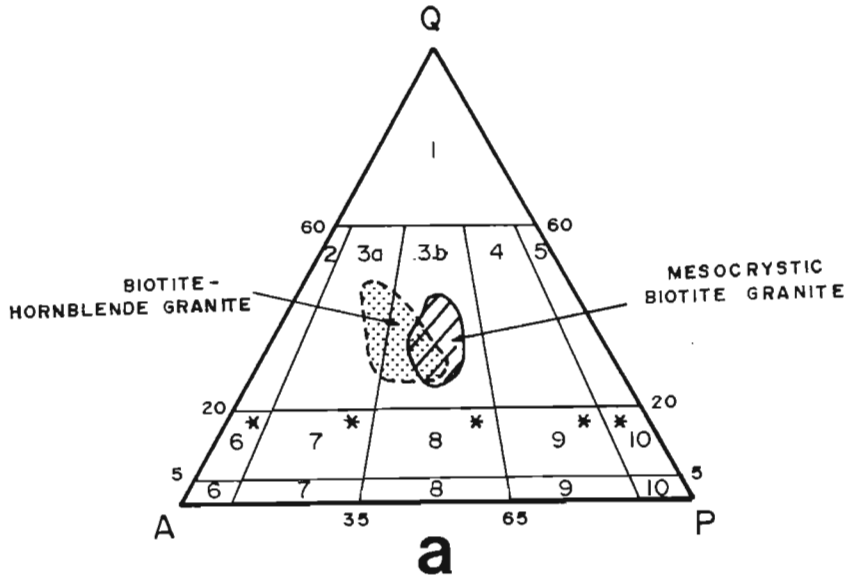


Figure 2.4. Classification of the Ngoye granitoids using the modal QAP diagram of Streckeisen (1976a): (a) biotite granite and biotite-hornblende granite, (b) syenite, peralkaline granites, magnetite-quartz rocks, (c) hornblende monzodiorite and muscovite-bearing granites. The fields are numbered as follows: 1 = quartzolite/quartz-rich granitoids, 2 = alkali-feldspar granite, 3a & 3b = granite, 4 = granodiorite, 5 = tonalite, 6* = quartz alkali-feldspar syenite, 7* = quartz syenite, 8* = quartz monzonite, 9* = quartz monzodiorite, 10* = quartz diorite, 6 = alkali-feldspar syenite, 7 = syenite, 8 = monzonite, 9 = monzodiorite, 10 = diorite.

and muscovite-bearing granites classify as alkali-feldspar granites. The mesocrystic biotite granite and biotite-hornblende granite, which contain some oligoclase in addition to albite, are of granitic composition. Three of the minor lithologies have widely-divergent modal characteristics, from the hornblende monzodiorite, through the two syenites that classify as alkali-feldspar syenite, to the magnetite-quartz veins that plot within the quartzolite field (Fig. 2.4).

A further observation concerning feldspars is that the Ngoye granites are essentially two-feldspar granites (albite + microcline, Table 2.2) and therefore classify as subsolvus types. However, small amounts of microcline perthite are generally present and suggest that the Ngoye granites originally crystallised as hypersolvus granites, with subsequent unmixing into two pure alkali-feldspar end-members as a result of metamorphic recrystallisation. Comparable mineralogical changes have been recorded in metamorphosed peralkaline granites elsewhere (Seyler 1986, Winchester & Max 1987).

Due to possible modification during brecciation and resilicification (Scogings 1985) the monzonite lithology, which occurs as a small plug on the northwest flank of the Ngoye Complex, has been removed from the current classification.

Detailed field and petrographic descriptions of the various granites have been given previously (Scogings 1985 1986 1990b) and only salient features are summarised below (see Fig. 2.3 for polished slabs of typical Ngoye granites). Representative microprobe mineral analyses are given as Tables 2.2 and 2.3.

2.2.2 Mesocrystic biotite granite

This rock-type, described previously as the typical Ngoye granite (McCarthy 1961, Charlesworth 1981), constitutes some 20% of the outcrop and forms the core of the complex (Fig. 2.1). In outcrop, this lithology is light grey, with pink microcline mesocrysts (25 to 35 modal%, Or₉₀) set in a matrix of quartz (23 to 33 modal%), oligoclase (26 to 34 modal%, An₁₂) and biotite (4 to 7 modal%). Accessory minerals include hornblende, epidote, sphene and allanite.

TABLE 2.2

MICROBROBE ANALYSES: NGOYE COMPLEX

PLAGIOCLASE

	N2o	N447a	N665a	N145a	N331a	N34a	N21o	A	B
SiO ₂	66.22	68.59	67.74	68.59	68.23	69.50	65.36	67.84	64.10
Al ₂ O ₃	21.32	19.50	20.38	18.18	18.83	19.33	21.77	19.65	22.66
FeO	0.01	0.05	0.01	0.54	0.41	--	0.06	0.05	0.30
CaO	2.47	0.32	1.45	--	--	0.18	2.94	--	3.26
Na ₂ O	10.45	11.98	10.33	12.12	12.35	11.21	9.96	11.07	9.89
K ₂ O	0.07	0.07	0.06	0.04	0.07	0.10	0.10	0.29	0.05
Total	100.54	100.51	99.97	99.47	99.89	100.32	100.19	98.90	100.26
ions on basis of 32 oxygens									
Si	11.581	11.945	11.837	12.096	11.988	12.067	11.483	11.964	11.267
Al	4.396	4.006	4.197	3.779	3.902	3.957	4.508	4.085	4.695
Fe ²⁺	0.001	0.007	0.002	0.079	0.060	--	0.008	0.007	0.042
Ca	0.463	0.063	0.271	--	--	0.033	0.554	--	0.614
Na	3.544	4.047	3.501	4.109	4.207	3.773	3.395	3.785	3.370
K	0.016	0.015	0.014	0.009	0.015	0.023	0.022	0.066	0.011
Total	20.001	20.083	19.822	20.072	20.172	19.853	19.970	19.907	19.999
Or	<.1	<.1	<.1	<.1	<.1	0.6	0.6	1.7	0.3
Ab	88.3	98.3	92.7	99.8	99.9	98.5	85.5	98.0	82.5
An	11.6	1.7	7.2	--	--	0.9	13.9	0.3	17.2

MICROCLINE

	N2m	N447m	N665m	N145m	N331m	N34m	N21m	C	D
SiO ₂	66.16	64.70	65.54	64.86	65.56	65.44	65.21	63.66	64.46
Al ₂ O ₃	18.18	18.20	18.06	17.88	17.79	18.13	18.17	19.54	18.55
FeO	--	0.02	--	0.28	0.20	0.04	0.08	0.10	0.14
CaO	0.01	--	--	--	--	0.01	0.01	0.50	0.17
Na ₂ O	1.09	0.42	0.45	0.31	0.85	0.39	0.46	0.80	0.40
K ₂ O	13.88	16.48	16.40	16.19	15.39	16.30	15.86	15.60	16.07
Total	99.32	99.82	100.45	99.52	99.79	100.31	99.79	100.20	99.88
ions on basis of 32 oxygens									
Si	12.141	12.001	12.059	12.053	12.098	12.051	12.049	11.759	11.938
Al	3.932	3.979	3.917	3.917	3.871	3.938	3.957	4.254	4.050
Fe ²⁺	--	0.003	--	0.043	0.031	0.006	0.012	0.014	0.019
Ca	0.001	--	--	--	--	0.002	0.002	0.099	0.033
Na	0.387	0.152	0.161	0.111	0.307	0.138	0.166	0.286	0.176
K	3.251	3.899	3.850	3.839	3.624	3.829	3.738	3.676	3.797
Total	19.712	20.034	19.987	19.963	19.931	19.964	19.924	20.088	20.013
Or	89.3	96.2	95.9	97.2	99.2	96.5	95.7	90.5	94.8
Ab	10.6	3.7	4.0	2.8	7.8	3.5	4.2	7.1	4.4
An	<.1	--	--	--	--	<.1	<.1	2.4	0.8

N2o, N21o = oligoclase

N447a to N34 a = albite

N2m to N21m = microcline

A = albite (Deer et al. 1966)

B = oligoclase (Deer et al. 1966)

C = orthoclase (Deer et al. 1966)

D = microcline (Deer et al. 1966)

TABLE 2.3

MICROPROBE ANALYSES: NGOYE COMPLEX

MAFIC MINERALS

	N447h	N665h	N21h	N145r	N330r	A	B	N331a	C	N21g	D
SiO ₂	40.95	38.95	40.21	49.50	50.19	38.89	51.01	52.76	51.64	35.5	37.03
TiO ₂	0.79	0.57	0.23	0.26	0.34	0.65	0.96	0.06	0.04	0.74	0.04
Al ₂ O ₃	8.19	11.54	10.88	1.60	2.33	11.88	0.80	0.64	1.05	4.96	8.92
FeO	30.02	28.62	26.87	35.49	35.25	28.68	32.39	29.18	29.82	23.18	18.76
MnO	0.94	1.12	0.82	0.70	0.46	0.66	0.48	0.24	0.26	1.51	1.09
MgO	2.34	2.52	4.79	0.07	0.12	2.68	0.22	0.05	0.38	0.04	0.83
CaO	10.79	11.04	11.03	0.09	0.02	10.66	0.19	1.68	0.60	31.64	30.26
Na ₂ O	1.62	1.01	1.69	7.60	6.65	1.75	7.98	12.76	12.21	0.02	nd
K ₂ O	1.57	1.83	1.67	0.96	1.20	1.99	1.80	--	0.06	--	nd
Total	97.21	97.20	98.19	96.27	96.56	97.84	95.83	97.37	96.06	97.59	96.93

ions on basis of 24 oxygens

ions on basis of 6 oxygens

Si	6.966	6.593	6.663	8.445	8.465	6.229	7.909	2.174	1.988	6.286	6.043
Ti	0.101	0.073	0.029	0.033	0.043	0.078	0.112	0.002	0.001	0.099	0.005
Al	1.642	2.303	2.126	0.322	0.463	2.242	0.146	0.031	0.048	1.036	1.716
Fe ²⁺	4.271	4.052	3.724	5.064	4.972	3.844	4.198	1.006	0.958	3.433	2.56
Mn	0.135	0.161	0.115	0.101	0.066	0.091	0.063	0.008	0.008	0.227	0.151
Mg	0.593	0.636	1.183	0.018	0.031	0.641	0.051	0.003	0.022	0.011	0.201
Ca	1.967	2.002	1.958	0.017	0.004	1.829	0.032	0.074	0.025	6.003	5.292
Na	0.534	0.332	0.543	2.514	2.175	0.543	2.398	1.019	0.912	0.007	nd
K	0.341	0.395	0.357	0.209	0.256	0.408	0.356	--	0.002	--	nd
Total	16.55	16.547	16.698	16.723	16.475	15.905	15.265	4.317	3.964	17.102	15.968

-- = not detected
nd = not determined

N447h = hastingsite: biotite-hornblende granite
N665h = hastingsite: biotite-hornblende granite
N21h = hastingsite: hornblende monzodiorite
N145r = riebeckite : riebeckite granite
N330r = riebeckite : riebeckite granite
N331a = aegirine : aegirine granite
N21g = andradite : hornblende monzodiorite

A = hastingsite (Deer et al. 1966)
B = riebeckite (Deer et al. 1966)
C = aegirine (Deer et al. 1966)
D = andradite (Deer et al. 1966)

2.2.3 Biotite-hornblende granite

This lithology comprises some 45% of the complex and crops out in the central and western parts of the massif. Subsequent to the original mapping by Scogings (1985), a narrow outcrop of this rock type was discovered to the east of the Mhlatuze River (Fig. 2.1). The biotite-hornblende granite is light pink, medium-grained and comprises quartz (23 to 35 modal%), microcline (30 to 40 modal%, Or₉₆), albite/oligoclase (20 to 30 modal%, Ab₉₃₋₉₈), hastingsitic

hornblende (3 to 8 modal%, see Table 2.3 for microprobe analysis) and biotite (<4 modal%). Sphene and opaque minerals are accessory phases.

2.2.4 Biotite granite

This leucocratic granite constitutes some 20% of the complex and crops out along the northern flanks of the complex, as well as rimming the south-western margin of the mesocrystic biotite granite body at Ninians. From the occurrence of biotite-hornblende granite xenoliths within the biotite granite, a relatively younger age for the latter lithology is indicated (Scogings 1985). In hand specimen, this fine- to medium-grained rock is light-pink to off-white and as indicated in Table 2.1, consists of microcline (25 to 35 modal%), albite (25 to 35 modal%), quartz (30 to 40 modal%) and biotite (<5 modal%), with accessory muscovite, fluorite and opaques.

2.2.5 Garnet-muscovite granite

Originally, outcrops of fine-grained garnet-muscovite granite were mapped as constituting about 5% of the Ngoye Complex (Scogings 1985). However, recent field mapping indicates that this peraluminous lithology is restricted to a far smaller area and forms a sheet some 2 km long and 50 to 100m in width which intrudes the biotite granite along the northeastern flank of the massif (Fig. 2.1). As indicated by the representative modal analysis (Table 2.1), the mineral assemblage typically comprises microcline (25 to 30 modal%, Or₉₇), albite (30 to 35 modal%, Ab₉₉), quartz (30 to 40 modal%) and muscovite (2 to 4 modal%). Biotite and pink almandine garnet occur as accessories, with garnet locally reaching concentrations of 1%. In the field, the garnet-muscovite granite has an aplitic appearance although local pegmatitic patches and "nests" of garnet-muscovite rock are encountered occasionally. It is considered that these mica-rich phases may represent greisen-like alteration zones related to late-stage fluid activity (Section 2.3).

2.2.6 Riebeckite-biotite granite

Exposures of this granite are restricted to an elongate sheet rimming the southern and southwestern margin of the Ngoye Complex (Fig. 2.1).

Modal analysis of this medium-grained leucocratic lithology indicates that it comprises quartz (30 to 40 modal%), albite (25 to 35 modal%), microcline (30 to 35 modal%), with characteristic clots and aggregates of riebeckite, aegirine, biotite and fluorite (5 to 10 modal%).

2.2.7 Magnetite granite

This lithology forms an apophysis that extends into the surrounding country rocks, on the southern margin of the complex (Figs 2.1, 2.2). It is fine-grained, light pink and consists of quartz (35 to 40 modal%), microcline (45 to 55 modal%) and albite (10 to 20 modal%). Magnetite (<5 modal%) is the characteristic mafic phase, accompanied by accessory biotite, zircon and fluorite. Although essentially equigranular, occasional larger microcline grains up to 4mm in diameter are encountered in thin section and probably represent relict microphenocrysts.

2.2.8 Riebeckite granite

Minor sheets of riebeckite granite, up to 5m in width and several hundred metres in length, are intrusive into the magnetite granite. Typically, riebeckite granite comprises quartz (30 to 40 modal%), microcline (c.30 modal%, Or₉₃₋₉₇), albite (c.30 modal%, Ab₉₉) and riebeckite (c.5 modal%, Table 2.3 for microprobe data). Accessory minerals are opaques and zircon, with zircon prevalent in pegmatitic patches near sample site N145. Samples of this lithology, as well as the riebeckite-biotite granite, have been used to assess the effects of mylonitisation on geochemistry (Section 2.3.2).

2.2.9 Aegirine granite

Only one outcrop of aegirine granite has been located (Fig. 2.2) and in thin section this rock type is very similar to the magnetite granite, except that aegirine occurs to the virtual exclusion of magnetite (Table 2.3 for microprobe analyses of microcline, albite and aegirine).

2.2.10 Chloritic syenite

Two narrow bands of syenite were intersected in a borehole drilled into magnetite granite, on the southern margin of the complex (Scogings 1985,

Fig. 2.2 for location of borehole NG2). As this lithology has never been observed in outcrop, despite an intensive search, it appears to have limited lateral extent and extremely variable thickness. The modal assemblage, which is dominated by microcline (60 to 73 modal%), albite (c.20 modal%) and chlorite (4 to 12 modal%), contains traces of quartz and pyrite. The development of chlorite, which apparently replaces quartz, suggests that the syenite is an alteration product of magnetite granite. Such a rock-type, more properly described as an "episyenite", is probably analagous to de-silicified granite associated with copper/tin mineralization in the upper part of the Nebo Granite of the Bushveld Complex (L.J. Robb pers. comm., 1991).

2.1.11 Magnetite-quartz rock

This is a coarse-grained rock of highly variable composition which forms veins and diffuse patches within both the magnetite granite and the amphibolitic country rocks (Fig. 2.2). Modally it consists of quartz (50 to 80 modal%), magnetite (5 to 20 modal%), alkali feldspar (<45 modal%) and zircon (<8 modal%), with fergusonite, biotite, sphene, fluorite, calcite and apatite as accessories. Gradational contacts with some of the surrounding magnetite granites indicate their derivation from residual Fe-rich fluids that crystallised late in the cooling history of the magnetite granite (Scogings 1985). It is noted that analagous veins are associated with peralkaline granites in Saudi Arabia and the USA (Harris & Marriner 1980, Al-Shaieb 1988).

2.1.12 Hornblende monzodiorite

This lithology forms a small plug-like body several hundred metres in diameter, within the biotite-hornblende granite (Fig. 2.1). It is a distinctive white to off-white, medium- to coarse-grained rock comprising oligoclase (60 to 70 modal%, An_{16}), microcline (10 to 20 modal%, Or_{96}), hastingsitic hornblende (4 to 8 modal%, microprobe data in Table 2.3), calcite (c.5 modal%), diopside (c. 2 modal%) and andraditic garnet (c. 2 modal%, microprobe data in Table 2.3). Accessory phases are quartz, epidote, allanite, sphene and apatite. As described previously (Scogings 1985), petrographic relationships indicate alteration of a primary oligoclase-diopside assemblage by late-stage CO_2 -rich volatiles. Reaction between CO_2 and oligoclase

produced calcite, andradite and epidote, with concomitant alteration of diopside to hastingsite. Textural relationships show microcline replacing plagioclase, suggesting potash metasomatism.

2.3 Geochemistry

2.3.1 Introduction

Representative whole-rock major- and trace-element geochemical data for the Ngoye granites are presented as Table 2.4, with a complete set of analyses in Appendix 2 (Table A2.1). Representative CIPW norms and mesonorms are presented as Table 2.6, with a complete data set in Appendix 3 (Table A3.1). Comparative granitoid analyses from literature sources are presented for reference as Table 2.7.

The 31 additional whole-rock samples collected subsequent to the original study (Scogings 1985) confirm the characteristics previously noted, viz. that compared with the average granite (Le Maitre 1976) the Ngoye granites generally are depleted in Al_2O_3 , MgO and CaO (Table 2.7, analysis H). A broad similarity is noted with granites from A-type central complexes (Table 2.7, analyses A, B, D & E) in that the Ngoye granites have high Nb, Zr and Y, and low Sr and Ba contents. The Ngoye magnetite-quartz veins are seen to comprise essentially silica and iron, with attendant enrichment in Zr, Zn, Nb, REE, Th and U. This is similar to the values recorded from analagous rocks of the Midian peralkaline complex of Saudi Arabia (Harris & Marriner 1980). One lithology in the Ngoye Complex that does not follow the above trends of alumina depletion and incompatible-element enrichment is the garnet-muscovite granite, which is more akin to felsic S-type granite than A-types (cf. analysis C, Table 2.7).

2.3.2 Effects of deformation on geochemistry

Every effort was made to collect the least-deformed samples for geochemical analysis. However, because of limited outcrop in certain areas, this approach was not always possible and therefore a test was run to compare mylonitised granites with granites displaying minimal fabric development (Table 2.5, Fig. 2.5). From this test it transpires that, with the exception of a slight loss of Na_2O , Nb, Zr and Zn

TABLE 2.5

PERALKALINE GRANITES: EFFECTS OF DEFORMATION ON GEOCHEMISTRY

	N468	N548	N145	N181	N142
SiO ₂	76.01	77.48	77.58	77.59	77.61
TiO ₂	0.19	0.11	0.11	0.09	0.10
Al ₂ O ₃	11.21	11.19	10.87	10.81	11.45
Fe ₂ O ₃	1.16	0.97	1.82	2.35	0.29
FeO	1.20	1.42	0.72	0.94	1.44
MnO	0.05	0.06	0.03	0.06	0.03
MgO	0.13	0.05	0.05	0.01	--
CaO	0.26	0.19	0.01	0.01	--
Na ₂ O	3.82	4.04	4.83	4.89	3.88
K ₂ O	4.80	4.62	4.08	4.25	4.65
P ₂ O ₅	0.02	--	--	0.02	--
LOI	0.29	0.13	0.14	0.13	0.31
Total	99.14	100.26	100.24	101.15	99.76
Zn	144	123	251	328	155
Ga	nd	27	nd	nd	28
Nb	59	39	43	26	15
Zr	527	443	704	690	367
Y	79	78	14	15	22
U	--	7	4	--	--
Th	14	10	4	--	--
Pb	20	12	1	--	--
Rb	144	126	227	267	191
Sr	8	14	--	--	--
Ba	212	195	11	11	49
P.I.	1.03	1.04	1.14	1.05	1.01
Na ₂ O+K ₂ O	8.62	8.66	8.91	9.14	8.53
Na ₂ O/K ₂ O	0.80	0.87	1.18	1.15	0.83
Y/Nb	1.34	2.00	0.33	0.58	1.47

nd = not determined

-- = not detected

N468 = poorly-foliated riebeckite-biotite granite

N548 = well-foliated riebeckite-biotite granite

N145 = poorly-foliated riebeckite granite

N181 = well-foliated riebeckite granite

N142 = mylonitized riebeckite granite

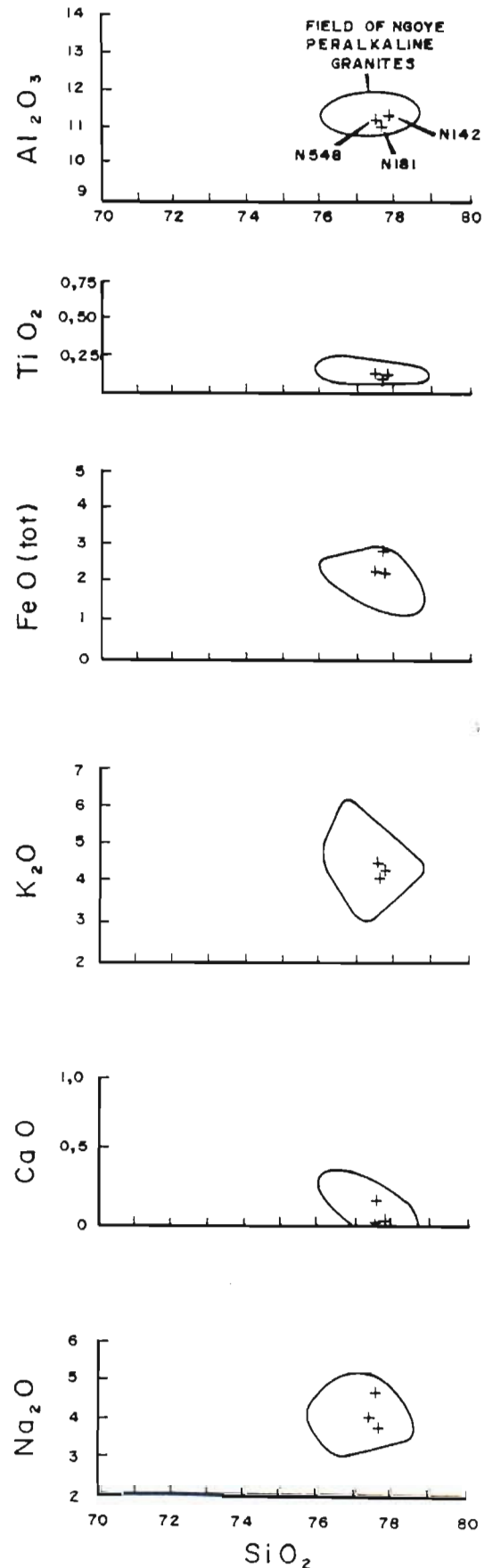


Fig. 2.5. Comparison of major-element geochemistry between well- and poorly-foliated Ngoye peralkaline granites

TABLE 2.7

REPRESENTATIVE GRANITOIDS FROM THE LITERATURE

	A	B	C	D	E	G	H
SiO ₂	72.60	74.25	73.72	75.60	75.37	74.01	71.30
TiO ₂	0.29	0.24	0.05	0.08	0.28	0.91	0.31
Al ₂ O ₃	14.07	13.30	14.79	9.60	10.71	7.51	14.32
Fe ₂ O ₃	0.90	0.57	0.17	2.60	4.08	5.17	nd
FeO	1.73	0.95	0.52	1.60	0.71	0.71	2.73
MnO	0.07	0.02	0.05	0.06	0.04	0.10	0.05
MgO	0.43	0.20	0.07	--	0.16	0.15	0.71
CaO	1.01	0.67	0.40	0.56	0.27	3.53	1.84
Na ₂ O	3.36	3.72	4.00	4.80	3.20	1.19	3.68
K ₂ O	5.74	5.28	4.11	4.42	4.88	1.99	4.07
P ₂ O ₅	0.07	0.02	0.42	0.04	0.02	0.50	0.12
LOI	0.47	0.64	1.30	0.56	0.29	0.44	0.77
Total	100.74	99.86	99.60	99.92	100.01	96.21	99.90
Zn	61	20	53	158	146	nd	nd
Ga	nd	20	26	48	29	nd	nd
Nb	57	18	47	54	255	5390	nd
Zr	246	251	27	710	1831	24089	nd
Y	63	47	12	42	238	2873	nd
U	nd	6	21	2	9	363	nd
Th	27	32	3	8	28	590	nd
Pb	22	14	18	12	45	nd	nd
Rb	185	174	945	155	162	124	nd
Sr	100	38	15	4	78	891	nd
Ba	362	340	2	38	156	nd	nd
Sn	8	nd	nd	nd	16	nd	nd
La	59	nd	nd	nd	331	1505	nd
Ce	144	91	10	121	608	3157	nd
Nd	nd	nd	nd	nd	179	1943	nd
Sm	nd	nd	nd	nd	nd	480	nd
Eu	nd	nd	nd	nd	nd	38	nd
Gd	nd	nd	nd	nd	nd	435	nd
Yb	nd	nd	nd	nd	nd	235	nd
Lu	nd	nd	nd	nd	nd	33	nd
P.I.	0.83	0.89	0.75	1.32	0.99	0.55	0.73
Na ₂ O+K ₂ O	9.10	9.00	8.11	9.22	8.08	3.18	7.75
Na ₂ O/K ₂ O	0.59	0.70	0.97	1.09	0.66	0.60	0.90
Rb/Sr	1.85	4.58	63.00	38.75	2.08	0.14	nd

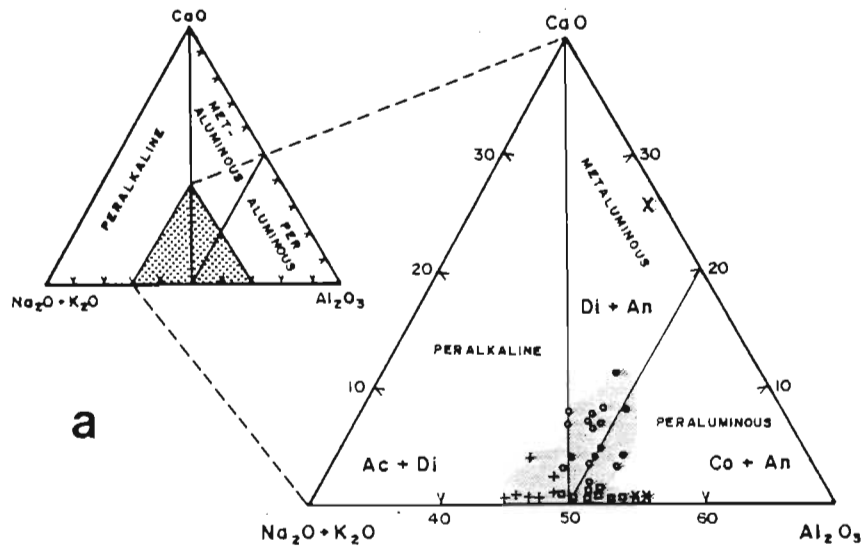
- A = biotite granite: Amo Complex, Nigeria (Bowden et al. 1987)
 B = biotite-hornblende granite: Topsails Complex, Canada (Whalen et al. 1987)
 C = muscovite granite: Sandy Cape, Tasmania (Whalen et al. 1987)
 D = aegirine granite: Shira Complex, Nigeria (Whalen et al. 1987)
 E = magnetite granite: Doolough, Ireland (Winchester & Max 1986)
 F = magnetite-quartz vein: Midian complex, Saudi Arabia (Harris & Marriner 1980)
 G = average granite (Le Maitre 1976)

during the mylonitisation process, no significant change has occurred in major- and trace- element chemistry although, with the limited database available, it is not possible to draw any statistically-valid numeric conclusions. As changes in chemistry are apparent only in the most-deformed and recrystallised mylonite (sample N142) it is concluded that, under conditions of moderate deformation, the various rock types at Ngoye behaved essentially as closed, isochemical, systems.

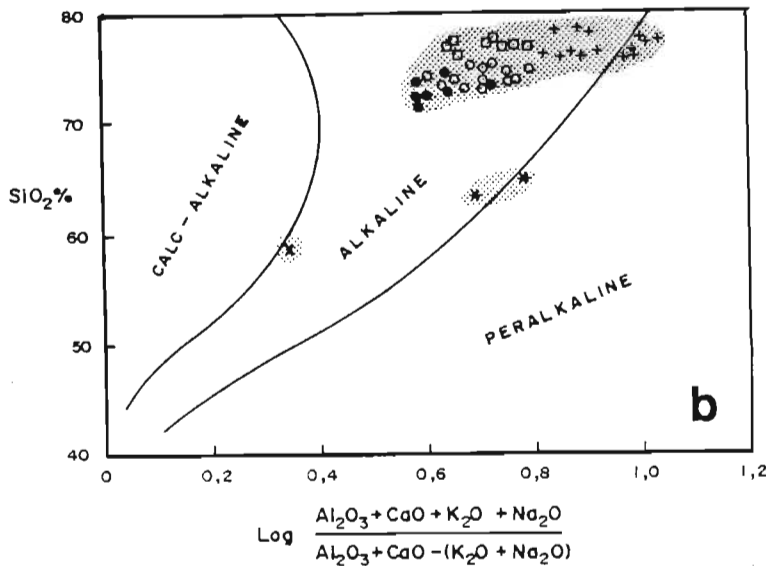
2.3.3 Alumina saturation

In terms of Bonin's (1986) classification (Fig. 2.6a), the Ngoye granitoids vary from peraluminous (muscovite granite and chloritic syenite) through metaluminous (biotite and hornblende granites, hornblende monzodiorite) to peralkaline (magnetite and riebeckite granites). This classification agrees with the CIPW-normative mineralogy (Table 2.6), in which peraluminous granites are corundum normative and peralkaline varieties contain acmite. However, two of the riebeckite-bearing granites are anorthite and/or corundum normative (Appendix 3, Table A3.1), suggesting some Na-loss as a result of metamorphic or magmatic alteration.

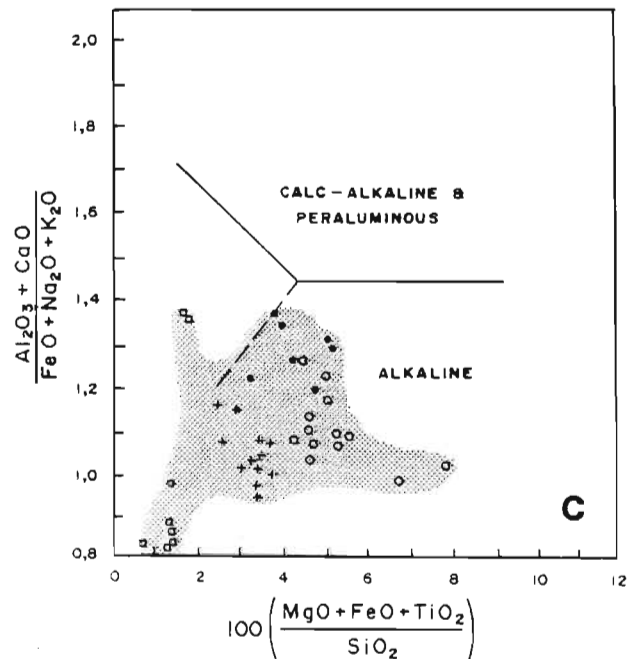
Na loss, as a result of metamorphic alteration, has been recorded from peralkaline granitoids deformed during the Grenville Orogeny (Floor 1974, Hill & Thomas 1983, Bourne 1986, Seyler 1986, Winchester & Max 1987). This process results in the breakdown of sodic Fe-rich amphiboles and pyroxenes to form magnetite, accompanied by a decrease in the peralkalinity index $(Na+K/Al)$. Thus, previously-peralkaline rocks display a peraluminous major-element chemistry. Alkali-loss also has been recorded from peralkaline volcanic suites, where it is ascribed to post-extrusion groundwater leaching or halide-rich vapour loss (MacDonald 1975a). Trace elements, notably Nb, Y, Zr and REE, are considered to be relatively immobile under metamorphic conditions and therefore, may provide a better method of indicating peralkaline or A-type chemistry, than major-element abundances (Bourne 1986, Seyler 1986, Winchester & Max 1987). A significant feature of "alkali-depleted," originally peralkaline granites is that Zr, which under normal peralkaline conditions is contained within riebeckite and



a



b



c

Figure 2.6. Alumina saturation and alkalinity of the Ngoye granitoids.

Fig. 2.6a. Alumina saturation relative to $\text{Na}_2\text{O}+\text{K}_2\text{O}$ and CaO (mol. props), diagram after Bonin (1986). The muscovite granite and chlorite syenite are peraluminous, the biotite and biotite-hornblende granites are metaluminous to peraluminous and the riebeckite- and/or magnetite-bearing granites are peralkaline.

Fig. 2.6b. Alkalinity vs silica diagram after Wright (1969), showing the predominantly alkaline to slightly peralkaline character of the Ngoye granitoids.

Fig. 2.6c. Classification of the Ngoye granitoids as alkaline, according to parameters suggested by Sylvester (1989).

Symbols: (●) mesocrystic biotite granite, (○) biotite-hornblende granite, (□) biotite granite & garnet-muscovite granite, (+) riebeckite/aegirine/magnetite granites, (*) chlorite syenite, (x) hornblende monzodiorite.

aegirine lattices, is released to form discrete zircon grains (Floor 1974).

2.3.4 Alkalinity

Sorensen (1974) classified rocks with normative and modal sodic mafic minerals and/or feldspathoids, as alkaline and on these grounds, the peralkaline Ngoye granites are alkaline. By this definition, the peraluminous and metaluminous granites are not strictly alkaline. However, as defined by Peacock (1931) alkaline igneous rock suites are depleted in Ca relative to Na + K. The Peacock concept has been modified (Wright 1969, Sylvester 1989), in which alkaline rocks are shown to be depleted in $(\text{Al}_2\text{O}_3 + \text{CaO})$ relative to $(\text{Na}_2\text{O} + \text{K}_2\text{O})$. According to these parameters the Ngoye granites range from alkaline to slightly peralkaline (Figs. 2.6b, 2.6c).

2.3.5 Degree of peralkalinity

As illustrated (Fig. 2.7) and described by Scogings (1985, 1986), the Ngoye riebeckite-, aegirine- and magnetite-bearing granites are mildly peralkaline ($\text{P.I.} < 1.2$) and using normative parameters, classify as comenditic granites (Fig. 2.7).

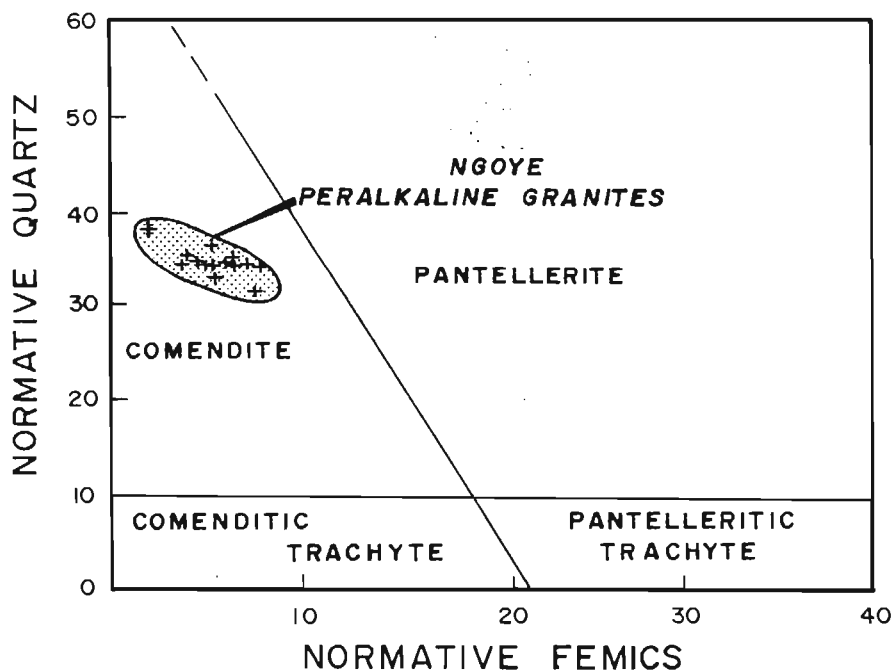


Figure 2.7. Classification of peralkaline Ngoye granites using normative quartz versus total normative femics. Diagram devised for silica-saturated peralkaline extrusive rocks by MacDonald & Bailey (1973). Symbols as in Fig. 2.6

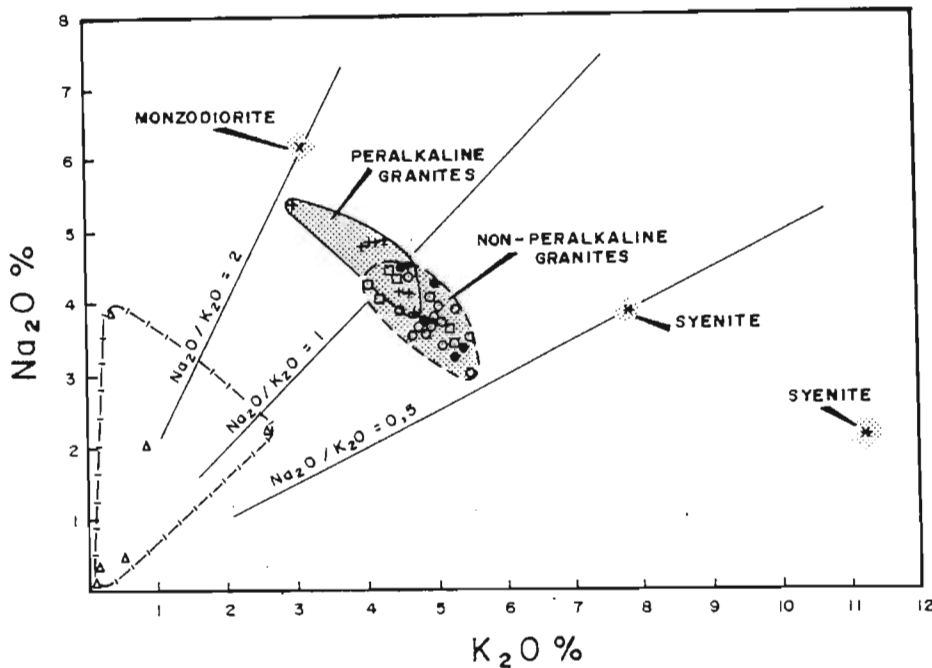


Figure 2.8. Discrimination of the various Ngoye lithologies according to their $\text{Na}_2\text{O}/\text{K}_2\text{O}$ ratios. Symbols as in Fig. 2.6.

2.3.6 $\text{Na}_2\text{O}/\text{K}_2\text{O}$ ratios

As shown in Figure 2.8, the peralkaline granites have higher $\text{Na}_2\text{O}/\text{K}_2\text{O}$ ratios than the metaluminous and peraluminous lithologies. The magnetite-quartz veins are highly depleted in total alkalis and have similar $\text{Na}_2\text{O}/\text{K}_2\text{O}$ ratios to the peralkaline samples.

2.3.7 Nomenclature based on geochemical parameters

The alkaline character of the Ngoye samples is clearly demonstrated by classifying the Ngoye granites according to their major element characteristics (Figs 2.9a, 2.9b).

- (i) **The R1-R2 diagram:** This diagram expresses all the major-element oxides as cations, in terms of mineralogical parameters (de la Roche *et al.* 1980). As indicated in Figure 2.9a an increase in the R1 component largely reflects increasing silica relative to alkalis, whereas variations in R2 values indicate mafic mineral and anorthite contents. Using this classification the biotite, hornblende and muscovite granites plot in the granite field and the peralkaline riebeckite and magnetite granites classify as alkali granite. Syenitic and syenodioritic compositions are indicated for the syenite and monzodiorite samples respectively.

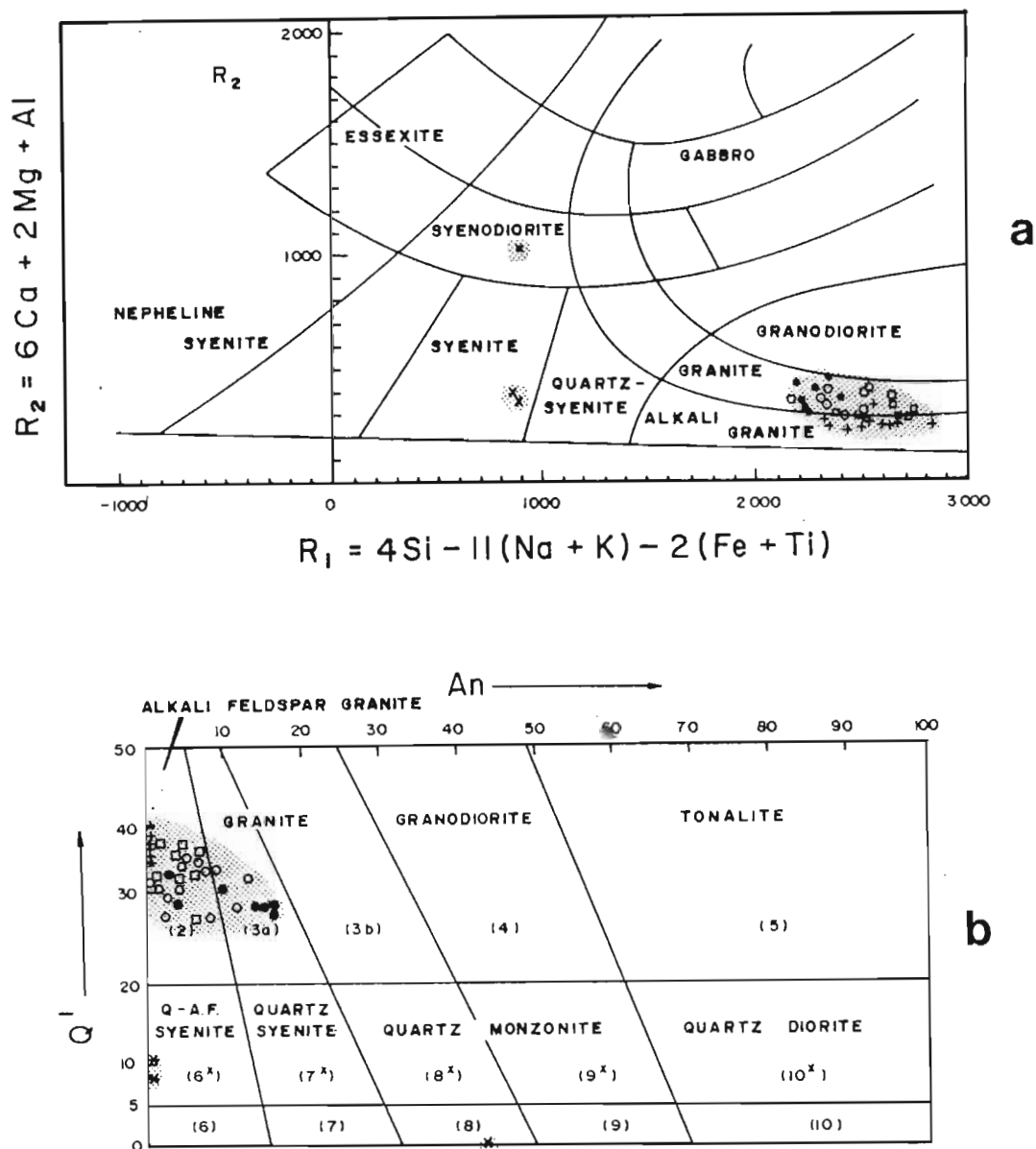


Figure 2.9. Classification of the Ngoye granitoids according to major-element characteristics.

Fig. 2.9a. Classification using the R1-R2 multicationic system devised by de la Roche *et al.* (1980).

Fig. 2.9b. Normative classification of the Ngoye granitoids, based on the Q' versus An' diagram of Streckeisen & le Maitre (1979). Numbered fields correspond to those of the modal QAP diagram (Fig. 2.4).

Symbols: (●) mesocrystic biotite granite, (○) biotite-hornblende granite, (□) biotite granite & garnet-muscovite granite, (+) peralkaline granites, (*) chlorite syenite, (x) hornblende monzodiorite.

- (ii) **Nomenclature derived using normative constituents:** The orthogonal plot given as Figure 2.9b was devised by Streckeisen & Le Maitre (1979) and follows an earlier attempt (Streckeisen 1976b) to classify igneous rocks according to normative constituents. Accordingly, the mesocrystic biotite granites are classified predominantly as granite (*sensu stricto*) whereas the hornblende-, riebeckite-, aegirine-, magnetite- and muscovite-bearing granites plot within the alkali-feldspar granite field in Figure 2.9b. The two syenites classify as alkali-feldspar quartz syenite and the single monzodiorite analysis falls within the monzonite field. This classification is largely in agreement with that derived using the QAP modal diagram (Fig. 2.4), with the exception of the biotite-hornblende granite that plots as alkali-feldspar granite in Figure 2.9b.

2.3.8 A-type classification (Ga/Al)

Whalen *et al.* (1987) successfully discriminated A-type granites from I-, S- and M-types using the elevated Ga/Al ratios typical of the former. When the Ngoye samples are plotted according to these parameters, a clear A-type character results from their enhanced incompatible-element contents (Fig. 2.10). However, some overlap between the Ngoye muscovite-bearing granites and the field of felsic S-type granites is noted, particularly with regard to depleted Zr, Ce and Y contents. The implication of this overlap is that the muscovite-bearing granites at Ngoye are contaminated and have some of the characteristics of an "S-type" partial melt.

2.3.9 Harker diagrams

Plotting of selected major- and trace-element data for the Ngoye granites on Harker diagrams (Harker 1909) shows the following trends (Figs 2.11 & 2.12):

- (i) SiO₂ values range between 72 and 79%, with the metaluminous biotite and hornblende granites essentially below 76% and the peraluminous muscovite- and peralkaline riebeckite-bearing granites restricted to values greater than 76%.

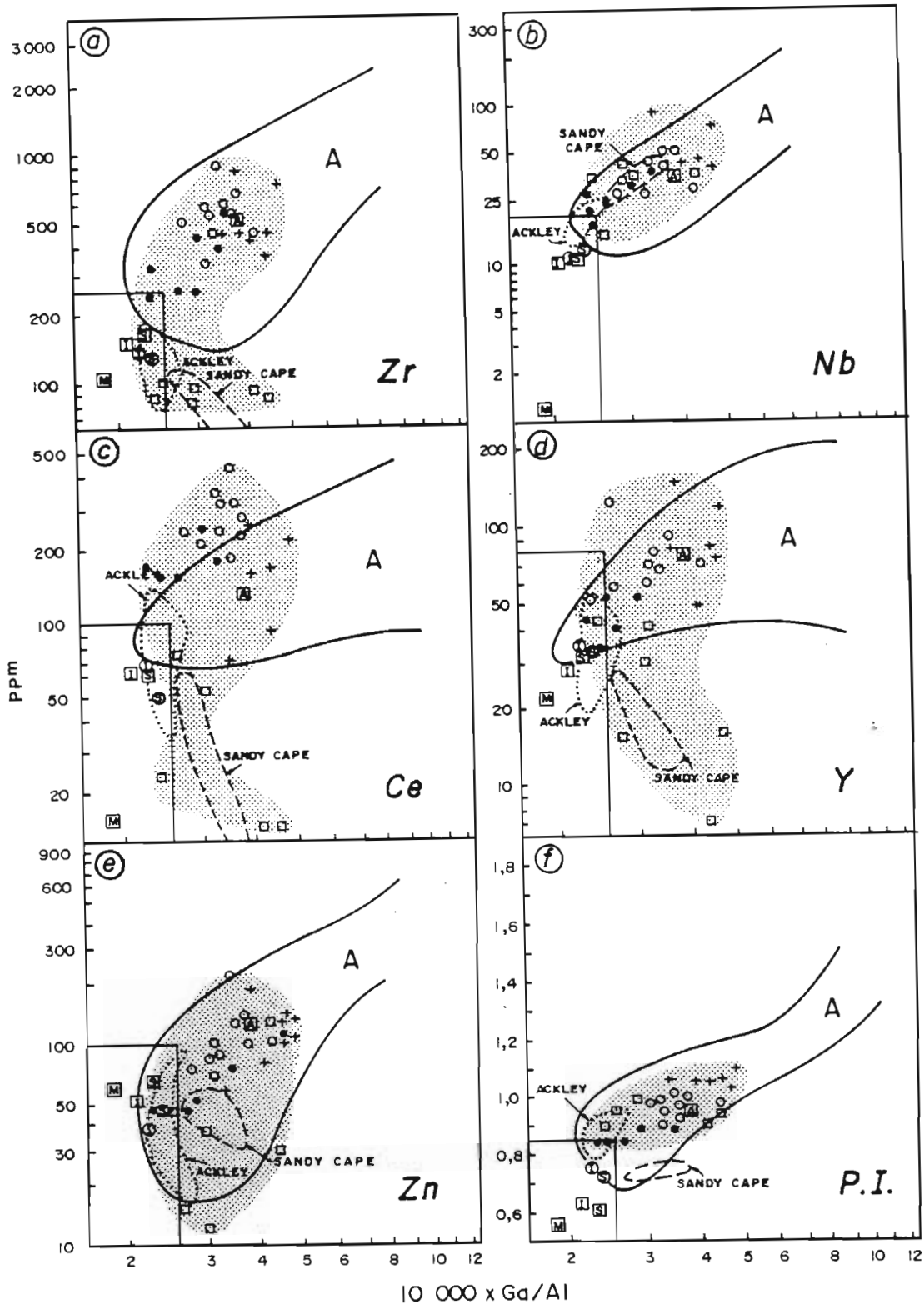


Figure 2.10. Plot of trace element and peralkalinity indices versus $10\,000 \times \text{Ga}/\text{Al}$ for the Ngoye granites. The rectangular field, with Ga/Al of less than 2.6, is the field of M-, I- and S- type granites. Average granite compositions are given as boxed letters. The field of A-type granites is delineated by the broad curved line and, for comparison, the fields of two fractionated felsic I- and S-type granites are shown as dashed outlines. Data for the various fields and granite types from Whalen *et al.* (1987). Symbols as in Figure 2.9.

- (ii) Al_2O_3 , TiO_2 , $\text{FeO}(\text{tot})$, MgO and CaO vary inversely with respect to SiO_2 .
- (iii) For given SiO_2 contents the riebeckite, magnetite and hornblende granites have lower Al_2O_3 and higher TiO_2 , Fe_2O_3 and $\text{FeO}(\text{tot})$ values than the biotite and muscovite-bearing varieties.
- (iv) The peralkaline granites are characterised by high Fe_2O_3 relative to FeO , reflecting the Fe_2O_3 -rich characteristics of sodic minerals such as hastingsitic hornblende, aegirine and riebeckite.
- (v) Na_2O and K_2O do not covary with SiO_2 to any significant degree, although a mild trend towards increased Na_2O and decreased K_2O with high SiO_2 is suggested. Total alkalis remain relatively constant, between 8 and 9%, with exceptions provided by the syenites (c. 12%) and the magnetite quartz veins (< 5%) (Table 2.4).
- (vi) When plotted against SiO_2 , Zr and Zn are diagnostic for each of the four major modal rock groupings, with the hornblende-, riebeckite- and magnetite-bearing granites enriched in Zn and Zr relative to the biotite and muscovite granites.
- (vii) The biotite and muscovite granites, although depleted in Zr and Zn, are enriched in Th (Fig. 2.11) as well as Pb, U and Sn (Table A2.1), relative to the hornblende-, riebeckite- and magnetite-bearing granites.
- (viii) Sr behaves in similar fashion to CaO, with the most siliceous of the peraluminous and peralkaline granites being highly depleted in Sr.
- (ix) Whereas Rb values for the biotite, hornblende and riebeckite/magnetite-bearing granites increase slightly with increasing SiO_2 , the muscovite-bearing granites show a distinct divergence from this trend, with extreme enrichment in Rb (up to 1047 ppm) characteristic of the garnetiferous type.

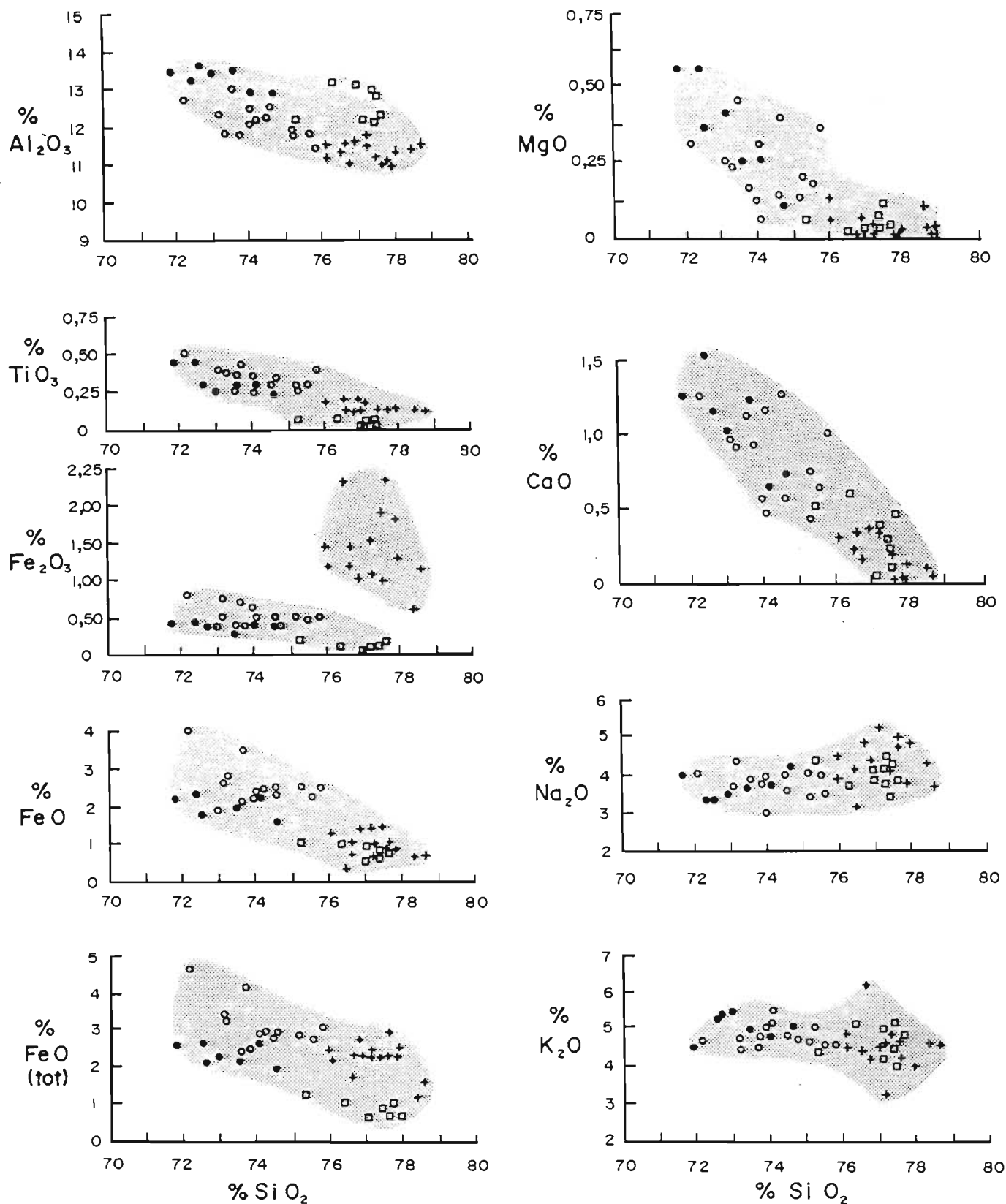


Figure 2.11. Ngoye major-element data plotted on Harker variation diagrams. Major-element oxides in %. Symbols: (●) mesocrystic biotite granite, (○) biotite-hornblende granite, (□) biotite granite & garnet-muscovite granite, (+) peralkaline granites.

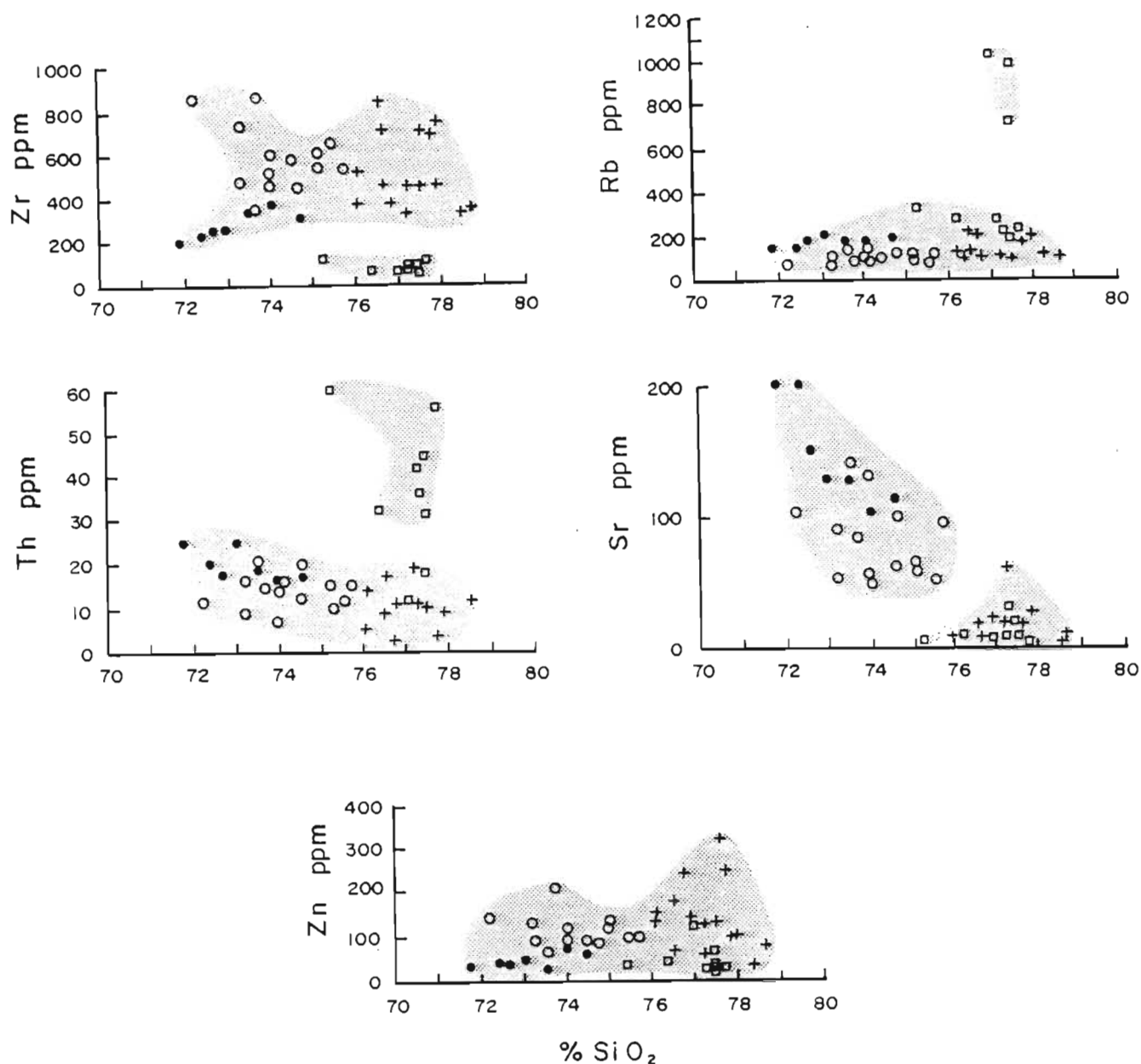


Figure 2.12. Selected Ngoye trace-element data (ppm) plotted on Harker variation diagrams. Symbols as in Figure 2.11.

2.3.11 K₂O/Rb relationships

Rb-enrichment of the garnet-muscovite granite is reflected in the K₂O/Rb plot (Fig. 2.13a). Whereas the peralkaline granites parallel the main trend of Shaw (1969), the biotite and muscovite-bearing lithologies define a classic cross-cutting pegmatitic-hydrothermal trend of decreasing K₂O/Rb. This suggests that the mica granites, particularly those rich in garnet and muscovite, have been altered by post-magmatic fluid activity (cf. Bowden & Kinnaird 1984). Such an

interpretation is corroborated by the development, within the garnet-muscovite granite, of muscovite-rich pods containing up to 570ppm Sn and 4460ppm Rb.

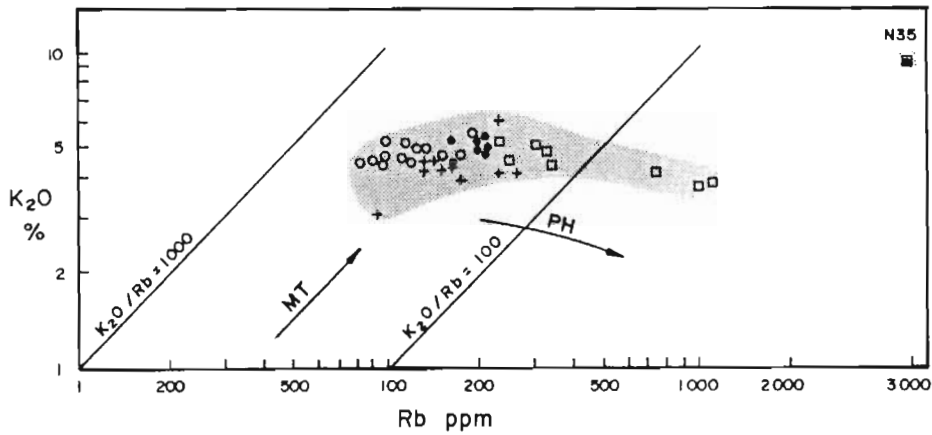


Figure 2.13. Plot of K_2O against Rb for the Ngoye granitoids, including sample N35 (muscovite-rich pod in garnet-muscovite granite). The main (MT) and pegmatitic-hydrothermal (PHT) trends of Shaw (1969) are shown for comparison. Symbols as in Figure 2.11.

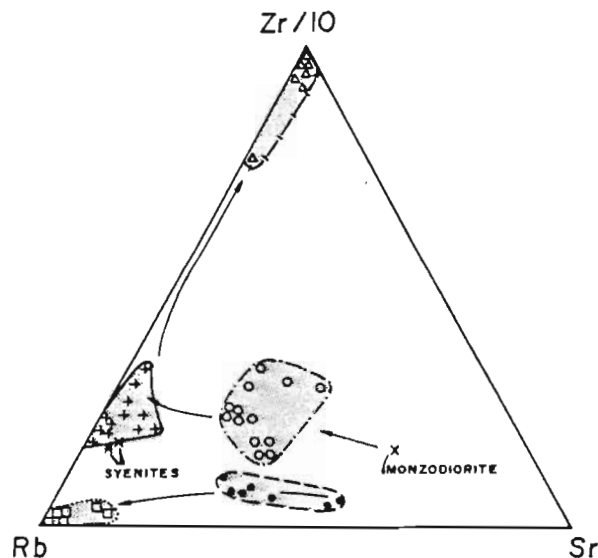


Figure 2.14. Discrimination of the Ngoye granitoids in Zr-Rb-Sr space. Two divergent paths are indicated, with peraluminous rocks tending towards increased Rb/Zr, whereas metaluminous/peralkaline differentiation results in a marked increase in Zr/Rb. Symbols as in Fig. 2.11.

2.3.12 Zr-Rb-Sr discrimination

Taking into consideration the trend of decreasing Sr with increasing differentiation in the Ngoye Complex and the tendency for peraluminous granites to be depleted in Zr relative to Rb, a plot that combines these three variables has been constructed (Fig. 2.14). This shows that:

- (i) The mesocrystic biotite, biotite and garnet-muscovite granites are depleted in Zr relative to the other granites in the complex, and that Zr decreases with increasing Rb from the mesocrystic biotite granite to the garnet-bearing types.
- (ii) The opposite relationship to (i) holds for the biotite-hornblende and peralkaline granites, with Zr either remaining constant or increasing in sympathy with Rb. The magnetite-quartz veins are extremely enriched in Zr and would thus, according to the petrological characteristics of peralkaline magmas (Watson 1971), represent residual fluids derived by fractional crystallisation of the Ngoye peralkaline granites.
- (iii) The chloritic syenites are similar to the peralkaline granites with respect to Zr-Sr-Rb ratios.

2.3.13 Nb-Y ratios

Constant ratios between incompatible elements such as Y and Nb are evidence for the comagmatic origin of different phases within an igneous intrusion (Nicholls 1988). However, as noted by Eby (1990) this ratio can vary as a result of metasomatic effects. Such dispersion has been reported from peralkaline complexes in Saudi Arabia and the Sudan (Harris & Marriner 1980, Harris et al. 1983). When the Ngoye data are plotted in Nb/Y space (Fig. 2.19a), it is seen that the Nb/Y ratio is fairly well constrained between 0.35 and 1.25, supportive of a comagmatic origin for the different granites. However the peraluminous muscovite-bearing granites and two of the riebeckite granite samples are depleted in Y and fall outside this field, possibly as a result of metasomatic alteration or contamination by crustal material.

2.3.14 Rare earth elements

Chondrite-normalised rare earth element (REE) data for 20 whole rock and 2 mineral separates from the Ngoye Complex (Figs 2.15 & 2.16) show that:

- (i) The mesocrystic biotite granite and biotite-hornblende granite samples (Fig. 2.15a) have moderately LREE-enriched patterns (La_N/Lu_N : 10.08 to 13.65) with negative Eu anomalies, (Eu/Eu^* : 0.33 to 0.64) indicative of some plagioclase fractionation. The higher total abundances of REE in the hornblende-bearing granites is commensurate with selective concentration of REE by modal hornblende and allanite.
- (ii) As illustrated in Figure 2.15b, the two samples of biotite granite have fairly flat REE patterns (La_N/Lu_N : 2.71 to 3.76) and marked negative Eu anomalies (Eu/Eu^* : 0.02 to 0.07) consistent with their fractionated major-element chemistry.
- (iii) The garnet-muscovite granite (Fig. 2.15b) has the lowest total-REE contents of all Ngoye lithologies, the "birdwing", HREE-enriched ($La_N/Lu_N = 0.23$) profile of N34 indicating concentration of HREE within garnet (Hanson 1978). This pattern may also relate to transport of HREE by post- or late-magmatic hydrothermal fluids (Baker 1985, Bowden *et al.* 1987, Cornell *et al.* 1989, Schade & Cornell 1989).
- (iv) Peralkaline riebeckite and magnetite granites (Fig. 2.15c) contain similar total REE's to the metaluminous biotite-hornblende granites, with slightly flatter chondrite-normalised patterns (La_N/Lu_N : 5.91 to 9.79) and larger negative Eu anomalies (Eu/Eu^* : 0.08 to 0.23). The magnitude of the Eu anomalies is consistent with extensive plagioclase fractionation, similar to that documented for riebeckite granites from Nigeria (Bowden & Whitley 1974).
- (v) Massive enrichment of total REE (up to 1.12%, or 4000 x chondrite), significant Eu depletion (Eu/Eu^* : 0.12 to 0.18), and "birdwing" HREE-enriched profiles (La_N/Lu_N : 0.12 to 1.18)

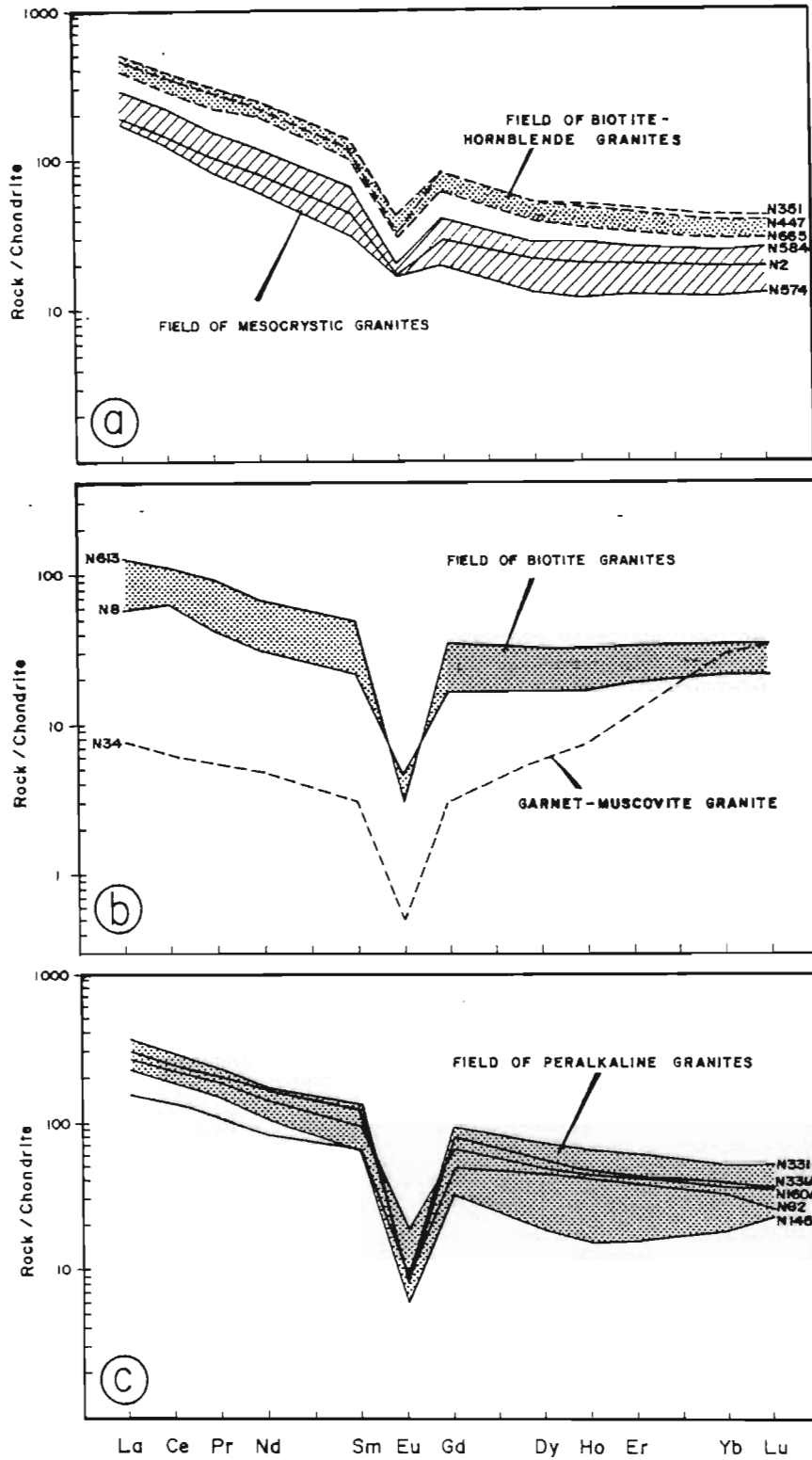


Figure 2.15. Chondrite-normalized REE patterns for the Ngoye granitoids. Fig. 2.15a biotite- and biotite-hornblende granites, Fig. 2.15b biotite and garnet-muscovite granites, Fig. 2.15c peralkaline granites. Chondrite values from Nakamura (1974).

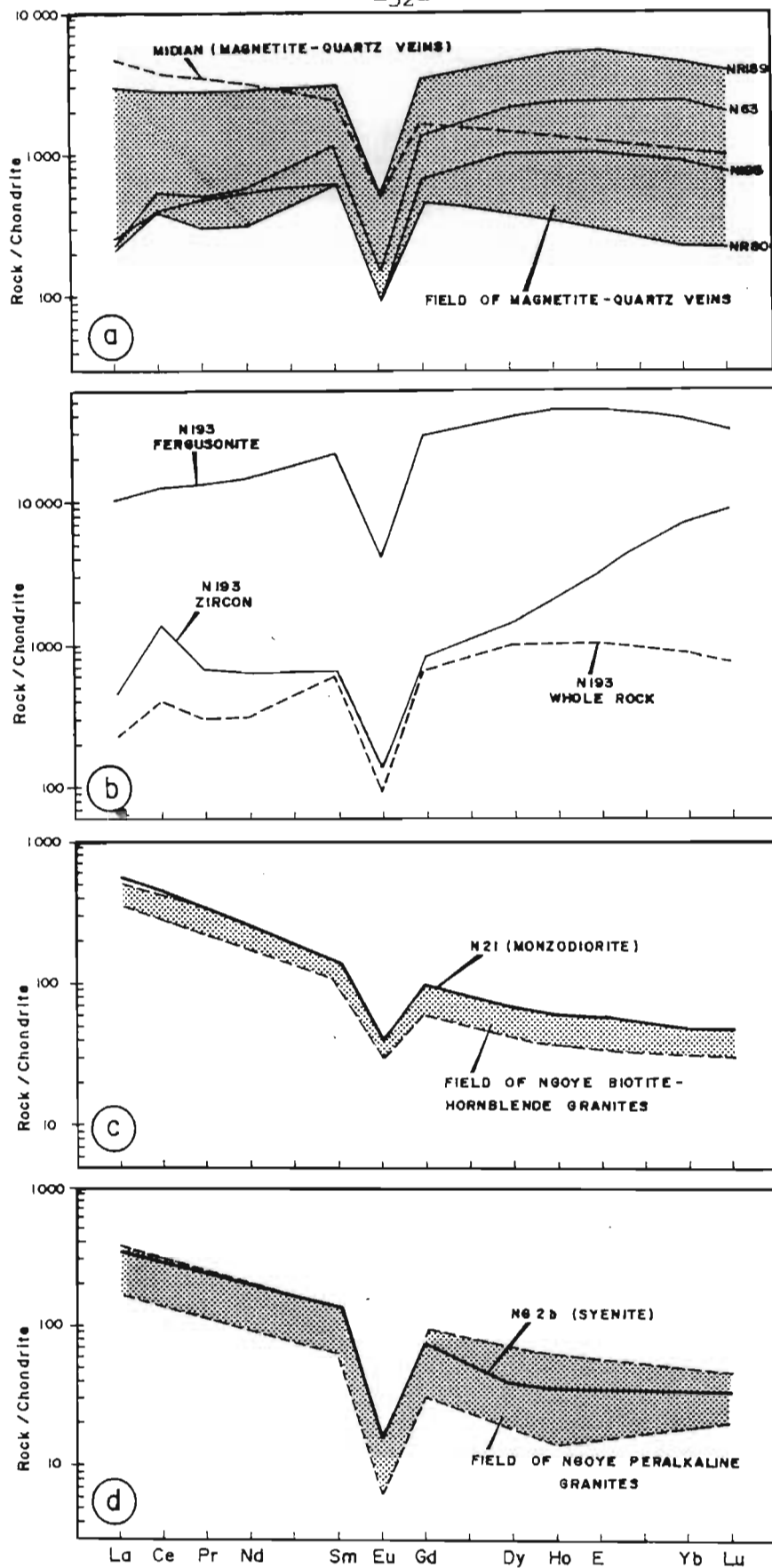


Figure 2.16. Chondrite-normalised REE patterns for the Ngoye granitoids. Fig. 2.16a magnetite-quartz veins and for comparison, a quartz vein from the Midian Complex (Harris & Marriner 1980), Fig. 2.16b zircon and fergusonite mineral concentrates from magnetite-quartz vein N193, Fig. 2.16c monzodiorite, Fig. 2.16d chloritic syenite.

characterises the four samples of magnetite-quartz rock (Fig. 2.16a). As illustrated in Figure 2.16b, the HREE are concentrated by zircon crystallisation ($La_N/Lu_N = 0.05$), similar to the garnet effect of sample N34. The remaining heavy-mineral concentrate from N193 demonstrates that the bulk of the REE are concentrated in fergusonite, which contains up to 7.15% and exhibits a similar HREE-enriched pattern to the whole-rock sample. The REE profile of a magnetite-quartz vein from the peralkaline Midian Granite Complex of Saudi Arabia is included (Fig. 2.16a) and has a comparable, though somewhat HREE-depleted, pattern.

- (vi) As shown in Figure 2.16c, the hornblende monzodiorite has a very similar LREE-enriched pattern to the biotite-hornblende granites (La_N/Lu_N : 11.71), with a moderate negative Eu anomaly (Eu/Eu^* : 0.35). The granite-like trend of the monzodiorite may result from infiltration of late-stage Eu-depleted granitic fluids into the original plagioclase-diopside assemblage, as evidenced by replacement textures observed in thin section (Section 2.1.12).
- (vii) The single syenite analysis exhibits a REE pattern (Fig. 2.16d) comparable with the field of Ngoye peralkaline granites, with moderate LREE enrichment (La_N/Lu_N : 10.49) and a marked negative Eu anomaly (Eu/Eu^* : 0.14). The similarity between the syenite and peralkaline granite patterns is supportive of a cogenetic relationship between the two lithologies.

2.4 Rb-Sr isotopes

2.4.1 Introduction

The radiogenic isotope characteristics of the Ngoye Complex were investigated previously by Barton (1983). Based on whole-rock Rb-Sr data an emplacement age of 1064 ± 19 Ma ($R_0 = 0.7058 \pm 0.002$) was obtained, with a maximum model age of 1100my. Although Barton considered the Ngoye granite to be homogeneous, her analytical results and sample positions (Fig. 2.17a) show that both the mesocrystic biotite granite and biotite granite were sampled.

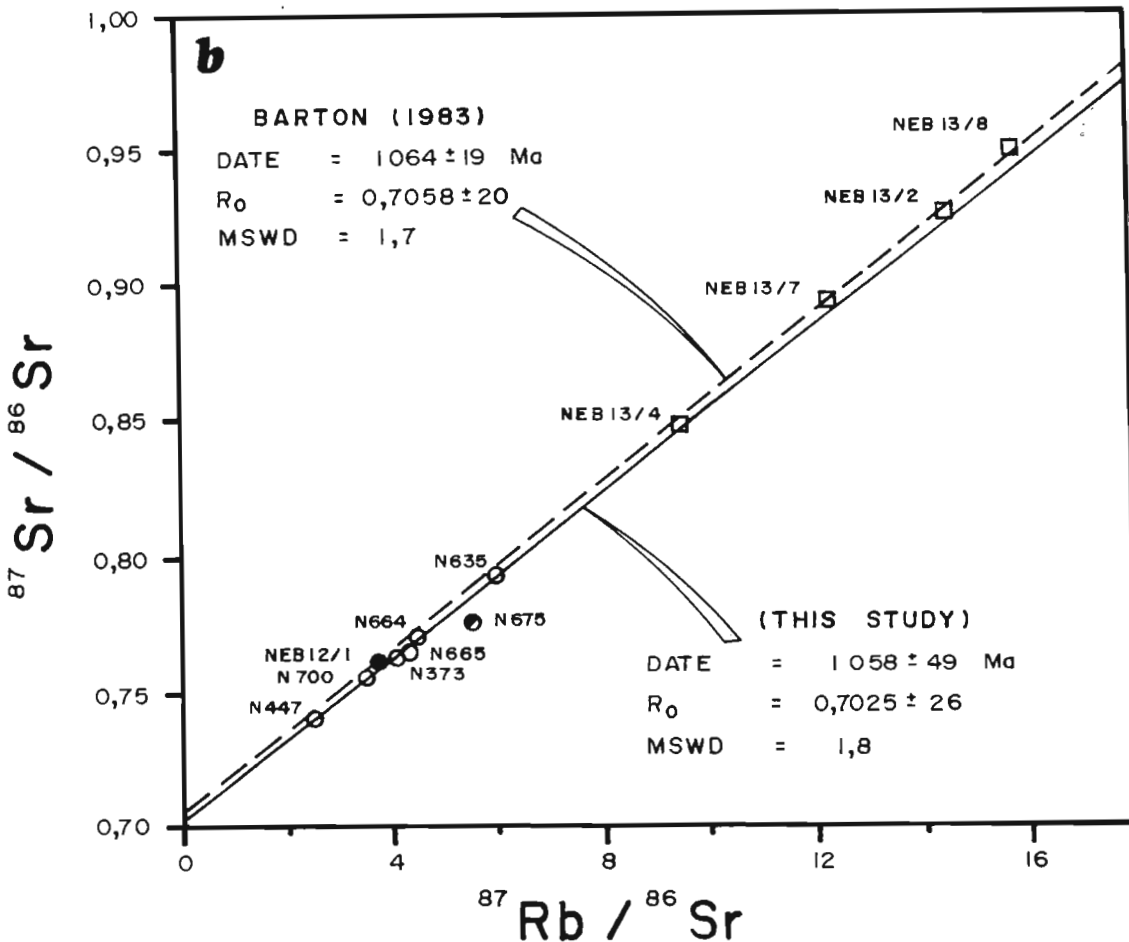
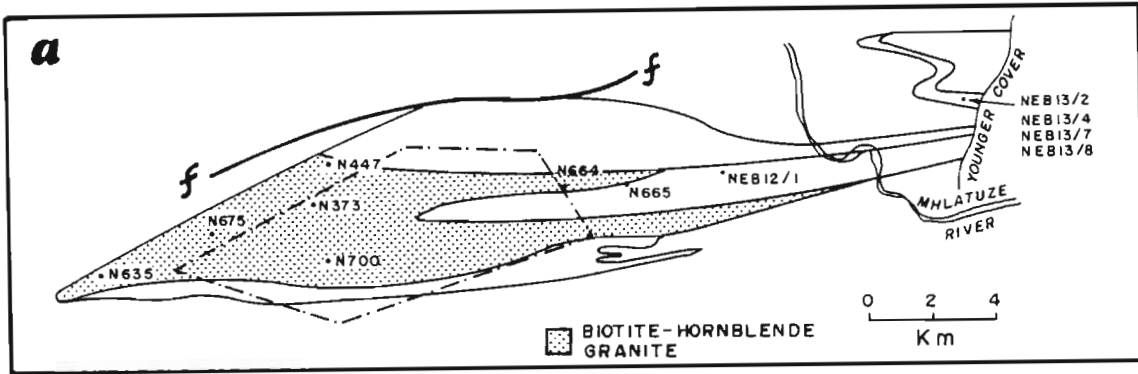


Figure 2.17. Locality of the biotite-hornblende granite samples analysed for Rb-Sr isotopes (Fig. 2.17a). The resulting Rb-Sr isochron is given as Fig. 2.17b, in which the open circles are biotite-hornblende granite. The solid circle is for mesocrystic biotite granite and the open squares are for biotite granite, from Barton (1983). One sample (N675, half-filled circle) was omitted to obtain the results of 1058 ± 49 Ma presented in this thesis.

The present investigation has been restricted to analysing seven samples of biotite-hornblende granite. This lithology was selected because it is the most abundant rock type in the complex, it is relatively undeformed and, furthermore, it was not sampled by Barton.

2.4.2 Analytical results

Rb, Sr and $^{87}\text{Sr}/^{86}\text{Sr}$ data for the various lithologies analysed are presented in Table 2.8 and plotted as Figure 2.17b. Six of the seven samples plotted regress to an isochron date of $1058 \pm 49\text{Ma}$ with an R_0 of 0.7025 ± 26 (MSWD = 1.8). The seventh sample (N675) deviates from this best-fit line by more than seven times the analytical uncertainty and was thus omitted from the regression. This result is within error of those previously obtained by Barton (1983) for samples of the mesocrystic biotite granite and biotite granite. Regression of the combined data, however, results in an errorchron, suggesting that there are real differences in R_0 of the lithology reported here and those analysed by Barton. Regression of various combinations of the data provides the results given in Table 2.9.

Barton (1983) reported U-Pb data for zircon concentrates from the biotite granite (NEB13/8). These data have been regressed and although the data are quite discordant, provide an upper-concordia intercept of $1093 +76/-66$ Ma. Until such time as more precise results are available, the preferred age for the Ngoye Complex is obtained from the weighted mean of 1064 ± 19 Ma and 1058 ± 49 Ma, ie. 1063 ± 17 Ma.

2.4.3 Discussion of Rb-Sr data

The isotopic data from Ngoye can be divided into two groups, with the hornblende-bearing granites having lower initial ratios ($R_0 = 0.7025$) than the biotite-bearing granites ($R_0 = 0.7058$). This indicates a mantle derivation for the hornblende granite, with little evidence for contamination by radiogenic ^{87}Sr . In contrast, the higher initial values of the second group support some degree of crustal assimilation during emplacement.

Table 2.8

Rb-Sr isotope data for Ngoye biotite-hornblende granite

Sample	Rb ppm	Sr ppm	$^{87}\text{Rb}/^{86}\text{Sr}$	$^{87}\text{Sr}/^{86}\text{Sr}$
N373	126	89	4.12	0.764698 ± 10
N447	90	104	2.51	0.740656 ± 12
N635	113	55	5.99	0.793353 ± 10
N664	146	95	4.47	0.771951 ± 12
N675	97	51	5.54	0.777407 ± 10
N700	103	85	3.52	0.755805 ± 11
N665	192	129	4.32	0.765865 ± 10

Table 2.9

Regressed results: biotite-hornblende granite

Granite type	Date	$^{87}\text{Sr}/^{86}\text{Sr}$
bi	$1121 \pm 63 \text{ Ma}$	0.6950 ± 11
bi + mesocrystic bi	$1064 \pm 19 \text{ Ma}$	0.7058 ± 20
bi-hbl	$1058 \pm 49 \text{ Ma}$	0.7025 ± 26
bi + bi-hbl	$1088 \pm 17 \text{ Ma}$	0.7009 ± 13
mesocrystic bi + bi-hbl	$1082 \pm 87 \text{ Ma}$	0.7021 ± 46
total data set	$1084 \pm 24 \text{ Ma}$	0.7020 ± 17

Table 2.10

Comparative ages and initial Sr ratios from selected A-type granite complexes.

Locality	Rock type	Age (Ma)	$^{87}\text{Sr}/^{86}\text{Sr}$
Oslo Rift, Norway	Peralkaline granite	275	0.7064
Sabaloka, Sudan	Peraluminous granite	383	0.711
Topsails, Canada	Peralkaline granite	419	0.707
Cape Anne, Canada	Hornblende granite	453	0.703
Ngoye	Hornblende granite	1058	0.7025
Ngoye*	Biotite granite	1064	0.7058

Note: Data for other alkaline occurrences from Blaxland *et al.* (1978); Eby (1984); Liegeois *et al.* (1983); Taylor *et al.* (1980). Ngoye data from this study. Ngoye* from Barton (1983).

2.5 Tectono-magmatic discrimination

The Ngoye lithologies have been plotted on selected tectonic-discrimination diagrams, in an effort to characterise the probable tectonic setting at the time of their emplacement. For background descriptions of the various diagrams the reader is referred to Section 1.5.4.

2.5.1 ORG-normalised patterns

With regard to the ORG-normalised patterns presented below (Fig. 2.18), only those samples that were analysed for Sm and Yb, in addition to the other elements, have been plotted. The following points are noted:

- (i) Whereas Zr, Sm, Y and Yb are close to the normalising values, K_2O , Rb and Th values are high in all the samples plotted. A general trend of decreasing values relative to ORG is thus apparent from K_2O across to Yb, a feature characteristic of WPG intrusives (Pearce et al. 1984).
- (ii) The fields delineated by the mesocrystic biotite granite and biotite-hornblende granite samples are comparable with the Skaergaard and Mull (attenuated continental margin) patterns (Figs 2.18a & b).
- (iii) Rb and Th are enriched relative to Nb in all the patterns, a feature which can be attributed to crustal involvement (Pearce et al. 1984).
- (iv) Selective enrichment ("spikes") of Ce and Sm, relative to their adjacent elements (Nb, Zr & Y) is particularly apparent in the patterns of the mesocrystic biotite granite, biotite-hornblende granite and the peralkaline granites (Figs 2.18a, b & c). Pearce et al. (op cit.) consider Ce and Sm enrichment to be characteristic of "crust-dominated" WPG patterns and, in this regard, it is instructive to compare the Sabaloka pattern with the patterns for Ngoye granites (Figs 2.18b & c). The Sabaloka A-type granite central intrusion of the Sudan shows selective enrichment of "crustal" components (eg. Rb, Th, Sm, Ce), consistent with lithospheric involvement during magma generation (Harris et al. 1983).
- (v) The pattern exhibited by the biotite granite and the garnet-muscovite granite is broadly comparable with the COLG pattern defined by Pearce et al. (1984) for S-type granites from Tibet and SW England (Fig. 2.18d). However the Ngoye granites have marked negative Ba spikes and higher HREE contents, more in common with WPG patterns.

From the above ORG-normalised patterns, the Ngoye granites have a clear WPG signature, with evidence for crustal contamination provided by enrichment in Rb and Th relative to Nb, as well as Ce and Sm relative to

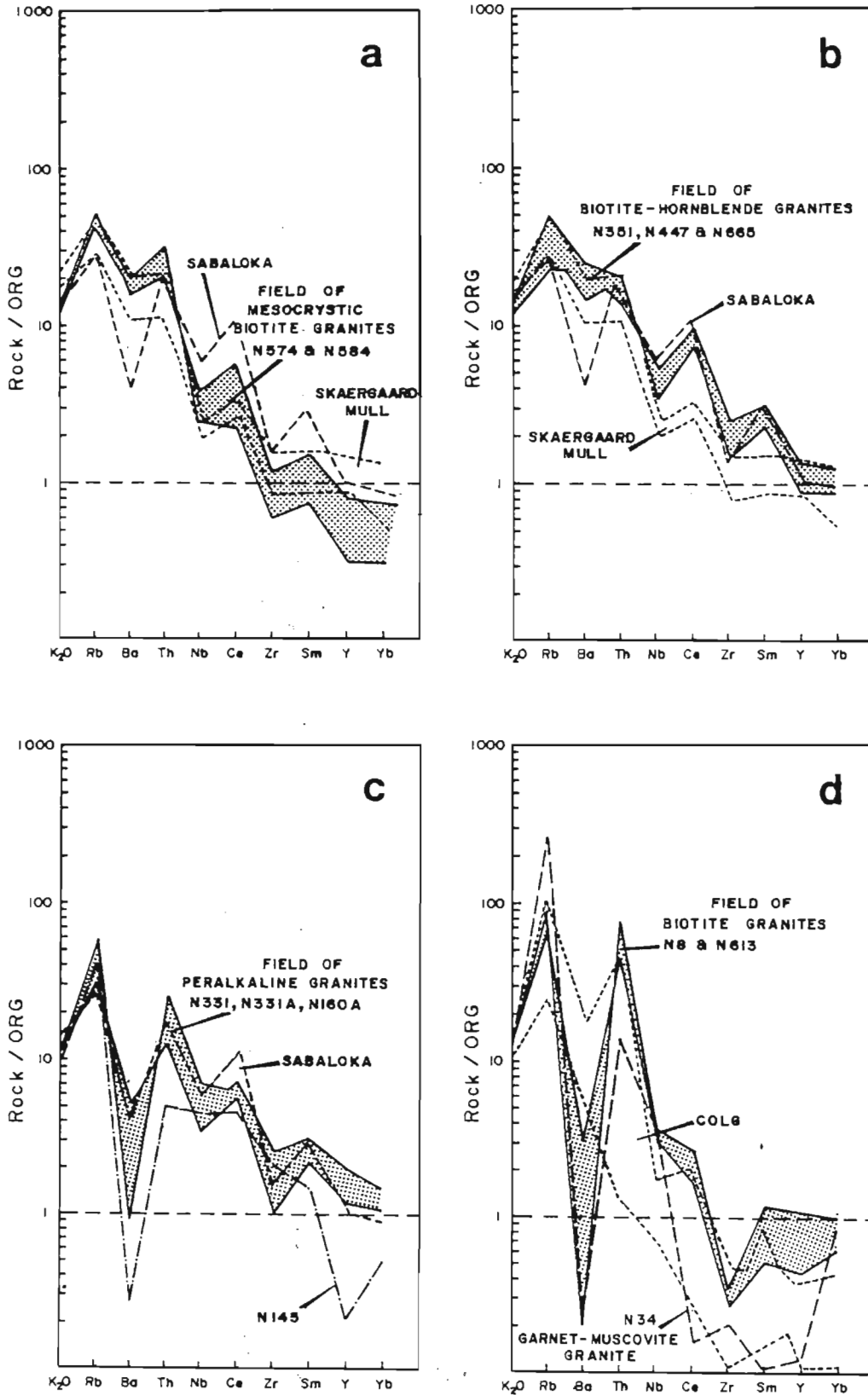


Figure 2.18. Plots of representative Ngoye granites, for which REE data are available, normalized against ocean-ridge granite (ORG). ORG values and the patterns for selected WPG's and COLG's are from Pearce *et al.* (1984). Fig. 2.18a mesocrystic biotite granite, Fig. 2.18b biotite-hornblende granite, Fig. 2.18c peralkaline granites, Fig. 2.18d biotite granite and garnet-muscovite granite.

Zr and Y. The implication therefore is that the Ngoye granites were intruded into continental crust.

2.5.2 Discrimination using Nb, Y and Rb

Within-plate granites (WPG) can be distinguished from volcanic- arc granites (VAG), ocean-ridge granites (ORG) and collision granites (COLG) by their Nb, Y and Rb contents (Pearce *et al.* 1984). When the Ngoye granites are plotted in Nb-Y space (Fig. 2.19a) they are predominantly WPG but, due to low Y contents, some of the peraluminous and peralkaline granites fall in the VAG+COLG field. The COLG character of these latter samples indicates crustal contamination, or alteration effects (Pearce *et al.* 1984).

The Ngoye granites are better constrained within the WPG field on the Pearce *et al.* (1984) Rb vs Nb+Y diagram (Fig. 2.19b). However the high Rb content of the muscovite-bearing granites again results in the spread of data towards the COLG field.

2.5.3 Maniar & Piccoli diagrams

The Ngoye data have been plotted on two of the major-element tectonic discrimination diagrams devised by Maniar & Piccoli (1989). As shown in Figure 2.20a, high Fe/Mg ratios result in the classification of the majority of Ngoye samples as Group II granites, ie. rift-related or continental epeirogenic-uplift types. With regard to Al₂O₃ contents the distinction is however not as clear (Fig. 2.20b) and a mixed Group II/Group III character is suggested.

2.5.4 Y/Nb discrimination

As outlined previously (Section 1.5.4), Y/Nb ratios for particular A-type granite intrusives tend to remain constant, even through protracted fractionation (Eby 1990). However, dispersed ratios may result from metasomatic effects common in peralkaline granites (Eby 1990). As shown in Figure 2.20, most of the Ngoye lithologies have Y/Nb ratios intermediate between ocean-island basalt (OIB) and island-arc basalt (IAB), and are comparable with the trend of Sabaloka granites. The low Y/Nb ratios displayed by two of the samples are attributed to alteration effects.

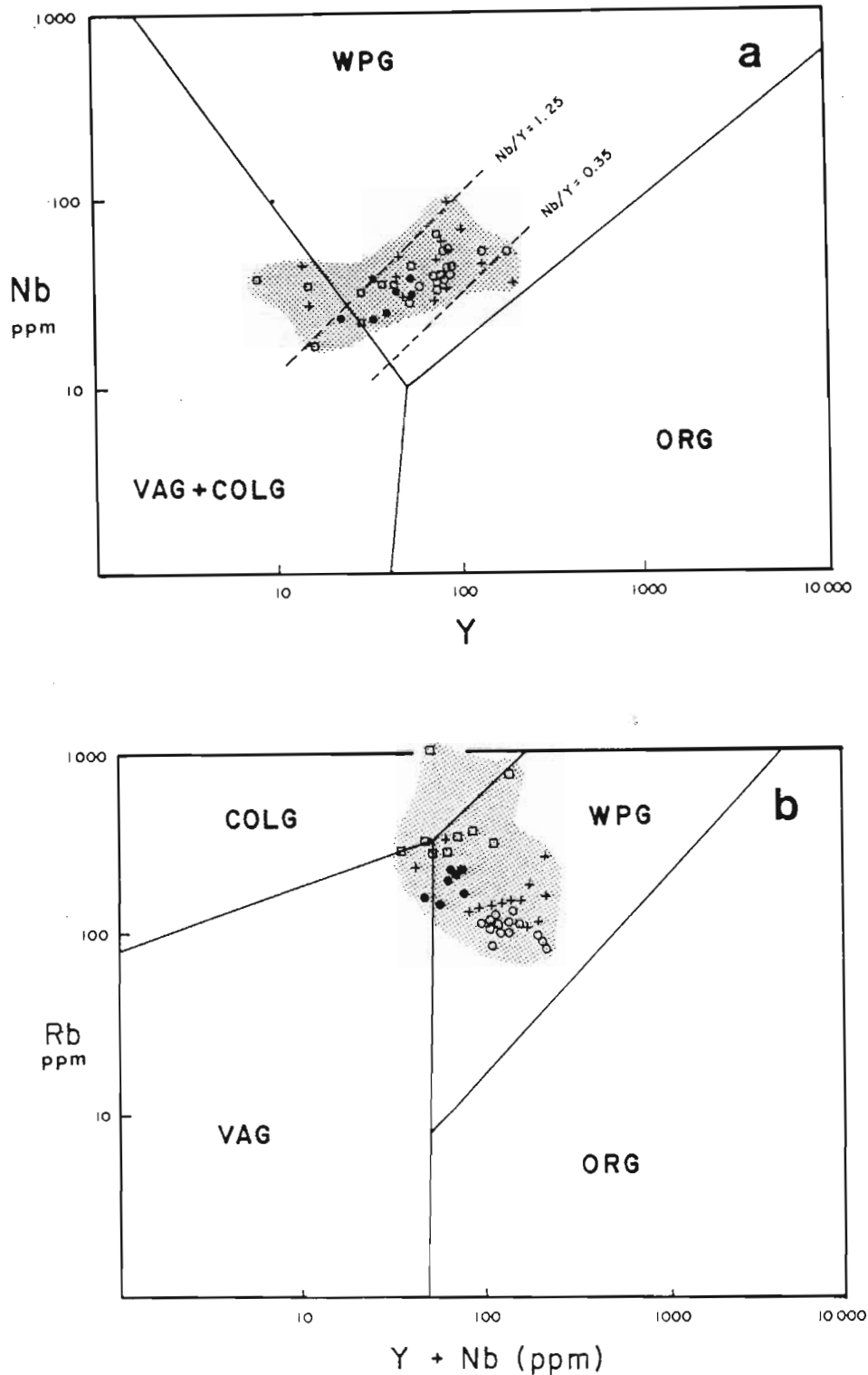


Figure 2.19. Tectonic discrimination plot of Nb/Y (Fig. 2.19a) and Rb vs Nb+Y (Fig. 2.19b). Fields for ORG, VAG, COLG and WPG from Pearce et al. (1984). Symbols: (●) mesocrystic biotite granite, (○) biotite-hornblende granite, (+) peralkaline granites, (□) biotite granite & garnet-muscovite granite. As illustrated in Fig. 2.19a, the majority of Ngoye samples have Nb/Y ratios between 0.35 and 1.25.

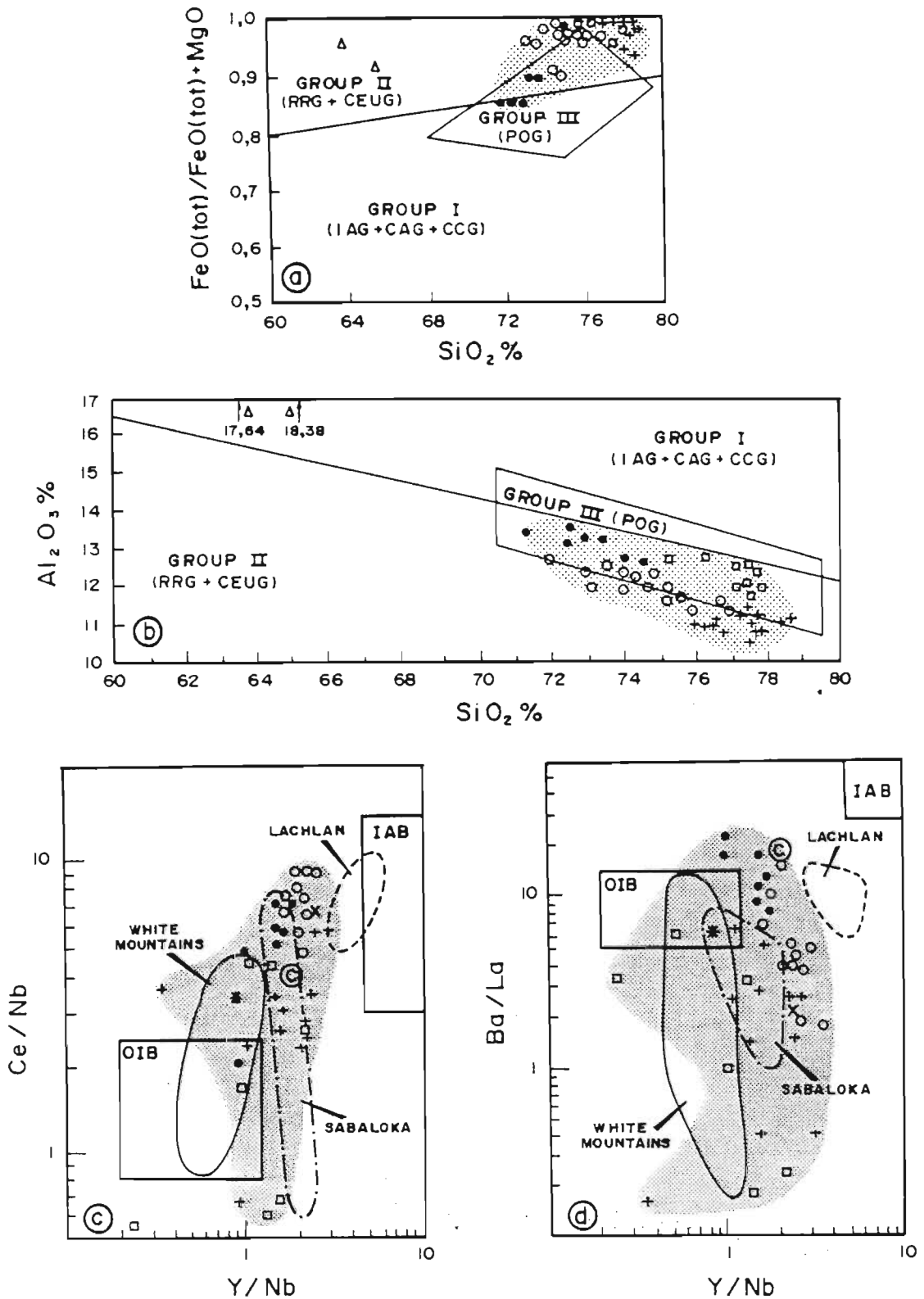


Figure 2.20. Tectonic discrimination of the Ngoye granitoids as Group II (Fig. 2.20a) and Group II/III (Fig. 2.20b) according to parameters suggested by Maniar & Piccoli (1989). Tectonic discrimination of the Ngoye granitoids in Ba/La vs Y/Nb (Fig. 2.20c) and Ce/Nb vs Y/Nb space (Fig. 2.20d). Fields for A-type granites of the Sabaloka, White Mountain and Lachlan complexes are from Eby (1990) and are included for comparison with the Ngoye data. Average crustal composition is given as ©, OIB = ocean-island basalt, IAB = island-arc basalt.

By analogy with the Sabaloka intrusion, it is inferred that the Ngoye Complex is an intra-continental ring complex.

2.6 Summary of salient features

- (i) Eleven gneissic alkaline granitoid types are recognised within the Ngoye Complex.
- (ii) The granitoids have been characterised according to modal and geochemical criteria and range from peraluminous through metaluminous, to peralkaline in composition.
- (iii) Structural and lithological considerations indicate that the Ngoye Complex is a deformed alkaline central complex, with an elongate outcrop pattern resulting from lateral shearing and stretching in an east-west direction.
- (vi) Rb-Sr isotopes support derivation of the metaluminous granites from a mantle source (low R_0).
- (v) Trace element ratios and ORG-normalized patterns indicate that the Ngoye lithologies have the geochemical characteristics of A-type, mantle-derived, within-plate-granite magmatism. High LIL/HFS element ratios are consistent with intrusion into, and some reaction with, continental crust.

CHAPTER 3

THE BULLS RUN COMPLEX

3.1 Introduction

The Bulls Run Complex is located approximately 20km northwest of the Ngoye Complex (Fig. 3.1). Physical aspects pertaining to this area are given by Scogings & Forster (1989) and Scogings (1991a). Access to this rugged area is poor, being hampered by dense vegetation, steep topography and the Mhlatuze River that flows along the southern margin of the complex (frontispiece). Therefore field traverses are generally lengthy and entail up to 15km of tough walking, which makes for arduous collection of geochemical samples.

Scogings & Forster (1989) reported in some detail on previous geological activity pertaining to the Bulls Run Complex, therefore only a summary is presented here:

- (i) Du Toit (1931) reported the area underlain by granitic rocks.
- (ii) De Villiers (1941) recorded the occurrence of niobium-bearing minerals in "albitite" at Bulls Run.
- (iii) Von Backstrom (1962) noted large zircons (c. 15cm long) in the gneisses on Bulls Run estate during an assessment of low-grade eluvial and alluvial deposits of zircon and monazite.
- (iv) Nicolaysen & Burger (1965, p. 508) suggested that the gneisses at

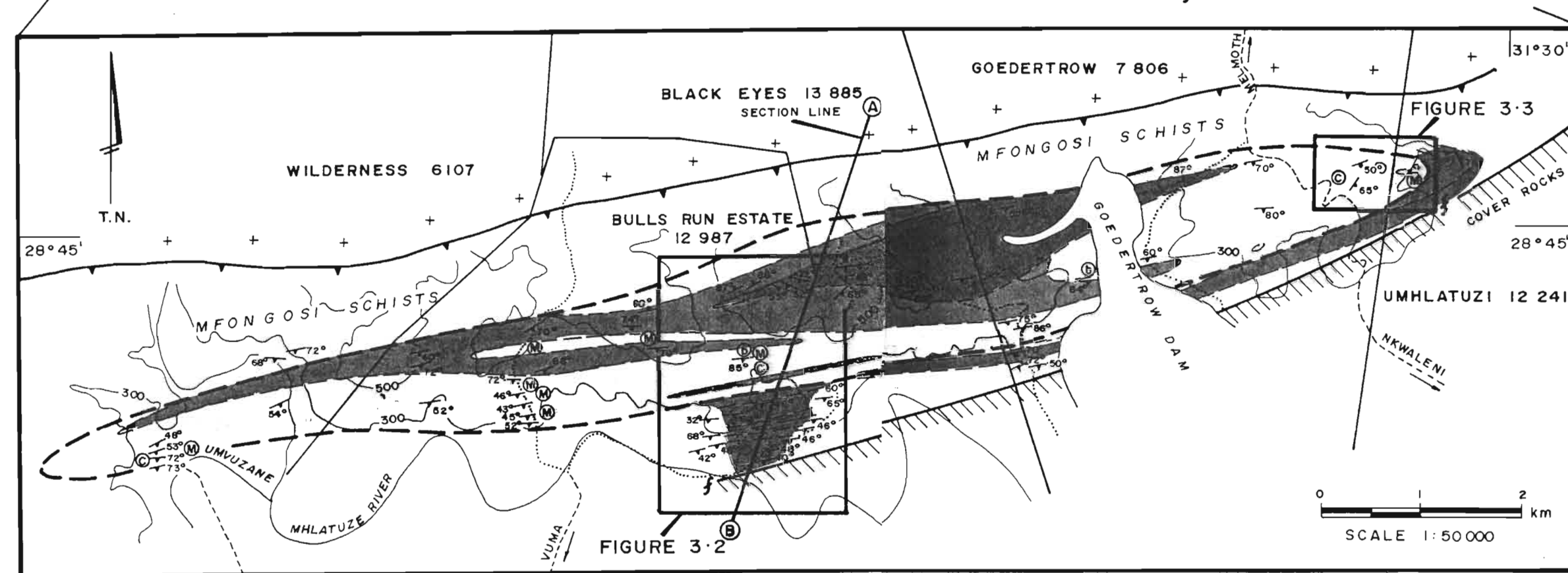
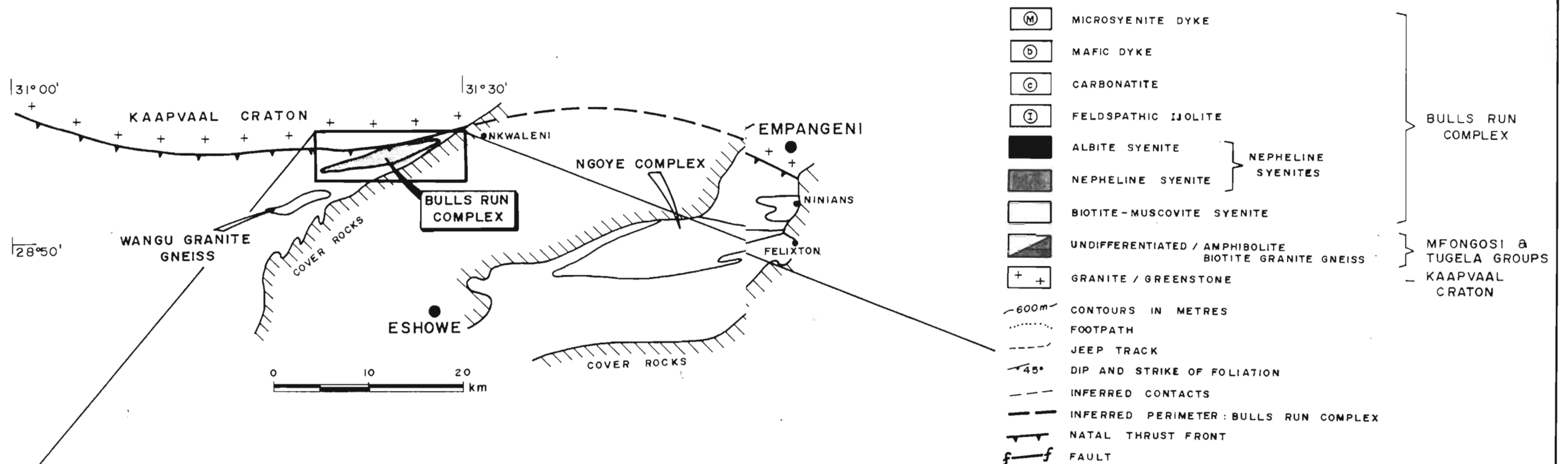
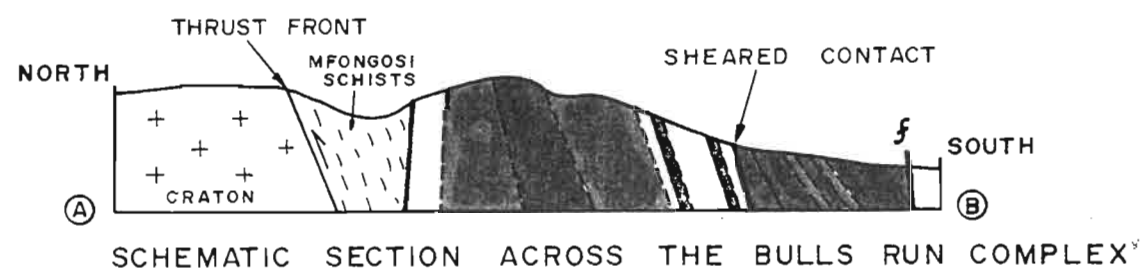


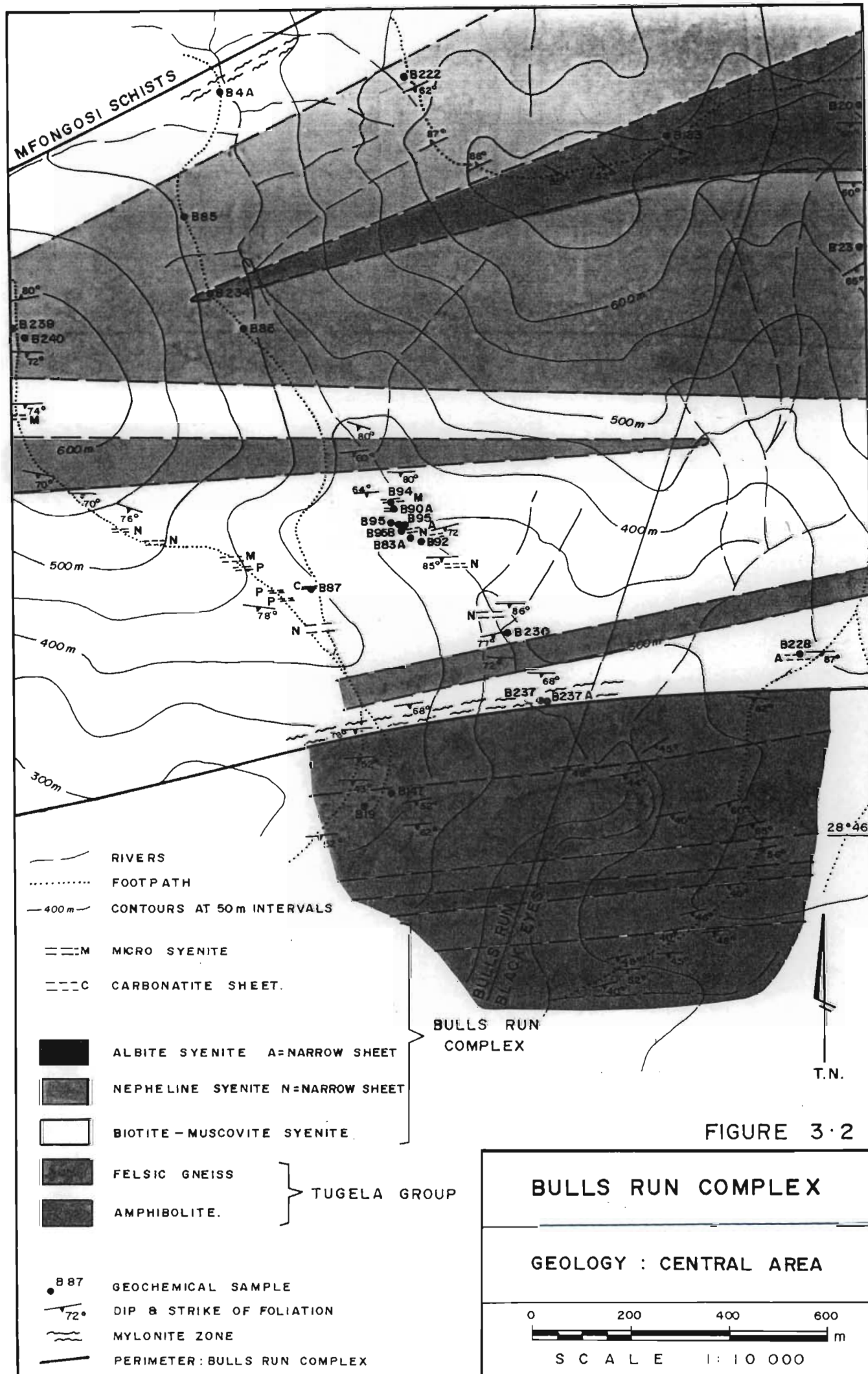
FIGURE 3.1



BULLS RUN COMPLEX

LOCALITY and GEOLOGY

SCALE: AS SHOWN



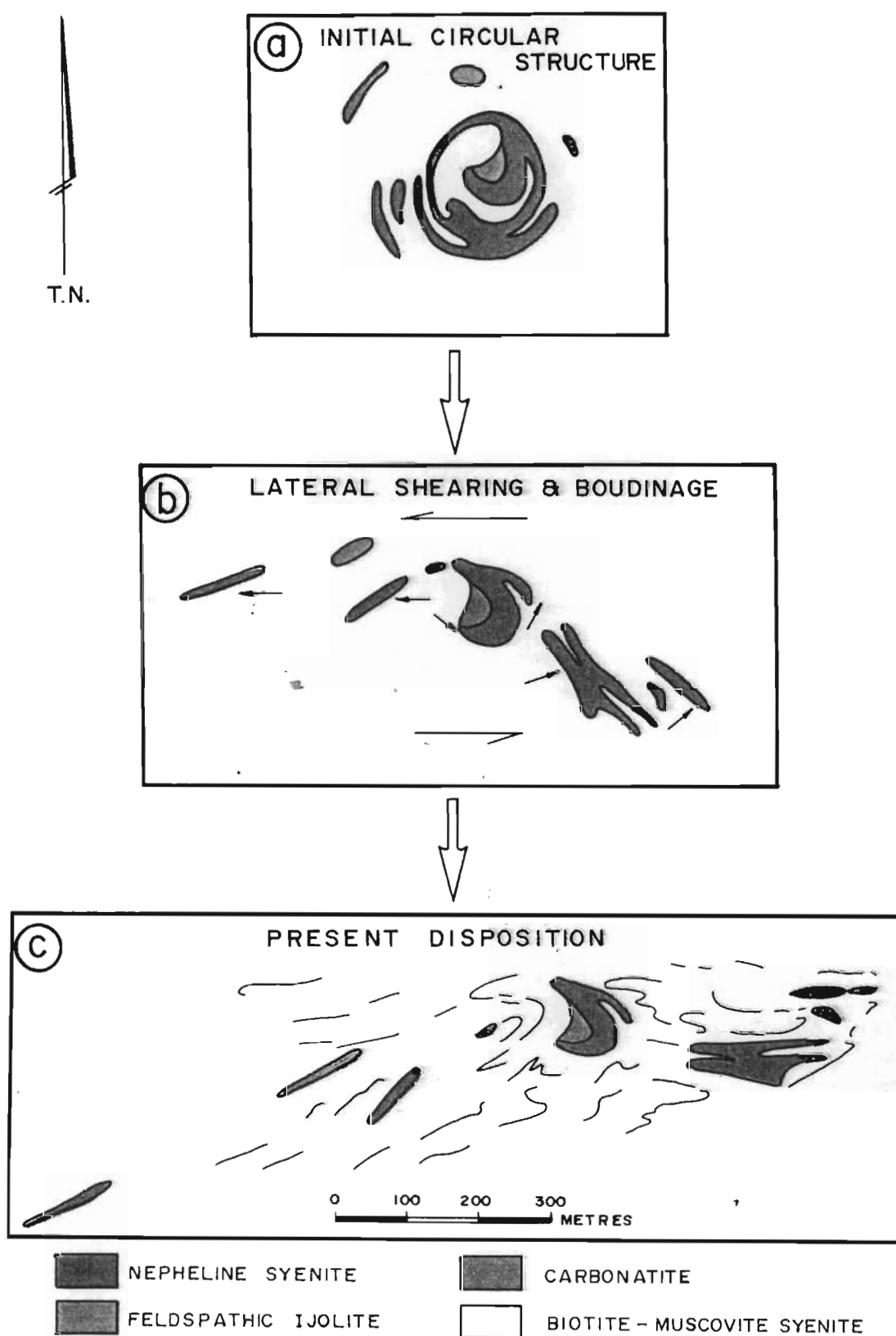


Figure 3.7. Cartoon diagram illustrating the proposed rupture of an initial circular ring complex by lateral shearing. This results in the present disposition, with boudinaged nepheline syenite remnants in a ductile matrix of biotite-muscovite syenite.

Bulls Run were syenitic and described them as "soda-rich Tugela migmatites and gneisses". Pb-isotope studies on a single zircon yielded an age of 1140 ± 35 Ma.

- (v) The name "Bulls Run Syenite Gneiss Formation" was proposed (SACS 1980).
- (vi) Charlesworth (1981) delineated the extent of the Bulls Run syenitic gneisses classifying them, on the basis of modal analyses, as varying from monzonite and syenite to quartz syenite. A mylonitized contact between the syenite gneisses and surrounding amphibolitic country rocks was cited as evidence for thrust tectonics during emplacement of the syenite body.
- (vii) Scogings & Forster (1989) recorded the discovery of carbonatites, nepheline syenites and albite syenite at Bulls Run. They interpreted the "formation" as a metamorphosed syenite/carbonatite central complex, emplaced into continental crust (Scogings & Forster op cit., Scogings 1990a).
- (viii) Daly et al. (1989) highlighted the economic potential of the Bulls Run nepheline syenite, for use as a flux in the ceramic and glass industries (see symposium abstract in Appendix 4).
- (ix) The proposal that the Bulls Run Formation be renamed the Bulls Run Complex (BRC), in accordance with generally-accepted terminology for alkaline central intrusions, was ratified by SACS (Scogings 1991a).

3.2 Structural considerations

3.2.1 Introduction

As mentioned previously (Section 1.1), the interpretation of post-emplacement deformational effects has not been accorded high priority during this investigation. This is because intensive structural analysis of the Tugela Terrane was carried out as part of the National Geodynamics Project, under the guidance of P.E. Matthews

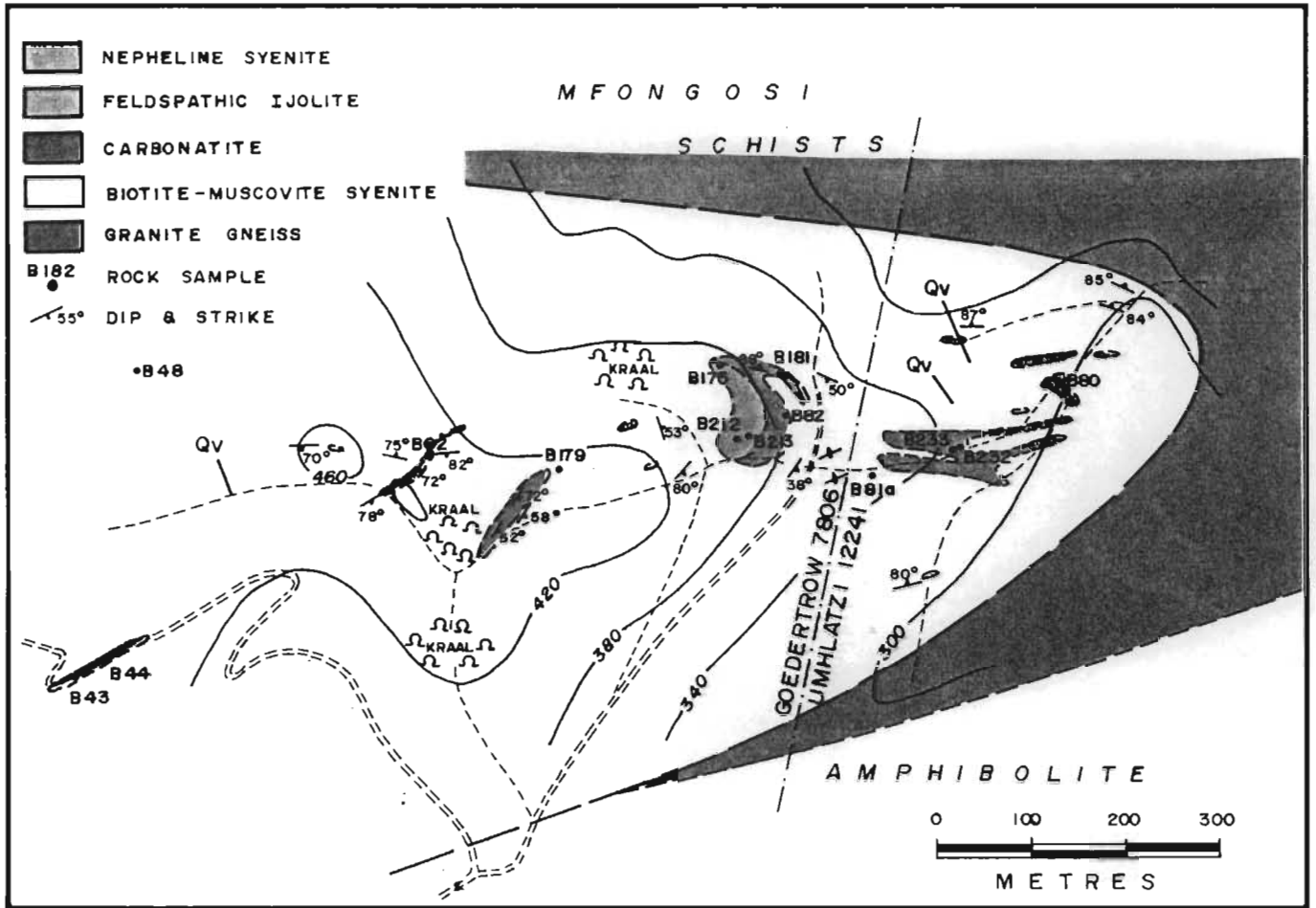


Figure 3.3. Geology of the eastern part of the Bulls Run Complex. For locality see Fig. 3.1.

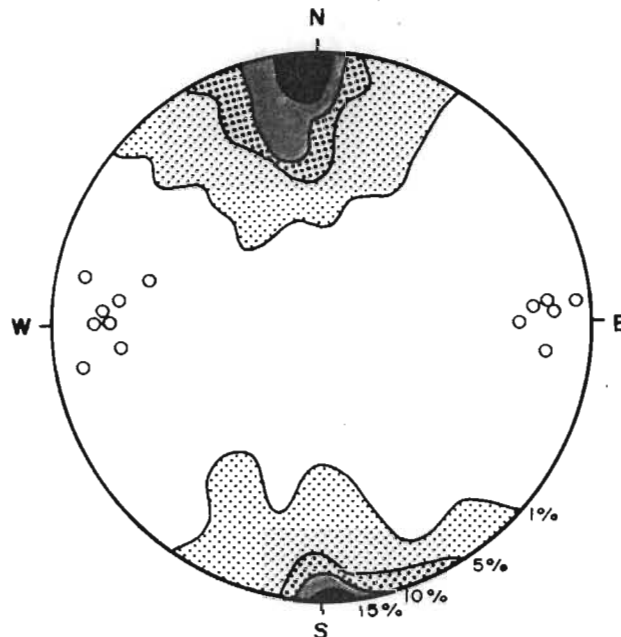


Figure 3.4. Stereographic plot of structural data from the Bulls Run Complex, showing contours of poles to foliation planes and the distribution of fold axes and lineations. Symbols: contours at 2.5, 5 and 10% per 1% area, () lineations and fold axes.

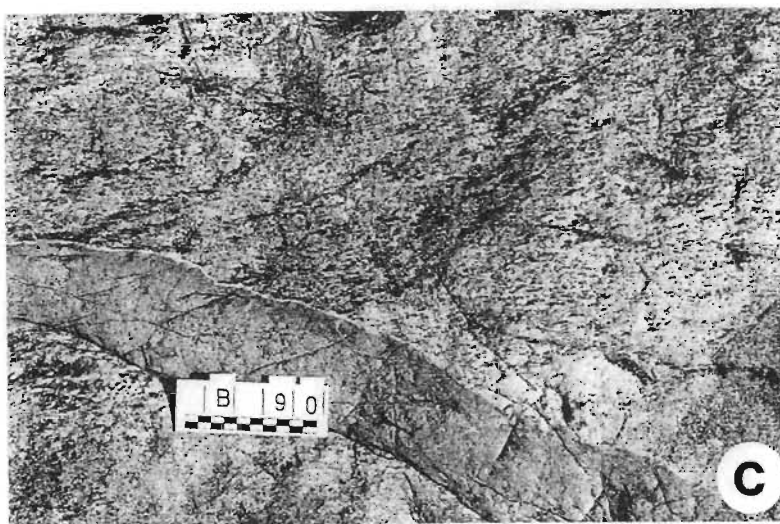
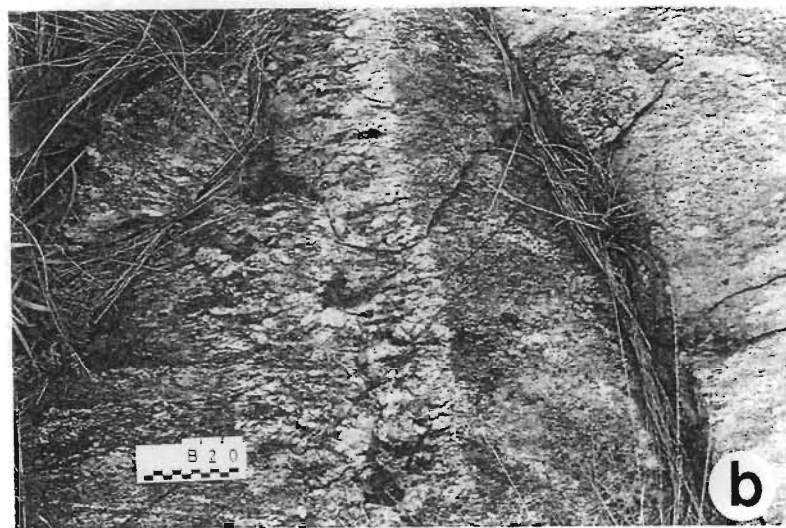
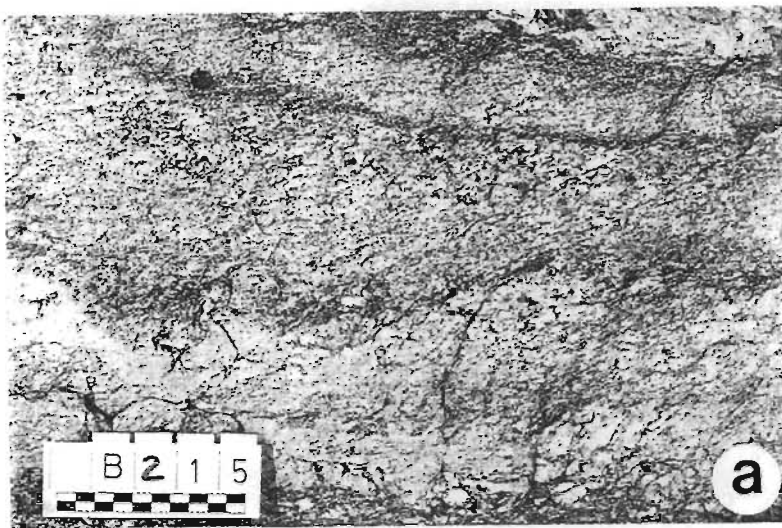


Figure 3.5. Field exposures illustrating transgressive structural fabrics that are superimposed on original magmatic features. Structural features highlighted on overlay. Fig. 3.5a: biotite-rich layers in nepheline syenite, Fig. 3.5b: contact between pegmatite and albite syenite, Fig. 3.5c: microsyenite dyke intruded into biotite-muscovite syenite. Scale in cm.

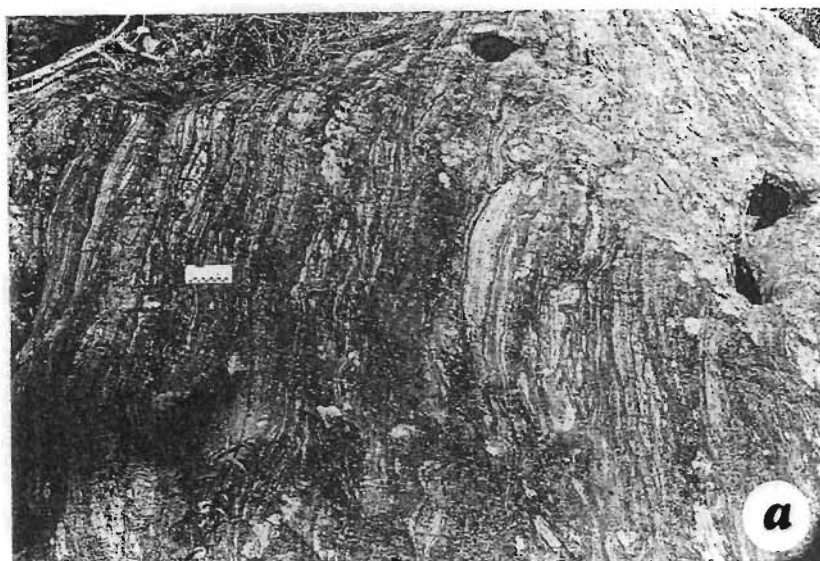


Figure 3.6. Outcrops of mylonitised biotite-muscovite syenite at locality B143/237. Scale in cm. Fig. 3.6a: mylonite zone looking east, Fig. 3.6b: microsyenite dyke boudin within mylonitised biotite-muscovite syenite. Looking southwest.

(Rigotti 1977, Schulze-Hulbe 1977, Harmer 1979, Smalley 1980, Charlesworth 1981, Matthews & Charlesworth 1981).

Although the emphasis during this study has been on the discrimination and delineation of lithologies, routine structural readings in the BRC were taken for comparison with the Ngoye structural data (Section 2.1 and Scogings 1985). From this database the following observations are made:

3.2.2 General structural fabric

The BRC is characterised by a pervasive east-west striking, upright, gneissose fabric that dips at high angles both to the north and south (Figs 3.1, 3.2). Features such as intrusive contacts and magmatic layering within the syenites, are transgressed by the gneissose fabric (Fig. 3.5) which increases in intensity towards the margins of the complex. The lithological banding in the felsic country rocks at the eastern extremity of the BRC defines an antiform that is sharply discordant to the foliation in the syenites (Fig. 3.1). This structural relationship is similar to that described from Ngoye (Scogings 1985), suggesting that the country rocks were metamorphosed and foliated prior to emplacement of the BRC (cf. Charlesworth 1981).

3.2.3 Contact relationships

As indicated (Fig. 3.2), the contact zone between the BRC and the surrounding country rock is mylonitised (Fig. 3.6). Shallower dips are apparent in the country rocks than in the complex itself (section, Fig. 3.1). Fold axes in the mylonites are subhorizontal and plunge at shallow angles both to the east and west (Fig. 3.4). A similar relationship was described for the Ngoye Complex (Scogings 1985), where the fold axes within mylonite zones have been rotated into parallelism with a lateral shear direction.

Apparently the biotite-muscovite syenite has responded relatively incompetently to strain within the mylonite zone, as exemplified by a boudinaged microsyenite dyke (Fig. 3.6). This example clearly indicates that mylonitization post-dated the intrusion of microsyenite.

3.2.4 Effects of competency contrast

Further evidence for deformation by a lateral shear couple is provided in the eastern part of the BRC (Fig. 3.7). At this locality the present disposition of nepheline syenite, carbonatite and feldspathic ijolite appears to result from shearing and boudinage of an original ring-dyke complex. It is suggested that the muscovite-syenite fenite to the nepheline syenite was relatively plastic during deformation and facilitated rupture of the more-competent ring dykes. This style of deformation is consistent with the high strain noted in the marginal mylonites to the BRC, and is in accord with the penetrative lateral-shear component described from the Ngoye Complex (Scogings 1985).

In conclusion, the BRC is envisaged as a set of concentric cylinders, or cones, of different syenites that were later compressed and stretched in an east-west direction by lateral shearing. The heterogeneous distribution of strain, from a relatively low-strain core to tectonised margins, is a result of competency contrast with the country rocks and ductile behaviour of the incompetent, muscovite-rich, envelope.

3.3 Field and petrographic descriptions

3.3.1 Introduction

Contrary to previous descriptions of the Bulls Run Complex as an homogeneous silica-oversaturated syenite body (Charlesworth 1981, Matthews & Charlesworth 1981), the BRC is shown to be lithologically complex and essentially undersaturated (Scogings & Forster 1989). The BRC is subdivided into three major lithotypes according to modal mineralogy, with an envelope of biotite-muscovite syenite surrounding a core of biotite-nepheline syenite and albite syenite (Figs. 3.1 & 3.8). Minor intrusive phases include peralkaline microsyenite dykes, carbonatite sheets, a feldspathic ijolite plug and biotite-rich mafic dykes.

Representative modal analyses are presented as Table 3.1 (complete data set in Appendix 1, Table A1.2) and QAPF modal classification is illustrated in Figure 3.9. Due to the virtual lack of anorthite

Figure 3.7. Cartoon diagram illustrating the proposed rupture of an initial circular ring complex by lateral shearing. This results in the present disposition, with boundinaged nepheline syenite remnants in a ductile matrix of biotite-muscovite syenite.

TABLE 3.1

REPRESENTATIVE MODES: BULLS RUN COMPLEX

	B179	B105	B81a	B175	B80	B222	B183	B220a	B217	B62	B46	B72
quartz	--	--	--	--	--	--	--	--	--	--	--	6
microcline	19	35	--	11	33	46	46	21	t		2	34
albite	34	36	5	1	22	19	36	52	39	--	t	47
nepheline	--	--	--	39	30	19	12	18	--	--	--	--
cancrinite	--	--	--	10	4	4	t	4	--	--	--	--
biotite	6	11	--	5	3	10	3	4	48	3	9	--
muscovite	40	14	95	--	--	--	t	--	--	--	--	--
hornblende	--	--	--	--	3	--	--	--	--	--	--	--
aegirine-augite	--	--	--	22	--	--	--	--	--	--	--	13
calcite	1	3	--	t	1	1	t	t	9	96	85	--
apatite	--	t	--	3	t	t	--	--	3	t	3	t
zircon	--	--	--	--	--	--	1	t	--	--	--	t
opaque	--	t	--	--	2	--	--	--	1	1	t	--
pyrochlore	--	--	--	--	--	--	1	--	--	--	t	--
garnet	--	--	--	7	--	--	--	--	--	--	--	--
sphene	--	--	--	1	2	--	--	--	--	--	--	--

- = not detected

t = trace amount, less than 1%

B179, B105 = biotite-muscovite syenite

B81a = muscovite-rich rock

B175

B80

B222

B183, B220a

= feldspathic ijolite

= hornblende-nepheline syenite

= biotite-nepheline syenite

= albite syenite

B217 = biotite-rich dyke

B62, B46 = carbonatite

B72 = microsyenite

component in the plagioclase, all the Bulls Run lithologies plot in the quartz alkali-feldspar syenite, alkali-feldspar syenite and feldspathoidal syenite fields.

Sorensen (1974), Currie (1976a) and Hall (1987) describe a mineralogical and geochemical classification of syenites related to alumina saturation. In this classification miaskitic syenites, with peralkalinity indices ($(Na+K)/Al$) less than 1.00, characteristically contain hornblende, biotite and zircon, sometimes with accessory pyrochlore and melanite garnet. Agpaitic syenites, on the other hand, are peralkaline and have mineral assemblages dominated by sodic amphiboles and pyroxenes, with unusual minerals such as eudialyte present as accessory phases. Modal data (Table 3.1) indicate that the Bulls Run lithologies are dominantly miaskitic.

Classification of the feldspathoidal syenites on the modal AFM diagram (Sorensen 1974, Le Bas 1977) indicates that the majority are feldspathoidal syenites (juvite and foyaite), with three relatively mafic samples plotting in the feldspathic-ijolite field (Fig. 3.9c).

Polished slabs of representative Bulls Run lithologies are illustrated in Figure 3.8, for reference during the following descriptions.

3.3.2 Biotite-muscovite syenite

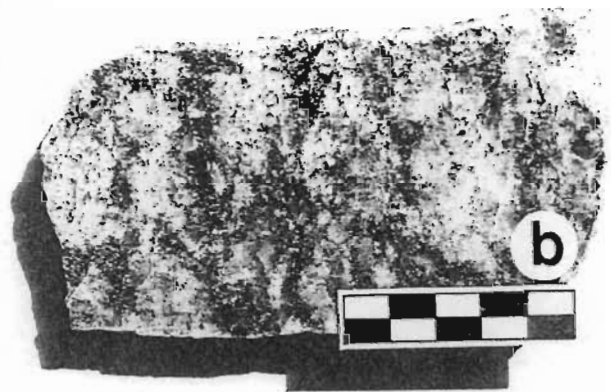
As depicted in Figure 3.1, this rock type forms an envelope to the nepheline syenite core. Due to high mica contents and susceptibility to weathering fresh outcrops are uncommon and encountered essentially to the east of Goedertrou Dam. Abundant muscovite (10 to 30 modal%) is characteristic of this rock type, and is particularly useful when mapping areas of poor exposure, as muscovite is easily recognised in residual soils.

This medium-grained lithology varies from off-white to pink, with the former colour restricted to the eastern and central parts of the complex. As the boundary between the two varieties of biotite-muscovite syenite has not yet been identified with certainty, they are not discriminated in Figure 3.1. Thin-section analysis of this rock type indicates the following modal assemblage: albite (30 to 50 modal%, Ab_{99}), microcline (10 to 35 modal%, Or_{94}), muscovite (5 to 35 modal%), Fe/Ti-rich biotite (<10 modal%) and calcite (<10 modal%), with accessory apatite and sphene. Modally, the biotite-muscovite syenite classifies as alkali-feldspar syenite and defines a restricted field near the "A" apex of the QAPF diagram.

Thin section examination reveals that the feldspars comprise 5mm-diameter domains of fine-grained polygonal material representing large crystals reduced in grain size during deformation. Almost invariably, muscovite is the dominant micaceous mineral and it commonly occurs as small books in nests up to 10mm diameter, in conjunction with pleochroic yellow to brown biotite; together these minerals define a gneissose fabric. Iron-stained calcite is a common accessory, especially near intrusive carbonatites, and forms interstitial patches and veinlets in the syenite.



BIOTITE - MUSCOVITE SYENITE



BIOTITE - NEPHELINE SYENITE



ALBITE SYENITE



FELDSPATHIC IJOLITE



MICROSYENITE



CARBONATITE

Figure 3.8. Polished slabs of representative lithologies from the Bulls Run Complex. Scale in cm.

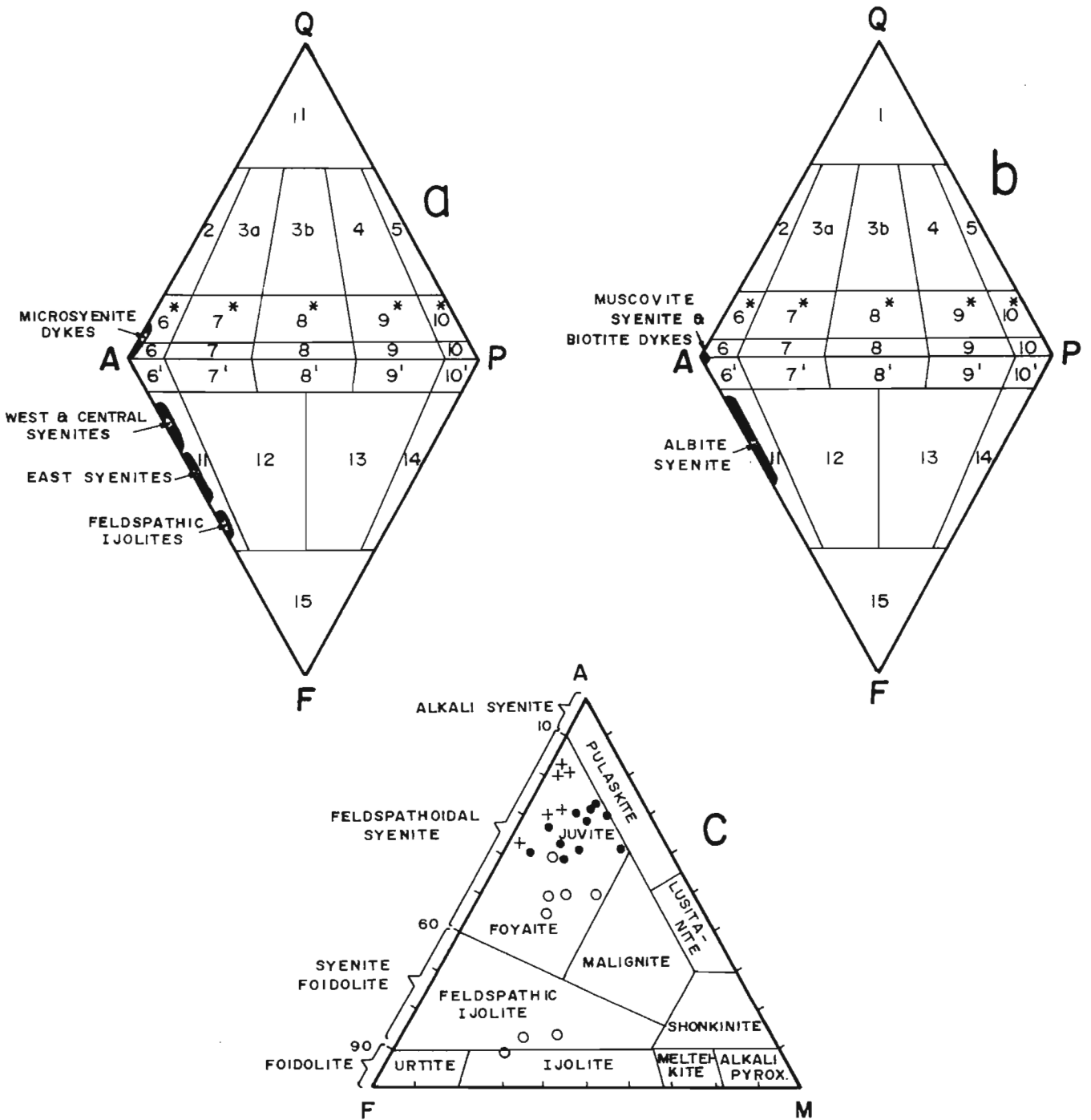


Figure 3.9. Classification of the Bulls Run lithologies using modal proportions. Figs 3.9 a & b: QAPF diagram of Streckeisen (1976a), with fields of Bulls Run syenites shown as solid black. The relevant QAPF fields are numbered as follows: 6* = quartz alkali-feldspar syenite, 6 = alkali-feldspar syenite, 6' = foid-bearing alkali-feldspar syenite, 11 = foid syenite. Fig. 3.9c: AFM diagram for the classification of feldspathoid-bearing rocks, from Sorensen (1974) and Le Bas (1977). Symbols: (o) nepheline syenites from the eastern part of the complex, (•) nepheline syenites from the central and western part of the complex, (+) albite syenite.

TABLE 3.2

MICROPROBE ANALYSES: BULLS RUN COMPLEX

ALBITE

	B179a	B175a	B80a	B23a	B183a	B72a	B46a	B217a	A
SiO ₂	68.94	67.92	69.28	68.81	69.38	68.57	68.66	69.16	67.84
Al ₂ O ₃	19.22	19.45	19.36	19.23	19.40	19.01	19.31	19.37	19.65
FeO	0.03	0.16	0.04	0.03	--	0.34	0.01	0.02	0.05
CaO	0.06	0.05	0.14	0.02	0.04	0.04	0.01	0.01	--
Na ₂ O	11.55	11.77	11.47	11.77	11.59	11.64	11.09	11.69	11.07
K ₂ O	0.07	0.06	0.07	0.09	0.04	0.31	0.57	0.15	0.29
Total	99.87	99.41	100.36	99.95	100.45	99.91	99.65	100.40	98.90
ions on basis of 32 oxygens									
Si	12.042	11.949	12.037	12.024	12.041	12.019	12.032	12.056	11.964
Al	3.958	4.036	3.066	3.960	3.969	3.928	3.989	3.970	4.085
Fe ²⁺	0.005	0.024	0.006	0.005	--	0.050	0.001	0.003	0.007
Ca	0.011	0.009	0.026	0.004	0.008	0.007	0.003	0.002	--
Na	3.918	4.018	3.875	3.987	3.901	3.955	3.769	3.940	3.785
K	0.016	0.014	0.016	0.019	0.009	0.069	0.127	0.033	0.066
Total	19.950	20.050	19.926	19.999	19.928	20.028	19.921	20.004	19.907
Or	0.4	0.3	0.4	0.4	0.2	1.7	3.3	0.9	1.7
Ab	99.3	99.5	98.9	99.4	99.6	98.1	96.7	99.1	98.0
An	0.3	0.2	0.7	0.1	0.2	0.2	<.1	<.1	0.3

MICROCLINE

	B175M	B80M	B23M	B183M	B72M	B46M	B
SiO ₂	65.45	65.40	64.59	65.18	64.36	64.60	63.66
Al ₂ O ₃	18.86	18.61	18.40	18.55	18.19	18.44	19.54
FeO	0.03	0.05	0.03	--	0.14	0.01	0.1
CaO	nd	0.03	0.04	0.01	0.02	0.01	0.5
Na ₂ O	0.66	1.26	0.77	0.58	0.39	0.07	0.8
K ₂ O	14.53	14.39	16.05	15.34	16.31	15.69	15.6
Total	99.53	99.74	99.88	99.66	99.41	99.52	100.2
ions on basis of 32 oxygens							
Si	12.020	12.014	11.964	12.027	11.986	11.979	11.759
Al	4.085	4.031	4.017	4.024	3.995	4.031	4.254
Fe ²⁺	0.005	0.007	0.005	--	0.022	0.001	0.014
Ca	--	0.006	0.007	0.001	0.004	0.002	0.099
Na	0.235	0.447	0.275	0.208	0.142	0.277	0.286
K	3.406	3.373	3.792	3.611	3.877	3.710	3.676
Total	19.751	19.878	20.060	19.871	20.026	20.000	20.008
Or	93.5	88.2	93.1	94.6	96.4	93.0	90.5
Ab	6.5	11.7	6.8	5.4	3.5	6.9	7.1
An	--	0.1	0.1	<.1	0.1	<.1	2.4

B179a = albite: biotite-muscovite syenite
 B175a = albite: feldspathic ijolite
 B80a = albite: hornblende-nepheline syenite
 B23a = albite: biotite-nepheline syenite
 B183a = albite: albite syenite
 B72a = albite: microsyenite
 B46a = albite: carbonatite
 B217a = albite: biotite-rich dyke

B175m = microcline: feldspathic ijolite
 B80m = microcline: hornblende nepheline syenite
 B23m = microcline: biotite-nepheline syenite
 B183m = microcline: albite syenite
 B72m = microcline: microsyenite
 B46m = microcline: carbonatite
 A = albite (Deer et al. 1966)
 B = orthoclase (Deer et al. 1966)

TABLE 3.3

MICROPROBE ANALYSES: BULLS RUN COMPLEX

	NEPHELINE				CANCRINITE			
	B175n	B80n	B23n	A	B175c	B80c	B23c	B
SiO ₂	42.11	42.84	42.10	43.97	36.36	36.52	38.33	35.22
Al ₂ O ₃	34.24	34.15	34.05	32.89	28.37	28.31	28.76	29.79
FeO	0.09	0.01	0.01	nd	0.15	--	0.03	--
CaO	0.13	0.28	0.09	0.43	6.69	7.91	6.77	8.17
Na ₂ O	16.25	15.94	15.99	15.73	17.83	15.97	16.65	18.16
K ₂ O	7.27	7.08	7.53	5.45	0.05	0.05	--	0.17
Total	100.09	100.30	99.77	98.47	89.45	88.76	90.54	91.51
ions on the basis of 32 oxygens								
Si	8.148	8.241	8.174	8.513	5.916	5.958	6.095	6.007
Al	7.809	7.744	7.792	7.764	5.442	5.446	5.391	5.990
Fe ²⁺	0.014	0.002	0.002	nd	0.020	--	0.004	--
Ca	0.028	0.057	0.019	0.090	1.166	1.383	1.153	1.493
Na	6.098	5.945	6.020	5.903	5.625	5.052	5.133	6.004
K	1.796	1.738	1.865	1.348	0.010	0.010	--	0.036
Total	23.893	23.727	23.872	23.618	18.179	17.849	17.776	19.530
Ne	73.98	73.54	72.81	75.1	nd	nd	nd	nd
Ks	24.58	23.93	25.51	19.1	nd	nd	nd	nd
Q	1.44	2.53	1.68	5.8	nd	nd	nd	nd

nd = not determined

-- = not detected

B175n = nepheline: feldspathic ijolite

B80n = nepheline: hornblende-nepheline syenite

B23n = nepheline: biotite-nepheline syenite

A = nepheline: nepheline syenite, Scotland

(Deer et al. 1966)

B175c = cancrinite: feldspathic ijolite

B80c = cancrinite: hornblende-nepheline syenite

B23c = cancrinite: biotite-nepheline syenite

B = cancrinite: nepheline syenite, Korea

(Deer et al. 1966)

TABLE 3.4

MICROPROBE ANALYSES: BULLS RUN COMPLEX

BIOTITE					PYROXENE				
	B179b	B183b	B46b	A	B175p	B72p	B94p	C	D
SiO ₂	34.35	33.80	33.03	35.84	53.35	53.28	52.90	50.44	49.73
TiO ₂	3.29	3.92	3.87	2.70	0.17	0.11	0.09	0.38	0.82
Al ₂ O ₃	18.93	19.48	17.24	14.21	6.81	0.87	0.66	2.20	4.25
FeO	28.18	28.06	28.98	29.98	16.68	16.66	18.07	20.77	20.51
MnO	0.49	0.45	0.17	0.29	0.48	0.25	0.19	0.61	0.38
MgO	3.90	2.20	4.18	2.91	4.47	7.39	6.59	5.31	3.82
CaO	--	--	0.08	0.99	11.92	15.16	13.86	13.40	13.32
Na ₂ O	0.09	0.06	0.04	0.19	5.76	2.29	5.41	5.34	5.45
K ₂ O	9.39	9.28	8.65	6.86	--	--	--	0.71	0.49
Total	98.62	97.25	96.24	93.97	99.64	96.01	97.77	99.16	98.77
ions on basis of 24 oxygens					ions on basis of 6 oxygens				
Si	5.765	5.751	5.719	5.73	2.021	2.105	2.084	1.944	1.915
Ti	0.415	0.502	0.504	0.32	0.005	0.003	0.003	0.011	0.024
Al	3.745	3.908	3.518	2.65	0.304	0.041	0.031	1.000	0.193
Fe ²⁺	3.956	3.993	4.196	3.97	0.529	0.551	0.595	0.648	0.664
Mn	0.069	0.065	0.025	0.04	0.015	0.008	0.006	0.020	0.012
Mg	0.976	0.558	1.079	0.69	0.252	0.435	0.387	0.305	0.219
Ca	--	--	0.015	0.17	0.484	0.642	0.585	0.553	0.549
Na	0.029	0.019	0.013	0.06	0.423	0.175	0.413	0.399	0.406
K	2.011	2.015	1.911	1.39	--	--	--	0.018	0.020
Total	16.966	16.811	16.980	15.02	4.033	3.960	4.104	4.898	4.002
HORNBLende					GARNET				
	B80h	B	B175G	E					
SiO ₂	39.15	40.88	35.04	35.22	--	=	not detected		
TiO ₂	0.69	0.22	1.55	3.44	nd	=	not determined		
Al ₂ O ₃	12.94	11.04	4.10	3.96	B179b	=	biotite: biotite-muscovite syenite		
FeO	22.76	24.21	21.54	21.13	B183b	=	biotite: albite syenite		
MnO	1.38	1.32	0.88	0.24	B46b	=	biotite: carbonatite		
MgO	6.60	5.92	0.07	0.45	B80h	=	amphibole: nepheline syenite		
CaO	7.34	10.46	34.08	33.21	B175p	=	pyroxene: feldspathic ijolite		
Na ₂ O	4.34	3.75	--	--	B72p	=	pyroxene: microsyenite dyke		
K ₂ O	2.20	0.78	--	--	B94p	=	pyroxene: microsyenite dyke		
Total	97.40	98.58	97.26	97.65	B175g	=	garnet, feldspathic ijolite		
ions on basis of 24 oxygens									
Si	6.447	6.377	6.227	nd	A	=	biotite (annite)		
Ti	0.086	0.025	0.207	nd	B	=	barkevikite (Deer <u>et al</u> 1966)		
Al	2.512	2.030	0.859	nd	C	=	aegirine-augite (Deer <u>et al</u> . 1966)		
Fe ²⁺	3.135	3.157	3.202	nd	D	=	aegirine-augite (Deer <u>et al</u> . 1966)		
Mn	0.193	0.174	0.133	nd	E	=	melanite garnet (Deer <u>et al</u> . 1982)		
Mg	1.619	1.376	0.019	nd					
Ca	1.295	1.748	6.489	nd					
Na	1.386	1.134	--	nd					
K	0.462	0.156	--	nd					
Total	17.135	16.177	17.136	nd					

3.3.3 Biotite-nepheline syenite

Biotite-nepheline syenite rims the undersaturated core of the BRC, and is well exposed on the farms Bulls Run, Black Eyes and the western part of Goedertrow (Fig. 3.1). Several small masses and elongate sheet-like bodies of hornblende-nepheline syenite, in association with an ijolitic plug at the eastern extremity of the BRC, are described separately (Section 3.3.5).

The biotite-nepheline syenite is medium to coarse grained, grey to pinkish-grey and, typically, has a "knobbly" outcrop surface due to preferential weathering of blue-grey nepheline mesocrysts. Irregular pegmatitic patches are developed occasionally and contain tabular nepheline megacrysts up to 5cm in length. The gneissose fabric varies, as described previously, from intense near the margins of the BRC to relatively weak towards the core of the massif.

As shown by the representative mode (Table 3.1, Sample B222, also Appendix 1, Table A1.2), this rock type consists predominantly of microcline (30 to 50 modal%, Or_{93}), pure albite (5 to 30 modal%, Ab_{99}), potassic nepheline (5 to 30 modal%, Ne_{73}) and cancrinite (<10 modal%), with biotite (5 to 15 modal%) the characteristic mafic phase. Accessory minerals include calcite, apatite and ilmenite.

Cancrinite, identified both by thin-section and microprobe techniques (analysis B23c, Table 3.3), usually occurs as aggregated polygonal grains and reaction rims between calcite and nepheline (Fig. 3.10b). According to Deer et al. (1966), cancrinite is typically formed by reaction between early-formed nepheline and CO_2 -rich residual fluids. The data presented in Table 3.3 shows the Bulls Run cancrinite has typical high volatile, Na_2O and Al_2O_3 contents.

3.3.4 Albite syenite

The core of the BRC comprises fine- to medium-grained, leucocratic, generally light-grey syenite with a siliceous "glassy" appearance in outcrop. Gradations in colour are apparent, from off-white, through to grey but it has not been feasible to map separate units on colour alone, particularly as the different colours form schlieren and grade

imperceptibly into one another. Contacts between albite syenite and the enclosing biotite-nepheline syenite envelope have not been observed but, from field relationships, the transition appears to be fairly rapid.

Due to the leucocratic nature of the albite syenite, with few mafic minerals, the pervasive east-west gneissosity is generally poorly defined in outcrop.

Modal analysis of thin sections reveals that the albite syenite mineral assemblage is dominated by albite (45 to 65 modal%, Ab_{99}), with subordinate microcline (25 to 45 modal%, Or_{95}), nepheline (<25 modal%), cancrinite (<20 modal%) and biotite (2 to 7 modal%). As indicated in Table 3.1 some of the albite syenites contain equal amounts of albite and microcline (sample B183). However, since they are physically indistinguishable in the field, they are grouped with the albite-rich types. Accessory minerals, generally more abundant in microcline-rich varieties of the albite syenite, are zircon and pyrochlore (Fig. 3.11).

Microprobe data for albite and microcline from sample B183 are presented in Table 3.2 and indicate essentially pure end-member compositions. A single biotite analysis (B183b, Table 3.4) is titaniferous and, with respect to FeO, approaches annite in composition.

Albite is the dominant mineral in most thin sections and occurs as relatively large single crystals and polygonal aggregates, enclosing interstitial microcline, nepheline and cancrinite. This textural relationship indicates that albite crystallised first, followed by the more potassic constituents.

Almost invariably, nepheline is altered to an aggregate of kaolin, sericite, muscovite and biotite hosting pyrochlore and zircon (Fig. 3.11). Cancrinite occurs both as reaction rims between nepheline and calcite as well as forming networks and veinlets through brecciated feldspar (Fig. 3.11). These textural relationships suggest that the albite syenite was invaded by volatile-rich fluids that reacted with nepheline, forming deuteric cancrinite and precipitating pyrochlore and

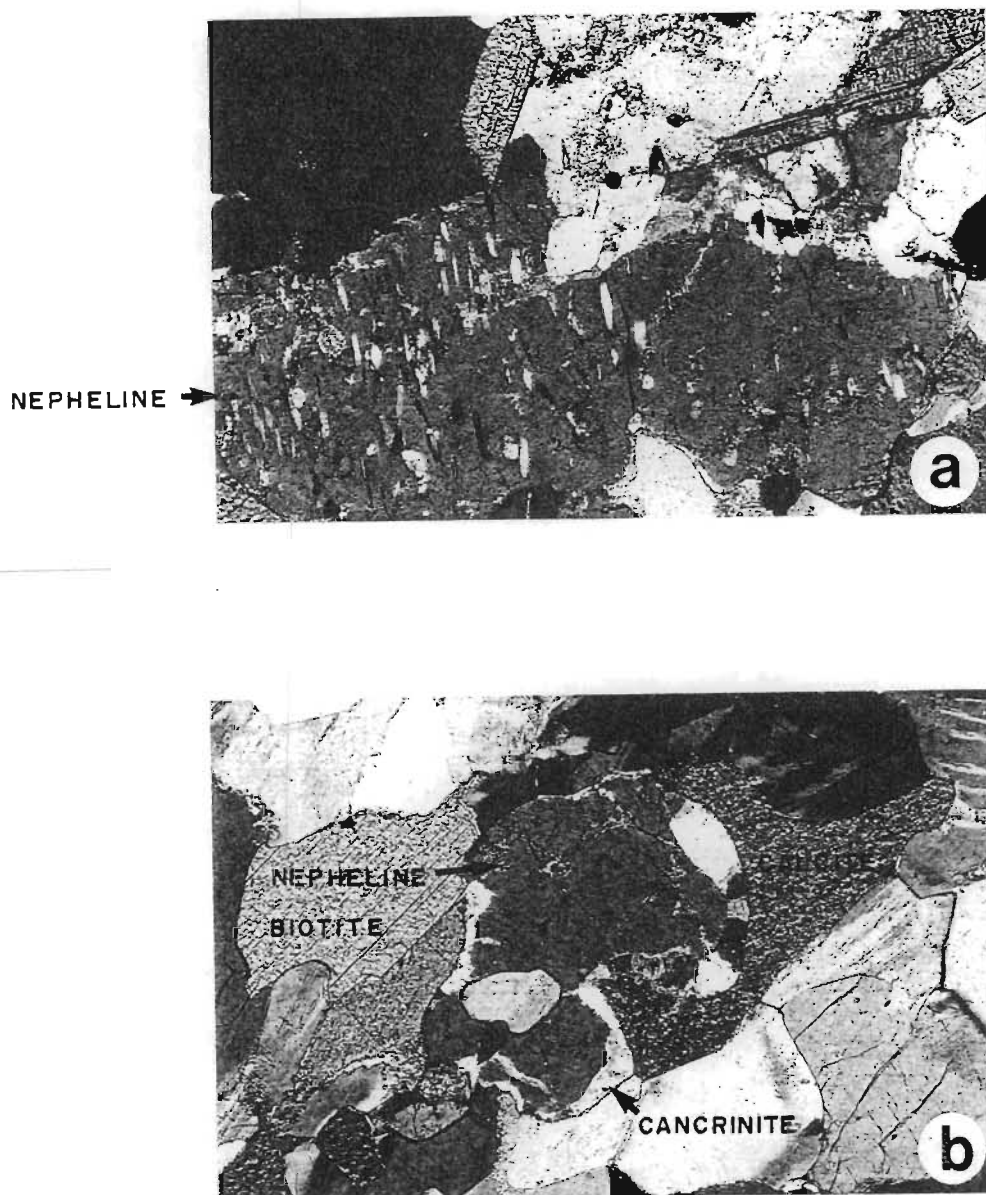


Figure 3.10. Photomicrographs of biotite-nepheline syenite, sample B23. Field of view 3 mm. Fig. 3.10b illustrates the formation of cancrinite due to the reaction between CO_2 -rich residual fluids and nepheline.

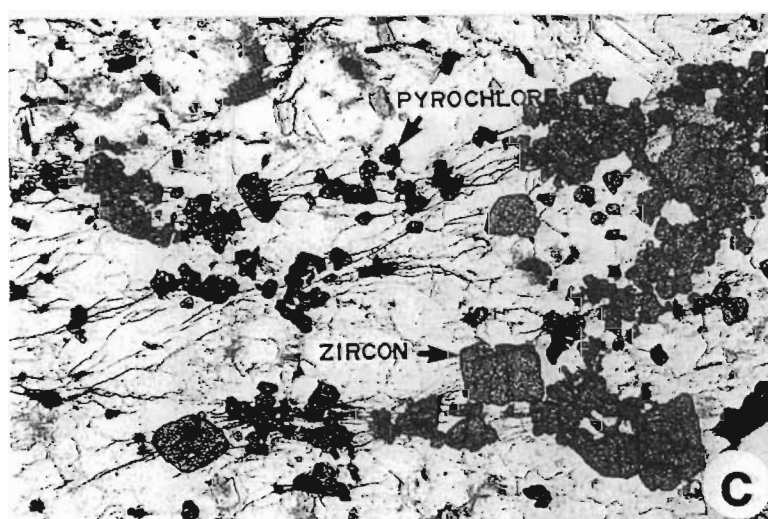
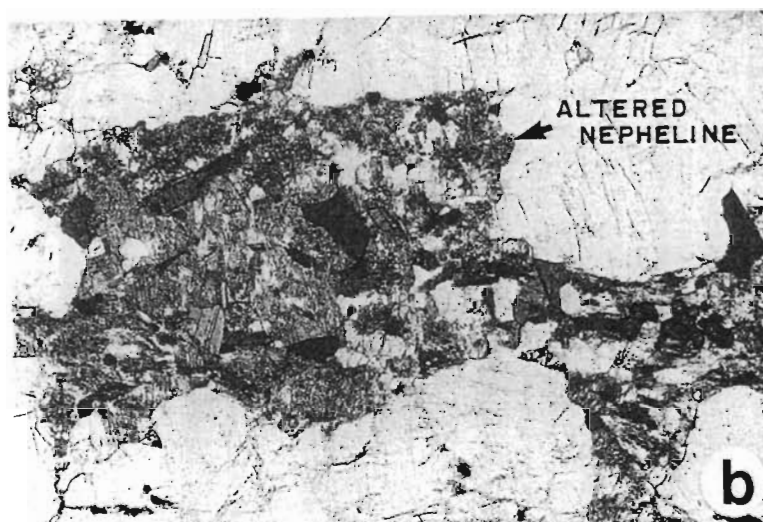
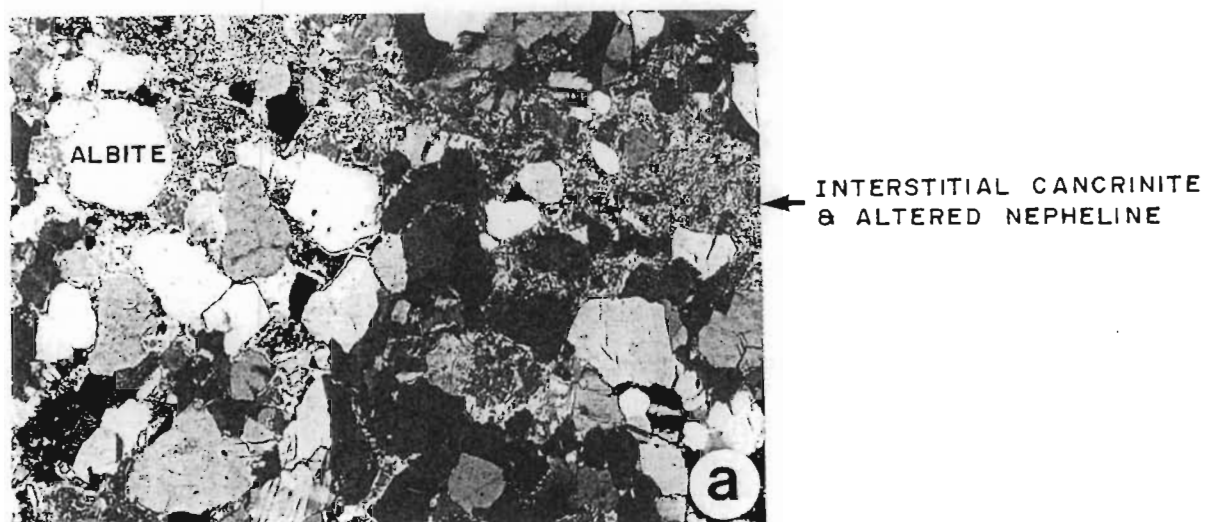


Figure 3.11. Photomicrographs of albite syenite. Field of view 3 mm. Fig. 3.11a: remnant albite crystals surrounded by cancrinite and altered nepheline (sample B20), Fig. 3.11b: altered nepheline (sample B183), Fig. 3.11c: pyrochlore and zircon surrounded by radioactively-induced cracks, in albite syenite B183.

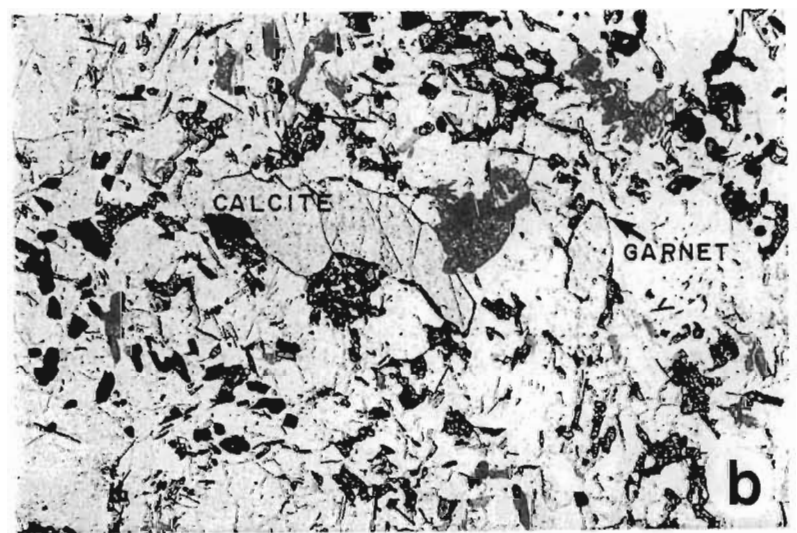
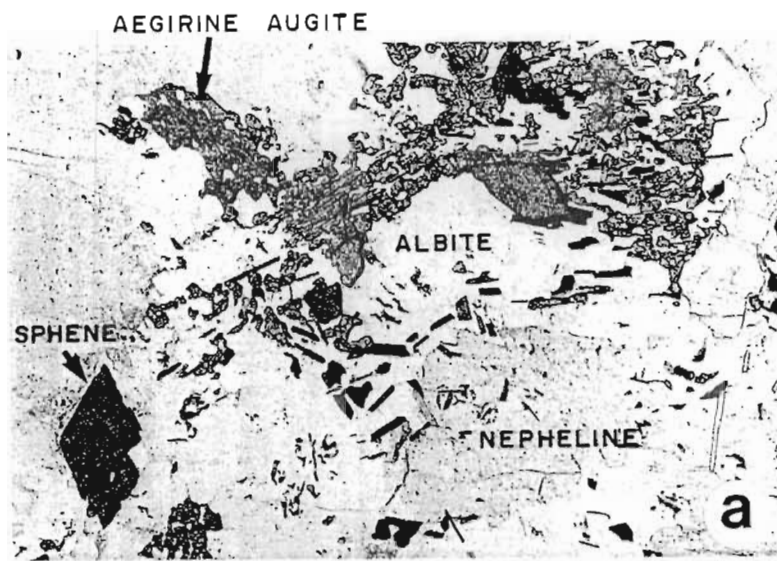


Figure 3.12. Photomicrographs to illustrate textural features in feldspathic ijolite B175. Field of view 3 mm. Fig. 3.12a: interstitial aegirine-augite, sphene and Ti-garnet, Fig. 3.12b: garnet reaction rim around calcite, Fig. 3.12c: euhedral nepheline surrounded by microcline.

zircon. This paragenetic sequence indicates the increasing importance of volatiles with progressive crystallization of the albite syenite.

3.3.5 Feldspathic ijolite

Feldspathic ijolite was discovered in the eastern extremity of the BRC, near the boundary between the farms Goedertrow and Umhlatuzi (Figs 3.1 & 3.3). This unusual lithology forms the centre of a small nepheline-syenite plug, some 100 m in diameter, and is associated with several elongate outcrops of hornblende-nepheline syenite, biotite-nepheline syenite and carbonatite. As described above, this assemblage is interpreted on structural grounds as a boudinaged and "unravellled" central-plug/ring-dyke association (Section 3.2.4, Fig. 3.7).

In outcrop the feldspathic ijolite is coarse-grained, noticeably mafic, distinctly green to green-black, and characterised by abundant negatively-weathered nepheline. The overall impression from outcrop evidence is that the pervasive east-west gneissosity is either absent or poorly developed and that the predominant structure is due to alignment of nepheline crystals in a concentric flow fabric that apparently parallels the plug margins. In hand specimen, tabular nepheline crystals 0.5 to 1.0 cm in length constitute a framework that hosts a network of interstitial green and black mafic minerals, with associated yellowish sphene (Fig. 3.12).

The Bulls Run ijolite classifies as feldspathic ijolite (Fig. 3.10), dominated by feldspathoids (nepheline and cancrinite 40 to 60 modal%), deep-green aegirine-augite (c. 20 modal%) and yellow-brown garnet (5 to 10 modal%). Accessory phases are microcline, albite, sphene, biotite, calcite, apatite and opaques (Table 3.1). Microprobe analyses of selected minerals are given in Tables 3.2, 3.3 and 3.4 and demonstrate that the albite (Ab_{99}) and microcline (Or_{94}) are essentially pure end-members, with nepheline relatively potassic (74%Ne, 25%Ks). Comparison of pyroxene analysis B175p with published data suggests an aegirine-augite composition (Table 3.4). The garnet is melanitic and characterised by TiO_2 contents up to 1.55%. This titaniferous composition is typical for ijolitic garnets (Bailey 1974).

Microscopic examination reveals that nepheline is surrounded by an intercumulus matrix of albite, cancrinite, unzoned green to brown pleochroic aegirine-augite, garnet, sphene, calcite and apatite (Fig. 3.12). The nephelines tend to be turbid and kaolinised along cleavage planes and, in addition, contain orientated needles of exsolved aegirine-augite and feldspar. Textural relationships indicate that euhedral nepheline crystallized early (Fig. 3.12c) and was then rimmed and sometimes corroded by later microcline. The voids between the nepheline and microcline crystals then trapped residual alkali-rich liquids that subsequently precipitated spongy, poikilitic intergrowths of sieve-textured aegirine-augite, surrounded and embayed by granular sphene and garnet. The textural evidence suggests that these latter minerals, ie. sphene and garnet, grew at the expense of pyroxene.

Garnet also forms rims between calcite and plagioclase, indicating reaction related to late-stage CO₂-rich fluid activity. A similar texture has been documented for the hornblende-monzodiorite plug in the Ngoye Complex, where Ti-bearing andraditic garnet has formed due to calcite plagioclase reaction (Scogings 1985).

3.3.6 Carbonatite

Carbonatites have been located at three sites in the BRC where they occur exclusively in areas underlain by biotite-muscovite syenite (Scogings & Forster 1989). The most extensive exposures are in the vicinity of the feldspathic ijolite plug in the eastern part of the complex (Locality A of Scogings & Forster 1989). Here, an elongate, north-east-striking, steep-dipping body of off-white to brown carbonatite (Figs 3.8f & 3.13b) some 100 m in length and up to 10 m wide, is clearly intrusive into the biotite-muscovite syenite (Fig. 3.13a). Bands and streaks of biotite define a probable relict flow fabric, with large books of biotite up to 5 cm in length characteristic of the brown carbonatite (samples B46 & B60).

The carbonatite in the central part of the BRC (Fig. 3.2 for locality, samples B87 & B92) occurs as an east-striking, essentially vertical sheet, some 200 m long and up to 1 m wide. Again, clear intrusive relationships are apparent, with sharp contacts and numerous well-rounded xenoliths of muscovite syenite.

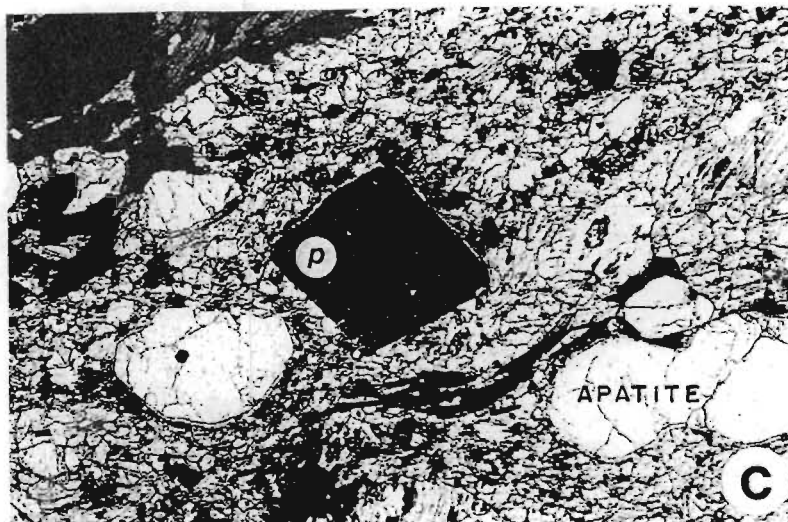
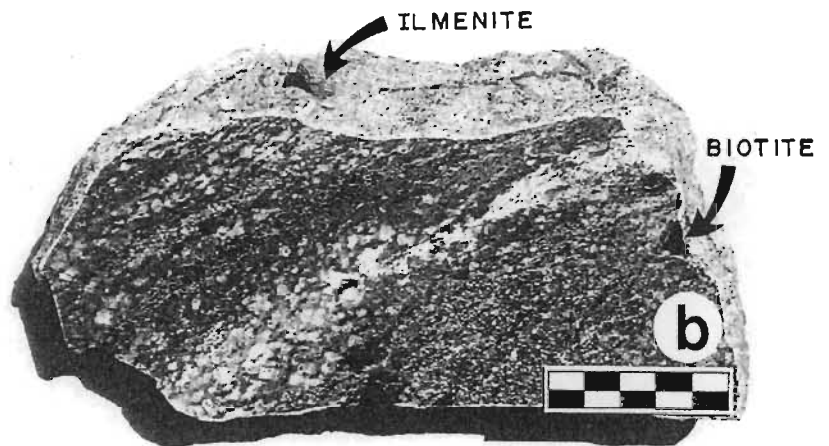
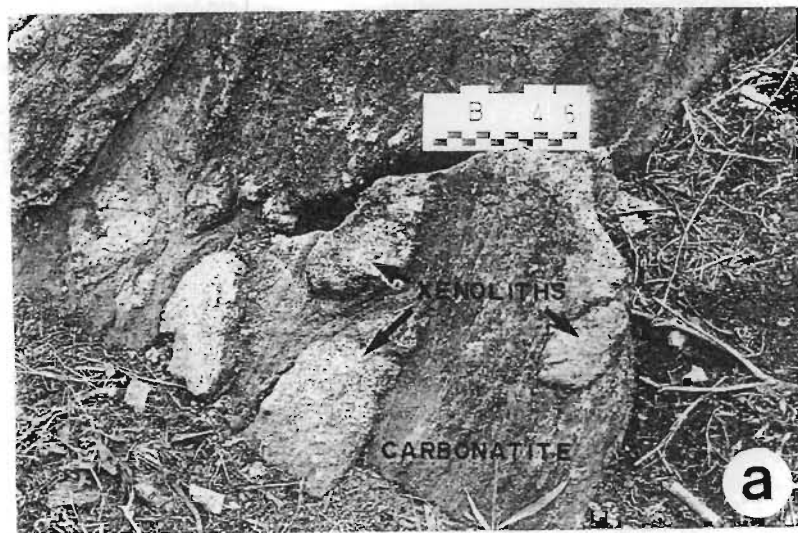


Figure 3.13. Bulls Run sövite carbonatites. Fig. 3.13a: outcrop of carbonatite with xenoliths of biotite-muscovite syenite, scale in cm, Fig. 3.13b: polished slab of brown carbonatite from sample site B60, scale in cm, Fig. 3.13c: photomicrograph of carbonatite B46, illustrating typical mineral assemblage (p = pyrochlore). Field of view 3 mm.

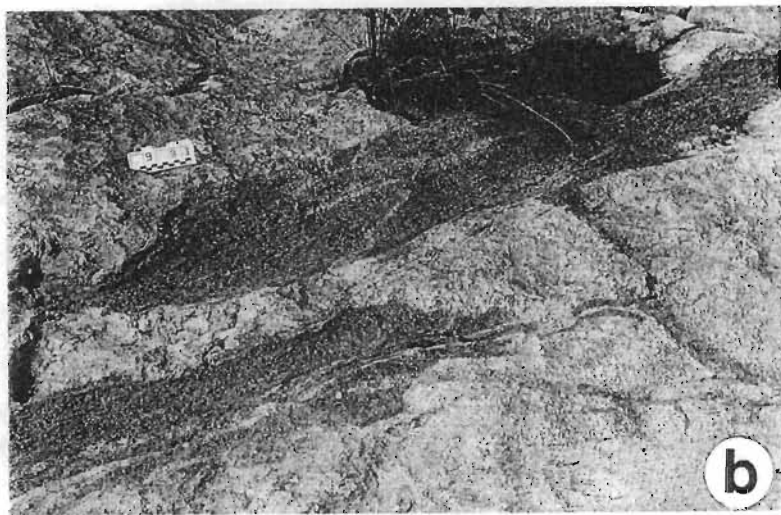


Figure 3.14. Field exposures of biotite-rich dyke with monomineralic inclusions (Fig. 3.14a). Field exposure in the central portions of the BRC, illustrating biotite-rich xenoliths enclosed in biotite-nepheline syenite (Fig. 3.14b).

The third locality (Locality C, sample B229 of Scogings & Forster 1989) is the smallest occurrence yet recorded in the BRC, with outcrops forming irregular pods and veins within biotite-muscovite syenite. Although composed predominantly of white medium-grained calcite, this occurrence is rich in biotite and a greenish hue is imparted to some specimens by high concentrations of apatite. This locality is of particular interest owing to the presence of red-brown, euhedral zircons up to about 0.5cm long within the carbonatite.

Petrographically the carbonatites are calcite carbonatite, or sövite (Streckeisen 1978, Woolley & Kempe 1989) and consist predominantly of calcite (50 to 95 modal%), biotite (2 to 20 modal%, Table 3.4 for microprobe data), and apatite (<10 modal%). Accessory constituents include microcline (Or_{93}), albite (Ab_{97}), pyrochlore and ilmenite, with traces of pyrite, zircon, and muscovite (Table 3.1). Biotite is the characteristic mafic mineral and commonly occurs as fish-shaped, sigmoidally-curved and often kinked books. The feldspars occur as rounded grains and aggregates which are most common in the xenolith-rich specimens from localities B and C. Rounded to subhedral apatite is a notable constituent of all specimens analysed. Pyrochlore is restricted to the brown carbonatite near the ijolitic plug and is distinguished in thin section by typical octahedral form, subtranslucent brown colour and isotropic behaviour under crossed polars (Fig. 3.13c).

3.3.7 Biotite-rich dykes

These mafic rocks are intrusive into biotite-muscovite syenite, particularly on the farm Goedertrow (Fig. 3.1). The dykes crop out as steep southerly-dipping sheets up to 2 m in width and are exposed over strike lengths of 5 to 10 m. The best exposures are on the western banks of the Goedertrou Dam (locality B217, Fig 3.14a), but are accessible only when the water level recedes. Elsewhere, due to the friable character of this biotite-rich lithology, outcrops are poor and highly weathered.

The dykes are dark grey to almost black in outcrop and, when freshly broken, glisten due to abundant small flakes of biotite. As illustrated

(Fig. 3.14a), the dykes are crowded with inclusions and wispy stringers of off-white feldspar aggregates.

In addition to the above intrusive dykes, macroscopically similar xenoliths of similar macroscopic appearances occur within nepheline syenite on the farm Bulls Run (Fig. 3.14b). However, these xenoliths lack the monomineralic inclusions that characterise the dykes.

In thin section the typical modal assemblage comprises equigranular, fine-grained (0.5 to 1.0 mm), red-brown to greenish-brown biotite (20 to 50 modal%), albite (40 to 50 modal%, Ab₉₉) and calcite (6 to 12 modal%). Microcline is a minor constituent of the dykes (<3 modal%), but is more abundant (c. 16 modal%) in the xenoliths. Apatite is a constant accessory (<3 modal%) and occurs as stumpy, rounded grains.

Examination of a felsic inclusion from the dyke at locality B217 reveals it to be essentially monomineralic, with 95 modal% polygonal albite and accessory calcite and biotite. Two generations of calcite are evident, with an early clear phase mantled by cloudy, iron-stained, overgrowths that also form interstitial networks between the silicate minerals.

3.3.8 Microsyenite dykes

Microsyenite dykes up to 2 m in width and several hundred metres in length intrude the biotite-muscovite syenite (Fig. 3.1 for locality). These steep-dipping dykes trend east-west, display sharp contacts with the surrounding rocks (Fig. 3.5c) and are characteristically flow-banded (Fig. 3.8e). Due to their fine grain size, these dykes do not exhibit the pervasive gneissosity of the surrounding muscovite syenite in the field (Fig. 3.5c), even when boudinaged (Fig. 3.6b).

Modal analyses (Table 3.1, B72) are dominated by albite (50 to 70 modal%, Ab₉₈) with lesser amounts of microcline (c. 20 modal%, Or₉₆), quartz (c. 5 modal%) and aegirine-augite (5 to 10 modal%, Table 3.4 for microprobe data). Accessory phases include interstitial calcite and rounded apatite grains. Texturally, the dykes are fine-grained (0.1 to 0.2 mm), essentially equigranular rocks, with occasional aggregates

of polygonal microcline up to about 2 mm in length. These aggregates may represent relict phenocrysts that recrystallised during metamorphism. The flow fabric is defined by aligned, elongate, polygonal aggregates and prisms of green to brown pleochroic aegirine-augite.

Although structural fabrics are not obvious in hand specimen, thin-section examination of a boudinaged dyke (sample site B237) reveals intense foliation, grain-size reduction, and metamorphic growth of blue riebeckite needles.

3.4 Geochemistry

3.4.1 Introduction

A total of 69 whole-rock samples were analysed for major- and trace-elements; 22 of these samples were also analysed for REE. A complete set of BRC data constitutes Tables A2.2 and 3.2 in the appendix. Representative geochemical and normative data for the Bulls Run Complex are presented as Tables 3.5 and 3.7, with comparative analyses from the literature as Table 3.8.

Comparison of the BRC nepheline syenites with average nepheline syenite and phonolite compositions (A and B, Table 3.8) confirms the relatively potassic character of the former. In this respect they are directly comparable with Blue Mountain nepheline syenite (J, Table 3.8) and, like the latter, are aluminous. Albite syenite (B183 and B220a, Table 3.5) from the BRC is generally sodic and, although relatively aluminous, is comparable with Le Maitre's (1976) average nepheline syenite and phonolite. Apart from somewhat higher SiO_2 and Na_2O contents, the microsyenite dykes within the BRC exhibit similar major-element compositions to Le Maitre's average syenite and trachyte compositions (C and D, Table 3.8).

Comparison with published analyses from the literature reveals similarities between the biotite-muscovite syenite from Bulls Run (B179 and B105, Table 3.5) and corundum syenite from Blue Mountain (I, Table 3.8), especially with respect to high Al_2O_3 contents and $\text{K}_2\text{O}/\text{Na}_2\text{O}$ ratios. Muscovite-rich material from the biotite-muscovite lithology (B81a, Table 3.5) has been analysed and comprises essentially

TABLE 3.5

REPRESENTATIVE MAJOR AND TRACE ELEMENT GEOCHEMISTRY: BULLS RUN COMPLEX

	B179	B105	B81a	B175	B80	B222	B183	B220a	B217	B62	B46	B72
SiO ₂	51.91	57.35	45.87	48.08	51.50	52.76	58.97	59.78	44.65	0.86	2.57	67.15
TiO ₂	0.65	0.80	0.59	1.36	0.82	0.65	0.22	0.07	2.24	0.01	0.23	0.31
Al ₂ O ₃	23.14	20.79	35.35	20.39	21.86	22.28	22.38	22.23	15.25	0.33	1.08	14.52
Fe ₂ O ₃	2.10	1.08	2.41	4.18	2.99	1.77	0.49	0.21	1.10	0.43	0.63	2.50
FeO	3.23	2.98	0.25	2.50	1.98	3.61	1.31	1.83	11.73	2.17	3.16	0.91
MnO	0.19	0.13	0.01	0.23	0.16	0.10	0.04	0.03	0.37	1.21	0.90	0.04
MgO	0.35	0.45	0.22	1.35	0.65	0.14	--	--	3.48	0.13	0.26	1.15
CaO	3.79	2.18	--	6.79	3.69	1.50	0.89	0.19	7.10	54.32	48.53	2.62
Na ₂ O	3.78	4.41	0.99	7.89	7.90	6.44	7.14	8.79	2.97	0.08	0.11	6.84
K ₂ O	6.05	7.03	10.58	5.58	6.50	8.01	7.18	5.80	4.52	0.12	0.49	3.98
P ₂ O ₅	0.31	0.10	0.07	0.61	0.30	0.17	0.07	0.01	1.27	0.03	2.75	0.19
LOI	2.08	0.77	4.36	0.64	0.62	0.45	0.55	0.25	0.22	0.00	0.36	0.03
CO ₂	2.39	1.61	0.04	0.55	0.90	1.17	0.88	0.37	4.51	41.62	37.79	0.22
Total	99.97	99.68	100.74	100.15	99.87	99.05	100.12	99.56	99.41	101.31	98.86	100.46
Zn	70	71	2	67	52	49	30	37	229	15	28	67
Ga	19	17	28	17	14	16	--	29	31	nd	nd	27
Nb	109	201	133	210	167	94	2280	494	256	68	2633	19
Zr	224	439	13	154	200	115	2129	1145	288	--	--	195
Y	15	7	4	21	14	4	6	2	26	82	100	12
U	nd	nd	--	3	nd	nd	239	32	nd	nd	nd	nd
Th	nd	nd	--	nd	6	nd	7	nd	nd	nd	17	22
Pb	112	nd	--	1	nd	nd	63	nd	nd	14	9	23
Rb	203	290	208	158	197	200	185	338	459	11	42	86
Sr	1311	743	211	1506	2055	1298	905	145	1060	9135	8077	563
Ba	1964	1325	1866	1793	2037	1335	872	91	610	81	132	1993
La	69.24	38.64	nd	120.38	83.23	15.32	15.55	5.22	103.08	265.60	361.37	78.79
Ce	136.37	72.02	nd	237.24	159.55	30.38	31.35	9.13	207.47	515.28	718.45	157.35
Pr	17.16	8.76	nd	27.29	21.20	--	--	--	24.10	55.44	76.29	16.25
Nd	54.90	24.90	nd	95.80	62.70	13.70	11.80	3.60	84.80	187.40	269.30	68.70
Sm	7.83	2.76	nd	13.58	8.34	1.62	1.29	0.27	13.34	28.99	41.63	11.42
Eu	2.34	0.75	nd	4.23	2.76	0.67	0.48	0.11	4.06	9.45	12.82	2.63
Gd	6.22	2.52	nd	10.14	6.60	1.70	1.40	0.47	10.59	23.33	32.19	7.33
Dy	3.89	1.51	nd	5.72	3.89	0.98	1.09	0.38	6.60	17.82	22.47	3.10
Ho	0.80	0.36	nd	1.07	0.77	0.20	0.29	0.11	1.28	3.63	4.50	0.55
Er	2.19	1.14	nd	2.77	2.02	0.67	0.99	0.51	3.46	10.48	12.67	1.51
Yb	1.91	1.08	nd	1.84	1.42	0.38	1.03	0.62	2.46	9.17	10.53	0.83
Lu	0.38	0.21	nd	0.31	0.26	0.07	0.20	0.14	0.38	1.43	1.62	0.13
P.I.	0.55	0.72	0.37	0.93	0.92	0.87	0.87	0.93	0.64	0.81	0.66	1.07
Na ₂ O+K ₂ O	9.83	11.44	11.57	13.47	14.41	14.45	14.32	14.59	7.49	0.20	0.60	10.82
Na ₂ O/K ₂ O	0.62	0.63	0.09	1.41	1.22	0.80	0.99	1.52	0.66	0.67	0.22	1.72
Rb/Sr	0.15	0.39	0.99	0.10	0.11	0.15	0.20	2.33	0.43	0.00	0.01	0.15

nd = not determined

-- = not detected

B179, B106 = biotite-muscovite syenite

B81a = muscovite-rich rock

B175 = feldspathic ijolite

B80 = hornblende-nepheline syenite

B222 = biotite-nepheline syenite

B183, N220a = albite syenite

B217 = biotite-rich dyke

B62, B46 = carbonatite

B72 = microsyenite dyke

SiO_2 , Al_2O_3 and K_2O . The only comparable potassic rock associated with carbonatite/syenite complexes is orthoclasite, developed as a result of K-metasomatism induced by sövite intrusion (K and L, Table 3.8). The carbonatites have been described previously (Scogings & Forster 1989) and have characteristic sövite chemistry (cf. Woolley & Kempe 1989) with high CaO, Nb and Sr contents (B62, B46 in Table 3.5).

The biotite-rich dykes that intrude the eastern parts of the BRC are potassic and essentially alkaline (Table 3.5, analysis B217). Similarities are exhibited with average basanite, nepheline basalt, nephelinite and tephrite (E, F, G and H, Table 3.8).

3.4.2 Effects of deformation on geochemistry

During the geochemical sampling programme every effort was made to collect the least-deformed specimens, ie. those with minimal gneissosity. However this approach was hampered by the availability of suitable outcrop and, therefore, the effect of deformation on major- and trace-element chemistry was assessed qualitatively (Table 3.6, Fig. 3.15). With respect to the major elements it is apparent that, apart from limited Al_2O_3 depletion in mylonite sample B237a, and K_2O depletion in mylonitised microsyenite B237, the remainder of the major elements plot within the fields defined by relatively poorly-foliated syenites. Likewise, trace elements do not show any appreciable change as a result of intense deformation (Table 3.6) and it therefore appears reasonable to assume that closed geochemical systems operated during deformation.

3.4.3 Alumina saturation

As discussed previously (Section 3.3.1), syenitic rocks are classified on mineralogical grounds as either agpaitic or miaskitic. A geochemical distinction, based essentially on relative proportions of alkalis to alumina, recognizes peralkaline agpaites and peraluminous miaskites (Sorensen 1974, Currie 1976a, Lurie 1985). Classification of the Bulls Run lithologies according to these parameters indicates that the biotite-muscovite syenites are peraluminous, the biotite-nepheline syenites peraluminous to metaluminous, and the microsyenite dykes metaluminous to peralkaline (Fig. 3.16a). A metaluminous character is

TABLE 3.6

EFFECTS OF DEFORMATION ON GEOCHEMISTRY

	B105	B237a	B43	B110	B98	B237
SiO ₂	57.35	57.74	49.49	51.36	68.94	69.58
TiO ₂	0.80	0.64	1.03	0.75	0.19	0.20
Al ₂ O ₃	20.79	18.45	22.18	22.50	16.68	16.27
Fe ₂ O ₃	1.08	0.48	1.32	1.52	0.91	0.41
FeO	2.98	3.83	3.51	2.92	0.41	1.08
MnO	0.13	0.14	0.18	0.17	0.01	0.02
MgO	0.45	0.75	0.73	0.68	0.27	0.32
CaO	2.18	3.03	3.96	3.77	0.18	0.57
Na ₂ O	4.41	6.02	6.56	7.22	7.11	7.47
K ₂ O	7.03	5.54	7.26	6.22	3.91	3.03
P ₂ O ₅	0.10	0.36	0.34	0.34	0.10	0.07
LOI	0.77	2.60	1.60	2.42	0.30	0.70
CO ₂	1.61	nd	1.68	1.00	0.08	nd
Total	99.68	99.58	99.84	100.87	99.09	99.45
Zn	71	65	65	51	24	39
Ga	17	18	12	15	22	21
Nb	201	151	166	153	23	14
Zr	439	422	172	212	128	124
Y	7	15	18	14	4	8
U	nd	8	nd	nd	nd	6
Th	nd	--	6	8	4	5
Pb	nd	6	10	nd	12	24
Rb	290	160	213	178	70	50
Sr	743	1271	1776	1543	63	311
Ba	1325	1451	2704	1875	1205	886
P.I.	0.72	0.72	0.84	0.83	0.96	1.01
Na ₂ O+K ₂ O	11.44	11.56	13.82	13.44	11.02	10.50
Na ₂ O/K ₂ O	0.63	1.09	0.90	1.16	1.82	2.47
Y/Nb	0.03	0.10	0.11	0.09	0.17	0.57

-- = not detected

nd = not determined

B105 = moderately-foliated biotite-muscovite syenite

B237a = mylonitised biotite-muscovite syenite

B43 = moderately-foliated biotite-nepheline syenite

B110 = well-foliated biotite-nepheline syenite

B98 = poorly-foliated microsyenite

B237 = mylonitised and boundinaged microsyenite

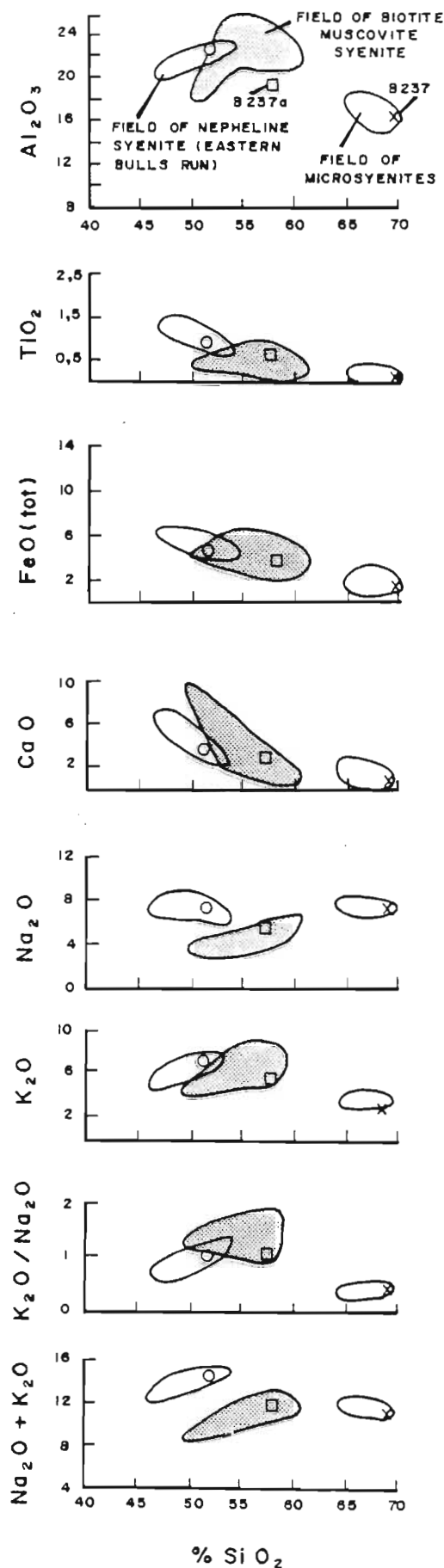


Fig. 3.15. Comparison of highly deformed syenites with fields of moderately deformed syenites, Bulls Run Complex

TABLE 3.7

REPRESENTATIVE NORMS: BULLS RUN COMPLEX

CIPW NORMS									
	B179	B105	B175	B80	B222	B183	B220a	B217	B72
Quartz	3.65	2.31	--	--	--	--	--	--	8.98
Corundum	9.65	5.80	--	--	3.06	2.87	1.50	5.52	--
Orthoclase	36.45	41.93	33.09	38.59	47.96	42.53	34.53	26.94	23.38
Albite	32.61	37.68	5.90	14.62	18.86	37.44	43.43	25.35	52.23
Anorthite	2.53	0.49	3.73	5.01	--	--	--	--	--
Nepheline	--	--	33.06	28.48	19.69	12.52	17.07	--	--
Acmite	--	--	--	--	--	--	--	--	4.69
Wollastonite	--	--	5.95	0.85	--	--	--	--	0.80
Diopside	--	--	7.27	3.72	--	--	--	--	7.10
Hypersthene	4.43	4.66	--	--	--	--	--	13.86	--
Olivine	--	--	--	--	3.60	1.33	2.43	9.48	--
Magnetite	3.10	1.58	4.88	4.36	2.60	0.71	0.31	1.59	1.26
Ilmenite	1.26	1.53	2.59	1.57	1.25	0.42	0.13	4.29	0.58
Haematite	--	--	0.83	--	--	--	--	--	--
Apatite	0.73	0.23	1.42	0.70	0.40	0.16	0.02	2.97	0.44
Calcite	5.54	3.70	1.25	2.06	2.56	1.59	0.35	9.94	0.50
Zircon	0.05	0.09	0.03	0.04	0.02	0.43	0.23	0.06	0.04
Total	100.00	100.00	100.00	100.00	100.00	100.00	100.00	100.00	100.00

MESONORMS									
Quartz	6.29	4.70	--	--	--	--	--	10.14	10.90
Corundum	10.49	5.98	--	--	3.06	2.87	1.50	5.52	--
Orthoclase	32.37	37.46	28.87	36.07	43.82	41.06	32.23	3.74	20.75
Albite	32.61	37.67	10.30	16.86	21.25	38.29	44.99	25.35	52.23
Anorthite	0.22	--	3.73	5.01	--	--	--	--	--
Nepheline	--	--	30.68	27.27	18.40	12.06	16.22	--	--
Biotite	6.97	7.57	6.42	3.98	7.23	2.60	4.08	38.41	3.77
Wollastonite	--	--	7.87	1.63	--	--	--	--	4.10
Riebeckite	--	--	--	--	--	--	--	--	4.72
Magnetite	3.10	1.58	6.08	4.36	2.60	0.71	0.31	1.61	--
Haematite	--	--	--	--	--	--	--	--	1.79
Sphene	1.63	0.35	3.35	2.02	--	--	--	--	0.76
Rutile	--	0.67	--	--	0.66	0.22	0.07	2.26	--
Apatite	0.73	0.23	1.42	0.70	0.26	--	--	2.57	0.44
Zircon	0.05	0.09	0.03	0.04	0.02	0.43	0.23	0.06	0.04
Calcite	5.54	3.70	1.25	2.06	2.70	1.76	0.37	10.34	0.50
Total	100.00	100.00	100.00	100.00	100.00	100.00	100.00	100.00	100.00

-- = not detected

B179, B105 = biotite-muscovite syenite

B175 = feldspathic ijolite

B80 = hornblende-nepheline syente

B222 = biotite-nepheline syenite

B183, B220a = albite syenite

B217 = biotite-rich dyke

B72 = microsyenite

TABLE 3.8

COMPARATIVE WHOLE-ROCK GEOCHEMISTRY FROM LITERATURE SOURCES

	A	B	C	D	E	F	G	H
SiO ₂	54.99	56.19	58.58	61.21	44.30	40.73	40.60	47.86
TiO ₂	0.60	0.62	0.84	8.70	2.51	2.17	2.66	1.76
Al ₂ O ₃	20.96	19.04	16.64	16.96	14.70	12.64	14.33	17.00
Fe ₂ O ₃	2.25	2.79	3.04	2.99	3.94	6.13	5.48	4.12
FeO	2.05	2.03	3.13	2.29	7.50	7.04	6.17	5.22
MnO	0.15	0.17	0.13	0.15	0.16	0.15	0.26	0.15
MgO	0.77	1.07	1.87	0.93	8.54	10.63	6.39	4.70
CaO	2.31	2.72	3.53	2.34	10.19	11.46	11.89	9.18
Na ₂ O	8.23	7.79	5.24	5.47	3.55	3.70	4.79	3.69
K ₂ O	5.58	5.24	4.95	4.98	1.96	2.12	3.46	4.49
P ₂ O ₅	0.13	0.18	0.29	0.21	0.74	0.89	1.07	0.63
LOI	1.47	1.94	1.22	1.62	1.62	2.12	2.19	1.25
CO	0.20	0.08	0.28	0.09	0.18	0.15	0.60	0.02
Total	99.69	99.86	99.74	99.94	99.89	100.93	99.89	100.07

	I	J	K	L	M	N
SiO ₂	59.56	58.84	48.40	65.04	47.16	50.25
TiO ₂	0.13	--	0.52	0.14	0.42	0.62
Al ₂ O ₃	24.69	23.26	14.22	19.21	18.34	19.50
Fe ₂ O ₃	0.44	1.43	7.96	0.25	6.68	2.42
FeO	1.28	0.52	nd	nd	2.84	2.51
MnO	0.04	0.05	0.36	0.05	0.33	0.20
MgO	0.03	0.03	0.29	0.01	1.93	0.41
CaO	0.43	0.66	8.57	0.09	6.73	5.67
Na ₂ O	3.89	4.75	0.42	4.45	9.40	6.90
K ₂ O	8.80	10.09	12.00	11.17	4.97	6.50
P ₂ O ₅	0.02	0.01	0.45	0.02	0.15	0.32
LOI	0.60	0.19	0.62	nd	0.85	2.87
CO	0.19	0.13	6.48	nd	0.35	1.86
Total	100.10	99.96	100.29	100.42	100.15	100.03

A = nepheline syenite (Le Maitre 1976)
 B = phonolite (Le Maitre 1976)
 C = syenite (Le Maitre 1976)
 D = trachyte (Le Maitre 1976)
 E = basanite (Le Maitre 1976)
 F = nepheline basalt (Le Maitre 1976)
 G = nephelinite (Le Maitre 1976)
 H = tephrite (Le Maitre 1976)

I = nepheline-corundum-albite-muscovite gneiss, Blue Mountain, Canada (Currie 1978)
 J = nepheline syenite gneiss, Blue Mountain, Canada (Currie 1978)
 K = orthoclase, Kenya (Le Bas 1977)
 L = orthoclase, Kenya (Le Bas 1977)
 M = feldspathic ijolite, Kenya (Le Bas 1977)
 N = nepheline syenite, Kenya (Le Bas 1977)

indicated for the biotite-rich dykes. It is noted that high modal calcite in B230 results in this sample plotting in the metaluminous field; in fact secondary calcite is a feature of many of the Bulls Run syenites and has caused displacement towards the Ca-apex of the Bonin diagram.

The classification of the majority of BRC syenites as peraluminous to metaluminous is commensurate with their normative character (Table 3.7). Both CIPW norms and mesonorms demonstrate that the biotite-muscovite syenites are corundum-normative, the nepheline and albite syenites are either corundum or diopside normative and the microsyenites are slightly acmite-normative. As the microsyenites are only mildly peralkaline ($P.I. < 1.07$) and do not contain agpaitic minerals such as eudialyte they should be classified as peralkaline, not agpaitic (Edgar 1977, Gittins 1979).

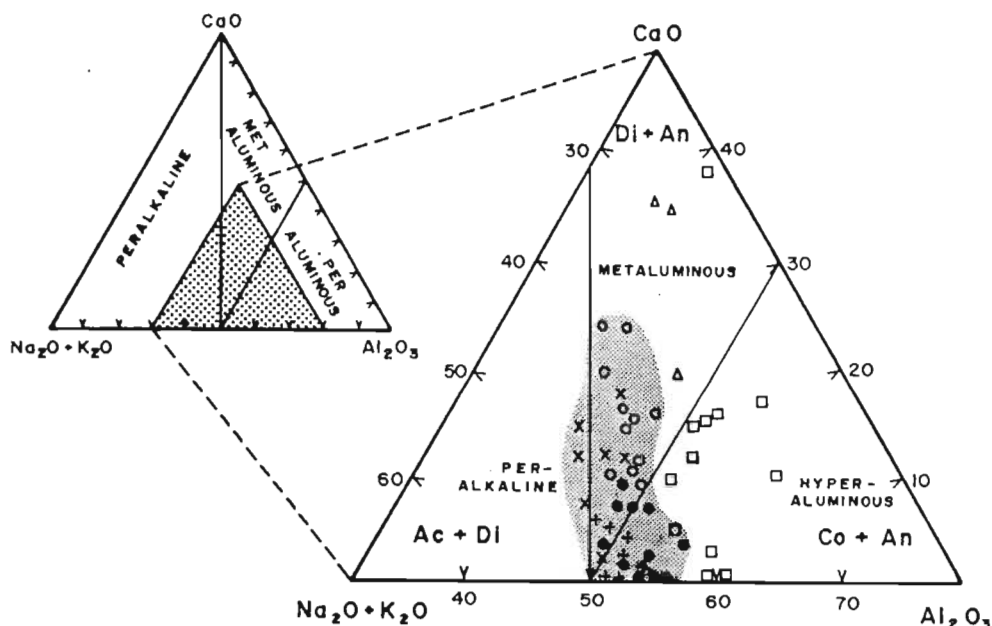


Figure 3.16. Alumina saturation relative to $\text{Na}_2\text{O} + \text{K}_2\text{O}$ and CaO (mol. props), diagram after Bonin (1986). The syenites are predominantly metaluminous to peraluminous, with three microsyenite dyke samples classified as peralkaline. The biotite-rich lamprophyric rocks are metaluminous. Symbols: (\square) biotite-muscovite syenite, (\circ) nepheline syenite/ijolite from the eastern BRC, (\bullet) nepheline syenite from the central and western BRC, (+) albite syenite, (\times) microsyenite, (Δ) biotite-rich lamprophyric rocks.

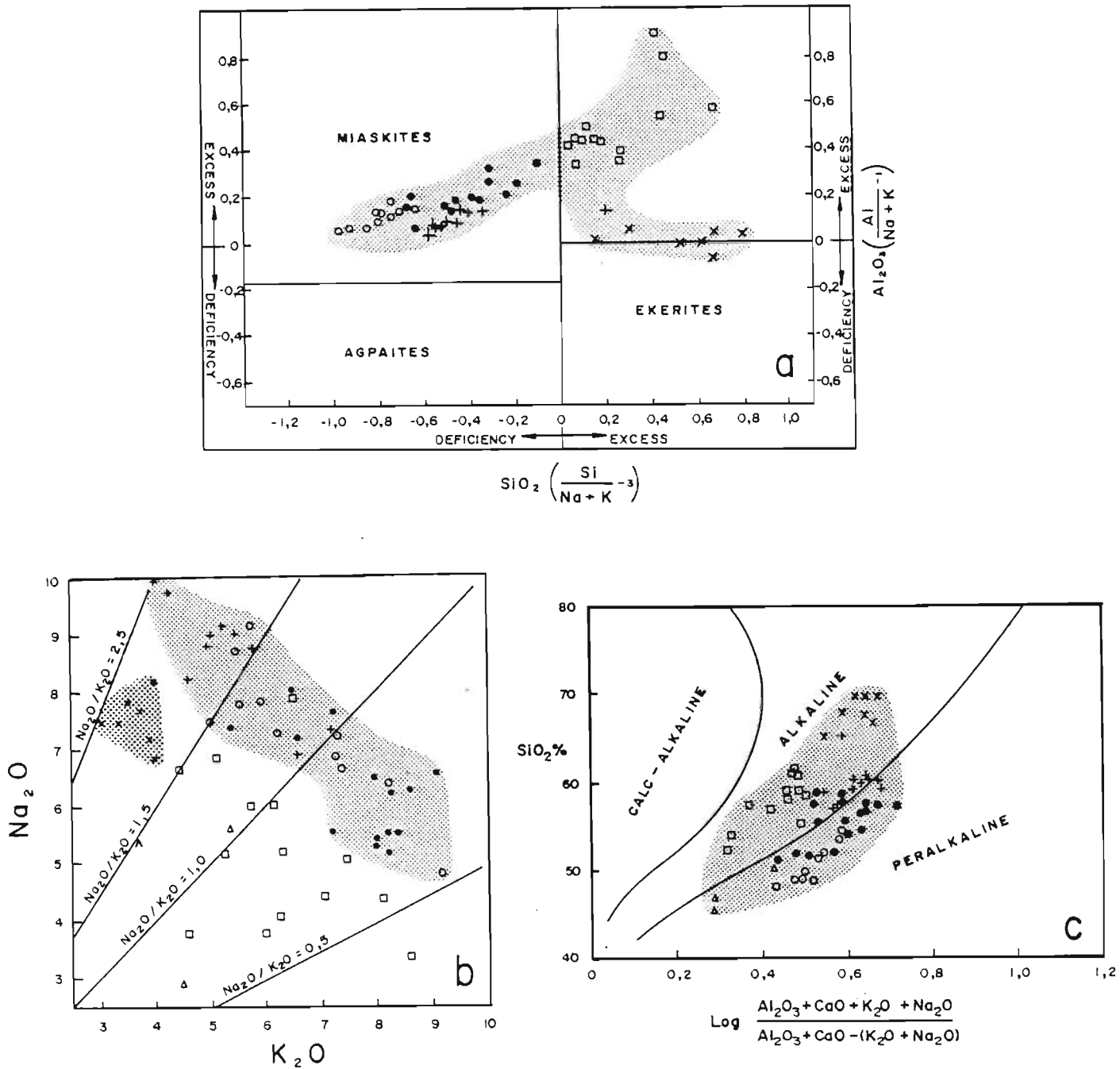


Figure 3.17. Alumina saturation relative to alkalis, and $\text{Na}_2\text{O}/\text{K}_2\text{O}$ ratios for the Bulls Run lithologies. Symbols as in Fig. 3.16.

Fig. 3.17a. Classification of the Bulls Run syenites as miaskites, as a result of their high alumina contents relative to alkalis. Diagram after Lurie (1985).

Fig. 3.17b. Discrimination of the Bulls Run lithologies using $\text{Na}_2\text{O}/\text{K}_2\text{O}$ ratios. The shaded area embraces nepheline-bearing syenites and the microsyenites dykes.

Fig. 3.17c: Alkalinity vs silica diagram after Wright (1969), showing the alkaline/peralkaline character of the Bulls Run lithologies.

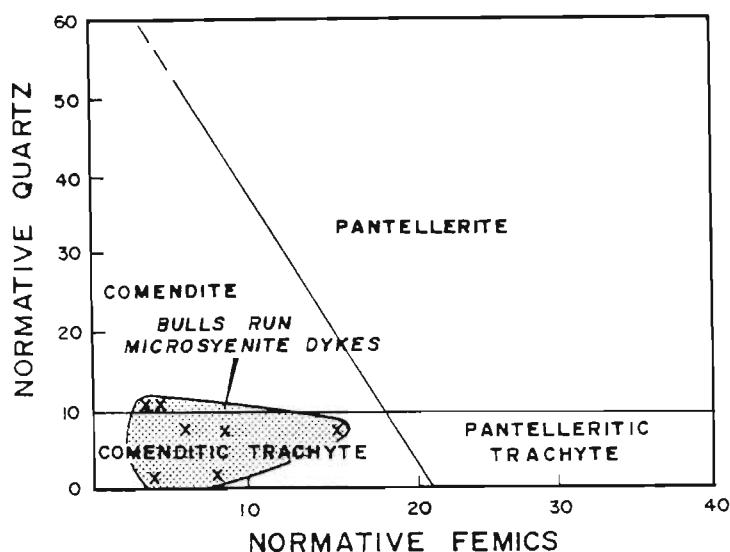


Figure 3.18. Classification of the BRC microsyenite dykes as comenditic trachyte, using normative quartz versus total normative femics. Diagram devised for the classification of silica-saturated peralkaline extrusive rocks by MacDondald & Bailey (1973). Symbols as in Fig. 3.16.

Although allocation of K^+ to biotite reduces orthoclase in the mesonorm relative to the CIPW-norm values, this effect is not significant for the nepheline-bearing syenites (Table 3.7). However, a noticeable difference between the two norms is apparent for the micaceous lithologies such as the biotite-muscovite syenite and biotite-rich dykes, where formation of mesonormative biotite results in excess SiO_2 and silica-oversaturated norms.

The alumina-rich character of the majority of Bulls Run samples results in their classification as miaskites (Fig. 3.17a).

3.4.4 Alkalinity

By definition, the Bulls Run syenites are alkaline as they have elevated alkalis relative to silica, modal and/or normative feldspathoids and alkali pyroxenes or amphiboles (Sorensen 1974, Currie 1976a). With respect to alkalis, Na_2O/K_2O ratios range from high values in the albite syenite and microsyenite (Na_2O/K_2O : 1.5 to 2.5), to relatively Na-depleted nepheline syenites in the western and central parts of the BRC (Na_2O/K_2O : 0.7 to 1.5, Fig. 3.17b). The biotite-muscovite syenites display a wide variation in this ratio but, generally, are K-rich (Na_2O/K_2O : 0.5 to 1.5) and have lower total alkalis than the nepheline syenites (Fig. 3.17b).

3.4.5 Degree of peralkalinity

As described above (Section 3.4.3) the BRC microsyenite dykes are very mildly peralkaline ($P.I. < 1.07$) and, according to normative mineral constituents, classify as comenditic trachyte (Fig. 3.18).

3.4.6 Nomenclature derived using geochemical parameters

For comparison with modally-derived terminology for the Bulls Run lithologies, several geochemical classifications have been used.

- (i) **The R1-R2 diagram:** As illustrated (Fig. 3.19a), the nepheline syenites and albite syenites classify as nepheline syenite, the majority of biotite-muscovite syenites plot along the nepheline syenite/syenite boundary and the microsyenites classify as syenite and quartz syenite. The three samples of biotite-rich dyke plot as nepheline syenite and essexite.
- (ii) **Normative classification:** A similar nomenclature to the R1-R2 classification is indicated when the mesonormative data are plotted (Fig. 3.19b). Thus, the nepheline syenites and albite syenites from the central and western portion of the BRC classify as feldspathoidal syenite, in contrast to the feldspathic ijolite and nepheline syenite lithologies from the eastern extremity of the BRC which classify as feldspathoidal monzosyenite. The microsyenite dykes and biotite-muscovite syenite plot as silica-oversaturated alkali-feldspar syenite and quartz alkali-feldspar syenite. As recommended by Streckeisen & Le Maitre (1979), the biotite-rich dykes were not plotted on Figure 3.19b, due to potential errors in the distribution of normative feldspar and foid molecules in mafic minerals such as biotite, which can be significant within rocks of high colour index.
- (iii) **Carbonatite classification:** When plotted on the triangular $CaO-MgO-(FeO+Fe_2O_3+MnO)$ diagram of Woolley (1982), the Bulls Run carbonatites classify as sövite (Fig. 3.20), which is in agreement with nomenclature derived from their modal mineralogy (Section 3.3.6) and trace-element chemistry (cf. Scogings & Forster 1989).

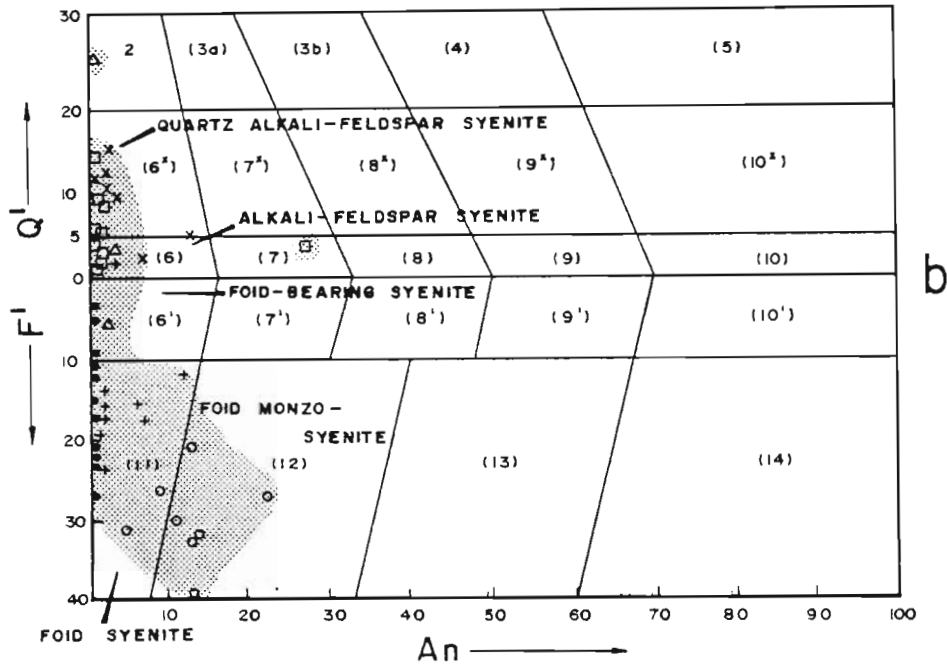
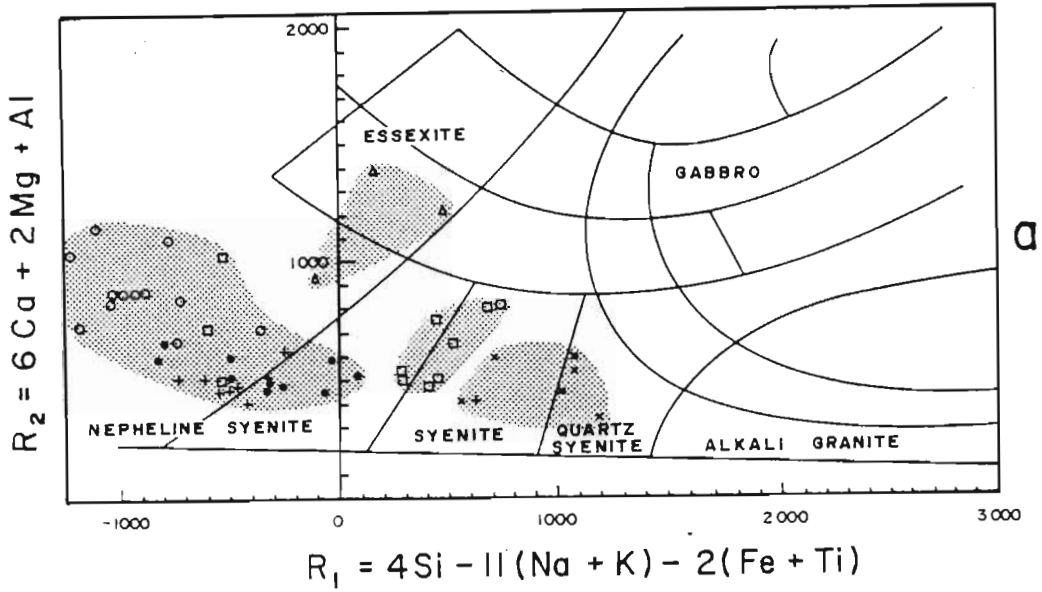


Figure 3.19. Classification of BRC lithologies according to their major-element and normative characteristics. Symbols as in Figure 3.16.

Fig. 3.19a. Classification of the BRC syenites and lamprophyric rocks, using the R1-R2 multicationic system devised by de la Roche *et al.* (1980).

Fig. 3.19b. Normative classification of the BRC syenites, based on the Q' vs An' diagram of Streckeisen & le Maitre (1979).

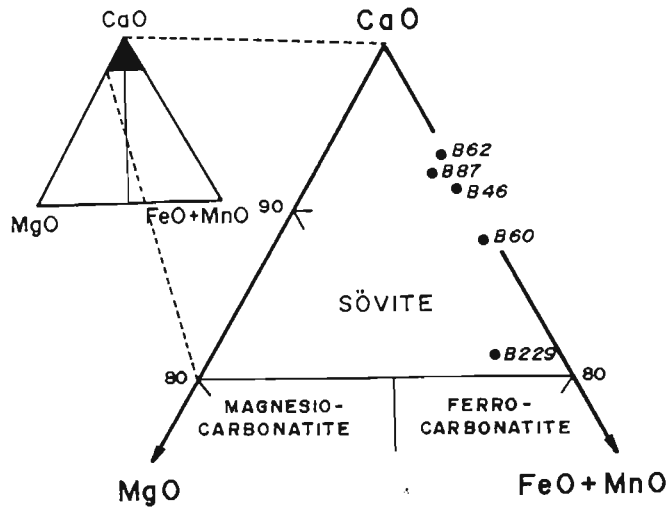


Figure 3.20. Classification of the BRC carbonatites using the triangular CaO-MgO-(FeO+Fe₂O₃+MnO) diagram of Woolley (1982). Carbonatites shown as filled circles.

3.4.7 Harker diagrams

Plotting of selected major- and trace-element data from the Bulls Run Complex on Harker diagrams (Figs 3.21 and 3.22) indicates the following trends:

- (i) SiO₂ contents are bimodally distributed, with the bulk of analyses between 45 and 60% SiO₂, separated by a 5% gap from a small cluster of analyses at 65 to 70% SiO₂. The ijolitic lithologies and the biotite-rich dykes, have the lowest SiO₂ contents (45 to 52%). Nepheline and albite syenites from the central and western core of the BRC are essentially phonolitic, with restricted SiO₂ values of between 52 and 60%. The trachytic microsyenite dykes are characterised by elevated SiO₂ values, between 65 and 70%, and separated by a prominent gap from the other lithologies in the complex. The biotite-muscovite syenite samples have highly variable SiO₂ values, largely related to the occurrence of modal calcite, and range from 48 to 57%.

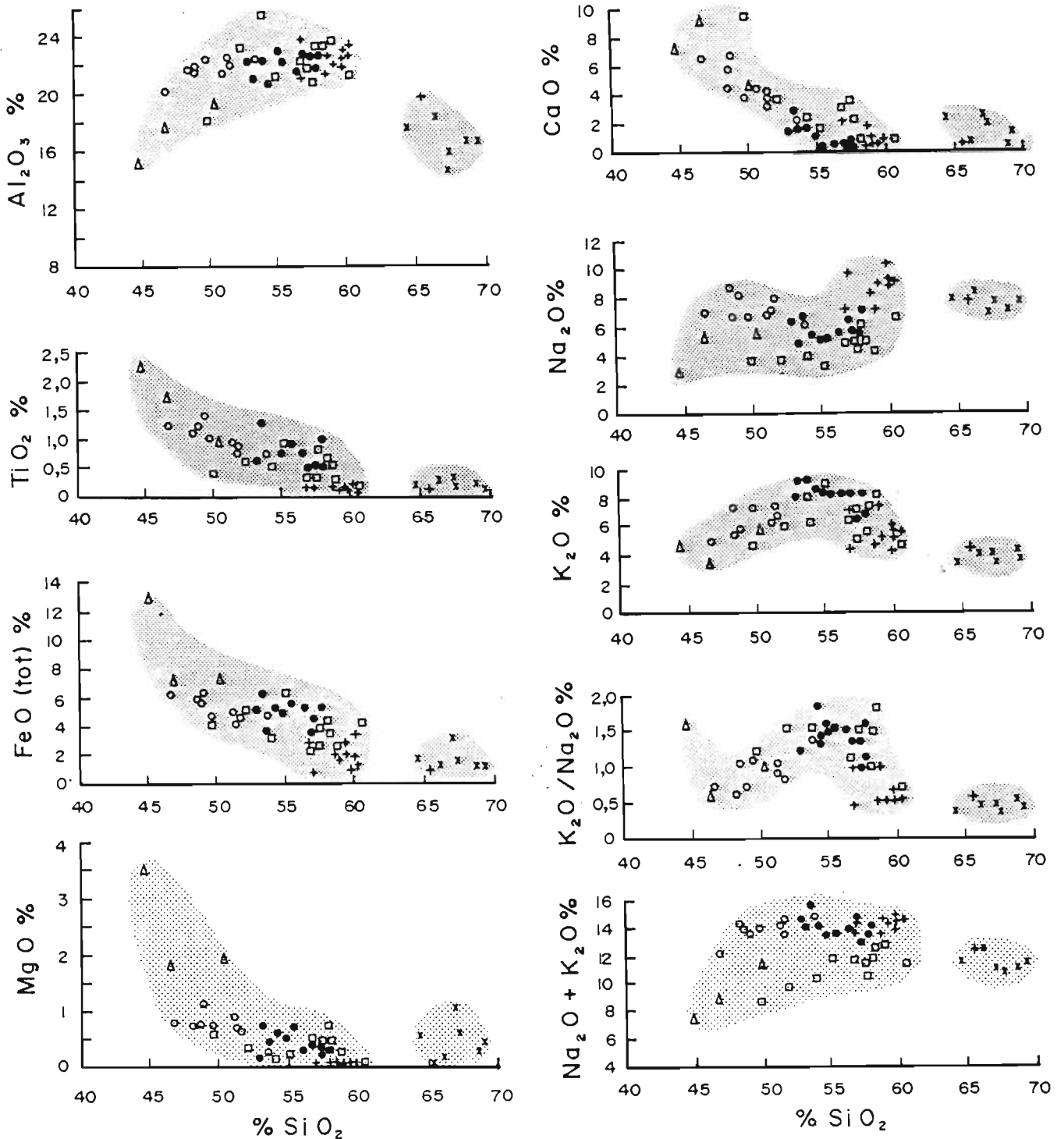


Figure 3.21. Bulls Run major-element data plotted on Harker variation diagrams. Major-element oxides in %. Symbols: (□) biotite-muscovite syenite, (○) nepheline syenite/ijolite from the eastern BRC, (●) nepheline syenite from the central and western BRC, (+) albite syenite, (×) microsyenite, (Δ) biotite-rich lamprophyric rocks. The carbonatites have not been included, due to their low SiO₂ contents.

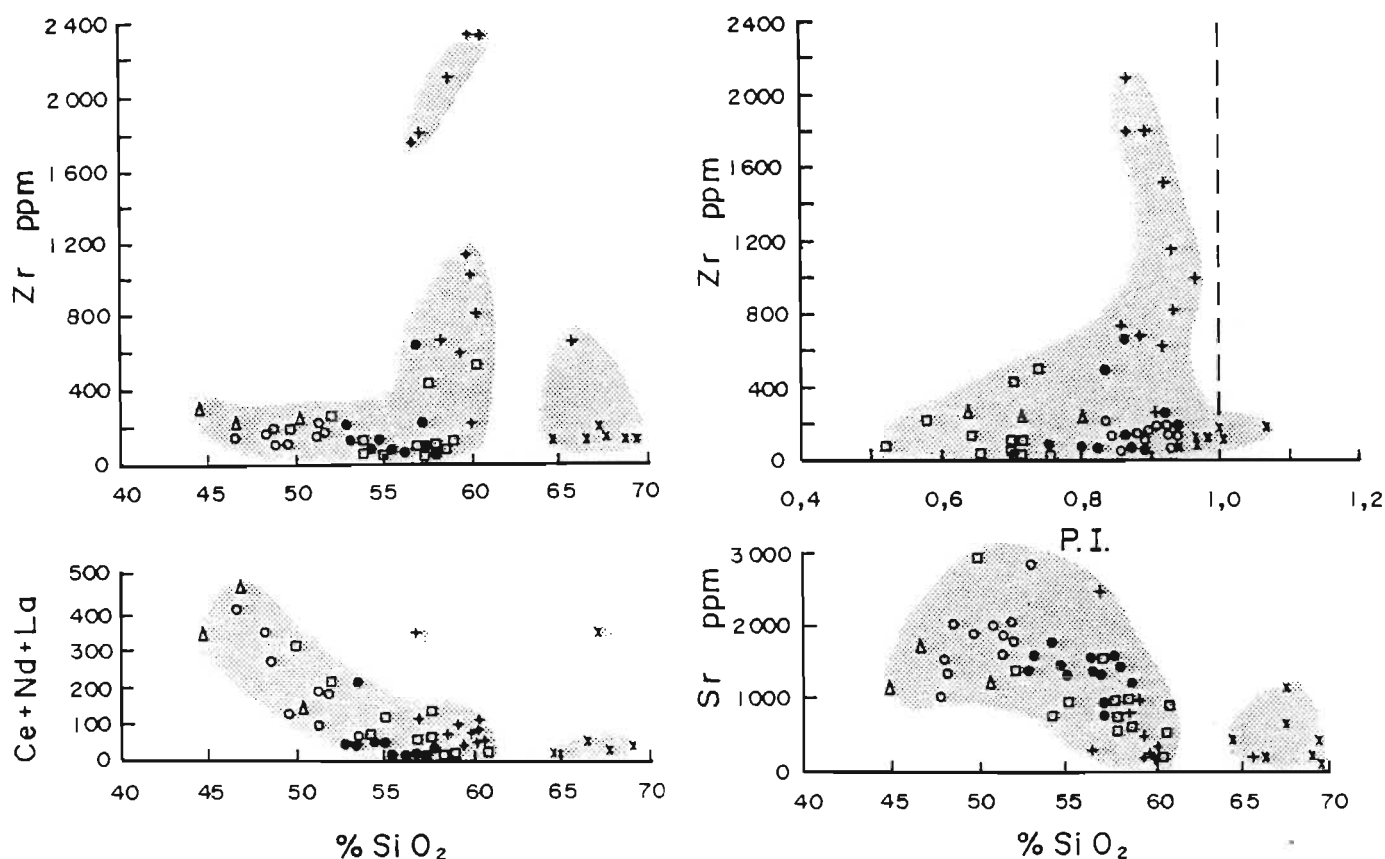


Figure 3.22. Selected Bulls Run trace-element data (ppm) plotted on Harker variation diagrams. Zr is plotted against both SiO_2 and P.I. (peralkalinity index). Symbols as in Fig. 3.21.

- (ii) Al_2O_3 contents tend to increase sympathetically with SiO_2 from the biotite-rich dykes (c. 18% Al_2O_3) and ijolites through to the nepheline and albite syenites (c. 21% Al_2O_3). A marked inflexion in this trend occurs between 60% and 65% SiO_2 , when Al_2O_3 contents decrease to c. 17% in the microsyenites. As a group, the biotite-muscovite syenites are enriched in Al_2O_3 relative to all other lithologies in the BRC, corroborating their corundum-normative character.
- (iii) TiO_2 , FeO , MgO , CaO are negatively correlated with SiO_2 , although the microsyenites are relatively enriched in CaO and MgO for their silica contents.
- (iv) Several trends are apparent for Na_2O and K_2O . Firstly, the ijolites and microsyenites are depleted in K_2O relative to Na_2O and display no obvious correlation of alkalis with SiO_2 . By contrast, the phonolitic syenites exhibit negative

correlation between K_2O and SiO_2 , and positive variation of Na_2O with SiO_2 . Hence, K_2O/Na_2O ratios probably decreased with increasing fractionation of the phonolitic syenites, from nepheline syenite through to albite syenite.

The ijolites, nepheline syenites and albite syenites have the highest total-alkali contents (Na_2O+K_2O : 12 to 16%), with the biotite-muscovite syenites containing between 9 and 12% Na_2O+K_2O . Whereas nepheline-bearing rocks display only a minor increase in total alkalis with SiO_2 , the alkali contents of the muscovite-bearing syenites correlate positively with SiO_2 .

- (v) With respect to incompatible trace elements such as Zr and Nb there is a negative trend between 45% and 57% SiO_2 . However, a marked inflexion occurs between 57% and 59% SiO_2 where Zr increases rapidly, against a background of c. 200 ppm in nepheline syenite, to a peak of c. 2300 ppm within albite syenite. This suggests that Zr (and Nb) were concentrated in differentiated liquids, towards the last stages of crystallization of the BRC phonolitic albite syenites. Similar concentration effects have been documented in differentiated phonolitic suites (Marsh 1987). This is in agreement with the petrographic data (Section 3.3.4) that indicate late-stage volatile-rich deuteric alteration related to zircon/pyrochlore mineralization in the albite syenite.
- (vi) Sr and the REE's (Ce+Nd+La) are negatively correlated with silica and do not follow the enrichment trend displayed by Zr and Nb. However, their similarity to the CaO pattern indicates hosting by calcite and possibly apatite and, therefore, depletion in the more differentiated, silica-rich syenites. This is reinforced by REE enrichment in the most CaO-rich rocks in the BRC, viz. carbonatites (Table 3.5).

3.4.8 K_2O fractionation in phonolites

As noted by Marsh (1987), the concentration of K_2O tends to decrease with fractional crystallization in phonolitic liquids, a phenomenon

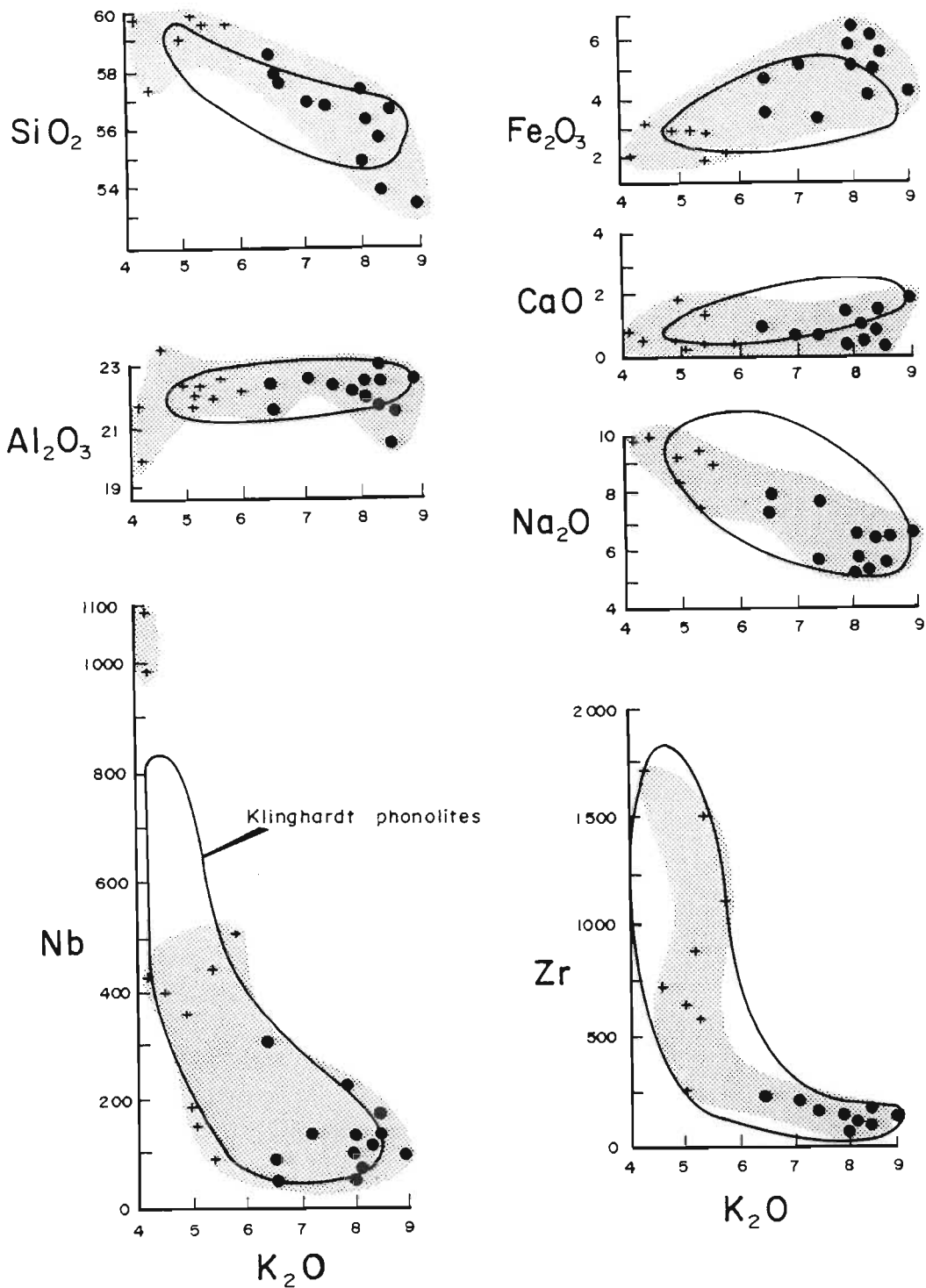


Figure 3.23. Selected major- and trace-element data from BRC phonolitic syenites plotted against K_2O , for comparison with the field of Klinghardt phonolites from Marsh (1987). Symbols: (●) biotite-nepheline syenite from central and western BRC, (+) albite syenite.

described as the "orthoclase effect". In order to test for this effect in Bulls Run phonolitic syenites, selected major-element oxides and trace elements have been plotted against K_2O (Fig. 3.23). These indicate that:

- (i) K_2O exhibits a negative correlation with SiO_2 , Na_2O , Nb and Zr, similar to the trend displayed by the Klinghardt phonolites.
- (ii) Fe_2O_3 is positively correlated with K_2O , whereas Al_2O_3 and CaO do not appear to covary with K_2O .

By analogy with the data from the Klinghardt Mountains, the above trends indicate that the siliceous, Na_2O -rich, albite syenites are differentiates of the nepheline syenite. Thus the observed compositional and textural variations, from nepheline syenite to albite syenite, are consistent with early fractional crystallisation of nepheline and microcline. This accumulated as medium- to coarse-grained nepheline syenite and resulted in concentration of Na, Si, Nb, Zr and volatiles in the residual liquid which, subsequently, crystallised to form albite syenite.

3.4.9 Incompatible elements and peralkalinity

A plot of Zr against the peralkinity index (P.I.) in Figure 3.22 reveals that the greatest concentrations of Zr are in rocks with peralkalinity indices of between 0.85 and 0.95 and that Zr tends to increase during fractionation in conjunction with increasing P.I. However, the mildly-peralkaline silica-oversaturated microsyenite dykes (P.I.>1.0) have the lowest Zr contents of any of the BRC lithologies, apart from the carbonatites. This feature is atypical, as peralkaline rocks are normally enriched in incompatibles such as Zr (Watson 1971). As noted previously, the microsyenites do not appear to be linked directly to the ijolite/phonolitic syenite fractionation trend (eg. Al_2O_3 and SiO_2 compositional gaps). Derivation of the microsyenite by a process other than crystallization of phonolitic magma is indicated and is referred to later in the discussion on fenitization processes (Section 3.6.4).

3.4.10 Rare earth elements

The analysis of 23 BRC whole-rock samples for REE's indicates that, although total REE contents are variable between different lithologies, the overall pattern is one of LREE enrichment relative to HREE. This general HREE-depletion, coupled with a lack of Eu depletion, is typical for alkaline syenites and carbonatites (Cullers & Graf 1984). It is noted that for each rock type, total REE's increase with decreasing SiO₂ (increasing mafic character), concomitant with REE concentration in mafic minerals as well as calcite and apatite. The various BRC lithologies display the following REE characteristics (Figs 3.24, 2.25):

- (i) The biotite-muscovite syenites are subdivided into two varieties, namely pink syenite from the western part of the complex and an off-white variety from the eastern outcrops (Section 3.3.2). Thus, as shown in Figure 3.24a, the western syenites have positive Eu anomalies (Eu/Eu^* : 1.17 to 1.65), are LREE-enriched (La_N/Lu_N : 13.69 to 28.30) and contain lower total REE (La : 20 to 100 x chondrite) than eastern syenites. In contrast, the three eastern syenites have very slight negative Eu anomalies (Eu/Eu^* : 0.85 to 0.95), steeper LREE-enriched patterns (La_N/Lu_N : 8.67 to 18.69) and are enriched both in total REE (La : 50 to 200 x chondrite) and HREE relative to the western types. The difference between HREE contents in the two syenites is highlighted when B179 is normalised against B34 (Fig. 3.24a).

As described above (Section 3.3.6) carbonatite dykes are spatially associated with biotite-muscovite syenite. Therefore a comparison has been drawn, by normalising a carbonatite from the western part of the BRC against both syenite types (Fig. 3.24a). Carbonatite B229 is clearly more like B34 (eg. HREE-depleted) than B179, which supports a genetic relationship between carbonatite B229 and syenite B34.

- (ii) The feldspathic ijolite is enriched in total REE relative to the phonolitic nepheline syenites from the central and western parts of the complex (Fig. 3.24b). Apart from this difference the overall patterns are similar, strongly LREE-enriched

(La_N/Lu_N : 9.31 to 39.65) and with positive Eu anomalies (Eu/Eu^* : 1.05 to 2.75).

Sample B41, which is a leucocratic nepheline syenite with very low total REE, has a pronounced positive Eu anomaly similar to biotite-muscovite syenite B54. As both B54 and B41 are leucocratic, with very little apatite or calcite that normally would carry REE, it is likely that biotite contains most of the REE in these rocks and will therefore significantly influence the REE patterns. Thus it is suggested that the positive Eu anomaly results from selective concentration of Eu in biotite, as described from the Oka Carbonatite Complex (Eby 1975).

- (iii) The albite syenite is subdivided into two types (Section 3.3.4). The predominant type is light grey, albite-rich, contains c.400 ppm Nb and 1000 ppm Zr and shows unusual LREE-depleted (La_N/Lu_N : 2.56 to 3.67; La: c. 20 x chondrite) "birdwing" patterns (Fig. 3.24c) that are characterised by negative Eu anomalies (Eu/Eu^* : 0.62 to 0.93).

The second, less common type of albite syenite is off-white and contains approximately equal amounts of albite and microcline, with significant modal zircon, pyrochlore and altered nepheline. Incompatible trace element concentrations reflect this modal assemblage, with up to 2129 ppm Zr and 16553 ppm Nb. Total REE are higher than for the grey albite syenite, due to an increase in light and middle REE (La_N/Lu_N : 7.85 to 61.0; La: 70 to 500 x chondrite), with Eu substantially increased to form a mild positive anomaly (Eu/Eu^* : 1.05 to 1.08).

The two different patterns described are indicative of fluid/volatile transport of LREE, possibly accompanied by removal of Na. The low total REE in albite syenite is rather surprising, considering the presence of modal pyrochlore and zircon that might be expected to preferentially accommodate REE. This anomaly may be ascribed to the extreme mobility of REE in CO_2 -rich volatile phases (Wendlandt & Harrison 1979, Cullers & Graf 1984), indicating preferential fractionation into a CO_2 -rich vapour

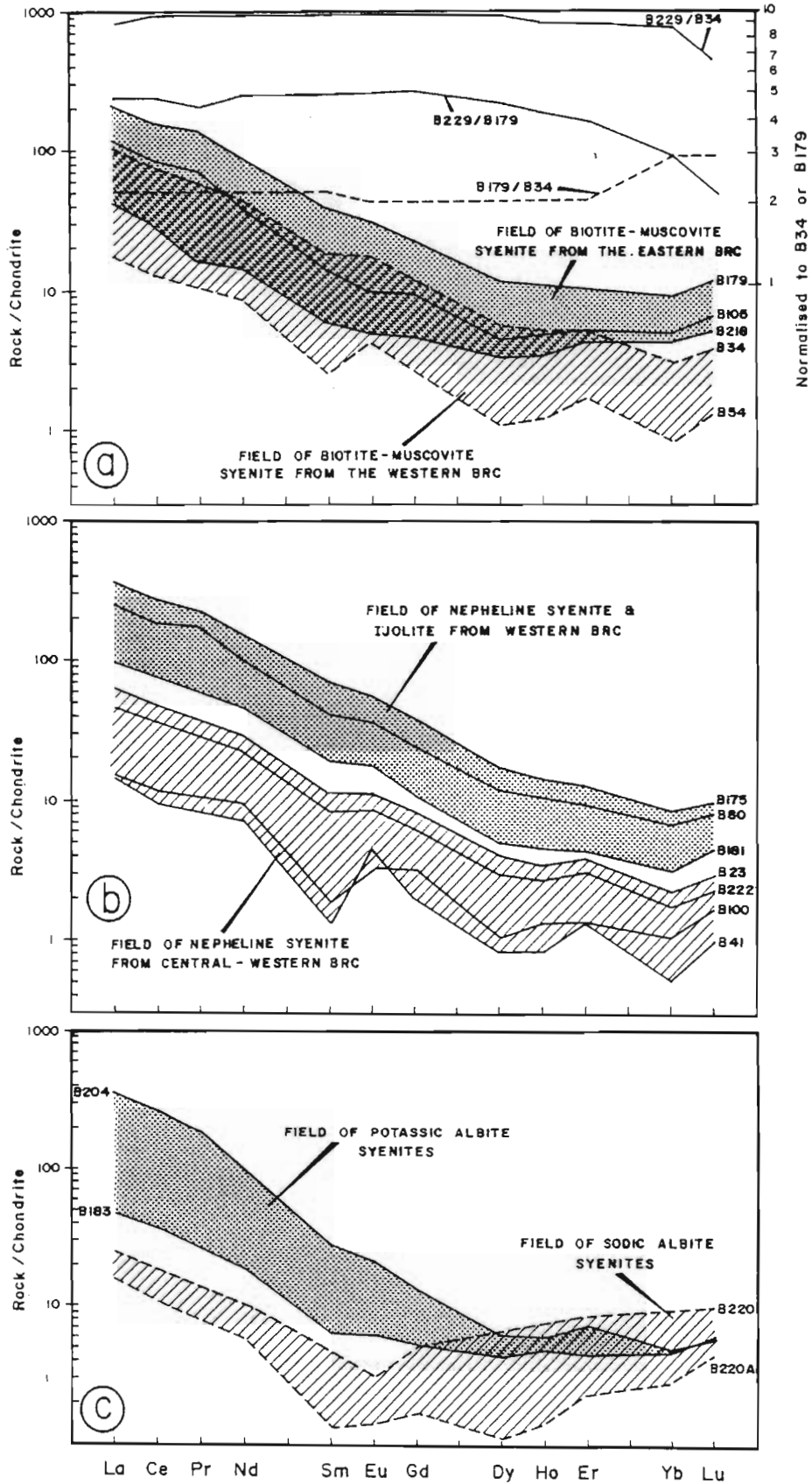


Figure 3.24. Chondrite-normalised REE patterns for Bulls Run Complex lithologies. Fig. 3.24a biotite-muscovite syenite, Fig. 3.24b nepheline syenite, Fig. 3.24c albite syenite. Chondrite values from Nakamura (1974).

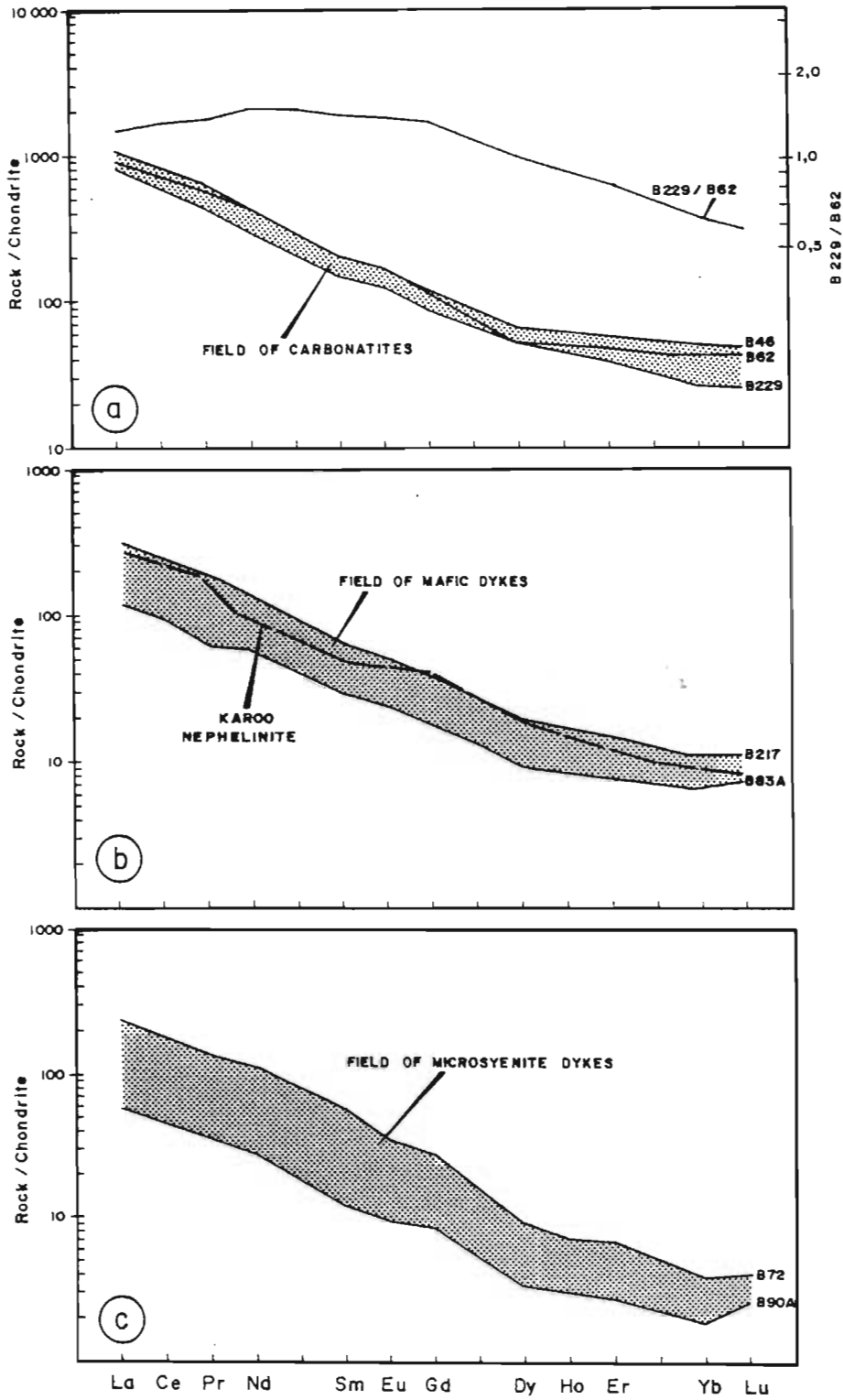


Figure 3.25. Chondrite-normalised REE patterns for Bulls Run lithologies. Fig. 3.25a carbonatite, Fig. 3.25b biotite-rich mafic lamprophyric rocks, Fig. 3.25c microsyenite.

that was removed as an immiscible phase from the albite syenite. This suggestion is compatible with the low abundances of both modal calcite and apatite in the albite syenite, indicating removal of these phases and REE after crystallisation of pyrochlore.

- (iv) The carbonatites have the highest REE abundances of all the BRC samples ($\text{La: } 1000 \times \text{chondrite}$) and are LREE-enriched (La_N/Lu_N : 19.07 to 37.79), with slight positive Eu anomalies (Eu/Eu^* : 1.03 to 1.07) (Fig. 3.25a). A general decrease in total REE is apparent, from the brown Fe-rich carbonatite (B46) east of Goedertrou Dam, through to B229 which is an off-white, apatite-rich, carbonatite intruded west of the Mhlatuze River. In addition to this trend, there is variation in LREE/HREE ratios where the apatite-rich carbonatite is enriched in LREE ($\text{La}_N/\text{Lu}_N = 37.79$) compared with, for example, B62 ($\text{La}_N/\text{Lu}_N = 19.07$). This variation is shown graphically in Fig. 3.25d by plotting normalised B229/B62 ratios; B229 is enriched in LREE by a factor of 1.5x, but contains only about half the HREE of B62.
- (v) REE data for the biotite-rich dykes are presented in Fig. 3.25e and show patterns of absolute-REE abundances very similar to those of the BRC ijolites, viz. LREE enrichment (La_N/Lu_N : 16.59 to 27.65) and virtually no inflexion at Eu (Eu/Eu^* : 1.01 to 1.06). A Karoo nephelinite is included for comparison with the REE trends exhibited by the biotite-rich dykes. The carbonatites B62 and B46, although enriched in total REE relative to the biotite-rich dykes, have the same range of LREE/HREE ratios, indicating a genetic relationship between the two.
- (vi) The microsyenite dykes are LREE-enriched (La_N/Lu_N : 23.20 to 59.7) and marked by slight negative Eu anomalies (Eu/Eu^* : 0.82 to 0.89). Total-REE contents are similar to those of the biotite-rich dykes ($\text{La: } 70 \text{ to } 160 \times \text{chondrite}$).

3.4.11 Nb/Y ratios

Constant ratios of incompatible elements such as Nb and Y are generally considered to indicate a comagmatic origin for different phases within

an intrusion (Nicholls 1988). When the BRC data are plotted on Figure 3.26 a wide scatter of Nb/Y ratios is apparent, suggesting that the various rock-types are not genetically related. Closer evaluation of Figure 3.26 shows however that the nepheline syenites, ijolites, biotite-rich dykes and biotite-muscovite syenites exhibit relatively well constrained ratios between 10 and 100. Lithologies that diverge from this cluster include albite syenite, microsyenite and carbonatite. Such dispersion is suggested to be due to partitioning of elements between immiscible carbonate and silicate liquids (eg. Cullers & Medaris 1977, Wendlandt & Harrison 1979) or CO₂ metasomatic alteration, evidence for which was presented in Section 3.3.

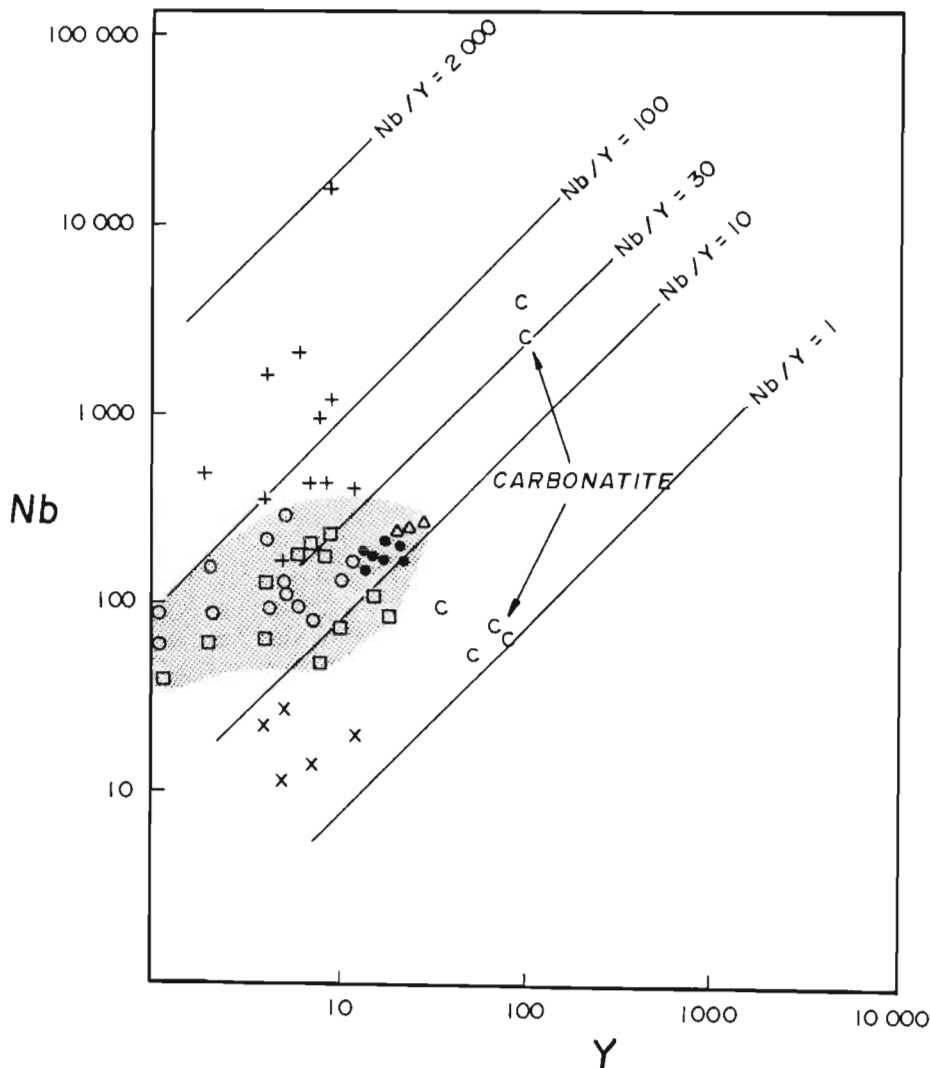


Figure 3.26. Plot of Nb vs Y for all the Bulls Run lithologies. Symbols: (□) biotite-muscovite syenite, (●) ijolite/nepheline syenite, (○) biotite-nepheline syenite, (+) albite syenite, (x) microsyenite, (Δ) biotite-rich dykes.

3.5 Rb-Sr isotopes

3.5.1 Introduction

The first isotopic data published for granitoids from the Tugela Terrane of the NMP were by Nicolaysen & Burger (1965). These indicated a U/Pb isotopic age of 1140 ± 35 Ma for a zircon from syenitic gneisses on Bulls Run Estate, although the exact locality and composition of the host syenite is unknown. The present investigation is aimed at elucidating the origin of the BRC syenites, particularly with regard to initial isotopic composition of the primary magma. As the biotite-muscovite syenite is interpreted as a fenite, and the albite syenite shows considerable evidence of late-magmatic fluid activity, the nepheline syenites were deemed most suitable for this exercise. Consequently, four samples of ijolitic nepheline syenite and seven of biotite-nepheline syenite from the eastern and central parts of the complex (Fig. 3.27a for locality), respectively, were analysed following the procedures outlined in Appendix 2.

3.5.2 Analytical results

The data from the four samples of ijolitic nepheline syenite regress to an isochron date of 1112 ± 133 Ma with an R_0 of 0.7033 ± 6 (MSWD = 0.2, Fig. 3.27b). The seven samples of biotite-nepheline syenite provide a statistically-identical result of 1101 ± 58 Ma and R_0 of 0.7035 ± 4 (MSWD = 1.8). Regression of the combined data provides an isochron date of 1138 ± 45 Ma and R_0 of 0.70322 ± 25 (MSWD = 1.6). This result is within error of the $^{207}\text{Pb}/^{206}\text{Pb}$ model date of 1140 ± 35 Ma reported by Nicolaysen & Burger (1965). Four carbonate separates from carbonatite dykes intrusive into the muscovite syenites of the complex provide an average R_0 of 0.70319 ± 15 (assuming the above date), identical to that obtained for the nepheline syenites.

3.5.3 Discussion of Rb-Sr data

The age obtained for the Bulls Run syenites (1138 ± 45 Ma) is similar to that obtained for the Tugela Rand Layered Suite (1189 ± 11 Ma, Wilson 1990) and the Tuma amphibolites (1242 ± 23 Ma, Harmer 1979). The low initial ratios indicated by the nepheline syenites ($R_0 = 0.70322$) and the carbonate separates from the carbonatites ($R_0 = 0.70319$) are essentially identical and support a comagmatic origin. Low initial

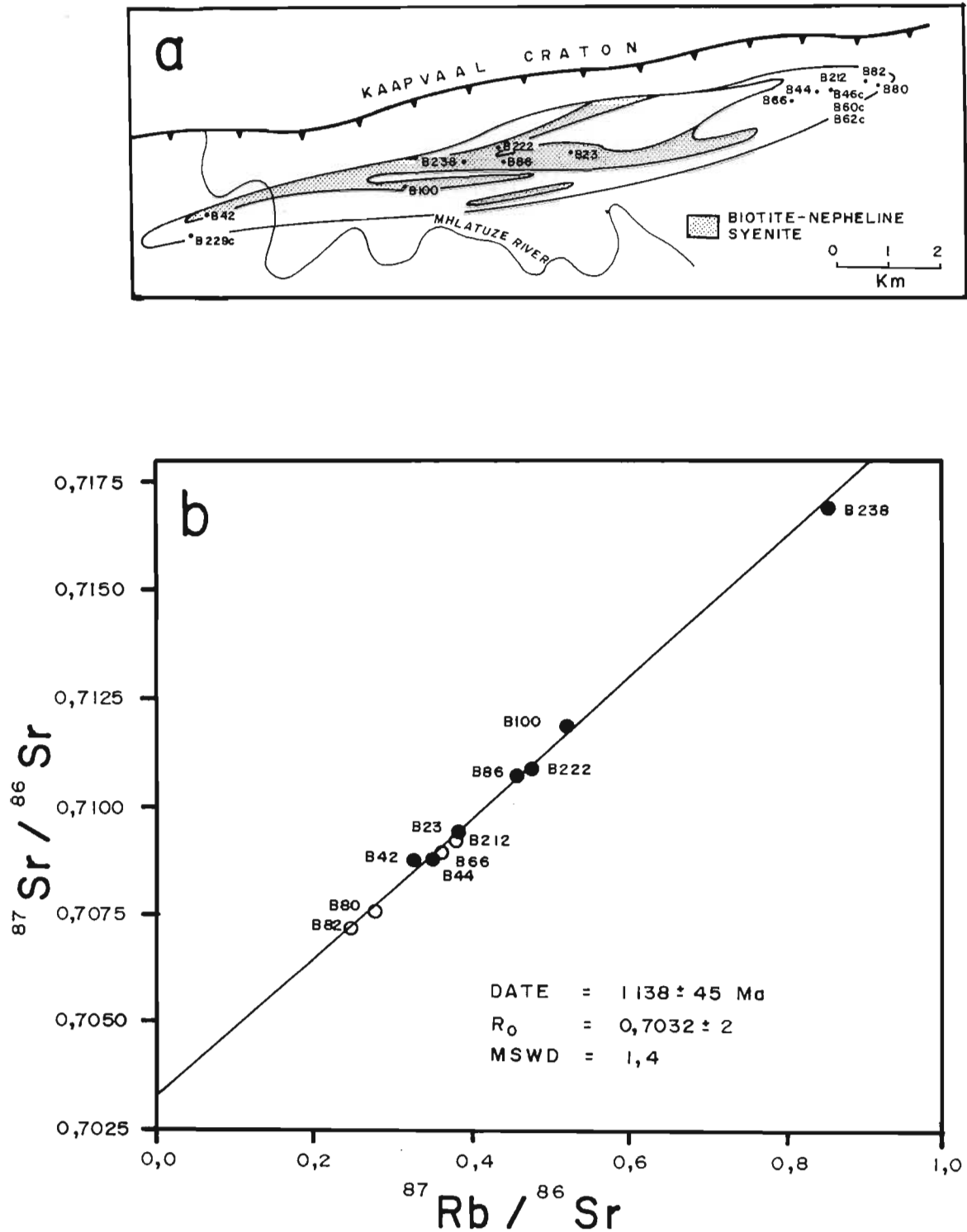


Figure 3.27. Locality of the nepheline syenite samples analysed for Rb-Sr isotopes (Fig. 3.27a). The resulting Rb-Sr isochron is given as Fig. 3.27b, in which the open circles are ijolitic nepheline syenite (eastern BRC) and the closed circles are biotite-nepheline syenite (western and central BRC).

ratios (0.703 to 0.704) are characteristic of most nepheline syenites world-wide (Table 3.11) and are taken to indicate a mantle origin.

Table 3.9

Rb-Sr isotope data for Bulls Run nepheline syenites

Sample	Rb ppm	Sr ppm	$^{87}\text{Rb}/^{86}\text{Sr}$	$^{87}\text{Sr}/^{86}\text{Sr}$
Ijolitic nepheline syenite				
B66	219	1767	0.359	0.708988 ± 13
B80	199	2065	0.279	0.707656 ± 12
B82	241	2811	0.248	0.707246 ± 10
B212	166	1266	0.380	0.709323 ± 23
Biotite-nepheline syenite				
B23	206	1560	0.382	0.709461 ± 11
B42	172	1523	0.327	0.708810 ± 12
B86	210	1327	0.458	0.710809 ± 12
B100	222	1231	0.521	0.711901 ± 13
B222	215	1298	0.478	0.710931 ± 10
B44	242	1996	0.351	0.716912 ± 12
B238	226	764	0.855	0.716912 ± 10

Note: Rb and Sr concentrations and Rb/Sr by XRF.

Table 3.10

Rb-Sr isotope data for Bulls Run carbonatites

Carbonate fraction

Sample	Rb ppm	Sr ppm	$^{87}\text{Rb}/^{86}\text{Sr}$	$^{87}\text{Sr}/^{86}\text{Sr}$
B46c	9.04	8472	0.003	0.70325 ± 7
B60c	2.33	9172	0.0007	0.70318 ± 6
B62c	3.00	9336	0.0009	0.70298 ± 5
B229c	3.98	6067	0.002	0.70338 ± 5

Rb and Sr concentrations and Rb/Sr by isotope dilution.

Table 3.11

Comparative ages and initial Sr ratios from other nepheline syenites reported in the literature.

Locality	Rock type	Age (Ma)	$^{87}\text{Sr}/^{86}\text{Sr}$
Mount Royal, Quebec	Nepheline syenite	118	0.7038
Tadhak, Mali	Nepheline syenite	262	0.7045
Oslo Rift, Norway	Nordmarkite	278	0.7042
Nunarssit, Greenland	Nepheline syenite	1154	0.7043
Gronnendal, Greenland	Nepheline syenite	1327	0.7032
Bulls Run*	Nepheline syenite	1133	---
Bulls Run	Nepheline syenite	1138	0.7032

Note: Data for other alkaline occurrences from Blaxland *et al.* (1978); Eby (1984); Liegeois *et al.* (1983); Taylor *et al.* (1980). Bulls Run* from Nicolaysen & Burger (1965).

3.6 Fenites and lamprophyres: discussion with reference to the BRC

The Bulls Run Complex comprises a variety of alkaline lithologies, for some of which direct analogues are not frequently described in the literature. This situation applies particularly to unusual rocks like the muscovite-bearing syenites and the biotite-rich dykes. Therefore, in view of the earlier suggestion that the former are aluminous fenites and that the latter have lamprophyric affinities, a review of fenites and lamprophyres is warranted for comparison with the Bulls Run occurrences.

3.6.1 Characteristics of fenites

Alkali-metasomatism (fenitisation) of country rocks is characteristic of carbonatite/nepheline syenite intrusions. Although Von Eckermann (1948) originally excluded remobilised altered rocks from his concept, Le Bas (1987, p.74) noted that the "products of fenitisation are mineralogically syenitic, with the result that they are sometimes misidentified as igneous syenites". Thus rheomorphic fenites are indistinguishable from normal alkaline magmatic rocks.

Von Eckermann (1948) related fenitisation to metasomatism by alkaline and CO_2 -rich fluids which, due to silica deficiency, tended to react with and absorb quartz in the country rock. In the classic fenite, therefore, quartz is replaced by sodic Fe-rich amphibole and/or pyroxene. Excess silica from this reaction goes into solution and may cause albitisation (Verwoerd 1967). As the fenitising process continues, biotite may react to form aegirine, thus releasing silica and alumina. At a late stage in the evolution of the fenite, when the metasomatising liquid is no longer deficient in silica and alumina, Verwoerd (op cit., p.333) notes that "feldspathisation", ie. growth of K-feldspar, can occur.

The opposite situation to the above is discussed by Verwoerd, who noted that at Fen the sequence of dissolution is reversed, and that the order of replacement is biotite - feldspar - quartz. This order was ascribed to fenitising fluids depleted in Fe which "could not form aegirine by

the replacement of quartz" (Verwoerd 1967, p.334). Therefore this situation suggests that a fenite need not always carry sodic mafic minerals.

Since calcite and apatite are accessory constituents in many fenites (Verwoerd 1967), their presence provides a link between fenitised rocks and the fluids expected to emanate from a CO_2 - and P_2O_5 -rich carbonatite source.

Le Bas (1977 1987) viewed fenitisation as a multiple process, involving variables such as the chemistry of the original magma, the composition of the country rock, and the type of fluids leaving the magma. Therefore, he distinguished between sodic fenites associated with ijolite intrusion and potassic fenites generated by carbonatites. With respect to carbonatites, in general, Le Bas (1977) noted that only sövites and dolomitic types cause fenitisation and that the most potassic fenites (often almost pure K-feldspar rock) form around the topmost parts of sövite intrusions. The process of potash metasomatism occurs ahead of the advancing sövite which subsequently brecciates and intrudes its own fenites. Therefore an intrusive sövite would be expected to contain xenoliths of earlier fenite.

That fenites formed at depth are sodic and albite-rich, is indicated by albitite xenoliths in carbonatites with K-rich fenites exposed at the surface (viz. Nyamaji-Wasaki, Kenya: Le Bas 1987). A similar zonation of fenites around the Novopoltavskoye carbonatite in the USSR has been described by Le Bas (op cit.), with albitic fenites enveloped by microcline-rich fenites. The feldspars in albitites developed around sövite are almost pure albite (Ab_{90}) and orthoclase (Or_{85}), compared with feldspars from fenites surrounding ijolites, which have intermediate compositions (Ab_{60-40} ; Or_{40-60}). Le Bas (1987) relates these differences in feldspar composition to the low temperature of fenitisation around carbonatite ($<550^\circ\text{C}$), compared with high temperature silicate-related fenitisation of more than 700°C .

In addition to the above observations on fenitisation, Le Bas (1977) reported intrusive trachyte veins associated with feldspathisation

accompanying sövite intrusives in Kenya and Uganda. These trachytes were not considered to be rheomorphic fenites, but rather to have formed by the crystallisation of fenitising fluids along fractures in rocks around the alkaline intrusions. This development suggests that, ultimately, fenitisation can produce silica-saturated and even silica-oversaturated rocks.

Another unusual feature of fenites, and one that has not often been documented, is the formation of aluminous minerals, viz. muscovite and corundum, where pelitic country rocks have suppressed the formation of sodic (alumina-undersaturated) minerals such as aegirine and riebeckite (Rock 1976).

3.6.2 Biotite-muscovite syenite - product of fenitisation?

As described previously (section 3.3.6) the sövites in the BRC are intruded exclusively into biotite-muscovite syenite. This suggests a genetic relationship, whereby potassic fenitisation of orthoclasite-type has produced K-rich minerals such as muscovite in pelitic country rocks.

3.6.3 Albite syenite - product of fenitisation?

An interesting comparison can be drawn with the discussion on fenites earlier in this chapter, where albitites form fenites around sövite intrusions. From this it is apparent that zonation, from an albite-rich core through to microcline-rich peripheral rocks, may occur (Le Bas 1987). This situation is remarkably similar to that encountered in the BRC, where albite syenite is surrounded by microcline-rich nepheline syenite. It suggests that the albite syenites may represent rheomorphic fenites.

3.6.4 Microsyenite - product of fenitisation?

By analogy with the development of trachytes described by Le Bas (1977), the suggestion is made that perhaps the late-stage, silica-saturated, microsyenite dykes within the BRC have a similar origin. This contention would support the silica gap separating the microsyenites from the remainder of the lithologies, as well as explaining their anomalously low incompatible-element contents.

3.6.5 Characteristics of lamprophyres

From the mineralogy and geochemistry of the biotite-rich dykes it is deduced that they are hydrous, alkaline, CO_2 - and P_2O_5 -rich rock types. In view of these features, and their glistening appearance in the field, it is tempting to classify them as lamprophyres or glimmerites (cf. Boer *et al.* 1990). From a review of the voluminous literature on the subject of lamprophyre classification (Rock 1979 1987 1991), the following points emerge:

- (i) The name lamprophyre derives from the Greek "lampros, porphyros" which means "glistening porphyry". Texturally, lamprophyres are generally porphyritic, without feldspar phenocrysts, although this criterion is not rated as importantly as the mineral assemblage (Rock 1987).
- (ii) Mineral assemblages includes amphibole, biotite/phlogopite, and other minerals rich in F, CO_2 and H_2O . Rock (1987) notes that, in lamprophyres, Mg-rich mafic minerals coexist with alkali feldspar and that low-Mg olivines and muscovite are absent.
- (iii) Monomineralic felsic globular structures are characteristic and may either be microscopic ocelli or macroscopic ovoids and schlieren. Essentially these globules are homogeneous and may contain a wide range of minerals, including alkali feldspar, calcite, feldspathoid, biotite and apatite.
- (iv) Lamprophyres are restricted to outcrops of less than a few square kilometres and generally form dykes, sills, plugs and diatremes.
- (v) The whole-rock chemistry of lamprophyres is highly variable, from calc-alkaline through alkaline, to ultramafic and lamproitic. For given SiO_2 contents, high levels of H_2O , CO_2 , alkalis, Sr, Th, Ba and LREE are characteristic (Rock 1987 1991).
- (vi) Hypabyssal intrusives satisfying the above conditions are restricted to several well-defined associations, with alkaline

lamprophyres characteristic of carbonatite/ syenite complexes, as well as occurring in regional dyke swarms unrelated to central magmatism.

According to Rock (in litt., January 1989), the mineralogy and geochemistry of the Bulls Run biotite-rich dykes suggests "lamprophyric affinities" and, if "...the mineralogy represents the igneous mineralogy, then the correct name would be sannaitite (alkaline lamprophyre), on the recommended Streckeisen terminology". Rock states that "...either the characteristic textures or the chemistry are preserved as far as lower amphibolite facies, but rarely both". He does note, however, note that " ...relict textural features such as globular structures (felsic patches)are often beautifully preserved".

From the above observations it seems highly probable, on the basis of mineralogy, geochemistry, presence of felsic globules, form of intrusion and associated alkaline rocks, that the mafic dykes of the BRC are metamorphosed alkaline lamprophyres.

3.7 Tectono-magmatic discrimination

Nepheline-syenite/carbonatite complexes are generally considered to be restricted to regions of intra-continental rifting (Bailey 1964, Middlemost 1974, Le Bas 1987). The common association of carbonatite/alkaline magmatism with continental rift zones has led to the suggestion that such magmatism is an integral part of rift formation and development (Saggerson 1970, Middlemost 1974). With regard to the tectonic setting of carbonatite magmatism, it is noted that carbonatites are also recorded from within-plate oceanic islands such as Cape Verde, as well as in association with high-K shoshonites along tectonically-active continental margins (Middlemost 1985, Le Bas 1987, Woolley 1989). However, these latter settings are comparatively rare (Le Bas op cit.).

The well-constrained tectonic setting indicated by the nepheline-syenite/carbonatite association has, in comparison with the voluminous literature generated concerning granite tectonic setting, resulted in a dearth of tectonic-discrimination diagrams. One diagram that is available is specifically for potassic rocks with less than 60% SiO₂

(Thompson & Fowler 1986). Thus, four potassic syenites and the three samples of biotite-rich alkaline lamprophyre from Bulls Run have been classified accordingly and, although their Zr contents are relatively low compared with the defined fields, Nb values are sufficiently elevated to indicate intrusion "unrelated to subduction" (Fig. 3.28).

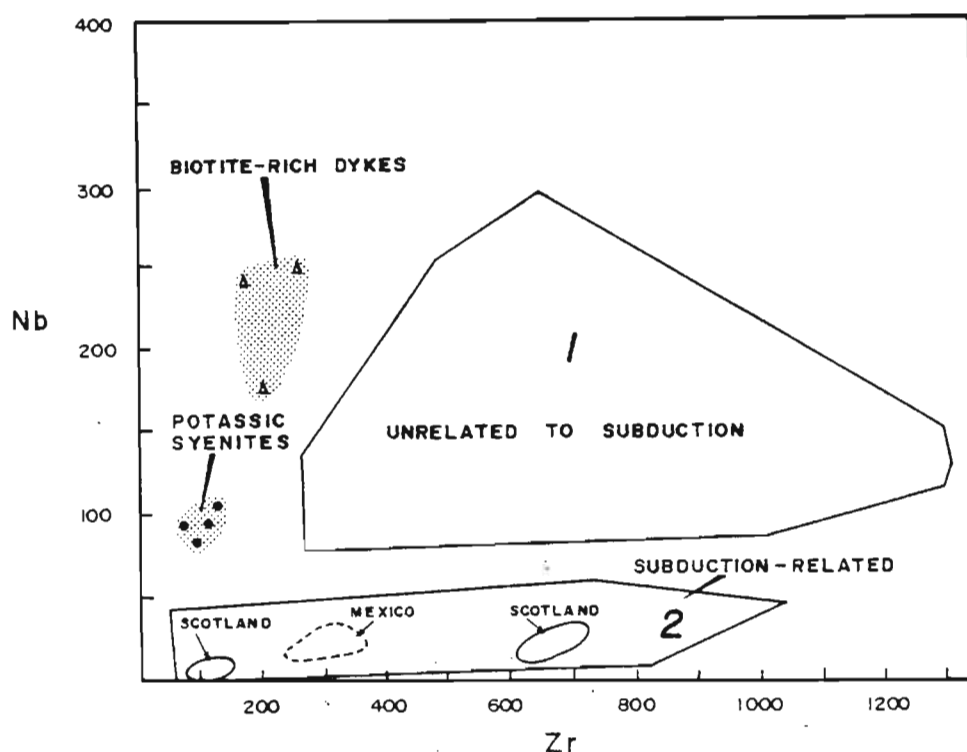


Figure 3.28. Tectonic classification of potassic BRC syenites and biotite-rich lamprophyric dykes, after Thompson & Fowler (1986).

3.7.1 Tectonic discrimination: syenite and carbonatite gneisses

As noted by Currie (1976a), gneissose nepheline syenites and carbonatites within metamorphosed terranes are neither well known nor apparently widely distributed, probably because their recognition in the field is problematic. In this regard, "many other occurrences probably exist, even within known belts" (Currie 1976a, p. 173). Gneissose syenite and/or carbonatite occurrences described in the literature include several Canadian Cordilleran examples (Currie 1976b, Höy & Kwong 1986, Pell & Höy 1989), the well-known Ontario miaskitic syenites (Keith 1939, Payne 1968, Appleyard 1967, 1969, Currie 1976a, 1976b, Windley 1989) and isolated occurrences in Africa (Gellatly & Hornung 1968, Lulin 1985).

The most extensive and best described nepheline-syenite/carbonatite gneiss belts are located in Canada, within the Cordilleran and

Grenvillian orogenic belts of western and eastern Canada respectively (Fig. 3.29). Attention is drawn here to similarities between the BRC and the syenite/carbonatite gneisses in Canada. Therefore, the more important features of the two belts are summarised below, with the emphasis placed on lithological associations and tectonic interpretation:

3.7.2 Cordilleran syenite/carbonatite gneisses

- (i) The alkaline intrusives were emplaced into continental crust prior to the major late Jurassic - early Tertiary Cordilleran Orogeny (Pell & Höy 1989).
- (ii) The igneous province comprises intrusive and extrusive gneissic carbonatites, nepheline syenites, ijolites, and lamprophyres (Currie 1976b, Höy & Kwong 1986, Pell & Höy 1989).
- (iii) The emplacement of these alkaline rocks is related to periodic rifting along the western margin of the North American continent, between c.750 Ma and 340 Ma (Pell & Höy 1989).
- (iv) Pell & Höy (1989) suggest that these extensional episodes relate to the initiation, and subsequent modification by thrusting, of the Cordilleran miogeocline.

3.7.3 Grenvillian miaskitic syenite gneisses

- (i) Pre-tectonic miaskitic alkaline syenites were emplaced into a linear belt of rifted and attenuated continental crust, along the margin of the proto-Grenville Ocean (Windley 1989). The belt extends along a strike length of some 800 km between Ontario and Quebec, immediately south of the Grenville Front (Fig. 3.29). Subsequent ocean closure resulted in northward-directed overthrusting within the rifted continental margin, and transformation of alkaline intrusives into gneissic complexes.

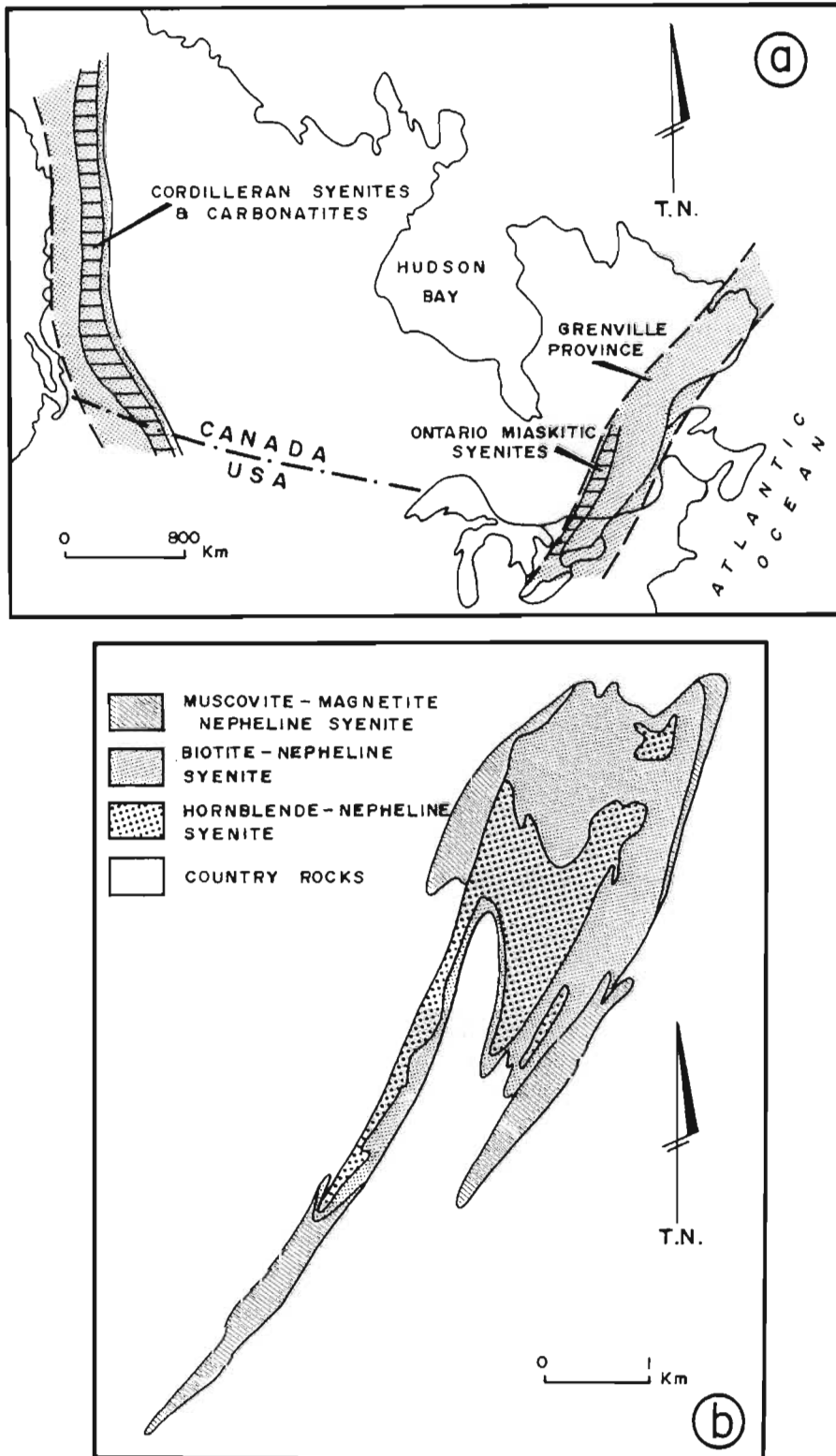


Figure 3.29. Location of the Cordilleran and Grenvillian (Ontario) syenite gneiss belts in Canada (Fig. 3.29a). Simplified geological map of the Blue Mountain syenite gneiss complex (Fig. 3.29b), after Payne (1968).

- (ii) The least-metamorphosed syenites give Rb-Sr ages of c.1285 Ma (eg. Blue Mountain), whereas the higher-grade gneisses have been metamorphically reset, and yield ages of c.1000 Ma (Payne 1968, Currie 1976a)
- (iii) The nepheline syenite bodies are generally rimmed by non-feldspathoidal syenites which may contain corundum and/or muscovite, in addition to magnetite and biotite (Currie 1976a). The Blue Mountain syenite gneiss is a typical example (Payne 1968), being regularly zoned from a core of hornblende-nepheline syenite, through a median shell of biotite-nepheline syenite, to a rim of muscovite syenite with traces of corundum (Fig. 3.29).
- (iv) The muscovite-bearing syenites are suggested either to be country rocks to the nepheline syenites (Currie 1976a), or in-situ differentiation products from an original nepheline syenite intrusive (eg. Blue Mountain: Payne 1968). Muscovite normally mantles corundum, indicating later replacement reactions possibly during metamorphism (Currie 1976a).
- (v) The origin of the Ontario nepheline syenite gneisses has long been controversial, with suggestions such as selective metasomatic replacement of country rocks (Appleyard 1967 1969) or metamorphism of pre-tectonic magmatic intrusives (Keith 1939, Payne 1968, Currie 1976a, Windley 1989). The least-deformed nepheline syenite gneiss in Ontario (viz. Blue Mountain) provides clear evidence for its origin as an alkaline intrusive (Currie 1976a).

From the data presented above, the similarities between the Bulls Run Complex and the Canadian nepheline syenite/carbonatite gneisses are notable. By analogy therefore, it is suggested that the BRC is of comparable origin and was intruded into rifted and attenuated crust, on a continental margin.

3.8 Summary of salient features

- (i) The Bulls Run "Formation" is shown to be complex and to comprise several alkaline rock types, including nepheline syenite, carbonatite and feldspathic ijolite.
- (ii) The useage of the term "complex" to describe the Bulls Run body is recommended in place of "formation".
- (iii) The elongate shape of the Bulls Run Complex is a result of lateral shearing and stretching in an east-west direction.
- (iv) A concentric outcrop pattern has been mapped, in which an envelope of muscovite-rich syenite surrounds a core of nepheline and albite syenites. This situation is similar to that described for the miaskitic syenite gneisses in the Ontario section of the Grenville Province.
- (v) The muscovite-rich syenites are thought to be pelitic country rocks fenitised by potassic fluids emanating from sövite carbonatite intrusions.
- (vi) Mafic biotite-rich dykes are interpreted as alkaline lamprophyres.
- (vii) Rb-Sr isotope data indicate a low initial-Sr ratio and an isochron age of 1138 ± 45 Ma for the nepheline syenites. Low initial Sr ratios for the carbonatites support a comagmatic mantle origin for the syenite and carbonatite.
- (viii) By analogy with miaskitic syenite complexes in Canada, the Bulls Run Complex was probably intruded into the rifted passive margin of a continent. The occurrence of carbonatite within the BRC supports this tectonic interpretation.

Chapter 4

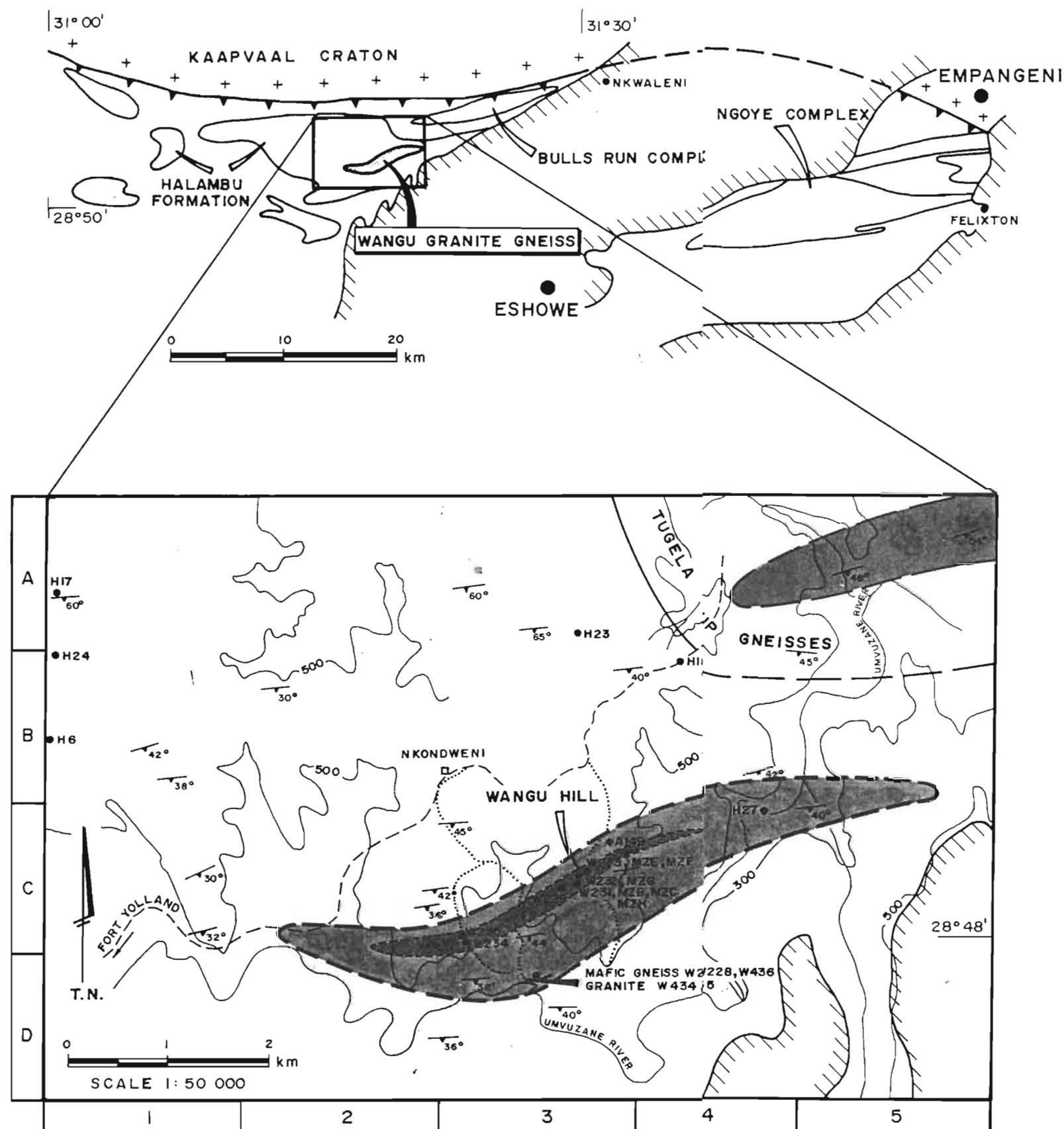
THE WANGU GRANITE

4.1 Introduction

The Wangu Granite is the westernmost of the three alkaline granitoids mapped to date and is located 20 km northwest of Eshowe (Fig. 4.1). Unlike the Ngoye and Bulls Run granitoids, which were identified as discrete entities prior to this study (Charlesworth 1981), the Wangu occurrence has only recently been distinguished from the surrounding Halambu granodiorites (Scogings 1988 1989). The name "Wangu" derives from Wangu Hill, where the peralkaline character of the granites was first recognised.

The Wangu Granite has been described in some detail during the course of this investigation (Scogings 1989 1991b). Therefore this chapter summarises the published data and describes additional unpublished data. In particular, seven additional whole-rock major- and trace-element analyses augment the thirteen samples originally documented (Scogings 1989). Due to financial and logistical constraints, an Rb-Sr isotopic investigation on samples from Wangu has not yet been carried out. This aspect will be dealt with during the next phase of this ongoing study and does not materially affect the compilation of this thesis. A summary of previous research in this area follows:

- (i) Du Toit (1931) assigned the gneisses on Wangu Hill to the predominantly amphibolitic "Tugela Series", in contrast to the granites of the so-called "Alambu mass" to the north of Wangu Hill.



L E G E N D

- W229 GEOCHEMICAL SAMPLE
- 600m CONTOURS IN METRES
- FOOTPATH
- JEEP TRACK
- 45° DIP AND STRIKE
- INFERRED CONTACT
- INFERRED PERIMETER: WANGU GRANITE GNEISS
- NATAL THRUST FRONT
- SANDSTONE, SHALE
- BIOTITE-RICH DYKES
- RIEBECKITE-AEGIRINE GRANITE
- MAGNETITE GRANITE
- SYENITE
- UNDIFFERENTIATED, HALAMBU FORMATION
- GRANITE/GREENSTONE
- PHANEROZOIC COVER
- WANGU GRANITE GNEISS
- BULLS RUN COMPLEX
- TUGELA GROUP
- KAAPVAAL CRATON

FIGURE 4.1

WANGU GRANITE GNEISS

LOCALITY, GEOLOGY AND
GEOCHEMICAL SAMPLE SITES

SCALE AS SHOWN

- (ii) Charlesworth (1981) confirmed the presence of granitoid gneisses within the "Alambu Mass" and incorporated some of Du Toit's "Tugela Series" from the Wangu area into the "Halambu Granite Gneiss Formation" (SACS 1980, Matthews & Charlesworth 1981). On the basis of limited mineralogical and geochemical evidence, Charlesworth classified the Halambu Formation as predominantly granodioritic to tonalitic. However, quartz-monzonite gneisses were noted to the south of Wangu Hill and, from the descriptions by both Charlesworth and Du Toit, it is clear that a compositional break was recognised in the vicinity of Wangu Hill.

Charlesworth (1981) suggested that the Halambu gneisses are deformed, intrusive, calc-alkaline I-type granitoids. Following detailed structural analysis of the Halambu area, he noted that the pervasive east-west foliation within the Halambu Formation as a whole, is axial-planar to northward-verging folds in the surrounding amphibolitic terrane. This suggested that the granodioritic precursors to the Halambu gneisses were intruded prior to the northward-directed compressional thrusting event.

- (iii) Scogings (1988 1989) discovered magnetite- and aegirine-bearing granite gneisses on Wangu Hill, in the southern part of the Halambu outcrop. These are comenditic to pantelleritic in composition, with typical A-type granite trace-element geochemistry. The magnetite granites were noted to be corundum-normative and peraluminous, due to magmatic or metamorphically-induced alkali depletion. The recognition of peralkalinity in this area was a marked departure from the calc-alkaline classification accorded the Halambu Formation by Charlesworth (1981). In addition to the discovery of peralkaline granites at Wangu, intrusive biotite-rich sheets of alkaline lamprophyre affinity were described.

An intracratonic tectono-magmatic setting was proposed for the Wangu granites and alkaline lamprophyres, similar to that envisaged for the Ngoye and Bulls Run Complexes (Scogings 1989, 1990a).

4.3 Field and petrographic descriptions

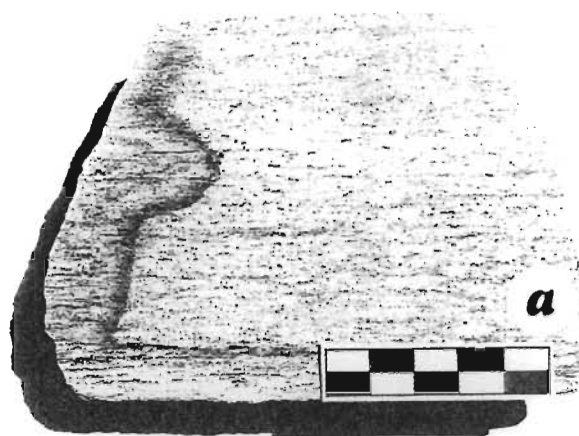
4.3.1 Introduction

Whereas systematic lithological zonation of the Wangu body was not recognised previously (Scogings 1989), the granites are now divided into two lithologies on the basis of distribution and modal mineralogy (Scogings 1991b). According to this division, the body comprises a core of pyroxene- and magnetite-bearing granite surrounded by an envelope of magnetite granite (Fig. 4.1). It has not been possible to define the exact position or nature of the contact between the two granite types in the field. Minor biotite-rich mafic dykes are intrusive into the southern part of the Wangu granite. Representative examples of the Wangu granite and biotite-rich mafic dykes are illustrated as Figure 4.2.

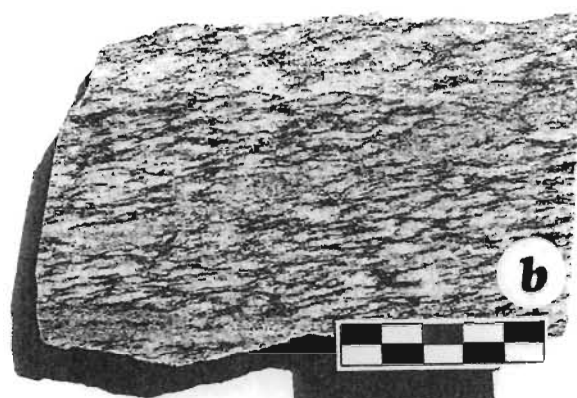
Representative modal analyses are presented as Table 4.1 (complete set of modal data in Appendix 1, Table A1.3), and classification according to the Streckeisen (1976a) QAP ternary diagram is illustrated in Figure 4.3. Microprobe analyses of aegirine-augite are given as Table 4.2. All the Wangu samples are alkali-feldspar rich and they plot along the alkali-feldspar - quartz join, within the alkali-feldspar syenite and alkali-feldspar granite fields. The field of granodioritic/tonalitic Halambu Formation lithologies sampled to the north of Wangu during the course of this study is shown in Figure 4.3 for comparison.

4.3.2 Aegirine-augite granite

This light pink to off-white, fine-grained, lithology forms sheet-like outcrops characterised by a prominent east-west planar foliation dipping at 40 to 50° to the south. Several elongate zones of relatively mafic granite, up to 20 m long and 10 cm wide, were noted on the crest of Wangu Hill. These layers, enriched in magnetite and aegirine-augite, may be cumulates resulting from mechanical concentration of heavy minerals in a highly fluid, volatile-rich melt. Such layering is common within peralkaline intrusions (eg. Illimaussaq, Greenland; Lovozero, USSR: Sorensen 1968).



WANGU MAGNETITE GRANITE



HALAMBU GRANODIORITE



Figure 4.2. Representative rock types from the Wangu area. The hand specimens are magnetite granite (Fig. 4.2a) and Halambu granodiorite (Fig. 4.2b). Characteristic outcrop of biotite-rich sheet, with xenoliths of magnetite granite in the Mvuzane Valley (Fig. 4.2c).

TABLE 4.1

REPRESENTATIVE MODES: WANGU

	H27	M2a	W235	W229	W232	W233	W228	W227	H18
microcline	36	33	42	15	15	10	5	6	17
albite	24	21	25	30	20	17	23	37	51
quartz	34	43	25	40	40	53	--	--	26
biotite	1	t	3	--	--	--	63	45	3
aegirine	--	--	4	4	15	12	--	--	--
opaque	4	3	t	10	8	9	t	t	t
calcite	--	--	--	--	--	--	6	8	--
apatite	--	--	--	--	--	--	3	2	t
spheue	--	--	--	--	t	--	t	t	t
hornblende	--	--	--	--	--	--	--	t	t
sericite	--	--	--	--	--	--	--	--	t
epidote	--	--	--	--	--	--	--	--	t

-- = not detected

H27 = magnetite granite (comenditic)

M2a = magnetite granite (comenditic)

W235 = aegirine granite (comenditic)

W229 = aegirine granite (comenditic)

W232 = aegirine-magnetite granite (pantelleritic cumulate)

W233 = aegirine-magnetite granite (pantelleritic cumulate)

W227, W228 = biotite-rich dykes

H18 = Halambu granodiorite

TABLE 4.2

MICROPROBE ANALYSES

	W323p	W233p
SiO ₂	50.29	52.53
TiO ₂	0.06	0.08
Al ₂ O ₃	0.84	0.95
FeO	24.25	24.02
MnO	1.19	1.32
MgO	3.42	3.20
CaO	11.45	10.64
Na ₂ O	6.15	6.48
Total	97.65	99.22

ions on basis of 6 oxygens

Si	2.056	2.094
Ti	0.002	0.002
Al	0.041	0.045
Fe ²	0.829	0.801
Mn	0.041	0.045
Mg	0.208	0.190
Ca	0.502	0.455
Na	0.488	0.501
Total	4.167	4.133

W232p, W233p = aegirine-augite
Wangu granite

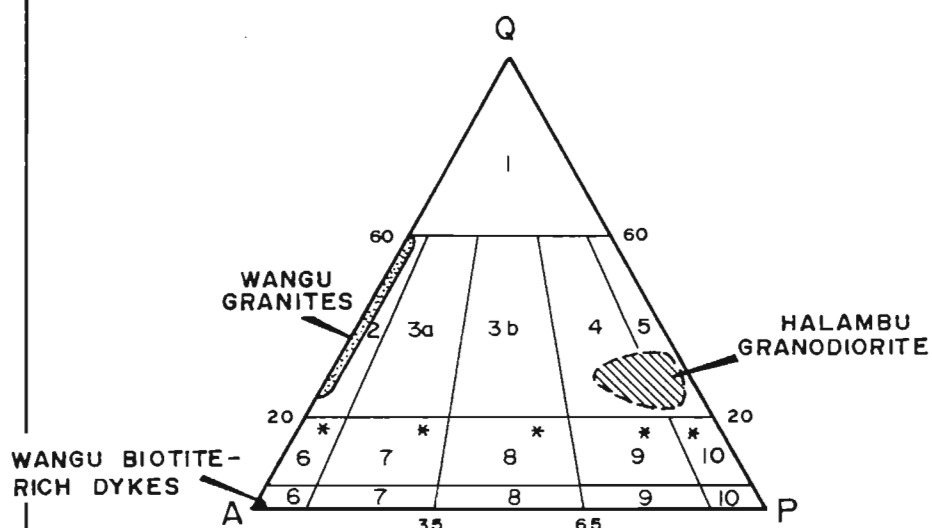


Fig. 4.3. Classification of the Wangu granites, Halambu granodiorite and Wangu biotite-rich dykes on the Streckeisen (1976) QAP diagram. The fields are numbered as follows: 2, alkali-feldspar granite; 3a & 3b, granite; 4, granodiorite; 5, tonalite; 6, alkali-feldspar syenite.

As shown by modal analyses (Table 4.1), the aegirine-augite granite comprises a fine-grained (0.2 to 0.5mm) polygonal assemblage of quartz (25 to 50 modal%), microcline (10 to 40 modal%), albite (20 to 50 modal%), aegirine-augite (up to 15 modal%, Table 4.2 for microprobe data) and magnetite (<10 modal%), with accessory biotite and riebeckite in some samples.

4.3.3 Magnetite granite

This leucocratic lithology forms a broad sheath around the aegirine-bearing granites and, apart from the absence of sodic pyroxene and amphibole, is petrographically very similar. Modally, it comprises quartz (25 to 49 modal%), albite (25 to 45 modal%), microcline (20 to 35 modal%) and magnetite (3 to 8 modal%), with accessory biotite and fluorite.

4.3.4 Biotite-rich dykes

Biotite-rich dykes, up to 30m long and 1m wide, appear to be restricted to the southern part of the Wangu outcrop, within the Mvuzane Valley (Fig. 4.1). These well-foliated mafic rocks intrude peralkaline granite and contain abundant xenoliths of this lithology (Fig. 4.2c). Thin-section examination confirms their well-foliated character and shows them to consist essentially of red-brown biotite flakes (45 to 63 modal%), albite (23 to 37 modal%), microcline (c. 6 modal%), irregular aggregates of calcite (4 to 8 modal%), and rounded apatite grains (c. 2 modal%). Although these rocks are mafic, because the sole felsic constituent is alkali feldspar, they classify as alkali-feldspar syenite on the QAP diagram (Fig. 4.3).

4.3.5 Halambu granodiorite

Five samples of Halambu granodiorite were collected at the sites indicated on Figure 4.1, for comparison with Wangu granitoids. Modal analysis (Table 4.1, Fig. 4.3) confirms Charlesworth's (1981) classification of the typical Halambu lithology as granodiorite or tonalite. Essentially they comprise saussuritised plagioclase (50 to 70 modal%), microcline (3 to 17 modal%) and chloritised biotite (1 to 5 modal%), with accessory hornblende.

4.4 Geochemistry

4.4.1 Introduction

Major- and trace-element geochemistry, together with CIPW norms and mesonorms for representative lithologies, are presented as Tables 4.3, 4.4 & 4.5. Five samples of Halambu granodiorite from north of Wangu Hill were analysed for comparative purposes: representative sample H18 is considered to be typical of this lithology (cf. Charlesworth 1981). A complete data set is to be found in Appendices 2 and 3 (Tables A2.3 and A3.3).

The magnetite- and aegirine-augite granites (excluding the mafic-rich cumulates) have moderately peralkaline geochemistry, with low Al_2O_3 , CaO, Sr and Ba, in conjunction with elevated Zn, Nb, Zr and REE, compared with average granites. In this respect they are similar to peralkaline comendites from the Naivasha volcanic field in the Kenya Rift Valley (Table 4.3). Compared with the average comendite and pantellerite, the Wangu granites are relatively potassic, a feature shared with some of the Naivasha comendites. The mafic-rich cumulates from the centre of the Wangu body have unusual geochemistry and, from the data presented in Table 4.3, are broadly comparable with the average pantellerite. This observation applies particularly to Al_2O_3 and K_2O depletion, elevated $\text{Na}_2\text{O}/\text{K}_2\text{O}$ ratios (Fig. 4.4a) and enrichment in $\text{Fe}_2\text{O}_3(\text{tot})$.

With reference to Table 4.4, the biotite-rich dykes are potassic (Fig. 4.4a), enriched with respect to total alkalis, CO_2 and incompatible elements (eg. Nb) and are broadly similar to such alkaline mafic rocks as nephelinite, alkaline lamprophyre and ultrapotassic rocks.

4.4.2 Alumina saturation

The Wangu granitoids are dominantly peralkaline in terms of the Bonin (1986) ternary plot (Fig. 4.4b), alkaline to peralkaline using Wright's (1969) alkalinity diagram (Fig. 4.5a), and alkaline according to the diagram devised by Sylvester (1989) (Fig. 4.5b). Their overall peralkalinity is corroborated by normative acmite and riebeckite in most of the samples (Table 4.5).

TABLE 4.3

REPRESENTATIVE GEOCHEMICAL ANALYSES: WANGU GRANITES)

	H27	MZa	W235	W229	W232	W233	A	B	C	D	H18
SiO ₂	70.88	79.75	68.41	79.20	61.16	73.12	73.9	71.9	75.70	73.50	72.27
TiO ₂	0.41	0.13	0.68	0.21	0.31	0.31	0.2	0.4	0.26	0.34	0.13
Al ₂ O ₃	10.89	10.11	11.96	8.94	5.79	5.19	12.4	9.4	11.09	10.59	14.80
Fe ₂ O ₃	1.52	2.73	5.91	4.10	20.15	11.37	1.1	2.4	2.65	1.67	0.29
FeO	6.22	ND	1.25	0.25	3.24	2.00	1.9	4.3	0.04	1.93	1.46
MnO	0.25	0.02	0.20	0.14	0.50	0.45	nd	nd	0.04	0.04	0.03
MgO	0.41	0.01	0.59	0.17	0.99	0.88	0.1	0.1	0.02	0.03	0.35
CaO	0.15	0.05	0.67	0.18	2.82	2.25	0.5	0.5	0.26	0.55	1.89
Na ₂ O	3.25	2.83	4.21	4.60	3.90	3.32	5.4	6.4	4.67	5.57	5.42
K ₂ O	5.09	4.06	6.38	2.08	1.18	0.60	4.6	4.5	4.52	4.46	2.63
P ₂ O ₅	--	--	0.01	--	0.04	0.04	--	0.1	--	--	0.04
LOI	0.17	0.51	0.20	0.40	0.86	0.82	nd	nd	0.55	1.51	0.24
CO	nd	nd	nd	nd	nd	nd	nd	nd	nd	nd	nd
Total	99.24	100.20	100.47	100.27	100.94	100.35	100.1	100.0	99.80	100.19	99.55
Zn	242	91	123	612	898	584	231	357	171	321	33
Ga	33	18	29	27	31	23	nd	nd	nd	nd	22
Nb	245	264	303	295	567	614	146	237	289	358	17
Zr	1095	1458	1549	1795	3076	3730	1019	1557	891	1419	155
Y	103	88	133	95	385	541	157	201	149	207	9
U	--	4	7	5	9	10	nd	nd	10	15	--
Th	42	37	109	47	78	115	24	27	52	71	5
Pb	32	15	82	166	19	13	nd	189	36	48	23
Rb	255	165	294	78	49	38	nd	189	368	408	67
Sr	22	13	9	4	20	29	11	4	2	--	1205
Ba	217	100	62	59	287	111	167	144	4	1	1312
La	208.1	nd	247.2	124.1	705.8	929	175	253	80	138	nd
Ce	403.2	nd	459.7	275.9	421.1	837	269	345	158	272	nd
Pr	40.6	nd	47.6	26.9	145.4	nd	nd	nd	nd	nd	nd
Nd	147.8	nd	169.8	100.1	603.8	1052	nd	nd	67	110	nd
Sm	25.5	nd	31.0	19.9	116.9	nd	nd	nd	17	28	nd
Eu	1.3	nd	2.4	1.7	21.0	nd	nd	nd	nd	nd	nd
Gd	21.5	nd	27.2	18.5	106.4	nd	nd	nd	21	30	nd
Dy	20.5	nd	30.9	23.2	93.3	nd	nd	nd	nd	nd	nd
Ho	4.3	nd	5.8	4.5	16.3	nd	nd	nd	nd	nd	nd
Er	12.8	nd	16.2	13.2	38.2	nd	nd	nd	nd	nd	nd
Yb	12.0	nd	15.3	13.4	34.4	nd	nd	nd	16	22	nd
Lu	1.8	nd	2.2	1.9	4.8	nd	nd	nd	2	3	nd
P.I.	0.99	0.90	1.16	1.10	1.33	1.18	1.12	1.64	1.14	1.32	0.79
Na ₂ O+K ₂ O	8.34	6.89	10.59	6.68	5.08	3.92	10.00	10.90	9.19	10.03	8.05
Na ₂ O/K ₂ O	0.64	0.70	0.66	2.21	3.31	5.53	1.17	1.42	1.03	1.25	2.06
Rb/Sr	11.59	12.69	32.67	19.50	2.45	1.31	0.00	47.25	184.00	0.00	0.66
Y/Nb	0.42	0.33	0.44	0.32	0.68	0.88	1.08	0.85	0.52	0.58	0.53

-- = not detected

nd = not determined

H27, MZa = magnetite granite (comenditic)

W235, W229 = aegirine granite (comenditic)

W232, W233 = aegirine-magnetite granite (pantelleritic)

A = average comendite (Hill & Thomas 1983)

B = average pantellerite (Hill & Thomas 1983)

C, D = Naivasha comendites (MacDonald et al. 1987)

H18 = Halambu granodiorite

TABLE 4.4

GEOCHEMISTRY: WANGU BIOTITE-RICH DYKES WITH COMPARATIVE ANALYSES

	W228	W436	W227	A	B	C	D	E	F	G
SiO ₂	39.23	47.04	51.24	42.50	51.00	40.60	52.70	39.06	43.15	46.74
TiO ₂	3.84	3.50	1.19	2.90	1.10	2.66	2.40	4.36	3.71	0.75
Al ₂ O ₃	12.25	13.46	12.75	13.70	14.00	14.33	10.80	8.18	12.24	12.30
Fe ₂ O ₃	1.71	1.66	1.33	12.00	8.20	5.48	nd	4.61	13.08	3.30
FeO	12.07	11.95	5.57	nd	nd	6.17	5.10	4.98	nd	4.59
MnO	0.51	0.26	0.35	0.20	0.13	0.26	0.09	0.26	0.20	0.19
MgO	9.96	5.39	5.54	7.10	7.00	6.39	8.40	17.66	8.54	8.96
CaO	6.83	5.71	7.42	10.30	7.00	11.89	6.70	10.40	11.83	15.35
Na ₂ O	1.55	2.75	3.82	3.00	2.70	4.79	1.30	0.18	2.03	0.81
K ₂ O	7.14	4.17	5.22	2.00	3.10	3.46	10.40	6.98	3.40	4.59
P ₂ O ₅	1.24	0.70	0.97	0.74	0.60	1.07	1.50	0.61	0.62	0.34
LQI	0.71	2.48	1.21	3.10	2.40	2.19	nd	1.92	nd	0.22
CO	2.44	nd	3.29	2.00	2.00	0.60	nd	--	nd	nd
Total	99.48	99.07	99.90	99.54	99.23	99.89	99.39	99.20	98.80	98.14
Zn	771	343	451	98	88	nd	nd	nd	nd	nd
Ga	40	25	24	19	18	nd	nd	nd	nd	nd
Nb	390	45	159	101	13	nd	74	nd	108	7
Zr	273	157	312	313	190	nd	1440	900	306	182
Y	86	34	114	31	23	nd	20	nd	29	28
U	9	1	5	nd	nd	nd	nd	nd	2	nd
Th	17	2	45	nd	nd	nd	nd	nd	11	nd
Pb	64	nd	25	nd	nd	nd	nd	nd	nd	nd
Rb	635	393	471	50	70	nd	253	450	127	396
Sr	341	495	1445	990	715	nd	2840	7000	1005	791
Ba	1325	969	1459	930	1050	nd	6600	7500	1119	738
La	146.8	nd	212.9	66	53	nd	213	80	81	52
Ce	278.2	nd	436.2	125	110	nd	427	nd	164	124
Pr	30.9	nd	49.1	14	11	nd	nd	nd	nd	56
Nd	124.6	nd	192.2	54	56	nd	166	nd	64	11
Sm	21.9	nd	29.9	11	11	nd	21	nd	11	2
Eu	5.3	nd	5.8	3	3	nd	5	nd	3	9
Gd	18.3	nd	20.7	8	11	nd	11	nd	8	nd
Dy	15.4	nd	16.5	5	4	nd	4	nd	nd	nd
Ho	2.8	nd	3.2	1	1	nd	nd	nd	nd	nd
Er	7.3	nd	9.1	3	2	nd	nd	nd	nd	nd
Yb	6.5	nd	9.4	2	2	nd	1	nd	2	2
Lu	0.9	nd	1.5	nd	nd	nd	nd	nd	nd	nd
P.I.	0.84	0.84	0.94	0.52	0.56	0.81	1.24	0.96	0.57	0.51
Na ₂ O+K ₂ O	8.69	6.92	9.04	5.00	5.80	8.25	11.70	7.16	5.43	5.40
Na ₂ O/K ₂ O	0.22	0.66	0.73	1.50	0.87	1.38	0.13	0.03	0.60	0.18
Rb/Sr	1.86	0.79	0.33	0.05	0.10	nd	0.09	0.06	0.13	0.50

-- = not detected

W228, W436, W227 = Wangu Dykes

A = average alkaline lamprophyre (Rock 1991)

B = average calc-alkaline lamprophyre (Rock 1991)

C = average nephelinite (Le Maitre 1976)

nd = not determined

D = Group 1 ultrapotassic lamproite (Wilson 1987)

E = Group 2 ultrapotassic Mafurite (Wilson 1987)

F = Potassic lava, East African Rift (Wilson 1987)

G = Group 3 ultrapotassic leucitite (Wilson 1987)

TABLE 4.5

REPRESENTATIVE NORMS: WANGU

CIPW NORMS

	H27	MZa	W235	W229	W232	W233	W228	W227	H18
Quartz	27.11	46.20	19.93	44.90	31.32	48.66	--	--	25.53
Corundum	--	0.97	--	--	--	--	--	--	--
Orthoclase	30.27	24.08	37.52	12.28	6.92	3.54	14.11	31.19	15.66
Albite	27.67	24.03	25.87	34.36	23.05	23.34	--	31.57	46.21
Anorthite	0.09	0.25	--	--	--	--	5.44	2.25	8.32
Leucite	--	--	--	--	--	--	22.39	--	--
Nepheline	--	--	--	--	--	--	7.18	0.60	--
Acmite	--	--	8.44	3.98	8.56	4.17	--	--	--
Wollastonite	--	--	--	--	2.89	2.03	--	--	--
Diopside	1.23	--	2.54	0.70	5.29	4.73	4.41	6.74	0.71
Hypersthene	10.40	3.33	0.28	0.10	--	--	--	--	2.81
Olivine	--	--	--	--	--	--	28.01	13.50	--
Magnetite	2.23	0.65	2.70	0.65	11.10	7.01	2.51	1.95	0.42
Ilmenite	0.78	0.21	1.29	0.40	0.58	0.59	7.37	2.29	0.25
Haematite	--	--	1.10	2.27	9.59	5.09	--	--	--
Sphene	--	--	--	--	--	--	--	--	--
Apatite	--	--	0.02	--	0.09	0.09	2.91	2.27	0.09
Calcite	--	--	--	--	--	--	5.61	7.58	--
Zircon	0.22	0.28	0.31	0.36	0.61	0.75	0.06	0.06	--
Total	100.00	100.00	100.00	100.00	100.00	100.00	100.00	100.00	100.00

MESONORMS

Quartz	32.29	47.57	21.27	45.94	28.87	47.80	0.56	6.36	27.11
Corundum	0.01	1.06	--	--	--	--	1.99	--	--
Orthoclase	21.80	21.51	36.17	11.89	4.66	1.52	4.05	11.34	13.07
Albite	27.67	24.02	25.87	34.36	23.05	23.34	13.26	32.69	46.18
Anorthite	0.06	--	--	--	--	--	--	2.25	8.34
Biotite	14.72	4.52	1.94	0.56	3.24	2.91	60.63	30.85	4.31
Wollastonite	--	--	0.38	0.07	5.27	4.11	--	1.71	0.16
Hypersthene	--	--	--	--	--	--	--	--	--
Riebeckite	--	--	7.57	2.50	16.00	8.29	--	--	--
Magnetite	2.22	0.80	--	--	--	1.64	2.51	1.95	0.42
Haematite	--	--	4.81	3.81	17.45	8.79	--	--	--
Sphene	1.01	0.18	1.66	0.51	0.76	0.76	7.65	2.95	0.32
Rutile	--	0.06	--	--	--	--	0.77	--	--
Apatite	--	--	0.02	--	0.09	0.09	2.91	2.27	0.09
Zircon	0.22	0.28	0.31	0.36	0.61	0.75	0.06	0.06	--
Calcite	nd	nd	nd	nd	nd	nd	5.61	7.57	nd
Total	100.00	100.00	100.00	100.00	100.00	100.00	100.00	100.00	0.00

nd = not determined
 -- = not detected
 H27, MZa = magnetite granite
 W235, W229 = aegirine granite

W232, W233 = aegirine-magnetite granite
 W228, W227 = biotite-rich dykes
 H18 = Halambu granodiorite

However, as displayed on the Bonin diagram (Fig. 4.4b) minor variations of alumina/alkali ratios in low-CaO rocks can produce significant shifts along the base of the diagram. In this context some of the Wangu granites, mainly the magnetite-bearing lithologies, are corundum-normative and plot just within the peraluminous field. However, this alumina-oversaturated character is inconsistent with their peralkaline trace-element geochemistry (Scogings 1989). Therefore, the current peraluminous status of the magnetite granites is interpreted as being a result either of alkali loss during metamorphism or post-magmatic halide-rich vapour loss, as described for extrusive peralkaline rhyolites (cf. MacDonald 1975, Hill & Thomas 1983, Bourne 1986, Seyler 1986, Winchester & Max 1987, Kumarapeli *et al.* 1989). With regard to the effects of alkali loss on mineralogy, Floor (1974) and Winchester & Max (1987) noted that this results in the conversion of alkali amphiboles and pyroxenes to magnetite, with the release of Zr to form discrete zircon. This minerals assemblage is not characteristic of peralkaline rocks, where zircon is an atypical modal phase.

The mafic dykes classify as metaluminous on the Bonin (1986) diagram, in keeping with the occurrence of CIPW-normative anorthite and diopside (Table 4.5). These rocks provide an insight into the effect on silica saturation when K^+ is used to form biotite in the mesonorm. For example, whereas the CIPW norm of sample W228 is undersaturated and contains leucite and nepheline, the mesonorm more accurately reflects the modal analysis and essentially comprises biotite and albite.

4.4.3 Degree of peralkalinity

Peralkaline granites are classified according to normative femic mineral contents either as comendite or pantellerite (MacDonald & Bailey 1973, MacDonald 1975, Seyler 1986). As shown in Figure 4.5c, the Wangu granites plot as two distinct groups; whereas the mildly peralkaline leucocratic granites fall in the comendite field, the relatively mafic aegirine-augite cumulates classify as pantellerite. However, in terms of their low total alkalis and exceptionally elevated iron content, the latter are not strictly comparable with pantellerites (Table 4.3, analysis B). Nonetheless, the term "pantellerite" is used to facilitate discussion and to highlight the marked differences between these and the comenditic lithologies.

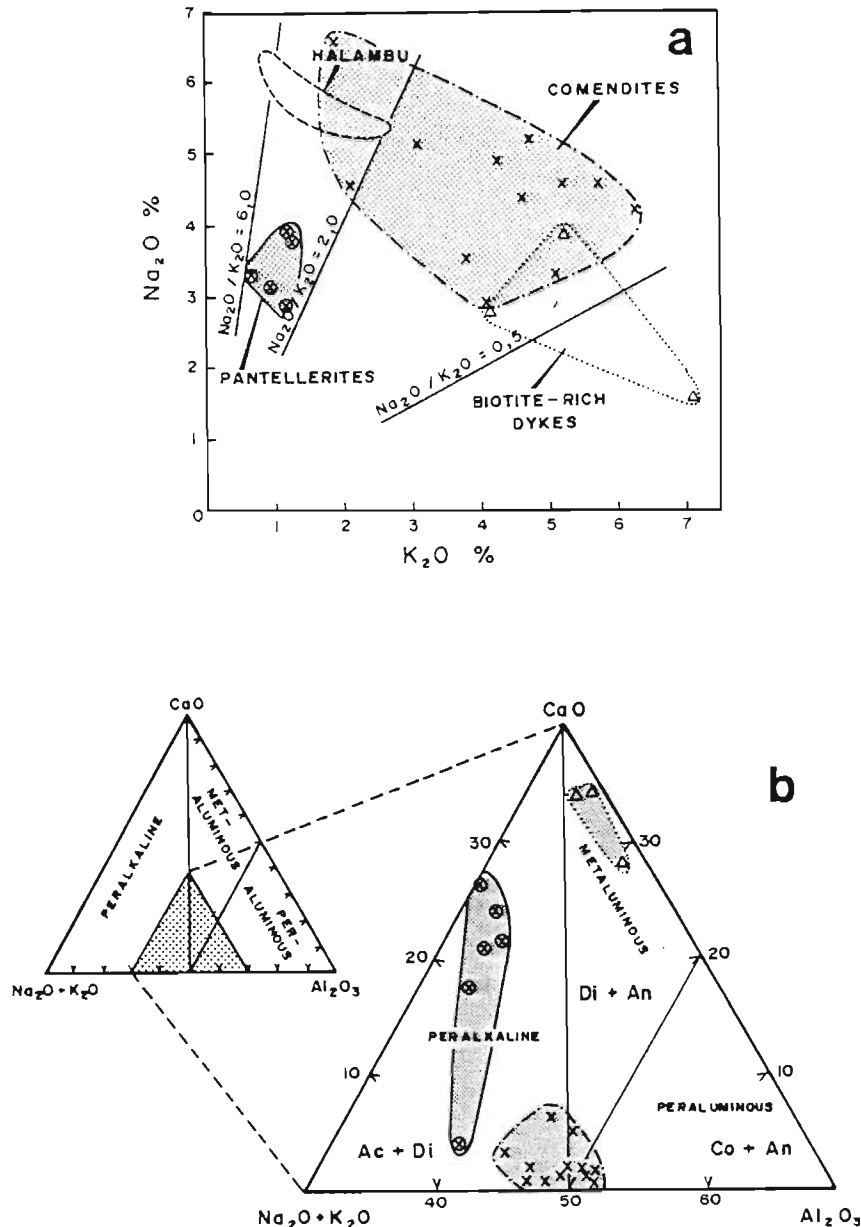


Figure 4.4. Alumina saturation and $\text{Na}_2\text{O}/\text{K}_2\text{O}$ characteristics of the Wangu granites, biotite-rich rocks and Halambu granodiorite.

Fig. 4.4a. Discrimination of the various Wangu lithologies according to their $\text{Na}_2\text{O}/\text{K}_2\text{O}$ ratios. The Halambu granodiorites are included for comparison.

Fig. 4.4b. Alumina saturation relative to $\text{Na}_2\text{O} + \text{K}_2\text{O}$ and CaO , after Bonin (1986). The Wangu granites plot predominantly within the peralkaline field, whereas the Halambu granodiorites are metaluminous.

Symbols: (x) magnetite/aegirine-augite granites, (⊗) mafic cumulates, (Δ) biotite-rich dykes.

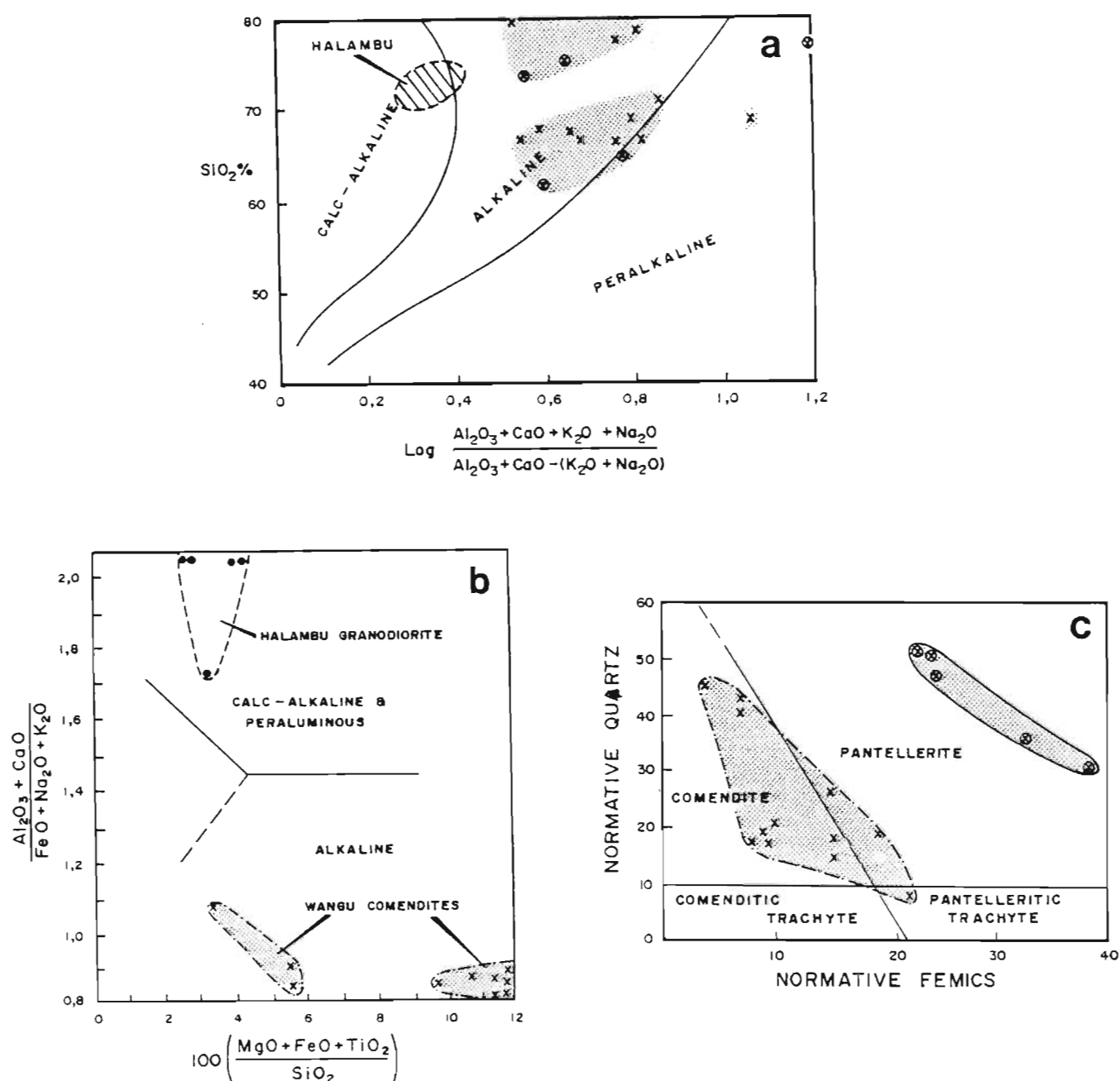


Figure 4.5. Alkalinity and degree of peralkalinity of the Wangu granites. Symbols as in Fig. 4.4

Fig. 4.5a. Alkalinity vs silica diagram after Wright (1969), showing the predominantly alkaline/peralkaline character of the Wangu granites, compared with the calc-alkaline nature of the Halambu granodiorites.

Fig. 4.5b. Classification of the Wangu granites as alkaline, according to the parameters suggested by Sylvester (1989). Due to their extremely low Al₂O₃ contents relative to FeO, the mafic-rich cumulates have not been plotted.

Fig. 4.5c. Classification of the Wangu granites using normative quartz vs total normative femics. Diagram for silica-saturated peralkaline extrusive rocks devised by MacDondald & Bailey (1973).

4.4.4 Nomenclature based on geochemical parameters

- (i) **R1-R2 classification:** When plotted on the R1-R2 diagram of de la Roche et al. (1980), the Wangu granites range in composition from quartz syenite to alkali granite, in contrast to the Halambu samples that fall within the granodiorite field (Fig. 4.6a). The three biotite-rich dyke samples classify as essexite and syenodiorite.
- (ii) **Normative classification:** The normative classification of Streckeisen & Le Maitre (1979) provides very similar nomenclature to the modal QAP diagram (Fig. 4.6b). Thus the Halambu rocks classify as granodiorite and tonalite and are distinctly different from the Wangu lithologies that plot as quartz alkali-feldspar and alkali-feldspar granite. As noted previously (Section 3.4.6) the biotite-rich dykes are not recommended for classification using normative constituents.
- (iii) **Classification using immobile elements:** In view of the observation that minor alkali-loss may have occurred in the magnetite granites, these lithologies have been compared with the other Wangu granites using relatively immobile elements, as suggested by Winchester & Floyd (1977) and Winchester & Max (1987). The broadly comenditic composition of the magnetite granites is confirmed on the SiO_2 vs Zr/TiO_2 discrimination diagram (Fig. 4.6c).

4.4.5 A-type classification (Ga/Al)

Good discrimination between I-, S-, M- and A-type granites is achieved using Ga/Al plotted against incompatible trace elements (Whalen et al 1987). According to these parameters the Wangu granites are clearly A-types, as a result of their elevated Ga/Al ratios and high incompatible-element contents (Fig. 4.7).

4.4.6 Harker diagrams

Selected major- and trace-element data for the Wangu granites are plotted on Harker diagrams (Fig. 4.8). The three biotite-rich dyke

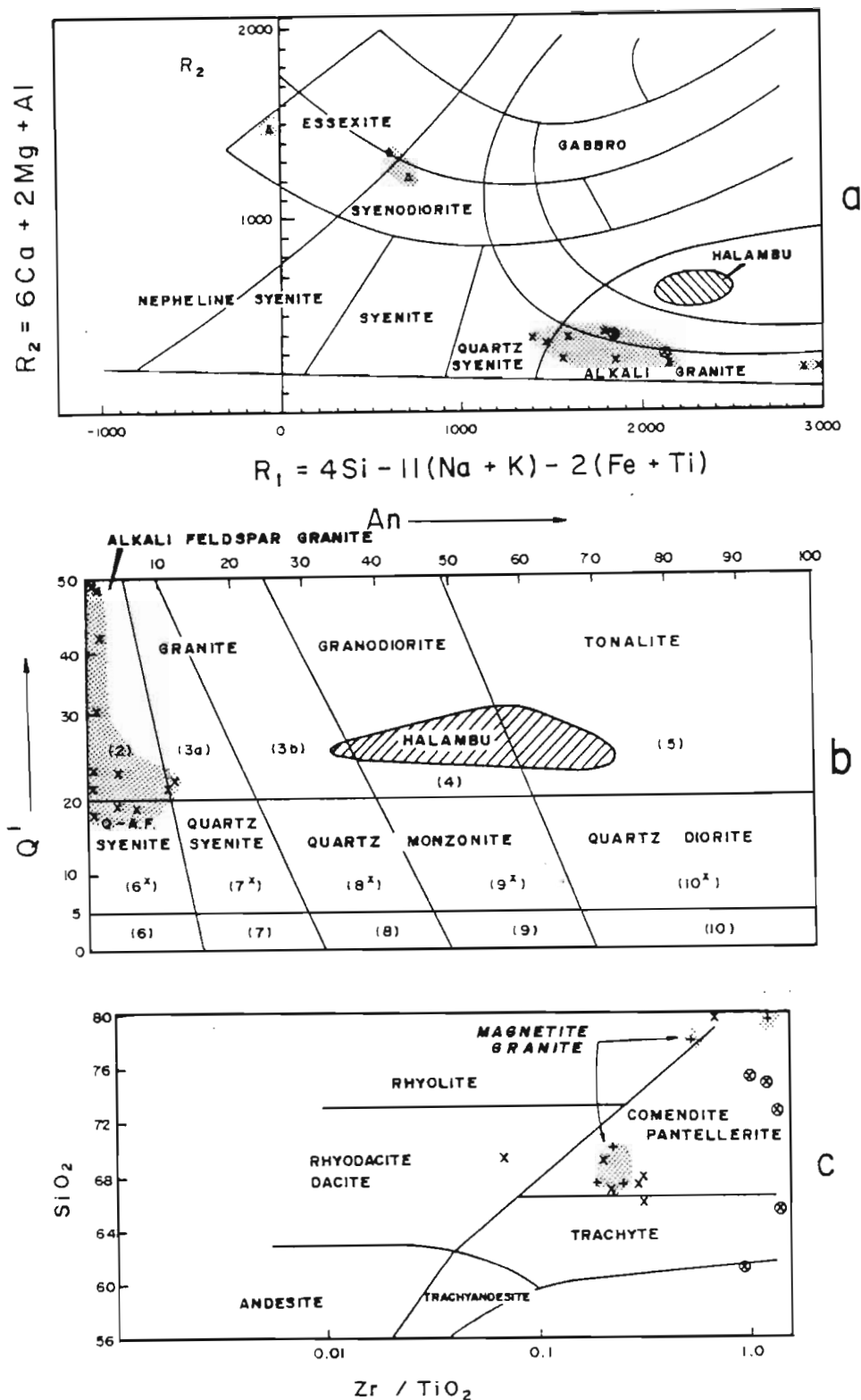


Figure 4.6. Classification of the Wangu granites and biotite-rich dykes according to major- and trace-element characteristics. Symbols as in Fig. 4.4

Fig. 4.6a. Classification using the R_1 - R_2 multicationic system devised by de la Roche *et al.* (1980).

Fig. 4.6b. Normative classification based on the Q' versus An' diagram of Streckeisen & Le Maitre (1979).

Fig. 4.6c. Classification of the Wangu lithologies using relatively immobile trace elements, with fields for volcanic rocks from Winchester & Floyd (1977).

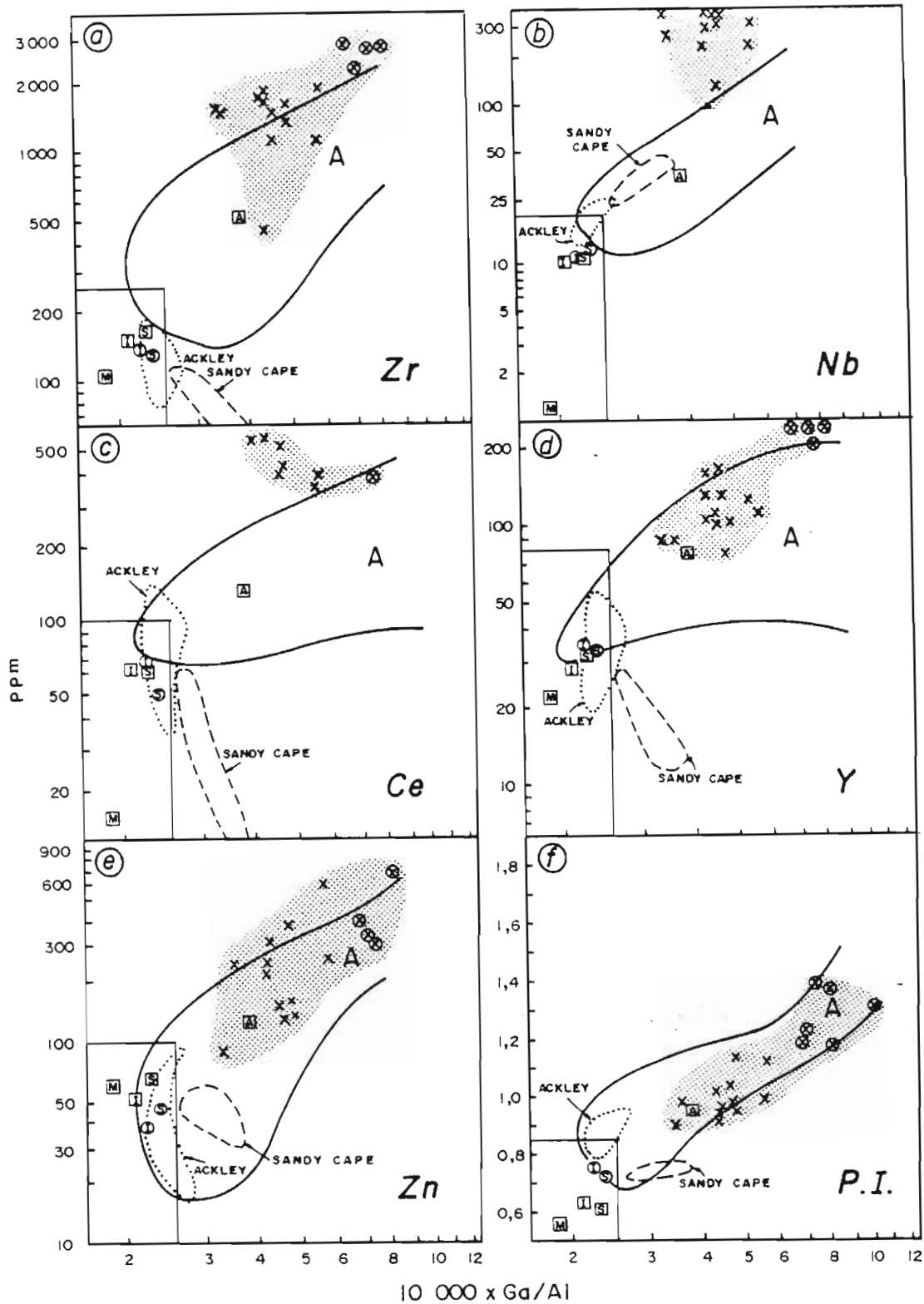


Figure 4.7. Plot of trace element and peralkalinity indices versus $10\,000 \times \text{Ga}/\text{Al}$ for the Wangu granites. The rectangular field, with Ga/Al of less than 2.6, is the field of M-, I- and S-type granites. Average granite compositions are given as boxed letters. The field of A-type granites is delineated by the solid curved line and, for comparison, the fields of two fractionated felsic I- and S-type granites are shown as dashed outlines. Data for the various fields and granite types from Whalen *et al.* (1987). Symbols: (x) comenditic granite, (⊗) pantelleritic granite.

samples have not been plotted on Figure 4.8 due to their low SiO_2 contents, but are referred to in the text below:

- (i) SiO_2 contents for the granites vary between 61 and 79%. The comenditic granites are bimodally distributed and essentially have silica values that are complimentary to the Fe-rich pantelleritic granite cumulates. Although the geochemical database for the biotite dykes is limited, they are characterised by much lower SiO_2 contents (40 to 50%) than the granites (Table 4.4).
- (ii) Within the granites, Al_2O_3 , TiO_2 , $\text{FeO}(\text{tot})$ and CaO vary inversely with respect to SiO_2 , a feature which is considered to reflect fractionation of feldspar and mafic minerals. The two samples of comenditic granite, with elevated CaO contents relative to silica, contain modal fluorite. Due to the limited number of mafic dyke analyses available it is not possible to comment on trends for these elements other than to note elevated TiO_2 , CaO and P_2O_5 values relative to the granites.
- (iii) Na_2O and K_2O in the granite analyses do not covary with SiO_2 to any marked degree, although a trend towards lower total-alkali contents with increasing SiO_2 is indicated. From Table 4.4 it is apparent that total alkalis are fairly constant (7 to 9%) in the mafic dykes, but that $\text{Na}_2\text{O}/\text{K}_2\text{O}$ ratios increase with increasing SiO_2 .
- (iv) For given SiO_2 contents the aegirine-rich pantelleritic granites have much lower Al_2O_3 , Na_2O and K_2O than the comendites, but are relatively enriched in FeO , CaO and MgO . From modal mineralogy it is clear that these trends are controlled by the relative abundance of aegirine and magnetite, in conjunction with low feldspar contents, in the pantelleritic lithologies.
- (v) A two-fold enrichment in incompatible trace elements, eg. Zr (cf. Nb, Zn, Y & REE, Table 4.2) characterises the pantellerites (c. 3000 ppm Zr) compared with the comendites (c. 1500 ppm Zr).

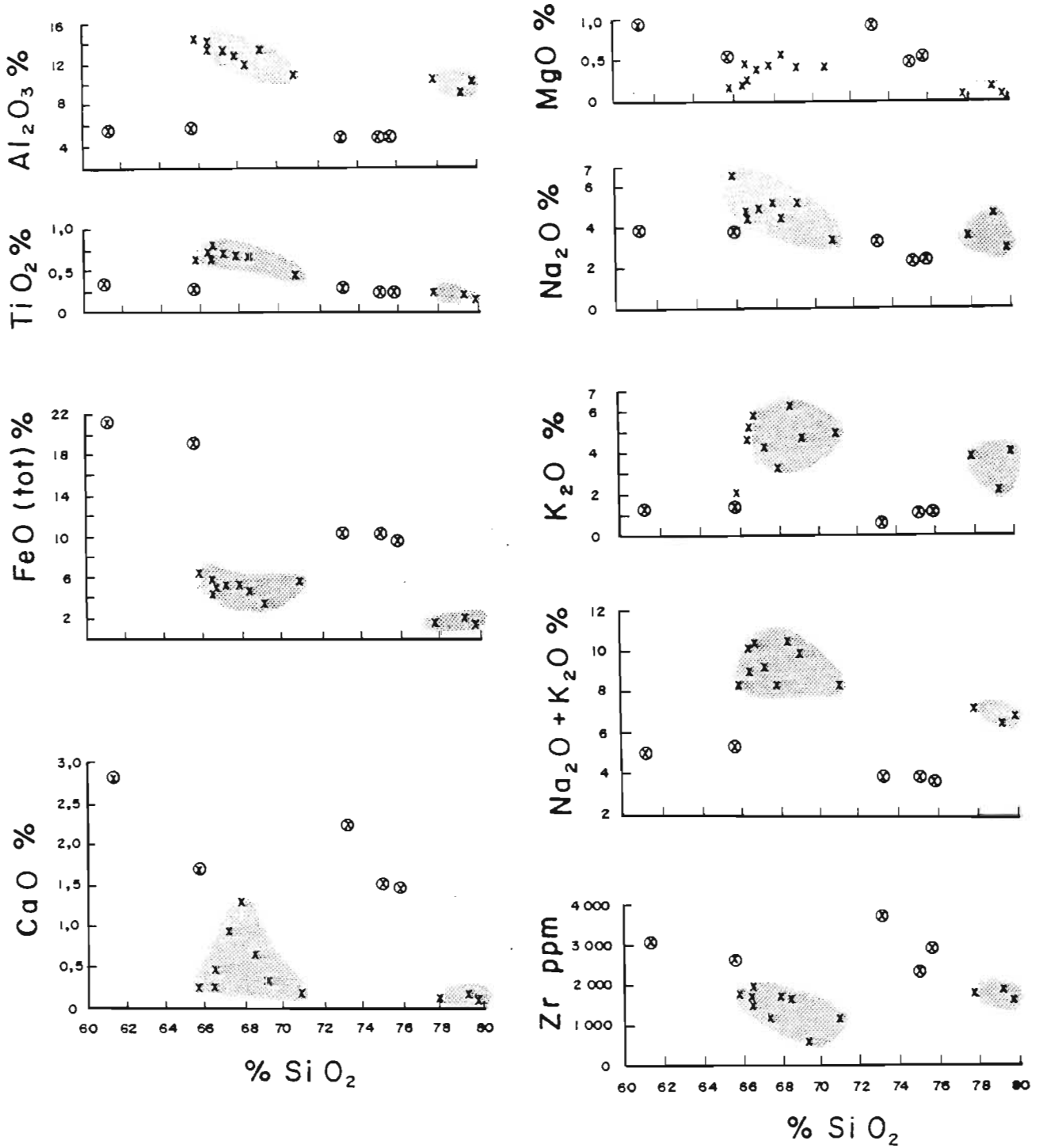


Figure 4.8. Selected major- and trace-element data from the Wangu granites plotted on Harker variation diagrams. Major-element oxides in %, trace elements in ppm. Symbols: (x) comenditic granite, (⊗) pantelleritic granite.

4.4.7 K₂O/Rb ratios

Constant K₂O/Rb ratios for the Wangu granites (Fig. 4.9) indicate evolution along a normal magmatic differentiation trend of constant K₂O/Rb ratios (Shaw 1969, Bowden & Kinnaird 1984). Thus these rocks do not show the Rb-enrichment trend noted in the Ngoye Complex, which is anomalous in view of the observation (Bowden & Kinnaird 1984) that Rb enrichment along the pegmatitic-hydrothermal trend is characteristic of subvolcanic alkaline granite complexes. This indicates that the Wangu granites may have crystallized soon after emplacement, precluding the development of pegmatitic-hydrothermal fluids by fractionation processes during protracted cooling. Their fine-grained character, if reflecting original textures, supports this contention of rapid cooling.

4.4.8 Incompatible-element ratios

For any particular suite of alkaline granites Nb/Y ratios tend to remain fairly constant during fractionation (Eby 1990). Nb/Y ratios for the Wangu granites and biotite-rich dykes are fairly well constrained (Fig. 4.13a) and, therefore, support a comagmatic origin (Nicholls 1988, Eby 1990).

4.4.9 Rare earth elements

Chondrite-normalized REE patterns for representative Wangu lithologies are presented (Figs 4.10a, b) and the following characteristics noted:

- (i) Apart from W232, the remainder of the granite samples exhibit comparable patterns, with moderate LREE enrichment (La/Lu: 3.67 to 18.43) and negative Eu anomalies (Eu/Eu*: 0,16 to 0,28). The unusual negative Ce anomaly exhibited by W232 may relate to its high Fe₂O₃/FeO ratio (Table 4.3) and to formation under highly oxidizing conditions (Cullers & Graf 1984).
- (ii) As indicated by their chondrite-normalized REE plots, the two mafic dykes display LREE-enriched patterns (La/Lu: 6.49 to 15.04), with slight negative Eu anomalies (Eu/Eu*: 0,68 to 0,79) typical of alkaline mafic rocks (Fig. 4.10b). A Karoo nephelinite and Bulls Run carbonatite have been included for comparison and define similar trends.

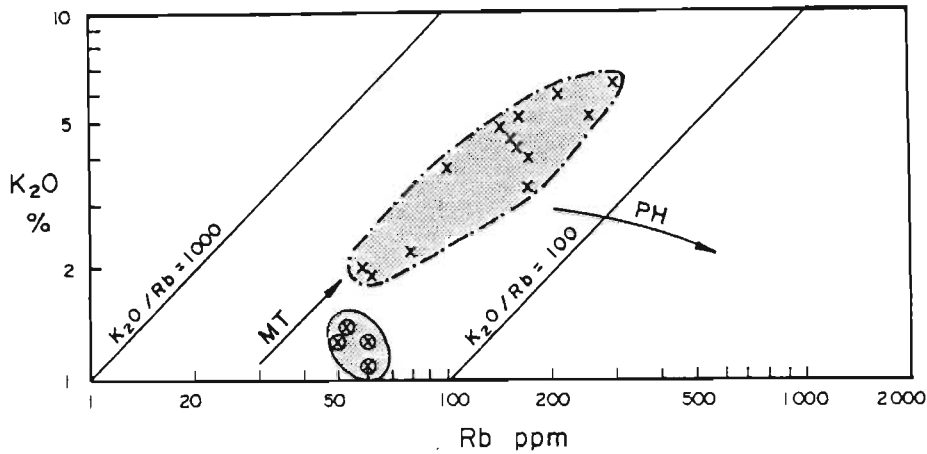


Figure 4.9. Plot of K_2O against Rb for the Wangu granites. The main (MT) and pegmatitic-hydrothermal (PH) trends of Shaw (1969) are shown for comparison.

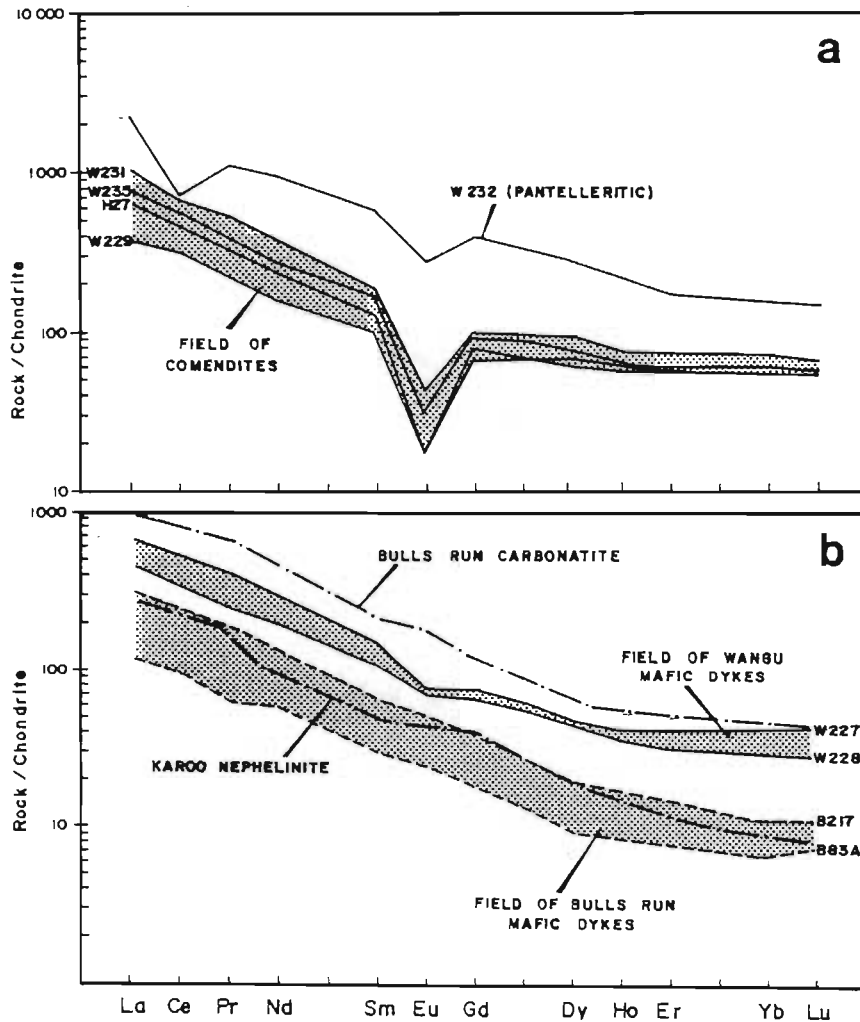


Figure 4.10. Chondrite-normalized REE patterns for the Wangu lithologies. Fig. 4.10a Wangu granites, Fig. 4.10b Wangu biotite-rich dykes with comparative data from the Bulls Run Complex. The Karoo nephelinite (Bristow 1984) is included for comparison, as are the Bulls Run carbonatite and biotite-rich mafic dykes.

4.5 Tectono-magmatic discrimination

The Wangu granites have been plotted on selected tectonic discrimination diagrams, in an effort to characterise the probable tectonic setting at the time of their emplacement. For background descriptions of the diagrams devised by Pearce *et al.* (1984), Maniar & Piccoli (1989) and Eby (1990), the reader is referred to Section 1.5.4. Where additional discrimination plots have been used they are outlined in the text below.

4.5.1 ORG-normalised patterns

With regard to the ORG-normalised patterns presented below (Fig. 4.11a, 4.11b), only those samples analysed for Sm and Yb in addition to the normal range of elements, have been plotted. The following characteristics are displayed:

- (i) The pattern defined by the comenditic granites (H27, W229, W231 & W235) is significantly enriched in Rb and Th relative to Nb, and accompanied by a large negative Ba anomaly. Apart from the Ba spike there is a general trend of decreasing values between Rb and Yb.
- (ii) The pattern exhibited by pantelleritic granite W232 is broadly similar to that of the comendites, especially with regard to Th enrichment relative to Nb. However the following exceptions are noted - K and Rb are depleted to about the same extent as Ba, probably as a result of low feldspar contents, and Sm is enriched relative to the adjacent elements Zr and Y.
- (iii) The Wangu comenditic granite pattern is comparable to that defined by comenditic rhyolites from the Naivasha volcanic complex, in the Kenya Rift valley. A representative sample of Naivasha comendite is plotted in Figure 4.11a and, apart from a larger negative Ba anomaly than the Wangu comendites, rocks from both areas have a very similar tenor of Th and Rb enrichment relative to Nb.

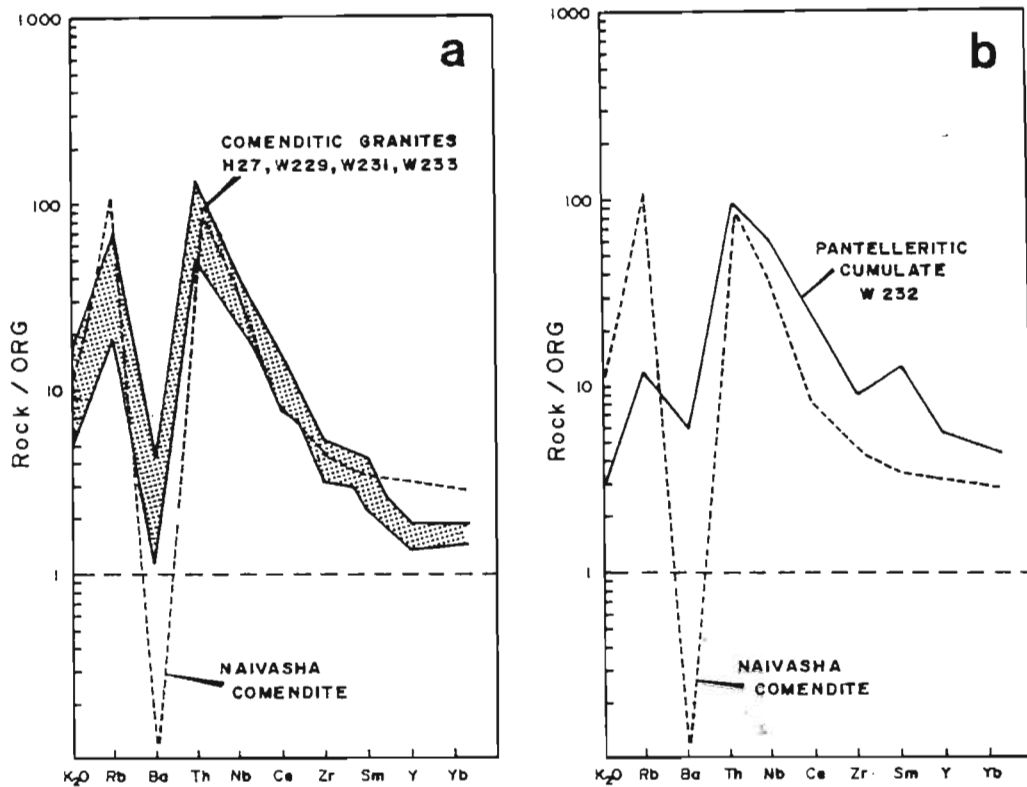


Figure 4.11. Plots of representative Wangu granites, for which REE data are available, normalized against ocean-ridge granite (ORG). ORG values and the patterns for selected WPG's and COLG's are from Pearce *et al.* (1984). Fig. 4.11a comenditic granites, Fig. 4.11b pantelleritic granite.

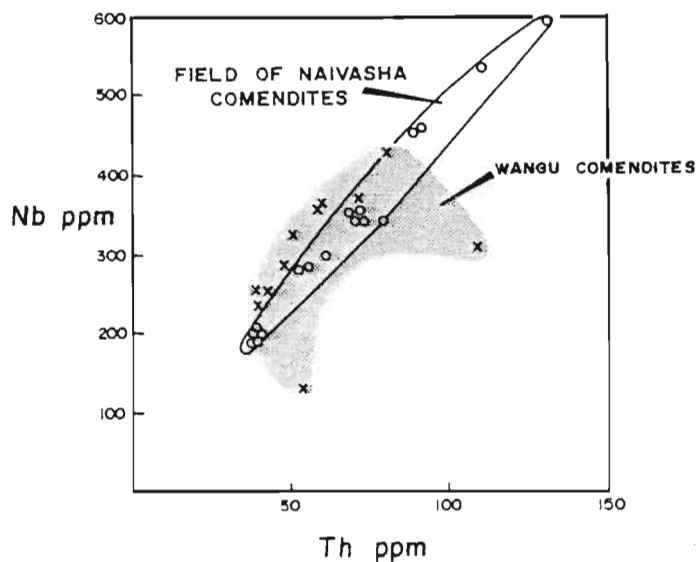


Figure 4.12. Binary plot comparing Wangu comendites with Naivasha Th-enriched comendites. Naivasha data from MacDondald *et al.* (1987).

The Naivasha pattern is considered to be crust-dominated, indicative of substantial crustal involvement during magma generation and/or emplacement (MacDonald 1987). The evidence for crustal involvement at Naivasha is provided by anomalous enrichment in "crustal elements" (large-ion-lithophiles such as Rb, Th, Pb, U) relative to high-field-strength components such as Nb, Zr, Zn and REE (MacDonald et al. 1987). The Wangu comendite data have been plotted on a binary LIL/HFS graph and exhibit comparable LIL-enriched character to the Naivasha comendites (Fig. 4.12). The Naivasha comendites are relatively potassic compared with oceanic comendites and, in this regard, it is noted that some of the Wangu comenditic granites are potassic ($K_2O > Na_2O$, Table 4.3). Continental comendites from other parts of the world share this feature, indicating addition of K_2O by interaction with sialic crust during magma generation (MacDonald et al. 1987).

4.5.2 Discrimination using Nb, Y and Rb

A-type granites are a typical magmatic feature of within-plate tectonic settings and can be distinguished from collision-related (COLG), volcanic-arc (VAG) and ocean-ridge (ORG) granites by their Y, Nb and Rb contents (Pearce et al. 1984, Whalen et al. 1987, Eby 1990). When the Wangu granites are plotted in Nb-Y space (Fig. 4.13a) they have clear WPG characteristics, as a result of elevated Nb and Y contents. However, a somewhat different pattern emerges when Rb is plotted relative to Nb+Y (Fig. 4.13b). In this diagram the comendites classify as WPG, whereas the pantelleritic cumulates have low Rb (due to low modal feldspar contents) and plot within the ORG field.

Although the Pearce diagrams are intended solely for granite classification, the alkaline mafic dykes have been plotted for comparison in Figure 4.13, indicating WPG characteristics. The Halambu granodiorite data have also been included in both the Pearce diagrams and, because of their much lower Rb, Nb and Y contents, fall within the VAG+COLG and VAG fields.

4.5.3 Maniar & Piccoli diagrams

Select major-element data for the Wangu granites have been plotted on

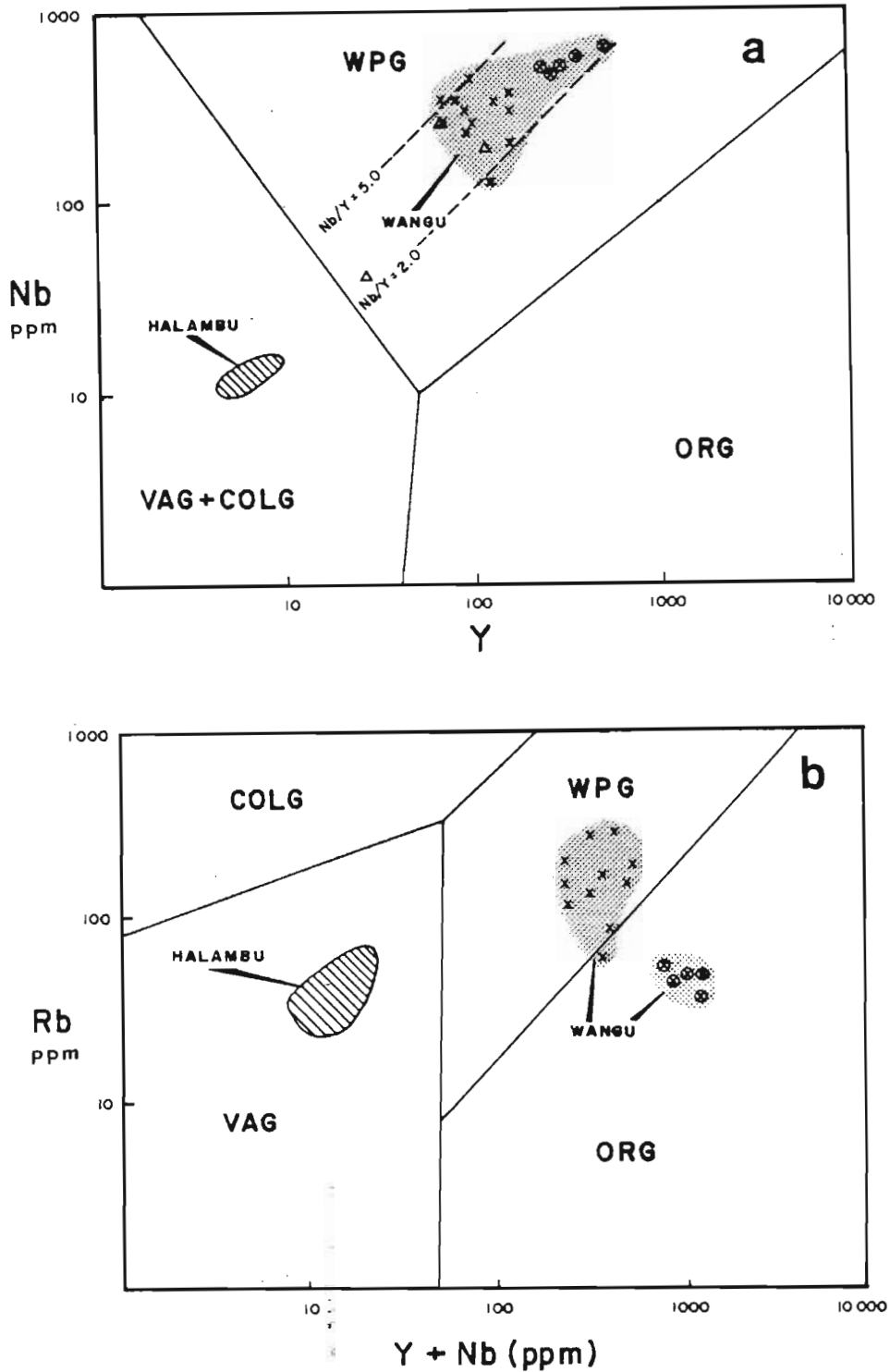


Figure 4.13. Tectonic discrimination of the Wangu granites using plots of Nb/Y (Fig. 4.13a) and Rb vs Nb + Y (Fig. 4.13b). Fields for ORG, VAG, COLG and WPG from Pearce *et al.* (1984). As illustrated in Fig. 4.13a, the majority of Wangu lithologies have Nb/Y between 2.0 and 5.0, suggesting that the granites and biotite-rich dykes are cogenetic.

two of the tectonic discrimination diagrams suggested by Maniar & Piccoli (1989). As illustrated (Fig. 4.14a, 4.14b) high FeO/MgO ratios, coupled with low Al₂O₃ contents, results in their classification as Group II anorogenic granites.

4.5.4 Y/Nb discrimination

Y/Nb ratios tend to remain constant, even through protracted fractionation, for A-type granite intrusives and are distinctive for particular tectono-magmatic settings (Eby 1990). When the Wangu granites are classified according to their Ce/Nb and Ba/La ratios relative to Y/Nb (Fig. 4.14c, 4.14d), a clear mantle signature is evident. This supports the contention that the Wangu granites are anorogenic and not post-orogenic (Section 4.5.3)

4.5.5 Tectonic setting indicated by the biotite-rich dykes

As described previously (Section 4.4.1), the biotite-rich dykes are potassic rocks enriched in CO₂ and incompatible elements. Potassic rocks, in which K₂O > Na₂O, are almost totally restricted to within-plate continental settings (Thompson & Fowler 1986, Wilson 1987) and are divided into three groups according to major-element geochemistry (Foley *et al.* 1987):

- (i) **Group 1:** Predominantly high-magnesian, ultrapotassic (K₂O/Na₂O > 5) lamproites, that range from 45 to 55% SiO₂. They are post-orogenic intrusions which generally intrude areas that have undergone continental collision. Lamproites are characterized by low Al₂O₃, CaO and Na₂O, but high overall abundances of incompatible elements (Table 4.4). With respect to modal mineralogy they carry very little calcite and, typically, lack nepheline and alkali feldspar which are characteristic minerals of Group 2 and 3 rocks.
- (ii) **Group 2:** These are the ultrapotassic rocks of continental rift zones, with the western branch of the East African Rift the type locality. As shown by the representative analysis (Table 4.4), this group is characterized by low SiO₂, Al₂O₃ and Na₂O, but high CaO, K₂O and Nb.

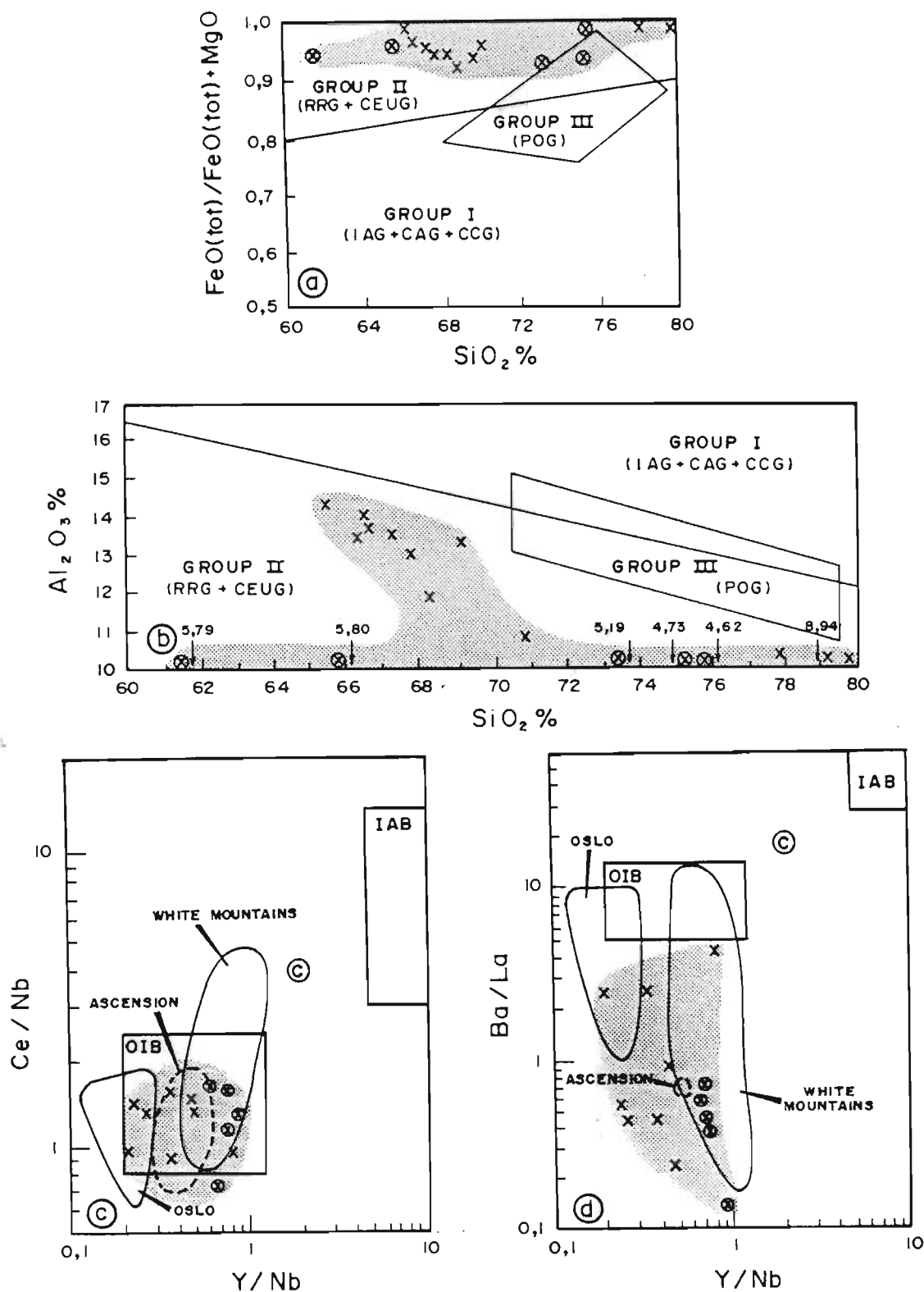


Figure 4.14. Tectonic discrimination of the Wangu granites as Group II ring-complex/continental epeirogenic-uplift granites (Fig. 4.14a, b). Tectonic discrimination of the Wangu granites when plotted in Ba/La vs Y/Nb space (Fig. 4.14c) and Ce/Nb vs Y/Nb (Fig. 4.14d). Fields for A-type granites of the Oslo Rift, Ascension Island and White Mountain complexes are from Eby (1990) and are included for comparison with the Wangu data. Average crustal composition is given as c, OIB = ocean-island basalt, IAB - island-arc basalt.

- (iii) **Group 3:** Ultrapotassic rocks of active orogenic zones, typically developed in the Roman Province of Italy, are characterized by high Al_2O_3 , higher SiO_2 than Group 2 rocks and most diagnostic, low Nb and TiO_2 .

In terms of the above characteristics, comparison of the Wangu potassic dykes with representative Group 1, 2 & 3 analyses suggests a rather mixed parentage. Thus the Wangu samples are aluminous and not very magnesian (Group 3), but enriched in calcite (Groups 2 and 3) and contain elevated incompatibles such as Nb and TiO_2 (Groups 1 and 2). Taking all variables into account, close affinities to Group 2 rocks are consistent with their high calcite, Nb and TiO_2 contents. From the above summary, it is apparent that potassic rocks related to subduction (Group 3) are most easily distinguished from those related to intraplate magmatism (Groups 1 and 2) by their Nb and TiO_2 contents (Table 4.4). Whereas subduction-related rocks contain less than 80ppm Nb, the Wangu biotite-rich dykes have variable, though fairly high Nb values, suggestive of within-plate emplacement (Fig. 4.15).

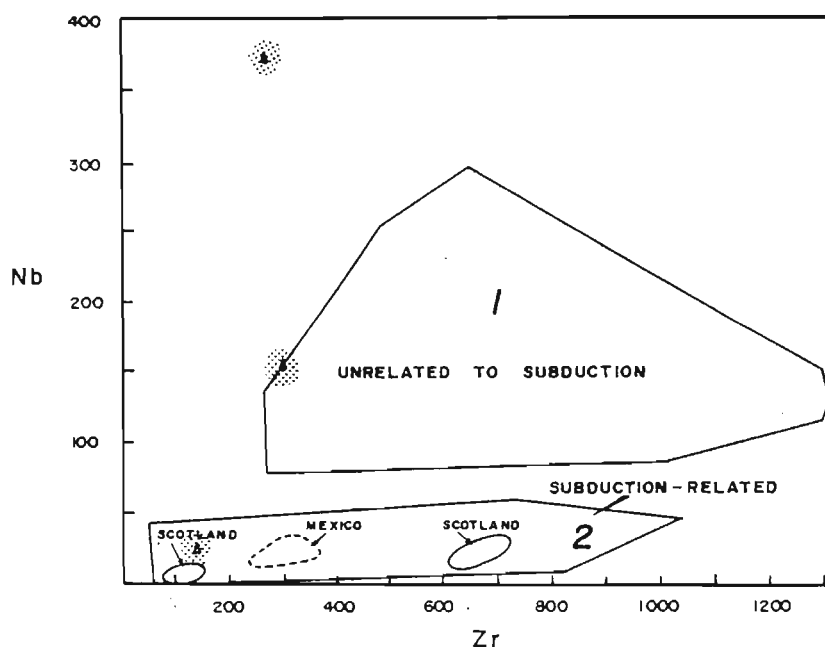


Figure 4.15. Tectonic discrimination of the Wangu biotite-rich mafic dykes, on the basis of Nb vs Zr for potassic and ultrapotassic rocks with less than 60% SiO₂. Diagram from Thompson & Fowler (1986), fields described as: 1, localities remote in space and/or time from subduction; 2, localities closely related to subduction tectonics.

As discussed earlier (Section 3.6.5), the comparable biotite-rich dykes in the Bulls Run Complex have characteristics of volatile-rich alkaline mafic rocks such as lamprophyres. It is therefore suggested that the Wangu biotite-rich rocks have a similar origin. Alkaline lamprophyres are most commonly emplaced into settings such as passive continental margins (transform faults), divergent margins (triple junctions and rifts) and intraplate settings (oceanic islands and continental hotspots). Therefore, although not specifically diagnostic, the alkaline lamprophyre character of the Wangu mafic dykes indicates an essentially non-compressional, or tensional, tectonic regime at the time of emplacement.

4.6 Summary of salient features

- (i) The Wangu Granite Gneiss is an elongate 6km-long body within the Nkomo nappe.
- (ii) The granites are fine-grained, contain aegirine-augite and/or magnetite and are intruded by biotite-rich dykes.
- (iii) Although the magnetite granites have peraluminous major-element chemistry, their high Ga/Al, Zn, Zr, Nb and REE contents are diagnostic of A-type peralkaline parentage. Alkali depletion, either as a result of post-magmatic volatile activity or metamorphic conditions, is thought to have caused breakdown of sodic mafic minerals to form magnetite.
- (iv) Localized iron-rich pantelleritic granitoids have enhanced REE, Zr, Nb, and Zn contents relative to the predominant comenditic granites, and are interpreted as magmatically-concentrated cumulate layers.
- (v) The biotite-bearing dykes are potassic, undersaturated and volatile-rich. They are interpreted as metamorphosed alkaline lamprophyres, with Group 2 affinities. A genetic relationship is indicated between the peralkaline granites and mafic sheets, according to their alkaline character, enrichment in Nb and well-constrained incompatible-element ratios.

- (vi) High LIL/HFS ratios and crust-dominated ORG-normalized patterns for the granites provide evidence of intrusion into continental crust, probably as high-level dykes.
- (vii) The lamprophyric dykes are geochemically comparable with Group 2 potassic rocks, signifying intrusion into rifted continental crust.

Chapter 5

SUMMARY, DISCUSSION AND CONCLUSIONS

Three alkaline intrusives have been mapped at Ngoye, Bulls Run and Wangu, within the Tugela Terrane of the Natal Metamorphic Province. These bodies have been described according to field relationships, petrography, major- and trace-element geochemistry, REE patterns and Rb-Sr isotopes, in an effort to understand their pre-deformational character. Salient characteristics of each of the intrusions are summarized below.

A discussion of unifying features is presented. These suggest that Ngoye, Bulls Run and Wangu intrusives are a cogenetic pre-tectonic alkaline suite, emplaced into rifted continental crust in a "within-plate" tectonic setting.

The currently accepted ophiolite-obduction model for the Tugela Terrane is briefly described. Comparisons with the Grenville Province are drawn. A model that embraces rifting of an attenuated continental margin is suggested in order to account for the presence of the alkaline Ngoye, Bulls Run and Wangu intrusives.

5.1 Summary

5.1.1 Ngoye Complex

As described in Chapter 2, eleven petrographically-distinct lithologies have been delineated within the Ngoye Complex, which is an elongate massif 30km in length located in the Nkomo nappe of the Tugela Terrane. Classification of these lithologies according to modal and geochemical

criteria indicates that they are predominantly metaluminous to peralkaline ($\text{Na}+\text{K}/\text{Al}$: 0.90 to 1.15), with a minor peraluminous component. Comparison of well- and poorly-foliated samples of peralkaline granite demonstrates that, under conditions of moderate deformation, the Ngoye lithologies behaved isochemically. However, slight depletion of Na_2O , as a result of post-magmatic vapour-loss processes, may have been responsible for the breakdown of riebeckite and aegirine to magnetite in certain of the peralkaline granites.

Metaluminous granites constitute the bulk of the Ngoye Complex and occupy the central and northern outcrops of the massif. Typically they contain hastingsite and biotite and classify as granite (*sensu stricto*) on the modal QAP diagram, although major-element/normative classifications indicate granite/alkali-feldspar granite compositions.

A small plug of metaluminous hornblende monzodiorite was mapped in the centre of the complex. Although volumetrically minor, this outcrop is considered significant as it provides evidence of CO_2 streaming and alkali-fluid activity during evolution of the Ngoye Complex, a phenomenon referred to later in this chapter.

Peralkaline Ngoye granites containing riebeckite, aegirine and/or magnetite are restricted to the southern part of the complex and classify as comenditic alkali-feldspar granites according to modal, major-element and normative plots. Compared with the metaluminous granites, these peralkaline lithologies are depleted in CaO , Al_2O_3 , Sr and Ba , but enriched in $\text{Na}_2\text{O}/\text{K}_2\text{O}$, Nb , Zr , Zn , REE and Y . REE patterns are flat and relatively HREE-enriched, with significant negative Eu anomalies, typical of peralkaline granites in other parts of the world.

The peralkaline granites host magnetite-quartz veins that are highly enriched in Zr , Nb , Th , U , HREE and Y ; these are interpreted as late-stage fractionates derived from crystallization of the peralkaline granites. Chloritic syenite intersected in a borehole is thought to be a desilicified episyenitic alteration product of peralkaline magnetite granite.

Peraluminous garnet- and muscovite-bearing granites are restricted to a thin intrusive sheet along the northeastern flank of the complex. The application of modal and geochemical criteria results in classification as alkali-feldspar granite. The peraluminous granites are geochemically distinct from the metaluminous and peralkaline granites, in that concentrations of incompatible elements (Nb, REE, Y and Zr) are relatively low. This is typical of peraluminous granitoids and is ascribed to the low solubility of incompatible HFS elements, a direct contrast to the trends noted in the peralkaline granites. Muscovite-rich pods associated with quartz-feldspar pegmatites in the peraluminous granites are enriched in Sn, Rb, U and Th. A "birds-wing" REE pattern, with low total REE and marked enrichment in HREE relative to LREE is consistent with retention of HREE by garnet and is possibly due to the effects of post-magmatic fluid activity.

Consideration of modal characteristics, major-element contents and trace-element ratios (eg. Y/Nb, Ga/Al, Rb v Y+Nb) indicates that the Ngoye lithologies have the characteristics of A-type, mantle-derived, within-plate granites. High LIL/HFS-element ratios within the peralkaline comenditic granites indicate that they were intruded into continental crust. Similarly the U, Th and Rb enrichment that characterises garnet-muscovite granite of the Ngoye Complex can be attributed to crustal contamination during magma generation and/or emplacement.

Rb-Sr isotope data for the metaluminous biotite-hornblende granite indicate a low initial ratio ($R_0 = 0.7025$) and an isochron age of 1058 ± 49 Ma.

It is concluded that the Ngoye Complex is a deformed A-type granite central complex, intruded into rifted continental crust.

5.1.2 Bulls Run Complex

The Bulls Run Complex is an elongate 15 km-long body located immediately south of the Kaapvaal Craton, within the lowermost part of the Nkomo nappe in the Tugela Terrane. Contrary to previous descriptions of the Bulls Run "Formation" as an homogeneous body of silica-oversaturated

syenite (Charlesworth 1981) this study has demonstrated that it is essentially silica undersaturated and lithologically complex. Seven types of alkaline rock have been discovered, resulting in the proposal that the term "Formation" be discarded in favour of "Complex" (Scogings & Forster 1989, Scogings 1991a). Lithologies are subdivided into three major and four minor types according to areal distribution, mineralogy and geochemistry. The major rock types are concentrically disposed, with an envelope of biotite-muscovite syenite surrounding a composite core of biotite-nepheline syenite and albite syenite. Minor phases, viz. carbonatite, lamprophyre, feldspathic ijolite and microsyenite are exposed only in areas underlain by biotite-muscovite syenite and generally are restricted to the eastern portion of the complex.

Biotite-muscovite syenite is classified as alkali-feldspar syenite according to modal and normative components, whereas major-element plots suggest a syenite to quartz-syenite composition. Derivation of the biotite-muscovite syenite by potassic fenitization of pelitic country rocks, as a result of sövite carbonatite intrusion, is proposed.

The core of the BRC is composite, with a rim of coarse-grained biotite-nepheline syenite surrounding an inner zone of fine-grained albite syenite. Alteration of nepheline to cancrinite, kaolin and sericite in the albite syenite indicates that volatiles such as CO_2 and H_2O became increasingly active as crystallization progressed. It is noted that this alteration is accompanied by deposition of incompatible-element enriched minerals such as zircon and pyrochlore.

Modal and geochemical classification of the biotite-nepheline and albite syenites indicates that they are alkaline, predominantly miaskitic, and of phonolitic composition. The biotite-nepheline syenite rim is relatively more potassic, silica deficient and contains lower incompatible-element concentrations than the inner albite-rich zone. The observed textural and compositional trends are consistent with phonolitic fractionation (the orthoclase effect) from early cumulate nepheline syenite, to residual volatile-rich albite syenite. REE patterns reflect paragenetic and geochemical fractionation trends, with HREE-enriched patterns characteristic of the altered albite syenites.

The positive Eu anomalies in the coarse-grained biotite-nepheline syenites are in agreement with their proposed cumulate origin.

Feldspathic ijolite forms the centre of a small hornblende-bearing nepheline syenite plug near the eastern end of the Bulls Run Complex. Geochemically the feldspathic ijolite and associated nepheline syenites are sodic and relatively depleted in silica and alumina, when compared with the nepheline syenites in the western part of the complex. The occurrence of several elongate, though disconnected bodies of nepheline syenite and carbonatite along strike from the ijolitic plug, within a ductile matrix of biotite-muscovite syenite, has led to the interpretation of these outcrops as a sheared and boudinaged ring-dyke complex.

Although exposed at a number of localities, the most extensive outcrops of carbonatite are in the vicinity of the boudinaged ijolitic plug in the eastern part of the Bulls Run Complex. Here, an elongate body of biotite-bearing sövite intrudes biotite-muscovite syenite and contains numerous xenoliths of the host rock. Trace-element contents are distinctive, with elevated Sr, Nb and REE contents comparable with sövites in other parts of the world.

Mafic biotite-rich dykes intrude biotite-muscovite syenite in the eastern part of the complex. With respect to major- and trace-element chemistry the mafic dykes are alkaline and classify as essexite. In view of their major- and trace-element chemistry, eg. high H₂O, CO₂, Na, K, Sr, Th, Ba and LREE/HREE, in addition to their association with carbonatite and syenite, it is probable that these biotite-rich rocks are metamorphosed alkali lamprophyres.

Microsyenite dykes, often flow-banded, are intrusive into biotite-muscovite syenite and have, at localities along the margins of the complex, been tectonically dismembered and boudinaged. According to modal and geochemical characteristics this lithology is classified as alkali-feldspar syenite to quartz alkali-feldspar syenite. An origin related to the action of fenitising fluids is suggested, akin to the production of intrusive trachytic veins around sövite intrusions in Kenya and Uganda.

Rb-Sr isotope data for the biotite- and hornblende-bearing nepheline syenites indicate a low initial-Sr ratio ($R_0 = 0.7032$) and an isochron date of 1138 ± 45 Ma. Carbonate separates from the carbonatite dykes provide an average R_0 of 0.70319, which supports a comagmatic mantle source for the carbonatite and syenite. The low initial-Sr ratios in the Bulls Run Complex are comparable with those from undeformed nepheline syenites in other parts of the world.

Plotting of the potassic BRC syenites and lamprophyric dykes on a Zr vs Nb tectonic-discrimination diagram indicates that they are unrelated to subduction. This is consistent with the widely-accepted view that the nepheline syenite/ijolite/carbonatite association is restricted to intra-continental rift zones. In this regard, similarities are noted between the BRC and mid-Proterozoic gneissose miaskitic syenite complexes in the Grenville Province; these are suggested to have been intruded into rifted crust along a continental margin.

The Bulls Run Complex is concluded to be a deformed syenite/carbonatite central complex, intruded under anorogenic conditions, into continental crust.

5.1.3 Wangu granite

The Wangu Granite Gneiss (Scogings 1991) is an elongate easterly-trending body 6 km long and up to 1 km wide, within the Halambu "Formation" of the Nkomo Nappe. Whereas previously the Halambu "Formation" was described as predominantly a calc-alkaline granodiorite, this study has demonstrated the presence of peralkaline granites and alkaline mafic dykes in the Wangu hill area, in the southern part of the Halambu outcrop.

The Wangu granites are subdivided into two types based on mineralogy, with a core of aegirine-augite granite surrounded by an envelope of magnetite granite. According to modal analyses they classify as alkali-feldspar granite and, on the basis of major- and trace-element contents, are of trachyte/quartz-syenite to comenditic alkali-granite composition. With respect to alumina saturation the magnetite-bearing granites of the outer envelope are wholly metaluminous ($(Na+K)/Al = 0.90$

to 0.99) whereas the pyroxene-bearing varieties are predominantly peralkaline ($\text{Na+K/Al} = 0.89$ to 1.38). Relatively mafic layers, rich in magnetite and aegirine-augite (c.20%), may be of cumulate origin and have a pantelleritic major-element chemistry, with low Al_2O_3 (c.7%) and high Fe_2O_3 (c.15%), Zn, Zr, Nb, REE and Y. REE patterns are similar to the Ngoye peralkaline granites, enriched in total REE, with low LREE/HREE ratios and significant negative Eu anomalies.

The biotite-rich dykes that intrude the southern part of the Wangu granite are similar to those described from the Bulls Run Complex although, relatively, they are more potassic and have lower alumina contents. They are metaluminous, nepheline- and/or leucite-normative, and classify as essexite according to their major-element geochemistry. By analogy with the Bulls Run occurrences, the Wangu biotite-rich dykes are thought to be metamorphosed alkaline lamprophyres.

Consideration of the modal and geochemical characteristics of the Wangu granites (viz. Y vs Nb, Ga/Al, Rb vs Nb+Y) indicates their origin as A-type, within-plate granites. High LIL/HFS-element ratios, allied with crust-dominated ORG-normalized patterns, provide evidence of intrusion through and some interaction with, continental crust.

On the basis of their fine grain size, if an inherited feature, and by analogy with comparable Hercynian and Grenvillian felsic rocks, it is considered likely that the Wangu granites were emplaced at high crustal levels, perhaps as hypabyssal dykes.

Comparison of the Wangu alkaline lamprophyric dykes with Group 1, 2 & 3 potassic and ultrapotassic rocks from the literature, especially with regard to low MgO and high K_2O , CaO, CO_2 , Nb and TiO_2 contents, indicates a Group 2 intraplate continental-rift tectonomagmatic setting at the time of intrusion.

5.2 Discussion

5.2.1 Unifying features

Following from the above summary, the characteristics of the Ngoye, Bulls Run and Wangu granitoids are discussed with the aim of highlighting common features. This provides a background to the proposal that the three bodies are a cogenetic suite of alkaline intrusives.

- (i) The alkaline intrusives at Ngoye, Bulls Run and Wangu are all located within the Nkomo Nappe of the Tugela Terrane, adjacent to the southern margin of the Kaapvaal Craton.
- (ii) The Ngoye, Bulls Run and Wangu intrusives all contain peralkaline granites and syenites, characterised by sodic and/or Fe-rich minerals such as riebeckite, aegirine, aegirine-augite and magnetite.
- (iii) All three bodies are essentially alkalic to alkaline and characterised by elevated concentrations of incompatible elements such as Nb, Zr, Y and REE.
- (iv) The Ngoye and Wangu intrusives are classified as A-type granites.
- (v) CO₂-volatile activity, reflected by the presence of modal calcite, has affected each of the three intrusions to a greater or lesser extent. Lithologies that illustrate this process are the monzodiorite at Ngoye, the carbonatites and lamprophyres of the Bulls Run Complex, and the lamprophyres at Wangu.
- (vi) Rb-Sr age determinations on selected lithologies within the Ngoye and Bulls Run Complexes indicate that they are broadly contemporaneous, intruded between c.1150 and 1050Ma. An age for the Wangu granite is not yet available.
- (vii) Initial-Sr ratios for the Ngoye and Bulls Run granitoids are low (0.703 to 0.706) and consistent with a mantle source. The Bulls Run carbonatites have similar initial ratios which support a comagmatic mantle origin.

- (viii) Classification of the Ngoye and Wangu granites on tectonic discrimination diagrams indicates that they are within-plate intrusions.
- (ix) Tectonic-discrimination diagrams are not generally applicable to nepheline syenite/carbonatite complexes, as such intrusions are widely believed to be characteristic of rifted continental crust.
- (x) ORG-normalised patterns for the Ngoye and Wangu granites indicate interaction with continental crust during magma generation and intrusion.
- (xi) The relatively potassic chemistry of some of the Wangu comenditic granites is, by comparison with Kenyan comendites, taken to indicate intrusion into continental crust.
- (xii) The Wangu potassic alkaline mafic dykes are geochemically similar to Group 2 potassic rocks, implying intrusion into rifted continental crust. Similarly, Nb-enrichment of the potassic rocks at Wangu and Bulls Run suggests intrusion in a tectonic environment unrelated to subduction.

From the above considerations, it is suggested that the Ngoye, Bulls Run and Wangu granitoids constitute a suite of metamorphosed alkaline intrusives emplaced anorogenically into continental crust. It is proposed to unite these intrusives formally as the Nkwaleni Suite, after the small farming centre situated midway between the Ngoye and Bulls Run Complexes.

The Nkwaleni Suite is pre-tectonic in origin and was emplaced into the Nkomo Nappe prior to the main fabric-forming event responsible for the Natal Metamorphic Province. The implication that the Nkomo Nappe is of continental derivation is clearly at odds with the presently-accepted ophiolite origin (Matthews 1972, 1981, Thomas 1990).

5.2.2 Tectonic implications for the Tugela Terrane

When the other alkaline granitoids discovered during the reconnaissance phase of this thesis (Fig. 1.1) are taken into account, the picture that unfolds is one of rifting and extensive anorogenic continental magmatism during development of the Tugela Terrane. This concept is supported by the broadly coeval emplacement of layered mafic intrusions such as the Tugela Rand Suite and Mambulu Complex which, likewise, are believed to reflect anorogenic magmatism (Cooper 1991, A. Wilson pers. comm.).

The widespread occurrence of anorogenic intrusives within the Nkomo Nappe places constraints on the presently-accepted model for this part of the Natal Metamorphic Province. The current model, which invokes ophiolite obduction during continent/continent collision, proposed by Matthews (1972 1981) and subsequently modified to include island-arc accretion (Thomas 1989 1990), is summarised below:

The nappes of the Tugela Terrane are interpreted as part of a metamorphosed ophiolite sequence that was obducted northwards onto the Kaapvaal Craton, along a basal decollément known as the Mfongosi Thrust. The southern limit of the Tugela Terrane (Tugela Group of Matthews 1981) is marked by the Matigulu Steep Belt, which was interpreted as the root zone to the Tugela nappes. The Mzumbe Terrane, which lies to the south of the Tugela Terrane, is regarded as a meta-greywacke "flysch apron" which was accreted onto the leading edge of a northward-moving continental plate, prior to collision with the southern foreland of the Kaapvaal Craton (Matthews 1972, 1981).

Tankard et al. (1982) noted that, in view of the infolded granitic infrastructure within the Tugela Group, the Tugela volcano-sedimentary sequence more likely accumulated in an ensialic back-arc basin than in an oceanic environment (Tankard et al. 1982).

Thomas (1989, 1990) modified Matthews' model and suggested that the Natal Metamorphic Province formed by the accretion of juvenile (<1300 Ma) island arcs onto the Kaapvaal Craton (Fig. 5.1a, b). The intervening oceanic floor between the craton and the island arcs was "probably studded with alkali basalt seamounts, the exposed roots of which are represented by the Tugela Rand Layered Suite and other mafic/ultramafic complexes" (Thomas & Eglington 1990, p. 764).

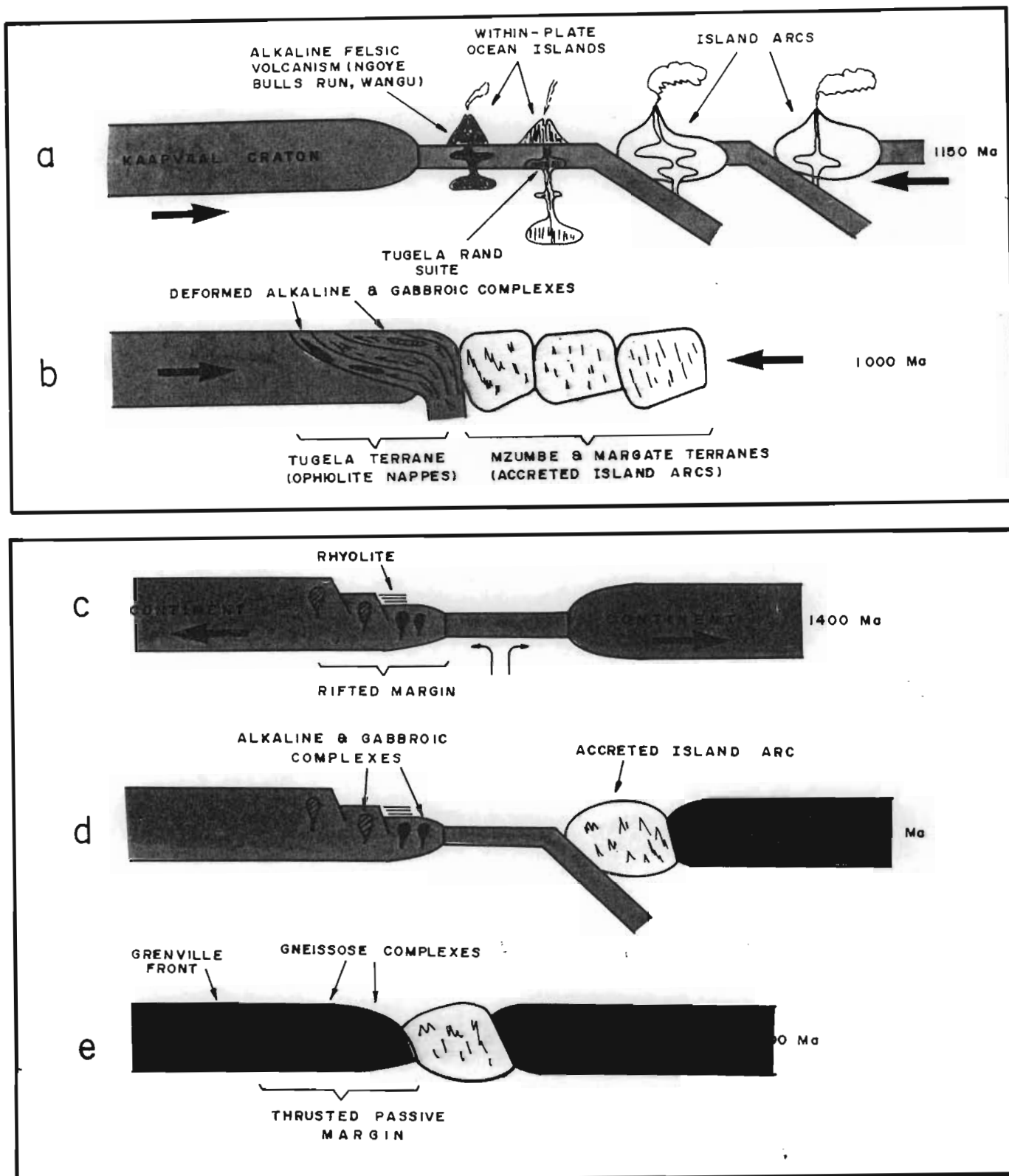


Figure 5.1. A series of cartoon diagrams illustrating the possible tectono-magmatic evolution of the Natal Metamorphic Province (Figs 5.1a, 5.1b), after Thomas (1990). This model invokes the accretion of island arcs onto the southern margin of the Kaapvaal Craton, preserving the Tugela Ocean as ophiolite nappes to the north of the suture zone. Figures 5.1c to 5.1e illustrate the possible evolution of the Grenville Orogeny in Ontario, after Windley (1989). Note that the pre-tectonic alkaline complexes are intruded into a rifted continental margin, eventually being preserved as gneissose complexes within the metamorphic belt.

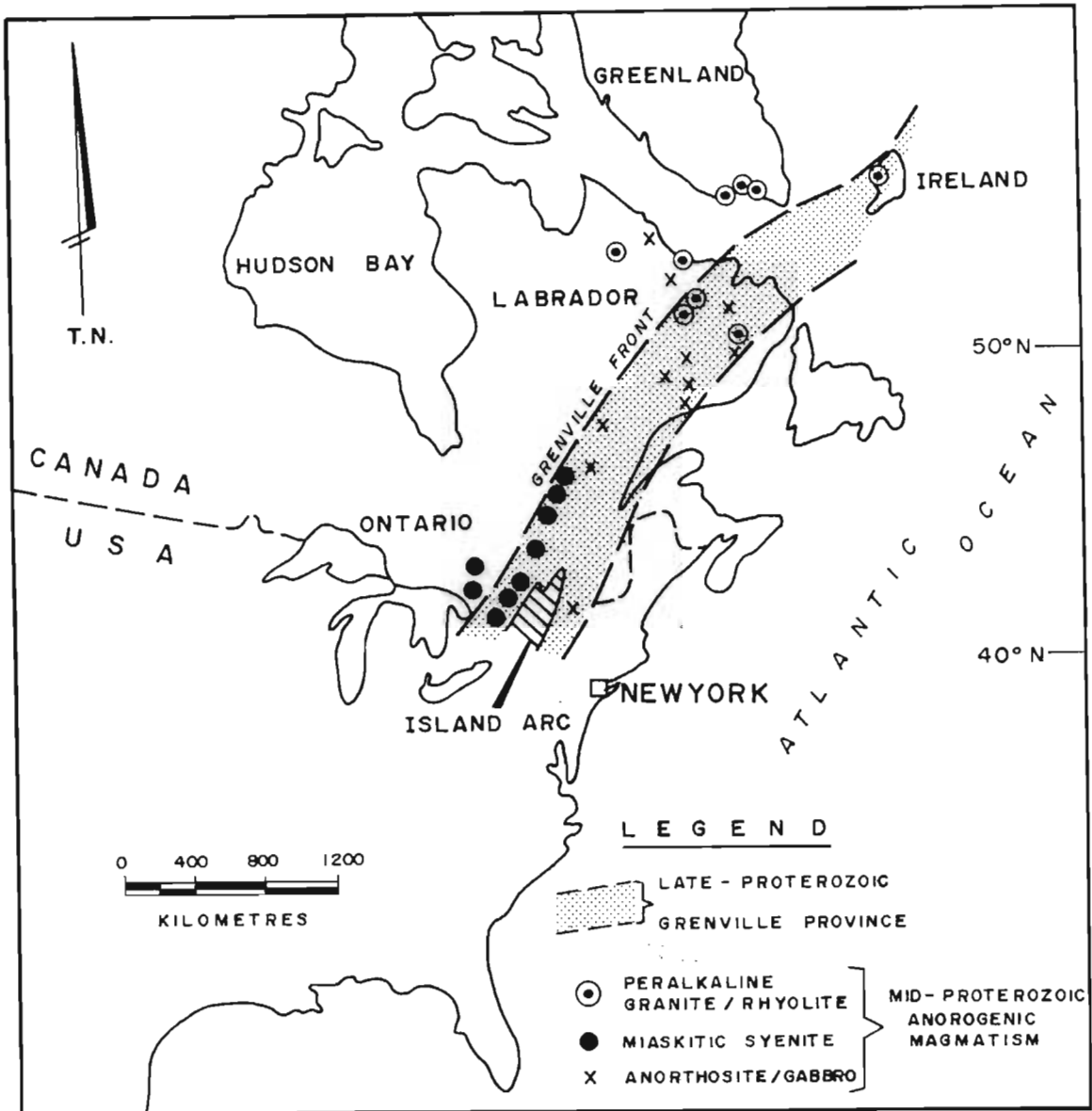


Figure 5.2. Map showing the distribution of mid-Proterozoic anorogenic magmatic centres in relation to the Grenville Metamorphic Province. Data from Windley (1989) and Winchester & Max (1987). Pre-drift positions of Greenland and Ireland from Winchester & Max (1987).

5.2.3 Comparison with the Grenville Province

The contrasting models outlined above recall the similar controversy surrounding the tectono-magmatic history of the Grenville Orogeny (Windley 1989).

The Grenville Province is located in southeast Canada and is part of an extensive mid- to late-Proterozoic mobile belt that extends from Mexico, through Canada, southern Greenland, Ireland and Scotland to Norway (Fig. 5.2). Several models have been proposed to explain the development of the Grenville Province in north America:

Dewey & Burke (1973) suggested that the Grenville Belt was the result of continent/continent collision, with thin slivers of ophiolite preserved along the suture zone. This model is analagous to Matthews' (1972 1981) interpretation of the Natal Metamorphic Province.

Subsequently, Windley (1989) stressed that anorogenic continental magmatism, during the period c.1500 to 1250 Ma, had preceeded the Grenvillian Orogeny. He suggested the following sequence of events in terms of an extensional/compressional Wilson cycle (Fig. 5.1c, d, e):

- (i) Emplacement of anorogenic rhyolites, peralkaline granites complexes, miaskitic nepheline-syenite complexes, basic dyke swarms and gabbros into rifted and thinned passive continental margin adjacent to the proto-Grenville Ocean.
- (ii) Subduction of ocean floor away from the passive continental margin caused the development of a calc-alkaline island arc within the Grenville Ocean.
- (iii) Ocean closure at c. 1100 Ma, with subsequent collision of the two continental blocks, sandwiching the island arc between them. Craton-directed overthrusting of the previously-thinned passive continental margin resulted in transformation of the alkaline intrusives into elongate gneissic bodies orientated parallel to the Grenville Front.

The occurrence of gneissose anorogenic granite and syenite complexes within both the Tugela Terrane and the Grenville Province, allied to their mid- to late-Proterozoic age, suggests that the Natal Metamorphic Province is but part of the Grenvillian system of mobile belts, with a similar origin. Therefore, it is proposed that the Tugela Terrane is a metamorphosed palaeorift system that evolved on the rifted passive margin of the Kaapvaal Craton during the initial stages of a Wilson cycle.

5.3 Conclusions

The anorogenic Nkwaleni Suite, comprising the alkaline Ngoye, Bulls Run and Wangu intrusives, was emplaced into continental crust prior to the c.1000 Ma fabric-forming event responsible for the Natal Metamorphic Province. The tectono-magmatic history of the Tugela Terrane resembles that of the Grenville Province, which is considered to be an appropriate analogue. The Tugela Terrane is interpreted therefore, not as obducted ophiolite, but as a metamorphosed palaeorift system.

REFERENCES

- Al-Shaieb, Z. (1988). Uranium mineralization in the peralkaline Quannah Granite and related pegmatite-aplite dikes, Wichita Mountains, Oklahoma. Ore Geol. Rev., **3**, 161-175.
- Anderson, W. (1901). Report on the reconnaissance survey of Zululand. Rep. geol. Surv. Natal - Zululand, **1**, 60-61.
- Appleyard, E.C. (1967). Nepheline syenite gneisses of the Wolfe Belt, Lyndoch Township, Ontario. (I). Structure, stratigraphy and petrography. Can. J. Earth. Sci., **4**, 374-395.
- Appleyard E.C. (1969). Nepheline gneisses of the Wolfe Belt, Lyndoch Township, Ontario. (II). Textures and mineral paragenesis. Can. J. Earth. Sci., **6**, 689-717.
- Bailey, D.K. (1964). Crustal warping - a possible tectonic control of alkaline magmatism. J. geophys. Res., **69**, 1103-1111.
- Bailey, D.K. (1974). Nephelinites and ijolites. In: Sorensen, H., ed., The alkaline rocks, 53-66, Wiley Interscience, NY.
- Baker, J.H. (1985). Rare earth and other trace element mobility accompanying albitization in a Proterozoic granite, Bergslagen, Sweden. Min. Mag., **49**, 107-115.
- Barton, E.S. (1983). The geochronology of the frontal zones of the Namaqua-Natal Mobile Belt. Ph.D. thesis (unpubl.), Univ. Witwatersrand, Johannesburg.

- Batchelor, R.A. & Bowden, P. (1985). Petrogenetic interpretation of granitoid rock series using multicationic parameters. Chem. Geol., **48**, 43-55.
- Blaxland, A.B., van Breemen, O., Emeleus, C.H. & Anderson, J.G. (1978). Age and origin of the major syenite centers in the Gardar province of south Greenland: Rb-Sr studies. Bull. geol. Soc. Am., **89**, 231-244.
- Boer, R.H., de Bruijn, H. & Schoch, A.E. (1990). Petrogenetic aspects of the copper-bearing Koperberg Suite, Namaqualand. Ext. Abstr. Geocongress '90. Geol. Soc. S. Afr., Cape Town.
- Bonin, B. (1986). Ring complex granites and anorogenic magmatism. North Oxford Academic, London.
- Bourne, J.H. (1986). Geochemistry of the felsic metavolcanic rocks of the Wakeham Group: a metamorphosed peralkaline suite from the eastern Grenville Province, Quebec, Canada. Can. J. Earth Sci., **23**, 978-984.
- Bowden, P. (1974). Oversaturated alkaline rocks : granites, pantellerites and comendites. In: Sorensen, H., ed., The alkaline rocks, 109-123. Wiley Interscience, NY.
- Bowden, P. & Whitley, J.E. (1974). Rare-earth patterns in peralkaline and associated granites. Lithos, **7**, 15-21.
- Bowden, P. & Kinnaird, J.A. (1984). The petrology and geochemistry of alkaline granites from Nigeria. Phys. Earth Planet. Int., **35**, 199-211.
- Bowden, P., Black, R. Martin, R.F., Ike, E.C., Kinnaird, J.A. & Batchelor, R.A. (1987). Niger-Nigerian alkaline ring complexes: a classic example of African Phanerozoic anorogenic mid-plate magmatism. Spec. Publ. geol. Soc. Lond., **30**, 357-380.

- Bristow, J.W. (1984). Nephelinites of the North Lebombo and south-east Zimbabwe. Spec. Publ. geol. Soc. S. Afr., **13**, 87-104.
- Brooks, C., Hart, S.R. & Wendt, I. (1972). Realistic use of two-error regression treatments applied to rubidium-strontium data. Rev. geophys. Space Phys., **10**, 551-577.
- Charlesworth, E.G. (1981). Tectonics and metamorphism of the northern margin of the Namaqua-Natal Mobile Belt, near Eshowe, Natal. Ph.D. thesis (unpubl.), Natal University, Durban.
- Collins, W.J., Beams, S.D., White, A.J.R. & Chappell, B.W. (1982). Nature and origin of A-type granites with particular reference to south-eastern Australia. Contrib. Mineral. Petrol., **80**, 189-200.
- Cooper, M.R. (1991). Tectonic cycles in southern Africa. Earth Sci. Rev., **28**, 321-364.
- Cornell, D.H., Schade, J. & Scheepers, R. (1989). Rare earth element geochemistry as a prospecting tool. S. Afr. J. Sci., **89**, 654-658.
- Cullers, R.L. & Medaris, G. (1977). Rare earth elements in carbonatite and cogenetic alkaline rocks: examples from Seabrook Lake and Callander Bay, Ontario. Contrib. Mineral. Petrol., **65**, 143-153.
- Cullers, R.L. & Graf, J.L. (1984). Rare earth elements in igneous rocks of the continental crust: predominantly basic and ultrabasic rocks. In : Henderson, P., ed., Rare earth element geochemistry, 237-274. Elsevier, Amsterdam.
- Currie, K.L. (1976a). The Alkaline rocks of Canada. Bull. 239, Geol. Surv. Canada.

- Currie, K.L. (1976b). Notes on the petrology of nepheline gneisses near Mount Copeland, British Columbia. Bull. 265, Geol. Surv. Canada.
- Daly, M.J., Germiquet, J-D. & Scogings, A.J. (1989). Bull's Run nepheline syenite, a new deposit - new products. Proc. 21st Ann. symp., 41 - 45. S. Afr. Ceramic Soc. Jhb.
- De la Roche, H., Leterrier, J., Grandclaude, P. & Marchal, M. (1980). A classification of volcanic and plutonic rocks using R_1 - R_2 diagram and major element analyses - its relationships with current nomenclature. Chem. Geol., 29, 183-210.
- Deer, W.A., Howie, R.A. & Zussman, J. (1966). An introduction to the rock-forming minerals. Longmans, London.
- De Villiers, J.E. (1941). Columbomicrolite from Eshowe, Natal. Amer. Min., 26, 501-506.
- Dewey, J.F. & Burke, K.C.A. (1973). Tibetan, Variscan and Precambrian basement reactivation: products of continental collision. J. Geol., 81, 683-692.
- Du Toit, A.L. (1931). The geology of the country surrounding Nkandla, Natal. Expl. Sheet 109, geol. Surv. S. Afr.
- Eby, G.N. (1975). Abundance and distribution of rare-earth elements and yttrium in the rocks and minerals of the Oka Carbonatite Complex, Quebec. Geochim. Cosmochim. Acta, 39, 597-620.
- Eby, G.N. (1984). Montereian Hills I. Petrography, major and trace element geochemistry, and strontium isotopic chemistry of the western intrusions: Mounts Royal, St. Bruno, and Johnson. J. Petrol., 25, 421-452.
- Eby, G.N. (1985). Montereian Hills II. Petrography, major and trace element geochemistry, and strontium isotopic chemistry of the eastern intrusions: Mounts Shefford, Brome, and Megantic. J. Petrol., 26(2), 418-448.

- Eby, G.N. (1990). The A-type granitoids: A review of their occurrence and chemical characteristics and speculations on their petrogenesis. Lithos, **26**, 115-134.
- Edgar, A.D. (1977). A comment on "Alkalinity revisited: pattern recognition in the chemistry of nepheline syenite rocks" by Dagbert et al. Geochim. Cosmochim. Acta, **41**, 439-440.
- Eglington, E.B. (1987). Field, geochemical and isotope studies of selected areas of Proterozoic crust in south-central Natal. Ph.D. thesis (unpubl.), Natal University, Durban.
- Eglington, B.M. & Harmer, R.E. (1989). GEODATE: a program for the processing and regression of isotope data using IBM-compatible microcomputers. CSIR Manual EMA-H8901, Pretoria.
- Eglington, B.M. & Kerr, A. (1989). Rb-Sr isotope and geochemical characteristics of intrusive units from the Port Edward-Port Shepstone area, Natal. Trans. geol. Soc. S. Afr., **89**, 199-213.
- Evans, M.J., Eglington, B.M., Kerr, A. & Saggerson, E.P. (1987). The geology of the Proterozoic rocks around Umzinto, southern Natal, South Africa. S. Afr. J. Geol., **90**, 471- 488.
- Fitton, J.G. (1987). The Cameroon line, West Africa: a comparison between oceanic and continental alkaline volcanism. Spec. Publ. geol. Soc. Lond., **30**, 273-291.
- Floor, P. (1974). Alkaline gneisses. In: Sorensen, H., ed., The alkaline rocks, 124-142. Wiley Interscience, NY.
- Foley, S.F., Venturelli, G., Green, D.H. & Toscani, L. (1987). The ultrapotassic rocks: characteristics, classification and constraints for petrogenetic models. Earth Sci. Rev., **24**, 81-134.

- Gellatly, D.C. & Hornung, G. (1968). Metasomatic nepheline-bearing gneisses from Darkainle, Somali Republic. J. Geol., **76**, 678-691.
- Gittins, J. (1979). The feldspathoidal alkaline rocks. In: Yoder, H.S. Jr., ed., The evolution of the igneous rocks, 351-390. Princeton University Press, NJ.
- Grantham, G. (1983). The tectonic, metamorphic and intrusive history of the Natal Mobile Belt between Glenmore and Port Edward. M.Sc. thesis (unpubl.), Natal University, Pietermaritzburg.
- Hall, A. (1987). Igneous petrology. Longman, England.
- Hanson, G.N. (1978). The application of trace elements to the petrogenesis of igneous rocks of granitic composition. Earth Planet Sci. Lett., **38**, 26-43.
- Harker, A. (1909). The natural history of igneous rocks. Macmillan, NY.
- Harmer, R.E. (1979). Pre-Cape geology of the Tugela Valley north of Kranskop, Natal. M.Sc. thesis (unpubl.), Natal University, Durban.
- Harmer, R.E. (1985). Rb-Sr isotopic study of units of the Pienaars River Alkaline Complex, north of Pretoria. Trans. geol. Soc. S. Afr., **88**, 215-224.
- Harris, N.B.W. & Marriner, G.F. (1980). Geochemistry and petrogenesis of a peralkaline granite complex from the Midian Mountains, Saudi Arabia. Lithos, **13**, 325-337.
- Harris, N.B.W., Duyverman, H.J. & Almond, D.C. (1983). The trace element and isotope geochemistry of the Sabaloka Igneous Complex, Sudan. J. geol. Soc. Lond., **140**, 245-256.

- Hill, J.D. & Thomas, A. (1983). Correlation of two Helikian peralkaline granite - volcanic centres in central Labrador. Can. J. Earth Sci., **20**, 753-763.
- Höy, T. & Kwong, Y.T.J. (1986). The Mount Crace carbonatite - an Nb and light rare earth element-enriched marble of probable pyroclastic origin in the Shuswap Complex, southeastern British Columbia. Econ. Geol., **81**, 1374- 1386.
- Hutchison, C.S. (1974). Laboratory handbook of petrographic techniques. Wiley Interscience, N.Y.
- Keith, M.L. (1939). Petrology of the alkaline intrusive at Blue Mountain, Ontario. Bull. geol. Soc. Am., **50**, 1795-1826.
- Kerr, A. (1985). Characterization of the granitic rocks from the Valley of a Thousand Hills area, Natal. S. Afr. J. Sci., **81**, 475-479.
- Kumarapeli, P.S., Dunning, G.R., Pinston, H. & Shaver, J. (1989). Geochemistry and U-Pb zircon age of comenditic metafelsites of the Tibbit Hill Formation, Quebec Appalachians. Can. J. Earth Sci., **26**, 1374-1383.
- Lameyre, J. & Bowden, P. (1982). Plutonic rock type series: discrimination of various granitoid series and related rocks. J. volcanol. geotherm. Res., **14**, 169-186.
- Le Bas, M.J. (1977). Carbonatite-nephelinite volcanism. Wiley Interscience, Lond.
- Le Bas, M.J. (1987). Nephelinites and carbonatites. Spec. Publ. geol. Soc. Lond., **30**, 53-83.
- Le Maitre, R.W. (1976). The chemical variability of some common igneous rocks. J. Petrol., **17**, 589-637.

- Liegeois, J.P. Bertrand, H., Black, R., Caby, R. & Fabre, J. (1983). Permian alkaline undersaturated and carbonatite province, and rifting along the West African craton. Nature, Lond., **305**, 42-43.
- Loiselle, M.C. & Wones, D.R. (1979). Characteristics of anorogenic granites. Abstr. with Programs, A.G.M. geol. Soc. Am., p.539.
- Lulin, J.M. (1985). Un Nouveau gite a Nb, Ta, U, T.R. d'origine magmatique en Afrique orientale: le complexe alcalin tectonise de Meponda, Precambrian de la Province du Niassa. Documents B.R.G.M., **87**, 1-352. Orleans, France.
- Lurie, J. (1985). Chemical classification of Pilanesberg rocks. Trans. geol. Soc. S. Afr., **88**, 472-473.
- Macdonald, R. (1975a). Nomenclature and petrochemistry of the peralkaline oversaturated extrusive rocks. Bull. Volcanol., **38**, 498-516.
- Macdonald, R. (1975b). Tectonic settings and magma associations. Bull. Volcanol., **38**, 575-593.
- Macdonald, R. (1987). Quaternary peralkaline silicic rocks and caldera volcanoes of Kenya. Spec. Publ. geol. Soc. Lond., **30**, 313-333.
- Macdonald, R. & Bailey, D.K. (1973). The chemistry of the peralkaline oversaturated obsidians. Prof. Pap. U.S. geol. Surv., **440**, N1-N37.
- MacDonald, R., Davies, G.R., Bliss, C.M., Leat, P.T., Bailey, D.K. & Smith, R.L. (1987). Geochemistry of high silica peralkaline rhyolites, Naivasha, Kenya Rift Valley. J. Petrol., **28**, 979-1008.

- Maniar, P.D. & Piccoli, P.M. (1989). Tectonic discrimination of granitoids. Bull. geol. Soc. Am., **101**, 635-643.
- Marsh, J.S. (1987). Evolution of a strongly differentiated suite of phonolites from the Klinghardt Mountains, Namibia. Lithos, **20**, 41-58.
- Matthews, P.E. (1972). Possible Precambrian obduction and plate - tectonics in southeast Africa, Nature, Lond., **240**, 37-39.
- Matthews, P.E. (1981). Eastern or Natal sector of the Namaqua-Natal Mobile Belt in southern Africa. In: Hunter, D.R., ed., Precambrian of the southern hemisphere, 705-725. Elsevier, Amsterdam.
- Matthews, P.E. & Charlesworth, E.G. (1981). 1 : 140000 Map, Northern margin of the Namaqua-Natal Mobile Belt in Natal. Compiled at Natal University. Colorgraphic Press, Durban.
- McCarthy, M.J. (1961). The geology of the Empangeni fault area. M.Sc. thesis (unpubl.), Natal University, Durban.
- Mendonidis, P. & Grantham, G.H. (1989). The distribution, petrology and geochemistry of the Munster Suite, south coast, Natal. S. Afr. J. Geol., **92**, 377-388.
- Mendonidis, P. & Strydom, D. (1989). Tectonic history of Proterozoic granulite gneisses between Glenmore and Southbroom, southern Natal. S. Afr. J. Geol., **92**, 352-368.
- Middlemost, E.A.K. (1974). Petrogenetic model for the origin of carbonatites. Lithos, **7**, 275-278.
- Middlemost, E.A.K. (1985). Magmas and magmatic rocks: an introduction to igneous petrology. Longman, London.

- Moller, P., Morteani, G. & Schley, F. (1980). Discussion of REE distribution patterns of carbonatites and alkalic rocks. Lithos **13**, 171-179.
- Nakamura, N. (1974). Determination of REE, Ba, Fe, Mg, Na and K in carbonaceous and ordinary chondrites. Geochim. Cosmochim. Acta, **38**, 757-775.
- Nicholls, J. (1988). The statistics of Pearce element diagrams and the Chayes closure problem. Contr. Mineral. Petrol., **99**, 11-24.
- Nicolaysen, L.O. & Burger, A.J. (1965). Note on an extensive zone of 1000 million year-old metamorphic and igneous rocks in southern Africa. Sci. Terre, **10**, 497-516.
- Nielsen, T.F.D. (1987). Tertiary alkaline magmatism in East Greenland: a review. Spec. Publ. geol. Soc. Lond., **30**, 489-515.
- Norrish, K. & Hutton, J.T. (1969). An accurate x-ray spectrographic method for the analysis of a wide range of geological samples. Geochim. Cosmochim. Acta, **33**, 431- 453.
- Payne, J.G. (1968). Geology and geochemistry of the Blue Mountain nepheline syenite. Can. J. Earth Sci., **5**, 259-273.
- Peacock, M.A. (1931). Classification of igneous rocks series. J. Geol., **39**, 54-67.
- Pearce, J.A., Harris, N.B.W. & Tindle, A.G. (1984). Trace element discrimination diagrams for the tectonic interpretation of granitic rocks. J. Petrol., **25**, 956- 983.
- Pell, J. & Höy, T. (1989). Carbonatites in a continental margin environment - the Canadian Cordillera. In, Bell, K., ed., Carbonatites - genesis and evolution, 200-220. Unwin Hyman, London.

- Petersen, J.S. (1978). Composite plutonic ring-complexes: a structural characteristic of rift zone plutonism. In: Neumann, E.R. & Ramberg, I.B., eds., Petrology and Geochemistry of Continental Rifts, 217-229. Riedel Publishing, Dordrecht.
- Petro, W.L., Vogel, T.A. & Wilband, J.T. (1979). Major-element chemistry of plutonic rock suites from compressional and extensional plate boundaries. Chem. Geol., **26**, 217-235.
- Rigotti, S.O. (1977). The geology of the Tugela Group in the Middledrift area, Natal. M.Sc. thesis (unpubl.), Natal University, Durban.
- Rock, N.M.S. (1976). Fenitization around the Monchique alkaline complex, Portugal. Lithos, **9**, 263-279.
- Rock, N.M.S. (1979). Petrology and origin of the type monchiquites and associated lamprophyre dykes of Serra de Monchique, Portugal. Trans. Royal Soc. Edinburgh, **70**, 149-170.
- Rock, N.M.S. (1987). The nature and origin of lamprophyres: an overview. Spec. Publ. geol. Soc. Lond., **30**, 191-226.
- Rock, N.M.S. (1991). Lamprophyres. Blackie & Son, London.
- Rogers, J.J.W. & Greenberg, J.K. (1990). Late-orogenic, post-orogenic, and anorogenic granites: distinction by major-element and trace-element chemistry and possible origins. J. Geol., **98**, 291-309.
- SACS (1980). Stratigraphy of South Africa. Part 1: Lithostratigraphy of the Republic of South Africa, South West Africa/Namibia and the Republics of Bophuthatswana, Transkei and Venda. Handbk geol. Surv. S. Afr., **8**.
- Saggerson, E.P. (1970). The structural control and genesis of alkaline rocks of central Kenya. Bull. Volcanol., **34**, 38-76.

- Sawkins, F.J. (1986). The recognition of palaeorifting in mid- to late-Proterozoic terranes: implications for the exploration geologist. Trans. geol. Soc. S. Afr., **89**, 223-232.
- Schade, J. & Cornell, D.H. (1989). Rare earth element and isotopic evidence for the genesis of the Prieska massive sulfide deposit, South Africa. Econ. Geol., **84**, 49-63.
- Schulze-Hulbe, A. (1977). A study of the structure and metamorphism of the rocks of the Tugela Group exposed in the Mambula-Mbongolwane area, Natal. M.Sc. thesis (unpubl.), Natal University, Durban.
- Scogings, A.J. (1985). The geology of the Ngoye Granite Gneiss Formation. M.Sc. thesis (unpubl.), Durban- Westville University, Durban.
- Scogings, A.J. (1986). Peralkaline gneissic granites in the Ngoye Granite-Gneiss Formation, Natal. Trans. geol. Soc. S. Afr., **89**, 361-365.
- Scogings, A.J. (1988). Geochemistry of the Wangu anomaly, Mvuzane rare elements project, KwaZulu. Int. Rep. 2554 (STK) Pretoria.
- Scogings, A.J. (1989). Peralkaline granitoid and associated mafic gneisses northwest of Eshowe, Natal. S. Afr. J. Geol., **92**, 339-351.
- Scogings, A.J. (1990a). Alkaline/peralkaline gneisses near the northern margin of the Natal Structural and Metamorphic Province. Ext. Abstr. Geocongress '90. 497-500, Geol. Soc. S. Afr., Cape Town.
- Scogings, A.J. (1990b). Ngoye Complex. In: M.R. Johnson, ed., Catalogue of South African Lithostratigraphic Units, **2**, 37-38. Pretoria.
- Scogings, A.J. (1991a). Bulls Run Complex. In, M.R. Johnson, ed., Catalogue of South African Lithostratigraphic Units, **3**, (in press).

- Scogings, A.J. (1991b). Wangu Granite Gneiss. In, M.R. Johnson, ed., Catalogue of South African Lithostratigraphic Units, 3, (in press).
- Scogings, A.J. & Forster, I.F. (1989). Gneissose carbonatites in the Bulls Run complex, Natal. S. Afr. J. Geol., 92(1), 1-10.
- Seyler, M. (1986). Petrology and genesis of Hercynian alkaline orthogneisses from Provence, France. J. Petrol., 27(5), 1229-1251.
- Shaw, D.M. (1969). A review of K-Rb fractionation trends by covariance analysis. Geochim. Cosmochim. Acta, 32, 573- 601.
- Smalley, T.J. (1979). Structure and metamorphism of the Tugela Group within the northern zone of the Natal Mobile Belt. Ph.D. thesis (unpubl.), Natal University, Durban.
- Sorensen, H. (1974). Introduction. In: Sorensen, H., ed., The alkaline rocks, 3-11. Wiley Interscience, NY.
- Sorensen, H. (1968). Rhythmic igneous layering in peralkaline intrusions. Lithos, 2, 261-283.
- Steiger, R.H. & Jager, E. (1977). Subcommittee on geochronology: convention on the use of decay constants in geo- and cosmochemistry. Earth Planet. Sci. Lett., 36, 359-362.
- Streckeisen, A. (1976a). To each plutonic rock its proper name. Earth Sci. Rev., 12, 1-33.
- Streckeisen, A. (1976b). Classification of the common igneous rocks by means of their chemical composition - a provisional attempt. N. Jb. Min., 1, 1-15.

- Streckeisen, A. (1978). Classification and nomenclature of volcanic rocks, lamprophyres, carbonatites and melilitic rocks, N. Jb. Min., 134, 1-14.
- Streckeisen, A. & Le Maitre, R.W. (1979). A chemical approximation to the modal QAPF classification of the igneous rocks. N. Jb. Min., 136, 169-206.
- Sylvester, P.J. (1989). Post-collisional alkaline granites. J. Geol., 97, 261-280.
- Tankard, A.J., Jackson, M.P.A., Erikson, K.A., Hobday, D.K., Hunter, D.R. & Minter, W.E.L. (1982). Crustal Evolution of southern Africa. Springer-Verlag, NY.
- Taylor, R.P., Strong, D.F. & Kean, B.F. (1980). The Topsails Igneous Complex: Silurian-Devonian peralkaline magmatism in western Newfoundland. Can. J. Earth Sci., 17, 425- 439.
- Thomas, R.J. (1989). A tale of two tectonic terranes. S. Afr. J. Geol., 92, 306-321.
- Thomas, R.J. (1990). Metallogensis in a Kibaran accreted terrane: the Natal Metamorphic Province, South Africa. Bull. I.G.C.P. No. 255 Newsletter, 3, 93-99.
- Thomas, R.J. & Mawson, S.A. (1989). Newly discovered outcrops of Proterozoic basement rocks in northeast Transkei. S. Afr. J. Geol., 92, 369-376.
- Thomas, R.J. & Eglington, B.M. (1990). A Rb-Sr, Sm-Nd and U-Pb zircon isotopic study of the Mzumbe Suite, the oldest intrusive granitoid in southern Natal, South Africa. S. Afr. J. Geol., 93, 761-765.

- Thomas, R.J., Bullen, W.D., de Klerk, I.D. & Scogings, A.J. (1990). The distribution and genesis of precious and base metal mineralization in the Natal Metamorphic Province, South Africa. S. Afr. J. Geol., **93**, 683-695.
- Thompson, R.N. & Fowler, M.B. (1986). Subduction-related shoshonitic and ultrapotassic magmatism: a study of Siluro-Ordovician syenites from the Scottish Caledonides. Contrib. Mineral. Petrol., **94**, 507-522.
- Upton, B.G.J. & Emeleus, C.H. (1987). Mid-Proterozoic alkaline magmatism in southern Greenland: the Gardar Province. Spec. Publ. geol. Soc. Lond., **30**, 449-471.
- Verwoerd, W.J. (1967). The carbonatites of South Africa and South West Africa. Handbk geol. Surv. S. Afr., **6**, 1-452.
- Von Backström, J.W. (1962). Zircon, ilmenite and monazite occurrences on Bull's Run Estate north-northwest of Eshowe, Natal. Ann. geol. Surv. S. Afr., **1**, 137-146.
- Von Eckermann, H. (1948). The alkaline and carbonatite dykes of the Alnö Formation on the mainland north-west of Alnö Island. K. Svenska Vetensk Akad. Handl., **7** (2).
- Watson, E.B. (1971). Zircon saturation in felsic liquids: experimental results and applications to trace element geochemistry. Contrib. Mineral. Petrol., **70**, 407-419.
- Wendlandt, R.F. & Harrison, W.J. (1979). Rare earth partitioning between immiscible carbonate and silicate liquids and CO₂ vapor: results and implications for the formation of light rare earth-enriched rocks. Contrib. Mineral. Petrol. **69**, 409-419.
- Whalen, J.B., Currie, L.C. & Chappell, B.W. (1987). A-type granites: geochemical characteristics, discrimination and petrogenesis. Contr. Miner. Petrol., **95**, 407-419.

- Wilson, A.H. (1990). Tugela Rand Layered Suite. In: M R Johnson, ed., Catalogue of South African Lithostratigraphic Units, 2, 47-48.
- Wilson, M. (1987). Igneous petrogenesis. Unwin Hyman, Lond.
- Winchester, J.A. & Floyd, P.A. (1977). Geochemical discrimination of different magma series and their differentiation products using immobile elements. Chem. Geol., 20, 325-343.
- Winchester, J.A. & Max, M.D. (1987). A displaced and metamorphosed peralkaline granite related to the late Proterozoic Labrador and Gardar suites: the Doolough Granite of County Mayo, northwest Ireland. Can. J. Earth Sci., 24, 631-642.
- Windley, B.F. (1989). Anorogenic magmatism and the Grenvillian Orogeny. Can. J. Earth Sci., 26, 479-489.
- Woolley, A.R. (1982). A discussion of carbonatite evolution and nomenclature, and the generation of sodic and potassic fenites. Min. Mag., 46, 13-17.
- Woolley, A.R. (1989). The spatial and temporal distribution of carbonatites. In: Bell, K. ed., Carbonatites - genesis and evolution, 15-37. Unwin Hyman, London.
- Woolley, A.R. & Kempe, D.R.C. (1989). Carbonatites: nomenclature, average chemical compositions, and element distribution. In: Bell, K., ed., Carbonatites - genesis and evolution, 1-14. Unwin Hyman, London.
- Wright, J.B. (1969). A simple alkalinity ratio and its application to questions of non-orogenic granite genesis. Geol. Mag., 106, 370-384.
- York, D. (1969). Least-squares fitting of a straight line with correlated errors. Earth Planet Sci. Lett., 5, 320-234.

APPENDICES

APPENDIX 1	Modal analyses
APPENDIX 2	Geochemical data
APPENDIX 3	Norms
APPENDIX 4	Publications and symposium abstracts

APPENDIX 1

MODAL ANALYSES

Modal analyses are presented for the majority of geochemical samples (Tables A1.1, A1.2 and A1.3). Some of the whole-rock samples collected during 1982, prior to the commencement of the Ngoye project, do not have accompanying modal data as the entire samples were crushed for geochemical analysis and no material retained for thin-sectioning. Modal analyses were not performed on samples of mylonite, as their fine-grain size does not permit efficient staining or accurate identification of felsic minerals.

Modal analyses were conducted on thin sections that were stained for K-feldspar, plagioclase and nepheline according to the methods described by Hutchison (1974). In the case of lineated, well-foliated samples, sections were cut both parallel and perpendicular to the lineation and the resulting mode is therefore an average of determinations in each direction. A minimum of 1 000 points were counted per samples, using a Swift counter.

The identification of mineral phases was done using conventional optical techniques. However, accurate determination of the anorthite content of plagioclase proved problematic, mainly as a result of deformational strain effects, so that microprobe analyses were carried out on selected samples as an aid to identification. Accurate anorthite contents are critical in the classification of alkaline rocks when using modal data, as all plagioclase with less than 5% An is combined with K-feldspar, in the QAP diagram (Streckeisen 1976a).

Maps showing the location of rock samples collected for modal and geochemical analyses are given as Figures A1 and 4.1. A list of sample descriptions is given in Tables I, II and III, with samples arranged in order of increasing silica content, per rock type. The sample numbers, which record fieldmapping stations, are therefore not in numerical order.

TABLE I: NGOYE COMPLEX

SAMPLE	DESCRIPTION	LOCALITY, FIG. A1 MAP REFERENCES
N574	Mesocrystic biotite granite	A8
N564	Mesocrystic biotite granite	A8
N2	Mesocrystic biotite granite	B6
N306	Mesocrystic biotite granite	C5
N708	Mesocrystic biotite granite	C6
N584	Mesocrystic biotite granite	B7
C47	Mesocrystic biotite granite	C6
N447	Biotite-hornblende granite	B3
C107	Biotite-hornblende granite	C2
N373	Biotite-hornblende granite	C3
N104	Biotite-hornblende granite	B4
N700	Biotite-hornblende granite	C3
C106	Biotite-hornblende granite	C3
N348	Biotite-hornblende granite	C3
N665	Biotite-hornblende granite	B5
N590	Biotite-hornblende granite	B8
N701	Biotite-hornblende granite	B4
N351	Biotite-hornblende granite	D3
N635	Biotite-hornblende granite	C1
N675	Biotite-hornblende granite	C2
N664	Biotite-hornblende granite	B5
N211	Biotite-hornblende granite	C5 (Fig. 2.2)
N613	Biotite granite	B5
N705	Biotite granite	B6
N568	Biotite granite	A8
N8	Biotite granite	B5
N604	Biotite granite	B5
N682	Biotite granite	B4
N34	Garnet-muscovite granite	B7
N11	Garnet-muscovite granite	B6
N710	Garnet-muscovite granite	B7
N35	Garnet-muscovite granite	B7

N272	Riebeckite-biotite granite	C5 (Fig. 2.2)
N468	Riebeckite-biotite granite	D1
N160	Riebeckite-biotite granite	C5 (Fig. 2.2)
N548	Riebeckite-biotite granite	D4
C46	Riebeckite-biotite granite	C5 (Fig. 2.2)
N58	Riebeckite-biotite granite	D2
N330	Riebeckite-granite	C5 (Fig. 2.2)
N145	Riebeckite-granite	C5 (Fig. 2.2)
N142	Riebeckite granite	C5 (Fig. 2.2)
N181	Riebeckite granite	C5 (Fig. 2.2)
N331	Aegirine granite	C5 (Fig. 2.2)
C110	Magnetite granite	C5 (Fig. 2.2)
NG2c	Magnetite granite	C5 (Fig. 2.2)
NG2	Magnetite granite	C5 (Fig. 2.2)
N331a	Magnetite granite	C5 (Fig. 2.2)
N712	Magnetite-quartz rock	C5 (Fig. 2.2)
NR189	Magnetite quartz rock	C5 (Fig. 2.2)
N63	Magnetite-quartz rock	C5 (Fig. 2.2)
N15	Magnetite-quartz rock	C5 (Fig. 2.2)
NR80	Magnetite-quartz rock	C5 (Fig. 2.2)
N17	Magnetite-quartz rock	C5 (Fig. 2.2)
N193	Magnetite-quartz rock	C5 (Fig. 2.2)
N19	Magnetite quartz rock	C5 (Fig. 2.2)
NG2b	Chlorite syenite	C5 (Fig. 2.2)
NG2a	Chlorite syenite	C5 (Fig. 2.2)
N21	Hornblende monzodiorite	B5

TABLE II: BULLS RUN COMPLEX

SAMPLE	DESCRIPTION	LOCALITY, FIG. A1
		MAP REFERENCES
B230	Biotite-muscovite syenite	H1
B179	Biotite-muscovite syenite	F7 (Fig. 3.3)
B48	Biotite-muscovite syenite	F7 (Fig. 3.3)
B231	Biotite-muscovite syenite	F7 (Fig. 3.3)
B34	Biotite-muscovite syenite	H1

B121	Biotite-muscovite syenite	G6
B105	Biotite-muscovite syenite	F6
B237a	Biotite-muscovite syenite (mylonite)	G4 (Fig. 3.2)
B95	Biotite-muscovite syenite	G4 (Fig. 3.2)
B54	Biotite-muscovite syenite	G3
B4a	Biotite-muscovite syenite	F4 (Fig. 3.2)
B218	Biotite-muscovite syenite	F6
B236	Biotite-muscovite syenite	G4 (Fig. 3.2)
B95a	Biotite-muscovite syenite	G4 (Fig. 3.2)
B81a	Muscovite rock	F7 (Fig. 3.3)
B213	Feldspathic ijolite	F7 (Fig. 3.3)
B175	Feldspathic ijolite	F7 (Fig. 3.3)
B212	Feldspathic ijolite	F7 (Fig. 3.3)
B44	Biotite-nepheline syenite	F7 (Fig. 3.3)
B43	Biotite-nepheline syenite	F7 (Fig. 3.3)
B233	Biotite-hornblende nepheline syenite	F7 (Fig. 3.3)
B66	Biotite-hornblende nepheline syenite	F7 (Fig. 3.3)
B110	Biotite-nepheline syenite	F6
B80	Biotite-hornblende nepheline syenite	F7 (Fig. 3.3)
B232	Biotite-nepheline syenite	F7 (Fig. 3.3)
B82	Biotite-hornblende nepheline syenite	F8 (Fig. 3.3)
B181	Biotite-hornblende nepheline syenite	F7 (Fig. 3.3)
B23	Biotite-nepheline syenite	F5
B222	Biotite-nepheline syenite	F4 (Fig. 3.2)
B96	Biotite-nepheline syenite	G3
B86	Biotite-nepheline syenite	G4 (Fig. 3.2)
B100	Biotite-nepheline syenite	G3
B42	Biotite-nepheline syenite	G1
B240	Biotite-nepheline syenite	G4 (Fig. 3.2)
B85	Biotite-nepheline syenite	G4 (Fig. 3.2)
B239	Biotite-nepheline syenite	G4 (Fig. 3.2)
B122	Biotite-nepheline syenite	G6
B238	Biotite-nepheline syenite	G4 (Fig. 3.2)
B41	Biotite-nepheline syenite	G1
B55	Biotite-nepheline syenite	G3
B241	Biotite-nepheline syenite	G4 (Fig. 3.2)
B203	Albite syenite	F5
B204	Albite syenite	F5

B95b		
B228	Albite syenite	G5 (Fig. 3.2)
B183	Albite syenite	F4 (Fig. 3.2)
B20	Albite syenite	F5
B103	Albite syenite	F7
B220a	Albite syenite	F6
B227	Albite syenite	G5 (Fig. 3.2)
B192	Albite syenite	F5
B190	Albite syenite	F5
B220	Albite syenite	F6
B217	Lamprophyre dyke	F6
B67	Lamprophyre dyke	F7
B83a	Lamprophyre xenolith	G4 (Fig. 3.2)
B90a	Microsyenite	G4 (Fig. 3.2)
B32	Microsyenite	H1
B72	Microsyenite	G4 (Fig. 3.2)
B94	Microsyenite	G4 (Fig. 3.2)
B98	Microsyenite	G3
B51	Microsyenite	G3
B237	Microsyenite (mylonite)	G5 (Fig. 3.2)

TABLE III: WANGU

SAMPLE	DESCRIPTION	LOCALITY, FIG. 4.1
		MAP REFERENCES
W435	Magnetite granite	D3
W434	Magnetite granite	D3
H27	Magnetite granite	C4
W149	Magnetite granite	C3
MZa	Magnetite granite	C3
MZc	Aegirine granite	C3
MZb	Aegirine granite	C3
MZh	Aegirine granite	C3
W231	Aegirine granite	C3
W235	Aegirine granite	C3

W234	Aegirine granite	C3
W229	Aegirine granite	C3
W232	Magnetite-aegirine granite	C3
MZg	Magnetite-aegirine granite	C3
W233	Magnetite-aegirine granite	C3
MZe	Magnetite-aegirine granite	C3
MZf	Magnetite-aegirine granite	C3
M228	Lamprophyre	D3
W436	Lamprophyre	D3
W227	Lamprophyre	D3
H24	Halambu Granodiorite	B1
H23	Halambu Granodiorite	A3
H17	Halambu Granodiorite	A1
H18	Halambu Granodiorite	B4
H6	Halambu Granodiorite	B1

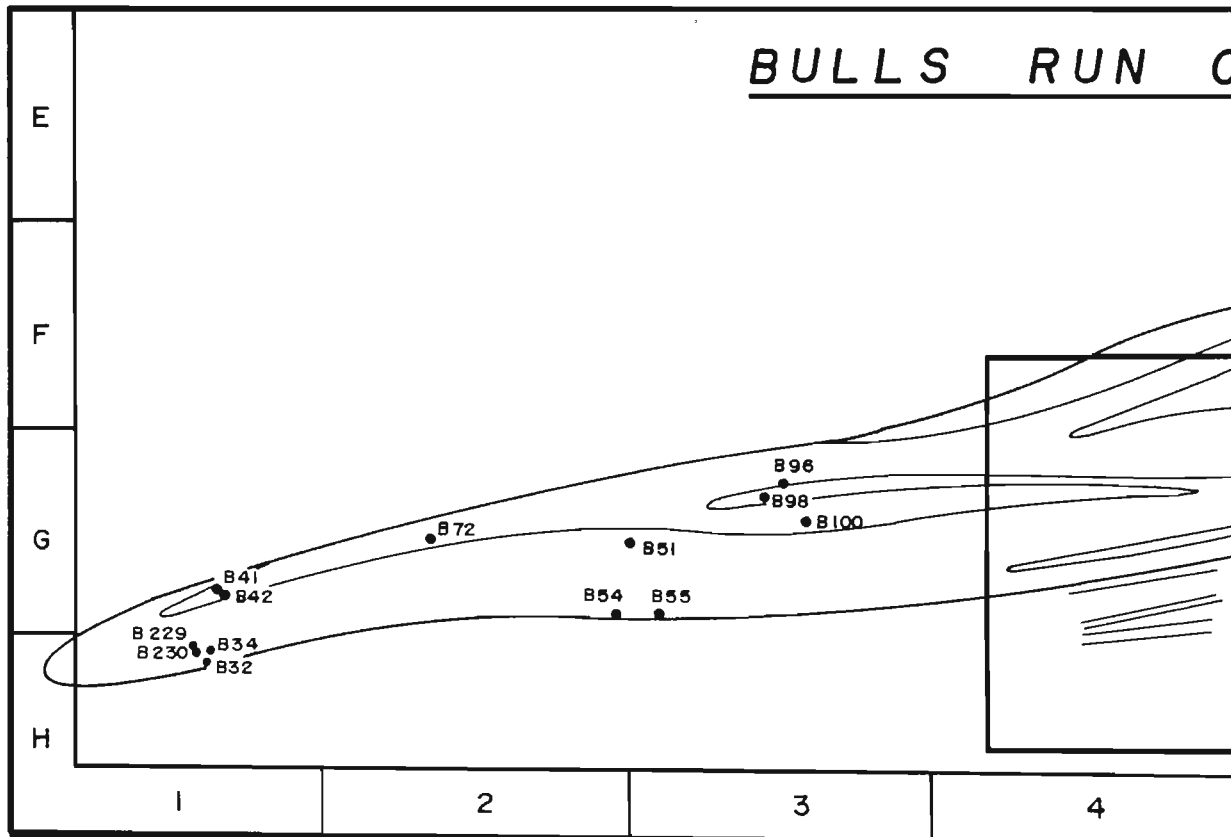
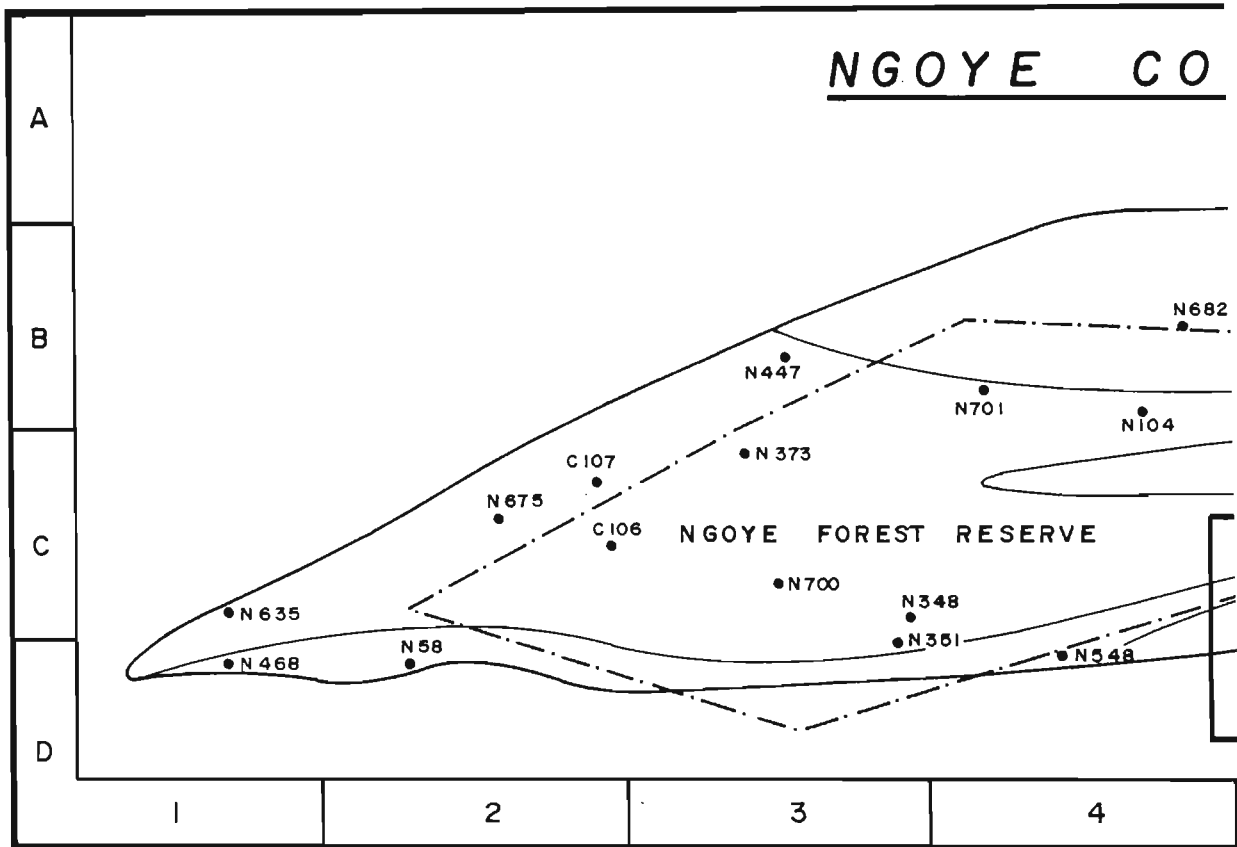
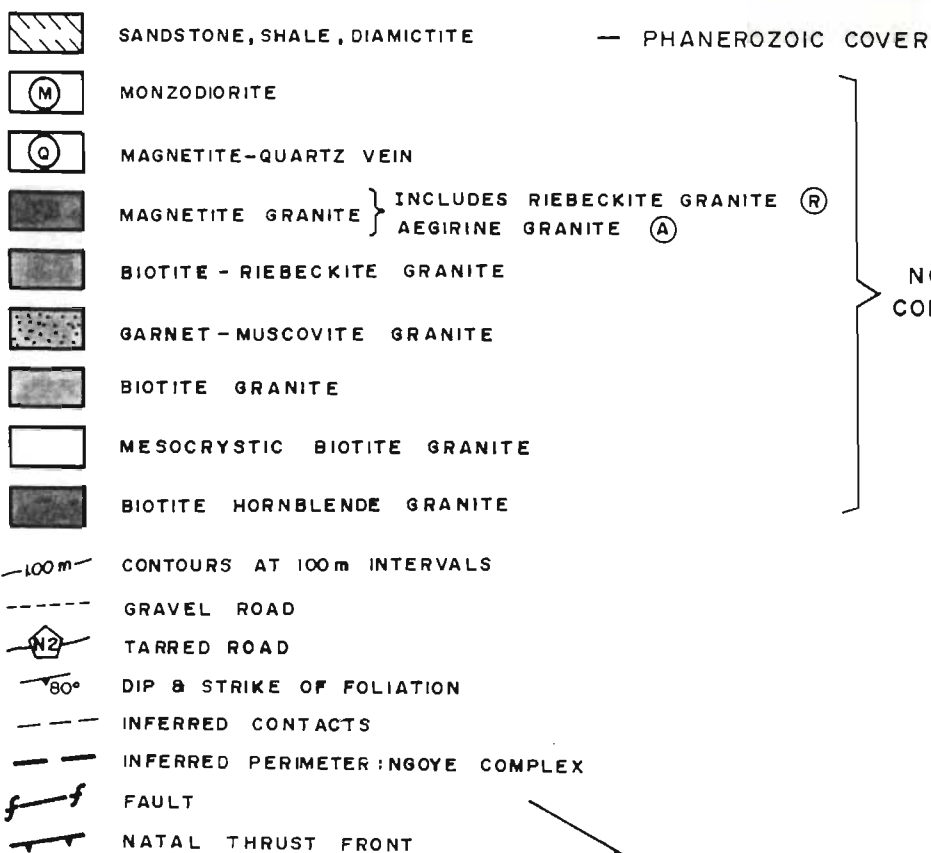
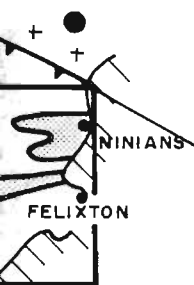


TABLE A1.1 (1)

[illegible][illegible]

EMPANGENI



NGOYE
COMPLEX

° 45'

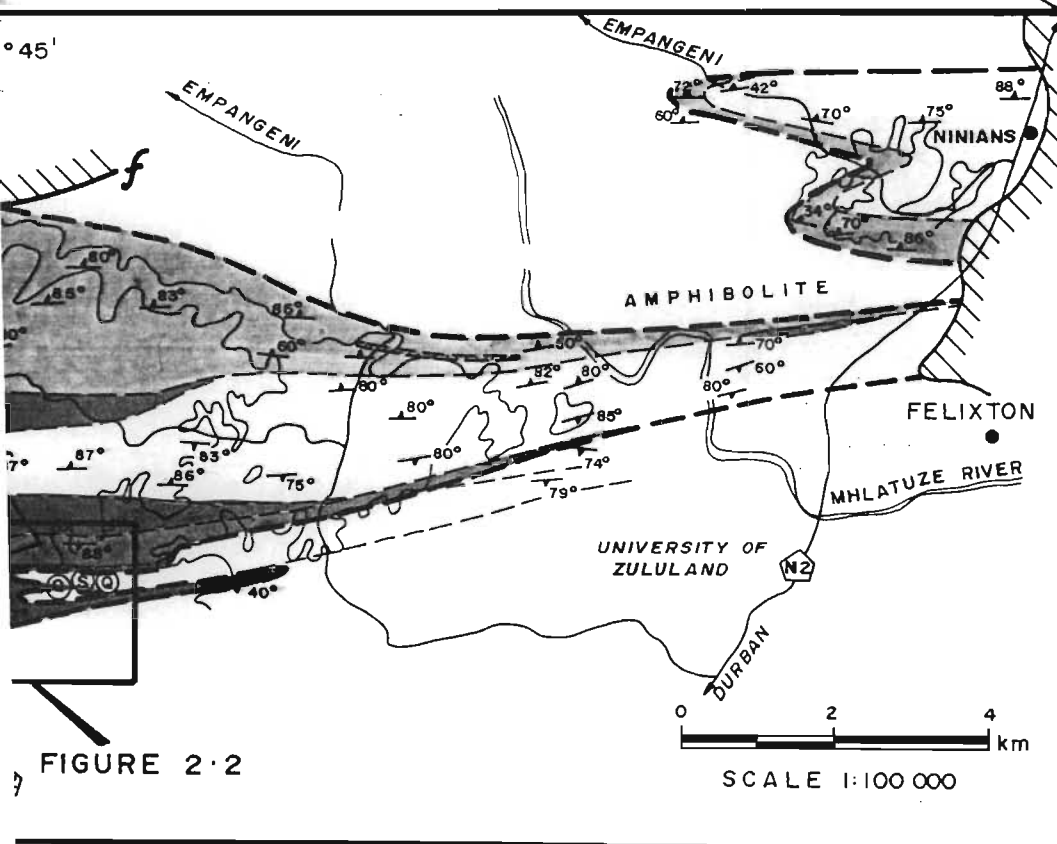


FIGURE 2.2

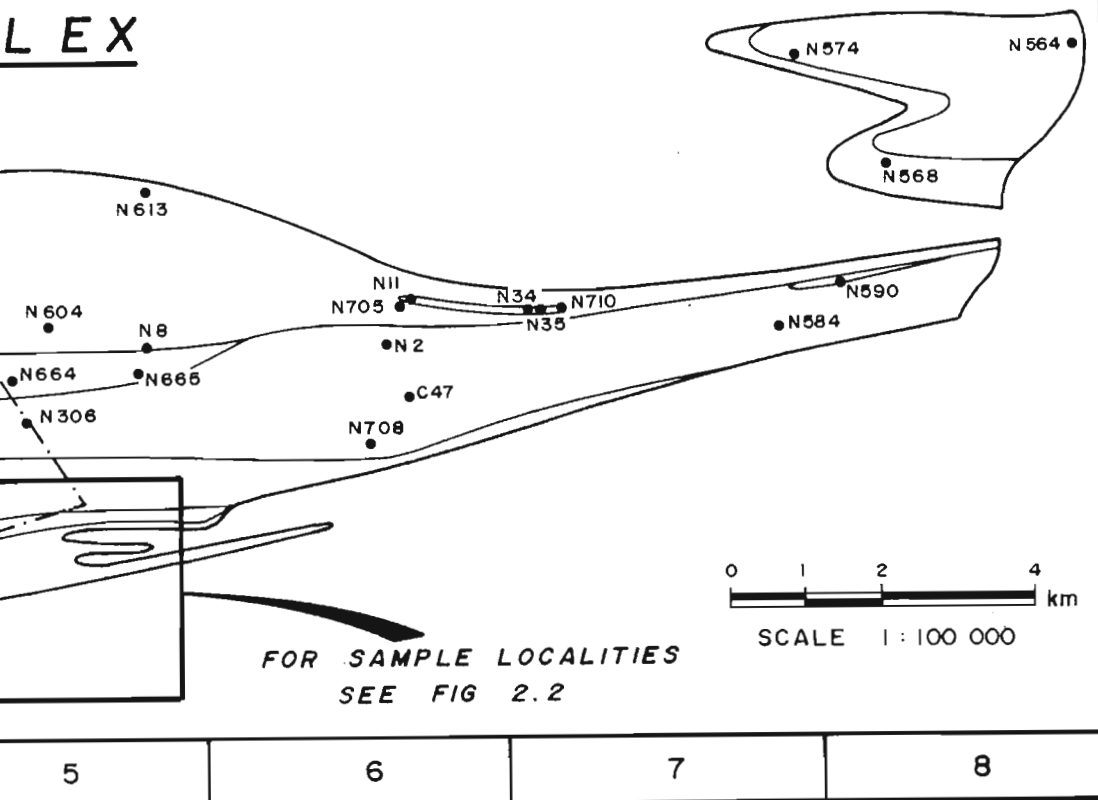
FIGURE 2.1

NGOYE COMPLEX

LOCALITY and GEOLOGY

SCALE : AS SHOWN

LEX



MPLEX

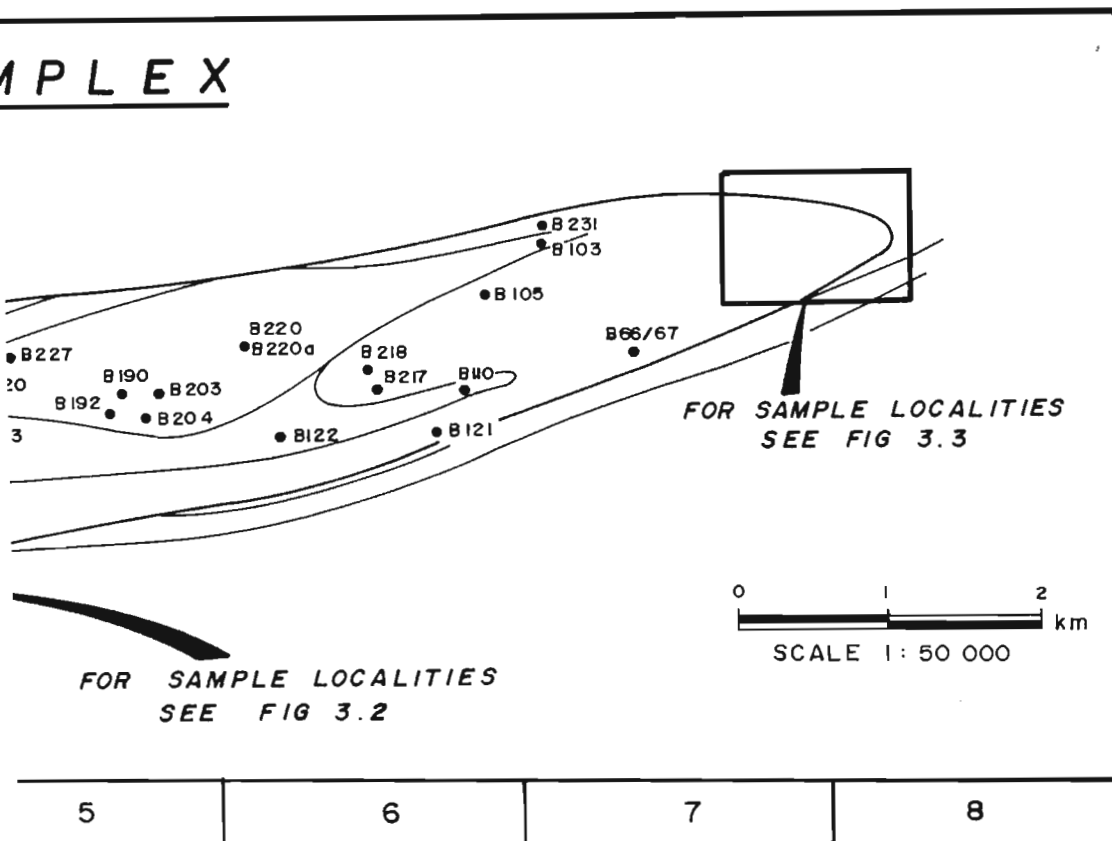
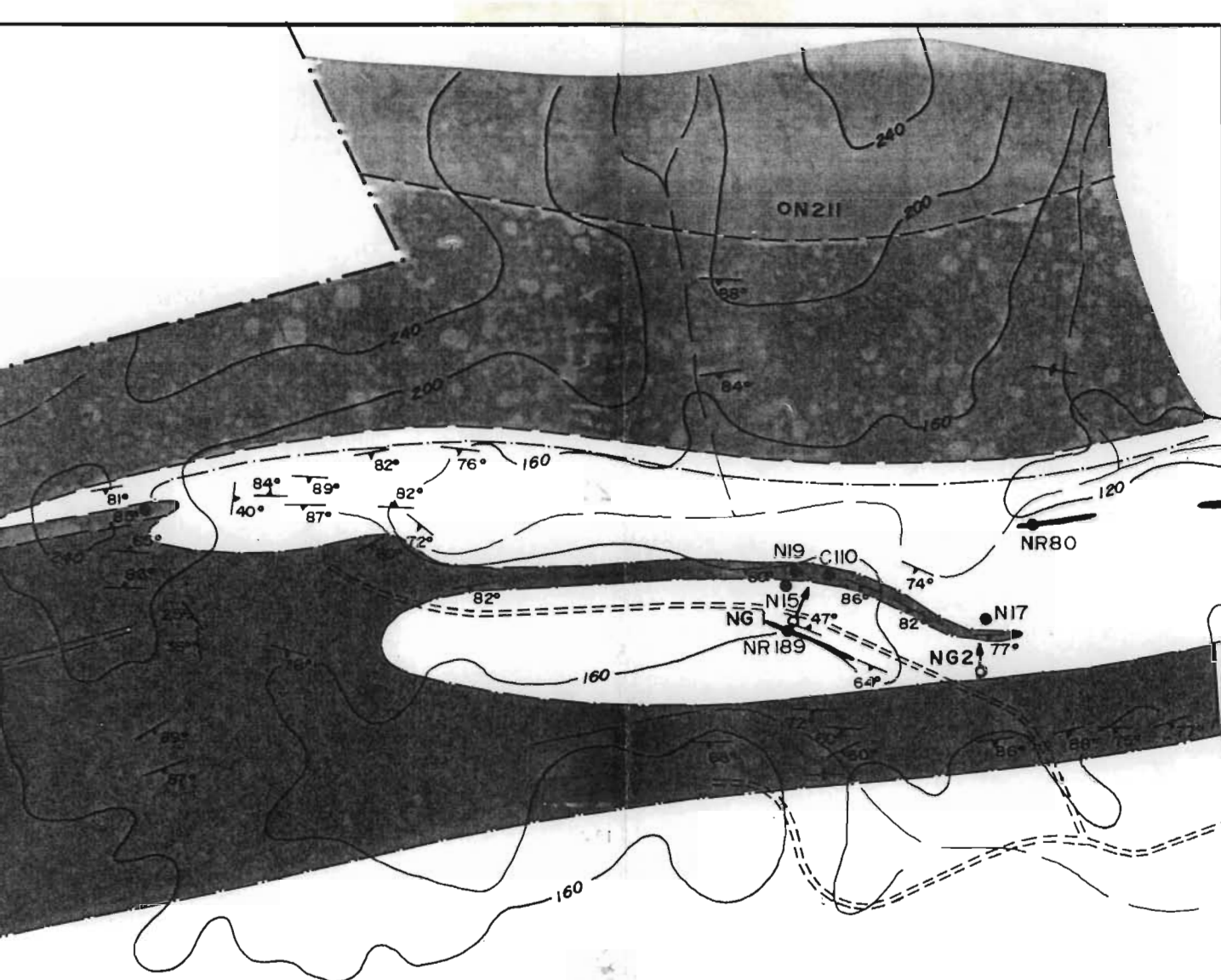


FIGURE A-1



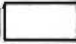


WHOLE-ROCK SAMPLE SITES

GEOLOGICAL BOUNDARIES AS IN
FIGURES 2.1 & 3.1

WANGU SAMPLES : SEE FIGURE 4.1



L E G E N D

-  MAGNETITE - QUARTZ VEIN
-  MAGNETITE GRANITE
-  AEGIRINE GRANITE
-  RIEBECKITE GRANITE
-  RIEBECKITE - BIOTITE GRANITE
-  BIOTITE - HORNBLLENDE GRANITE
-  AMPHIBOLITE



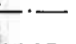

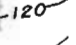


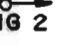
-  75° DIP & STRIKE OF FOLIATION
-  INFERRED CONTACT
-  PERIMETER : NGOYE COMPLEX
-  N145 WHOLE ROCK SAMPLE
-  120 CONTOURS AT 40m INTERVALS
-  STREAMS
-  TRACK
-  NG2 BOREHOLE

FIGURE 2.2

GEOLOGY OF THE AMANZAMNYAMA AREA SOUTHERN NGOYE COMPLEX

SCALE : AS SHOWN

(2)

[illegible][illegible]

(3)

	N62	N331a	N712	NR189	N63	N15	NR88	N193	N62b	N62a	N21
microcline	51	29	t	t	t	19	1	7	63	73	15
plagioclase	9	32	13	2	t	26	1	15	24	22	64
quartz	37	36	49	74	76	49	84	73	4	1	2
biotite	-	-	-	t	t	-	-	-	8	4	-
muscovite	-	-	-	-	-	-	-	-	t	t	-
hornblende	-	-	-	-	-	-	-	-	-	-	7
riebeckite	-	-	-	-	-	-	-	-	-	-	-
aegirine	-	-	-	-	-	-	-	-	-	-	1
epidote	-	-	-	-	-	-	-	-	-	-	3
sphene	-	-	1	1		t	t	-	-	-	1
opaque	2	2	27	18	15	5	14	3	t	t	-
garnet	-	-	-	-	-	-	-	-	-	-	1
calcite	-	-	-	-	-	-	-	-	-	-	4
fluorite	-	-	5	-	-	-	-	-	-	-	-
zircon	-	t	3	3	8	t	t	2	-	-	-
fergusonite	-	-	1	2	1	t	t	-	-	-	-

BULLS RUN

TABLE A1.2 (1)

	B230	B179	B48	B231	B34	B121	B105	B95	B54	B4a	B218	B236
quartz	-	-	-	-	-	-	-	-	-	-	-	-
microcline	32	19	13	45	21	31	35	7	34	39	9	30
plagioclase	40	34	39	28	54	45	36	53	34	43	70	50
nepheline	-	-	-	-	-	-	-	-	-	-	-	-
cancrinite	-	-	-	-	-	-	-	-	-	-	-	-
biotite	15	6	10	12	3	2	11	14	8	8	9	t
muscovite	1	40	33	14	22	16	14	25	24	10	11	20
hornblende	-	-	-	-	-	-	-	-	-	-	-	-
aegirine	-	-	-	-	-	-	-	-	-	-	-	-
riebeckite	-	-	-	-	-	-	-	-	-	-	-	-
calcite	11	1	4	t	t	6	3	t	t	t	t	-
apatite	-	-	t	-	-	t	t	-	-	t	-	-
zircon	-	-	-	-	-	-	-	-	-	-	-	-
opaque	-	-	t	t	-	-	t	-	t	t	-	-
pyrochlore	-	-	-	-	-	-	-	-	-	-	-	-
garnet	-	-	-	-	-	-	-	-	-	-	-	-
sphene	-	-	-	-	-	-	-	-	-	-	t	-

	B95a	B81a	B213	B175	B212	B44	B43	B233	B66	B110	B80	B232
quartz	-	-	-	-	-	-	-	-	-	-	-	-
microcline	40	-	12	11	7	43	35	40	46	25	33	29
plagioclase	48	5	19	1	29	11	24	10	19	31	22	24
nepheline	-	-	36	39	30	28	8	21	19	8	30	23
cancrinite	-	-	t	10	3	7	17	14	-	17	4	12
biotite	10	t	23	5	8	7	11	3	3	12	3	8
muscovite	2	95	-	-	-	-	t	-	-	3	-	-
hornblende	-	-	-	-	-	-	-	5	4	-	3	-
aegirine	-	-	t	22	6	-	-	-	1	-	-	-
riebeckite	-	-	-	-	-	-	-	-	-	-	-	-
calcite	t	-	6	t	1	2	3	t	3	4	1	2
apatite	-	-	t	3	t	t	-	t	t	t	t	t
zircon	-	-	-	-	-	-	-	-	-	-	-	-
opaque	-	-	3	-	2	1	2	2	t	t	2	2
pyrochlore	-	-	-	-	-	-	-	-	-	-	-	-
garnet	-	-	-	7	11	-	-	3	1	-	-	-
sphene	-	-	-	1	2	t	-	2	3	-	2	-

(2)

	B222	B82	B23	B181	B96	B86	B100	B42	B240	B85	B239	B122
quartz	-	-	-	-	-	-	-	-	-	-	-	-
microcline	46	52	35	40	48	52	36	31	38	44	48	29
plagioclase	19	4	26	19	18	21	33	37	34	18	32	42
nepheline	19	35	14	14	1	7	18	18	5	30	15	3
cancrinite	4	2	9	13	10	8	t	-	15	6	t	-
biotite	10	4	13	5	19	10	11	11	8	1	5	14
muscovite	-	-	t	-	-	-	1	t	-	-	-	12
hornblende	-	1	-	7	-	-	-	-	-	-	-	-
aegirine	-	-	-	-	-	-	-	-	-	-	-	-
riebeckite	-	-	-	-	-	-	-	-	-	-	-	-
calcite	1	1	2	-	3	1	t	-	-	t	t	t
apatite	t	t	t	-	-	-	-	-	-	t	-	-
zircon	-	-	-	-	-	-	-	-	-	-	-	-
opaque	-	t	-	t	t	t	-	2	-	-	-	-
pyrochlore	-	-	-	-	-	-	-	-	-	-	-	-
garnet	-	-	-	-	-	-	-	-	-	-	-	-
sphene	-	t	-	1	-	-	-	-	-	-	-	-

[illegible]

(3)

	B227	B192	B190	B220	B217	B67	B83a	B60	B62	B46
quartz	-	-	-	-	-	-	-	-	-	-
microcline	16	26	19	21	t	3	16		t	2
plagioclase	60	42	48	78	39	50	43	-	t	t
nepheline	20	23	25	-	-	-	5	-	-	-
cancrinite	t	-	2	-	-	6	-	-	-	-
biotite	3	8	5	1	48	29	27	3	12	9
muscovite	t	1	-	-	-	-	-	-	-	-
hornblende	-	-	-	-	-	-	-	-	-	-
aegirine	-	-	-	-	-	-	-	-	-	-
riebeckite	-	-	-	-	-	-	-	-	-	-
calcite	t	-	t	t	9	12	9	96	80	85
apatite	-	-	-	t	3	t	t	t	5	3
zircon	t	t	t	t	-	-	-	-	-	-
opaque	-	-	-	-	1	t	-	1	1	t
pyrochlore	-	-	t	-	-	-	-	-	1	t
garnet	-	-	-	-	-	-	-	-	-	-
sphene	-	-	-	-	-	-	t	-	-	-

[illegible]

WANGU

TABLE A1.3

	W435	W434	H27	W149	MZa	MZc	MZb	MZh	W231	W235	W234	W229
microcline	26	17	36	29	33	23	36	38	30	42	35	15
albite	39	47	24	25	21	45	31	33	35	25	27	30
quartz	26	28	34	40	43	22	24	23	25	25	30	40
biotite	t	1	1	t	t	1	t	t	-	3	4	-
aegirine	-	-	-	-	-	6	7	5	5	4	3	4
riebeckite	-	-	-	-	-	t	t	-	1	-	-	-
opaque	8	6	4	6	3	3	2	-	5	t	t	10
calcite	1	t	-	-	-	-	-	-	-	-	-	-
apatite	-	-	-	-	-	-	-	-	-	-	-	-
fluorite	-	t	-	-	-	-	-	-	-	-	-	-
sphene	-	-	-	-	-	-	-	-	-	-	-	-
hornblende	-	-	-	-	-	-	-	-	-	-	-	-
sericite	-	-	-	-	-	-	-	-	-	-	-	-
epidote	-	-	-	-	-	-	-	-	-	-	-	-

	W232	MZg	W233	MZe	MZf	W228	W436	W227	H24	H23	H17	H18
microcline	15	16	10	17	14	5	7	6	2	7	4	18
albite	20	19	17	13	15	23	34	37	61	63	69	52
quartz	40	43	52	40	55	-	-	-	27	24	24	26
biotite	-	-	-	t	2	63	52	45	5	5	3	3
aegirine	15	12	12	15	9	-	-	-	-	-	-	-
riebeckite	-	t	-	t	t	-	-	-	-	-	-	-
opaque	8	10	9	7	5	t	t	t	-	t	-	t
calcite	-	-	-	-	-	6	4	8	-	-	-	-
apatite	-	-	-	-	-	3	2	2	-	t	-	t
fluorite	-	-	-	-	-	-	-	-	-	-	-	-
sphene	t	-	-	t	t	t	t	t	-	-	t	t
hornblende	-	-	-	-	-	-	-	-	t	-	t	t
sericite	-	-	-	-	-	-	-	-	1	t	t	t
epidote	-	-	-	-	-	-	-	-	3	t	t	t

APPENDIX 2

MAJOR, TRACE ELEMENT AND ISOTOPE ANALYSES

A2.1 Major and trace elements

Major- and trace-element geochemical data for whole-rock samples from Ngoye, Bulls Run and Wangu are presented in Tables A2.1, A2.2 and A2.3. Sample size varied according to the grain size of the individual rocks, with approximately 3 kg collected in the case of fine-grained specimens such as Bulls Run microsyenite and albite syenite and the Wangu granites. Coarser-grained granitoids like the Ngoye biotite/hornblende granites and the Bulls Run nepheline syenites necessitated the collection of larger samples of some 10 kg, in order to obtain representative geochemical analyses. All samples were dressed in the field to remove oxidised material, prior to crushing and milling in the Geology Department at UDW. Representative aliquots were submitted to Dr M R Sharpe at Pretoria University for XRF analysis using standard techniques described by Norrish & Hutton (1969).

REE determinations were carried out on selected representative powders submitted to Dr J N Walsh, Bedford New College, UK, using ICP techniques. Realistic working detection limits by this method are approximately 1 x chondritic abundance (C.A.) for most REE, excepting Er (2 x C.A.) and Pr (10 x C.A.). The precision is noted as 5 to 10%, unless working close to detection limits. The high levels of Sr and Ba in some of the Bulls Run samples caused problems with Pr detection and these analyses are denoted as "not detected" in the table. The REE-enriched magnetite-quartz veins from Ngoye were analysed to within 10 ppm. All values were normalised relative to chondritic abundance data given by Nakamura (1974).

During 1989 all samples containing modal calcite were submitted to the Geological Survey for CO₂ and FeO determinations by Mr G Trojack, using infrared spectroscopy and redox titration analysis respectively. In addition to the calcite-bearing samples, all peralkaline rocks were analysed for FeO, in view of the fact that peralkaline rocks typically have higher Fe₂O₃/FeO ratios than metaluminous and peraluminous varieties. Samples collected subsequent to 1989, mainly from Wangu,

have not been analysed for CO_2 or FeO . Thus for these samples, Fe is presented as total Fe_2O_3 .

In those samples for which CO_2 was determined, the value given for "LOI" is the difference between the mass lost during fusion and total CO_2 .

A2.2 Rb and Sr Isotopes

Rb and Sr concentration measurements and Rb/Sr ratios for mineral separates were determined by isotope dilution mass-spectrometry (ID) at the CSIR, whereas the granitoid powders were analysed by XRF at the University of Pretoria using an ARL 8420 with rhodium tube. The Rh Compton peak was monitored and used to correct for matrix effects. Data reduction was performed by means of software developed by Rocklabs Development CC. $^{87}\text{Sr}/^{86}\text{Sr}$ ratios were generally determined from unspiked aliquots. All $^{87}\text{Sr}/^{86}\text{Sr}$ ratios are normalised to $^{86}\text{Sr}/^{88}\text{Sr} = 0.1194$. Rb and Sr blanks measured during the course of this study were less than 1 ng and are thus negligible relative to the concentrations in the samples. Values obtained for strontium standard NBS 987 were 0.71026 ± 2 .

Data were regressed using the method of York (1969), as implemented in version 2.0 of the GEODATE computer package (Eglington & Harmer 1989, modified 1990). The value of MSWD (= MSUM, Brooks *et al.*, 1972) was used to distinguish isochrons from errorchrons and was assumed on the basis of 60 replicates at the 5% level of significance. Uncertainty limits quoted for dates and initial $^{87}\text{Sr}/^{86}\text{Sr}$ (hereafter R_0) are for 95% confidence. The decay constant for ^{87}Rb is $1.42 \times 10^{-11} \text{ yr}^{-1}$ (Steiger & Jager, 1977).

Harmer (1985), Eglington (1987) and Eglington and Harmer (1989) provide more detailed descriptions of the analytical and data processing techniques followed at the CSIR.

A2.3 Ngoye Complex

Whole-rock major- and trace-element data for 58 Ngoye samples are presented as Table A2.1 This includes the 27 analyses previously described by Scogings (1985), in conjunction with an additional set of 31 samples col-

lected during the present study. REE were determined on 20 selected samples. The low totals for "major elements" in the magnetite-quartz veins are due to high concentrations of the "trace elements" Nb, Zr, Zn, REE, U and Th.

A2.4 Bulls Run Complex

A total of 69 whole-rock samples from Bulls Run were analysed for major- and trace-element concentrations and are presented as Table A2.2. REE were determined on 22 representative samples.

A2.5 Wangu Granite

In addition to the data presented by Scogings (1990), 7 extra samples were analysed for major- and trace-elements to bring the total number of analyses at Wangu to 20, as given in Table A2.3. REE were determined on 7 representative specimens.

NGOYE

TABLE A2.1 (1)

	N574	N564	N2	N386	N708	N584	C47	N447	C187	N373	N184	N788
SiO ₂	71.79	72.44	72.58	72.98	73.51	74.03	74.68	72.12	73.15	73.18	73.51	73.68
TiO ₂	0.43	0.42	0.27	0.22	0.30	0.29	0.22	0.49	0.37	0.32	0.29	0.44
Al ₂ O ₃	13.54	13.14	13.60	13.41	13.52	12.84	12.86	12.78	11.83	12.37	12.98	11.80
Fe ₂ O ₃	0.44	0.46	0.36	0.38	0.23	0.47	0.40	0.81	0.74	0.55	0.41	0.71
FeO	2.19	2.29	1.82	1.91	2.00	2.33	1.59	4.04	2.65	2.77	2.06	3.56
MnO	0.04	0.06	0.05	0.05	0.07	0.06	0.05	0.11	0.10	0.07	0.05	0.10
MgO	0.56	0.55	0.35	0.39	0.24	0.27	0.08	0.28	0.25	0.21	0.40	0.18
CaO	1.25	1.57	1.10	1.01	1.24	0.66	0.74	1.24	0.90	0.86	1.11	0.93
Na ₂ O	4.08	3.28	3.44	3.59	3.68	3.74	4.24	4.06	3.62	4.39	3.82	3.95
K ₂ O	4.52	5.26	5.39	5.48	4.92	4.85	5.03	4.66	4.66	4.53	4.90	4.66
P ₂ O ₅	0.14	0.12	0.04	-	0.06	0.02	0.06	0.08	0.06	0.05	-	0.05
LOI	0.36	0.19	0.31	0.12	0.28	0.26	0.29	0.34	0.53	0.21	0.14	0.25
Total	99.34	99.78	99.31	99.54	100.05	99.82	100.16	101.01	98.86	99.51	99.67	100.31
Zn	34	44	43	50	18	75	56	148	128	84	61	219
Ga	nd	17	20	21	17	24	nd	nd	nd	nd	22	22
Nb	23	22	24	30	32	37	37	51	50	42	28	52
Zr	198	225	257	268	322	385	297	839	713	478	333	847
Y	22	34	39	55	45	54	34	83	181	55	52	138
U	4	-	5	7	3	-	5	-	-	4	-	-
Th	25	19	17	25	18	16	17	11	8	16	20	14
Pb	9	21	20	21	26	24	29	11	16	6	19	17
Rb	166	157	197	209	199	207	210	90	84	126	175	183
Sr	202	202	148	122	125	99	114	104	52	89	143	85
Ba	937	1208	1086	817	731	765	753	1086	711	825	1931	1730
Sn	-	nd	nd	nd	nd	nd	nd	nd	nd	-	nd	nd
La	57.66	112	63.19	100	78	96.78	31	57.66	423	nd	122	348
Ce	109.65	154	123.49	213	174	191.80	82	109.65	868	nd	241	474
Pr	10.27	nd	12.39	nd	nd	19.35	nd	10.27	nd	nd	nd	nd
Nd	38.60	65	50.80	83	71	75.60	41	38.60	nd	nd	104	228
Sm	6.47	nd	9.28	nd	nd	13.45	nd	6.47	nd	nd	nd	nd
Eu	1.29	nd	1.32	nd	nd	1.52	nd	1.29	nd	nd	nd	nd
Gd	5.48	nd	8.36	nd	nd	11.46	nd	5.48	nd	nd	nd	nd
Dy	4.50	nd	7.53	nd	nd	9.75	nd	4.50	nd	nd	nd	nd
Ho	0.91	nd	1.56	nd	nd	2.02	nd	0.91	nd	nd	nd	nd
Er	2.81	nd	4.64	nd	nd	6.02	nd	2.81	nd	nd	nd	nd
Yb	2.63	nd	4.21	nd	nd	5.62	nd	2.63	nd	nd	nd	nd
Lu	0.44	nd	0.64	nd	nd	0.88	nd	0.44	nd	nd	nd	nd
P.I.	0.86	0.84	0.84	0.88	0.84	0.89	0.97	0.92	0.93	0.98	0.89	0.98
Na ₂ O+K ₂ O	8.60	8.54	8.83	9.07	8.60	8.59	9.27	8.72	8.28	8.92	8.72	8.61
Na ₂ O/K ₂ O	0.90	0.62	0.64	0.66	0.75	0.77	0.84	0.87	0.78	0.97	0.78	0.85
Rb/Sr	0.82	0.78	1.33	1.71	1.59	2.09	1.84	0.87	1.62	1.42	1.22	1.21
Y/Nb	0.96	1.55	1.63	1.83	1.41	1.46	0.92	1.63	3.62	1.31	1.86	2.65

(2)

	C106	N348	N665	N590	N701	N351	N635	N675	N664	N211	N613	N705
SiO ₂	73.91	74.02	74.07	74.53	74.57	75.18	75.18	75.52	75.76	76.86	75.20	76.30
TiO ₂	0.30	0.26	0.33	0.27	0.32	0.22	0.27	0.28	0.38	0.18	0.07	0.07
Al ₂ O ₃	12.06	12.48	12.22	12.23	12.59	11.96	11.75	11.77	11.40	11.63	13.07	13.16
Fe ₂ O ₃	0.63	0.46	0.49	0.48	0.50	0.50	0.50	0.47	0.53	1.05	0.21	0.12
FeO	2.26	2.30	2.44	2.40	2.50	2.48	2.50	2.36	2.67	1.35	1.05	1.00
MnO	0.06	0.05	0.09	0.08	0.06	0.08	0.09	0.07	0.09	0.05	0.03	0.03
MgO	0.12	0.05	0.30	0.15	0.38	0.12	0.19	0.16	0.36	0.06	0.05	-
CaO	0.57	0.47	1.16	0.58	1.25	0.73	0.43	0.63	0.99	0.36	0.55	0.62
Na ₂ O	3.71	3.93	3.02	3.98	3.56	3.39	4.10	3.97	3.54	4.30	4.40	3.67
K ₂ O	5.08	5.21	5.47	4.95	4.72	5.05	4.65	4.48	4.59	4.41	4.41	5.14
P ₂ O ₅	0.04	-	0.02	-	0.02	-	-	0.02	0.05	0.01	-	0.01
LOI	0.51	0.44	0.22	0.14	0.26	0.12	0.21	0.28	0.16	0.17	0.33	0.30
Total	99.25	99.67	99.83	99.79	100.73	99.83	99.87	100.01	100.52	100.43	99.37	100.42
Zn	92	109	74	89	86	136	130	96	99	136	30	43
Ga	nd	28	18	21	21	23	24	24	19	nd	nd	17
Nb	51	32	34	37	38	42	43	39	39	20	37	33
Zr	592	455	496	578	430	603	541	646	522	374	112	60
Y	86	77	59	82	71	90	88	89	76	51	73	43
U	-	-	7	7	5	-	-	4	-	-	40	11
Th	15	7	16	12	20	15	10	11	15	11	62	32
Pb	21	22	27	20	24	24	16	18	19	4	23	36
Rb	122	97	195	131	151	133	113	97	146	136	345	305
Sr	56	52	135	57	100	61	55	51	95	21	5	7
Ba	622	596	1208	699	751	708	646	1207	779	256	10	18
Sn	8	nd	nd	nd	nd	nd	nd	nd	nd	-	-	nd
La	152	nd	120.85	201	193	156.25	136	237	190	nd	42.60	7
Ce	360	nd	250.58	347	355	309.73	242	260	185	nd	97.30	22
Pr	nd	nd	29.30	nd	nd	35.06	nd	nd	nd	nd	11.08	nd
Nd	170	nd	124.01	130	133	142.00	124	111	88	nd	42.20	3
Sm	nd	nd	20.17	nd	nd	25.89	nd	nd	nd	nd	10.05	nd
Eu	nd	nd	2.27	nd	nd	2.52	nd	nd	nd	nd	0.24	nd
Gd	nd	nd	16.98	nd	nd	22.20	nd	nd	nd	nd	9.65	nd
Dy	nd	nd	13.17	nd	nd	18.25	nd	nd	nd	nd	11.00	nd
Ho	nd	nd	2.64	nd	nd	3.74	nd	nd	nd	nd	2.42	nd
Er	nd	nd	7.39	nd	nd	10.66	nd	nd	nd	nd	7.53	nd
Yb	nd	nd	6.43	nd	nd	9.29	nd	nd	nd	nd	7.55	nd
Lu	nd	nd	1.01	nd	nd	1.44	nd	nd	nd	nd	1.17	nd
P.I.	0.96	0.97	0.89	0.97	0.87	0.92	1.00	0.97	0.95	1.02	0.99	0.88
Na ₂ O+K ₂ O	8.79	9.14	8.49	8.93	8.28	8.44	8.75	8.45	8.13	8.71	8.81	8.81
Na ₂ O/K ₂ O	0.73	0.75	0.55	0.80	0.75	0.67	0.88	0.89	0.77	0.98	1.00	0.71
Rb/Sr	2.18	1.87	1.44	2.30	1.51	2.18	2.05	1.90	1.54	6.48	69.00	43.57
Y/Nb	1.69	2.41	1.74	2.22	1.87	2.14	2.05	2.28	1.95	1.82	1.97	1.30

(3)

	N568	N8	N604	N682	N34	N11	N710	N35	N272	N468	N160	N548
SiO ₂	77.12	77.33	77.38	77.57	76.96	77.38	77.44	47.87	76.83	76.01	77.16	77.48
TiO ₂	0.02	0.04	0.06	0.09	0.01	0.02	0.01	0.00	0.19	0.19	0.17	0.11
Al ₂ O ₃	12.18	11.97	12.08	12.25	13.02	12.96	12.84	27.50	11.53	11.21	11.45	11.19
Fe ₂ O ₃	0.14	0.13	0.15	0.21	0.07	0.17	0.08	1.47	1.41	1.16	1.09	0.97
FeO	0.69	0.67	0.75	1.05	0.54	0.60	0.68	7.35	1.28	1.20	1.46	1.42
MnO	0.02	0.02	0.01	0.02	0.11	0.08	0.06	1.05	0.05	0.05	0.06	0.06
MgO	0.06	0.05	0.02	0.04	0.03	0.11	0.10	0.03	0.06	0.13	0.03	0.05
CaO	0.38	0.31	0.32	0.48	0.05	0.25	0.07	-	0.31	0.26	0.43	0.19
Na ₂ O	4.11	3.87	3.39	3.84	4.07	4.48	4.31	0.64	4.54	3.82	3.85	4.04
K ₂ O	4.91	4.75	5.30	4.83	4.14	4.41	3.91	9.07	4.59	4.80	4.65	4.62
P ₂ O ₅	-	-	-	0.02	-	0.01	-	0.02	0.11	0.02	-	-
LOI	0.10	0.17	0.18	0.26	0.36	0.22	0.40	3.82	0.21	0.29	0.19	0.13
Total	99.73	99.31	99.64	100.66	99.36	100.69	99.98	98.82	100.31	99.14	100.54	100.26
Zn	10	33	16	29	122	33	28	925	147	144	121	123
Ga	19	19	17	nd	29	nd	30	112	nd	nd	27	27
Nb	35	31	16	22	37	64	35	90	28	59	33	39
Zr	89	88	96	122	65	97	64	55	366	527	339	443
Y	38	29	16	29	8	76	15	0	74	79	82	78
U	12	10	8	28	5	14	4	-	-	-	5	7
Th	41	36	45	56	11	32	18	5	5	14	10	10
Pb	26	41	24	19	92	68	60	119	8	20	17	12
Rb	305	249	226	266	1047	724	1005	4460	151	144	123	126
Sr	5	30	24	1	3	4	2	16	8	8	17	14
Ba	41	147	24	16	10	3	19	67	214	212	248	195
Sn	nd	nd	nd	-	81	7	nd	572	-	-	nd	nd
La	nd	19.29	18	nd	2.52	17	3	-	nd	79	88.67	86
Ce	nd	54.82	73	nd	5.30	41	2	-	nd	192	190.21	86
Pr	nd	5.02	nd	nd	1.22	nd	nd	nd	nd	nd	22.13	nd
Nd	nd	19.20	-	nd	3.00	27	-	-	-	89	91.20	44
Sm	nd	4.43	nd	nd	0.63	nd	nd	nd	nd	nd	19.48	nd
Eu	nd	0.35	nd	nd	0.04	nd	nd	nd	nd	nd	1.40	nd
Gd	nd	4.45	nd	nd	0.85	nd	nd	nd	nd	nd	18.20	nd
Dy	nd	5.65	nd	nd	1.99	nd	nd	nd	nd	nd	16.55	nd
Ho	nd	1.25	nd	nd	0.54	nd	nd	nd	nd	nd	3.38	nd
Er	nd	4.27	nd	nd	2.65	nd	nd	nd	nd	nd	9.51	nd
Yb	nd	4.75	nd	nd	6.51	nd	nd	nd	nd	nd	7.90	nd
Lu	nd	0.73	nd	nd	1.14	nd	nd	nd	nd	nd	1.19	nd
P. I.	0.99	0.96	0.94	0.94	0.86	0.94	0.88	0.40	1.08	1.03	0.99	1.04
Na ₂ O+K ₂ O	9.02	8.62	8.69	8.67	8.21	8.89	8.22	9.71	9.13	8.62	8.50	8.66
Na ₂ O/K ₂ O	0.84	0.81	0.64	0.80	0.98	1.02	1.10	0.07	0.99	0.80	0.83	0.87
Rb/Sr	61.00	8.30	9.42	266.00	349.00	181.00	502.50	278.75	18.88	18.00	7.24	9.00
Y/Nb	1.09	0.94	1.00	1.32	0.22	1.19	0.43	0.00	2.64	1.34	2.48	2.00

(4)

	C46	N58	N338	N145	N142	N181	N331	C110	N62c	N62	N331a	N712
SiO2	78.47	78.64	76.70	77.58	77.61	77.59	76.45	76.55	77.15	77.65	77.68	50.24
TiO2	0.11	0.11	0.10	0.11	0.10	0.09	0.16	0.12	0.04	0.13	0.10	1.72
Al2O3	11.40	11.56	10.93	10.87	11.45	10.81	11.32	11.52	11.73	10.92	11.13	1.80
Fe2O3	0.60	1.09	1.44	1.82	0.29	2.35	2.36	1.12	1.53	1.79	1.28	3.90
FeO	0.62	0.71	1.05	0.72	1.44	0.94	0.25	0.66	0.91	0.76	1.26	31.54
MnO	0.02	0.02	0.01	0.03	0.03	0.06	0.04	0.01	0.02	0.02	0.01	0.38
MgO	0.00	0.01	-	0.05	-	0.01	-	0.03	0.01	0.03	0.02	0.22
CaO	0.06	0.01	0.15	0.01	-	0.01	0.34	0.21	0.38	0.13	0.11	4.01
Na2O	4.28	3.68	4.04	4.03	3.88	4.09	4.11	3.08	5.38	3.78	4.82	0.14
K2O	4.52	4.59	4.14	4.00	4.65	4.25	4.47	6.14	2.99	4.82	3.93	0.07
P2O5	0.01	-	-	-	-	0.02	0.01	0.02	-	0.01	-	0.27
LOI	0.21	0.23	0.27	0.14	0.31	0.13	0.33	0.49	0.13	0.09	0.23	1.29
Total	100.38	100.65	99.63	100.24	99.76	101.15	99.84	99.95	100.27	100.13	100.57	95.58
Zn	35	78	241	251	155	328	181	57	52	89	101	1775
Ga	nd	25	nd	nd	28	nd	23	nd	21	nd	29	-
Nb	48	38	35	43	15	26	45	38	94	46	69	3843
Zr	344	444	699	704	367	690	831	458	445	462	774	8721
Y	46	45	196	14	22	15	132	87	86	76	101	2459
U	-	-	-	4	-	-	3	-	12	-	8	202
Th	12	11	3	4	-	-	18	9	20	9	20	1123
Pb	8	7	1	1	-	0	39	26	16	3	34	94
Rb	156	133	242	227	191	267	153	240	93	155	175	5
Sr	2	8	3	-	-	-	8	14	64	26	5	24
Ba	49	145	11	11	49	11	50	120	288	289	41	76
Sn	19	nd	-	14	9	-	nd	6	nd	-	nd	nd
La	19	101	nd	75.30	nd	nd	119.64	81	44	51.91	99.09	nd
Ce	120	163	nd	161.13	nd	nd	247.06	132	64	113.88	209.53	3226
Pr	nd	ndn	nd	17.50	nd	nd	27.95	nd	nd	13.06	25.03	nd
Nd	26	53	nd	67.60	nd	nd	111.30	86	23	53.31	101.41	1473
Sm	nd	nd	nd	13.09	nd	nd	27.02	nd	nd	13.60	25.05	nd
Eu	nd	nd	nd	0.46	nd	nd	0.72	nd	nd	0.69	0.63	nd
Gd	nd	nd	nd	8.93	nd	nd	26.08	nd	nd	13.94	22.17	nd
Dy	nd	nd	nd	6.10	nd	nd	24.59	nd	nd	15.28	18.91	nd
Ho	nd	nd	nd	1.18	nd	nd	4.97	nd	nd	3.19	3.58	nd
Er	nd	nd	nd	3.57	nd	nd	13.56	nd	nd	8.71	9.75	nd
Yb	nd	nd	nd	4.01	nd	nd	11.22	nd	nd	7.01	8.41	nd
Lu	nd	nd	nd	0.79	nd	nd	1.75	nd	nd	0.89	1.21	nd
P. I.	0.99	1.05	1.14	1.14	1.01	1.05	1.03	1.02	1.03	1.05	1.00	0.17
Na2O+K2O	0.80	0.27	0.98	0.91	0.53	0.14	0.58	0.22	0.37	0.60	0.75	0.21
Na2O/K2O	0.95	0.00	1.17	1.18	0.83	1.15	0.92	0.50	1.00	0.78	1.23	2.00
Rb/Sr	78.00	16.63	80.67	nd	nd	nd	19.13	17.14	1.45	5.96	35.00	0.21
Y/Nb	0.96	1.18	5.60	0.33	1.47	0.58	2.93	2.29	0.91	1.65	1.46	0.64

(5)

	NR189	N63	N15	NR88	N17	N193	N19	N62b	N62a	N21
SiO ₂	63.49	66.55	71.32	71.30	71.92	76.92	78.81	63.79	65.12	58.99
TiO ₂	1.35	0.60	0.24	0.91	0.87	0.48	0.35	0.14	0.22	0.55
Al ₂ O ₃	1.29	1.00	6.07	0.44	6.50	0.86	0.29	17.64	18.38	18.72
Fe ₂ O ₃	18.53	12.30	9.51	15.14	8.17	9.92	2.79	2.19	1.32	1.93
FeO	10.67	8.26	6.39	9.73	5.50	6.93	13.97	3.36	2.02	2.86
MnO	0.14	0.10	0.17	0.18	0.18	0.08	0.16	0.12	0.05	0.18
MgO	0.06	-	-	-	-	-	-	0.25	0.28	0.39
CaO	0.86	0.02	0.16	0.05	0.30	-	0.07	0.07	0.15	6.03
Na ₂ O	0.43	0.34	2.29	0.14	3.94	2.01	0.08	3.89	2.18	6.20
K ₂ O	0.45	0.13	2.58	0.04	0.32	0.85	0.01	7.84	11.16	3.07
P ₂ O ₅	0.18	0.17	0.04	0.03	0.10	0.03	0.08	0.02	0.02	0.05
LOI	0.24	0.59	0.10	0.11	0.36	0.42	0.05	0.76	0.57	0.78
Total	97.69	90.06	98.87	98.07	98.16	98.50	96.66	100.07	101.47	99.75
Zn	985	2270	622	681	116	201	744	75	45	76
Ga	-	nd	-	-	-	nd	nd	nd	nd	33
Nb	8797	13539	1886	56	4215	3572	5920	74	104	58
Zr	29605	49771	3443	3285	4196	6511	6535	587	955	717
Y	4780	2127	265	584	856	1016	1332	64	81	129
U	394	1004	141	85	405	267	708	5	-	4
Th	1065	1108	54	84	3353	360	576	11	32	28
Pb	253	289	42	24	409	274	129	2	8	21
Rb	27	16	95	2	23	38	4	276	408	109
Sr	15	7	6	-	61	10	-	17	31	247
Ba	50	0	56	21	105	87	14	217	658	452
Sn	115	57	113	24	1936	nd	34	-	12	-
La	960.00	76.75	402	82.31	nd	70.00	24	nd	113.62	193.65
Ce	2350.00	458.42	763	342.61	335	337.66	389	nd	247.41	390.22
Pr	330.00	61.05	nd	58.27	nd	36.06	nd	nd	28.35	42.17
Nd	1760.00	360.61	669	334.38	210	194.12	178	nd	112.8	168.4
Sm	650.00	231.11	nd	121.61	nd	122.23	nd	nd	25.97	31.56
Eu	40.00	10.95	nd	6.98	nd	6.96	nd	nd	1.14	3.49
Gd	940.00	358.85	nd	119.91	nd	178.66	nd	nd	21.07	27.49
Dy	1530.00	710.23	nd	122.14	nd	332.91	nd	nd	13.63	24.46
Ho	380.00	172.65	nd	24.66	nd	74.37	nd	nd	2.72	4.98
Er	1150.00	507.85	nd	64.24	nd	222.59	nd	nd	8.06	14.02
Yb	970.00	508.59	nd	52.21	nd	192.86	nd	nd	7.44	11.82
Lu	130.00	65.15	nd	7.16	nd	23.96	nd	nd	1.11	1.7
P. I.	0.93	0.71	1.08	0.63	1.05	1.11	0.46	0.85	0.85	0.72
Na ₂ O+K ₂ O	0.88	0.47	4.87	0.18	4.26	2.86	0.09	11.73	13.34	9.27
Na ₂ O/K ₂ O	0.96	2.62	0.89	3.50	12.31	2.36	0.00	0.50	0.20	2.02
Rb/Sr	1.00	2.29	15.83	nd	0.38	3.00	nd	16.24	13.16	0.44
Y/Nb	0.54	0.16	0.14	10.43	0.20	0.28	0.23	0.86	0.78	2.22

BULLS RUN

TABLE A2.2 (1)

	B230	B179	B48	B231	B34	B121	B105	B237a	B95	B54	B4a	B218
SiO ₂	49.58	51.91	53.78	54.89	56.69	57.22	57.35	57.74	57.77	58.04	58.56	60.25
TiO ₂	0.46	0.65	0.56	0.89	0.34	0.31	0.80	0.64	0.63	0.56	0.26	0.16
Al ₂ O ₃	18.28	23.14	25.57	21.18	22.12	21.88	20.79	18.45	23.18	23.16	23.89	21.18
Fe ₂ O ₃	1.44	2.10	1.86	1.35	1.13	0.92	1.08	0.48	0.79	1.37	1.03	1.39
FeO	2.97	3.23	1.51	4.91	1.50	1.76	2.98	3.83	3.53	2.33	1.56	3.10
MnO	0.17	0.19	0.11	0.13	0.05	0.08	0.13	0.14	0.06	0.07	0.03	0.12
MgO	0.62	0.35	0.14	0.25	0.48	0.44	0.45	0.75	0.73	0.43	0.25	0.00
CaO	9.50	3.79	2.16	1.49	2.99	3.52	2.18	3.03	0.68	0.46	0.09	0.84
Na ₂ O	3.88	3.78	4.02	3.26	5.11	5.13	4.41	6.02	5.93	4.94	4.37	6.57
K ₂ O	4.69	6.05	6.22	8.61	6.32	5.24	7.03	5.54	5.77	7.49	8.10	4.49
P ₂ O ₅	1.74	0.31	0.04	0.03	0.28	0.06	0.10	0.36	-	-	-	0.03
LOI	0.72	2.08	2.33	1.05	1.16	2.50	0.77	2.60	1.37	1.40	1.46	0.73
CO ₂	5.97	2.39	1.41	1.13	2.01	1.20	1.61	nd	0.45	0.37	0.12	0.69
Total	100.02	99.97	99.71	99.17	100.18	100.26	99.68	99.58	100.09	100.62	99.72	99.55
Zn	55	70	40	65	28	32	71	65	57	43	24	87
Ga	20	19	17	18	19	18	17	18	21	16	19	23
Nb	89	109	76	129	49	191	201	151	207	60	73	249
Zr	183	224	65	71	106	59	439	422	90	91	107	531
Y	18	15	10	-	8	6	7	15	-	2	-	9
U	-	-	-	-	-	46	-	8	49	-	-	-
Th	-	-	-	-	-	-	-	-	-	-	-	-
Pb	6	112	11	-	-	10	-	6	9	-	8	5
Rb	118	203	183	290	106	134	290	160	199	176	193	248
Sr	2950	1311	766	915	1529	935	743	1271	586	959	591	168
Ba	2371	1964	2283	528	4139	1465	1325	1451	1404	863	1110	86
La	73	69.24	nd	52	34.56	nd	38.64	nd	nd	5.88	nd	14.03
Ce	166	136.37	47	50	65.82	82	72.02	nd	nd	11.19	nd	25.28
Pr	nd	17.16	nd	nd	-	nd	8.76	nd	nd	-	nd	1.93
Nd	64	54.90	-	19	28.60	51	24.90	nd	nd	5.50	nd	9.10
Sm	nd	7.83	nd	nd	3.68	nd	2.76	nd	nd	0.51	nd	1.17
Eu	nd	2.34	nd	nd	1.35	nd	0.75	nd	nd	0.32	nd	0.38
Gd	nd	6.22	nd	nd	3.25	nd	2.52	nd	nd	0.71	nd	1.25
Dy	nd	3.89	nd	nd	1.89	nd	1.51	nd	nd	0.36	nd	1.09
Ho	nd	0.80	nd	nd	0.38	nd	0.36	nd	nd	0.09	nd	0.25
Er	nd	2.19	nd	nd	1.12	nd	1.14	nd	nd	0.37	nd	0.95
Yb	nd	1.91	nd	nd	0.65	nd	1.00	nd	nd	0.17	nd	0.91
Lu	nd	0.38	nd	nd	0.13	nd	0.21	nd	nd	0.04	nd	0.16
P.I.	0.63	0.55	0.52	0.69	0.69	0.65	0.72	0.72	0.69	0.71	0.71	0.74
Na ₂ O+K ₂ O	8.57	9.83	10.24	11.87	11.43	10.37	11.44	11.56	11.70	12.43	12.47	11.06
Na ₂ O/K ₂ O	0.83	0.62	0.65	0.38	0.81	0.98	0.63	1.09	1.03	0.66	0.54	1.46
Rb/Sr	0.04	0.15	0.24	0.32	0.07	0.14	0.39	0.13	0.34	0.18	0.33	1.48
Y/Nb	0.20	0.14	0.13	0.00	0.16	0.03	0.03	0.10	0.00	0.03	0.00	0.04

(2)

	B236	B95a	B81a	B213	B175	B212	B44	B43	B233	B66	B110	B80
SiO ₂	60.46	60.69	45.87	47.85	48.08	48.23	48.48	49.49	50.87	51.10	51.36	51.50
TiO ₂	0.24	0.17	0.59	1.21	1.36	1.10	1.21	1.03	0.78	0.91	0.75	0.82
Al ₂ O ₃	23.95	22.42	35.35	20.20	20.39	21.57	21.59	22.18	22.15	21.50	22.50	21.86
Fe ₂ O ₃	0.85	0.44	2.41	2.41	4.18	2.27	2.59	1.32	0.77	2.65	1.52	2.99
FeO	0.25	0.76	0.25	4.12	2.50	3.86	3.41	3.51	3.83	2.59	2.92	1.98
MnO	0.01	0.03	0.01	0.22	0.23	0.20	0.19	0.18	0.19	0.17	0.17	0.16
MgO	0.11	0.18	0.22	0.78	1.35	0.73	0.71	0.73	0.49	0.91	0.68	0.65
CaO	0.12	1.25	0.00	6.49	6.79	5.72	4.18	3.96	4.04	4.04	3.77	3.69
Na ₂ O	6.08	6.84	0.99	7.48	7.89	8.72	6.61	6.56	7.91	6.88	7.22	7.90
K ₂ O	6.11	5.12	10.58	5.03	5.58	5.47	7.39	7.26	6.04	7.32	6.22	6.50
P ₂ O ₅	0.03	0.04	0.07	0.53	0.61	0.40	0.63	0.34	0.43	0.31	0.34	0.30
LOI	1.51	1.12	4.36	0.76	0.64	0.47	0.72	1.60	1.99	0.53	2.42	0.62
CO ₂	0.11	1.02	0.04	3.70	0.55	0.90	1.93	1.68	nd	0.82	1.00	0.90
Total	99.83	100.08	100.74	100.78	100.15	99.64	99.64	99.84	99.49	99.73	100.87	99.87
Zn	6	10	2	86	67	57	74	65	49	56	51	52
Ga	18	21	28	14	17	15	15	12	10	12	15	14
Nb	39	64	133	224	210	171	181	166	169	177	153	167
Zr	39	13	13	147	154	159	182	172	152	184	212	200
Y	1	4	4	17	21	22	21	18	8	12	14	14
U	1	11	-	-	3	5	-	-	-	7	-	-
Th	-	-	-	-	-	3	8	6	-	-	8	6
Pb	6	7	-	-	1	4	-	10	4	-	-	-
Rb	100	114	208	197	158	153	246	213	209	218	178	197
Sr	537	854	211	1079	1506	1284	1982	1776	2009	1754	1543	2055
Ba	2582	1171	1866	1624	1793	1745	2406	2704	1656	2342	1875	2037
La	6	8	nd	115.00	120.38	92	113	63	114	24	52	83.23
Ce	nd	nd	nd	240.00	237.24	193	101	68	177	50	89	159.55
Pr	nd	nd	nd	nd	27.29	nd	nd	nd	nd	nd	nd	21.20
Nd	nd	2	0.00	74.00	95.00	70	62	-	106	29	53	62.70
Sm	nd	nd	nd	nd	13.58	nd	nd	nd	nd	nd	nd	8.34
Eu	nd	nd	nd	nd	4.23	nd	nd	nd	nd	nd	nd	2.76
Gd	nd	nd	nd	nd	10.14	nd	nd	nd	nd	nd	nd	6.60
Dy	nd	nd	nd	nd	5.72	nd	nd	nd	nd	nd	nd	3.89
Ho	nd	nd	nd	nd	1.07	nd	nd	nd	nd	nd	nd	0.77
Er	nd	nd	nd	nd	2.77	nd	nd	nd	nd	nd	nd	2.02
Yb	nd	nd	nd	nd	1.04	nd	nd	nd	nd	nd	nd	1.42
Lu	nd	nd	nd	nd	0.31	nd	nd	nd	nd	nd	nd	0.26
P. I.	0.69	0.75	0.37	0.88	0.93	0.94	0.87	0.84	0.88	0.89	0.83	0.92
Na ₂ O+K ₂ O	12.19	11.96	11.57	12.51	13.47	14.19	14.00	13.82	13.95	14.20	13.44	14.40
Na ₂ O/K ₂ O	1.00	1.34	0.09	1.49	1.41	1.59	0.89	0.90	1.31	0.94	1.16	1.22
Rb/Sr	0.19	0.13	0.99	0.18	0.10	0.12	0.12	0.12	0.10	0.12	0.12	0.10
Y/Nb	0.03	0.06	0.03	0.00	0.10	0.13	0.12	0.11	0.05	0.07	0.09	0.08

(3)

	B232	B82	B181	B222	B23	B96	B86	B180	B42	B240	B85	B239
SiO ₂	51.57	53.07	53.54	52.76	53.45	54.12	54.78	55.16	56.21	56.26	56.83	57.02
TiO ₂	0.60	1.28	0.73	0.65	0.50	1.00	0.83	0.92	0.76	0.38	0.50	0.42
Al ₂ O ₃	22.68	20.99	22.34	22.28	22.71	20.58	23.03	22.12	21.61	21.71	22.38	22.21
Fe ₂ O ₃	0.55	2.76	0.79	1.77	0.65	0.70	0.84	0.89	3.03	1.03	0.61	0.75
FeO	2.75	3.80	3.95	3.61	3.24	4.55	4.19	4.92	2.75	2.97	2.99	2.12
MnO	0.10	0.14	0.13	0.10	0.08	0.12	0.08	0.09	0.06	0.09	0.06	0.06
MgO	0.33	0.74	0.26	0.14	0.39	0.62	0.57	0.74	0.31	0.19	0.41	0.30
CaO	2.61	2.63	2.22	1.50	1.96	1.61	1.08	0.18	0.40	1.06	0.54	0.85
Na ₂ O	9.10	4.81	6.37	6.44	6.54	5.50	5.14	5.30	5.56	8.06	6.31	7.82
K ₂ O	5.67	9.10	8.20	8.01	9.18	8.49	8.16	8.04	8.26	6.43	8.29	7.32
P ₂ O ₅	0.28	0.28	0.02	0.17	0.13	0.05	0.01	-	-	0.11	0.06	0.21
LOI	2.95	0.59	1.07	0.45	0.23	0.74	1.96	0.81	1.08	0.49	0.47	0.67
CO ₂	nd	0.33	nd	1.17	1.69	1.24	nd	0.26	0.41	0.81	0.62	0.48
Total	99.19	100.52	99.62	99.05	100.75	99.32	100.67	99.43	100.44	99.59	100.07	100.23
Zn	34	65	44	49	43	63	56	73	38	47	42	32
Ga	16	13	16	16	18	14	17	18	15	20	15	20
Nb	126	139	91	94	102	140	133	95	130	310	131	218
Zr	120	154	106	115	128	97	111	84	84	245	656	178
Y	5	10	6	4	5	-	-	1	-	5	-	4
U	6	-	-	-	-	-	-	-	-	11	7	10
Th	-	7	-	-	-	-	-	-	-	2	7	1
Pb	-	-	6	-	-	-	nd	-	-	-	-	2
Rb	195	245	217	200	206	221	215	221	180	158	209	182
Sr	1726	2820	1402	1298	1560	1737	1344	1236	1544	977	1188	897
Ba	1341	4721	771	1335	1835	1627	2134	1518	1333	824	961	788
La	nd	123	31.73	15.32	21.06	48	30	4.93	nd	13	nd	13
Ce	nd	42	65.34	30.38	41.29	nd	nd	10.05	nd	nd	nd	9
Pr	nd	nd	-	-	nd	nd	nd	-	nd	nd	nd	nd
Nd	nd	49	28.40	13.70	18.00	nd	nd	6.00	nd	nd	nd	12
Sm	nd	nd	3.78	1.62	2.26	nd	nd	0.36	nd	nd	nd	nd
Eu	nd	nd	1.30	0.67	0.85	nd	nd	0.25	nd	nd	nd	nd
Gd	nd	nd	3.01	1.70	2.23	nd	nd	0.89	nd	nd	nd	nd
Dy	nd	nd	1.64	0.98	1.30	nd	nd	0.35	nd	nd	nd	nd
Ho	nd	nd	0.33	0.20	0.26	nd	nd	0.10	nd	nd	nd	nd
Er	nd	nd	0.94	0.67	0.82	nd	nd	0.30	nd	nd	nd	nd
Yb	nd	nd	0.66	0.38	0.48	nd	nd	0.15	nd	nd	nd	nd
Lu	nd	nd	0.15	0.07	0.09	nd	nd	0.06	nd	nd	nd	nd
P. I.	0.93	0.85	0.65	0.87	0.87	0.89	0.75	0.79	0.84	0.93	0.87	0.94
Na ₂ O+K ₂ O	14.77	13.91	14.57	14.45	15.72	13.99	13.30	13.34	13.82	14.49	14.60	15.14
Na ₂ O/K ₂ O	1.60	0.53	0.78	0.80	0.71	0.65	0.63	0.66	0.67	1.25	0.76	1.07
Rb/Sr	0.11	0.09	0.15	0.15	0.13	0.13	0.16	0.18	0.12	0.16	0.18	0.20
Y/Nb	0.04	0.07	0.07	0.04	0.05	0.00	0.00	0.01	0.00	0.02	0.00	0.02

(4)

	B122	B238	B41	B55	B241	B203	B204	B95b	B228	B183	B20	B103
SiO2	57.07	56.81	57.46	57.81	58.68	56.75	57.78	58.44	58.88	58.97	59.26	59.77
TiO2	0.55	0.66	0.98	0.56	0.35	0.15	0.14	0.37	0.17	0.22	0.16	0.03
Al2O3	22.61	21.50	21.87	22.62	22.12	23.68	21.02	21.67	21.33	22.38	22.00	21.86
Fe2O3	0.94	1.58	1.53	0.68	0.99	0.75	0.58	0.63	0.42	0.49	0.59	0.18
FeO	3.71	3.19	3.97	3.17	2.12	2.02	0.25	1.92	1.73	1.31	2.34	1.87
MnO	0.00	0.06	0.10	0.07	0.04	0.04	0.04	0.05	0.06	0.04	0.04	0.04
MgO	0.43	0.50	0.36	0.30	0.13	0.00	0.00	0.39	0.00	0.00	0.09	0.13
CaO	0.65	0.22	0.23	0.30	0.30	0.44	2.16	1.50	1.78	0.89	0.49	0.77
Na2O	5.48	6.26	5.28	7.11	8.24	9.74	6.93	7.37	8.28	7.14	8.94	10.14
K2O	7.10	8.59	8.02	6.57	6.51	4.24	6.60	5.34	4.96	7.18	4.98	4.05
P2O5	0.01	0.01	-	-	0.01	-	0.01	0.00	0.03	0.07	-	-
LOI	0.85	0.67	0.62	0.89	0.36	1.03	1.42	1.49	0.88	0.55	0.94	0.52
CO2	0.68	0.12	0.39	0.42	0.28	0.28	1.39	0.97	0.84	0.88	0.49	0.84
Total	100.16	100.17	100.81	100.50	100.13	99.12	98.32	100.22	99.36	100.12	100.32	100.20
Zn	55	62	54	42	25	37	27	38	20	30	33	34
Ga	17	17	15	20	18	26	-	24	27	-	31	23
Nb	135	151	60	61	88	1224	16553	78	165	2280	350	420
Zr	222	140	88	79	62	1780	1793	485	669	2129	613	1017
Y	-	2	1	-	2	9	9	7	5	6	4	7
U	5	11	-	-	3	71	535	3	19	239	19	52
Th	-	-	-	-	-	-	61	-	-	7	-	-
Pb	5	4	-	-	-	21	127	-	10	63	9	8
Rb	211	223	180	181	150	199	193	144	129	185	182	194
Sr	700	810	1588	1356	102	236	2378	1200	875	905	393	212
Ba	578	1173	1189	1095	535	76	856	833	644	872	168	112
La	nd	11	4.79	nd	6	23	114.74	17	18	15.55	41	31
Ce	nd	nd	0.25	30	nd	69	223.61	6	42	31.35	nd	nd
Pr	nd	nd	-	nd	nd	nd	22.52	nd	nd	-	nd	nd
Nd	nd	nd	4.40	nd	nd	17	60.20	4	17	11.80	nd	16
Sm	nd	nd	0.26	nd	nd	nd	5.49	nd	nd	1.29	nd	nd
Eu	nd	nd	0.34	nd	nd	nd	1.62	nd	nd	0.48	nd	nd
Gd	nd	nd	0.51	nd	nd	nd	3.55	nd	nd	1.40	nd	nd
Dy	nd	nd	0.26	nd	nd	nd	2.06	nd	nd	1.09	nd	nd
Ho	nd	nd	0.06	nd	nd	nd	0.46	nd	nd	0.29	nd	nd
Er	nd	nd	0.30	nd	nd	nd	1.64	nd	nd	0.99	nd	nd
Yb	nd	nd	0.10	nd	nd	nd	1.08	nd	nd	1.03	nd	nd
Lu	nd	nd	0.04	nd	nd	nd	0.20	nd	nd	0.20	nd	nd
P. I.	0.74	0.91	0.79	0.83	0.93	0.87	0.88	0.83	0.87	0.87	0.92	0.96
Na2O+K2O	12.58	14.85	13.30	13.68	14.75	13.98	13.53	12.71	13.24	14.32	13.92	14.19
Na2O/K2O	0.77	0.73	0.66	1.00	1.27	2.30	1.05	1.38	1.67	0.99	1.00	2.50
Rb/Sr	0.30	0.28	0.11	0.13	1.47	0.84	0.08	0.12	0.15	0.20	0.46	0.92
Y/Nb	0.00	0.01	0.02	0.00	0.02	0.01	0.00	0.09	0.03	0.00	0.01	0.02

(5)

	B220a	B227	B192	B190	B220	B217	B67	B83a	B62	B60	B46	B87
SiO2	59.78	59.83	59.98	60.17	65.51	44.65	46.51	50.24	0.86	2.34	2.57	16.90
TiO2	0.07	0.03	0.18	0.03	0.01	2.24	1.73	0.92	0.01	0.28	0.23	0.33
Al2O3	22.23	22.79	21.72	22.19	19.68	15.25	17.60	19.02	0.33	0.99	1.08	6.01
Fe2O3	0.21	0.08	0.52	0.53	0.09	1.10	1.18	0.72	0.43	0.05	0.63	0.47
FeO	1.83	0.65	2.81	0.76	0.90	11.73	5.90	6.65	2.17	4.27	3.16	2.37
MnO	0.03	0.03	0.05	0.03	0.03	0.37	0.27	0.17	1.21	1.10	0.90	0.28
MgO	0.00	0.00	0.00	0.00	0.00	3.48	1.79	1.93	0.13	0.27	0.26	0.50
CaO	0.19	0.32	0.10	0.48	0.53	7.10	9.17	4.41	54.32	49.40	48.53	39.70
Na2O	8.79	9.05	8.84	9.12	7.65	2.97	5.38	5.55	0.08	0.01	0.11	0.90
K2O	5.80	5.55	5.05	5.26	4.44	4.52	3.46	5.49	0.12	0.53	0.49	2.32
P2O5	0.01	-	-	-	0.07	1.27	0.81	0.38	0.03	2.94	2.75	0.69
LOI	0.25	0.51	0.45	0.57	0.06	0.22	0.76	0.71	0.00	0.00	0.36	0.00
CO2	0.37	0.29	0.15	0.07	0.44	4.51	5.73	3.08	41.62	37.77	37.79	30.55
Total	99.56	99.13	99.05	99.21	99.41	99.41	100.29	99.27	101.31	100.75	98.86	101.02
Zn	37	11	40	21	14	229	68	109	15	34	28	29
Ga	29	31	31	5	26	31	6	19	-	-	-	-
Nb	494	441	153	1774	403	256	247	176	68	3993	2633	52
Zr	1145	1460	209	818	667	288	214	234	0	0	0	0
Y	2	9	-	4	13	26	22	13	82	94	100	56
U	32	57	5	102	12	-	-	-	-	-	-	-
Th	-	-	-	3	-	-	5	-	-	-	17	-
Pb	-	12	3	24	-	-	-	-	14	20	9	9
Rb	338	233	203	213	220	459	119	215	11	48	42	54
Sr	145	165	221	267	131	1060	1620	1105	9135	8956	8077	7206
Ba	91	129	85	112	99	610	339	924	81	142	132	900
La	5.22	nd	20	65	8.12	103.08	97.00	39.45	265.60	306	361.37	286
Ce	9.13	30	35	45	15.69	207.47	218.00	82.97	515.28	606	718.45	455
Pr	-	nd	nd	nd	-	24.10	nd	7.64	55.44	nd	76.29	nd
Nd	3.60	nd	15	nd	6.30	84.00	140.00	37.10	187.40	275	269.30	199
Sm	0.27	nd	nd	nd	0.95	13.34	nd	5.77	28.99	nd	41.63	nd
Eu	0.11	nd	nd	nd	0.23	4.06	nd	1.87	9.45	nd	12.82	nd
Gd	0.47	nd	nd	nd	1.37	10.59	nd	4.80	23.33	nd	32.19	nd
Dy	0.38	nd	nd	nd	2.26	6.60	nd	3.20	17.82	nd	22.47	nd
Ho	0.11	nd	nd	nd	0.54	1.28	nd	0.63	3.63	nd	4.50	nd
Er	0.51	nd	nd	nd	1.91	3.46	nd	1.71	10.48	nd	12.67	nd
Yb	0.62	nd	nd	nd	2.04	2.46	nd	1.40	9.17	nd	10.53	nd
Lu	0.14	nd	nd	nd	0.32	0.38	nd	0.24	1.43	nd	1.62	nd
P. I.	0.93	0.92	0.92	0.93	0.88	0.64	0.72	0.81	0.81	0.59	0.66	0.67
Na2O+K2O	14.59	14.60	13.89	14.38	12.09	7.49	8.84	11.04	0.20	0.54	0.60	3.22
Na2O/K2O	1.52	1.63	1.75	1.73	1.72	0.66	1.55	1.01	0.67	0.02	0.22	0.39
Rb/Sr	2.33	1.41	0.92	0.80	1.68	0.43	0.07	0.19	0.00	0.01	0.01	0.01
Y/Nb	0.00	0.02	0.00	0.00	0.03	0.10	0.09	0.07	1.21	0.02	0.04	1.08

(6)

	B229	B92	B90a	B32	B72	B94	B98	B51	B237
SiO ₂	21.68	42.45	64.58	66.33	67.15	67.45	68.94	69.27	69.58
TiO ₂	0.74	0.26	0.16	0.23	0.31	0.20	0.19	0.16	0.20
Al ₂ O ₃	8.75	15.59	17.56	18.27	14.52	15.82	16.68	16.78	16.27
Fe ₂ O ₃	1.01	1.22	1.17	1.27	2.50	0.98	0.91	0.54	0.14
FeO	5.03	1.92	0.83	0.29	0.91	0.75	0.41	0.61	1.08
MnO	0.28	0.23	0.03	-	0.04	0.02	0.01	0.03	0.02
MgO	1.06	0.30	0.57	0.22	1.15	0.61	0.27	0.42	0.32
CaO	31.34	17.24	2.40	0.66	2.62	2.10	0.18	1.25	0.57
Na ₂ O	0.87	3.13	7.80	8.24	6.84	7.51	7.11	7.78	7.47
K ₂ O	3.14	4.53	3.47	3.97	3.98	3.24	3.91	3.61	3.03
P ₂ O ₅	6.28	0.43	0.05	0.09	0.19	0.03	0.10	0.05	0.07
LOI	0.65	0.00	0.05	0.20	0.03	0.38	0.30	0.10	0.70
CO ₂	18.92	13.57	1.25	0.10	0.22	0.66	0.08	0.08	nd
Total	99.75	100.87	99.84	99.87	100.46	99.75	99.09	100.68	99.45
Zn	82	24	45	27	67	53	24	39	39
Ga	15	16	23	26	27	21	22	21	21
Nb	72	99	29	11	19	14	23	13	14
Zr	87	151	148	125	195	170	128	134	124
Y	70	34	5	5	12	-	4	7	8
U	6	12	-	6	-	9	-	-	6
Th	7	-	7	-	22	10	4	8	5
Pb	-	17	19	13	23	16	12	6	24
Rb	125	103	70	60	86	74	70	34	50
Sr	5701	4194	425	107	563	1193	63	60	311
Ba	837	838	1029	1051	1993	1522	1205	1037	886
La	309.27	170	19.13	39	78.79	nd	nd	nd	nd
Ce	637.19	247	37.39	nd	157.35	nd	23	nd	nd
Pr	71.00	nd	-	nd	16.25	nd	nd	nd	nd
Nd	271.60	57	16.90	nd	68.70	nd	nd	nd	nd
Sm	40.99	nd	2.44	nd	11.42	nd	nd	nd	nd
Eu	12.86	nd	0.70	nd	2.63	nd	nd	nd	nd
Gd	30.60	nd	2.29	nd	7.33	nd	nd	nd	nd
Dy	17.82	nd	1.12	nd	3.10	nd	nd	nd	nd
Ho	3.36	nd	0.22	nd	0.55	nd	nd	nd	nd
Er	8.69	nd	0.57	nd	1.51	nd	nd	nd	nd
Yb	5.67	nd	0.39	nd	0.83	nd	nd	nd	nd
Lu	0.84	nd	0.08	nd	0.13	nd	nd	nd	nd
P.I.	0.55	0.65	0.94	0.98	1.07	1.01	0.96	1.01	1.01
Na ₂ O+K ₂ O	4.01	7.66	11.27	12.21	10.82	10.75	11.02	11.39	10.50
Na ₂ O/K ₂ O	0.28	0.69	2.25	2.08	1.72	2.32	1.02	2.16	2.47
Rb/Sr	0.02	0.02	0.16	0.56	0.15	0.06	1.11	0.57	0.16
Y/Nb	0.97	0.34	0.17	0.45	0.63	0.00	0.17	0.54	0.57

WANGU

TABLE A2.3 (1)

	W234	W229	W232	MZg	W233	MZe	MZf	W228	W436	W227
SiO ₂	69.10	79.20	61.16	65.58	73.12	75.09	75.67	39.23	47.04	51.24
TiO ₂	0.57	0.21	0.31	0.25	0.31	0.23	0.25	3.84	3.50	1.19
Al ₂ O ₃	13.41	8.94	5.79	5.80	5.19	4.73	4.62	12.25	13.46	12.75
Fe ₂ O ₃	5.37	4.10	20.15	20.79	11.37	13.48	12.95	1.71	1.66	1.33
FeO	0.75	0.25	3.24	nd	2.00	nd	nd	12.07	11.95	5.57
MnO	0.12	0.14	0.50	0.42	0.45	0.29	0.34	0.51	0.26	0.35
MgO	0.41	0.17	0.99	0.56	0.88	0.50	0.57	9.96	5.39	5.54
CaO	0.36	0.18	2.82	1.70	2.25	1.60	1.52	6.83	5.71	7.42
Na ₂ O	5.23	4.60	3.90	3.95	3.32	2.74	2.58	1.55	2.75	3.82
K ₂ O	4.75	2.08	1.18	1.41	0.60	1.20	1.19	7.14	4.17	5.22
P ₂ O ₅	0.10	-	0.04	0.05	0.04	0.02	0.04	1.24	0.70	0.97
LOI	0.37	0.40	0.86	0.97	0.82	1.17	0.93	0.71	2.48	1.21
CO ₂	nd	nd	nd	nd	nd	nd	nd	2.44	nd	3.29
Total	100.54	100.27	100.94	101.48	100.35	101.05	100.66	99.48	99.07	99.90
Zn	150	612	898	704	584	321	411	771	343	451
Ga	30	27	31	25	23	18	17	40	25	24
Nb	189	295	567	641	614	465	542	390	45	159
Zr	450	1795	3076	2652	3730	2257	2857	273	157	312
Y	159	95	385	464	541	334	315	86	34	114
U	3	5	9	11	10	8	17	9	1	5
Th	14	47	78	81	115	83	89	17	2	45
Pb	13	166	19	28	13	50	24	64	nd	25
Rb	145	78	49	54	38	64	60	635	393	471
Sr	13	4	20	16	29	24	30	341	495	1445
Ba	553	59	287	334	111	266	242	1325	969	1459
La	121	124.10	705.00	752	929	411	516	146.00	nd	212.90
Ce	193	275.91	421.11	692	837	704	952	278.17	nd	436.20
Pr	nd	26.91	145.41	nd	nd	nd	nd	30.93	nd	49.09
Nd	143	100.10	603.00	793	1052	445	554	124.60	nd	192.20
Sm	nd	19.93	116.06	nd	nd	nd	nd	21.91	nd	29.93
Eu	nd	1.66	21.02	nd	nd	nd	nd	5.29	nd	5.80
Gd	nd	18.45	106.42	nd	nd	nd	nd	18.26	nd	20.66
Dy	nd	23.20	93.27	nd	nd	nd	nd	15.37	nd	16.48
Ho	nd	4.48	16.30	nd	nd	nd	nd	2.76	nd	3.17
Er	nd	13.16	38.23	nd	nd	nd	nd	7.27	nd	9.07
Yb	nd	13.40	34.35	nd	nd	nd	nd	6.47	nd	9.36
Lu	nd	1.97	4.81	nd	nd	nd	nd	0.92	nd	1.46
P. I.	1.03	1.10	1.33	1.38	1.18	1.23	1.20	0.84	0.67	0.94
Na ₂ O+K ₂ O	9.98	6.68	5.08	5.36	3.92	3.94	3.77	8.69	6.92	9.04
Na ₂ O/K ₂ O	1.10	2.21	3.31	2.00	5.53	2.28	2.17	0.22	0.66	0.73
Rb/Sr	11.15	19.50	2.45	3.38	1.31	2.67	2.00	1.86	0.79	0.33
Y/Nb	0.84	0.32	0.68	0.72	0.88	0.72	0.58	0.22	0.76	0.72

(2)

	W435	W434	H27	W149	MZa	MZc	MZb	MZh	W231	W235
SiO ₂	67.27	67.97	70.88	77.86	79.75	65.78	66.43	66.44	66.48	68.41
TiO ₂	0.65	0.63	0.41	0.24	0.13	0.62	0.61	0.71	0.77	0.68
Al ₂ O ₃	13.36	12.79	10.89	10.44	10.11	14.40	13.55	14.04	13.74	11.96
Fe ₂ O ₃	7.95	7.98	1.52	0.42	2.73	9.01	8.66	6.98	6.66	5.91
FeO	nd	nd	6.22	3.46	nd	nd	nd	nd	0.25	1.25
MnO	0.16	0.22	0.25	0.06	0.02	0.24	0.27	0.18	0.16	0.20
MgO	0.39	0.40	0.41	0.08	0.01	0.14	0.19	0.21	0.42	0.59
CaO	0.96	1.34	0.15	0.06	0.05	0.25	0.22	0.33	0.46	0.67
Na ₂ O	4.91	5.21	3.25	3.51	2.83	6.53	4.41	4.79	4.68	4.21
K ₂ O	4.23	3.11	5.09	3.77	4.06	1.96	4.63	5.34	5.75	6.38
P ₂ O ₅	-	-	-	0.02	-	0.02	0.03	0.07	0.08	0.01
LOI	0.23	0.35	0.17	0.20	0.51	1.52	1.57	1.18	0.84	0.20
CO ₂	nd	nd	nd	nd	nd	nd	nd	nd	nd	nd
Total	100.11	100.00	99.24	100.12	100.20	100.47	100.57	100.27	100.29	100.47
Zn	146	341	242	168	91	206	241	229	323	123
Ga	30	30	33	26	18	33	32	26	30	29
Nb	228	373	245	128	264	366	332	384	423	303
Zr	1141	1672	1095	1694	1458	1754	1654	1493	1836	1549
Y	97	161	103	128	88	73	116	87	100	133
U	10	13	-	6	4	9	6	11	10	7
Th	38	57	42	52	37	56	49	71	80	109
Pb	nd	nd	32	38	15	137	328	50	41	82
Rb	155	176	255	104	165	59	143	167	205	294
Sr	163	116	22	33	13	14	18	20	20	9
Ba	113	36	217	157	100	249	403	136	145	62
La	nd	nd	208.06	nd	nd	103	151	231	334.70	247.20
Ce	nd	nd	403.20	nd	nd	392	496	543	570.39	459.65
Pr	nd	nd	40.60	nd	nd	nd	nd	nd	66.06	47.61
Nd	nd	nd	147.80	nd	nd	80	132	204	232.70	169.80
Sm	nd	nd	25.51	nd	nd	nd	nd	nd	38.39	31.00
Eu	nd	nd	1.28	nd	nd	nd	nd	nd	3.13	2.37
Gd	nd	nd	21.49	nd	nd	nd	nd	nd	27.04	27.23
Dy	nd	nd	20.53	nd	nd	nd	nd	nd	26.23	30.91
Ho	nd	nd	4.30	nd	nd	nd	nd	nd	4.90	5.77
Er	nd	nd	12.77	nd	nd	nd	nd	nd	12.68	16.22
Yb	nd	nd	12.00	nd	nd	nd	nd	nd	12.66	15.33
Lu	nd	nd	1.81	nd	nd	nd	nd	nd	1.88	2.21
P.I.	0.95	0.94	0.99	0.94	0.90	0.89	0.91	0.95	1.01	1.16
Na ₂ O+K ₂ O	9.14	8.32	8.34	7.28	6.89	8.49	9.04	10.13	10.43	10.59
Na ₂ O/K ₂ O	1.16	1.68	0.64	0.93	0.70	3.33	0.95	0.90	0.81	0.66
Rb/Sr	0.95	1.52	11.59	3.15	12.69	4.21	7.94	8.35	10.25	32.67
Y/Nb	0.43	0.43	0.42	1.00	0.33	0.20	0.35	0.23	0.24	0.44

(3)

	H24	H23	H17	H18	H6
SiO2	70.57	71.17	71.97	72.27	73.85
TiO2	0.21	0.15	0.11	0.13	0.13
Al2O3	16.41	16.01	16.30	14.80	14.53
Fe2O3	0.31	0.26	0.20	0.29	0.19
FeO	1.57	1.29	1.00	1.46	0.93
MnO	0.02	0.02	0.01	0.03	0.01
MgO	0.59	0.52	0.39	0.35	0.39
CaO	3.15	2.40	2.72	1.89	2.80
Na2O	5.81	5.53	6.41	5.42	5.48
K2O	1.04	1.77	0.90	2.63	1.29
P2O5	0.04	0.07	0.06	0.04	0.08
LOI	0.30	0.32	0.22	0.24	0.28
CO2	nd	nd	nd	nd	nd
Total	100.02	99.51	100.29	99.55	99.96
Zn	38	41	24	33	26
Ga	20	21	17	22	20
Nb	13	10	10	17	10
Zr	142	150	130	155	147
Y	6	6	-	9	6
U	-	-	-	-	-
Th	6	-	-	5	-
Pb	8	13	8	23	10
Rb	35	34	34	67	29
Sr	1207	1366	1102	1205	1115
Ba	1494	1166	412	1312	600
La	nd	nd	nd	nd	nd
Ce	nd	nd	nd	nd	nd
Pr	nd	nd	nd	nd	nd
Nd	nd	nd	nd	nd	nd
Sm	nd	nd	nd	nd	nd
Eu	nd	nd	nd	nd	nd
Gd	nd	nd	nd	nd	nd
Dy	nd	nd	nd	nd	nd
Ho	nd	nd	nd	nd	nd
Er	nd	nd	nd	nd	nd
Yb	nd	nd	nd	nd	nd
Lu	nd	nd	nd	nd	nd
P. I.	0.65	0.68	0.71	0.79	0.72
Na2O+K2O	6.85	7.30	7.31	8.05	6.77
Na2O/K2O	5.59	3.12	7.12	2.06	4.25
Rb/Sr	0.03	0.02	0.03	0.06	0.03
Y/Nb	0.46	0.60	0.00	0.53	0.60

APPENDIX 3

CIPW- AND MESO-NORMS

Normative constituents for whole-rock analyses from Ngoye, Bulls Run and Wanga are presented as Tables A3.1, A3.2 and A3.3 respectively. Both CIPW normas and Mesonorms were calculated by B M Eglington and R.E. Harmer of the CSIR (Pretoria). The following points are noted:

- i) All analyses were recalculated to 100%, H₂O-free.
- ii) Fe₂O₃/FeO ratios for those peralkaline samples from Wangu that had not had FeO determined, were adjusted to correspond to known ratios from other Wangu rocks with similar mineralogy.
- iii) The elements Sr, Ba, and Zr have been incorporated in the norm calculations and reflect in feldspar and zircon contents. CO₂ has been assigned to calcite, although it must be borne in mind that some CO₂ is probably contained in the cancrinite lattice. The incorporation of Ca into normative calcite is of paramount importance, so as to allocate the correct amount of Ca to An. Failure to follow this routine results in an excess of An and mis-classification, especially when dealing with alkaline rocks.
- iv) Calculation of the mesonorm is required when classifying rocks on the Streckensien & Le Maitre (1979) normative plot.
- v) By converting CIPW-normative diopside and hypersthene into minerals such as biotite and hornblende in the mesonorm, excess SiO₂ is released and reflects in additional normative quartz.

NGOYE

TABLE A3.1 (1)

[illegible][illegible]

(2)

[illegible][illegible]

(3)

[illegible][illegible]

(4)

[illegible][illegible]

(5)

[illegible][illegible]

TABLE A3.2 (1)

[illegible][illegible]

(2)

[illegible][illegible]

(3)

	B110	B80	B232	B222	B82	B23	B181	B96	B86	B100	B42
Quartz	-	-	-	-	-	-	-	-	-	-	-
Corundum	-	-	-	3.06	-	2.00	-	2.11	3.53	4.76	3.48
Orthoclase	37.26	38.59	34.76	47.96	53.60	53.94	49.12	50.80	48.76	48.11	49.04
Albite	16.79	14.62	15.34	18.86	6.96	9.25	8.24	19.33	20.26	26.48	28.94
Anorthite	10.76	5.01	4.45	-	8.78	-	8.25	0.71	6.22	-	0.15
Nepheline	24.45	28.48	34.95	19.69	18.20	24.81	25.13	15.06	12.85	10.26	9.93
Acmite	-	-	-	-	-	-	-	-	-	-	-
Wollastonite	-	0.85	-	-	-	-	-	-	-	-	-
Diopside	0.36	3.72	6.87	-	1.82	-	2.97	-	-	-	-
Hypersthene	-	-	-	-	-	-	-	-	-	-	-
Olivine	3.56	-	0.93	3.60	2.80	4.31	3.68	6.06	5.52	6.73	1.64
Magnetite	2.23	4.36	0.83	2.60	3.99	0.94	1.16	1.03	1.23	1.31	4.41
Ilmenite	1.44	1.57	1.18	1.25	2.42	0.94	1.40	1.92	1.59	1.77	1.45
Haematite	-	-	-	-	-	-	-	-	-	-	-
Apatite	0.80	0.70	0.67	0.40	0.65	0.30	0.05	0.12	0.02	-	-
Calcite	2.31	2.06	nd	2.56	0.75	3.48	nd	2.86	nd	0.58	0.94
Zircon	0.04	0.04	0.02	0.02	0.03	0.03	-	0.02	0.02	-	0.02
Total	100.00	100.00	100.00	100.00	100.00	100.00	100.00	100.02	100.00	100.00	100.00

Quartz	-	-	-	-	-	-	-	-	-	-	-
Corundum	0.82	-	-	3.06	0.83	2.00	-	2.37	4.60	4.76	3.54
Orthoclase	32.52	36.07	30.47	43.82	48.43	49.16	43.62	43.65	42.35	40.36	46.45
Albite	20.67	16.86	19.72	21.25	11.15	12.22	12.30	23.88	25.48	31.19	30.22
Anorthite	8.53	5.01	4.45	-	6.50	-	8.25	-	3.30	-	-
Nepheline	22.35	27.27	32.58	18.40	15.94	23.19	22.93	12.59	10.02	7.70	9.24
Biotite	7.86	3.98	7.32	7.23	8.60	8.17	9.52	12.17	10.92	13.17	4.35
Wollastonite	-	1.63	2.41	-	-	-	0.34	-	-	-	-
Riebeckite	-	-	-	-	-	-	-	-	-	-	-
Magnetite	2.23	4.36	0.83	2.60	3.99	0.94	1.16	1.03	1.23	1.31	4.41
Haematite	-	-	-	-	-	-	-	-	-	-	-
Sphene	1.87	2.02	1.53	-	3.13	-	1.82	0.50	2.06	-	0.11
Rutile	-	-	-	0.66	-	0.50	-	0.81	-	0.93	0.72
Apatite	0.80	0.70	0.67	0.26	0.65	-	0.05	0.12	0.02	-	-
Zircon	0.04	0.04	0.02	0.02	0.03	0.03	0.02	0.02	0.02	-	0.02
Calcite	2.31	2.06	nd	2.70	0.75	3.79	nd	2.86	nd	0.58	0.94
Total	100.00	100.00	100.00	100.00	100.00	100.00	100.01	100.00	100.00	100.00	100.00

[illegible][illegible]

(5)

[illegible][illegible]

TABLE A3.3 (1)

[illegible][illegible]

(2)

[illegible][illegible]

(3)

	H24	H23	H17	H18	H6
Quartz	24.40	25.91	24.29	25.53	30.65
Corundum	0.18	0.83	-	-	-
Orthoclase	6.14	10.52	5.31	15.66	7.62
Albite	49.32	47.13	54.23	46.21	46.53
Anorthite	15.15	11.55	13.02	8.32	11.29
Leucite	-	-	-	-	-
Nepheline	-	-	-	-	-
Acmite	-	-	-	-	-
Wollastonite	-	-	-	-	-
Diopside	-	-	0.06	0.71	1.78
Hypersthene	3.79	3.25	2.45	2.81	1.43
Olivine	-	-	-	-	-
Magnetite	0.44	0.37	0.29	0.42	0.27
Ilmenite	0.40	0.28	0.21	0.25	0.25
Haematite	-	-	-	-	-
Sphene	-	-	-	-	-
Apatite	0.18	0.16	0.14	0.09	0.18
Calcite	-	-	-	-	-
Zircon	-	-	-	-	-
Total	100.00	100.00	100.00	100.00	100.00

Quartz	26.39	27.62	25.65	27.11	31.83
Corundum	0.36	1.00	0.12	-	-
Orthoclase	2.92	7.78	3.23	13.07	5.64
Albite	49.30	47.18	54.20	46.18	46.52
Anorthite	14.60	11.02	12.71	8.34	11.27
Biotite	5.29	4.49	3.39	4.31	3.26
Wollastonite	-	-	-	0.16	0.69
Hypersthene	-	-	-	-	-
Riebeckite	-	-	-	-	-
Magnetite	0.45	0.38	0.29	0.42	0.28
Haematite	-	-	-	-	-
Sphene	0.52	0.37	0.27	0.32	0.32
Rutile	-	-	-	-	-
Apatite	0.09	0.16	0.14	0.09	0.19
Zircon	-	-	-	-	-
Calcite	nd	nd	nd	nd	nd
Total	100.00	100.00	100.00	100.00	100.00

APPENDIX 4

Published papers and symposium abstracts

PERALKALINE GNEISSIC GRANITES IN THE NGOYE GRANITE-GNEISS FORMATION, NATAL

by

A.J. SCOGINGS

ABSTRACT

The Ngoye Granite-Gneiss Formation is located in the Natal sector of the Namaqua–Natal Mobile Belt. Eight different granite types have been recognized within the formation. These range from peraluminous to peralkaline in composition. The peralkaline granites underlie about 10 per cent of the formation and are essentially restricted to its southern contact with surrounding amphibolitic country rocks. Peraluminous granites are typically muscovite- and garnet-bearing whereas metaluminous varieties contain pale-green biotite and hornblende. Riebeckite and aegerine, with zircon and fluorite as common accessory minerals, are characteristic of the peralkaline granites. Geochemically, the peralkaline samples analysed display a range in agpaitic index (A.I. = mole $\text{Na}_2\text{O} + \text{K}_2\text{O}/\text{Al}_2\text{O}_3$) from 1.02 to 1.08. They are generally depleted in Al, Ca, and Mg relative to average granites, whereas Na and K are relatively high. Trace element analyses show enrichment of Nb, Zr, and Zn and depletion of Ba and Sr in the peralkaline granites. Stream sediment samples have delineated several mineralization targets around the margin of the massif. Those along the southern contact are associated with magnetite–quartz-rich rocks, which are highly enriched in Nb, Zr, Y, Zn, U, Th and to a lesser extent Sn and W. One target on the north-eastern margin of the formation has enhanced Sn contents.

The Ngoye Granite-Gneiss Formation is similar in size, morphology and composition to the younger anorogenic granite complexes of Nigeria, Sudan, and Saudi Arabia. It may be classified as an “A” type or “within-plate” granite complex.

CONTENTS

	<i>Page</i>
I. INTRODUCTION	361
A. Location	361
B. Previous Investigation	361
C. Geologic Setting	361
D. Present Study	361
II. LITHOLOGY	362
III. GEOCHEMISTRY	363
IV. DISCUSSION	363
ACKNOWLEDGMENTS	364
REFERENCES	364

I. INTRODUCTION

A. Location

The Ngoye Granite-Gneiss Formation is a prominent whaleback massif at the north-eastern extremity of the Natal portion of the Namaqua–Natal Mobile Belt. Situated to the south-west of Eshowe it has been subdivided into a main body which extends westerly for 30 km from Felixton and a smaller 3 km long Ninians body just north of Felixton (Fig. 1).

B. Previous Investigations

The granitic nature of the “Engoye [sic] Mountains” was first noted by Anderson (1901) who also observed that these hills occupy “the axis of the metamorphic belt”. Subsequent research by McCarthy (1961) and Charlesworth (1981) confirmed Anderson’s original appraisal of the area. Whereas McCarthy (1961) noted that biotite was the predominant mafic mineral, with local development of garnetiferous types, Charlesworth, in 1981, described hornblende-bearing granite gneisses in the main body. However, due to insufficient field data, he had to conclude that the hornblende granites were not restricted to any particular part of the formation and that the dominant lithology was characterized by biotite. Furthermore, Charlesworth (1981) proposed a transition from remnant augen-gneiss pods in the centre of the main body, through predominant strongly gneissose types, to bounding mylonites. The sharp, in places, mylonitized contacts of the

granite were cited as evidence for the thrust nature of the Ngoye Granite-Gneiss Formation. This was depicted by Charlesworth as an antiformal thrust sheet of igneous, mantle-derived granite gneiss.

C. Geological Setting

The Ngoye Granite-Gneiss Formation is situated at the north-eastern end of the 1 100 Ma Namaqua–Natal Mobile Belt, just to the south of the Natal Thrust-Front (Charlesworth, 1981). It has been assigned to the Nkomo Nappe at the base of the Tugela Group (Matthews and Charlesworth, 1981). The formation has a characteristic east–west-striking foliation, with steep southerly dips along the southern margins and moderate to steep northerly dips along the northern flanks of the massif.

D. Present Study

Interest in the area was generated in 1981 with the discovery by Mining Corporation of radioactive, quartz-rich, magnetite-bearing rocks along the southern contact zone of the Ngoye Granite-Gneiss Formation. Subsequent stream sampling and geophysical work delineated several targets along this zone which were trenching and assessed. Reconnaissance mapping by the author, whilst employed by Mining Corporation, indicated the presence of at least four distinctly different, mappable, granite units within the formation. The aim of the study has therefore been to:

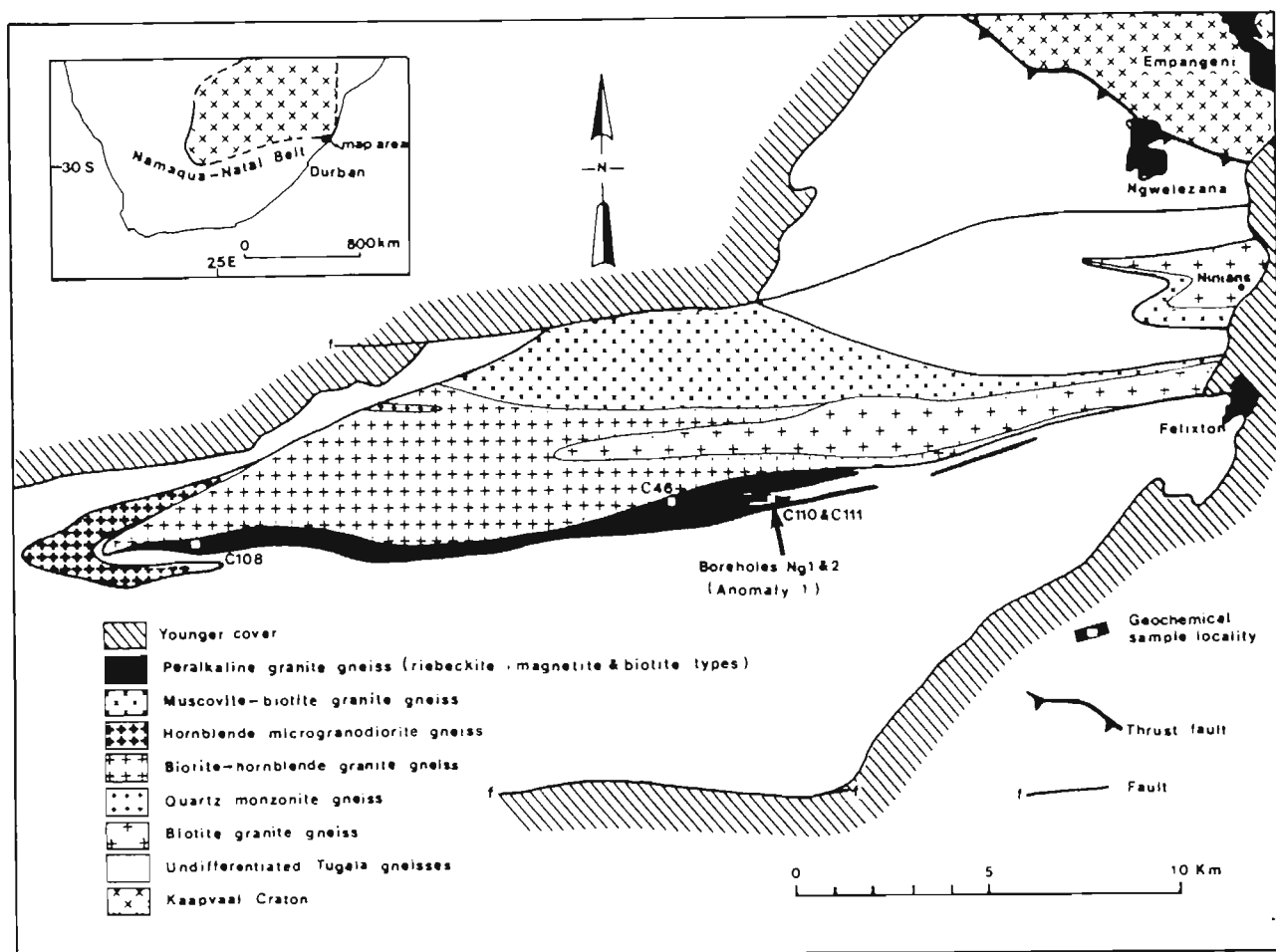


Figure 1

Simplified geological map of the Ngoye Granite-Gneiss Formation. Younger cover and Kaapvaal Craton data from Matthews and Charlesworth (1981).

1. map (at a scale of 1 : 10 000) the various lithologies and their field relationships;
2. establish compositional variations by microscopic and geochemical techniques and to define granitic types;
3. investigate the structural aspects, in particular the mylonites and shear zones; and
4. establish the relationship of the radioactive magnetite-rich rocks to the Ngoye Granite-Gneiss Formation.

This paper outlines the petrographic and geochemical results so far achieved.

II. LITHOLOGY

Eight gneissic granite types were distinguished during field mapping and thin section examinations (Fig. 1). Average modal analyses are presented in Table I, and for simplicity the terms "gneiss and gneissic" have been omitted from the following brief descriptions.

1. *Biotite granite* occurs in the eastern part of the main massif as well as in the Ninians Body (Fig. 1) and is the entity described by McCarthy (1961) and Charlesworth (1981) as the "Ngoye Granite-Gneiss". It is grey to pinkish in colour, with ovoid pink microcline megacrysts set in a groundmass of plagioclase, quartz and biotite. The microcline crystals, which range up to 2 cm in length, are often mantled by white plagioclase. Microscopically, microcline and plagioclase (An_{20-30}) are present in almost equal amounts (Table I) whilst pale-yellow to olive-green biotite with associated epidote and sphene are characteristic of this lithology. Muscovite and fluorite are present in places.

2. *Quartz monzonite* forms a small body on the north-western flanks of the main massif. It is a pinkish-grey, medium-grained rock superficially similar to the biotite

granite. Quartz contents are, however, low, and modal analyses (Table I) reveal almost equal contents of microcline and plagioclase (An_{30-35}). Accessories comprise chlorite, biotite, epidote, and sphene.

3. *Biotite-hornblende granite* crops out over most of the western half of the main body (Fig. 1). In the field this medium-grained rock type is distinguished from the biotite granite by a lack of microcline megacrysts and by the occurrence of clots and streaks of greenish-black hornblende. Modal analyses (Table I) show microcline to be more abundant than plagioclase (An_{20-30}), with hornblende and biotite the dominant mafic minerals. Sphene, epidote, and fluorite are accessories.

4. *Hornblende microgranodiorite* forms a sheet up to 1 km in thickness and defines a westerly plunging antiformal closure at the western extremity of the main massif (Fig. 1). It is essentially fine grained and contains microcline subordinate to plagioclase (An_{35-40}) with hornblende the dominant mafic mineral (Table I). Epidote and garnet are accessories.

5. *Muscovite-biotite granite* occurs along the northern portion of this main massif as well as in the southern part of the Ninians body (Fig. 1). It is off-white in colour, medium-grained, and contains microcline and plagioclase (An_{10-15}) in almost equal amounts, with biotite the principal mafic mineral. Muscovite may occur to the exclusion of biotite; with the muscovite-rich varieties characterized by small reddish garnets. This granite hosts microcline-quartz pegmatites, with occasional muscovite pods, along the northern-western margin of the main massif.

6. *Riebeckite-biotite granite* crops out along most of the southern part of the main massif and is a pinkish, medium-grained granite characterized by discrete aggregates of

TABLE I
Average Modal Analyses (vol. per cent) for Rocks from the Ngoye Granite-Gneiss Formation

	Biotite granite	Quartz monzonite	Biotite-hornblende granite	Hornblende microgranodiorite	Muscovite*-biotite granite	Riebeckite-biotite granite	Riebeckite granite	Magnetite microgranite	Radioactive aplite/pegmatite
Samples Analysed	n=22	2	16	3	13	7	3	5	4
Quartz	32,0	12,1	33,8	36,7	36,6	36,3	33,3	36,0	72,1
Microcline	29,1	34,7	36,7	14,1	30,5	31,1	31,9	52,3	5,6
Plagioclase	30,1	36,8	22,5	42,3	29,4	28,7	29,4	9,7	7,7
Hornblende	0,3		3,5	4,6					
Biotite	6,1	0,6	2,5	t	2,3	1,8		t	
Chlorite		4,7							
Muscovite	t				0,6				
Riebeckite						1,1	4,8		
Aegerine						0,3			
Sphene	0,5	1,4	0,3	t					
Epidote	0,6	7,2	0,3	0,4					t
Garnet				0,3					
Opaque	0,3	1,5		0,8	t	t	t	1,8	11,8
Zircon		0,4		t		t	t	t	2,4
Fluorite					t	t		t	t
Allanite	t				t				t
Total	99,0	99,4	99,6	99,2	99,4	99,3	99,4	99,8	99,6
% Outcrop	20,0	0,2	45,0	4,0	20,0	8,0	0,2	2,6	
Peraluminous/metalluminous granites 89,2 % of area									
Peralkaline granites 10,8 % of area									

* Include muscovite-rich varieties

t = Trace, less than 0,25 %

Modal analyses performed on sections stained for K-feldspar and plagioclase (Hutchison, 1974).

biotite, riebeckite, and occasional aegerine. The riebeckite and aegerine are strongly pleochroic (α = prussian blue, β = grey blue, γ = yellow) and (α = emerald green, β = green, γ = yellow-green), respectively. The biotite (α = yellow, γ = brown) is sometimes present to the complete exclusion of riebeckite and aegerine. Microcline and plagioclase (An_{0-12}) are present in subequal amounts (Table I). Clear to purplish fluorite is a common accessory and may form up to 1,5 per cent of the mode.

7. *Riebeckite granite* occurs as thin (<50 m wide) bands closely associated with the magnetite microgranite. This medium-grained rock is characterized by colourless to white feldspars and shiny blue-black riebeckite crystals, with microcline and plagioclase (An_{0-12}) present in almost equal amounts. Zircon is an ubiquitous accessory. A few pegmatitic portions contain riebeckite and zircon crystals up to 1 cm in length.

8. *Magnetite microgranite* is located along the south-central to south-eastern margins of the main body and also forms sheets within the country rocks (Fig. 1). It is a light-pink, fine-grained granitoid characterized by magnetite as the predominant mafic mineral. Microcline perthite greatly exceeds plagioclase (An_{5-15}) and zircon is a common accessory. Streaks and knots of quartz and magnetite-rich aplitic/pegmatitic material are encountered, in places, in the microgranite and are commonly radioactive. Minerals present in such rocks include abundant zircon, minor amounts of a yellow-brown mineral tentatively identified as fergusonite, biotite, and rare fluorite.

III. GEOCHEMISTRY

Whole-rock analyses and CIPW norms for riebeckite-biotite and magnetite-bearing granites from the southern part of the massif (Fig. 1) are presented in Table II. Based on Shand's (1947) classification they are peralkaline, as the combined molecular proportions of Na_2O and K_2O exceed Al_2O_3 , i.e.: $Na + K/Al > 1$. This ratio varies from 1,02 to 1,08 and is given as the agpaic index (A.I.) in Table II. These rather low indices are similar to that of the Nigerian riebeckite-biotite granite given in Table II and classified by Bowden and Turner (1974) as of

intermediate peralkalinity. The analyses presented in Table II show the Ngoye samples to be depleted in Al_2O_3 , MgO , and CaO , as well as the trace elements Ba and Sr relative to the average granite of Le Maitre (1976). These features, coupled with relative enrichments in $Na_2O + K_2O$, as well as enhanced Nb and Zr are characteristic of peralkaline granites (Radain and Kerrich, 1980). Similarly, the presence of acmite and the absence of normative anorthite for the Ngoye analyses is typical of Al_2O_3 -depleted granites (Nockolds *et al.*, 1978).

Trench samples at the highest grade target (Anomaly 1) showed highly variable concentrations of Nb (220–3 135 ppm), Ta (up to 194 ppm), Sn (up to 621 ppm), W (up to 124 ppm) and U (up to 309 ppm), over widths of between 0,4 and 3 m. Samples randomly analysed for Th and Zr yielded values of up to 1800 and 15 400 ppm, respectively. Data from two boreholes (NG1 and NG2) provided additional evidence that the mineralization is apparently of narrow width and low, irregular grade. Anomalous Sn values were detected in samples from streams draining the north-eastern flanks of the massif. Subsequent investigations indicated their derivation from small muscovite-rich pods in muscovite-biotite granite (a single analysis yielded 572 ppm Sn). According to the parameters described by Loiselle and Wones (1979), and Collins *et al.* (1982) the Ngoye samples analysed have all the geochemical characteristics of "A"-type granites. These authors describe "A"-type granites as typically enriched in Na_2O and K_2O whilst containing low CaO and MgO contents. They are also commonly enriched in Zr, Nb, REE, Zn, Sn, and W. Characteristic modal minerals include aegerine and riebeckite, with zircon and fluorite as common accessories (Loiselle and Wones, 1979).

IV. DISCUSSION

Petrographic evidence clearly indicates that the granites of the Ngoye Granite-Gneiss Formation vary from peraluminous to peralkaline in composition. Moreover, the peralkaline nature of the riebeckite- and biotite-bearing varieties is corroborated by the major element analyses which show the excess of ($Na_2O + K_2O$) relative to Al_2O_3

TABLE II
Major (wt %) and Trace Element (ppm) Abundances and CIPW
Norms for Peralkaline Rocks from the Ngoye Granite-Gneiss
Formation (Sample Localities on Fig. 1)

	C110	C46	C108	C111	A	B
SiO ₂	76.55	78.47	76.06	71.32	76.84	71.30
TiO ₂	0.12	0.11	0.19	0.24	0.07	0.31
Al ₂ O ₃	11.52	11.40	11.21	6.07	11.24	14.32
Fe ₂ O ₃	0.37	0.24	0.49	3.33	1.06	1.21
FeO	1.34	0.94	1.79	11.97	1.27	1.64
MnO	0.01	0.02	0.05	0.17	0.02	0.05
MgO	0.03	0.08	0.13	0.00	0.11	0.71
CaO	0.21	0.06	0.26	0.16	0.54	1.84
Na ₂ O	3.08	4.28	3.82	2.29	4.29	3.68
K ₂ O	6.14	4.52	4.80	2.58	4.28	4.07
P ₂ O ₅	0.02	0.01	0.02	0.04	0.01	0.12
LOI	0.22	0.11	0.19	0.02	0.08	0.64
H ₂ O	0.27	0.10	0.09	0.10	0.04	0.13
Total	99.88	100.34	99.13	98.29*	99.93	100.07
A.I.	1.02	1.05	1.03	1.08	1.04	0.73
Q	34.22	36.78	34.38	40.20	35.05	29.06
or	36.47	26.69	28.91	15.57	25.29	24.50
ab	25.15	33.54	30.92	17.29	33.98	31.13
an						8.04
c						0.92
ac	0.88	0.46	1.39	2.31	1.11	
ns		0.49				
di	0.87	0.24	0.98	0.49	2.15	
hy	1.88	1.65	2.96	19.80	0.85	3.37
mt				3.71	0.98	1.75
il	0.15	0.15	0.30	0.46	0.13	0.58
ap	0.03		0.19	0.10	0.02	0.28
cc						0.12
Nb	38	48	59	1 886	—	20
Zr	458	344	527	3 443	—	200
Y	87	46	79	1 265	—	34
Sr	14	2	8	6	—	300
Rb	240	156	144	95	—	200
Ba	120	49	212	56	—	830
Zn	57	35	142	622	—	60
U	n.d.	n.d.	n.d.	141	—	3.5
W	n.d.	n.d.	n.d.	14	—	1.5
Sn	6	19	n.d.	113	—	3

— not available

n.d. — not detected

* total excludes 0.19 % Nb; 0.34 % Zr; 0.13 % Y; and 0.18 % REE.

A.I. — Alkalic Index, or mol. pops Na₂O + K₂O/Al₂O₃

C110 — magnetite microgranite, Ngoye

C46, C108 — riebeckite-biotite granite, Ngoye

C111 — magnetite-quartz aplite/pegmatite, Ngoye

A — riebeckite-biotite granite, Nigeria, from Bowden and Turner (1974).

B — average granite, Le Maitre (1976) and average trace element contents from Rösler and Lange (1972).

Sample C46 collected by S.B. Gain in 1982. Remainder collected by Gain and Scogings in 1983. Analyses by M.R. Sharpe, Pretoria University.

CIPW norms from recalculated 100 % volatile-free analyses.

concentrations, as well as depleted MgO and CaO (Shand, 1947; Bowden and Turner, 1974; Nockolds *et al.*, 1978; Radain and Kerrich, 1980). Similarly, enrichments of the trace elements Nb, Zr, Th, Y, and U as well as Ba and Sr depletion at Ngoye are characteristic of peralkaline chemistry (Gerasimovsky, 1974; Bowden and Turner, 1974; Harris and Marriner, 1980).

According to the parameters suggested by Loiselle and Wones (1979) and Collins *et al.* (1982), the Ngoye specimens so far analysed are typical "A"-type granites. These authors, as well as Gass (1982) and Pitcher (1983) have noted that "A"-type granites (often as ring-complexes) are intruded into stable intracratonic or back-arc settings. Furthermore, Brown *et al.* (1984) proposed that such granites are intruded at increased distances

(continentwards) from subduction zones relative to calc-alkaline magmas. They suggest that the incompatible elements Nb, Zr, and Y are introduced into "A"-type magmas from within-plate mantle sources. Comparison of the Ngoye Granite-Gneiss Formation with the well-known "younger" granitic complexes of Nigeria, Saudi-Arabia (Fig. 2), and the Sudan reveals marked similarities, particularly with regard to lithologies, size of complex, geochemistry, and economically important minerals (Bowden and Turner, 1974; Harris and Marriner, 1980; Radain and Kerrich, 1980).

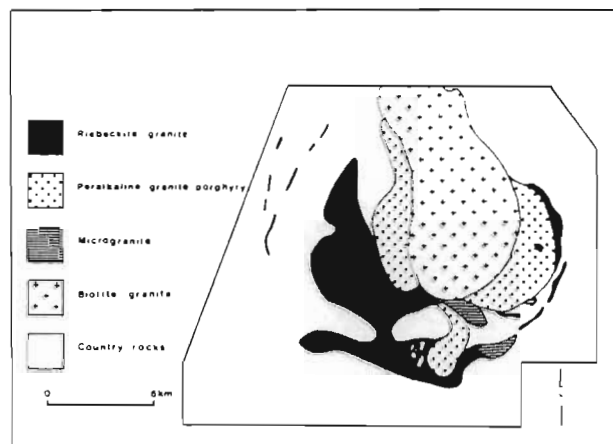


Figure 2

Simplified geological map of the Hadb-Aldyaheen peralkaline granite complex, Saudi Arabia from Radain and Kerrich (1980).

The inference, therefore, is that the Ngoye Granite-Gneiss Formation is a metamorphosed granite ring complex, and according to Loiselle and Wones (1979) should have been intruded in a post-orogenic (late kinematic) or anorogenic tectonic environment. Thus, in accordance with Matthews' (1981) model, the Ngoye Complex may be related to the final stages of a continent-arc collision and cratonization sequence, similar to that proposed by Gass (1982) for the Saudi-Arabian shield.

ACKNOWLEDGMENTS

The author would like to thank Mining Corporation (now part of the SA Development Trust Corporation), in particular Dr H.J. Hanekom and S.B. Gain for their enthusiasm and permission to use data from the Ngoye Project. The author is also grateful for the helpful advice of Prof. P.E. Matthews and his colleagues, Drs I.F. Forster, G.A. Zelt, M.R. Cooper, and C.A. Finlay in the Department of Geology at the University of Durban-Westville. Many thanks to my wife Renee for capturing this text onto the word-processor.

REFERENCES

- Anderson, W. (1901). Report on the reconnaissance survey of Zululand. *Rep. geol. Surv. Natal, Zululand*, 1, 60-61.
- Bowden, P., and Turner, D.C. (1974). Peralkaline and associated ring complexes in the Nigeria-Niger Province, West Africa. 330-351. In: Sørensen, H., Ed., *The Alkaline Rocks*. Wiley Interscience, New York, 662 pp.
- Brown, G.C., Thorpe, R.S., and Webb, P.C. (1984). The geochemical characteristics of granitoids in contrasting arcs and comments on magma sources. *J. geol. Soc. Lond.*, **141**, 413-426.
- Charlesworth, E.G. (1981). *Tectonics and metamorphism of the northern margin of the Namaqua-Natal Mobile Belt, near Eshowe, Natal*. Ph.D. thesis (unpubl.), Univ. Natal, Durban, 433 pp.
- Collins, W.J., Beams, S.D., White, A.J.R., and Chappell, B.W. (1982). Nature and origin of "A"-type granites with particular reference to Southeastern Australia. *Contr. Miner. Petrol.*, **80**, 189-200.

- Gass, I.G. (1982). Upper proterozoic (Pan-African) calc-alkaline magmatism in north-eastern Africa and Arabia, 591–609. In: Thorpe, R.S., Ed., *Andesites*. John Wiley and Sons, London, 690 pp.
- Gerasimovsky, V.I. (1974). Trace elements in selected groups of alkaline rocks, 402–410. In: Sørensen, H., Ed., *The Alkaline Rocks*. Wiley Interscience, New York, 622 pp.
- Harris, N.B.W., and Marriner, G.F. (1980). Geochemistry and petrogenesis of a peralkaline granite complex from the Midian Mountains, Saudi Arabia. *Lithos*, 13, 325–337.
- Hutchison, C.S. (1974). *Laboratory Handbook of Petrographic Techniques*. Wiley Interscience, New York, 527 pp.
- Le Maitre, R.W. (1976). The chemical variability of some common igneous rocks. *J. Petrol.*, 17, 589–637.
- Loiselle, M.C., and Wones, D.R. (1979). Characteristics of anorogenic granites. *Abstr. with Programs, geol. Soc. Amer.*, p. 539.
- Matthews, P.E. (1981). A new tectonic model for the northern region of the Namaqua–Natal Belt in Natal, 150–151. In: *Abstracts of Papers, South African Geodynamics Symposium*. Geol. Soc. S. Afr.
- , and Charlesworth, E.G. (1981). 1 : 140 000 Map, Northern Margin of the Namaqua–Natal Mobile Belt in Natal. *Geol. Dept. Univ. Natal*.
- McCarthy, M.J. (1961). *The geology of the Empangeni Fault area*. M.Sc. thesis (unpubl.), Univ. Natal, Durban, 81 pp.
- Nockolds, S.R., Knox, R.W.M., and Chinner, C.A. (1978). *Petrology for Students*. Cambridge University Press, 435 pp.
- Pitcher, W.S. (1983). Granite type and tectonic environment, 19–40. In: Hsu, K., Ed., *Mountain Building Process*. Academic Press, London, 263 pp.
- Radain, A., and Kerrich, R. (1980). Peralkaline granite in the western part of the Arabian Shield, 117–130. In: Al Shanti, A.M.S., Ed., *Evolution and Mineralization of the Arabian-Nubian shield*, 2, Pergamon Press, U.K., 205 pp.
- Rösler, H.J., and Lange, H. (1972). *Geochemical Tables*. Elsevier, Amsterdam, 468 pp.
- Shand, S.J. (1947). *The Eruptive Rocks*. Thomas Murby and Co., London, 488 pp.
- Geology Department,
University of Durban-Westville,
Private Bag X54001,
4000 Durban.

Accepted for publication by the Society on 30.10.1986.

Gneissose carbonatites in the Bull's Run Complex, Natal

A.J. Scogings

Mineral Development, STK, P.O.Box 213, Pretoria 0001, Republic of South Africa

I.F. Forster

Geology Department, University of Durban-Westville, Private Bag X54001, Durban 4000, Republic of South Africa

Accepted 28 December 1988

During 1986 several gneissose carbonatites of sövite composition were discovered in the northern portion of the 1100 Ma Natal Structural and Metamorphic Province, where they form an integral part of the Bull's Run Syenite Gneiss Complex. The latter is a complex body of syenite and nepheline-syenite gneisses with minor intrusive phases of carbonatite and peralkaline microsyenite. The carbonatites comprise principally calcite, apatite and biotite with ilmenite, pyrite, pyrochlore and zircon as accessory phases. Geochemically, the samples have typical sövite major-element concentrations, with low SiO_2 , Al_2O_3 , MgO , Na_2O , and K_2O while enhanced CaO and P_2O_5 reflect the presence of essential modal calcite and apatite. Enrichment of Nb, Y, Ba, and Sr in the Bull's Run carbonates, relative to sedimentary limestone, is considered indicative of their magmatic origin. Chondrite-normalized REE data support a magmatic derivation for the carbonate gneisses, with high LREE/HREE ratios and lack of Eu anomaly. A muscovite-rich syenite gneiss envelope around the nepheline syenite is interpreted as a possible fenite, in which the high alumina content of the pelitic country rocks suppressed the formation of aegirine and riebeckite. Because the carbonatite/ nepheline syenite association is generally considered diagnostic of a rifted intracratonic or taphrogenic environment at the time of intrusion, its discovery within the Natal Structural and Metamorphic Province has significant implications with respect to the tectonic history of this metamorphic belt.

Gedurende 1986 is verskeie gneisagtige karbonatiete van sövietsamestelling in die noordelike deel van die Natal Strukturele en Metamorfe Provinsie van 1 100 Ma ontdek waar hulle 'n integrale deel van die Bull's Run Siëniëtgneiskompleks vorm. Laasgenoemde is 'n ingewikkelde liggaam van siënië en nefeliënsiëniëtgneise met geringe intrusiefases van karbonatiet en peralkaliese mikrosiënië. Die karbonatiete bestaan hoofsaaklik uit kalsiet, apatiet en biotiet met ilmeniet, pinië, pirochloor en sirkoon as bykomende fases. Geochemies het die voorbeelde tipiese söviethoofelementekonsentrasie, met lae SiO_2 , Al_2O_3 , MgO , Na_2O en K_2O , terwyl verhoogde CaO en P_2O_5 die teenwoordigheid van belangrike modale kalsiet en apatiet aandui. Verryking in Nb, Y, Ba en Sr in die Bull's Run-karbonate met betrekking tot sedimentêre kalksteen, word beskou as aanduidend van hulle magmatiese oorsprong. Chondrietgenormaliseerde REE-data onderskryf 'n magmatiese herkoms vir die karbonaatgneise met hoë LREE/HREE-verhoudings en 'n gebrek aan Eu-anomalie, 'n muskoviëtryke siëniëtgneis wat die nefeliënsiënië omhul word geïnterpreteer as 'n moontlike feniet waarin die hoë alumina-inhoud van die pelitiese newegesteentes die vorming van aegirien en riebeckiet onderdruk het. Aangesien die karbonatiet/nefeliënsiënië-assosiasie oor die algemeen beskou word as diagnosties van 'n gekerfde intrakatoniese of tafrogeniese omgewing ten tye van intrusie, het die ontdekking daarvan in die Natal Strukturele en Metamorfe Provinsie betekenisvolle implikasies met betrekking tot die tektoniese ontwikkeling van hierdie metamorfiese gordel voorgestel is.

Introduction

The Bull's Run Syenite Gneiss Complex (BRSGC) is located some 180 km east-northeast of Durban, Natal (Figure 1) where it forms a prominent easterly trending ridge rising to some 400 m above the north bank of the Mhlathuze River. Geologically the BRSGC is situated within the northern marginal zone of the ~ 1100 Ma (Kibaran) Natal Structural and Metamorphic Province (NSMP), just south of the Natal Thrust Front and the Kaapvaal Craton (Charlesworth, 1981). Matthews & Charlesworth (1981) interpreted this complex as a thrust sheet of syenitic gneiss within the Nkomo Nappe, at the base of the Tugela Group. The latter is suggested to comprise imbricate-thrust slices of metamorphosed ocean floor and island-arc material obducted northwards onto the Kaapvaal Craton (Matthews, 1981).

Du Toit (1931) was the first to report on the granitic nature of the terrane immediately north of the Mhlathuze River. Subsequently, De Villiers (1941, p. 501) recorded

the occurrence of niobium-bearing minerals in 'a somewhat weathered albitite which occurs in basement about 15 miles north of the village of Eshowe'. The discovery of eluvial and alluvial deposits of zircon and monazite during the 1940s drew the attention of the Geological Survey to the economic potential of this area. These occurrences were described several years later by Von Backström (1962) who noted extremely large zircons up to several inches in length within decomposed gneisses on Bull's Run Estate. He concluded that the potential deposits were of low grade and although fairly extensive, of limited economic potential. Reconnaissance sampling by the author during 1987 confirmed Von Backström's appraisal, with grades of up to 0,66% combined ilmenite, zircon, and pyrochlore in eluvial soil deposits.

The syenitic character of the gneisses on Bull's Run Estate was first suggested by Nicolaysen & Burger (1965, p. 508) which they described as 'soda-rich Tugela migmatites and gneisses'. Historically this unit is of

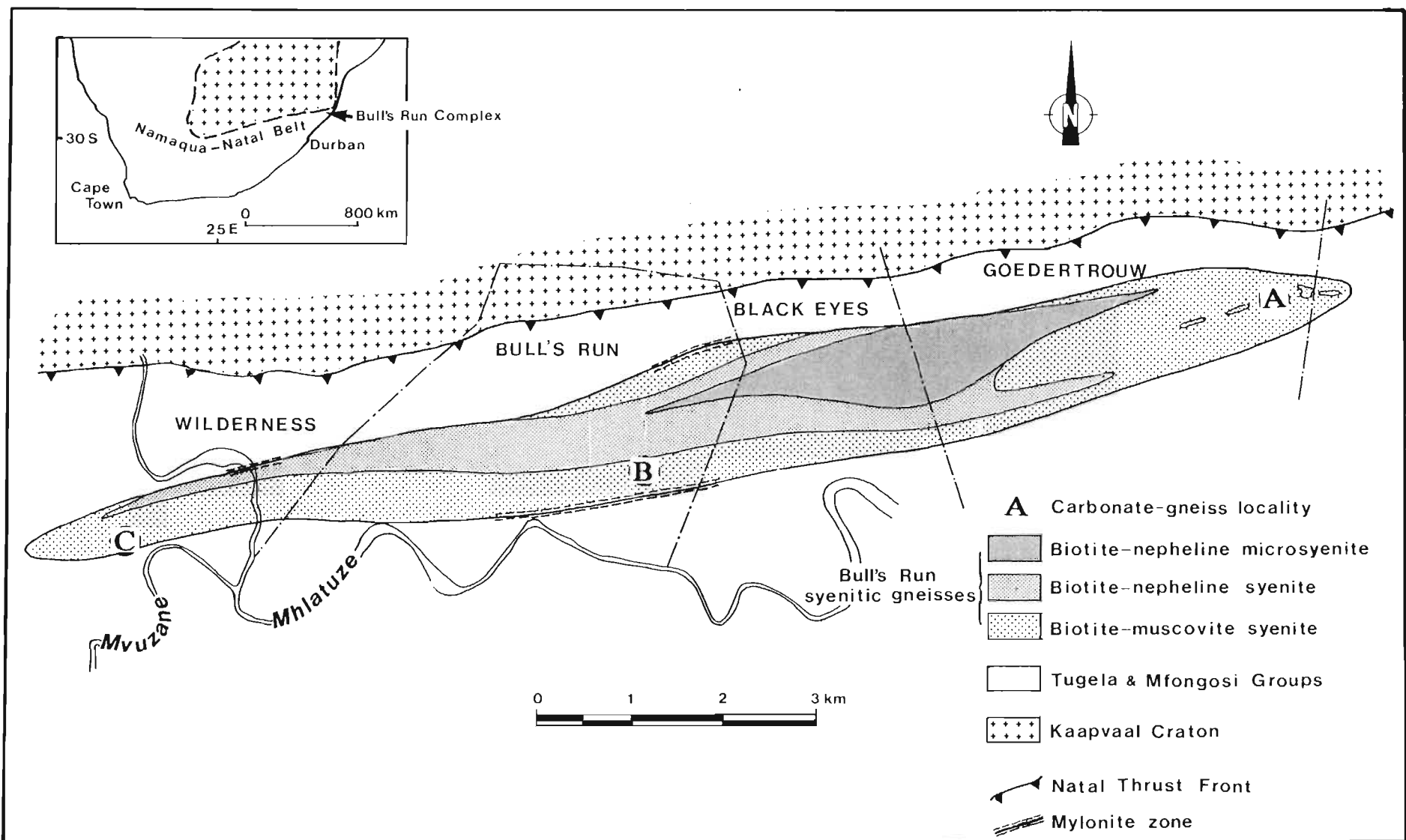


Figure 1 Simplified geological map of the Bull's Run Syenite Gneiss Complex, showing location of the carbonate gneiss outcrops.

interest, as it provided one of four rock types selected for the first age determinations in Natal by these authors. U-Th-Pb dates on a single zircon from Bull's Run gave ages of 1140 ± 35 Ma and 1100 ± 40 Ma, while K/Ar dating of biotite yielded an age of 900 Ma.

Although Nicolaysen & Burger (1965, p. 505) proposed the name 'Bull's Run Syenitic Gneiss' to describe the lithology, they did not delimit the body or make specific observations concerning its modal or chemical composition. Charlesworth (1981) subsequently delineated the complex and was able to demonstrate that the BRSGC is some 15 km long and up to 2 km wide. On the basis of modal analyses, Charlesworth classified the BRSGC as predominantly syenitic to quartz-syenitic in composition, with biotite the characteristic mafic phase. Scapolite was noted in several thin sections and suggested to be a metamorphic mineral, often occurring as replacement veinlets in K-feldspar megacrysts.

As recorded by Charlesworth (1981, p. 53) 'contacts (of the Bull's Run syenite) with the adjacent lithotypes are rarely observed', although highly mylonitized syenitic gneisses were noted to outcrop in the Mhatuze Valley along the northern margin of the BRSGC. This mylonite occurrence, in conjunction with mylonites observed on the southern margin, were interpreted by Charlesworth as representing thrust contacts between the BRSGC and adjacent amphibolitic and granitoid gneisses. A comprehensive review of the structural features of this area is given by Charlesworth (1981) and therefore, as Figure 1 is a simplified lithological map, structural data have been omitted for purposes of this discussion.

Present study

This investigation forms part of a research programme aimed at describing alkaline granitoids and establishing their tectonic significance with respect to the northern part of the NSMP. Current field work, petrography and geochemistry indicate that, contrary to previous interpretations, the BRSGC is lithologically complex and comprises a wide spectrum of syenitic gneisses with minor intrusive phases. As shown in Figure 1, the BRSGC may be subdivided into two broad lithotypes, with an envelope of biotite-muscovite syenite gneiss surrounding a core complex of biotite-nepheline syenite gneisses. Minor phases include peralkaline microsyenite dykes and the various carbonate-gneiss sheets and bodies which form the subject of this paper. The syenitic lithologies are briefly described below as an introduction to the setting of the carbonate gneisses.

Syenitic gneisses

Biotite-muscovite syenite gneiss forms an envelope around the central nepheline syenite gneiss core (Figure 1). It is an off-white to pink medium-grained granitoid gneiss rich in biotite and muscovite, with the accessory minerals calcite, apatite, and sphene. Silica contents range from about 52 to 59%, total alkalis vary between 10 and 13% while CaO is highly variable and reflects the

Table 1 Major elements (wt.%), CIPW norms (wt.%) and modes (vol.%) for representative syenitic gneisses, Bull's Run Syenite Gneiss Complex

	B34	B23	B20	B94
SiO ₂	56.69	53.45	59.26	67.45
TiO ₂	0.34	0.50	0.16	0.20
Al ₂ O ₃	22.12	22.71	22.00	15.82
Fe ₂ O ₃	0.43	0.65	0.49	0.28
FeO	2.13	3.24	2.43	1.38
MnO	0.05	0.08	0.04	0.02
MgO	0.48	0.39	0.09	0.61
CaO	2.99	1.96	0.49	2.10
Na ₂ O	5.11	6.54	8.94	7.51
K ₂ O	6.32	9.18	4.98	3.24
P ₂ O ₅	0.28	0.13	0.00	0.03
LOI	3.17	1.92	1.43	1.04
Total	100.11	100.75	100.31	99.68
A.I.	0.69	0.91	0.91	1.00
K ₂ O/Na ₂ O	1.24	1.40	0.56	0.43
				7.79
or	38.52	54.48	29.66	19.38
ab	35.78	5.64	48.00	64.04
an	13.43	3.92	0.21	
ne	4.77	27.01	15.29	
c	2.17	0.59	1.83	
di				7.24
ol	3.33	4.35	3.16	
cc		1.81	0.80	0.59
mt	0.63	0.94	0.71	0.32
il	0.67	0.96	0.30	0.38
ap	0.68	0.30		0.07
ac				0.15
Quartz				5.8
Microcline	21.2	34.8	20.9	18.9
Plagioclase	54.0	26.4	57.4	68.6
Nepheline		14.4	13.0	
Scapolite		9.3		
Biotite	2.8	13.1	7.7	
Muscovite	21.8	tr		
Aegirine				4.5
Riebeckite				1.0
Calcite	tr	1.8	0.8	0.6
Apatite		tr		
Zircon			tr	0.5
Pyrochlore			tr	

LOI includes CO₂, H₂O and other volatiles

tr = less than 0.2%

A.I. = agpaitic index (mol. prop. Na₂O + K₂O/Al₂O₃)

CIPW norms from recalculated 100% H₂O-free analyses. Major element analyses by M.R. Sharpe, University of Pretoria. For the purposes of norm calculations the CO₂ content of the samples was estimated from modal analyses. Modal analyses performed on thin sections stained according to the methods outlined by Hutchison (1974).

B34 = biotite-muscovite syenite gneiss

B23 = medium-/coarse-grained biotite nepheline syenite gneiss

B20 = fine-grained biotite nepheline syenite gneiss

B94 = peralkaline microsyenite dyke

modal occurrence of calcite and, to a lesser extent, apatite. Diagnostic CIPW normative constituents include minor amounts of quartz or nepheline and corundum. The latter indicates the excess of Al_2O_3 to $\text{Na}_2\text{O} + \text{K}_2\text{O}$ characteristic of this peraluminous saturated to mildly undersaturated lithology (see representative analysis, sample B34, Table 1).

Nepheline syenite gneisses form the core of the BRSGC (Figure 1) and are subdivided on the basis of textural, mineralogical, and geochemical features into two main lithotypes:

(1) an outer zone of *medium- to coarse-grained, dark grey to pinkish-grey, biotite nepheline-syenite gneiss*. As shown by the representative mode (Sample B23, Table 1), this rock type consists predominantly of microcline, albite, and nepheline, with biotite the characteristic mafic phase. Scapolite is a common accessory and characteristically occurs as reaction rims between nepheline and calcite. This mineral assemblage is reflected by the chemistry of the group which, with SiO_2 contents ranging from about 48 to 58%, is notably silica undersaturated. Alkali contents (12 – 15%) are considerably higher relative to Al_2O_3 than in the muscovite syenite gneisses, this character being manifested by lower normative corundum contents and elevated agpaite indices (Table 1). Furthermore, K_2O generally exceeds Na_2O , with $\text{K}_2\text{O}/\text{Na}_2\text{O}$ ratios above unity and ranging to as high as 2,64.

(2) An inner zone of fine-grained *leucocratic light-grey biotite-nephelinesyenite gneiss* is characterized by a high albite content and ubiquitous small zircon crystals. As indicated by the representative analysis in Table 1, SiO_2 contents are elevated, while CaO , FeO , and MgO are depleted relative to the coarser-grained nepheline syenites. Possibly the most distinctive geochemical character of this lithology is enrichment of Na_2O relative to K_2O , with low $\text{K}_2\text{O}/\text{Na}_2\text{O}$ ratios of between 0,44 and 1,01. This is reflected in the CIPW norm where albite occurs far in excess of orthoclase, while calcite and anorthite are only minor components. Most samples are only slightly corundum normative and therefore mildly peraluminous; this is corroborated by generally high agpaite ratios which approach unity (representative analysis B20, Table 1).

Gneissose microsyenite dykes up to 2 m wide and several hundred metres long are intrusive into the BRSGC, though apparently are most abundant in areas underlain by muscovite syenite gneiss. These dykes are steep dipping and display sharp contacts with the surrounding gneisses. A typical modal analysis (B94, Table 1) consists predominantly of albite with minor microcline and quartz. The agpaite minerals aegirine and riebeckite are essential constituents while calcite is a common accessory. Geochemically, the microsyenite dykes are characterized by enhanced SiO_2 contents of between 64 and 69%, low $\text{K}_2\text{O}/\text{Na}_2\text{O}$ ratios, and reduced Al_2O_3 (14 – 18%) relative to total alkalis. CaO values are highly variable and follow modal calcite occurrence. With agpaite indices of 1,0 or higher, the microsyenite

dykes are mildly peralkaline and consequently, with acmite in the norm, have no normative anorthite or corundum (B94, Table 1).

Carbonate gneisses — location and field relationships

Three carbonate gneiss occurrences have so far been discovered, the largest of which (locality A: samples B46, B60, and B62) crops out near the eastern extremity of the BRSGC. Two smaller bodies (locality B: sample B87; and locality C: sample B229) are described from the central and western parts of the complex (Figure 1). Field aspects of each occurrence are outlined below:

Locality A (samples B46, B60, B62): This is an elongate, north-east-striking, steep-dipping body of carbonate gneiss some 100 m long and up to 10 m wide. The carbonate gneiss is clearly intrusive into the muscovite syenite gneiss host as it contains 5 – 50 cm long ellipsoidal xenoliths of the latter (Figure 4). Contacts of the carbonate gneiss with the country rock have not been observed at this locality, although from available field

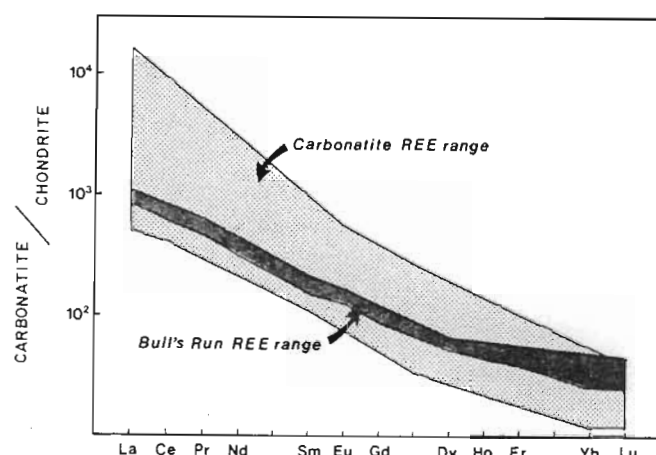


Figure 2 The range of chondrite-normalized REE contents for Bull's Run carbonate rocks. The range of REE contents for magmatic carbonatites is shown for comparison, from Cullers & Graf (1984).

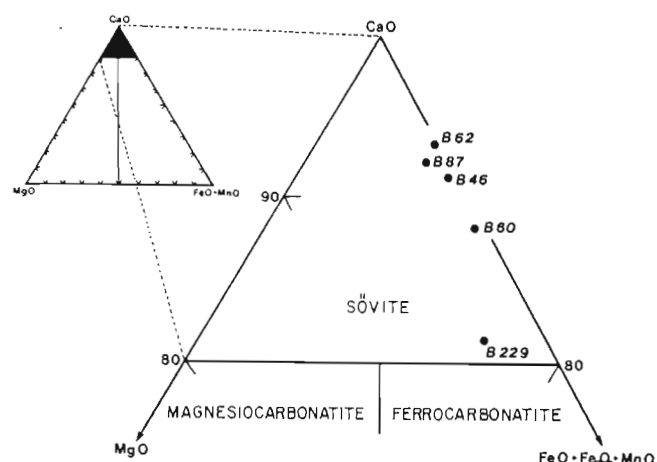


Figure 3 Classification of Bull's Run carbonatites according to the triangular $\text{CaO} - \text{MgO} - (\text{Fe}_2\text{O}_3 + \text{FeO} + \text{MnO})$ diagram of Woolley (1982). BRSGC samples shown as solid circles.



Figure 4 Carbonate gneiss outcrop B60 at locality A, displaying typical xenolithic inclusions of muscovite syenite gneiss. Scale in cm.



Figure 5 Carbonate gneiss outcrop B62 at locality A, displaying biotite-rich bands and streaks. Scale in cm.

evidence these are assumed to be quite sharp and probably steep dipping. Bands and streaks of biotite (Figure 5) may define a relic flow fabric. The carbonate is typically medium grained, reacts readily with dilute HCl, and displays a wide range in colour from white (B62, Figure 6) to brown (B46 and B60, Figure 7). Large books of shiny black biotite up to 5 cm in length, as well as centimetre-long ilmenite grains are characteristic of the brown carbonate gneiss outcrops.

Locality B (sample B87): The carbonate gneiss at this locality occurs as an east-west-striking, steep-dipping sheet, some 200 m long and up to 1 m wide. Clearly intrusive relationships are apparent, with sharp contacts and numerous xenoliths of syenite gneiss within the carbonate gneiss dyke.

Locality C (sample B229): This is the smallest occurrence of carbonate gneiss reported on here, and takes the form of metre-long pods and veins within biotite-muscovite syenite gneiss. Outcrops are restricted to a stream bed, about 1 km to the west-northwest of the confluence of the Mvuzane and Mhlatuze rivers, at the western end of the BRSGC. Although predominantly of medium-grained white calcite, this rock type is rich in biotite, while a greenish hue is imparted to some specimens due to high apatite concentrations. This locality is of particular interest owing to the occurrence of red-brown zircon crystals up to 1 cm long within the carbonate gneiss.



Figure 6 Polished specimen of white carbonate gneiss from sample site B62, locality A. Scale in cm.

Carbonate gneisses — petrography

Under the microscope, the carbonate gneisses are seen to comprise predominantly calcite, feldspar, biotite, and apatite (Table 2). Accessory constituents include pyrochlore and ilmenite, while traces of pyrite, zircon, and muscovite are present.

Polygonal calcite is the predominant mineral in all thin sections examined, comprising 56 – 96% by volume of

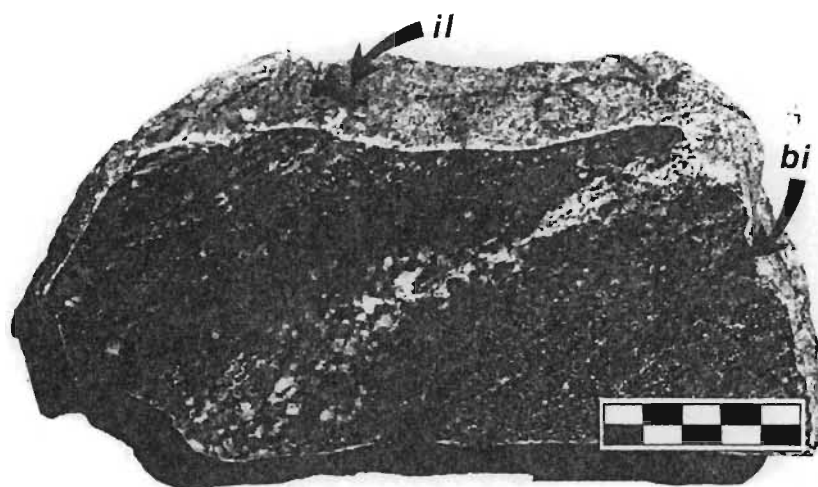


Figure 7 Polished specimen of brown carbonate gneiss from sample site B60, locality A. The rock is well foliated and characterized by coarse biotite books (bi), streaks of white calcite, and occasional large ilmenite grains (il).

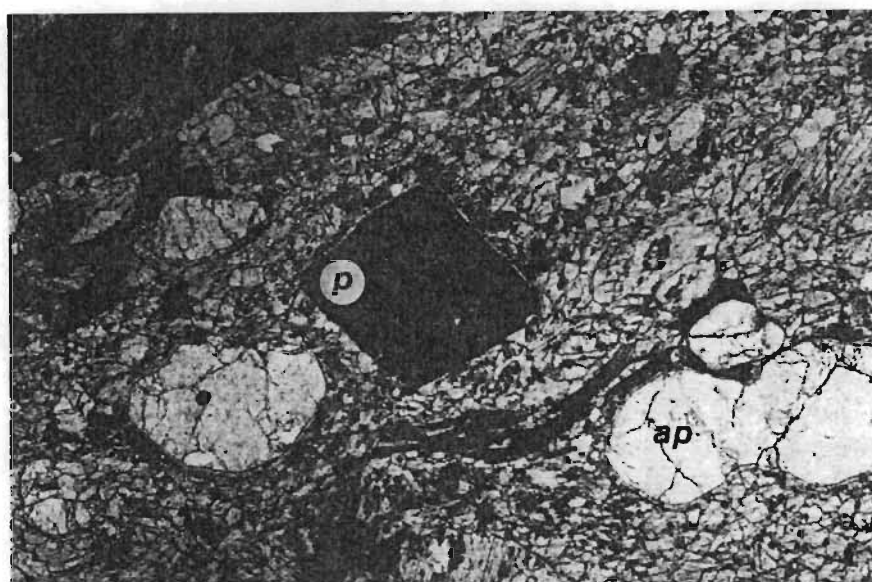


Figure 8 Photomicrograph of carbonate gneiss sample B46 taken under transmitted plane-polarized light. Minerals considered diagnostic of the carbonatitic ancestry of this lithology include pyrochlore (p) and rounded apatite grains (ap). The groundmass comprises calcite while in the upper left are flakes of biotite. Field of view is 8 mm × 5 mm.

this lithology. Grain size is highly variable, often with larger grains (up to 14 mm diameter) surrounded by an aggregate of finer grains (0,2 mm diameter). Polygonized calcite stringers are also notably developed along kinked twin planes in the larger calcite grains and possibly represent grain size reduction in response to deformational stresses. Polygonization of calcite is best developed in specimens of well-foliated carbonate gneiss (Figure 9), whereas equigranular calcite is typical of the more massive outcrops such as those of locality C.

Biotite is the characteristic mafic mineral of all specimens examined, occurring as pleochroic greenish to yellow-brown flakes and books up to 2 cm long. As shown in Figure 9, the biotite books are commonly fish shaped with sigmoidally curved and often kinked cleavage planes. Feldspars (microcline and plagioclase)

occur as rounded grains and aggregates and are most common in the xenolith-rich specimens from localities B and C. Microprobe analyses of biotite, microcline, and plagioclase are presented as Table 3. The biotite is notably Fe-rich, while the plagioclase is pure albite with very low CaO and K₂O content. The low analytical total obtained for the biotite is suggested to be due to all Fe having been assigned as FeO, in addition to the high volatile content typical of biotite.

Rounded to subhedral apatite is a notable constituent of all specimens analysed and generally comprises up to 5% of modal values (Table 2). One exception is sample B229 from locality C where 10% modal apatite is recorded. Accessories include euhedral yellow-brown pyrochlore octahedra of 0,2 mm diameter (Figure 8), subhedral ilmenite and euhedral pyrite cubes. Pyrochlore is restricted in distribution to the brown



Figure 9 Photomicrograph of carbonate gneiss sample B46 taken in transmitted plane-polarized light. Large sigmoidally curved biotite books in polygonized calcite. Remnant large calcite grains (cc) indicated at top right. Note dilated cleavage planes in biotite (arrowed). Field of view is 8 mm × 5 mm.

Table 2 Modal analyses (vol %) of Bull's Run carbonate gneisses

	B62	B60	B46	B87	B229
Calcite	96,0	79,7	84,8	71,3	56,4
K-Feldspar		0,5	2,0	9,9	3,4
Plagioclase		tr	tr	11,0	6,7
Biotite	3,2	12,3	9,4	6,9	23,0
Apatite	tr	4,8	3,2	0,6	10,0
Opaque	0,7	1,2	0,2	tr	tr
Pyrochlore		1,2	0,3		
Zircon					tr
Muscovite					0,2
Total	99,9	99,7	99,9	99,9	99,7

B62 — white carbonate gneiss, locality A

B60 — brown carbonate gneiss, locality A

B46 — brown carbonate gneiss, locality A

B87 — white carbonate gneiss, locality B

B229 — white carbonate gneiss, locality C

tr — trace amount less than 0,2%

Modal analyses performed on thin sections stained for K-feldspar, plagioclase, and carbonate, after the methods described by Hutchison (1974). A minimum of 1 200 points counted per section

Table 3 Preliminary microprobe analyses of biotite and feldspar — sample B46, locality A

	B46A	B46B	B46C
SiO ₂	33,03	68,66	64,60
TiO ₂	3,87	—	—
Al ₂ O ₃	17,24	19,31	18,44
FeO*	28,98	0,01	0,01
MnO	0,17	—	—
MgO	4,18	—	—
CaO	0,08	0,01	0,01
Na ₂ O	0,04	11,09	0,77
K ₂ O	8,65	0,57	15,60
Total	96,24	99,65	99,52

— = not analysed

FeO* = total Fe as FeO

B46A = biotite

B46B = albite

B46C = microcline

Microprobe analyses performed at Rhodes University on a JEOL 6330 Superprobe, under the supervision of Rob Skae

carbonate gneisses of locality A and is distinguished in thin section by typical octahedral form, subtranslucent brown colour and isotropic behaviour under crossed polars. Further evidence for the identification of pyrochlore is provided by the whole rock trace element data which show marked enrichment of Nb whenever this mineral is present.

The ilmenite has been positively identified using polished sections under reflected light. Traces of zircon and muscovite are present in sample B229.

Geochemistry

Whole-rock major and trace element analyses of five Bull's Run carbonate gneiss samples are presented, with comparative data, as Tables 4 and 5. Samples B46, B60, and B62 are very similar to the average calcite-carbonatite (sövite) of Le Bas (1981) in which SiO₂, Al₂O₃, MgO, Na₂O and K₂O are low while CaO and CO₂ constitute the major portion of each analysis. The feldspar-rich samples B87 and B229 are typified by higher SiO₂, Al₂O₃, and alkali contents. A consistent feature of all five samples is their very low MgO content

Table 4 Major (wt.%) and trace element (ppm) abundances for carbonate gneisses from the Bull's Run Complex

	B62	B60	B46	B87	B229	A	B	C	D
Si ₂ O	0,86	2,34	2,57	16,90	21,68	5,67	0,88	5,14	4,84
Ti ₂ O	0,01	0,28	0,23	0,33	0,74	0,50	0,18	0,07	0,07
Al ₂ O ₃	0,33	0,99	1,08	6,01	8,75	1,77	1,40	0,40	0,99
Fe ₂ O ₃	0,43	0,85	0,63	0,47	1,01	8,00	3,81	0,49	4,19
FeO	2,17	4,27	3,16	2,37	5,03	n.a.	0,36	n.a.	n.a.
MnO	1,21	1,10	0,90	0,28	0,28	0,78	0,65	0,14	0,39
MgO	0,13	0,27	0,26	0,50	1,06	6,10	0,38	7,79	5,10
CaO	54,32	49,40	48,53	39,70	31,34	37,06	50,83	42,30	43,79
Na ₂ O	0,08	0,01	0,11	0,90	0,87	1,09	0,48	0,03	0,33
K ₂ O	0,12	0,53	0,49	2,32	3,14	0,87	0,04	0,16	0,75
P ₂ O ₅	0,03	2,94	2,75	0,69	6,28	1,73	1,02	0,05	1,60
CO ₂	41,83	37,77	37,79	30,55	18,92	35,18	39,62	n.a.	34,70
Total	101,52	100,75	98,50	101,02	99,10	98,75	99,20	n.a.	96,75
Nb	68	3993	2633	52	72	560	n.a.	0,3	200
Y	86	94	102	56	78	114	n.a.	9	n.a.
Ce	1128*	606	1564*	455	1411*	5300*	n.a.	12	1020
Nd		275		199			n.a.	n.a.	430
La		306		286			n.a.	8	500
Sr	9135	8956	8077	7206	5701	7500	n.a.	600	5800
Ba	81	142	132	900	837	400	n.a.	90	3600
Rb	11	48	42	54	125	n.a.	n.a.	n.a.	n.a.
Sc	60	51	24	27	—	n.a.	n.a.	n.a.	n.a.

B62 = white carbonate gneiss, locality A

B60 = brown carbonate gneiss, locality A

B46 = brown carbonate gneiss, locality A

B87 = white carbonate gneiss, locality B

B229 = white carbonate gneiss, locality C

A = average carbonatite (Le Bas, 1981)

B = average calcite-carbonite, western Kenya (Le Bas, 1981)

C = average limestone (Hyndman, 1972; Middlemost, 1985)

D = Mount Grace carbonatite gneiss (Hoy & Kwong, 1986)

— = not detected; n.a. = not available

* = total REE (individual values for B62, B46, B229 in Table 4)

Bull's Run samples analysed by M.R. Sharpe, University of Pretoria.

CO₂ analysed by Building Research Institute, CSIR. Samples arranged in order of increasing silica content**Table 5** Rare earth element contents (ppm) of Bull's Run carbonate gneisses

	B62	B46	B229
La	265,60	361,37	309,27
Ce	515,28	718,45	637,19
Pr	55,44	76,29	71,80
Nd	187,40	269,30	271,60
Sm	28,99	41,63	40,99
Eu	9,45	12,82	12,86
Gd	23,33	32,19	30,60
Dy	17,82	22,47	17,82
Ho	3,63	4,50	3,36
Er	10,48	12,67	8,69
Yb	9,17	10,53	5,67
Lu	1,43	1,62	0,84
Total REE	1128,02	1563,84	1410,69

Analyses by J.N. Walsh, Bedford New College, U.K.

magmatic carbonatites by Cullers & Graf (1984) is presented as Figure 2. As noted by these authors, true carbonatites have the largest REE contents (REE = 72 - 15,515 ppm) and LREE/HREE ratios ((La/Lu)_{CN} = 7,1 - 1240) of any rock types, as well as no Eu anomalies. Although the BRSGC samples plot towards the lower limit of these ranges (Figure 2), the preponderance of LREE to HREE ((La/Lu)_{CN} = 19 - 38) and the lack of an Eu anomaly are strongly suggestive of their magmatic origin.

Discussion

Field and petrographic evidence indicates that the Bull's Run carbonate gneisses are intrusive into syenitic gneisses and consist primarily of calcite with variable amounts of biotite, apatite, pyrochlore, ilmenite, and zircon. The major- and trace element concentrations reflect this mineralogy, with high CaO, P₂O₅ and significant enrichments of Nb. According to the mineralogical and geochemical characteristics of magmatic carbonatites (Le Bas, 1981; Middlemost, 1985; Verwoerd, 1986), the BRSGC carbonate gneisses have the hallmarks of magmatic carbonatites. Thus, they contain the following diagnostic minerals: apatite, pyrochlore and zircon, they show pronounced enrichment of various trace elements such as P, Sr, Y, Nb and Ba, have high LREE/HREE ratios, and they are associated with nepheline syenites and related alkaline intrusives within the BRSGC.

Alkali metasomatism (finitization) of country rocks is characteristic of carbonatite/nepheline syenite intrusions. Such fenites result from the introduction of Na and K into the country rocks, which causes enhancement of Na and K relative to Al, and feldspathization and/or the formation of sodic minerals such as aegirine. Classic fenites, however, are notably absent from the BRSGC, although the close spatial association of the carbonatites with muscovite-rich syenite gneisses may indicate a genetic relationship.

corroborating the absence of dolomite, as suggested by stained thin sections. Although a similarity exists between CaO contents of these samples and the average sedimentary limestone (Table 4, column C), other major elements, especially Ti, Fe and P, are clearly enriched.

Further differences are highlighted by trace element geochemistry, with the BRSGC carbonate gneisses displaying massive enrichments of Nb, Y, Sr, and Ba relative to sedimentary limestone (Table 4). The Nb enrichment is clearly linked to the occurrence of pyrochlore (Table 2, samples B46 and B60), while P₂O₅ is directly related to modal apatite concentrations.

A comparison of the BRSGC carbonate gneiss REE data (see Table 5) with the REE range suggested for

Therefore, by analogy with similar muscovite-bearing alteration zones associated with nepheline syenite complexes, e.g. Blue Mountain, Ontario (Payne, 1968) Monchique, Portugal (Rock, 1976) it is suggested that the muscovite-rich envelope around the BRSGC represents a fenite halo derived by metasomatic alteration of pelitic (aluminous) country rocks. This interpretation is in accordance with conclusions reached by Rock (1976), who noted that the formation of highly sodic minerals, such as aegirine, tends to be suppressed around alkaline complexes intrusive into pelitic country rocks.

All the evidence suggests that the Bull's Run carbonate gneiss occurrences are gneissic carbonatites. They are thus classified as calcite-carbonatites (sövites) by their modal mineralogy (Streckeisen, 1978), as well as by their major-element chemistry according to the triangular CaO - MgO - (Fe₂O + FeO + MnO) diagram of Woolley (1982) (Figure 3).

Attention is drawn to the discovery of rather similar carbonatite gneisses within the Shuswap Complex of British Columbia (Hoy & Kwong, 1986). These authors have interpreted a thin, though extensive marble unit, as representing a metamorphosed pyroclastic carbonatite horizon within a sequence of calc-silicate and pelitic gneisses. Evidence cited for the magmatic parentage of this marble, referred to as the Mount Grace carbonatite, includes high concentrations of Mn, Sr, Ba, Nb, and LREE in addition to modal apatite, phlogopite, and sodic amphiboles. A representative analysis is included in Table 4 for comparison with the Bull's Run carbonatite gneiss data.

Tectonic significance

The discovery of gneissose carbonatites within the BRSGC has particular significance for the interpretation of the Natal Structural and Metamorphic Province (NSMP). This is due to the fact that the nepheline syenite/carbonatite association is widely considered to be restricted to regions of intra-continental rifting (Bailey, 1954; Middlemost, 1985). However, it must be pointed out that carbonatites are also recorded from oceanic islands such as those of the Cape Verde Archipelago, as well as in association with high-K shoshonites around tectonically active continental margins (Middlemost, 1985). Although alkaline rocks are not restricted to rift zones, 'where continental rifting is known, alkaline magmatism is strongly in evidence' (Bailey, 1964, p. 150). This common association has led to the proposal that carbonatite/alkaline magmatism is an integral part of rift formation and development (Middlemost, 1974; Saggerson, 1970).

A feature of the magmatism associated with intracratonic rift and epeirogenically domed settings is a wide variety of alkaline rocks, ranging from carbonatite and nepheline syenites through to peralkaline granite ring complexes. Examples of continental rifts with this characteristic magma association include the Gardar palaeorift in Greenland, the Oslo Rift of Norway, the African Niger-Nigerian Province and the St Lawrence

palaeorift in Canada (Bowden & Turner, 1974; Barberi & Varet, 1978; Petersen, 1978; Philpotts, 1978; Upton & Blundell, 1978.)

It is noteworthy, therefore, that the Ngoye Granite Gneiss Formation, some 30 km east of the Bull's Run Complex, has recently been interpreted (Scogings, 1985, 1986) as a gneissic 'A-type' alkaline/peralkaline granite ring complex similar to the classic occurrences of Nigeria and Saudi Arabia. Although the discovery of carbonatite gneisses in the NSMP is not on its own necessarily diagnostic of a particular tectonic setting, when viewed in conjunction with the associated Ngoye ring complex, it is considered indicative of emplacement into a rifted or epeirogenically domed continental environment.

Conclusions

The Bull's Run carbonate gneisses represent gneissose carbonatites within a nepheline-syenite gneiss complex. They display the hallmarks of magmatic carbonatites, i.e. enhanced P₂O₅, Sr, Ba, Nb, and REE concentrations, and the diagnostic mineral phases apatite, zircon, and pyrochlore. They are furthermore clearly intrusive and, although not associated with classic peralkaline fenites, are surrounded by muscovite-rich syenite gneisses that may represent metasomatized pelites. When interpreted in conjunction with other alkaline rocks in the Tugela Group of the NSMP, the BRSGC gneissose carbonatites are considered to be indicative of an intracratonic rifted tectonic setting at the time of intrusion.

Acknowledgements

Sincere thanks are extended to Anglo American Corporation, the South African Development Trust Corporation, and Kidogo Mining for permission to use geological information from the Bull's Run Complex. The assistance rendered to us by fellow members of staff in the Geology Department at the University of Durban-Westville is gratefully acknowledged.

References

- Bailey, D.K. (1964). Crustal warping — a possible tectonic control of alkaline magmatism. *J. geophys. Res.*, **69**, 1103 – 1111.
- Barberi, F. & Varet, J. (1978). The Afar rift junction, 55 – 69. In: Neumann, E.R. & Ramberg, I.B., Eds., *Petrology and Geochemistry of Continental Rifts*. Riedel Publishing, Holland.
- Bowden, P. & Turner, D.C. (1974). Peralkaline and associated ring complexes in the Nigeria-Niger Province, West Africa. 330–351. In: Sørensen, H., Ed., *The Alkaline Rocks*. Wiley Interscience, New York, 622 pp.
- Charlesworth, E.G. (1981). *Tectonics and metamorphism of the northern margin of the Namaqua Natal Mobile Belt near Eshowe, Natal*. Ph.D thesis (unpubl.), Univ. Natal, Durban, 433 pp.
- Cullers, R.L. & Graf, J.L. (1984). Rare earth elements in igneous rocks of the continental crust: predominantly basic and ultrabasic rocks, 237–274. In: Henderson, P., Ed., *Rare Earth Element Geochemistry*. Elsevier, Amsterdam, 515pp.

- De Villiers, J.E. (1941). Columbomicrolite from Eshowe, Natal. *Amer. Min.*, **26**, 501–506.
- Du Toit, A.L. (1931). *The geology of the country surrounding Nkandla, Natal*. Expl. Sheet 109, Geol. Surv. S. Afr., 111 pp.
- Hoy, T. & Kwong, Y.T.J. (1986). The Mount Crace carbonatite- an Nb and light rare earth element-enriched marble of probable pyroclastic origin in the Shuswap Complex, Southeastern British Columbia. *Econ. Geol.*, **81**, 1374–1386.
- Hutchison, C.S. (1974). *Laboratory Handbook of Petrographic Techniques*, Wiley Interscience, New York, 527 pp.
- Hyndman, D.W. (1972). *Petrology of Igneous and Metamorphic Rocks*. McGraw-Hill, New York, 533 pp.
- Le Bas, M.J. (1981). Carbonatite magmas. *Min. Mag.*, **44**, 133–140.
- Matthews, P.E. (1981). *A new tectonic model for the northern margin of the Namaqua-Natal Belt in Natal*. Abstr. Geocongr. Geol. Soc. S. Afr.
- & Charlesworth, E.G. (1981). 1:140 000 map, *Northern Margin of the Namaqua-Natal Mobile Belt in Natal*. Compiled at Natal University.
- Middlemost, E.A.K. (1974). Petrogenetic model for the origin of carbonatites. *Lithos*, **7**, 275 – 278.
- (1985). *Magmas and Magmatic Rocks: an Introduction to Igneous Petrology*. Longman, London, 266 pp.
- Nicolaysen, L.O. & Burger, A.J. (1965). Note on an extensive zone of 1 000 million year-old metamorphic and igneous rocks in Southern Africa. *Sci. de la Terre*, **10**, 497–516.
- Payne, J.G. (1968). Geology and geochemistry of the Blue Mountain nepheline syenite. *Can. J. Earth Sci.*, **5**, 259 – 273.
- Petersen, J.S. (1978). Composite plutonic ring-complexes: a structural characteristic of riftzone plutonism, 217–229. In: Neumann, E.R. & Ramberg, I.B., Eds., *Petrology and Geochemistry of Continental Rifts*. Riedel Publishing, Holland.
- Philpotts, A.R. (1978). Rift-associated igneous activity in Eastern North America, 133–154. In: Neumann, E.R. & Ramberg, I.B., Eds., *Petrology and Geochemistry of Continental Rifts*. Riedel Publishing, Holland.
- Rock, N.M.S. (1976). Fenitization around the Monchique alkaline complex, Portugal. *Lithos*, **9**, 263 – 279.
- Saggerson, E.P. (1970). The structural control and genesis of alkaline rocks of central Kenya. *Bull. Volcanol.*, **34**, 38 – 76.
- Scogings, A.J. (1985). *The geology of the Ngoye Granite Gneiss Formation*. M.Sc. thesis (unpubl.), Univ. Durban-Westville, Durban, 186 pp.
- (1986). Peralkaline gneissic granites in the Ngoye Granite-Gneiss Formation, Natal. *Trans. geol. Soc. S. Afr.*, **89**, 361–365.
- Streckeisen, A. (1978). Classification and nomenclature of volcanic rocks, lamprophyres, carbonatites and melilitic rocks, *Neues Jb. Miner.*, **134**, 1–14.
- Upton, B.G.J. & Blundell, D.J. (1978). The Gardar Igneous Province: evidence for Proterozoic continental rifting. 163–172. In: Neumann, E.R. & Ramberg, I.G., Eds., *Petrology and Geochemistry of Continental Rifts*. Riedel Publishing, Holland.
- Verwoerd, W.J. (1986). Mineral deposits associated with carbonatites and alkaline rocks, 2173–2191. In: Anhaeusser, C.R. & Maske, S., Eds., *Mineral Deposits of Southern Africa*. Geol. Soc. S. Afr., Johannesburg.
- Von Backström, J.W. (1962). Zircon, ilmenite and monazite occurrences on Bull's Run Estate north-northwest of Eshowe, Natal. *Ann. geol. Surv. S. Afr.*, **1**, 137 – 146.
- Woolley, A.R. (1982). A discussion of carbonatite evolution and nomenclature, and the generation of sodic and potassic fenites. *Min. Mag.*, **46**, 13–17.

Peralkaline granitoid and associated alkaline mafic gneisses northwest of Eshowe, Natal

A.J. Scogings*

Geology Department, University of Durban-Westville, Private Bag X54001, Durban 4000, Republic of South Africa

Accepted 30 September 1989

Peralkaline granitoid and alkaline mafic gneisses have recently been discovered within the Halambu Formation, near the northern margin of the *ca.* 1100 Ma Natal Structural and Metamorphic Province. The Halambu Formation has previously been described as predominantly of granodioritic composition with some monzonitic elements. The peralkaline gneisses crop out on Wangu Hill as an elongate mylonite-bounded body about 6 km long and up to 1 km wide and are leucocratic, fine-grained rocks characterized by the presence of aegirine-augite, riebeckite and magnetite. The Wangu gneisses are depleted in Al_2O_3 relative to alkalis and have peralkaline indices ranging between 0.94 and 1.33. Trace element contents are typical of peralkaline granitoids with elevated Ga/Al, Zn, Zr, Nb, Y and REE, and low Ba and Sr. Based on various major and trace element geochemical classification schemes these gneisses are shown to have 'within-plate' or 'A-type' granite characteristics and were probably intruded into a post-collisional or anorogenic tectonic setting. The gneissose biotite-rich mafic sheets display intrusive relationships with the peralkaline Wangu granite gneisses and, on the basis of major and trace element signatures, are suggested to be metamorphosed volatile-rich alkaline mafic rocks. The above interpretations are in marked contrast to the calc-alkaline, granodioritic affinities of the Halambu Formation described by previous researchers.

Peralkaliese granitoïed en alkalies-mafiese gneise is onlangs naby die noordelike grens van die *ca.* 1100 Ma Natal Strukturele en Metamorfie Provinsie ontdek en word ingesluit in die Formasie Halambu. Die Formasie Halambu is voorheen beskryf as van oorheersend granodioritiese samestelling met sekere monzonitiese elemente. Die peralkaliese gneise dagsoom as 'n verlengde milloniet-begrensde liggaam van ongeveer 6 km lank en tot 1 km wyd en is 'n leukokratiese fynkorrelrige gesteente gekarakteriseer deur die teenwoordigheid van aegirien-augiet, riebeckiet en magnetiet. Die gneise is verarm in Al_2O_3 relatief tot alkalies met peralkaliese indekse wat wissel tussen 0.94 en 1.33. Die spoorelementinhoud is tipies van peralkaliese granitoïedes met verhoogde Ga/Al, Zn, Zr, Nb, Y en REE asook lae Ba en Sr. Gebaseer op verskeie hoof- en spoorelement geochemiese klassifikasies, vertoon hierdie gneise of 'tussenplaatse'- of 'A-tipe' graniet karaktertrekke en is hulle moontlik ingedring in 'n voor-kontinent botsing of 'n anorogenetiese tektoniek. Gneisagtige biotietryke mafiese plate vertoon intrusiewe verwantskappe met die peralkaliese Wangu granietgneise en op grond van hulle hoof- en spoorelement kenmerke word hulle beskou as gemetamorfiseerde, vlugstofryke alkalies-mafiese gesteentes. Volgens bogenoemde interpretasies staan hierdie gesteentes in duidelike kontras met die kalk-alkaliese-granodioritiese verwantskappe van die Formasie Halambu soos beskryf deur vorige navorsers.

* **Present address:** Mineral Development Division, STK, P.O. Box 213, Pretoria 0001, Republic of South Africa

Introduction

The purpose of this communication is to record the discovery of peralkaline granitoid and alkaline mafic gneisses in the Wangu Hill area to the northwest of Eshowe, Natal. These distinctive rocks had previously not been recognized and had been grouped within the granodioritic Halambu Granite Gneiss Formation Charlesworth (1981).

The Halambu Granite Gneiss Formation, as outlined by Charlesworth (1981), occupies an extensive area along the northern margin of the *ca.* 1100 Ma Natal Structural and Metamorphic Province (NSMP) (Figure 1). The geology of this region was first described by Du Toit (1932). He noted that granites of the so-called 'Alambu mass' form 'a belt averaging 2 miles wide running eastwards along the watershed between the Inyawoshane and Mvusana (rivers)' (Du Toit, 1931, p.55). The lithologies south of the 'Alambu Mass', and including those on 'Iwangu Hill' were ascribed by Du Toit to the predominantly amphibolitic 'Tugela Series' (see location of Wangu Hill in Figure 1).

Subsequent mapping confirmed the presence of

granitoid gneisses within the 'Alambu Mass' (Charlesworth, 1981). Charlesworth incorporated some of Du Toit's Tugela Series rocks of the Wangu area into the proposed 'Halambu Granite Gneiss Formation' (Matthews & Charlesworth, 1981). On the basis of regional mapping and limited mineralogical and geochemical evidence, Charlesworth (1981) classified the Halambu Formation as predominantly of granodioritic to tonalitic composition, with lesser amounts of monzonitic gneiss (see Table 1 for representative modal analysis of the predominant granodioritic gneiss).

Although these two rock types are not differentiated on the map compilation of Matthews & Charlesworth (1981), Charlesworth (1981) suggested that the monzonitic variety is restricted to the area south of a line between Wangu and Khomo Hills (see localities on Figure 1). Therefore, from the descriptions by both Charlesworth and Du Toit (1932), it is clear that a compositional break in the vicinity of Wangu Hill was recognized, although neither author appreciated the peralkalinity of the gneisses south of the main body of

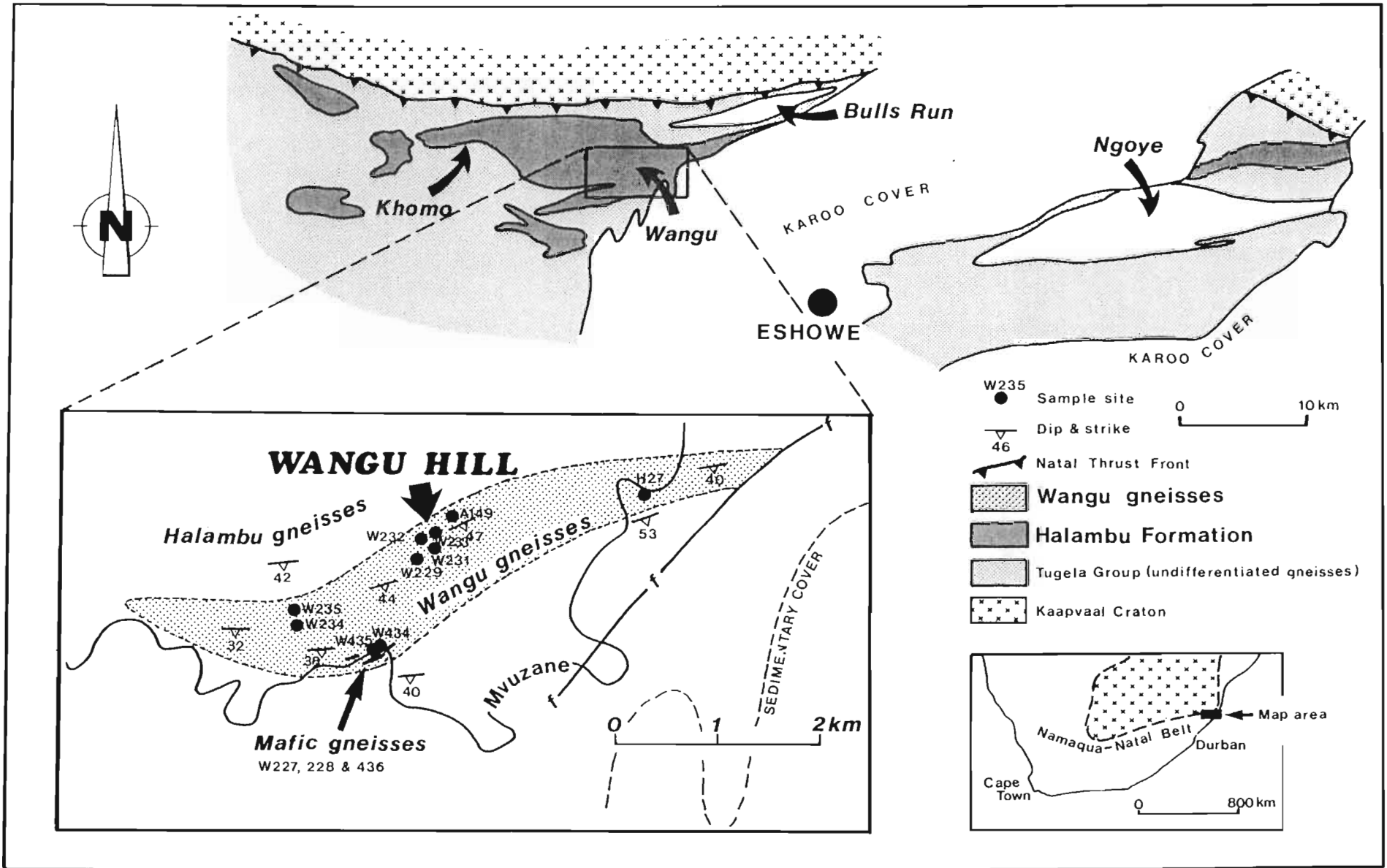


Figure 1 Simplified geological map of the north-eastern margin of the Natal Structural and Metamorphic Province showing the distribution of the Halambu Granite Gneiss Formation, from Matthews & Charlesworth (1981). The inset shows the locality of peralkaline granitoid and mafic gneiss samples collected over the Wangu Hill area.

Table 1 Modal mineralogy (vol.%) of the Wangu Hill lithologies

	W231	W435	W434	W235	W234	H27	W149	W229	W232	W233	H18	W228	W436	W227
Quartz	25	26	28	25	30	34	40	40	40	53	26			
Microcline	30	26	17	42	35	36	30	15	15	10	17	5	7	6
Albite	35	39	47	25	27	24	25	30	20	17	51*	21	34	37
Biotite		t	1	3	4	1	t				4	63	52	45
Aegirine augite	5			4	3			4	15	12				
Riebeckite	1													
Opaque	5	8	6	t	t	3	6	10	8	9	2	t	t	t
Pyrochlore						t								
Calcite		1	t									6	4	8
Apatite											t	3	2	2
Fluorite			t											
Sphene									t		t	t	t	t

Modal analyses performed on thin sections stained for K-feldspar, plagioclase and quartz

t = trace amount, less than 0.2%

* = the plagioclase feldspar in H18 is oligoclase

W231 to W229 = Wangu granitoid gneisses

W232 and W233 = Wangu magnetite-rich granitoid gneisses

W228 to W227 = Wangu mafic gneisses

H18 = granodioritic gneiss from north of Wangu Hill

Halambu granodioritic gneisses.

According to his geochemical data, Charlesworth (1981) suggested that the Halambu gneisses represent deformed intrusive granites of calc-alkaline affinity with both I- and S-type signatures, based on the parameters of Chappell & White (1974). Following a detailed structural analysis of the Halambu area, it was suggested that the granodioritic precursors to the Halambu gneisses were intruded during post-D₁ times and prior to a northward-directed D₂ compressional thrusting event (Charlesworth, 1981). Metamorphic conditions were shown by Charlesworth to have attained upper amphibolite grade during the D₁ compressional event, while lower grades were suggested during D₂ thrusting. The pervasive east-west foliation, within the Halambu Formation as a whole, was ascribed by Charlesworth (1981) to deformational stresses developed during the D₂ event and was noted to be axial planar to northward-verging D₂ folds in the surrounding amphibolitic terrane.

Peralkaline gneisses to the northwest of Eshowe were first identified by the author during 1986, when geochemical analysis of a fine-grained granitoid gneiss collected east of Wangu Hill (H27, Figure 1) showed typical peralkaline characteristics such as low Al₂O₃, Cao and SrO, with enhanced contents of Nb, Zr, Zn, and REE (see Tables 2 and 3). Subsequent fieldwork early in 1988 confirmed the alkaline/peralkaline chemistry of felsic gneisses in the Wangu Hill area (Scogings, 1988a, b). The granitoid gneisses of the Wangu Hill area are hereafter referred to as the Wangu granitoid gneisses in order to distinguish them from the granodioritic gneisses typical of the Halambu Formation to the north of Wangu Hill.

Field and petrographic descriptions

Wangu granitoid gneisses

The Wangu gneisses occupy a 6 km-long zone approximately 1.0 km wide that trends east-west across Wangu Hill, being bounded to the north and south by granodioritic gneisses of the Halambu Formation (Figure 1). Contact and age relationships (e.g. xenoliths of country rock or cross-cutting features) between the Wangu gneisses and the surrounding lithologies are poorly defined at present. This is partly due to the fairly limited scale of field mapping so far done in this area, as well as to the highly sheared character of the outcrops which tends to mask lithological variations. However, it is apparent from an increase in the intensity of foliation and the development of mylonites near the margins of the wangu gneiss body, that the contacts have been tectonically modified and that the Wangu gneisses may be a thrust-bound unit. This interpretation is consistent with descriptions of similar mylonite-bounded granitoid bodies in the NSMP by Charlesworth (1981) where the mylonites are suggested to be of D₂ age.

The Wangu gneisses are fine-grained, light-pink rocks of aplitic character that form sheet-like outcrops and demonstrate by a prominent east-west planar foliation (D₂ of Charlesworth, 1981) that dips at between 40 and 50° to the south (Figures 1 and 2). Several elongate zones of relatively mafic magnetite-rich radioactive gneiss up to 20 m long and 10 cm wide were noted on the crest of Wangu Hill. These heavy mineral-rich layers (ca. 20–30% magnetite + pyroxene) are suggested to be cumulate phases, derived by mechanical concentration in a highly fluid, volatile-rich peralkaline melt. Such layering is common within peralkaline intrusions (e.g.

Table 2 Wangu granitoid gneisses — major elements (wt.%) and CIPW norms (wt.%)

	W231	W435	W434	W235	W234	H27	W149	W229	W232	W233	H18	Sh	N331
SiO ₂	66,48	67,27	67,97	68,41	69,10	70,88	77,86	79,20	61,16	73,12	72,27	69,10	76,45
TiO ₂	0,77	0,65	0,63	0,68	0,57	0,41	0,24	0,21	0,31	0,31	0,13	0,46	0,16
Al ₂ O ₃	13,74	13,36	12,79	11,96	13,41	10,89	10,44	8,94	5,79	5,19	14,80	12,80	11,32
Fe ₂ O ₃	6,66	0,88	0,89	5,91	5,37	1,52	0,42	4,10	20,35	11,37	0,29	2,30	2,36
FeO	0,25	6,37	6,39	1,25	0,75	6,22	3,46	0,25	3,24	2,00	1,46	3,50	0,25
MnO	0,16	0,16	0,22	0,20	0,12	0,25	0,06	0,14	0,50	0,45	0,03	0,14	0,04
MgO	0,42	0,39	0,40	0,59	0,41	0,41	0,08	0,17	0,99	0,88	0,35	0,23	0,00
CaO	0,46	0,96	1,34	0,67	0,36	0,15	0,06	0,18	2,82	2,25	1,89	0,95	0,34
Na ₂ O	4,68	4,91	5,21	4,21	5,23	3,25	3,51	4,60	3,90	3,32	5,42	6,00	4,11
K ₂ O	5,75	4,23	3,11	6,38	4,75	5,09	3,77	2,08	1,18	0,60	2,63	4,78	4,47
P ₂ O ₅	0,08	0,00	0,00	0,01	0,10	0,00	0,02	0,00	0,04	0,04	0,04	0,07	0,01
LOI	0,84	0,23	0,35	0,20	0,37	0,17	0,20	0,40	0,86	0,82	0,24	0,46	0,33
Total	100,29	99,41	99,30	100,47	100,54	99,24	100,12	100,27	101,14	100,35	99,55	100,79	99,84
P.I.	1,01	0,95	0,94	1,16	1,03	0,99	0,94	1,10	1,33	1,18	0,79	1,18	1,03
Ga/Al	4,12	4,24	4,42	4,57	4,22	5,72	4,70	5,70	10,10	8,36	2,81	5,68	3,91
CIPW norms													
Qz	16,38	15,87	18,54	19,93	19,93	27,11	40,03	44,90	31,32	48,66	25,35	15,81	35,47
Co							0,51						
Or	34,08	25,16	18,53	37,52	28,00	30,27	22,24	12,28	6,92	3,54	15,63	28,12	26,51
Ab	38,78	41,82	44,45	25,87	42,42	27,67	29,65	34,36	23,05	23,34	46,11	39,04	33,46
An		1,93	2,35			0,09	0,21				8,33		
Ac	0,83			8,44	1,51			3,98	8,56	4,17		6,62	1,27
Ns												0,9	
Wo									2,89	2,03			0,66
Di	0,55	2,58	3,87	2,54	0,97	1,23		0,70	5,28	4,73		3,80	0,05
Hy	0,79	9,88	9,43	0,29	0,57	10,40	5,91	0,10			1,27	4,47	
Mt		1,22	1,30	2,70	1,15	2,22	0,61	0,65	11,10	7,01	2,52		0,47
Il	0,87	1,24	1,21	1,29	1,08	0,78	0,46	0,40	0,58	0,59	0,42		0,30
Hm	6,39			1,10	4,04			2,27	9,59	5,09	0,25	0,87	1,60
Sp	0,77												
Ap	0,19			0,02	0,23		0,05		0,09	0,09	0,09	0,16	0,02
Z	0,37	0,23	0,34	0,31	0,09	0,22	0,34	0,36	0,61	0,75	0,03	0,17	0,17
Total	100,00	100,00	100,00	100,00	100,00	100,00	100,00	100,00	100,00	100,00	100,00	100,00	100,00

W231 to W229 = Wangu granitoid gneisses, in order of increasing SiO₂

W232 and W233 = Wangu magnetite-rich granitoid gneisses

H18 = Representative Halambu gneiss (author's own data)

Sh = Aegirine granite, Shira Complex, Nigeria, from Whalen *et al.* (1987)

N331 = Aegirine granite gneiss, Ngoye (author's own data)

Major element XRF analyses of W231, W235, W234, W149, W229, W232, W233 by A. Wilson, Natal Univ. Pmb. Samples W435, W434 and H27 by M.R. Sharpe, Rocklabs, Pretoria

FeO determined by the Geological Survey, Pretoria, on all samples except W435 and W434

P.I. = Peralkaline index (mol. prop. Na₂O + K₂O/Al₂O₃)

Ga/Al = Ga × 10000/Al

LOI includes CO₂, H₂O, and other volatilesCIPW norms from H₂O-free analyses recalculated to 100%

Ilmaussaq, Greenland; Lovozero, USSR: Sorensen, 1968).

Petrographically the granitoid gneisses are seen to comprise a fine-grained (0,2 – 0,5mm) polygonal assemblage of quartz, microcline, albite, aegirine-augite, biotite, magnetite, and riebeckite (Table 1). The pervasive east-west D₂ foliation (Figure 3) is highlighted in thin section by elongate aggregates of mafic

constituents such as aegirine-augite (Figure 5). According to their modal mineralogy the Wangu granitoid gneisses are classified as alkali-feldspar granites on the QAP diagram of Streckeisen (1976) (Figure 7). This is in marked contrast to Halambu gneisses sampled by the author from north of Wangu Hill, which are classified in Figure 7 as having tonalite to granodiorite compositions (see H18, Table 1).

Table 3 Wangu granitoid gneisses — trace element contents (ppm)

	W231	W435	W434	W235	W234	H27	W149	W229	W232	W233	H18	Sh	N331
Zn	323	146	341	123	150	242	168	612	898	584	33	240	181
Ga	30	30	30	29	30	33	26	27	31	23	22	38	23
Nb	423	228	373	303	89	245	128	295	567	614	17	154	45
Zr	1836	1141	1672	1549	450	1095	1694	1795	3076	3730	155	865	831
Y	100	97	161	133	159	103	128	95	385	541	9	107	158
U	10	10	13	7	3	0	6	5	9	10	0	4	3
Th	80	38	57	109	14	42	52	47	78	115	5	25	18
Rb	205	155	176	294	145	255	104	78	49	38	67	145	153
Sr	20	163	116	9	13	22	33	4	20	29	1205	44	8
Ba	145	113	36	62	553	217	157	59	287	111	1312	375	50
La	334.7	—	—	247.2	—	208.1	—	124.1	705.8	—	—	—	119.6
Ce	570.4	—	—	459.7	—	403.2	—	275.9	421.1	—	—	—	247.1
Pr	66.1	—	—	47.6	—	40.6	—	26.9	145.4	—	—	—	27.9
Nd	232.7	—	—	169.8	—	147.8	—	100.1	603.8	—	—	—	111.3
Sm	38.4	—	—	31.0	—	25.5	—	19.9	116.9	—	—	—	27.0
Eu	3.1	—	—	2.4	—	1.3	—	1.7	21.0	—	—	—	0.7
Gd	27.0	—	—	27.2	—	21.5	—	18.5	106.4	—	—	—	26.1
Dy	26.2	—	—	30.9	—	20.5	—	23.2	93.3	—	—	—	24.6
Ho	4.9	—	—	5.8	—	4.3	—	4.5	16.3	—	—	—	4.9
Er	12.7	—	—	16.2	—	12.8	—	13.2	38.2	—	—	—	13.6
Yb	12.7	—	—	15.3	—	12.0	—	13.4	34.4	—	—	—	11.2
Lu	2.0	—	—	2.2	—	1.8	—	1.9	4.8	—	—	—	1.8

W231 to W229 = Wangu granitoid gneisses, in order of increasing SiO₂. W232 & W233 are iron-rich Wangu gneisses identified as cumulates
H18 = Representative Halambu gneiss (author's own data)

Sh = aegirine granite, shira Complex, Nigeria, from Whalen *et al.* (1987)

331 = Aegirine granite gneiss, Ngoye (author's own data)

Trace elements Zn to Ba analysed by XRF at Natal University: Pmb. and Rocklabs: Pretoria

REE by ICP at Bedford New College UK, analyst J.N. Walsh

— = not determined

Wangu mafic gneisses

The development of sheet-like bodies (up to 30 m long and 1 m thick) of biotite-rich gneiss appears to be restricted to the southern part of the peralkaline granite gneiss outcrops, within the Mvuzane River Valley (Figure 1). These well-foliated gneissose mafic rocks are

believed to have been intruded into the Wangu peralkaline gneisses and, as illustrated in Figure 4, contain abundant peralkaline granitoid gneiss xenoliths.

Thin section examination confirms the well-foliated character of these fine-grained biotite-rich rocks (Figure 6) which consist essentially of red-brown biotite laths,



Figure 2 Typical outcrops of peralkaline granitoid gneiss on Wangu Hill, looking West. Note the moderate southerly dip of the outcrop, due to well-developed D₂ foliation.



Figure 3 Polished slab of Wangu granitoid gneiss, scale in centimetres.

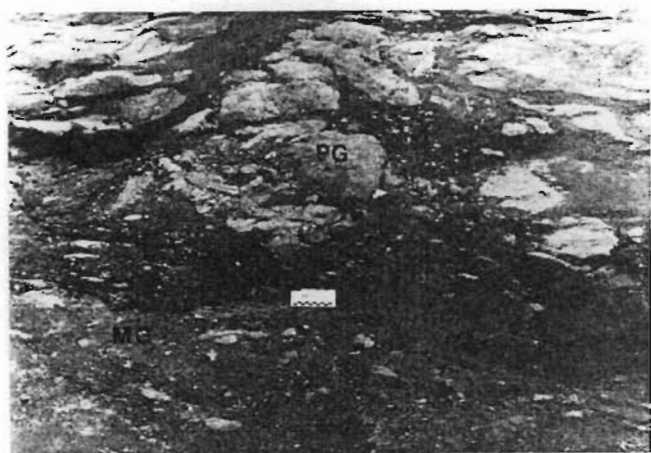


Figure 4 Contact zone between mafic biotite-rich gneiss (MG) and peralkaline granitoid gneiss (PG), showing granitoid xenoliths within the mafic gneiss sheet. Locality: Mvuzane River Valley, southwest of Wangu Hill.

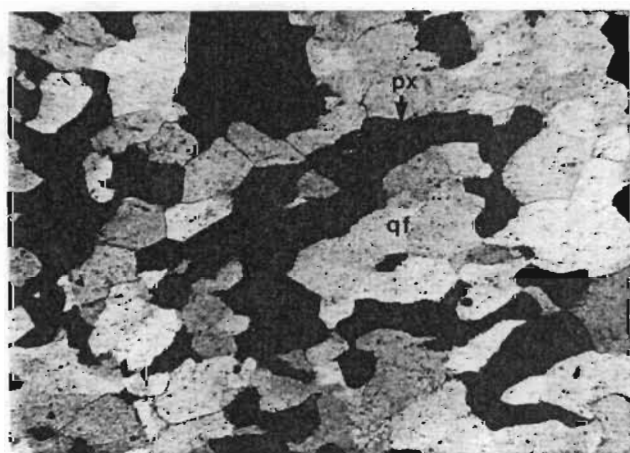


Figure 5 Photomicrograph of typical Wangu peralkaline granitoid gneiss showing fine grain size and aegirine augite (px) in polygonal quartz and feldspar matrix (qf). Field of view 3 mm, plane light.

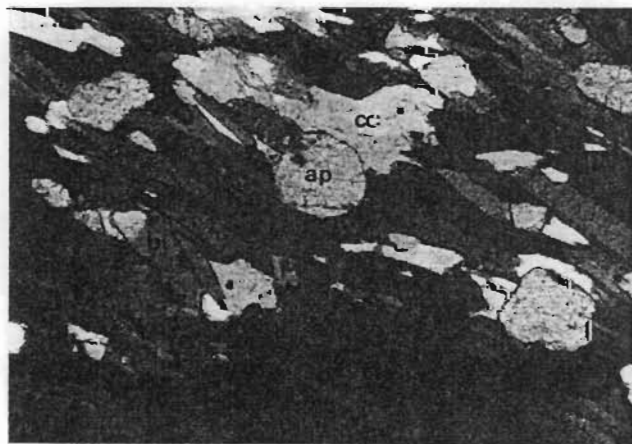


Figure 6 Photomicrograph of mafic Wangu gneiss (sample W228) showing prominent foliation. Mineral constituents include dark laths of biotite (bi), rounded grains of apatite (ap), and irregular aggregates of calcite (cc). Field of view 3 mm, plane light.

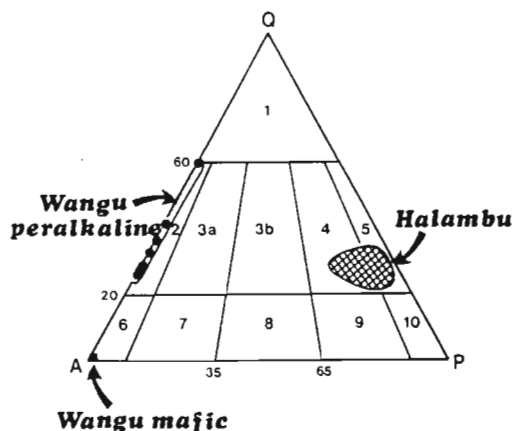


Figure 7 Classification of the Wangu granitoid gneisses (solid circles), Halambu granodioritic gneisses (cross-hatched field) and Wangu mafic gneisses (solid square) on the Streckeisen (1976) QAP diagram. The fields are numbered as follows: 2, alkali-feldspar granite; 3a & 3b, granite; 4, granodiorite; 5, tonalite; 6, alkali-feldspar syenite.

albite, microcline, irregular aggregates of calcite, and rounded apatite grains (Table 1). Although mafic rocks, as a result of the sole felsic constituent being alkali feldspar, they are classified on the QAP diagram as alkali-feldspar syenite (Figure 7).

Geochemistry

Whole-rock major and trace element geochemical data and CIPW norms for ten granitoid and three biotite-rich mafic gneisses from Wangu Hill are presented in Tables 2, 3, 4, and 5. Five samples of Halambu granodiorite gneiss from north of Wangu Hill were also analysed for comparative purposes: representative sample H18 presented in Tables 2 and 3 is considered to be a typical example of this lithology as described by Charlesworth (1981).

Samples W435, W434, H27 and H18 were analysed for major and trace elements by M.R. Sharpe of Rocklabs, Pretoria: samples W231, W235, W234, W149, W229, W232, W233 and N331 were analysed for major and trace elements by A. Wilson of Natal University, Pietermaritzburg. All major elements, excepting Na, were analysed using fused discs prepared after the method described by Norrish & Hutton (1969). Pressed powder briquettes were analysed for Na and trace elements by XRF techniques. Samples W231, W235, H27, W229, W232, W228, W227 and N331 were analysed for REE using ICP, by J.N. Walsh at Bedford New College, UK. CO_2 was determined by Infrared Spectroscopy, and FeO by Redox Titration at the Geological Survey in Pretoria.

Wangu granitoid gneisses

Broad geochemical characteristics of the Wangu granitoid gneisses are summarized below. In addition, comparisons have been drawn with the Halambu granodiorite gneisses to the north of Wangu Hill:

1. the Wangu granitoid gneisses are enriched in Fe_2O_3 , FeO, MnO, and K_2O relative to the Halambu

Table 4 Wangu biotite dykes — major elements (wt%) and CIPW norms (wt%)

	W228	W436	W227	KN	ML
SiO ₂	39,23	47,04	51,24	41,30	50,20
TiO ₂	3,84	3,50	1,19	4,18	0,66
Al ₂ O ₃	12,25	13,46	12,75	12,47	10,30
Fe ₂ O ₃	1,71	1,66	1,33	15,26	3,90
FeO	12,07	11,95	5,57	1,80	
MnO	0,51	0,26	0,35	0,22	0,10
MgO	9,96	5,39	5,54	5,84	10,70
CaO	6,83	5,71	7,42	8,13	5,09
Na ₂ O	1,55	2,75	3,82	6,74	1,25
K ₂ O	7,14	4,17	5,22	2,67	7,77
P ₂ O ₅	1,24	0,70	0,97	1,14	1,14
H ₂ O	0,71	2,48	1,21	2,00	2,68
CO ₂	2,44	—	3,29	—	2,80
Total	99,48	99,07	99,90	99,95	98,39
CIPW norms					
Or	14,11	25,49	31,19	16,07	47,82
Ab		20,61	31,57	11,93	10,12
An	5,44	12,48	2,25		
Ac				6,96	0,78
Lc	22,39				
Ne	7,18	1,87	0,60	20,73	
Di	4,41	10,35	6,74	15,91	1,11
Hy					17,21
Ol	28,01	18,13	13,50	5,21	7,03
Mt	2,51	2,49	1,95		4,39
Hm				13,14	0,76
Il	7,37	6,88	2,29	0,48	1,31
Pf				6,82	
Ap	2,91	1,68	2,27	2,69	2,75
Cc	5,61	—	7,57		6,63
Z	0,06	0,03	0,06	0,06	0,09
Total	100,00	100,00	100,00	100,00	100,00

W228, W436, W227 = Wangu biotite-rich dykes, in order of increasing SiO₂

KN = Karoo nephelinite. NTS12: from Bristow (1984)

ML = Mica-rich lamprophyre, Keewatin, Canada: from Le Cheminant *et al.* (1987)

Major element XRF analyses of W228 and W227 by A. Wilson, Natal Univ., Pmb. Sample W436 analysed by M.R. Sharpe, Rocklabs, Pretoria

FeO and CO₂ determinations (W228 and W227) by the Geological Survey of South Africa, Pretoria

H₂O = LOI (loss on ignition) - CO₂. CIPW norms from H₂O-free analyses recalculated to 100%

— = not determined

Table 5 Wangu biotite dykes — trace element contents (ppm)

	W228	W436	W227	KN	ML
Zn	771	343	451	137	—
Ga	40	25	24	—	—
Nb	390	45	159	187	9
Zr	273	157	312	271	416
Y	86	34	114	23	31
U	9	1	5	—	3
Th	17	2	45	—	21
Rb	635	393	471	63	205
Sr	341	495	1445	1663	1321
Ba	1325	969	1459	1713	4180
La	146,8	—	212,9	—	153
Ce	278,2	—	436,2	—	304
Pr	30,9	—	49,1	—	—
Nd	124,6	—	192,2	—	127
Sm	21,9	—	29,9	—	22,71
Eu	5,3	—	5,8	—	4,91
Gd	18,3	—	20,7	—	—
Dy	15,4	—	16,5	—	—
Ho	2,8	—	3,2	—	0,51
Er	7,3	—	9,1	—	—
Yb	6,5	—	9,4	—	1,51
Lu	0,9	—	1,5	—	0,41

W228, W436, W227 = Wangu biotite dykes

KN = Karoo nephelinite, NTS12: from Bristow (1984)

ML = Mica-rich lamprophyre, Keewatin, Canada: from Le Cheminant *et al.* (1987)

Trace elements Zn to Ba analysed by XRF at Natal University (Samples W228 & W227) and Rocklabs, Pretoria (Sample W436)

REE by ICP at Bedford New College UK, analyst J.N. Walsh

— = not determined

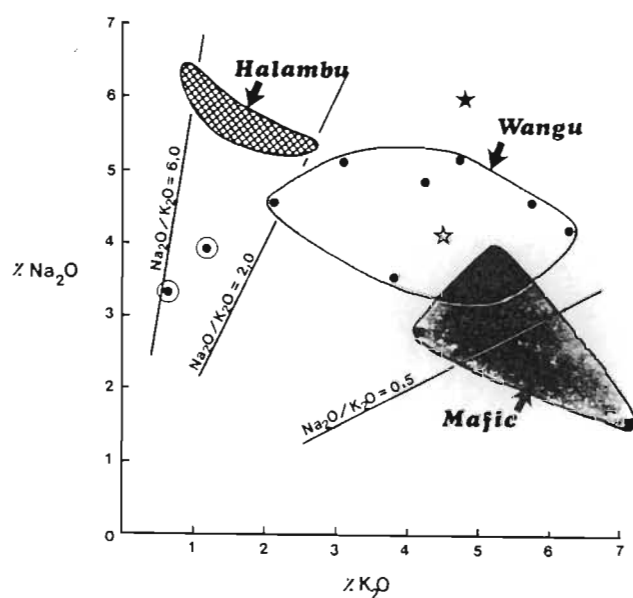


Figure 8 Discrimination of the various Wangu gneisses according to Na₂O:K₂O ratios. Solid circles in lightly stippled field = Wangu peralkaline gneisses; solid squares in heavily stippled field = Wangu mafic gneisses; open circle with dot = Wangu iron-rich cumulates; cross-hatched field = Halambu gneisses; open star = Ngoye peralkaline granite gneiss; solid star = Nigerian aegirine granite.

gneisses. Samples W232 and W233, which are possible cumulate phases, are noted to have exceptionally high contents of Fe₂O₃ (total), at 24,70 and 13,59% respectively;

2. ratios of Fe₂O₃:FeO are highest within the aegirine and riebeckite granitoid gneisses, reflecting the high

- oxidation state of these sodic minerals;
- as shown in Figure 8, the Wangu gneisses have low $\text{Na}_2\text{O}:\text{K}_2\text{O}$ ratios (*ca.* 0,5 – 2) which is similar to the representative peralkaline Nigerian and Ngoye samples, whereas the Halambu gneisses are characterized by high $\text{Na}_2\text{O}:\text{K}_2\text{O}$ ratios (*ca.* 2 – 6). Two exceptions are the iron-rich cumulate rocks W232 and W233 which have low total alkalis and relatively high $\text{Na}_2\text{O}:\text{K}_2\text{O}$ ratios (Figure 8);
 - Al_2O_3 contents within the Wangu gneisses are low (*ca.* 9 – 13%), compared with the Halambu gneisses which contain between about 14 and 16% Al_2O_3 . Samples W232 and W233 are highly depleted in Al_2O_3 (*ca.* 5 – 6%) which reflects low modal feldspar contents and the lack of aluminous mafic minerals (Table 1);
 - the Wangu gneisses are characterized by a wide range of SiO_2 contents (*ca.* 61 – 79%), while the Halambu granodioritic gneisses are restricted to a narrow range of between about 70 and 74% SiO_2 ;
 - the Wangu granitoid gneisses generally contain normative acmite, reflecting low alumina relative to alkali contents and which is similar to the aegirine granite and granite gneiss norms from Nigeria and Ngoye presented in Table 2;
 - marked enrichment in incompatible and large-ion lithophilic elements such as Zn, Nb, Zr, Th, Y, and Rb is common to all the Wangu granitoid gneisses, relative to the representative Halambu granodiorite gneiss. As shown in Table 3, the Wangu gneisses contain similar amounts of these elements to a typical aegirine granite from a Nigerian central complex. Of potential economic interest are the high concentrations of Nb (614 ppm), Y (541 ppm) and REE (2300 ppm) in W232 and W233, although due to the lack of discrete REE minerals in these rocks, it is suggested that these incompatible elements are hosted by sodic minerals such as aegirine augite.
 - the Wangu gneisses contain much lower amounts of Sr and Ba than the Halambu granodioritic gneisses;
 - ratios of $\text{Ga} \times 10000:\text{Al}$ within the Wangu gneisses are high (*ca.* 4–10) when compared with the Halambu gneisses (*ca.* 2 – 3); and
 - REE chondrite-normalized ratios for samples W231, W235, H27 W229, and W232 are presented in Figure 9. Apart from W232 the Wangu samples display LREE-enriched patterns ($\text{La}/\text{Yb} = 6,18 - 17,64$) with significant negative Eu anomalies ($\text{Eu}/\text{Eu}^* = 0,16 - 0,28$). A representative peralkaline granite gneiss from the Ngoye complex has been plotted for comparison in Figure 9 ($\text{La}/\text{Yb} = 7,11$ and $\text{Eu}/\text{Eu}^* = 0,08$). The unusual pattern exhibited by W232 may be due to the probable cumulate origin of this aegirine- and magnetite-rich rock. Furthermore, in keeping with its high $\text{Fe}_2\text{O}_3/\text{FeO}$ ratio (Table 2) the negative Ce anomaly may be related to formation under highly oxidizing conditions (Cullers & Graf, 1984).

Wangu mafic gneisses

Geochemical data and CIPW norms for the three samples analysed are presented in Tables 4 and 5.

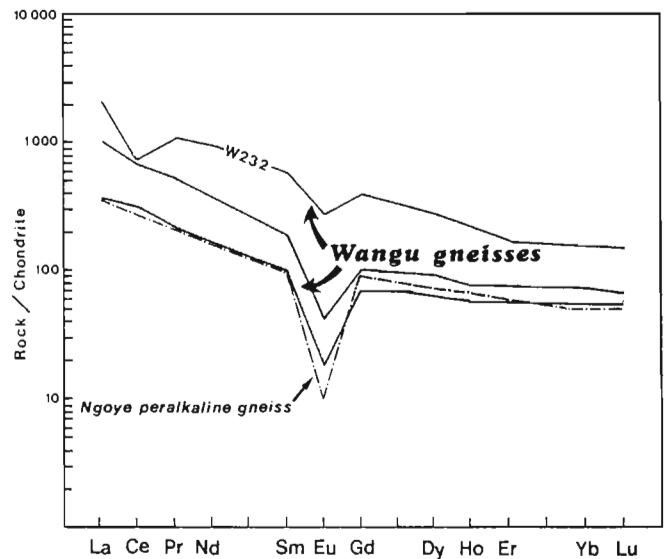


Figure 9 Chondrite-normalized REE patterns illustrating the typical peralkaline trend of the Wangu granitoid gneisses (stippled field). W232 is a magnetite- and aegirine augite-rich cumulate phase with both Ce and Eu anomalies. The Ngoye sample has been included for comparison. Chondrite values from Nakamura (1974).

Although this is a limited data base, the following major and trace element characteristics are apparent:

- SiO_2 contents are much lower than in the peralkaline granite gneisses (*ca.* 40 – 50%);
- total alkalis (7 – 9%) are high for the relatively low silica contents in these samples, and are similar to the levels reported in alkaline igneous rocks such as the Karoo nephelinite and Canadian lamprophyre given in Table 4. The Wangu mafic gneisses are potassic rocks, with low $\text{Na}_2\text{O}:\text{K}_2\text{O}$ ratios of less than 0,7 (Figure 8);
- the CIPW norms are characterized by the presence of nepheline, leucite and olivine, a reflection of the

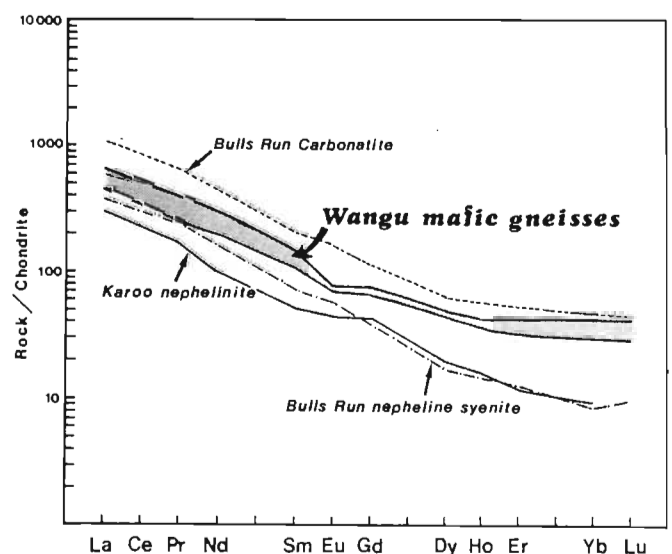


Figure 10 Chondrite-normalized REE patterns illustrating the LREE-enriched nature of the Wangu mafic gneisses (stippled field). Data from the nearby Bull's Run alkaline gneisses, as well as a Karoo nephelinite, are included for comparison. Chondrite values from Nakamura (1974).

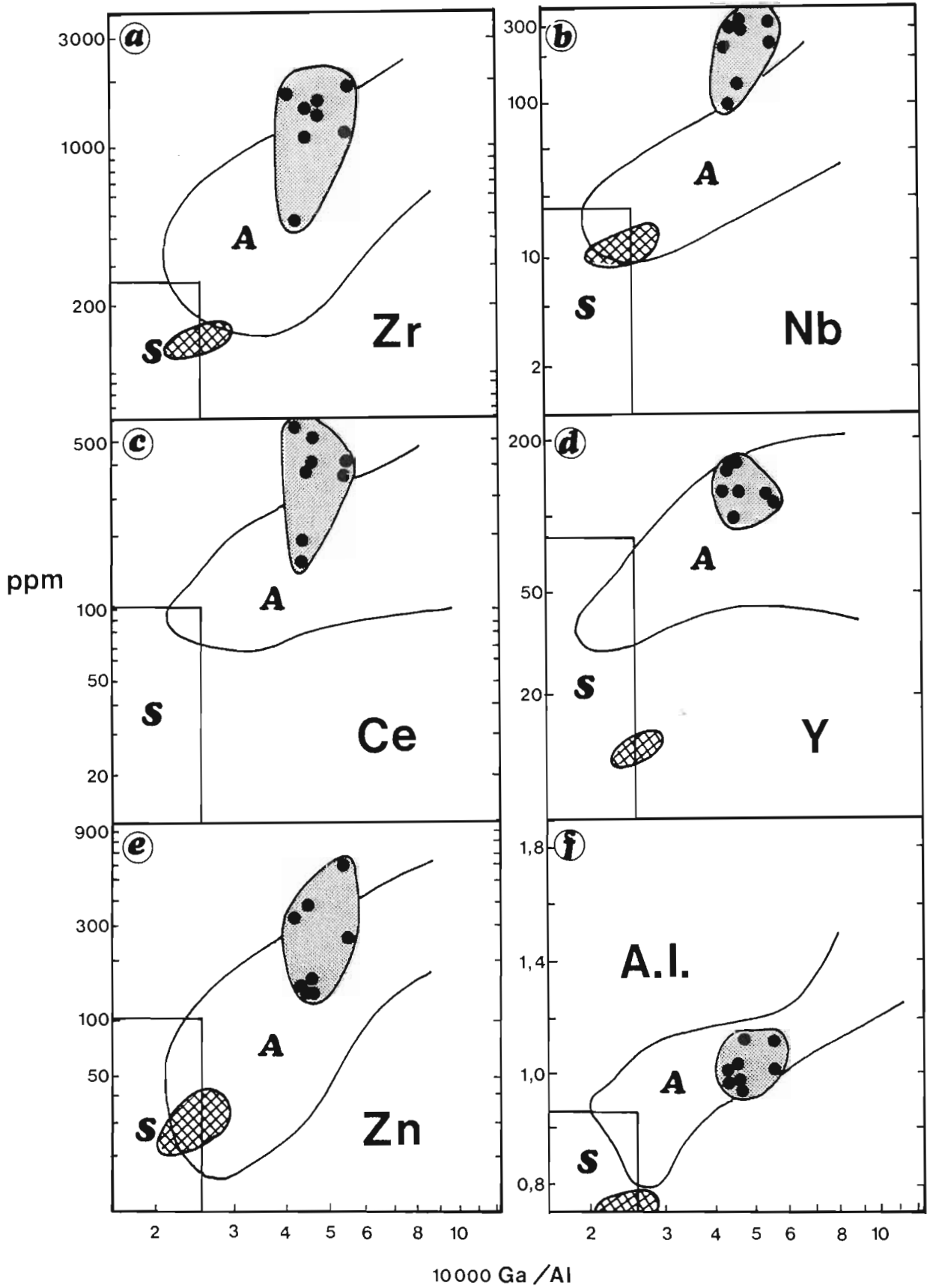


Figure 14 Comparison of trace element and Ga:Al ratios for Wangu gneisses, with S- and A-type granite fields from Whalen *et al.* (1987). S-type compositions characterize the rectangular field designated S, while A- types plot predominantly within the field marked A, as derived from Whalen *et al.* 1987. The Mvuzane samples are shown as solid circles within the stippled fields. The Halambu granodiorite gneisses (cross-hatched fields) have been plotted for comparison.

(1980) and the normative classification of Streckeisen & Le Maitre (1979), respectively. The Halambu granodiorite / tonalite gneiss field is shown for

comparison in both Figures 12 and 13, where a distinct difference in composition is apparent between the Halambu and Wangu gneisses. It is noted that the

nomenclature derived from the Streckeisen (1976) modal QAP ternary diagram of Figure 7 is virtually identical to that based on the normative classification of Figure 13.

Granites have been classified by various authors into three major genetic groups, namely I-, S- and A-types according to parameters such as tectonic setting, derivation from various precursors, mineralogy, and geochemistry. Chappell & White (1974) proposed a partial-melting model for granites of orogenic belts, with derivation from igneous (I-type) or sedimentary (S-type) precursors. Thus I-type granites are defined as hornblende-bearing, metaluminous rocks with high $\text{Na}_2\text{O}/\text{K}_2\text{O}$ ratios, whereas S-type granites are characterized by peraluminous chemistry, low $\text{Na}_2\text{O}/\text{K}_2\text{O}$ ratios and the occurrence of aluminous minerals like muscovite. Loiselle & Wones (1979) extended the I & S concept to embrace what they proposed should be termed A-type granites, with the 'A' prefix derived from features considered common to this group such as Alkaline, Anorogenic, Anhydrous and After (in that they normally succeed I- and S- type plutonism).

Whalen *et al.* (1987) summarized the characteristics of A-type granites, noting that good discrimination can be obtained between A-types and I- and S-type granites on plots using Ga/Al ratios versus, for example, Zr, Nb, Ce, Y, and Zn contents, as well as the peralkalinity index. The Wangu gneisses, as illustrated in Figure 14, coincide with the A-type fields derived by Whalen *et al.* (1987), whereas the Halambu gneisses plot within the area of overlap between S-type and A-type granites.

Pearce *et al.* (1984) showed that undeformed Phanerozoic within-plate (WPG) or A-type granitic rocks can be distinguished from collision-related (COLG) and volcanic-arc (VAG) granites by using a binary plot of Rb v $\text{Y}+\text{Nb}$. When the Wangu granitoid gneisses are plotted on this diagram they fall well within the WPG field due to enhanced contents of $\text{Y}+\text{Nb}$

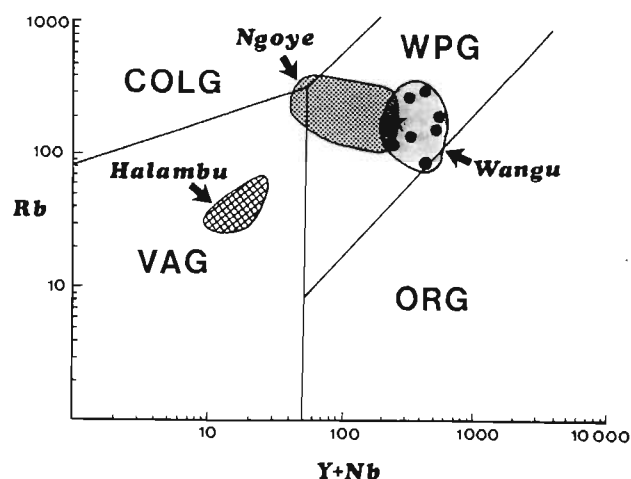


Figure 15 Tectonic discrimination plot of Rb against $\text{Y}+\text{Nb}$ for the Wangu granitoid gneisses (solid circles), based on Pearce *et al.* (1984). Fields of peralkaline Ngoye gneisses (coarse stipple) and Halambu granodioritic gneisses (cross-hatched) are included for comparison, as is a typical aegirine granite from Nigeria (solid star).

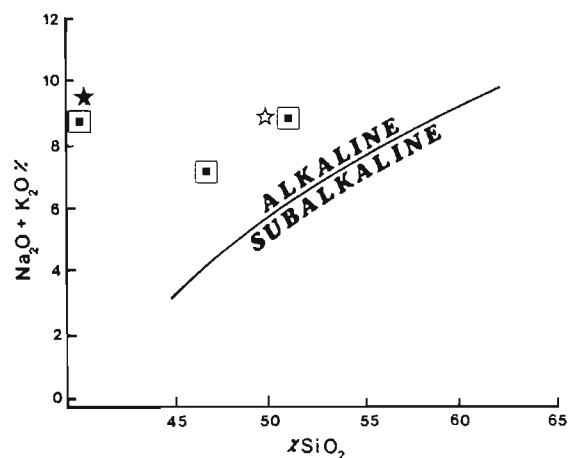


Figure 16 Total alkalis v. silica plot to show the alkaline character of the mafic Wangu gneisses (solid squares in boxes). The division into alkaline and subalkaline fields is after Kuno (1966). For comparison a Karoo nephelinite (solid star) and Canadian mica lamprophyre (open star) are plotted, data from Table 4.

relative to Rb, rather similar to the representative aegirine granite from the Nigerian Shira Complex (Figure 15). The field of peralkaline granite gneisses from the Ngoye granite gneiss massif has been included in Figure 15 and also shows a WPG signature. The Halambu granodioritic gneisses have been plotted for comparison in Figure 15 and are suggested to have a VAG signature.

Wangu mafic gneisses

These have been classified using major elements and REE data. Thus, on the R1-R2 diagram (Figure 12) the three samples analysed are classified as having an essexite (or tephrite) composition, which is essentially a consequence of their high alkali contents relative to silica, as shown by their position within the alkaline field of Kuno (1966) in Figure 16.

The Streckeisen & Le Maitre normative classification scheme has been used to classify sample W227, which as shown in Figure 13, plots just below Field 7, and may therefore be classified as a 'foid-bearing syenite'. Due to a lack of CO_2 data for W436 (resulting in the normative allocation of Ca from calcite to anorthite) this sample has not been plotted in Figure 13. Sample W228 has abnormally high normative leucite and hence no normative orthoclase, as a result of its high biotite content and is therefore unable to be plotted in Figure 13.

REE chondrite-normalized data for samples W227 & W228 are given in Figure 10, and display the LREE-enriched trend, with only minor Eu depletion, typical of alkaline rocks. REE-normalized values for nepheline syenite and carbonatitic gneisses from the Bull's Run area (Scogings, own data) and a Karoo nephelinite (Duncan *et al.*, 1984) have been included as examples of alkaline igneous rocks for comparison.

Discussion

The Wangu granitoid gneisses have many of the

petrographic and geochemical characteristics of peralkaline granites. On the basis of field evidence, geochemistry, and by comparison with similar Hercynian felsic gneisses described by Seyler (1986), it is suggested that the Wangu gneisses represent deformed A-type peralkaline microgranitic or aplitic rocks. Although alkali depletion may have occurred during deformation, the presence of modal aegirine-augite, normative acmite, in addition to high concentrations of Zn, Zr, and Nb are considered diagnostic of peralkaline parentage. Localized iron-rich highly peralkaline siliceous gneisses with enhanced REE, Zr, Nb, and Zn contents are interpreted as magmatically concentrated cumulate layers within the Wangu gneisses.

It is also suggested that the intrusive biotite-rich gneisses represent deformed volatile-rich alkaline mafic rocks. A genetic relationship is indicated between the peralkaline gneisses and mafic sheets on the basis of their alkaline character, as well as spatial association.

Peralkalinity is a condition typical of granites and rhyolites of oceanic islands and intra-cratonic rift environments, and has recently been recognized in post-collisional plate tectonic settings (Bowden, 1974; Sylvester, 1989; Whalen *et al.*, 1987). This suggests that the Wangu gneisses have particular significance with respect to the interpretation of the tectonic setting of the NSMP at the time of intrusion of the Wangu gneiss precursors. Therefore, it is necessary to consider them in association with other alkaline/peralkaline gneisses recently described from the northern margin of the NSMP. As proposed by Scogings (1985, 1986) the Ngoye Granite Gneiss Formation (Figure 1 for locality) probably represents a tectonically deformed A-type granite central complex, very similar to the Nigerian 'younger granite' central complexes. Furthermore, the Bull's Run Syenite Gneiss Formation (see Figure 1) has been demonstrated to be lithologically complex, comprising a range of nepheline syenite gneisses with minor carbonatite and peralkaline dyke phases (Scogings & Forster, 1989), suggesting that the Bull's Run Formation represents a deformed syenite-carbonatite central complex.

Following from the above, it is proposed that the Wangu, Ngoye, and Bull's Run alkaline/peralkaline gneiss occurrences constitute the remnants of a metamorphosed alkaline magmatic province, near the northern margin of the NSMP. This is in marked contrast to the calc-alkaline character suggested previously for the Halambu Formation by Charlesworth (1981).

Acknowledgements

Permission by the South African Development Corporation Ltd. (STK) to use data from the Mvuzane Rare Elements Project is gratefully acknowledged, as is the assistance given to the author by the Geology Department at the University of Durban-Westville. The Geological Survey is thanked for helping with FeO and CO₂ data.

References

- Bowden, P. (1974). Oversaturated alkaline rocks : granites, pantellerites and comendites, 109–123. In: Sorensen, H., (Ed.), *The Alkaline Rocks*, Wiley Interscience, New York, 622 pp.
- Bristow, J.W. (1984). Nephelinites of the North Lebombo and South-East Zimbabwe, 87–104. In: Erlank, A.J., (Ed.), *Petrogenesis of the Volcanic Rocks of the Karoo Province*. Spec. Publ. geol. Soc. S. Afr., **13**, 395 pp.
- Chappell, B.W. & White, A.J.R. (1974). Two contrasting granite types. *Pacific Geol.*, **8**, 173–174.
- Charlesworth, E.G. (1981). *Tectonics and metamorphism of the northern Margin of the Namaqua Natal Mobile Belt near Eshowe, Natal*. Ph.D. thesis (unpubl.), Univ. Natal, Durban, 433pp.
- Cullers, R.L. & Graf, J.L. (1984). Rare earth elements in igneous rocks of the continental crust: predominantly basic and ultrabasic rocks, 237–274. In: Henderson, P., (Ed.), *Rare Earth Element Geochemistry*. Elsevier, Amsterdam, 515 pp.
- De la Roche, H., Leterrier, J., Grandclaude, P. & Marchal, M. (1980). A classification of volcanic and plutonic rocks using the R1-R2 diagram and major element analyses — its relationship with current nomenclature. *Chem. Geol.*, **29**, 183–210.
- Duncan, A.R., Erlank, A.J. & Marsh, J.S. (1984). Regional geochemistry of the Karoo Province, 355–388. In: Erlank, A.J., (Ed.), *Petrogenesis of the Volcanic Rocks of the Karoo Province*. Spec. Publ. geol. Soc. S. Afr., **13**, 395 pp.
- Du Toit, A.L. (1931). *The geology of the country surrounding Nkandla, Natal*. Expl. sheet 109, Geol. Surv. S. Afr., 111 pp.
- Kuno, H. (1966). Lateral variation of basalt magma type across continental margins and island arcs. *Bull. Vulcanol.*, **29**, 195–222.
- Le Cheminant, A.N., Miller, A.R. & Le Cheminant, G.M. (1987). Early Proterozoic alkaline igneous rocks, District of Keewatin, Canada: petrogenesis and mineralization, 219–240. In: Pharaoh, T.C., *et al.*, (Eds.), *Geochemistry and Mineralization of Proterozoic Volcanic Suites*. Spec. Publ. geol. Soc. Lond., **33**, 577 pp.
- Loiselle, M.C. & Wones, D.R. (1979). *Characteristics and origin of anorogenic granites*. Abstr. Prog. geol. Soc. Amer., **11**, 468.
- Matthews, P.E. & Charlesworth, E.G. (compilers) (1981). *Northern Margin of the Namaqua-Natal Mobile Belt in Natal*. 1:140 000 scale geological map, Colorgraphic, Durban. 1 sheet.
- Nakamura, N. (1974). Determination of REE, Ba, Fe, Mg, Na and K in carbonaceous and ordinary chondrites. *Geochim. Cosmochim. Acta*, **38**, 757–775.
- Norrish, K. & Hutton, J.T. (1969). An accurate x-ray spectrographic method for the analysis of a wide range of geological samples. *Geochim. Cosmochim. Acta*, **33**, 431–453.
- Pearce, J.A., Harris, N.B.W. & Tindle, A.G. (1984). Trace element discrimination diagrams for the tectonic interpretation of granitic rocks. *J. Petrol.*, **25**, 956–983.

- Scogings, A.J. (1985). *The geology of the Ngoye Granite Gneiss Formation*. M.Sc. thesis (unpubl.), Univ. Durban-Westville, Durban, 186pp.
- (1986). Peralkaline gneissic granites in the Ngoye Granite-Gneiss Formation, Natal. *Trans. geol. Soc. S. Afr.*, **89**, 361–365.
- (1988a). *Geochemistry of the Mvuzane granitoids, Kwa Zulu*. STK int. rep. 2495. (STK data bank, Pretoria).
- (1988b). *Geochemistry of the Wangu anomaly, Mvuzane rare elements project, Kwa Zulu*. STK int. rep. 2554 (STK data bank, Pretoria).
- & Forster, I.F. (1989). Gneissose carbonatites in The Bulls Run Complex, Natal. *S. Afr. J. Geol.*, **92**(1), 1–10.
- Seyler, M. (1986). Petrology and genesis of Hercynian alkaline orthogneisses from Provence, France. *J. Petrol.*, **27**(5), 1229–1251.
- Shand, S.J. (1947). *The Eruptive Rocks*, 228–230. Thomas Murby & Co., London. 488pp.
- Sorensen, H. (1968). Rhythmic igneous layering in peralkaline intrusions. *Lithos*, **2**, 261–283.
- Streckeisen, A. (1976). To each plutonic its proper name. *Earth Sci. Rev.*, **12**, 1–33.
- & Le Maitre, R.W. (1979). A chemical approximation to the modal QAPF classification of the igneous rocks. *N. Jb. Miner. Abh.*, **136**, 169–206.
- Sylvester, P.J. (1989). Post-collisional alkaline granites. *J. Geol.*, **97**, 261–280.
- Whalen, J.B., Currie, L.C. & Chappell, B.W. (1987). A-type granites: geochemical characteristics, discrimination and petrogenesis. *Contr. Miner. Petrol.*, **95**, 407–419.
- Wright, J.B. (1969). A simple alkalinity ratio and its application to questions of non-orogenic granite genesis. *Geol. Mag.*, **106**, 370–384.

1. PROPOSER OF NAME

McCarthy (1961) proposed the name "Ngoye Granite Gneiss."

2. DERIVATION OF NAME

Ngoye Hills southwest of Empangeni, Natal (Fig. 1), which largely consist of rocks of the Ngoye Complex.

3. TYPE AREA

Terrain between Ngoye Forest Reserve and Mhlatuze River (Fig. 1).

4. STRATIGRAPHIC POSITION AND AGE

Situated within the Nkomo Nappe (Tugela Group) near the northern margin of the Natal Structural and Metamorphic Province (Charlesworth, 1981). Dated by Barton (1983) at 1067 ± 20 Ma (Rb-Sr whole-rock isochron).

5. GEOLOGIC DESCRIPTION

Basic concept and unifying features: Geochemically related alkaline to peralkaline A-type granitoid gneisses, with minor monzodioritic and syenitic gneiss phases.

Form and size of intrusion: Prominent easterly-trending whaleback massif 30 km in length and up to 4 km wide, rising to 300 m above the surrounding terrane. A smaller 3-km-long satellite body is poorly exposed around Ninians, northeast of the main massif (Fig. 1). Apophyses of microgranite gneiss extend into the country rocks along the southern margin of the main massif.

Lithology: Three broad varieties of granitoid gneiss are recognized, on the basis of alumina saturation relative to alkalis (for distribution see Fig. 1).

Metaluminous gneisses (65%): Can be mineralogically subdivided into three types: (i) *Biotite granite gneiss*. Grey to pinkish, with pink microcline megacrysts (25–36%) set in a matrix of quartz (23–33%), plagioclase (26–34%) and biotite (4–7%). Accessory phases include hastingsite, epidote, sphene and allanite. (ii) *Biotite-hornblende granite gneiss*. Light pinkish; medium-grained; comprises quartz (23–35%), microcline (30–40%), plagioclase (20–30%), hornblende (3–8%) and biotite ($\leq 4\%$). Sphene and opaques are common accessory minerals. (iii) *Hornblende monzodiorite gneiss*. Coarse-grained; white with black hornblende aggregates; comprises plagioclase (60–70%), microcline (10–20%), hornblende (4–8%), and calcite ($< 5\%$). Accessory constituents include quartz, diopside,

garnet, sphene, allanite and apatite.

Peraluminous gneiss (20%): Consists essentially of *muscovite-biotite granite gneiss*: Light pinkish to white; fine- to medium-grained; well foliated; comprises quartz (30–39%), microcline (25–35%), albite (25–35%), biotite ($\leq 5\%$), muscovite ($\leq 4\%$), and accessory garnet, opaques and fluorite.

Peralkaline gneisses (15%): Two types have been recognized:

- (i) *Riebeckite granite gneiss*. Medium-grained; white; prominent foliation defined by blue-black riebeckite crystals or aggregates of biotite, riebeckite and aegirine. Composed of quartz (30–40%), microcline (30%), albite (25–35%), riebeckite ($\leq 6\%$), biotite ($\leq 4\%$) and aegirine ($\leq 5\%$). Common accessories include fluorite and zircon.
- (ii) *Magnetite microgranite gneiss*. Fine-grained; light pink; consists of microcline (45–55%), albite (10%), quartz (35–40%), with magnetite ($< 5\%$) as the diagnostic mafic phase. Zircon and fluorite are present in trace amounts. Minor variants within the microgranite gneiss include coarse-grained lenses rich in quartz, magnetite, zircon, sphene and fergusonite, in addition to *syenitic gneisses* consisting mainly of microcline (60–70%), albite (20–25%), quartz ($< 5\%$) and chlorite (5–10%).

Geochemistry: The Ngoye granitoid gneisses display a wide range of SiO_2 contents (65–77%) and are generally very depleted in Al_2O_3 , MgO, CaO, Ba and Sr, but enriched in Na_2O , K_2O , Zr, Zn, Nb and REE relative to average granites (Scogings, 1985; 1986). Although subeconomic, the quartz-magnetite lenses within the magnetite granite gneiss unit contain significant amounts of Zr (0.3–5%), Nb (0.18–1.3%), Sn ($\leq 0.2\%$), Y (0.02–0.48%), Zn (0.02–0.23%), U (0.01–0.1%), Th (0.01–0.3%) and REE (0.1–1.12%).

Genesis: The Ngoye gneisses have many of the mineralogical and chemical characteristics typical of A-type late stage "granite central complexes" according to the parameters suggested by Whalen *et al.* (1987). Comparison of the Ngoye Complex with the "younger granite" complexes of Nigeria, Saudi Arabia and the Sudan reveals marked similarities with regard to rock types, size of complex, geochemistry and economically important elements (Scogings, 1985). By analogy, therefore, it probably represents a metamorphosed and structurally deformed granite central complex.

Other aspects: The Ngoye Complex has a pervasive east-striking planar structural fabric, with steep southerly dips along its southern margins and moderate to steep northerly dips along the northern flanks of the massif.

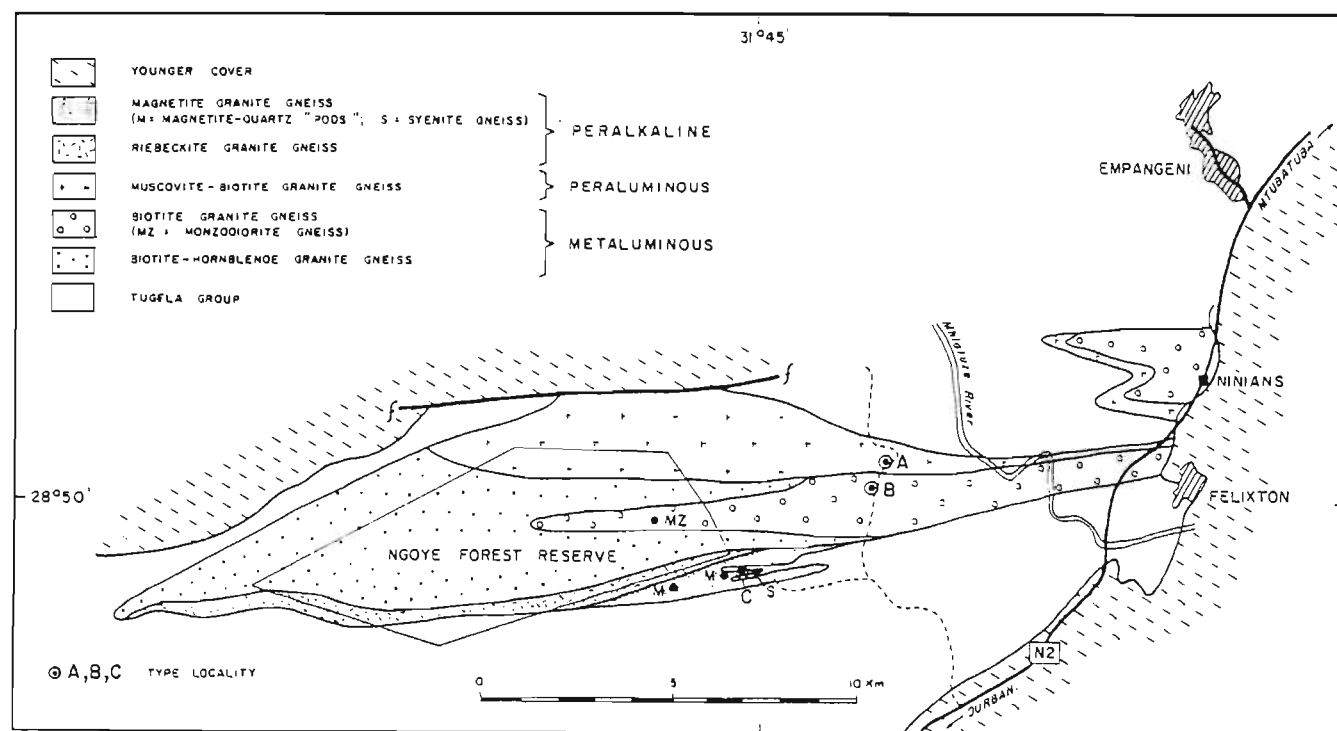


Fig. 1. Distribution of the Ngoye Complex and its constituent rock types.

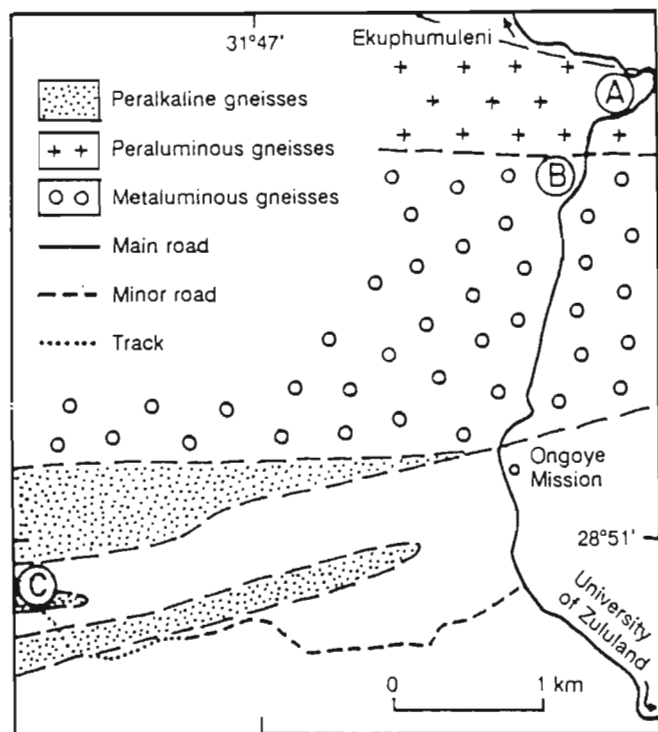


Fig. 2. Type localities (A, B, C) of the Ngoye Complex.

6. BOUNDARIES

Contacts of the Ngoye Complex with the surrounding amphibolites are sharp, discordant and frequently mylonitized. Internal contacts are generally sharp and suggested to be intrusive, although the well developed structural fabric tends to mask age relationships (Scogings, 1985).

7. HISTORICAL BACKGROUND

The name Ngoye Granite Gneiss was proposed by McCarthy (1961). Charlesworth (1981) further defined the extent and composition of granitic rocks in the Ngoye Hills and introduced the term Ngoye Granite Gneiss Formation (cf. SACS, 1980). The variation of alkaline/peralkaline granitoid gneisses within the unit was first recognized by Scogings (1985; 1986). The use of the term "complex" is in accordance with nomenclature used to describe similar alkaline/peralkaline granite central complexes (e.g. Nigeria; Bowden *et al.*, 1987), although some of the referees favoured calling the unit a "suite".

8. SUBDIVISION

No subdivision into named rock units is envisaged.

9. REGIONAL ASPECTS

Geographic distribution: See Figure 1.

Lateral variation: As noted above and in Figure 1.

Correlation: Similar, though more peralkaline, granitoid gneisses have been described by Scogings (1989) from the Wangu area, some 40 km west of the Ngoye Complex. Alkaline and peralkaline syenitic and carbonatitic gneisses have also been recorded from the Bull's Run area, 30 km west of Ngoye (Scogings and Forster, 1989). It has been suggested that these three occurrences are the remnants of a metamorphosed "alkaline province" (Scogings, 1989).

10. STRATOTYPES

A composite type locality has been defined that shows typical examples of the three major granitoid gneiss varieties at component type localities A (peralkaline gneisses), B (metaluminous gneisses) and C (peralkaline gneiss) (Figs 1 and 2). Type locality A comprises natural outcrops on northern side of road, type locality B consists of a road cutting and small quarry west of road, and type locality C (which can only be reached using a light truck or four-wheel-drive vehicle) displays natural outcrops near the access track.

11. LITERATURE REFERENCES

- BARTON, E.S., 1983. The geochronology of the frontal zones of the Namaqua-Natal Mobile Belt: Ph.D. thesis, Univ. Witwatersrand, Johannesburg (unpubl.).
- BOWDEN, P., BLACK, R., MARTIN, R.F., IKE, E.C., KINNAIRD, J.A., and BATCHELOR, R.A., 1987. Niger-Nigerian alkaline ring complexes: a classic example of African Phanerozoic anorogenic mid-plate magmatism, in *Alkaline Igneous Rocks* (J.G. Fitton and B.J.G. Upton, eds.): Geol. Soc. Lond. Spec. Publ. 30, p. 357-380.
- CHARLESWORTH, E.G., 1981. Tectonics and metamorphism of the northern margin of the Namaqua Natal Mobile Belt in Natal: Ph.D. thesis, Univ. Natal, Durban (unpubl.).
- McCARTHY, M.J., 1961. The geology of the Empangeni fault area: M.Sc. thesis, Univ. Natal, Durban (unpubl.).
- SACS: SOUTH AFRICAN COMMITTEE FOR STRATIGRAPHY, 1980. Stratigraphy of South Africa. Part 1: Lithostratigraphy of the Republic of South Africa, South West Africa/Namibia and the Republics of Bophuthatswana, Transkei and Venda (L.E. Kent, comp.): Handbk. geol. Surv. S. Afr., 8, 690 pp.
- SCOGINGS, A.J., 1985. The geology of the Ngoye Granite Gneiss Formation: M.Sc. thesis, Univ. Durban-Westville, Durban (unpubl.).
- , 1986. Peralkaline gneissic granites in the Ngoye Granite Gneiss Formation, Natal: Trans. geol. Soc. S. Afr., 89, p. 361-365.
- , 1989. Peralkaline granitoid and alkaline mafic gneisses northwest of Eshowe, Natal: S. Afr. J. Geol., 92, p. 339-351.
- , and FORSTER, I.F., 1989. Gneissose carbonatites in the Bull's Run Complex, Natal: S. Afr. J. Geol., 92, p. 1-10.
- WHALEN, J.B., CURRIE, L.C., and CHAPPEL, B.W., 1987. A-type granites: geochemical characteristics, discrimination and petrogenesis: Contrib. Mineral. Petrol., 95, p. 407-419.

Received: April 1989

Accepted: March 1990

Referees: D.R. Hunter, E.P. Saggerson, D. Strydom, R.J. Thomas

¹SA Development Trust Corp., Pretoria

1. PROPOSER OF NAME

Nicolaysen and Burger (1965 – "Bulls Run Syenitic Gneiss"); revised by present author (this publication).

2. DERIVATION OF NAME

The farm Bulls Run Estate 12987, 17 km NNW of Eshowe, Natal.

3. TYPE AREA

Northeast of Goedertrou Dam (Fig. 1).

4. STRATIGRAPHIC POSITION AND AGE

Located within the Nkomo Nappe of the Tugela Group, near the northern margin of the Natal Metamorphic Province (Charlesworth, 1981). Intrusive into the Tugela Group. Nicolaysen and Burger (1965) obtained a U-Pb age of 1140 ± 35 Ma from a single zircon. More recent work (author's unpublished whole-rock Rb-Sr data) indicates an age of 1138 ± 45 Ma for the nepheline syenite gneiss.

5. GEOLOGICAL DESCRIPTION

Basic concept and unifying features: Geochemically related undersaturated to saturated alkaline/peralkaline syenitic and minor carbonatitic gneisses.

Form and size of body: Prominent easterly-trending ridge 15 km long and up to 1.5 km wide, rising some 400 m above the Mhlathuze River (Fig. 1).

Lithology: A broad subdivision into three major syenitic gneiss types (muscovite syenite, nepheline syenite and albite syenite gneiss) is proposed for the bulk of the complex (Fig. 1). Three minor rock types (carbonatite, peralkaline microsyenite and alkaline mafic gneiss) occur as dyke- or sheet-like bodies in the muscovite syenite gneiss (Scogings & Forster, 1989).

Muscovite syenite gneiss (50%): Medium-grained; white to yellowish grey. Consists of muscovite (5–35%), microcline (20–35%), albite (30–40%) and biotite (<10%); calcite, apatite and sphene are accessory minerals.

Nepheline syenite gneiss (30%): Medium- to coarse-grained; blue-grey to dark grey. Comprises nepheline (5–40%), microcline (30–50%), albite (5–30%) and biotite (2–15%). Cancrinite, calcite, apatite and ilmenite are characteristic accessories. Nepheline syenite gneisses within the eastern portion of Goedertrow contain aegirine augite (5–20%) and are more mafic than those on Black Eyes and Bulls Run; they can be classified as feldspathic ijolite.

Albite syenite gneiss (20%): Fine-grained; light grey to white; has

siliceous appearance in outcrop. Composed of albite (45–65%), microcline (25–45%), nepheline (<25%) and biotite (2–7%). Accessory minerals include zircon, pyrochlore, cancrinite and sericite; nepheline is commonly kaolinized.

Carbonatite gneiss (<1%): Medium-grained; white to brown. Consists of calcite (60–96%), alkali feldspars (<20%), biotite (3–25%), apatite (<10%). Accessory minerals are ilmenite, pyrochlore and zircon.

Peralkaline microsyenite gneiss (<1%): Fine-grained; white to blue-green. Consists of albite (60–70%), microcline (10–20%), quartz (2–6%) and aegirine-augite (2–5%). Calcite and riebeckite occur in accessory amounts.

Alkaline mafic gneiss (<1%): Fine-grained; dark grey to black. Consists of biotite (20–50%), albite (35–50%), microcline (2–15%), calcite (8–12%) and apatite (<3%).

Geochemistry: Muscovite syenite gneisses are silica-saturated (SiO_2 : 52–59%), peraluminous and have moderate alkali contents ($\text{Na}_2\text{O} + \text{K}_2\text{O}$: 10–13%), with K_2O generally in excess of Na_2O ($\text{Na}_2\text{O}/\text{K}_2\text{O}$ c. 0.75). Nepheline syenite gneisses are undersaturated (SiO_2 : 48–58%; normative nepheline 10–30%), metaluminous to peraluminous and have elevated alkali contents ($\text{Na}_2\text{O} + \text{K}_2\text{O}$: 12–15%). Potassic and silica-rich in central and western outcrops ($\text{Na}_2\text{O}/\text{K}_2\text{O}$ c. 0.75) but more sodic and undersaturated in the east ($\text{Na}_2\text{O}/\text{K}_2\text{O}$ c. 1.25). Albite syenite gneisses have the highest silica contents of the major lithologies (SiO_2 : 57–65%) and due to their sodic character ($\text{Na}_2\text{O}/\text{K}_2\text{O}$: 1–2.5) are moderately undersaturated (normative nepheline 10–20%). FeO (<2%) and CaO (<1%) contents are low. Enrichment in trace elements such as Zr (700–2000 ppm) and Nb (200–16500 ppm) is diagnostic. Carbonatite gneisses have typical syenite chemistry: CaO (30–55%), MgO (c. 0.5%), P_2O_5 (<6%), Sr (6000–9000 ppm), Nb (50–4000 ppm). Peralkaline microsyenite gneisses are silica-saturated (SiO_2 : 60–70%, normative quartz 2–12%), sodic ($\text{Na}_2\text{O}/\text{K}_2\text{O}$ c. 2) and mildly peralkaline ($\text{Na} + \text{K}/\text{Al}$ c. 1.02). Alkaline mafic gneisses have high alkali contents ($\text{Na}_2\text{O} + \text{K}_2\text{O}$: 8–11%) for relatively low SiO_2 (45–50%); trace elements Zn, Nb, Zr, Rb, Sr, Ba, F, CO_2 and LREE are enriched and typical of nephelinitic or alkaline lamprophyre.

Genesis: The Bulls Run gneisses have many of the mineralogical and geochemical characteristics typical of nepheline syenite/ijolite carbonatite central complex magmatism. Nepheline syenite complexes are generally intruded into anorogenic or rifted continental settings, but minor occurrences have also been noted in within-plate oceanic settings. By analogy with undeformed

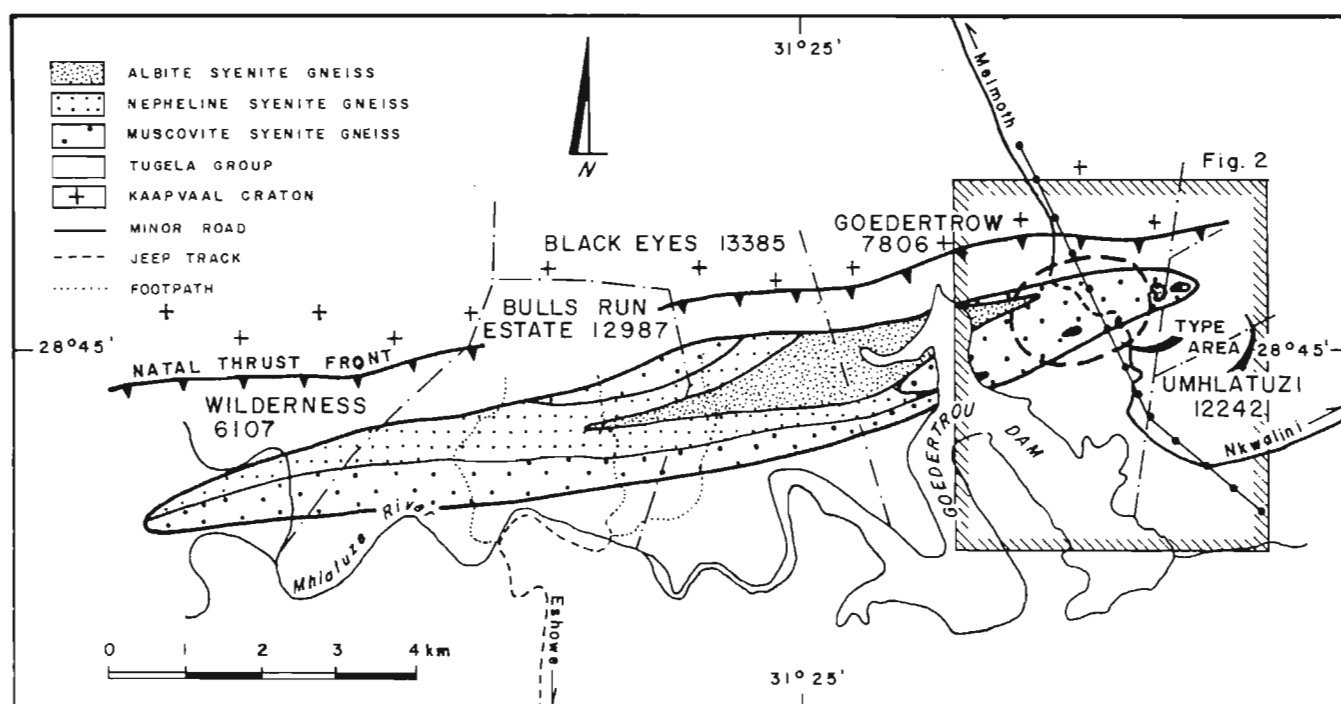


Fig. 1 Distribution of the Bulls Run Complex and location of its type area.

complexes, the Bulls Run gneisses probably represent a metamorphosed and deformed nepheline syenite/carbonatite central complex. Rb-Sr isotopes (author's data) indicate that the nepheline syenite gneisses had a low initial $87\text{Sr}/86\text{Sr}$ ratio of 0.7028 at the time of intrusion, indicating a mantle-derived alkaline magma. Available field data suggest that the sequence of magmatic emplacement was: (i) muscovite syenite, (ii) carbonatite, (iii) nepheline syenite, (iv) albite syenite. The muscovite syenite may be a fenitized aureole around the nepheline syenites (Scogings and Forster, 1989).

Other aspects: The Bulls Run Complex has a pervasive east-striking planar structural fabric that transgresses lithological contacts and dips to the south at between 50° and 70° .

6. BOUNDARIES

Contacts of the Bulls Run Complex with the surrounding amphibolites are not exposed, but the known field relationships indicates that they are sharp and mylonitized. Charlesworth (1981) suggested that the mylonites are located along thrust faults around the Bulls Run body. Internal contacts are rarely exposed, but where observed are sharp and intrusive, although the well developed structural fabric tends to obscure age relationships.

7. HISTORICAL BACKGROUND

The syenitic character of the gneisses on Bulls Run Estate, described as "soda-rich Tugela migmatites and gneisses," was first noted by Nicolaysen & Burger (1965, p. 508) who proposed the name Bulls Run Syenitic Gneiss. Charlesworth (1981) subsequently outlined the syenitic gneisses which he termed the Bulls Run Syenite Gneiss Formation (cf. SACS, 1980). Scogings & Forster (1989) redefined the outer limits of the body (their Bull's Run Syenite Gneiss Complex), particularly in the east on Goedertrow 7806 and Umhlathuzi 12242, and described the undersaturated character of the gneisses.

8. SUBDIVISION

No subdivision into named rocks units is envisaged.

9. REGIONAL ASPECTS

Geographic distribution: See Figure 1.

Lateral variation: See 5 above and Figure 1.

Correlation: Geochemically-related alkaline granitoid gneisses have been described from the Ngoye Hills 30 km east of Bulls Run (Scogings, 1986; 1990) and also from Wangu Hill some 5 km west of Bulls Run (Scogings, 1989). It has been suggested that these three occurrences are the remnants of a metamorphosed alkaline province (Scogings, 1989).

10. STRATOTYPES

Type localities of the three major syenite gneiss varieties, in addition to carbonatite gneiss, have been defined in the eastern part of the complex (Fig. 2). Together these constitute a composite type locality. Type locality A: natural outcrops of muscovite syenite gneiss on summit of hill; type locality B: road cutting in nepheline syenite gneiss below Eskom powerlines; type locality C: natural outcrops of albite syenite gneiss on westerly trending spur; type locality D: natural outcrops of brown carbonatite 25 m southeast of type locality A.

11. LITERATURE REFERENCES

CHARLESWORTH, E.G., 1981. Tectonics and metamorphism of the northern margin of the Namaqua Natal Mobile Belt in Natal: Ph.D.

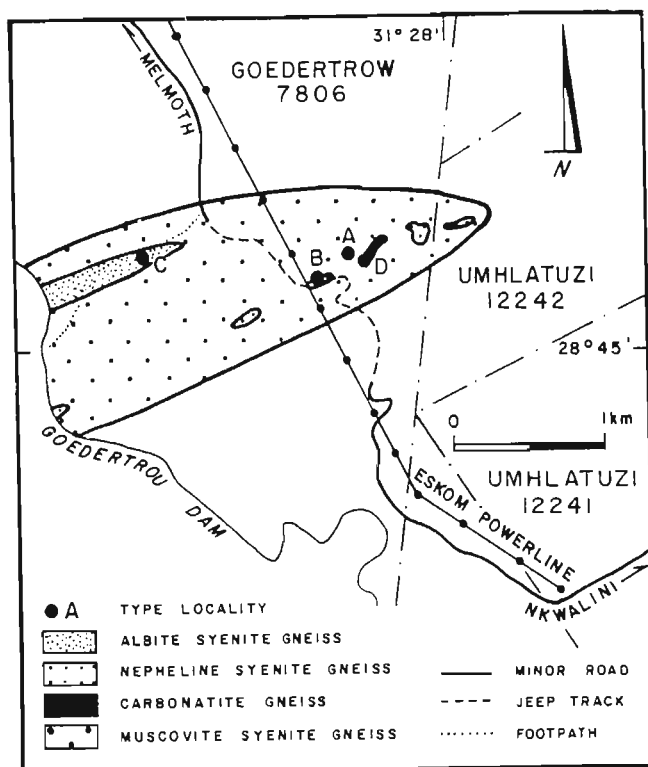


Fig. 2 Type localities A-D of the Bulls Run Complex.

thesis, Univ. Natal, Durban (unpubl.).

NICOLAYSEN, L.O., and BURGER, A.J., 1965. Note on an extensive zone of 1000 million year-old metamorphic and igneous rocks in southern Africa: *Sci. de la Terre*, 10, p. 497-516.

SACS: South African Committee for Stratigraphy, 1980. *Stratigraphy of South Africa. Part 1: Lithostratigraphy of the Republic of South Africa, South West Africa/Namibia and the Republics of Bophuthatswana, Transkei and Venda* (L.E. Kent, comp.). *Handbk. geol. Surv. S. Afr.*, 8, 690 pp.

SCOGINGS, A.J., 1986. Peralkaline gneissic granites in the Ngoye Granite-Gneiss Formation, Natal: *Trans. geol. Soc. S. Afr.*, 89, p. 361-365.

——, 1989. Peralkaline granitoid and associated alkaline mafic gneisses northwest of Eshowe, Natal: *S. Afr. J. Geol.*, 92, p. 339-351.

——, 1990. Ngoye Complex, in *Catalogue of South African Lithostratigraphic Units, Volume 2* (M.R. Johnson, ed.): *S. Afr. Comm. Strat.* p. 37-38.

——, and FORSTER, I.F., 1989. Gneissose carbonatites in the Bull's Run Complex, Natal: *S. Afr. J. Geol.*, 92, p. 1-10.

Received: April 1990

Accepted: August 1991

Referees: D.H. Cornell, D.R. Hunter, R.J. Thomas

¹ SA Development Trust Corp., Pretoria

1. PROPOSER OF NAME

Scogings (1989 – "Wangu granitoid gneisses"); modified by author (this publication).

2. DERIVATION OF NAME

Wangu Hill, 20 km NW of Eshowe, Natal (Fig. 1).

3. TYPE AREAS

Wangu Hill to the Mvuzane River 1,5 km to the southwest of Wangu Hill (Fig. 1).

4. STRATIGRAPHIC POSITION AND AGE

Situated within the Nkomo Nappe near the northern margin of the c. 1100 Ma Natal Metamorphic Province. No age determinations available.

5. GEOLOGICAL DESCRIPTION

Basic concept and unifying features: Predominantly alkaline/peralkaline granite gneisses, with very minor alkaline mafic intrusive phases.

Form and size of intrusion: Elongate easterly-trending body 6 km long and up to 1 km wide. Three-dimensional form unknown.

Lithology: Three varieties of gneiss are recognised on the basis of modal mineralogy, two being granitic and the third mafic.

Magnetite granite gneiss (78%): Fine-grained, light pink to pink. Consists of quartz (25–40%), microcline (20–35%), albite (25–45%)

and magnetite (3–8%). Biotite and fluorite are accessory phases. QAP classification (Streckeisen, 1976): alkali-feldspar granite (Fig. 2).

Aegirine granite gneiss (20%): Fine-grained, light pinkish to white. Consists of quartz (25–50%), microcline (10–40%), albite (20–50%), magnetite (<10%) and aegirine (<15%). Classified as alkali-feldspar granite on the QAP diagram (Fig. 2).

Mafic gneiss (2%): Occurs as sheets up to 30m long and 1m thick, containing xenoliths of peralkaline granitoid gneiss implying an intrusive relationship. Fine-grained; grey to dark grey, with glistening appearance in hand specimen due to high biotite content. Comprises biotite (45–65%), albite (20–40%) microcline (5–10%), calcite (5–10%) and apatite (<5%). Accessory minerals are opaque oxides, pyrite and sphene. Classified as alkali-feldspar syenite on the QAP diagram (Fig. 2).

Geochemistry: Aegirine granite gneiss is peralkaline ($Na+K/Al = 1,01-1,33$) and silica oversaturated ($SiO_2: 67-79\%$). Scogings (1989) reported low levels of MgO, CaO, Ba and Sr, elevated Ga/Al ratios and enrichment in incompatible trace elements such as Zn (123–612 ppm), Zr (450–1836 ppm), Y (95–159 ppm) and Nb (89–423 ppm). These are characteristic of peralkaline granite chemistry as defined by Whalen *et al.* (1987).

Magnetite granite gneiss is metaluminous to almost peralkaline ($Na+K/Al = 0,94-0,99$) and silica oversaturated ($SiO_2: 67-78\%$). Major and trace element chemistry very similar to the aegirine granite gneisses.

Mafic gneiss has low SiO_2 contents (c. 40–50%) with relatively

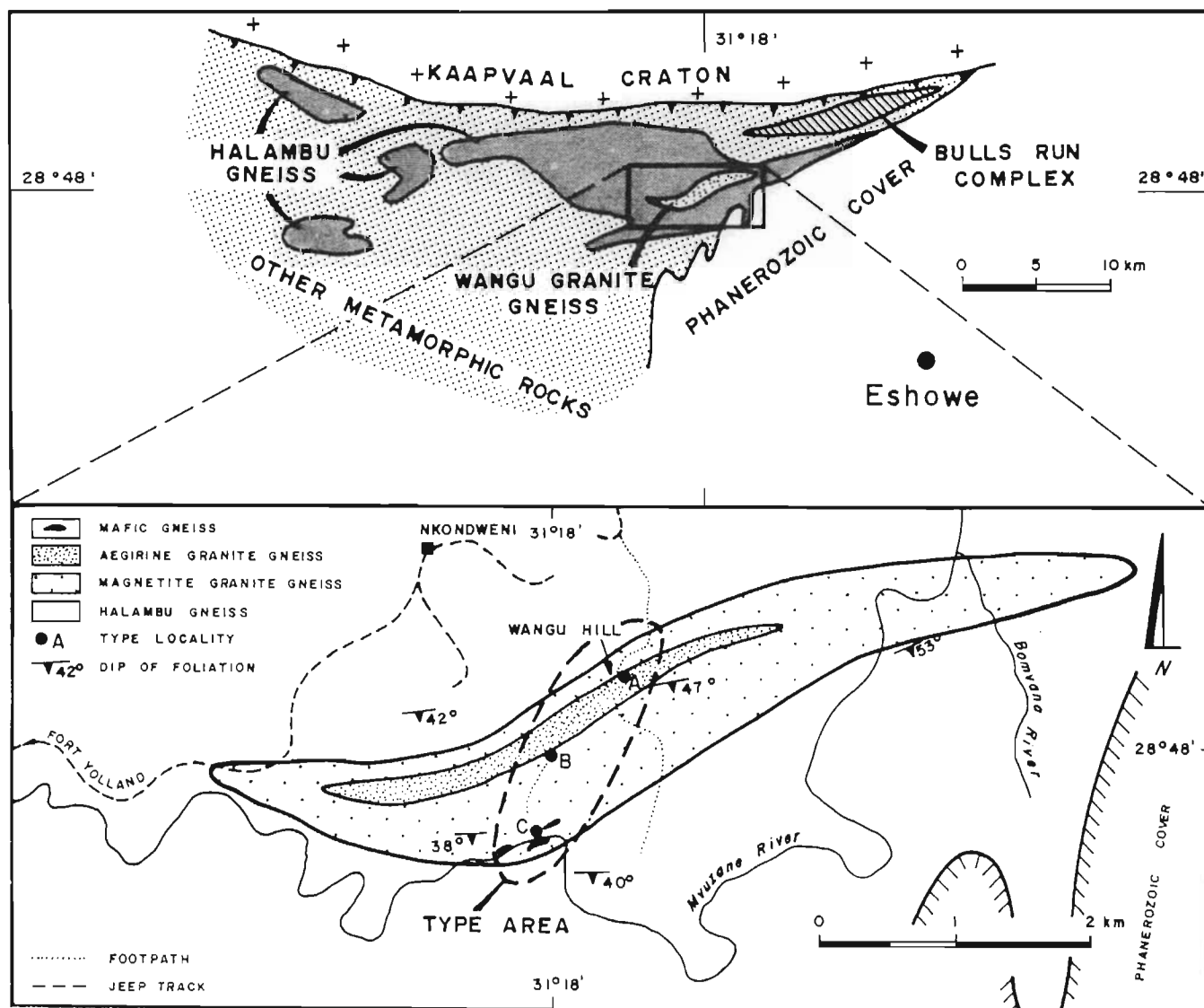


Fig. 1 Distribution of the Wangu Granite Gneiss and location of its type area and type localities.

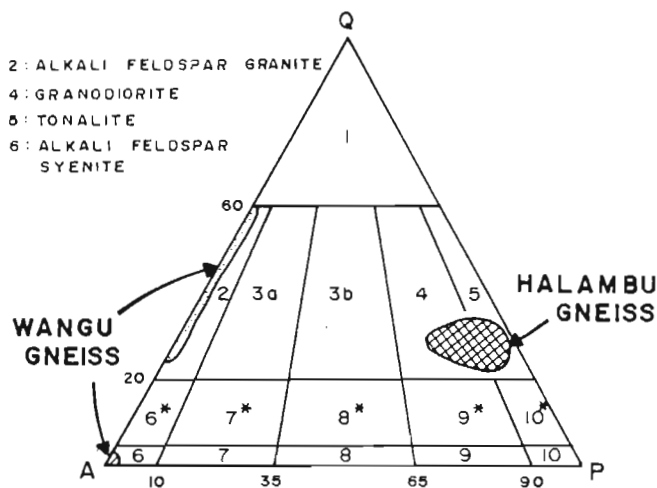


Fig. 2 Classification of the Wangu gneisses and Halambu granodioritic gneisses on the Streckeisen (1976) QAPF modal diagram.

high total alkalis ($\text{Na}_2\text{O} + \text{K}_2\text{O}$: 7–9%) similar to nephelinite and mica lamprophyre (Scogings, 1989). Dominantly potassic, with $\text{K}_2\text{O}/\text{Na}_2\text{O}$ c. 2.5. Trace element contents such as Zn (450–750 ppm), Nb (45–390 ppm), Rb (390–635 ppm), Sr (340–1445 ppm) and Ba (970–1460 ppm) are similar to alkaline mafic rocks such as nephelinite and mica lamprophyre (see Scogings, 1989).

Genesis: The Wangu granite gneisses represent deformed peralkaline microgranitic or aplitic rocks. The Wangu gneisses range in composition from quartz syenite to alkali granite on the R1-R2 diagram of de la Roche et al (1980) and are clearly different from the field of Halambu gneisses (Scogings, 1989). "A-type", or "within plate" trace element chemistry corroborates major element character and contrasts markedly with the surrounding calc-alkaline Halambu Formation gneisses. Therefore the Wangu granitoid gneisses probably represent deformed "A-type" microgranitic or aplitic rocks. The fine grain size, if an inherited feature, indicates high-level, possibly subvolcanic, intrusion of a rapidly-cooled granitic body. The biotite-rich mafic gneisses are possibly derived from alkaline mafic rocks of essexite composition, with a genetic relationship to the peralkaline gneisses suggested on the basis of their alkaline nature and close spatial association.

Other aspects: The Wangu gneisses have a pervasive east-striking structural foliation that dips southwards at moderate angles (c. 45°).

6. BOUNDARIES

Contacts of the Wangu gneisses with the surrounding Halambu Gneiss are not exposed but from intense foliation are thought to be tectonic or thrust, similar to those around the Ngoye and Bulls Run Complexes (Scogings and Forster, 1989; Scogings, 1990).

7. HISTORICAL BACKGROUND

The area was first mapped by du Toit (1931) when he assigned the rocks on 'Wangu Hill' to the predominantly amphibolitic 'Tugela Series'. The rocks north of this hill were described as granites of the 'Alambu Mass'. Subsequent mapping by Charlesworth (1981) resulted in the incorporation of Du Toit's Tugela Series rocks of the Wangu area into the 'Halambu Granite Gneiss Formation' (cf. SACS, 1980). The Halambu Formation was described as predominantly of calc-alkaline granodioritic to tonalitic composition, with minor amounts of monzonitic gneiss in the southern part of the formation (Charlesworth, 1981). The presence of alkaline/peralkaline gneisses

on Wangu Hill was first recognised by Scogings (1989), who referred to them as the 'Wangu granitoid gneisses'.

8. SUBDIVISION

No subdivision into named rock units is envisaged.

9. REGIONAL ASPECTS

Geographic distribution: See Figure 1.

Lateral variation: As noted above and in Figure 1.

Correlation: Similar alkaline/peralkaline granite gneisses have been recorded in the Ngoye Complex, 40 km east of Wangu Hill (Scogings, 1985; 1986; 1990). Geochemically related, though undersaturated, syenitic and carbonatitic gneisses have also been described in the Bulls Run area, to the northeast of Wangu (Scogings and Forster, 1989). These occurrences of alkaline gneiss may be the remnants of an 'alkaline province' (Scogings, 1989).

10. STRATOTYPES

Typical examples of the three gneiss varieties are to be seen at type localities A (aegirine granite), B (magnetite granite) and C (mafic gneiss) (Fig. 1). All are natural outcrops and are best reached on foot traverse from A to C. Access to point A is by foot path from the Fort Yolland road, with use of four-wheel drive vehicle recommended in the rainy season.

11. LITERATURE REFERENCES

- CHARLESWORTH, E.G., 1981. Tectonics and metamorphism of the northern margin of the Namaqua-Natal Mobile Belt near Eshowe, Natal: Ph.D. thesis, Univ. Natal, Durban, 433 pp. (unpubl.).
- DE LA ROCHE, H., LETERRIER, J., GRANDCLAUDE, P., and MARCHAL, M., 1980. A classification of volcanic and plutonic rocks using the R1 - R2 diagram and major element analyses - its relationship with current nomenclature: *Chem. Geol.*, 29, p. 183-210.
- DU TOIT, A.L., 1931. The geology of the country surrounding Nkandla, Natal: Expl. sheet 109, Geol. Surv. S. Afr., 111 pp.
- SACS: SOUTH AFRICAN COMMITTEE FOR STRATIGRAPHY, 1980. Stratigraphy of South Africa. Part 1: Lithostratigraphy of the Republic of South Africa, South West Africa/Namibia and the Republics of Bophuthatswana, Transkei and Venda (L.E. Kent, comp.): *Handbk. geol. Surv. S. Afr.*, 8, 690 pp.
- SCOGINGS, A.J., 1985. The geology of the Ngoye Granite Gneiss Formation: M.Sc. thesis (unpubl.), Univ. Durban-Westville, Durban, 186 pp.
- , 1986. Peralkaline gneissic granites in the Ngoye Granite Gneiss Formation, Natal: *Trans. geol. Soc. S. Afr.*, 89, p. 361-365.
- , 1989. Peralkaline granitoid and associated alkaline mafic gneisses northwest of Eshowe, Natal: *S. Afr. J. Geol.*, 92, p. 339-351.
- , 1990. Ngoye Complex, in *Catalogue of South African Lithostratigraphic Units, Volume 2* (M.R. Johnson, ed.): *S. Afr. Comm. Strat.*, p. 37-38.
- , and FORSTER, I.F., 1989. Gneissose carbonatites in the Bull's Run Complex, Natal: *S. Afr. J. Geol.*, 92, p. 1-10.
- STRECKEISEN, A., 1976. To each plutonic rock its proper name: *Earth Sci. Rev.*, 12, p. 1-33.
- WHALEN, J.B., CURRIE, L.C., and CHAPPELL, B.W., 1987. A-type granites: geochemical characteristics, discrimination and petrogenesis: *Contr. Miner. Petrol.*, 95, p. 407-419.

Received: November 1990

Accepted: August 1991

Referees: D.H. Cornell, P.B. Groenewald, D.R. Hunter, E.P. Saggerson, R.J. Thomas, M.K. Watkeys.

¹ SA Development Trust Corp., Pretoria

The distribution and genesis of precious and base metal mineralization in the Natal Metamorphic Province, South Africa

R.J. Thomas

Geological Survey, P.O. Box 900, Pietermaritzburg 3200, Republic of South Africa

W.D. Bullen

Geological Survey, P.O. Box 900, Pietermaritzburg 3200, Republic of South Africa

I. de Klerk*

Rhodes University, P.O. Box 94, Grahamstown 6140, Republic of South Africa

A.J. Scogings

Mineral Development Division, South African Development Trust Corporation, P.O. Box 213, Pretoria 0001, Republic of South Africa

Accepted 21 July 1990

Mineralization in the three major tectonostratigraphic terranes of the Late Proterozoic Natal Metamorphic Province can be subdivided into a number of distinct types. In the greenschist to amphibolite grade Tugela Terrane (in the north), shear zone-hosted epigenetic precious metal mineralization, a gold-bearing volcanogenic exhalative massive sulphide body, and primary magmatic mineralization are recognised. There is a stepwise decrease in metallic ore occurrences southwards into the higher-grade terranes, such that no occurrences have been recognised in the granulite facies Margate Terrane. The mineralization is consistent with models which have been proposed to account for the evolution of the belt as a whole, including northward obduction of the Tugela Terrane ophiolite (seen as an oceanic basin situated to the south of the Archaean Kaapvaal Craton), and accretion of discrete magmatic arcs which developed to the south of the Tugela Ocean.

Mineralisasie in die drie hoof-tektonostratigrafiese terreine van die Laat-Proterosoïese Natal Metamorfie Provinsie kan onderverdeel word in 'n aantal duidelik onderskeibare tipes. In die groenskis- tot amfibolietgraad Tugelaterrein (in die noorde), word epigenetiese metaalmineralisasie in skeursones, 'n gouddraende vulkanogeniese ekshalerende massiewe sulfiedliggaam, en primêre magmatiese mineralisasie, herken. Daar is 'n trapgewyse afname in metaalhoudende ertsvoorkomste suidwaarts in die hoër-graad terreine in, sodanig dat geen voorkomste in die Margateterrein se granulietfasies herken kan word nie. Die mineralisasie stem ooreen met modelle wat voorgestel is om die evolusie van die gordel as 'n geheel, insluitende noordwaartse obduksie van die Tugelaterrein-opholiet (gesien as 'n oseaaniese kom na die suide van die Argeïese Kaapvaalkraton gesitueer), en die akkresie van afsonderlike magmatiese boë wat na die suide van die Tugelaoseaan ontwikkel het, te verklaar.

*Present address: Anglo American Prospecting Services, P.O. Box 561, Bethal, 2310.

Introduction and geological setting

The Late Proterozoic Natal Metamorphic Province crops out in a series of poorly exposed basement inliers which cover some 10 000 km² of Natal / KwaZulu. The belt stretches ca. 300 km from the Tugela Valley to northern Transkei (Figure 1). The rocks, which have a broadly east-trending structural grain, have undergone intense polyphase deformation and medium- to high-grade regional metamorphism. It has been widely assumed, since the geochronological studies of Nicolaysen & Burger (1965), that the Natal and Namaqualand Metamorphic Provinces are contiguous beneath the Karoo cover of central southern Africa. Isotopic dates from the Natal Province (chiefly Rb-Sr, whole-rock, and U-Pb, zircon) fall within the range ~1250 to ~900 Ma (Eglington *et al.*, 1989; Thomas & Eglington, 1990). In the Tugela Valley, the rocks of the Natal Province are in tectonic contact with those of the Archaean Kaapvaal Craton. It has been suggested that this northern part of the belt represents a deformed and metamorphosed Proterozoic obduction zone, involving a package comprising mafic/ultramafic oceanic crust with overlying pelagic metasediments and metalavas (Matthews, 1972). These rocks, interpreted as the middle and upper parts of an ophiolite complex, were transported northwards

in a series of thrust nappes onto the stable foreland of the Kaapvaal Craton along a sole décollement known as the Mfongosi thrust (Matthews & Charlesworth, 1981). The southern, western, and eastern limits of the belt are obscured beneath Palaeozoic cover rocks. However, a 100–200 km wide, east-trending geophysical anomaly (the Southern Cape Conductive Belt) strikes westwards from the Transkei coast, some 60 km south of the southernmost outcrops of the Natal Metamorphic Province (Figure 1). This anomaly has been interpreted as a large slab of highly conductive and magnetic, partially serpentized rock which represents oceanic lithosphere that was subducted during the Proterozoic (De Beer *et al.*, 1982). The Southern Cape Conductive Belt thus probably marks the unseen southern limit of the belt.

The Natal Metamorphic Province has not been an important source of metallic minerals, particularly in comparison with the numerous rich deposits which are exploited from the western continuation of the belt, the Namaqualand Metamorphic Province. However, the relatively mountainous terrain, deep weathering, thick vegetation cover and poor outcrop which characterise the Natal Province, have doubtless hindered mineral exploration. In addition, there is very little literature on

Table 2 Classification of the metalliferous mineralization in the Natal Metamorphic Province

	METAL	HOST LITHOLOGY	MINERALIZATION TYPE	REFERENCES
TUGELA TERRANE	Au, Ag, Pb, Cu, Zn	Mainly schists of the Mfongosi Group and amphibolites of the Tugela Group	Gold associated with quartz in shear zones	This work
	Au, Ag, Cu, Pb, Zn	Amphibolites and schists of the Tuma Formation (Tugela Group)	Deformed, stratiform, sediment-hosted exhalative massive sulphide	This work
	Cr, Fe, V, Ti, (Cu, Ni Co)	Mafic and ultramafic rocks of the Sithilo, Sebenzani, Mambula and Tugela Rand complexes	Vanadiferous and titaniferous magnetite layers and chromite-bearing pods in layered mafic/ultramafic intrusions	Wuth & Archer, (1986), Reynolds, (1986), Knoetze, (1988)
	Zr, Nb	Syenitic and carbonate gneiss (Bull's Run Complex)	Local concentrations in gneissic carbonatite	Scogings & Forster (1989)
	Nb, Zr, Y, REE	Peralkaline granitoid gneiss of Ngoye Complex	Quartz-magnetite 'blows'	Scogings, (1986)
	Zr, Nb, Zn, REE	Peralkaline gneiss in Halambu Formation	Disseminated in peralkaline granitoid gneisses	Scogings, (1989)
MZUMBE TERRANE	Au	Granite gneiss (Mzimlilo Suite) and fine-grained siliceous gneisses (Mapumulo Group)	<i>En echelon</i> quartz veins associated with sulphides in wide zones of shearing	Thomas & Gain, (1989)
	W, Mo,	Calc-silicates and amphibolites (Mapumulo Group)	Stratiform, sediment-hosted exhalative	Scogings, (1984)
	U, Th	Alaskitic granites and pegmatites	Xenotime, allanite etc, in alaskitic granite and pegmatites	Evans (1984) Hart & Barton, (1984)
	Cu, Ni, Cu, Mo	Gneisses of Mapumulo Group, granites	Small serpentinite pods	
MARGATE TERRANE		NO METALLIFEROUS OCCURRENCES KNOWN		

are locally developed. The metalavas are composed of 40–60% chlorite and up to 15% epidote with varying amounts of sericite, albite, quartz, carbonate, clinozoisite, and biotite. Rare undeformed amygdals, first recognized by Matthews (1959), have cores of epidote, surrounded by granular quartz and calcite. The pelites consist of sericite, quartz, chlorite, and albite.

Weak to pervasive carbonate alteration is evident in all the metalavas, being most strongly developed in zones of intense shearing. This alteration is late in the paragenetic sequence, post-dating the Au mineralization. The secondary carbonate occurs as concordant, fine- to medium-grained patches, or as thin (~1 mm) carbonate veins which cross-cut the foliation. Carbonate is also present in late-stage, 1–10 cm-thick, undeformed quartz veins. It is suggested that this alteration was caused by the passage of late-stage CO₂-rich fluids. An early, pre-tectonic, generation of unmineralized, highly deformed quartz veins is locally conspicuous.

The graphitic schist units in the Ngubevu area are typically developed along the contacts between metalavas and metasediments, or enclosed within the latter. These layers contain zones, up to several metres in thickness, of intense carbonation, associated quartz and sericite, with abundant fine-grained tourmaline, which locally constitutes

more than 20% of the rock. These rocks conform to the definition of 'tourmalinites', as proposed by Slack (1982), who pointed out that such rocks are often spatially associated with, and genetically related to, stratabound base metal sulphide, gold, tin, and tungsten deposits, as a result of submarine exhalative processes. Thus, the location of such tourmaline-rich rocks may possibly be used as a prospecting tool (one tourmalinite sample from the Ngubevu area returned a value of 350 ppb Au). This mineralization is considered to be syngenetic in origin. It is therefore possible that some of the later shear zone-hosted epigenetic gold mineralization may have been derived, at least in part, from a syngenetic, stratabound, exhalative protore rich in tourmaline.

The mineralization at all the old workings consists of epigenetic gold-rich quartz veins confined to west-striking zones of intense shearing. These thin (up to 3 cm), weakly deformed, discontinuous quartz veins and stringers contain up to ~7 000 ppb Au, whereas the late stage, undeformed carbonate-bearing quartz veins contain only minor amounts of gold (up to 20 ppb). To summarize, at Ngubevu, the following sequence of events important to the genesis of the mineralization is recognised:

1. an early phase of barren, highly deformed quartz veins;

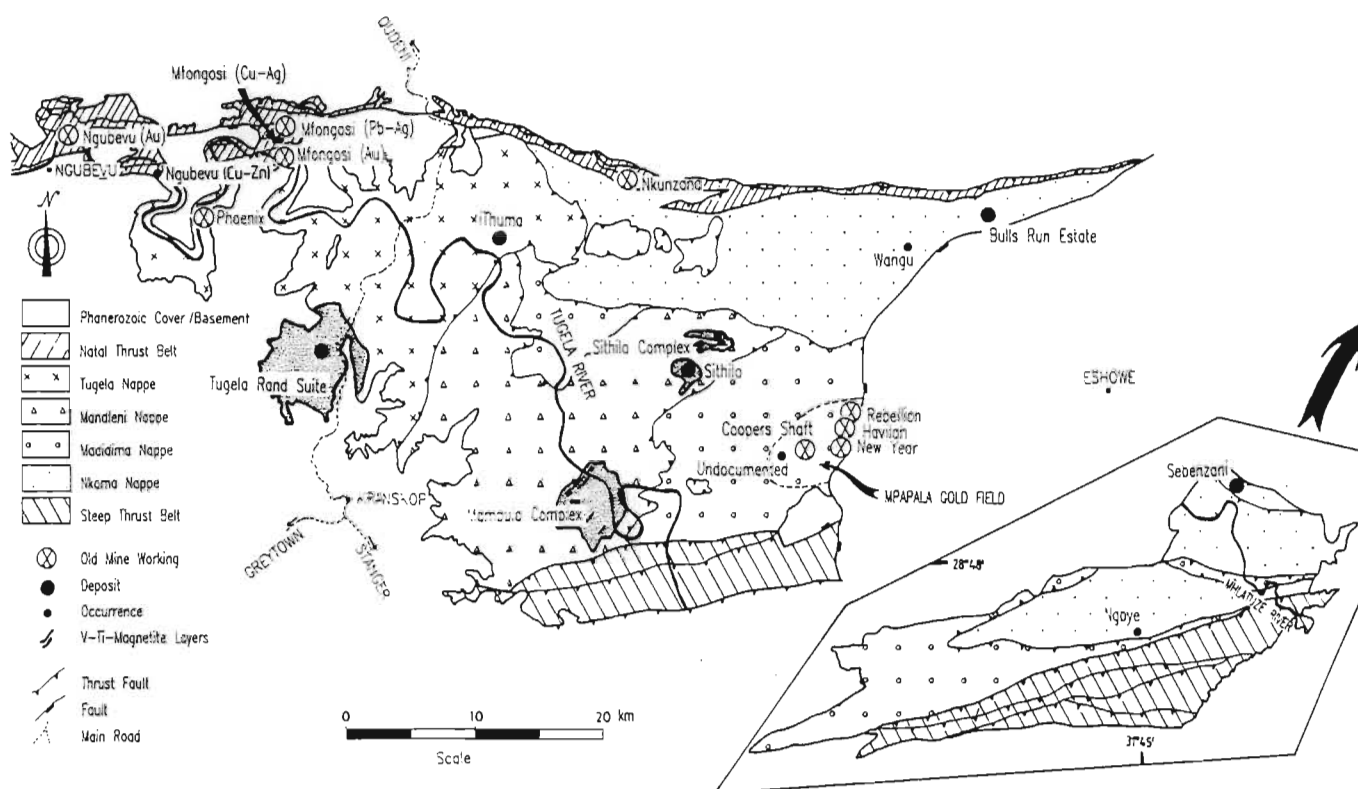


Figure 2 Metallic mineral occurrences in the Tugela Terrane. (Tectonic data from Matthews & Charlesworth, 1981).

2. intense shearing, probably associated with northward-directed thrusting;
3. mineralizing hydrothermal fluids, which were channelled through shear zones, deposited gold in quartz veins during the metamorphic event that was synchronous with, or possibly post-dated the last major deformation; and
4. the late generation of virtually barren veining is related to late-stage influx of CO_2 -rich fluids along shear zones, resulting in extensive carbonate alteration.

In addition to precious metal mineralization at Ngubevu several Cu-Zn showings have been identified some 6 km to the east of the goldfield (Figures 2 & 3). The host rocks are deformed, southerly dipping, quartz-mica schists and chlorite-epidote schists with quartz-calcite veins containing coarse-grained pyrite. Relic textures in the rocks led Brown (1988) to suggest that the Mfongosi schists at this locality represent highly deformed metalavas and tuffs, and that the mineralization was of submarine volcanogenic exhalative type, with a chloritized and carbonatized stringer zone to the south, and a stratigraphically higher, Cu-Zn sulphide zone to the north. Gossanous outcrops have given values up to 0,85% Cu and 1% Zn.

Mfongosi Gold Mine

The Mfongosi Mine workings are situated on the north bank of the Tugela River, 1 km east of its confluence with the Mfongosi River (Figure 2). Numerous ore zones, consisting of thin quartz stringers in Mfongosi chlorite schists, are developed along the southerly dipping foliation. 'Ayers Reef', a steep, west-pitching, poorly defined ore body up to 1,1 m thick yielded, in 1909, 1 325,3 g Au (Du Toit, 1931) at an average grade of 5,2 g/t.

Mfongosi Pb-Ag workings

These workings are situated 2 km north of the Mfongosi Gold Mine, in Mfongosi chlorite schists (Figure 2). The mineralization is associated with a 1,7 m thick quartz vein, containing argentiferous galena. Hedges (1909) noted that the galena was disseminated throughout the ore body which is otherwise zoned; Cu sulphides concentrated towards the hanging wall, and pyrrhotite towards the footwall. The workings could not be located in 1988.

Mfongosi Cu-Ag occurrence

This occurrence takes the form of deformed, concordant lenses of mineralized granitoid which intrude chlorite schists, magnetite quartzites, and limestones of the Mfongosi Group, 1 km NW of the confluence of the Mfongosi and Tugela Rivers (Figure 2). The lenses are up to 5 m in length and 3 m in thickness but of unknown width (Theart, 1981). The granitoids are extremely sodic (up to 6,75% Na_2O) and grab samples from these rocks gave values up to 1,6% Cu and 9 ppm Ag. It is clear that the mineralization is directly related to the introduction of cupriferous sodic granite veins and dykes.

Nkunjana Gold Mine

The mine is situated on the east and west banks of the Nkunjana River, some 40 km NW of Eshowe (Figure 2). The two workings, which were abandoned in 1922, produced some 24 kg Au from 8 672 t of ore at ~2,8 g/t (Du Toit, 1931). Apparently, this low recovery rate reflects dilution of higher-grade ore from the ore-shoots by lower-grade material, a suggestion verified both by the absence of waste dumps, and records of high Au values within stope

Table 3 Shear zone-hosted precious metal deposits in the thrust front

MINE	HOST LITHOLOGY (Mfongosi Group)	MINERALIZATION/ ALTERATION	STRUCTURE OF ORE BODY	KNOWN GRADE
NGUBEVU GOLDFIELD				
H.M.S.	Quartz sericite schist, quartz chlorite schist	Some carbonate alteration. Gold in quartz veinlets with disseminated pyrite. Pervasive silicification.	Silicified shear zone dipping 63°S	Best value 5,2 ppm Au in veinlets
Champion Reef	Quartz sericite schist, associated graphite schist	Intense late-stage sericite-calcite alteration. Minor pyrite. No quartz veining. Propylitic alteration around shear (epidote-albite-chlorite-sericite)	4m-wide shear zone dipping 60°S Minor Au-bearing quartz veins in the shear.	5,4g/t over 1,2m (Hatch, 1910)
Golden Dove	Chlorite and quartz-chlorite schist (metalavas)	Gold in fine quartz veinlets. Chlorite-calcite-sericite-pyrite alteration in shear zone. Alteration halo not mineralized. Late carbonatization.	Shear zone dips 55°S	Quartz stringer: 7,1 ppm Shearzone rock: 45 ppm
Buffalo River	Quartz-sericite schist and phyllite	Sideritic alteration. Gold associated with pyrite in gossanous enclaves in quartz veins with Cu, Pb, and Zn and Ni sulphides.	Mineralized veins 70 cm thick dip steeply to south	Gossanous enclave: 1,6 ppm Au, 2,23% Cu, 811 ppm Ni, 2 ppm Ag.
MFONGOSI WORKINGS				
Mfongosi Gold Mine	Chlorite schist	Numerous quartz stringers	Southerly dipping ore zone ~1 m thick	5,2g/t over 1,1 m (Du Toit, 1931)
Mfongosi Pb-Ag	Chlorite schist	Ore zone contains argentiferous galena, minor chalcopyrite, pyrrhotite	S-dipping quartz vein up to 1,7 m thick in shear zone	
Mfongosi Cu-Ag	Chlorite schist, limestone, magnetite quartzite sodic granite	Mineralization in sodic granite and host-rock schists	Concordant sodic granite lenses dip to south	1,6% Cu, 9 g/t Ag (Theart, 1981)
NKUNZANA GOLD MINE				
Nkunzana	Chlorite-sericite schist	Au with base metals in ferruginized zone	Steeply plunging pencil-like bodies	11 ppm Au

pillars (eg. 11 g/t Au over 1,2 m; Hatch, 1910).

The gold mineralization is hosted in sericite and chlorite schists of the Mfongosi Group. The schists are intensely sheared and display steep, southerly dipping, C- and S-planar fabrics in addition to steeply plunging lineations and fold closures. According to old mine plans and sections, the auriferous lodes are steeply plunging, pencil-like bodies that were mined 70 m downplunge to the level of the Nkunzana River. Figure 4 shows a cross-section through the workings. Reconnaissance sampling of the adits has shown that elevated precious and base metal contents are contained within a ferruginous, highly oxidized reef zone, with the

following maxima recorded over 1 m intersections: Au (4,4 ppm); Ag (0,9 ppm); Cu (235 ppm); Pb (1 260 ppm); Zn (370 ppm) and As (333 ppm). In addition, Ba, Y, Rb, and Co are enriched across the auriferous zone, relative to the surrounding schists. An example of a typical sampling profile is given in Figure 5. Whereas the eastern workings have a Cu-As signature, the western workings are distinguished by a Pb-As-Zn association. The general tenor of gold mineralization in unstoped 'off-shoot' sections of the adits is in the 0,5 to 2 ppm range. Values outside stope areas are comparable with the 11 g/t recorded by Hatch (1910), in an area now inaccessible due to fallen ground. The

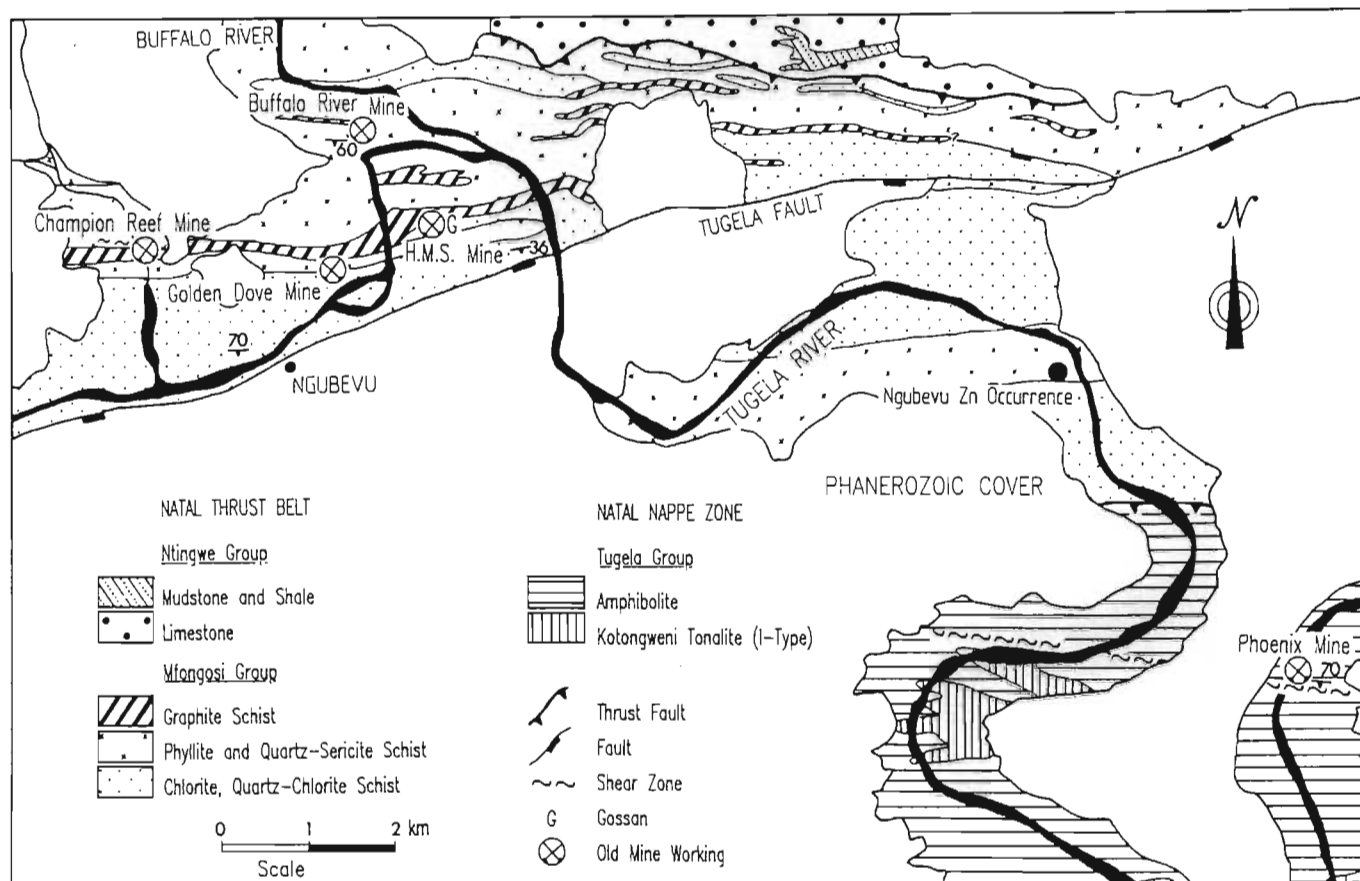


Figure 3 Geological map of the Ngubevu Goldfield.

reef zone itself can only be distinguished from the country rocks by its somewhat ferruginous nature. Unlike other shear-related gold deposits within the Tugela Terrane, there is apparently no correlation between gold mineralization and intensity of vein quartz development.

Shear zone-hosted precious metals in the Nappe zone *Phoenix Mine*

The Phoenix Mine is the most important gold occurrence in the so-called 'Umvoti Goldfield', which is situated on the Tugela River, 12 km ESE of Ngubevu (Figures 2 & 3). At Phoenix, the style of mineralization is similar to that observed at Ngubevu, although the gold-bearing quartz veins are thicker (up to 75 cm). The mineralized shear zone, which is about 3 m wide, occurs in medium-grained actinolite-clinzoisite-sericite metagabbro dipping 65°S. Hatch (1910) reported a grade of 5.49 g/t Au over 0.6 m along a 50 m strike length. Significant gold mineralization is confined to relatively undeformed quartz veins within the shear zone, where the metagabbro is retrogressed to a chlorite-biotite schist containing up to 20 ppb gold.

The Mpapala Goldfield

The goldfield is situated in a poorly exposed area, some 22 km west of Eshowe (Figure 2). It comprises four small workings (Rebellion, New Year, Havilah, and Cooper's Shaft) which were in operation at the turn of the century (Table 4). The gold is disseminated in quartz veins in amphibolites of the Silambo Formation (Tugela Group) and in a later, sheared aplitic dyke. The quartz veins lie within

narrow shear zones, one of which is continuous for over 2 km, from the Rebellion to the New Year workings. The Au in the Mpapala Goldfield is clearly of hydrothermal, epigenetic origin, similar to that at Ngubevu.

Gold-bearing, massive to semi-massive sulphides

The mineralization in the i'Thuma River area (Figures 2 & 6) is associated with two lithologies: amphibolitic metalavas composed of hornblende and plagioclase with minor quartz, epidote, chlorite, biotite, and pyrite; and pelitic/psammitic metasediments. The psammitic rocks consist of quartz and plagioclase with subordinate muscovite and biotite, whereas the metapelites contain more mica, along with variable quantities of garnet, staurolite, kyanite, and chlorite. Clearly, most of the originally amphibolite-grade assemblages have been pervasively retrogressed. Harmer

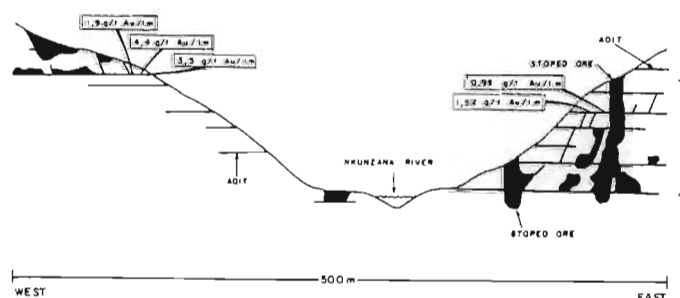


Figure 4 Schematic cross-section through the gold workings at Nkunzana Mine (courtesy of the Government Mining Engineer, Johannesburg).

Table 4 The Mpapala Goldfield statistics

WORKING	TOTAL TONS CRUSHED	GRADE (g/t)	KNOWN EXTENT OF ORE BODY	MAX. WIDTH OF ORE BODY (m)	ORIENTATION OF ORE BODY
Rebellion	508	1,7	16,8m Strike 15,9m Depth	1,7	045/80 SE
Havilah	189	6,9	Strike not known 19,8 Depth	1,5	037/Vertical
New Year	436	5,2	Strike not known 11,0 m Depth	5,5	037/Vertical
Coopers Shaft	1	40,5	450m Strike 7,6m Depth	2,0	045/85 SE
New Occurrence (this work)	—	>9	—	—	—

(1979) pointed out that assemblages reflecting the peak metamorphism are rare because of this retrogressive event which was associated with the later northward-directed thrusting. Smalley (1980) recognized three phases of folding in the area. The mineralization takes the form of a stratabound massive to semi-massive sulphide layer, hosted by the psammitic and pelitic schists and gneisses. The 2 m wide mineralized sulphide unit is strongly sheared and contains abundant secondary fuchsite. It has been folded into a major, NE-plunging, F_1 antiform, with both limbs dipping NW at about 40° (Figure 6). Shearing has occurred at the sulphide/host-rock interface due to their competency

contrast. The intensity of this shearing decreases towards the core of the sulphide unit. Thin magnetite quartzite layers are developed in the hanging wall. Pyrite (10–50% of the rock) is the dominant sulphide, with minor galena and sphalerite. The following results were obtained from the best mineralized 1 m width of the sulphide zone over a 120 m strike length south of the westernmost waterfall (Figure 6):

	Cu (%)	Pb (%)	Zn (%)	Ba (%)	Au (ppm)	Ag (ppm)
Highest	0,83	1,79	0,81	1,10	2,76	87,0
Mean (n=25)	0,29	0,32	0,18	0,43	1,25	27,0

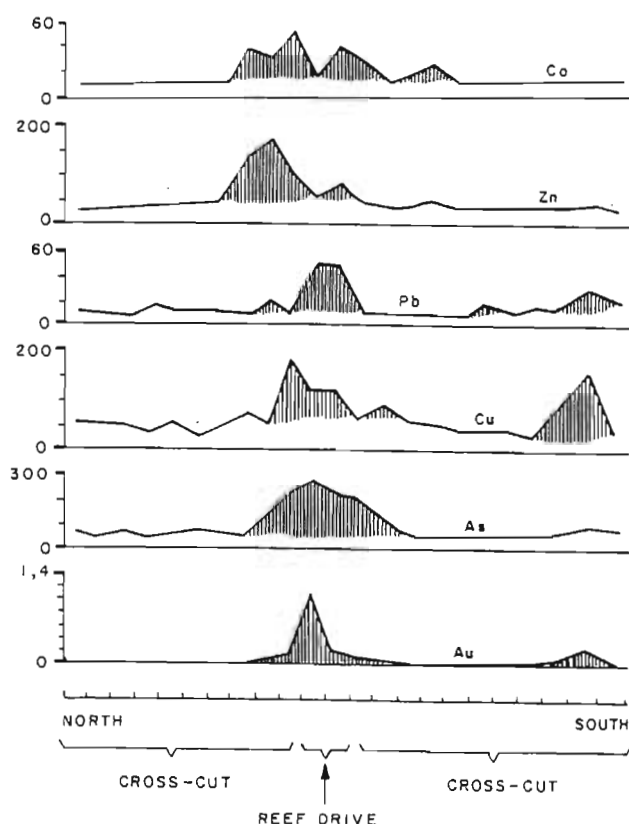


Figure 5 Channel sample metal values across level three crosscut, east Nkuzana Mine. Values in ppm, samples over 1 m intervals.

The high base metal, Ba, and Ag values are characteristic of large sediment-hosted syngenetic exhalative base-metal deposits, e.g. Aggeneys, NW Cape Province (Ryan *et al.*, 1986). Enhanced gold and silver values were also obtained from the sheared sulphide rock and the immediately adjacent host rocks. The biotite-chlorite-phlogopite schist which forms the footwall, southeast of the sulphide layer, contains abundant, concordant pyrite-chalcopryrite segregations up to several centimetres in length, along with numerous thin, phlogopite-rich, sulphide veinlets. Minor tourmaline and andalusite are locally present in this horizon, which is interpreted as a feeder zone for the overlying exhalative-type mineralization. The passage of fluids through the footwall schist unit gave rise to observed biotite-chlorite-phlogopite-calcite-andalusite alteration assemblage. Silica introduced by premetamorphic, exhalative, mineralizing fluids forms medium-grained veins and segregations associated with the sulphides. Gold is enriched in the feeder zone sulphides up to 230 ppb, thus indicating that the mineralizing fluids were themselves gold-bearing. In other words, the gold mineralization is syngenetic in origin and not the result of a late epigenetic event, though, the extent to which mobilization and possible further concentration of the gold during shearing is not clear. At the Maranda J Cu-Zn deposit in the Murchison greenstone belt, comparable sulphide lenticles (pyrite-pyrrhotite-chalcopryrite-sphalerite) are interpreted as volcanogenic

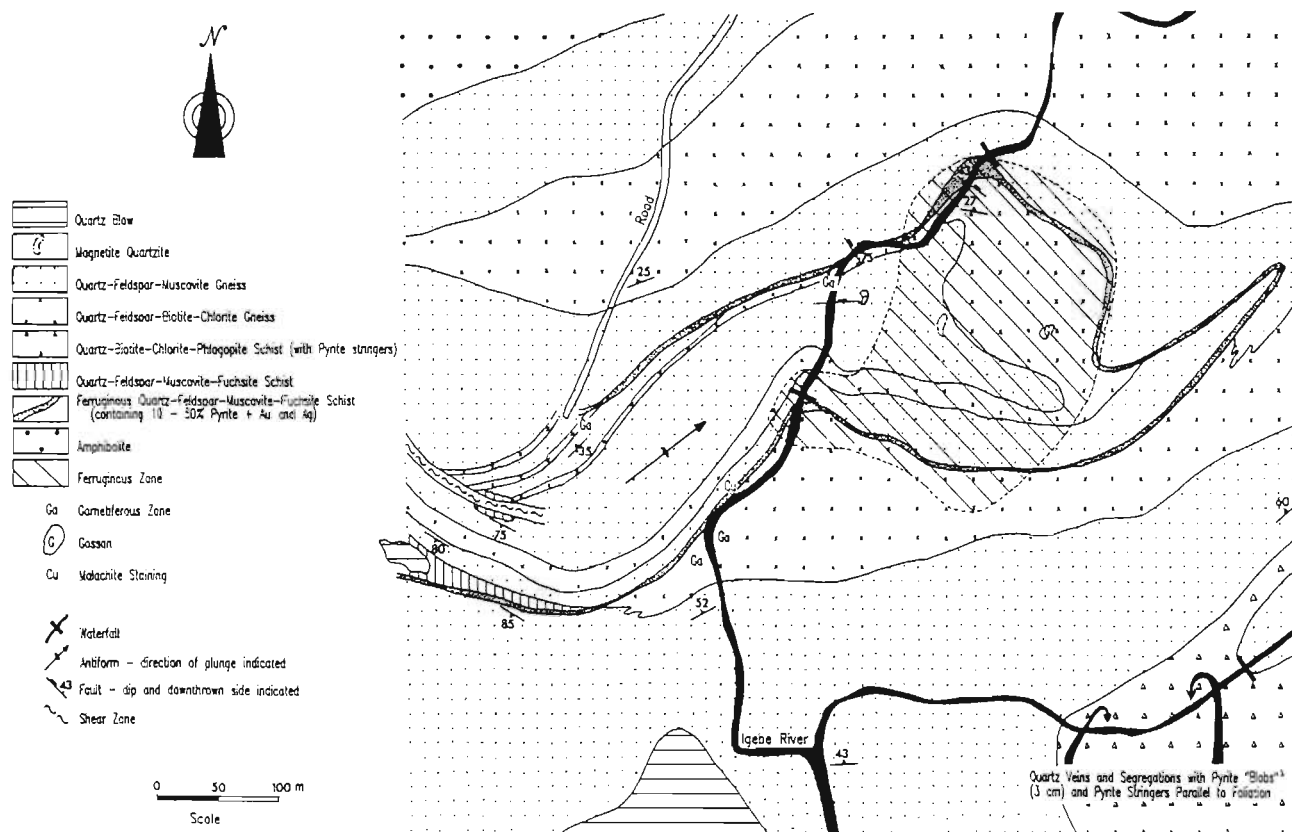


Figure 6 Geological map of the area surrounding the i'Thuma massive / semimassive sulphide body.

'stringers' that were transposed into the foliation during deformation (Maiden, 1984).

Large *et al.* (1988) recognized two distinct spatial and mineralogical Au associations in some Australian volcano-genic massive sulphide deposits: 1) a Au-Zn-Pb-Ag association with gold concentrated in the stratigraphic hanging wall; and 2) a Au-Cu association typically occurring in the footwall stringer zone. A similar situation is apparent at i'Thuma where the Pb-Zn-Ag-Au association occurs in the massive to semi-massive sulphide body, whereas the footwall stringer zone consists of pyrite and chalcopyrite only. Gold values in the sulphides from this latter zone vary from 20 to 230 ppb Au. It is therefore proposed that the i'Thuma River mineralization represents the first example of a syngenetic, sediment-hosted, volcanogenic, submarine-exhalative, auriferous, massive sulphide deposit to be recognised in the Natal Metamorphic Province.

Magmatic ores

Sithilo Complex

The Sithilo ultramafic complex intrudes amphibolites of the Tugela Group about 27 km west of Eshowe (Figure 2). The complex, which consists largely of serpentized dunite, initially assumed economic importance in 1904 when veins of good quality chrysotile asbestos were discovered (Hedges, 1906). Interest in the Sithilo massif was renewed in the early 1950's when four, low-alumina chromite ore bodies were delineated (Wuth & Archer, 1986). The chromite was subsequently exploited from four adits driven into the northeastern flank of Sithilo Hill. During 1952-53, 2 000 t of high-grade chrome concentrates were produced.

In three of the workings chromite occurs in lenticular bodies measuring 1,5 m by 30, 12 and 20 m respectively, whereas in the fourth working a 15 m diameter, southeast-pitching, pipe-like chromitite body is developed. The chromite itself forms irregular or banded stringers, irregular stockworks and isolated pods. These typically podiform chromitite ore bodies are limited in extent owing to faulting as well as to rapid lateral and downdip variations in Cr concentration. Chromite grades within the four ore bodies vary from 9 to 50% Cr₂O₃ while Cr/Fe ratios range from 1 in lower grade ores, up to 3,3 in the highest grade ores (Wuth & Archer, 1986). A similar, smaller, deposit occurs in the Ntulwane serpentinite, some 4 km northeast of Sithilo.

Cu-Ni sulphides at Sebenzani

Anomalous Cu-Ni values have recently been recorded from the Sebenzani area, 8 km west of Empangeni (Figure 2). The occurrence is situated just south of the Natal Thrust Front, in amphibolites, talc schists and actinolite schists, which have been intruded by later gabbros (Schutte & Schurink, 1986). The mineralization takes the form of pyrrhotite, pyrite, chalcopyrite, and pentlandite (Knoetze, 1988). Borehole results (0,32% Ni and 0,09% Cu over 1 m at 63 m depth) suggest that supergene enrichment of the metals has taken place in the oxidised zone (0,8% Ni, 0,6% Cu, 0,1% Co over 5 m at 25 m depth).

Mathews (1972) considered the Sithilo Complex to be a segment of lower oceanic crust which was emplaced along, or proximal to, an active thrust zone during the Natal tectonothermal event, ie. it is an Alpine-type, ophiolitic chromite deposit (Wuth & Archer, 1986). A similar origin was suggested for the Sebenzani body (Knoetze, 1988).

Tugela Rand Layered Suite

The Tugela Rand Layered Suite (Wilson, 1990) forms a differentiated mafic to ultramafic body which intrudes amphibolitic gneisses of the Tugela Nappe, 10 km north of Kranskop (Figure 2). Small, irregular chromite ore bodies occur within the serpentinite, but the ore is of rather low grade, containing a maximum of only about 25% Cr₂O₃ (Hatch, 1910). Possibly more significant, however, are the Cu, Ni and Co sulphides which are disseminated within the lowermost pyroxenitic and peridotitic rocks. A diamond drill hole sunk in the NE portion of the complex gave peak results of 0,12% Cu, 0,25% Ni, and 0,027% Co over 3,1 m (Versveld, 1981). The Tugela Rand Suite represents the product of alkali basalt magmatism at ~1200 Ma which was intruded prior to the main deformation and metamorphism (Wilson, 1990).

Mambula Complex

The Mambula layered mafic complex intrudes amphibolites of the Tugela Group near the confluence of the Tugela and Mambula Rivers, 20 km east of Kranskop (Figure 2). It consists largely of medium-grained gabbro with subordinate norite, websterite, and vanadium-bearing titaniferous magnetite layers, together with concordant, coarse-grained to pegmatitic diallagite and anorthosite dykes and sills (Schulze-Hulbe 1979). Contacts dip radially towards the centre of the body, implying a broadly saucer-shaped geometry. At least six magnetite-rich layers from 1 m to 5 m thick are recognized (Reynolds, 1986). These consist of up to 90% V-Ti-magnetite, ilmenite, and pleonaste. Trace amounts of sulphides (pyrrhotite, pentlandite, cubanite, chalcopyrite and pyrite) have been recorded. The lateral and vertical extents of the ore horizons are uncertain, but Luyt (1976) estimated ore reserves to be 22 Mt at an average grade of 45,92% Fe, 11,53% TiO₂ and 0,56% V₂O₅. The Mambula Complex formed by the fractional crystallization of a mafic magma and the ores themselves accumulated during the latter stages of the crystallization sequence (Reynolds, 1986). The more felsic and Fe-rich nature of the Mambula Complex suggests that it represents the higher part of a layered complex than the Tugela Rand body (Reynolds, 1986). It is uncertain whether both bodies are the result of the same magmatic episode, though both were intruded prior to the main regional tectonometamorphic event, and dismembered by northward-directed thrusting.

Alkaline complexes

Three distinct localities of peralkaline rocks have been recognized in the northeastern part of the Tugela Terrane. Each contains subeconomic occurrences of various elements which are typically associated with alkaline and A-type granite complexes (Scogings, 1989). These include localized Zr and Nb (zircon and pyrochlore) concentrations in syenitic and carbonatitic gneisses at Bull's Run (Von Backström, 1962; Scogings & Forster, 1989); Nb, Zr, Y, Sn and REE anomalies in quartz-magnetite-zircon 'blows' in peralkaline rocks of the Ngoye Complex (Scogings, 1986), and local concentrations of Zr, Nb, Y, Zn, and REE in the alkaline gneisses of the Wangu Hill area (Figure 2).

Mineralization in the Mzumbe Terrane

The northern part of the Mzumbe Terrane, from the Mapumulo thrust to Durban, has been neither geologically mapped in detail, nor systematically prospected. The late-tectonic rapakivi granites and sulphide-bearing charnockites of the Oribi Gorge Granitoid Suite, which constitute ca. 60% of the surface area of this region, appear to be barren. South of the latitude of Durban, the belt has been more comprehensively studied, and minor Cu-Ni (in gneisses of the Mapumulo Group), U-Th (in alaskitic and pegmatitic rocks) and W (in calc-silicate rocks) occurrences have been documented. The most interesting deposits, however, are the enigmatic gold occurrences of the 'Umzinto Goldfield', the western sector of which boasts the only intermittently working gold mine in the Natal Metamorphic Province - the Dumisa Mine.

Shear zone-hosted gold

In the southern part of the Mzumbe Terrane, the 'Umzinto Goldfield' comprises 16 Au occurrences, prospects and, old mines, including the partially reopened Dumisa Mine (Figure 1). The nearby Alfreda Mine is reportedly reopening in the near future. The host rocks of the 10 known Au occurrences in the western sector are highly sheared, leucocratic, syntectonic granite gneisses of the Mzimlilo Suite, and fine-grained pink, acid gneisses of uncertain origin (Thomas & Gain, 1989). In the eastern sector of the 'goldfield', the Mzimlilo granites and banded gneisses of the Quha Formation constitute the host rocks. In general, the gold in all the occurrences appears to be both disseminated in the sheared host rocks and concentrated in later *en echelon* quartz-sulphide vein arrays. Thomas & Gain (1989) noted that the geological setting at Dumisa is similar to that at the Renco Mine, Zimbabwe.

W-Mo in Ca-rich gneisses

Minor scheelite mineralization in amphibolites, diopside-rich gneisses and magnetite quartzites in the Mvoti River valley, constitute the only known metalliferous occurrences north of Durban (Figure 1). Schutte (1976) and Du Preez (1976) considered this mineralization to be of pegmatitic origin, whereas Stephan (1977) argued that the scheelite (which is hosted in Ca-rich gneisses) resulted from the metasomatic interaction of W-bearing pegmatitic fluids with the country rocks. The scheelite takes the form of white, subhedral grains and stringers in saccharoidal, greyish-green, diopside-hornblende gneisses. These rocks are associated with cherts and magnetite quartzites which are possibly of chemical origin. There is a significant dearth of granitic or pegmatitic rocks in the immediate vicinity of known mineralization. Consequently, Scogings (1984), found no significant amounts of W in the pegmatites of the general area and concluded that the mineralization was of stratiform, sedimentary-exhalative type. A similar mode of origin has been proposed for most of the tungsten deposits in Namaqualand (Bowles, 1988), and the Mittersill scheelite deposit in Austria (Thalhammer *et al.*, 1989). Minor Mo showings have been recorded from the Mvoti River area, but the scheelite itself is Mo-poor.

The presence of alluvial scheelite in the Mpambanyoni

River valley west of Umzinto, has long been known (Hatch, 1910). Additionally, a loose boulder of calc-silicate gneiss containing >300 ppm W has been collected from this general area (Andreoli & Hart, 1985). These anomalies are probably associated with fairly extensive tourmaline-bearing, calc-silicate horizons which have been identified in the Mpambanyoni River (Thomas, 1989b).

Cu-Mo in granitoids and Cu-Ni in ultramafic rocks

A Cu-Mo showing is known from the Mfume area, 30 km SW of Durban (Figure 1). The copper occurs as chalcopyrite disseminated in banded gneisses of the Mapumulo Group and as secondary malachite. Scattered values of up to 0,78% Cu were obtained with minor Mo, along an old adit. Two small Cu-Ni anomalies have been documented from the area West of Durban (Figure 1), hosted by small serpentinite bodies within gneisses of the Mapumulo Group (Schutte, 1976). However, the Ni and Cu is contained within silicate minerals.

U-Th in pegmatites and alaskites

In the Umzinto area, 60 km SW of Durban (Figure 1), a number of U and U-Th anomalies have been discovered as a result of recent exploration projects (Evans, 1984). Most of these are associated with biotite-bearing pegmatites and alaskites, with localized U concentrations up to 900 ppm (Hart & Barton, 1984). An occurrence of a quartz-xenotime rock with 53% modal xenotime gave U and Th concentrations of 1,26% and 1,88% respectively (Evans, 1984). Andreoli & Hart (1985) concluded that the U-Th mineralization in this area was concentrated in the pegmatites themselves and/or associated with shear zone-related polymetallic vein systems.

Mineralization in the Margate Terrane

The granulite facies Margate Terrane is the most barren area of the Natal belt. No metalliferous occurrences have, to date, been identified within it. Ironically however, the most important economic deposit of the Natal Metamorphic Province is located in the Margate Terrane - the extensive and valuable marbles which are exploited at 'Marble Delta', near Port Shepstone.

Discussion, conclusions and some speculations

The main findings of this study can be summarized as follows:

1. Mineralization in the Natal Metamorphic Province is not uniformly distributed in the three major tectonostratigraphic terranes recognized. The greenschist to amphibolite facies Tugela Terrane is the most well-endowed with metals. Mineral occurrences become more sparse to the south, into the higher-grade terranes, such that no metalliferous showings are known from the granulite-charnockite Margate Terrane. So little of the recently discovered amphibolite terrane in northern Transkei is exposed that no occurrences have been identified there (Thomas & Mawson, 1989).

2. Eighty percent of the Mzombe and Margate Terranes are made up of granitoids which, except for very localized U (Th) showings in pegmatites and alaskites, are barren. Other mineralization is hosted in supracrustal gneisses which

constitute less than twenty percent of the Mzombe and Margate Terranes, but a far higher proportion of the Tugela Terrane.

3. The abundance of epigenetic gold occurrences in the Tugela Terrane can possibly be attributed to the voluminous, oceanic basic metalavas of the Mfongosi and Tugela Groups, which may represent the original source of the gold (eg. Anhaeusser, 1986). It is suggested that the precious metals were leached from the mafic rocks, firstly by seawater interaction, and then by prograde metamorphic dewatering. These mineralized fluids would have migrated upwards along syntectonic thrust planes during the obduction event. Ore deposition subsequently occurred at shallower levels in shear zones. Syntectonic sodic granitoids were a source of some of the metals (Cu-Ag at Mfongosi), whereas other deposits may be related to early volcanogenic exhalative activity. Yet another possible source for the gold could have been the greenstone remnants which are exposed along the southern margin of the Kaapvaal Craton, and which may presently underlie the imbricate thrust front. Recent gravity modelling by Barkhuizen & Matthews (1990) suggested that the Archaean rocks extend for at least 30 km to the south of the thrust front, beneath the Tugela Terrane.

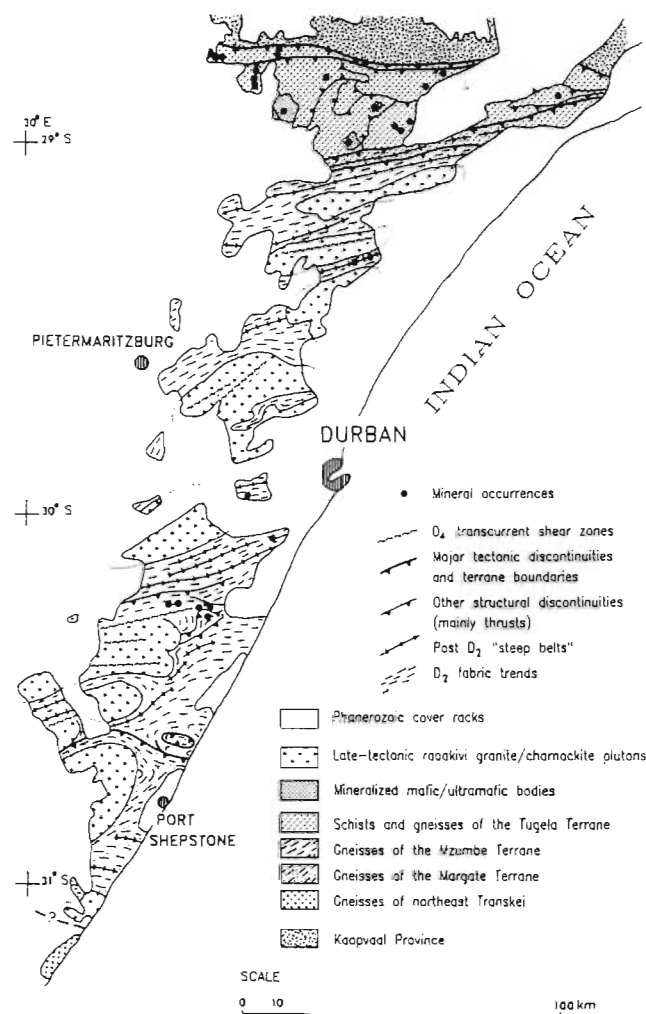


Figure 7 Major tectonic features and mineral occurrences in the Natal Metamorphic Province (features in the Tugela Terrane from Matthews & Charlesworth, 1981).

4. The final location of the mineralization is structurally controlled (Figure 7). As previously outlined, the epigenetic precious metals are thrust and shear-zone related. In the Tugela Terrane, the mineralized Alpine-type, syntectonic serpentinite bodies were probably intruded along major structural discontinuities (Matthews, 1972). The Tugela Terrane is characterized by extensive thrusting and shearing, as a result of oceanic obduction during the Proterozoic, particularly in the thrust front (Matthews, 1972). It thus contains a large number of important structural discontinuities, with the imbricate thrust front in the north and the flat-lying, thrust-bounded nappes to the south (Figure 7). Structural control on mineralization is also evident in the Mzumbe Terrane. The most heavily mineralized part of this area is located west of Umzinto, where Au, W, and U-Th anomalies have been recorded. This is a tectonically complex region with many local structural discontinuities of different ages (Figure 7). It is suggested that the various thrusts and shear zones within the Province acted as zones of crustal weakness and channels not only for the migration of metalliferous fluids and uranium-bearing late-stage differentiates, but also for the emplacement of mineralized, Alpine-type, ultramafic intrusions. The layered complexes of the Tugela Terrane are pre-thrusting in age, and are thus probably separated from their roots. This feature is clearly important in the estimation of ore reserves. It also leaves open the possibility of further allochthonous thrust slices of similarly mineralized rocks at relatively shallow depths within the nappe zone of the Tugela Terrane.

5. Although the Natal Metamorphic Province has not been an important source of metallic minerals, it appears that the area is not without potential, with the i'Thuma body being especially significant. In addition, the fairly extensive schist and gneiss belts of the Mzumbe Terrane north of Durban have never been systematically examined, neither have the remoter parts of the Tugela Terrane. It is furthermore clear that the areas along strike, both east and west from the Umzinto Goldfield deserve further investigation. The apparently barren, granulite facies, Margate Terrane in the far south, would appear to have the least potential with respect to metalliferous ores, though the extremely poorly exposed Mellville shear zone area should possibly be the subject of a more detailed economic study.

6. In conclusion, the mineralization described here is consistent with envisaged models for the evolution of the Natal Metamorphic Province. The northern part of the belt has been interpreted as a Proterozoic oceanic ophiolite complex (Matthews, 1972; 1981a), with a coeval volcanic arc in the Mzumbe Terrane to the south (Matthews, 1981b; Thomas & Eglington, 1990). Thomas & Eglington suggested, furthermore, that this magmatic arc evolved in response to southward-directed subduction of the 'Tugela Ocean'. Thus, the Tugela Terrane is seen in terms of an oceanic basin, with localized sea-floor spreading giving rise to the tholeiitic lavas of the i'Thuma Formation. Volcanogenic exhalations on the ocean bed, adjacent to spreading centres, gave rise to the massive/semimassive sulphide body at i'Thuma. Limited hot-spot activity led to the development of alkali basalt seamounts, the roots of

which are now exposed as the Tugela Rand and Mambula intrusions (A.H. Wilson, pers. comm.). The production of peralkaline granitoids and associated mineralization took place at this time of localized tensional tectonics immediately to the south of the Kaapvaal Craton. In this regard, it is significant that the alkaline-type mineralization is confined to the Nkomo Nappe, the lowest structural unit of the nappe zone, and the one which is closest to the craton margin. Terrane accretion, northward thrusting, and obduction of the Tugela ophiolite onto the Kaapvaal Craton then ensued, accompanied by the emplacement of mineralized, alpine-type serpentinites. During this main tectogenesis, metamorphic dewatering caused mobilization and concentration of precious and base metals in extensive shear zones.

The tectonic evolution of the southern terranes is not as well understood. It has been suggested that the entire belt evolved from the accretion of successive tectonic fragments from the south, and that the Mzumbe and Margate Terranes may both have had comparable early histories as calc-alkaline magmatic arcs (Thomas, 1989a; Thomas & Eglington, 1990). Localized Ca-rich mafic volcanic and sedimentary rocks in this arc-type setting hosted restricted tungsten mineralization (cf. Thalhhammer *et al.*, 1989). The gold in the Mzumbe Terrane was mobilized and concentrated in shear zones, as in the Tugela Terrane, but the source rocks are more likely to have been acid igneous rocks (Thomas & Gain, 1989). The high thermal input from voluminous granitoid melts in the Mzumbe and particularly the Margate Terranes have rendered these areas far more barren than the Tugela Terrane.

Acknowledgements

RJT and WDB thank the Chief Director, Geological Survey, for permission to publish this article. The authors are also grateful to Kobus Minnaar for translating the abstract into Afrikaans. Professors D.R. Hunter and R. Jacob kindly reviewed the original manuscript and made many valuable suggestions for its improvement.

References

- Andreoli, M.A.G. & Hart, R.J. (1985). *Mineral potential of the Braemar area, S. Natal*. Unpubl. NRRU. Rep., 85/03, 4 pp.
- Anhaeusser, C.R. (1986). Archaean gold mineralization in the Barberton Mountain Land, 113-154. In: Anhaeusser, C.R. & Maske, S. (Eds.), *Mineral Deposits of Southern Africa*, I, Geol. Soc. S. Afr., Johannesburg, 2335 pp.
- Barkhuizen, J.G. & Matthews, P.E. (1990). Gravity modelling of the Natal thrust-front: A mid-Proterozoic crustal suture in southeastern Africa. *Ext. Abstr. Geocongress '90, Geol. Soc. S. Afr., Cape Town*, 32-35.
- Bowles, M. (1988). Metallogeny of stratabound tungsten mineralization in the Namaqualand Metamorphic Complex, northwest Cape, South Africa - a consanguineous view. *S. Afr. J. Geol.*, **91**, 248-258.
- Brown, G.J. (1988). *Ngubevu Zinc, Msinga, KwaZulu*. Rep. (unpubl.), South African Development Trust, 2543, 18 pp.
- De Beer, J.H., Van Zijl, J.S.V. & Gough, D.I. (1982). The southern Cape Conductive Belt: its composition, origin and tectonic significance. *Tectonophysics*, **83**, 205-225.

- Du Preez, J.W. (1976). *Mineral occurrences in KwaZulu*. Unpubl. Rep., Geol. Surv. S. Afr., 1976-0017, 8 pp.
- Du Toit, A.L. (1931). The geology of the country surrounding Nkandla, Natal. *Expl. sheet 109 (Nkandla)*. Geol. Surv. S. Afr., 105 pp.
- Eglington, B.M., Harmer, R.E. & Kerr, A. (1989). Isotope and geochemical constraints on Proterozoic crustal evolution in south-eastern Africa. *Precambrian Res.*, 45, 159-174.
- Evans, M.J. (1984). *Precambrian geology west of Scottburgh, Natal*. M.Sc. thesis (unpubl.) Univ. Natal, Durban, 158 pp.
- Harmer, R.E. (1979). *Pre-Cape geology of the Tugela Valley north of Kranskop, Natal*. M.Sc. thesis (unpubl.) Univ. Natal, Durban, 235 pp.
- Hart, R.J. & Barton, E.S. (1984). The application of U-Th-Pb isotope systematics in the investigation of potential uranium source rocks in the Natal Precambrian basement. *Trans. geol. Soc. S. Afr.*, 87, 73-78.
- Hatch, F.H. (1910). *Report on the Mines and Mineral Resources of Natal (other than Coal)*. Clay & Sons, London, 155 pp.
- Hedges, J.S. (1906). Annual Report of the Inspector of Mines, Eastern Mines Department District, 8. In: Gray, C.J., *Report on the Mining Industry of Natal for the Year 1905*. Times Printing & Publishing, Pietermaritzburg.
- (1909). Annual Report of the Inspector of Mines, Eastern Mines Department District, 41. In: Gray, C.J., *Report on the Mining Industry of Natal for the Years 1907 and 1908*. Times Printing & Publishing, Pietermaritzburg.
- Knoetze, J.S.P. (1988). *Finale verslag: eksplorasi op die ysterhoed voorkomste en nikkell/koper mineralisasie te Sebezani, Kwazulu*. Unpubl. FOSKOR Rep., 26 pp.
- Large, R., Huston, D., McGoldrick, P., Mc Arthur, G. & Ruxton, P. (1988). Gold distribution and genesis in Palaeozoic volcanogenic massive sulphide systems, eastern Australia. In: Goode, A.D.T. & Bosma, L.I. (Compilers), *Bicentennial Gold, '88, Ext. Abstr.*, Geol. Soc. Aust., 121-126.
- Luyt, J.F.M. (1976). Vanadium, 241-245. In: Coetzee, C.B., (Ed.), *Mineral Resources of South Africa*. Handbk. geol. Surv. S. Afr., 7, 478 pp.
- Maiden, K.J. (1984). Metamorphic features of the Maranda J copper-zinc deposit, Murchison greenstone belt, Transvaal. *Trans. geol. Soc. S. Afr.*, 87, 335-345.
- Matthews, P.E. (1959). The metamorphism and tectonics of the pre-Cape formations in the post-Ntingwe Thrust-Belt, S.W. Zululand, Natal. *Trans. geol. Soc. S. Afr.*, 62, 257-322.
- (1972). Possible Precambrian obduction and plate tectonics in southeastern Africa. *Nature*, 240, 37-39.
- (1981a). Eastern or Natal sector of the Namaqua-Natal mobile belt in southern Africa, 705-715. In: D.R. Hunter (Ed.), *Precambrian of the Southern Hemisphere*. Elsevier, Amsterdam, 882 pp.
- (1981b). A new tectonic model for the northern region of the Namaqua-Natal belt in Natal. *Abstr. S. Afr. geodyn. Symp., Geocongress '81*, Geol. Soc. S. Afr., 150-151.
- & Charlesworth, E.G. (Compilers) (1981). *Northern margin of the Namaqua-Natal mobile belt in Natal*. 1:140 000 scale geological map, Colorgraphic, Durban, 1 sheet.
- Nicolaysen, L.O. & Burger, A.J. (1965). Note on an extensive zone of 1 000 million-year old metamorphic and igneous rocks in southern Africa. *Sciences de la Terre*, 10, 497-518.
- Reynolds, I.M. (1986). The mineralogy and petrography of some vanadium-bearing titaniferous iron ores of the Mambula Complex, Zululand, 1695-1708. In: Anhaeusser, C.R. & Maske, S. (Eds.), *Mineral Deposits of Southern Africa*, II, Geol. Soc. S. Afr., Johannesburg, 2335 pp.
- Ryan, P.J., Lawrence, A.L., Lipson, R.D., Moore, J.M. Paterson, A. & Stedman, D.P. (1986). The Aggeneys base metal sulphide deposits, Namaqualand district, 1447-1473. In: Anhaeusser, C.R. & Maske, S., (Eds.), *Mineral Deposits of Southern Africa*, II, Geol. Soc. S. Afr., Johannesburg, 2335 pp.
- Schulze-Hulbe, A. (1979). *A study of the structure and metamorphism of the rocks of the Tugela Group exposed in the Mambula-Mbogolwane area, Natal*. M.Sc. thesis (unpubl.), Univ. Natal, Durban, 229 pp.
- Schutte, D.J. (1976). *The mineral potential of KwaZulu*. Unpubl. Rep. geol. Surv. S. Afr., 1976-0019, 23 pp.
- & Schurink, H. (1986). *Gossan occurrences and copper-nickel mineralization in the Sebezani area, KwaZulu*. Rep. (unpubl.), South African Development Trust, 2265, 30 pp.
- Scogings, A.J. (1984). *Final report on the Mvoti scheelite deposit*. Rep. (unpubl.), South African Development Trust, 1987, 12 pp.
- (1986). Peralkaline gneissic granites in the Ngoye Granite-Gneiss Formation, Natal. *Trans. geol. Soc. S. Afr.*, 89, 361-366.
- (1989). Peralkaline granite and alkaline mafic gneisses, northwest of Eshowe, Natal. *S. Afr. J. Geol.*, 92, 339-351.
- & Foster, I.F. (1989). Gneissose carbonatites in the Bull's Run Complex, Natal. *S. Afr. J. Geol.*, 92, 1-10.
- Slack, J.F. (1982). Tourmaline in Appalachian-Caledonian massive sulphide deposits and its exploration significance. *Inst. Min. Metall.*, 91, B81-B89.
- Smalley, T.J. (1980). *Structure and metamorphism at the Tugela Group within the northern zone of the Natal Mobile Belt*. Ph.D. thesis (unpubl.), Univ. Natal, Durban, 220 pp.
- Stephan, L.A. (1977). *Report on the Mvoti scheelite occurrence in Natal*. Unpubl. Rep. geol. Surv. S. Afr., 1977-0030, 3 pp.
- Thalhammer, O.A.R., Stumpf, E.F. & Jahodah, R. (1989). The Mittersill scheelite deposit, Austria. *Econ. Geol.*, 84, 1153-1171.
- Theart, H. (1981). *The Tugela Fault project*. Rep. (unpubl.), South African Development Trust, 1190, 17 pp.
- Thomas, R.J. (1989a). A tale of two tectonic terranes. *S. Afr. J. Geol.*, 92, 306-321.
- (1989b). *Geological mapping of high-grade terranes in a sub-tropical environment - the Proterozoic rocks of southern Natal*. Winter Field School Guide, Geol. Soc. S. Afr., 46 pp.
- (1990). Metallogenesis in a Kibaran accreted terrane: the Natal Metamorphic Province, South Africa. *I.G.C.P. No.255, Newsletter/Bulletin*, 3, 93-99.
- & Gain, S.B. (1989). The geological setting of gold mineralization at Dumisa, Natal. *S. Afr. J. Geol.*, 92, 410-419.
- & Mawson, S.A. (1989). Newly discovered outcrops of Proterozoic basement rocks in northeast Transkei. *S. Afr. J. Geol.*, 92, 369-376.
- & Eglington, B.M. (1990). A Rb-Sr, Sm-Nd and U-Pb zircon isotopic study of the Mzumbe Suite, the oldest intrusive granitoid in southern Natal, South Africa. *S. Afr. J. Geol.*, 93, (in press).
- Wilson, A.H. (1990). Tugela Rand Layered Suite. In: M.R. Johnson, (Ed.), *Catalogue of South African Lithostratigraphic Units*. S. Afr. Comm. Strat. 2, 47-48.

- Wuth, M.G. & Archer, P.D. (1986). Chromite mineralization at Sithilo, Northern Zululand, 1689–1694. *In*: Anhaeusser, C.R. & Maske, S. (Eds.), *Mineral Deposits of Southern Africa*, II, Geol. Soc. S. Afr., Johannesburg, 2335 pp.
- Versveld, A (1981). *Final report on a portion of the Tugela*

- Location, Kranskop District, Kwazulu*. Int. Rep., Anglo American Prospecting Services, 23 pp.
- Von Backström, J.W. (1962). Zircon, ilmenite and monazite occurrences on Bull's Run Estate, north-northwest of Eshowe, Natal. *Ann. Geol. Surv. S. Afr.*, 1, 137–146.

23RD EARTH SCIENCE CONGRESS OF THE
GEOLOGICAL SOCIETY OF SOUTH AFRICA

ABSTRACTS



2 - 6 JULY 1990

**ALKALINE / PERALKALINE GNEISSES NEAR THE NORTHERN MARGIN
OF
THE NATAL STRUCTURAL AND METAMORPHIC PROVINCE**

A.J. Scogings. Mineral Development, STK, P.O.Box 213
Pretoria 0001.

INTRODUCTION

Alkaline / peralkaline gneisses occur within three granitoid complexes at Ngoye, Bull's Run and Wangu, near the northern margin of the 1100 Ma Natal Structural and Metamorphic Province (NSMP). A wide range of rock types is present, from nepheline syenite gneisses through to peralkaline granite gneisses, with minor carbonatite and monzodiorite gneiss intrusive phases noted within two of the bodies. It is suggested that the three alkaline gneiss occurrences so far mapped constitute the remnants of a metamorphosed alkaline magmatic province, and that such magmatism occurred either in a post-collisional or anorogenic post-D1, pre-D2 tectonic setting. The three complexes are described below with respect to mineralogy and chemistry, followed by a brief overview of the possible tectonic setting at the time of their intrusion, on the basis of research by Scogings (1986, 1989) and Scogings & Forster (1989).

NGOYE

This is a whaleback massif 30 km in length located at the eastern extremity of the NSMP and, on the basis of alumina saturation relative to alkalis, there are three granitoid gneiss varieties within the Ngoye Complex*:

Peraluminous gneisses; consisting of quartz, albite and microcline with minor amounts of biotite, muscovite and garnet. Geochemically distinct, these rocks are silicic, moderately peraluminous and characterised by high Rb, Th and U contents, but have low Zr, Sr and Ba values (N11, Table 1).

Metaluminous gneisses; consisting of quartz, albite / oligoclase and microcline with biotite and hastingsite the characteristic mafics. The HFS elements Nb, Zr, Y and REE, in addition to Ba and Sr, are enriched relative to the peraluminous gneisses. Rb, U and Th however relatively depleted (N675, Table 1). A plug-like body of monzodiorite crops out within the metaluminous gneisses, and comprises plagioclase, microcline, diopside, hornblende and calcite.

Peralkaline gneisses; comprising quartz, albite and microcline, with the diagnostic sodic minerals riebeckite and aegirine. Magnetite may occur to the exclusion of the sodic mafics, especially along the southern flanks of the massif. The magnetite gneisses are fine grained and host

coarse-grained quartz-magnetite pods enriched in zircon, sphene and fergusonite. Both major and trace element chemistry reflect the peralkaline heritage of this group of gneisses; namely depletion in alumina relative to alkalis ($\text{Na}+\text{K}/\text{Al} = 1,05$), extremely low CaO & Sr and enhanced Zn, Nb, Zr & Y contents (N331, Table 1). Chondrite-normalised REE patterns are typical for peralkaline granites. The quartz-magnetite pods have quite unusual trace element chemistry, containing highly anomalous amounts of Zn, Nb, Zr, Y, REE (particularly the HREE), U, Th, Pb and Sn (NR189, Table 1).

BULL'S RUN

The Bull's Run Complex* (BRC) forms an easterly-trending ridge rising to 400m above the Mhlathuze River and is located 15km north of Eshowe. The BRC has been subdivided into two broad lithotypes, in which an envelope of biotite-muscovite syenite gneiss surrounds a core of various nepheline syenite gneisses. Minor intrusive phases include gneissose peralkaline microsyenite dykes and carbonatite sheets, generally restricted to areas underlain by biotite-muscovite syenite gneiss.

Biotite-muscovite syenite gneiss; granitoid gneisses comprising microcline, albite, muscovite and biotite, with accessory calcite, apatite and sphene. Chemically this unit is silica-saturated and depleted in alkalis relative to alumina ($\text{Na}+\text{K}/\text{Al} = 0,70$), with low concentrations of incompatible elements such as Zr, Y, REE, U and Th (B105, Table 1). High Sr values in this lithotype are related to modal calcite, suggesting derivation of the calcite from a carbonatitic source.

Nepheline-syenite gneisses form the core of the BRC and are compositionally zoned, from an outer zone of coarse-grained highly undersaturated syenites, through to an inner zone of fine-grained relatively siliceous material. The gneisses of the outer zone consist predominantly of nepheline, microcline, albite and cancrinite with biotite and hornblende the diagnostic mafic phases. Geochemically the outer zone is distinguished from the inner zone on the basis of lower silica contents (B80, Table 1) and from the muscovite-bearing gneisses by higher alkali to alumina ratios ($\text{Na}+\text{K}/\text{Al} = 0,85$). Chondrite normalised REE patterns are typical for alkaline rocks. The inner zone gneisses, comprising albite, nepheline and microcline, are sodic (B220A, Table 1) and have peralkaline tendencies ($\text{Na}+\text{K}/\text{Al} = 0,95$) with high concentrations of HFS elements such as Nb and Zr hosted by pyrochlore and zircon.

Carbonatite gneiss sheets; these are of particular interest as metamorphosed carbonatites are not a widely recognised

rock type. Field relationships, mineralogy and chemistry have been described by Scogings & Forster (1989) and it suffices to note their rock composition, comprising modal calcite, apatite, biotite, pyrochlore and zircon. Trace elements are distinctive, with typical magmatic carbonatite Sr, Nb and REE contents (B46, Table 1).

WANGU

Peralkaline gneisses have recently been described from a 6km long granitoid body on Wangu Hill, to the west of Bull's Run (Scogings, 1989). These fine-grained rocks were previously incorporated into the Halambu Formation, a widely distributed unit of calc-alkaline granodioritic gneisses. Mafic biotite-rich gneisses are also noted and apparently intrude the peralkaline granitoids.

Peralkaline granitoid gneisses; modally they have a wide range in compositions, but essentially comprise quartz, albite, microcline, aegirine-augite, magnetite and riebeckite. They are depleted in alumina relative to alkalis (Na+K/Al up to 1.33), are enriched in iron (FeO up to 22%), and have trace element contents typical of peralkaline granitoids with elevated Zn, Zr, Nb, Y and REE, and low Ba and Sr (W235 & W232, Table 1). Chondrite-normalised REE patterns are similar to the Ngoye peralkaline gneisses.

Alkaline mafic gneisses; sheets of biotite-rich gneiss up to 30m long exhibit intrusive relationships and comprise modal biotite, albite, microcline, apatite and calcite. Chemically quite distinct, some samples are highly undersaturated with normative leucite and high Zn, Nb, Rb, Sr and Ba contents typical of alkaline mafic rocks (W228, Table 1). REE patterns are typical of alkaline mafic rocks.

TECTONIC SETTING

The major and trace element data from Ngoye and Wangu have been plotted on a wide variety of tectonic discrimination diagrams. These indicate that the peralkaline and associated granitoid gneisses are metamorphic derivatives of A-type granites which generally occur as anorogenic central complexes, such as the Nigerian younger granites. A-type granites are also noted to intrude into post-collisional tectonic settings and on attenuated continental margins. The nepheline syenite / carbonatite association of Bull's Run is also typical of central complex magmatism, often developed within rift zones and in relatively stable continental settings. The discovery of alkaline gneisses in the NSMP indicates a magmatic event related to continental crust relaxation, or possibly even a rifting stage, prior to

northward obduction of the Tugela ophiolite onto the Kaapvaal Craton.

REFERENCES

Scogings, A.J. (1986). Peralkaline gneissic granites in the Ngoye Granite Gneiss Formation, Natal. Trans. geol. Soc. S. Afr., 89, 361-365.

----- (1989). Peralkaline granitoid and associated alkaline mafic gneisses northwest of Eshowe, Natal. S. Afr. J. Geol., 92, 339-351.

Scogings, A.J. and Forster, I.F. (1989). Gneissose carbonatites in the Bull's Run Complex, Natal. S. Afr. J. Geol., 92, 1-10.

Note:

* The term "complex" has not yet been accepted by SACS.

TABLE I

PARTIAL ANALYTICAL DATA: NGOYE, BULL'S RUN, WANGU GNEISSES

	N11	N675	N331	NRL89	B105	B80	B220A	B46	W235	W232	W228
SiO ₂	77,38	75,52	76,45	64,89	57,35	51,50	59,78	2,57	68,41	61,16	39,23
Al ₂ O ₃	12,96	11,77	11,32	1,29	20,79	21,86	22,23	1,08	11,96	5,79	12,25
FeO	0,75	2,78	2,38	27,36	3,95	4,67	2,02	3,73	6,57	21,55	12,57
CaO	0,25	0,63	0,34	0,86	2,18	3,69	0,19	48,53	0,67	2,82	6,83
Na ₂ O	4,48	3,97	4,11	0,43	4,41	7,90	8,79	0,11	4,21	3,90	1,55
K ₂ O	4,41	4,48	4,47	0,45	7,03	6,50	5,80	0,49	6,38	1,18	7,14
P ₂ O ₅	0,01	0,02	0,01	0,18	0,10	0,30	0,01	2,75	0,01	0,04	1,24
Zn	33	96	181	985	71	52	37	28	123	898	771
Nb	64	39	45	8797	201	167	494	2633	303	567	390
Zr	97	646	831	29605	439	200	1145	nd	1549	3076	273
Y	76	89	132	4780	11	12	3	102	133	385	86
U	14	4	3	394	nd	nd	32	nd	7	9	9
Th	32	11	18	1065	nd	6	nd	17	109	78	17
Rb	724	97	153	27	290	197	338	42	294	49	635
Ba	3	1207	50	50	1325	2037	91	132	62	287	1325
Sr	4	51	8	15	743	2055	145	8077	9	20	341
REE	124	434	616	11190	162	353	21	1564	1055	2305	659

NOTE: Major elements in %, traces in ppm; nd = not detected; REE = total REE



S.A. CERAMIC SOCIETY
21st ANNUAL SYMPOSIUM

PROCEEDINGS

IMPROVED CERAMIC MATERIALS

WEDNESDAY 28 JUNE 1989

BULL'S RUN NEPHELINE SYENITE

A NEW DEPOSIT - NEW PRODUCTS

Daly M.J., Germiquet J.D. and Scogings A.J.
Kidogo Mining CC, and SA Development Trust Corporation Ltd

SYNOPSIS

The Bull's Run Syenite Complex is situated in Kwazulu some 6 kms west of the railhead at Nkwaleni and approximately 60 kms from Richard's Bay.

Geological and metallurgical work carried out to date indicate that products suitable for glass and ceramic manufacture, comparable in quality to commercial nepheline syenites produced in Norway and Canada, can be obtained from recently explored areas of the Complex.

These materials, together with ilmenite and apatite which occur in small amounts, and possibly alumina and alkali products, demonstrate the potential of the Bull' Run Complex in terms of import substitution and export; its location and vast resources enhance this perception.

1.0 INTRODUCTION

Nepheline syenite is a silica-deficient crystalline rock consisting of albite, microcline feldspars and nepheline, together with varying but small amounts of mafic silicates and other accessory minerals. Nepheline-bearing rocks are widely distributed around the world but only in Canada, Norway, the Union of Soviet Socialist Republics, and the United States of America are deposits worked commercially on a large scale.

The majority of nepheline syenite produced in Canada and Norway is used in glass and ceramic manufacture; however, it is now finding increased acceptance in Europe and North America as an extender/filler in the paint and plastic industries. A similar pattern of use is anticipated for the nepheline syenite products from Bull's Run.

Since the U.S.S.R. production is geared primarily towards usage as a source of alumina, only Canada and Norway can be considered as strictly commercial producers; they currently export some 440 000 tons and 220 000 tons per annum respectively out of a total combined production of some 780 000 tons per annum.

In glass and ceramic sectors nepheline syenite faces competition from a variety of other natural and artificial feldspathic fluxes, whilst it competes with talc, barytes, kaolin and calcium carbonate in the filler applications.

Over the past few years, small quantities of nepheline syenite with a high iron content have been produced from a deposit near Pretoria and used locally in ceramic manufacture. Currently the primary feldspathic flux used in the glass and ceramic industries within South Africa is potassium feldspar from the Northern Cape and/or Eastern Transvaal. Reported local sales of feldspar in 1987 and

1988 were 60 000 tons and 75 000 tons per annum respectively.

Current work shows that nepheline syenite products - with varying iron levels - can be produced from the rocks making up the Bull's Run Syenite Complex; a low-iron soda feldspar rich product can also be obtained from within the same Complex. In the future, with further development and with an established track record in Southern Africa, the various nepheline syenite products should also be able to compete successfully overseas.

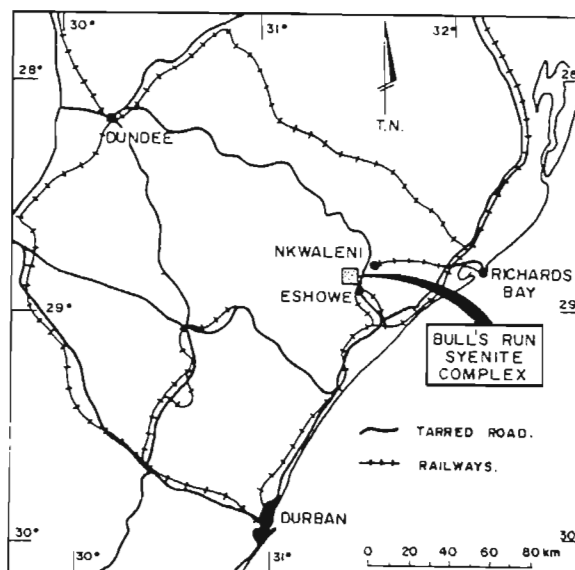


Figure 1

Figure 1 shows the location of the Complex, highlighting its ideal situation for both overseas and local markets.

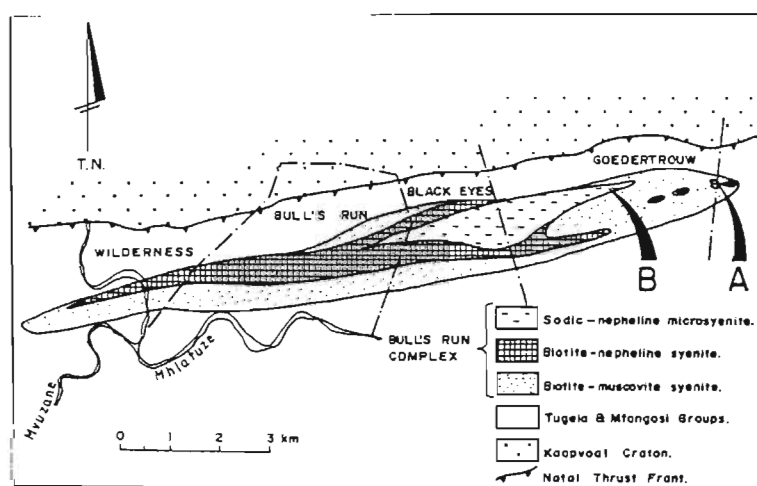
2.0 GEOLOGY

The Bull's Run Syenite Complex is situated in the Natal Mobile Belt where it forms an east-west elongated body approximately 15 kms long and up to 1,8 kms in width. A simplified lithological map is shown in figure 2. A detailed description of the various rock types is given by Scogings and Forster (1989, in press) while a comprehensive review of the structural features of the area has been made by Charlesworth (1981). In brief, the Bull's Run Complex displays a concentric outcrop pattern, with an envelope of biotite-muscovite syenite gneiss enclosing a core complex of nepheline-bearing syenite gneisses. Isolated carbonatite gneiss lenses occur at intervals along the length of the complex. The syenitic gneisses are characterised by a penetrative east-west planar fabric which dips to the south at an average of about 60°.

As indicated in figure 2 the Bull's Run Complex is surrounded by amphibolitic and granitoid schists and gneisses of the Tugela and Mfongosi Groups. A major structural feature of this area is the Natal Thrust Front, which delineates the boundary between the northern limits of the Natal Mobile Belt and the southern margin of the much older Kaapvaal Craton.

At present, the simplest geological model to explain the attitude and fabric of the complex is a series of vertical cylinders, made up of concentric rings of the different rock types, which have been compressed and stretched in an east-west direction.

The structure and mineralogy of the bodies are complex and further detailed geological, geochemical and geophysical work will need to be carried out in order to present the true picture of the geology of the Bull's Run Syenite Complex.



(AFTER SCOGINGS AND FORSTER 1989)

Figure 2. Bull's Run Syenite Complex : Geology

3.0 EXPLORATION

Reconnaissance mapping and sampling was carried out by Germiquet (1985, 1986a, 1986b) of the South African Development Trust Corporation Ltd (STK) over the Bull's Run Syenite Complex, which is situated in a particularly mountainous and rugged part of KwaZulu. Initial beneficiation tests indicated that a suitable glass-grade product could be produced from the coarse-grained nepheline syenite occurring within the complex.

Consequently, further mapping of the complex was carried out by STK (Mngomezulu, 1986) as well as by Scogings and Forster (1989); this latter study identified two previously unrecorded nepheline syenite occurrences on the eastern limits of the Complex (Target A, Figure 2).

In 1987 and 1988 more detailed mapping, surface sampling and processing were carried out by Kidogo Mining on the nepheline syenites from the eastern part of the complex; followed by the drilling of an inclined borehole funded by STK.

Petrographic studies were made of selected surface and borehole samples to assist in delineating the various lithologies and also to provide a link with magnetic separation data.

Based on the above information, recoverable reserves of nepheline syenite in the easternmost deposits are considered to be more than adequate to meet local market demand for feldspathic fluxes for at least the next 20 years, and provide a platform to penetrate overseas markets.

Resources of several hundred million tons of coarse-grained nepheline syenite occur in the central body of the complex over the farms Bull's Run Estate and Black Eyes. These areas are, however, currently inaccessible and will require detailed exploration and development work before they can be successfully exploited.

In addition, extensive but unproven reserves of a soda feldspar-rich nepheline syenite - also with flux potential have been identified in other deposits in the eastern part of the Bull's Run Complex as shown by Scogings and Forster (1989) (Target B, Figure 2).

4.0 BENEFICIATION

During the initial reconnaissance survey conducted by STK in 1985, the selected samples of predominantly coarse-grained nepheline syenite were obtained from various parts of the complex and submitted to Mintek to determine whether they could be upgraded by either wet or dry magnetic separation. The results were as follows:

Wet Magnetic Separation

Samples of coarse-grained nepheline syenite and of a leucocratic dyke were upgraded on a wet batch solenoid magnetic separator (WHIMS). The resultant products had iron contents and recoveries of 0.12% Fe_2O_3 and 54.3%, and 0.063% Fe_2O_3 and 82.2% respectively.

Dry Magnetic Separation

Two further samples of coarse-grained nepheline syenite (one from the west and the other from the east of the Complex) were obtained and beneficiated over a Neodymium Permroll; the resulting grades are shown in Table I. These initial results indicate that the major deleterious minerals (biotite, garnet, magnetite, ilmenite and sphene) can be successfully removed and a product suitable for flint glass and high quality ceramic manufacture produced which, as shown, is comparable to the Norwegian North Cape nepheline syenite (Table I, analysis 1).

Although it occurs only in minor amounts, the rejected ilmenite can be further upgraded to export quality.

Subsequent beneficiation of surface and borehole samples from the easternmost deposits carried out by Kidogo Mining, using a laboratory Carpcu dry high intensity induced roll separator, has validated the Mintek results and demonstrated that despite variations in recoveries and grades of the various types of nepheline syenite an acceptable low iron product can be achieved by blending.

Samples from the central and easternmost deposits contain varying amounts of apatite giving P_2O_5 levels ranging from 0,05% to 2,30%. Heavy media separation tests indicate that these levels can be reduced to less than 0,05% yielding a phosphate product suitable for the local or export market.

Dry magnetic separation of samples from the eastern soda-rich nepheline syenite deposit (Target B) yields a low iron product (sample c) generally similar to the 'B' glass-grade product (sample 2) from Indusmin of Canada, as shown in Table I.

The detailed metallurgical and petrographic work carried out therefore indicates that the introduction of a process plant comprising a wet high induced magnetic separator and spirals/cyclones will provide a range of nepheline syenite products from the Bull's Run Syenite Complex at high yields, and with marketable by-products of ilmenite and apatite. The product specifications, in particular the iron contents, can be tailored to meet market requirements both locally and overseas.

In addition to affording high recoveries and grades, wet processing improves the efficiency of milling and classifying the nepheline syenite and minimises potential health and environmental problems.

TABLE I

Magnetically Beneficiated Syenites, Major Element Oxides (%).

	A	B	C	1	2
SiO ₂	56,80	55,71	62,8	55,7	59,7
TiO ₂			0,00		0,00
Al ₂ O ₃	23,56	23,45	20,6	23,9	23,5
Fe ₂ O ₃	0,12	0,08	0,35	0,12	0,35
MgO			0,23		0,10
CaO			0,64		0,50
Na ₂ O	9,12	8,69	9,20	8,20	10,20
K ₂ O	7,54	7,25	4,69	8,57	5,00
P ₂ O ₅			0,04		0,00
LOI	1,68	1,96	1,03	0,91	0,60

NOTES: A = Nepheline syenite, western Bull's Run Complex
 B = Nepheline syenite, eastern Bull's Run Complex
 C = Soda-rich nepheline syenite, Bull's Run Complex
 1 = Norwegian North Cape nepheline syenite
 2 = "B" glass-grade product, Indusmin, Canada

All Bull's Run analyses by fused disc XRF techniques.

5.0 END USES

Nepheline syenite from the Canadian and Norwegian producers is used primarily in the manufacture of glass and ceramics, and in micronised form as an extender and filler in paint, plastics and rubber. In the Soviet Union it is used in increasing quantities in the manufacture of alumina, alkali carbonates, and portland cement and, to a lesser degree, in the manufacture of coloured container glass. Nepheline syenite is also used in the manufacture of mineral wool and fibreglass, and as an ornamental stone for internal decoration.

Glass

By far the largest use of nepheline syenite is in the manufacture of a range of glass products including container glass, opal glass, flat glass and tableware glass. Nepheline syenite provides necessary additions of alumina and alkalis in the glass batch as it is low in silica and contains no free quartz. Nepheline syenite-bearing glass batches have lower viscosity and easier workability compared with those containing potash feldspar.

The lower fusion point of nepheline syenite lowers the melting temperature of the glass batch with attendant faster melting, higher productivity and fuel savings.

Its high alumina content acts as a stabiliser and improves the durability of the finished product by increasing resistance to impact, bending and thermal shock. Because of these characteristics, significantly less nepheline syenite need be used in the batch than is the case with other feldspathic fluxes, resulting in favourable overall cost savings.

In Canada about 70% of nepheline syenite is used for glass manufacture and the majority of the export product is used for glass-making in the United States. Some 85% of Norwegian production is glass grade nepheline syenite - used mostly in the UK and Europe.

Ceramic Ware

Nepheline syenite is used in making a wide range of ceramic products where it contributes to the production of the glassy phase which binds other constituents together and gives strength to the ware.

In Europe and North America, the main ceramic application of nepheline syenite lies in the manufacture of a large variety of vitreous whitewares, which have iron contents of 0,1% or less. These include institution - and some fine - tableware, sanitaryware, floor and wall tiles, and a range of porcelain bodies. In the case of electrical porcelain, the strict requirements of whiteness, translucency and refractoriness are often relaxed in order to use fluxes like nepheline syenite that provide better electrical properties.

Apart from these applications, nepheline syenite is used as a frit ingredient in glazes, enamels and structural clay products.

The ready fusibility and abundant fluxing capacity of nepheline syenite enable economies to be made by permitting reduced body flux content and lower firing temperatures or faster firing schedules.

Extender Pigment and Fillers

Applications for nepheline syenite in micronised form as extender pigments and inert fillers have been found and developed. These include exterior and interior latex and alkyd paint systems, traffic paints, metal primers, exterior wood stains, sealers, undercoats and hardboard

ground coats. In these applications nepheline syenite has desirable high dry brightness, high bulking value, low vehicle demand, extreme ease of wetting and dispersion and a stabilising ph value. In paint formulations nepheline syenite has exceptionally good tint retention characteristics.

In plastics, nepheline syenite has found increasing use in rigid, flexible, and plastisol-type polyvinyl chloride and in epoxy and polyester resin systems. It exhibits extremely low resin demand thus making high loadings possible. In PVC resins it exhibits extremely low tinting strength, has a refractive index close to that of vinyl resin and has a very low optical dispersion.

Mineral Wool and Fibreglass

Mineral wool is a term applied to manufactured fibres of silicate glass with useful properties of thermal and acoustic insulation. It is a low priced commodity and purity standards are generally low. Since crude nepheline syenite in lump form has been found to impart useful properties to the fibres as well as assisting the melting process, it has been used increasingly in North American mineral wool production.

Fibreglass is a special type of high quality mineral wool and the raw material requirements are as stringent as for colourless glass. Beneficiated glass grade nepheline syenite imparts desirable qualities of durability and resistance to devitrification to the glass fibres, in addition to acting as a flux, and consequently is used extensively in Europe and North America for this purpose.

Ornamental Use

The coarse-grained nepheline syenites have an attractive appearance due to the presence of coloured (cancrinite) or darker ferromagnesian (biotite) minerals in a light coloured mass of nepheline and alkali feldspar, which makes them suitable for ornamental use.

The poor resistance of the feldspathoids to weathering process, and restricted reserves, have generally inhibited their large scale use as an ornamental stone for external decoration in Europe and North America. Within the Bull's Run Complex there are, however, sufficient reserves of decorative quality stone which could be exploited for internal use.

Alumina, Cement and Alkali Products

Rocks rich in nepheline have attracted interest as possible sources of alumina, particularly in those countries where bauxite resources are limited or supplies are unreliable. The U.S.S.R. is understood, however, to be the only country where nepheline is actually used to produce alumina. This began in 1951 by treating nepheline concentrates from the Kola apatite mines. Valuable by-products of this treatment are cement and alkali products which make an important contribution to the economic viability of the extremely capital intensive process.

In South Africa, preliminary tests were carried out by Mintek in 1967 to concentrate nepheline from ijolite of the Spitskop Complex and then extract alumina from it. Acid leaching was used to extract Al_2O_3 , K_2O and Na_2O , but this process was considered uneconomic. Sintering with lime also resulted in the extraction of these oxides at a lower cost and this is the method adopted by the Russians.

In view of the strategic and export potential of the alumina which could be obtained from treating the Bull's Run nepheline syenite, further research and development appear to be warranted, especially as the Bull's Run syenites are relatively rich in alumina when compared to other syenites in South Africa.

6.0 PRODUCTION AND TRADE

World production of processed nepheline syenite (excluding the U.S.S.R.) has grown steadily, as indicated in Fig.3, from some 250 000 tons in 1961 to current levels of around 780 000 tons. Major expansion in the glass and ceramic markets in Europe and the U.S. has been responsible for much of the growth in demand.

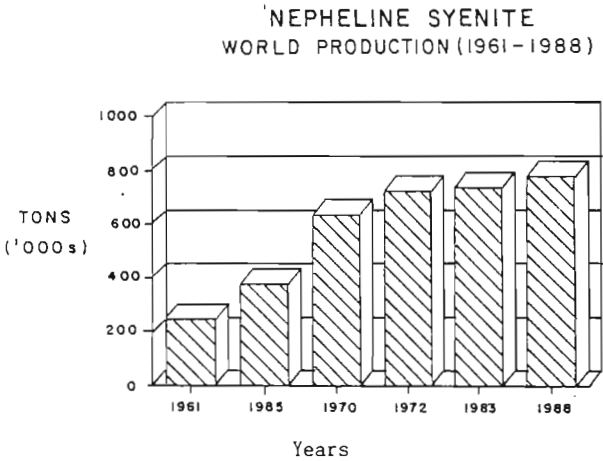


Figure 3

Canadian production increased steadily from 240 000 tons in 1961 to some 500 000 tons in 1970, and to around 600 000 tons in 1980 despite a brief decline in 1984/85. Approximately 80% of Canadian production is exported, the majority to the U.S. and the balance to the U. K. and Europe.

Norwegian production increased from 8 000 tons in 1960 to approximately 150 000 tons in 1971, gradually edging up to its current level of 230/240 000 tons per annum. Some 90% of its production is exported, primarily to Europe (West Germany, France, the Netherlands and the U.K.).

World-wide the annual growth rate in the production and sales of processed nepheline syenite is forecast in the range of 2 - 4% (16 - 32 000 tons).

Both locally and overseas there has been a similar upward trend in the production and sales of nepheline syenite's main competitor - feldspar. World production of feldspar rose from 2 million tons in 1966 to 3,6 million tons in 1980 and 4,1 million in 1984. Whilst local sales, as shown in Figure 4, have risen from 22 000 tons in 1961 to 74 000 tons in 1988.

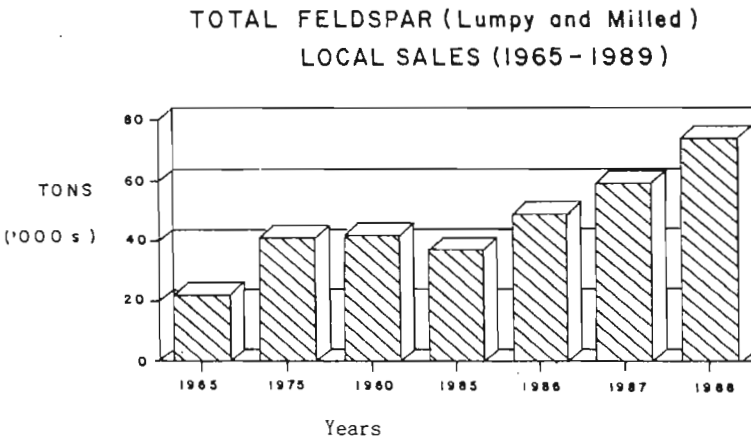


Figure 4

This data gives an indication of the potential market for the Bull's Run nepheline syenites, providing that all the technical criteria for substitution can be satisfied and the pricing is competitive.

7.0 CONCLUSIONS

Current geological and metallurgical work has shown that a range of nepheline syenite products suitable for glass and ceramic manufacture, locally and overseas, can be obtained from the recently explored Bull's Run Syenite Complex.

With further research and development other marketable products such as phosphate, ilmenite, possibly alumina and alkali carbonates will result. The location and vast resources of the Complex enhance its potential for long term mineral development.

8.0 REFERENCES

- Allen, J.B. and Charsley, T.J. (1968). Nepheline Syenite and Phonolite, Institute of Geological Sciences, Minerals Resources Division, London. p.169
- Charlesworth, E.G. (1981). Tectonics and metamorphism of the northern margin of the Namaqua-Natal Mobile Belt near Eshowe, Natal. Ph.D. thesis (unpublished). University of Natal, Durban.
- Germiquet, J.D. (1985). The mineral flux potential of the Bull's Run Syenite Complex, N.W. of Eshowe, KwaZulu. South African Development Trust Corporation Ltd., Pretoria. STK library ref. 2215
- Germiquet, J.D. (1986). Preliminary cost study for the production of nepheline syenite from Bull's Run Syenite Gneiss Complex near Eshowe. South African Development Trust Ltd., Pretoria, STK library ref. 2246
- Germiquet, J.D. (1986). The Industrial Mineral Potential of the Bull's Run Syenite Complex North-West of Eshowe, KwaZulu. South African Development Trust Corporation Ltd., Pretoria, STK library ref. 2312
- Hansen, K.R.N., Romm, J.H., McCulloch, H.W. and Laschinger J.E. (1967). The Extraction of Alumina, Potash and Soda from a Nepheline Concentrate. Report No. 149, Mintek, Randburg.
- Scogings, A.J. and Forster, I.F. (1989). Gneissose Carbonatites in the Bull's Run Complex, Natal. J. Geol. Soc. of S.A., Vol. 92, 1, in press.
- Minnes, D.G. (1975). Nepheline Syenite. In, Lefond, S.J., et al., Eds., Industrial Minerals and Rocks, 861-893. Port City Press, Baltimore, U.S.A., 1360 pp.
- Mngomezulu, M.A. (1986). Bull's Run Nepheline Syenite : Reserve No. 19, Wilderness, Bull's Run Estate, Black Eyes and Goedertrouw, Mtonjaneni, KwaZulu. South African Development Trust Corporation Ltd., Pretoria, STK library ref. 2311.

samancor limited

Delmas Silica Mine

Registration No. 64/03272/07

**P.O. BOX 65
DELMAS 2210
TELEPHONE 0157 2204/2287
TELEX 747241
TELEFAX 0157 2787**

**METALLURGICAL SILICA
GRADED REFRACTORY AND
INDUSTRIAL SILICA SAND**